EMERGING INFECTIOUS DISEASES®

U.S. CENTERS FOR DISEASE CONTROL AND PREVENTION

The Diversity of Life

August 2024

Gustav Klimt (1862–1918). *The Tree of Life, Stoclet Frieze* (1905–1909). Oil, gold leaf, mosaic on canvas, 77 in x 40 in/195 cm x 102 cm (combined dimensions for 3 panels). Museum of Applied Arts, Vienna, Austria. Photo credit: Album/Art Resource. Digital image from Art Resource, New York, New York, USA.

EMERGING INFECTIOUS DISEASES®

Emerging Infectious Diseases is published monthly by the Centers for Disease Control and Prevention, 1600 Clifton Rd NE, Mailstop H16-2, Atlanta, GA 30329-4018, USA. Telephone 404-639-1960; email, eideditor@cdc.gov

EMERGING INFECTIOUS DISEASES®

The Diversity of Life

August 2024

On the Cover

Gustav Klimt (1862–1918). *The Tree of Life*, *Stoclet Frieze* (1905–1909). Oil, gold leaf, mosaic on canvas, 77 in x 40 in/ 195 cm x 102 cm (combined dimensions for 3 panels). Museum of Applied Arts, Vienna, Austria. Photo credit: Album/ Art Resource. Digital image from Art Resource, New York, New York, USA.

About the Cover p. 1740

Perspective

Synopses

Research

EMERGING INFECTIOUS DISEASES®
August 2024

Dispatches

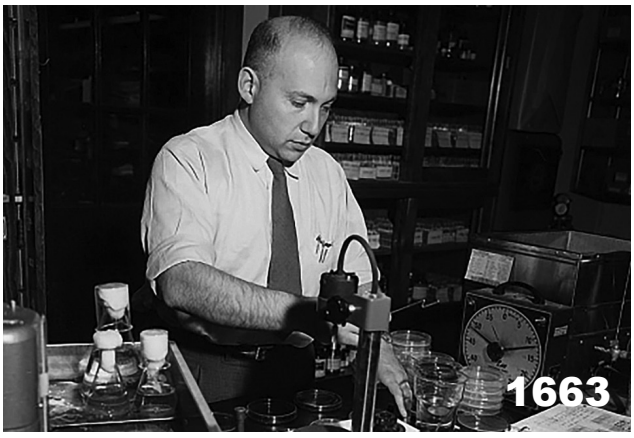

Research Letters

EMERGING INFECTIOUS DISEASES®
August 2024

Comment Letter

About the Cover

Etymologia

Online Reports

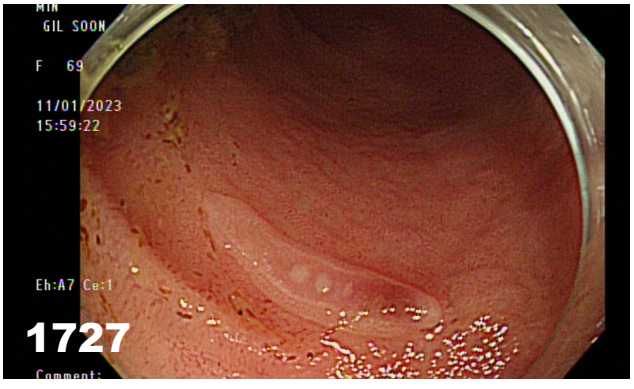

Emerging Infectious Diseases
Photo Quiz Articles

Volume 14, Number 9
September 2008

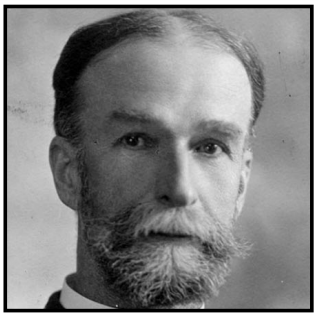

Volume 14, Number 12
December 2008

Volume 15, Number 9
September 2009

Volume 15, Number 10
October 2009

Volume 16, Number 6
June 2010

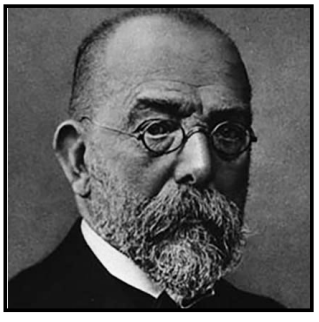

Volume 17, Number 3
March 2011

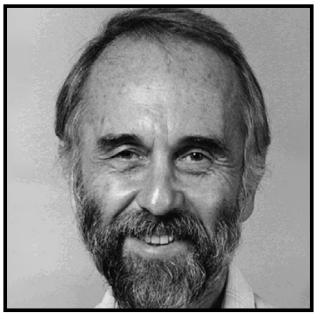

Volume 17, Number 12
December 2011

Volume 19, Number 4
April 2013

Volume 20, Number 5
May 2014

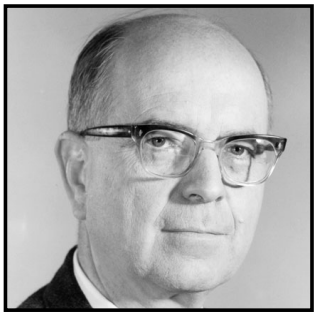

Volume 21, Number 9
September 2015

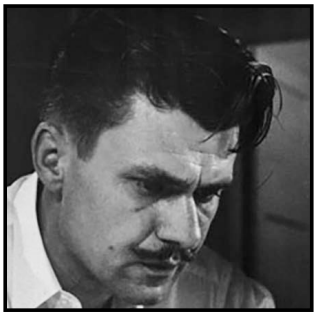

Volume 22, Number 8
August 2016

Volume 28, Number 3
March 2022

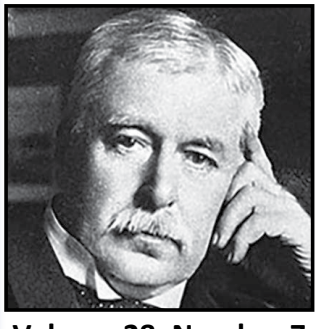

Volume 28, Number 7
July 2022

Click on the link below to read about the people behind the science.

https://bit.ly/3LN02tr

See requirements for submitting a photo quiz to EID.

https://bit.ly/3VUPqfj

EID Journal

Archaea in the Human Microbiome and Potential Effects on Human Infectious Disease

Stefanie Duller, Christine Moissl-Eichinger

Medscape CME Activity

In support of improving patient care, this activity has been planned and implemented by Medscape, LLC and Emerging Infectious Diseases. Medscape, LLC is jointly accredited with commendation by the Accreditation Council for Continuing Medical Education (ACCME), the Accreditation Council for Pharmacy Education (ACPE), and the American Nurses Credentialing Center (ANCC), to provide continuing education for the healthcare team.

Medscape, LLC designates this Journal-based CME activity for a maximum of 1.00 ***AMA PRA Category 1 Credit(s)™***. Physicians should claim only the credit commensurate with the extent of their participation in the activity.

Successful completion of this CME activity, which includes participation in the evaluation component, enables the participant to earn up to 1.0 MOC points in the American Board of Internal Medicine's (ABIM) Maintenance of Certification (MOC) program. Participants will earn MOC points equivalent to the amount of CME credits claimed for the activity. It is the CME activity provider's responsibility to submit participant completion information to ACCME for the purpose of granting ABIM MOC credit.

All other clinicians completing this activity will be issued a certificate of participation. To participate in this journal CME activity: (1) review the learning objectives and author disclosures; (2) study the education content; (3) take the post-test with a 75% minimum passing score and complete the evaluation at https://www.medscape.org/ qna/processor/72141? Show StandAlone=true&src=prt_jcme_eid_mscpedu; and (4) view/print certificate. For CME questions, see page 1744.

NOTE: It is Medscape's policy to avoid the use of Brand names in accredited activities. However, in an effort to be as clear as possible, trade names are used in this activity to distinguish between the mixtures and different tests. It is not meant to promote any particular product.

Release date: July 15, 2024; Expiration date: July 15, 2025

Learning Objectives

Upon completion of this activity, participants will be able to:

- Distinguish the most common species of archaea found in human stools
- Assess biochemical byproducts of colonization with archaea
- Evaluate the pathogenic potential of archaea
- Identify the anatomic site most associated with archaea in pathological processes

CME Editor

Dana C. Dolan, BS, Technical Writer/Editor, Emerging Infectious Diseases. *Disclosure: Dana C. Dolan, BS, has no relevant financial relationships.*

CME Author

Charles P. Vega, MD, Health Sciences Clinical Professor of Family Medicine, University of California, Irvine School of Medicine, Irvine, California. *Disclosure: Charles P. Vega, MD, has the following relevant financial relationships: served as an advisor or consultant for Boehringer Ingelheim; GlaxoSmithKline.*

Authors

Stefanie Duller, MSc; Christine Moissl-Eichinger, Dr. rer. nat.

Author affiliations: Medical University of Graz, Graz, Austria (S. Duller, C. Moissl-Eichinger); BioTechMed Graz, Graz (C. Moissl-Eichinger)

DOI: http://doi.org/10.3201/eid3008.240181

Archaea represent a separate domain of life, next to bacteria and eukarya. As components of the human microbiome, archaea have been associated with various diseases, including periodontitis, endodontic infections, small intestinal bacterial overgrowth, and urogenital tract infections. Archaea are generally considered nonpathogenic; the reasons are speculative because of limited knowledge and gene annotation challenges. Nevertheless, archaeal syntrophic principles that shape global microbial networks aid both archaea and potentially pathogenic bacteria. Evaluating archaea interactions remains challenging, requiring clinical studies on inflammatory potential and the effects of archaeal metabolism. Establishing a culture collection is crucial for investigating archaea functions within the human microbiome, which could improve health outcomes in infectious diseases. We summarize potential reasons for archaeal nonpathogenicity, assess the association with infectious diseases in humans, and discuss the necessary experimental steps to enable mechanistic studies involving archaea.

Archaea are a group of single-celled microorganisms with distinct characteristics, and constitute 1 of the 3 domains of life, along with bacteria and eukarya. Although they were thought to live only in extreme environments such as hot springs, archaea have emerged as important components of the human microbiome. Despite their potential importance to human health and disease, archaea are studied less than other members of the microbiome, such as bacteria and fungi. The human microbiome harbors a variety of archaeal species from different phyla (*1*). Archaeal representatives have been found in various body sites, including the skin, the respiratory tract, the urogenital tract, and the gastrointestinal tract (*2*,*3*). Human-associated archaeal communities exhibit spatial patterns similar to those of bacteria; notable examples are the predominant signatures of ammonia-oxidizing Nitrososphaeria on the skin, methane-producing (methanogenic) Archaea in the urogenital and gastrointestinal tracts, and unknown Nanoarchaeota (formerly Woesearchaeota) in the respiratory tract (*1*–*3*).

Given that the gastrointestinal tract contains 99% of all microbial biomass in the human body and serves as the gateway for numerous diseases, research on human-associated archaea, as with bacteria, has primarily focused on fecal samples. In human feces, the most prevalent (>90%) archaeal representatives are *Methanobrevibacter smithii* and *Candidatus* Methanobrevibacter intestini, (*1*,*4*,*5*). In particular, *M. smithii* is highly abundant, especially in persons emitting high levels of methane (*6*). Because many studies primarily concentrate on fecal samples rather than in vivo samples, and because of general methodological challenges associated with archaea detection (*7*,*8*), our understanding of the human archaeome (all archaea residing in the human body) still lacks comprehensive insights into diversity, taxonomic classification, and, importantly, the functional and mechanistic roles of archaea.

Pathogenic Traits

Pathogenicity, the ability to cause disease in multicellular hosts, is widespread in various domains of life. In total, >1,500 human pathogenic bacterial species belonging to 10 phyla and 24 classes are known (*9*). The pure ratio observed in the bacterial domain indicates that >16 archaeal pathogens should exist (*10*); however, despite individual case reports and possible correlations with certain polymicrobial diseases (e.g., periodontitis), archaea are mostly considered nonpathogenic. No single representative of archaea known to date possesses capabilities consistent with Koch's postulates, which has led to several discussions about possible reasons for that observation (*10*–*13*).

In theory, archaea have the prerequisites to evolve into pathogens because they are genetically and metabolically diverse, ubiquitous in the environment, and able to conflict with close relatives by using compounds directed against archaea (*10*). It is possible that our limited ability to accurately recognize them in disease conditions (not-yet-been-discovered hypothesis) is the reason no archaeal pathogens have been identified (*8*,*11*). Other perspectives have proposed that archaeal pathogens might not exist, potentially because they use different cofactors than those found in eukaryotes (*14*) or are unable to use the organic resources of the host, which are typically exploited by bacterial pathogens on a large scale (metabolism hypothesis) (*15*; D.J. Harrison, master's thesis, 2022, https://researchspace.auckland.ac.nz/handle/2292/63414). Alternatively, some argue that pathogenesis in archaea does not exist because they do not possess the required virulence factor genes (gene-absence hypothesis) (D.J. Harrison, master's thesis, 2022). Related hypotheses suggest that archaea cannot acquire virulence factors from bacteria or eukaryotes, possibly because their viruses and cell walls do not permit transfer between domains (virus hypothesis) (*10*). All those hypotheses warrant discussion. However, considering the huge lack of knowledge regarding gene annotation (virulence factors might be present, but we cannot identify them; or the metabolic capacities of methanogenic archaea have not yet been fully assessed, and we do not understand

their behavior in the host with respect to metabolites taken up), a more superficial view on the principles of bacterial pathogenic traits might be useful.

Several steps are necessary for bacterial pathogenicity to develop: invasion, colonization, damage, and transmission (*16*) (Figure 1). Some of those traits overlap with archaeal characteristics, including exposure to the host (archaea are commensals) and the ability to adhere to and colonize the host (archaea form biofilms and might be able to attach to surfaces through their adhesins). Furthermore, the immunogenic reaction is highly species-specific; immunogenic potential is low for *Methanobrevibacter* spp. but stronger for *Methanosphaera* spp. (*17*). Transmission to other hosts seems probable; Pausan et al. demonstrated that methanogens can survive extended periods under oxygenated conditions (*18*). Archaea can team up with bacterial pathogens in harmful groups that can enter hosts' tissues and benefit from invasion or cause damage to the host. In this context, we should mention the keystone pathogen hypothesis (*19*), in which some microorganisms could orchestrate the microbiome toward a disease status even in low numbers. Indeed, their metabolic capacity at the end of the food chain, consuming fermentation waste products, indicates that methanogens can influence the entire microbiome; their extraordinarily strong pull toward methane production can result in a microbial community optimized for fiber degradation and coping with B12 shortage (*6*).

Overall, the discussion on the potential of archaea for bearing pathogenic action at this stage remains highly speculative, underscoring the need for further research to elucidate their role in disease. We will address the different examples for infectious state in the human body that involve archaea and warrant deeper studies.

Potential Contribution to Infectious Diseases

The involvement of pathogenic bacteria in various infectious diseases is often the focus of studies, but our understanding of the role of archaea in this context is still limited. Although no pathogenic archaea are known to date, the literature has presented some evidence of links between archaea and various infectious diseases (*4*,*20*,*21*) (Figure 2).

Principles of archaeal syntrophy may play a role in shaping specific microbial networks that influence the overall condition but do not cause disease. Studies suggest that methanogenic archaea engage in a symbiotic relationship with bacteria; they use hydrogen (H_2) and other byproducts of bacterial fermentation for methanogenesis, thereby reducing H_2 pressure

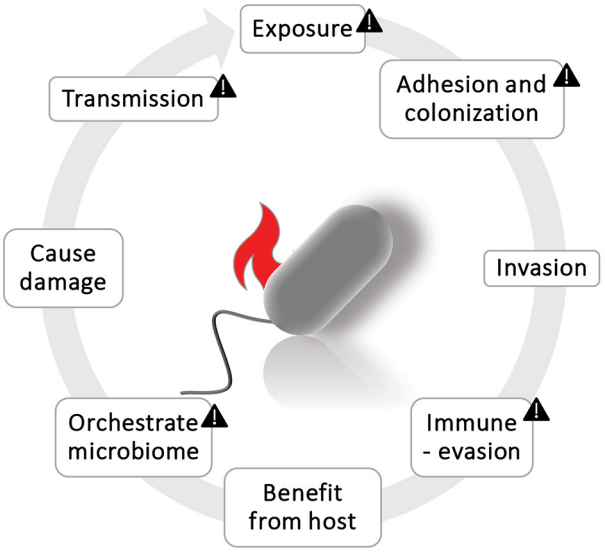

Figure 1. Cycle of pathogen actions. Triangles indicate pathogenic potentials for archaea. The other actions still require attention and strategic research. Figure created with BioRender (https://www.biorender.com).

(*1*). In addition, they produce metabolites, including short-chain fatty acids or vitamins (e.g., formate, B12) (*6*) that could support the growth of both archaea and potentially pathogenic bacteria (*1*,*4*,*21*).

We will explore the potential role of archaea in human infectious diseases in the oral cavity, gastrointestinal tract, and urogenital tract. Archaea have also been detected in other parts of the body, such as the skin (*22*) and the respiratory tract (*3*). However, for both those sites, the information available is too sparse to elaborate on potential infectious traits.

Oral Cavity

A diverse microbial community thrives in the oral cavity; it includes various microorganisms, among which archaea, specifically the genus *Methanobrevibacter*, should be emphasized. The archaea have been identified in both healthy and sick persons (*1*,*4*). Of note, the strain and species resolution of archaeal diversity associated with humans is only partially satisfactory so far. Most of the studies we cite used 16S rRNA gene sequencing (partially with short reads), which does not allow differentiation of the major *Methanobrevibacter* species. Therefore, any subsequent information provided at the species level should be carefully scrutinized and requires reevaluation.

Periodontitis

Periodontitis is one of the most common bacterial infections in humans and the 6th most common disease worldwide (*23*). It is a complex dysbiotic disease

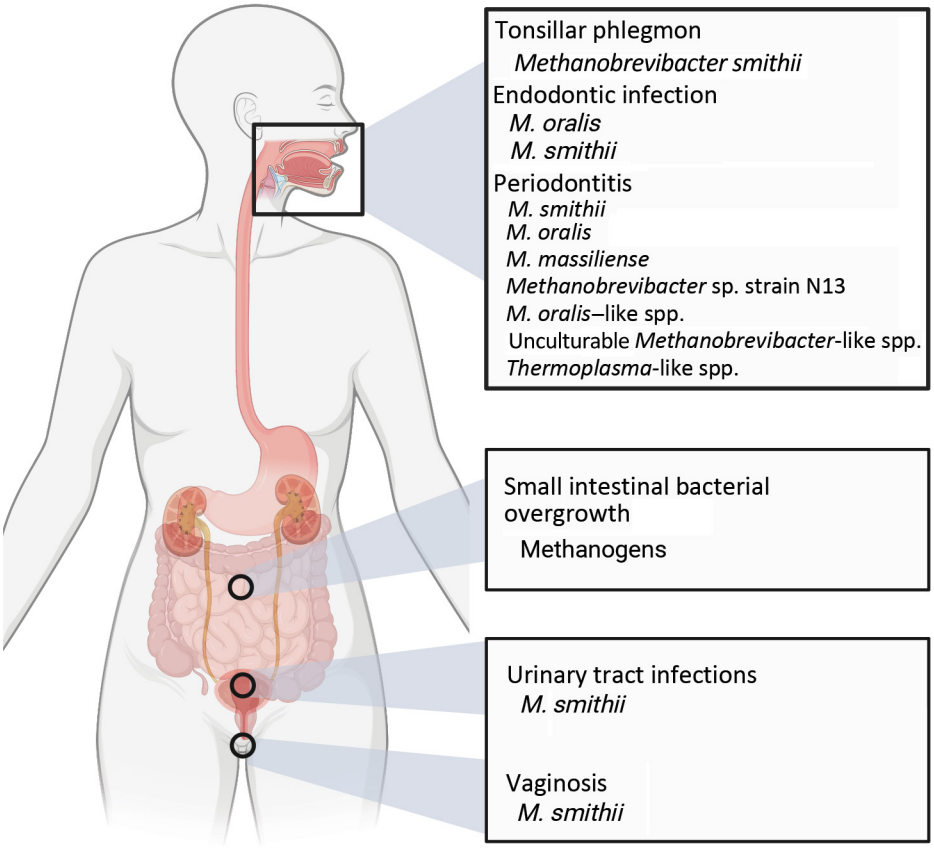

Figure 2. Infectious diseases in areas of the body in which archaea may have an effect. Figure created with BioRender (https://www.biorender.com).

that develops over a longer timeframe and is the consequence of destructive host immune response to pathogenic, biofilm-forming microorganisms (*24*). It is characterized by the gradual loss of bone, the development of periodontal pockets, and the progressive decline in tooth function (*25*,*26*). Untreated periodontitis is recognized as a risk factor for life-threatening systemic diseases, such as endocarditis, atherosclerosis, and stroke. In addition, it is considered a co-factor for preterm birth (*25*).

Various microorganisms have been implicated in the onset of periodontitis, including different bacteria (e.g., *Tannerella*, *Treponema*, *Prevotella*, *Fusobacterium*), and potentially methanogenic archaea (*25*,*26*). In particular, *M. oralis*, *M. smithii*, and *M. massiliense* were identified in periodontitis patients within subgingival plaques and deep periodontal pockets (*27*). It has been shown that *M. oralis* is more prevalent and abundant in severe periodontitis but was not detected in healthy sites close-by and was not found after healing (*27*). Methanogenic archaea can comprise up to 18% of all community members in severe periodontitis (*1*,*28*,*29*).

Archaea have a completely different biology from bacteria. Most of the methods used in microbiology and microbiome research have been developed to optimally study and analyze bacteria, which means archaeal signatures are overlooked in most studies, so knowledge about the involvement of archaea is very limited (*8*). To date, the microbiology of periodontitis has been poorly studied and often remains descriptive. The reasons for the development of the various complex stages and disorders, and the influence of therapy and treatment, remain largely unexplored.

Endodontic Infection

Endodontic infection refers to a microbial infection that develops within the pulp of a tooth, the central part containing nerves, blood vessels, and connective tissues. Typically caused by bacterial invasion, such infections often stem from factors such as tooth decay, dental trauma, incorrect cavity preparation during dental procedures, or use of contaminated restorative materials. Bacteria can infiltrate the root canal primarily through caries, dental anomalies, lateral canals, or damaged cementum. The predominant bacterial phyla identified in infected root canals are Firmicutes, Proteobacteria, Spirochaetes, Bacteroidetes, and Actinobacteria (*30*).

Efenberger et al. detected methanogenic archaea, especially *M. smithii* and *M. oralis*, in 85% of infected

pulp tissues using 16S rRNA gene sequencing. That finding suggests that archaea may play a role in the development of endodontic infection, potentially in collaboration with bacteria (*30*). Given that methanogens are involved in deep oral and dental infections, and considering the associated barrier breach, they could spread from that location to other closely located body areas and possibly lead to brain and muscular abscesses, as described in single cases (*31*).

Tonsillar Phlegmon

Tonsillar phlegmon, a retropharyngeal abscess, mainly affects adolescents and young adults and is caused by an infection originating from the peritonsillar space and the pharyngeal sphincter. The infection can spread to adjacent tissues and, if not treated promptly, this condition, which often involves pathogens such as *Streptococcus pyogenes* and *Fusobacterium necrophorum*, can escalate and become a serious threat (*32*).

Within tonsillar phlegmon, archaea, particularly *M. smithii*, may foster the growth of pathogenic bacteria through syntrophic interactions. In addition, archaeal methanogenesis activity, leading to methane (CH_4) production, could contribute to radiologically visible gas in tonsillar phlegmon cases (*32*). Djemai et al. identified *M. smithii* using 16S rRNA gene sequencing with coexisting bacteria commonly found in *M. smithii* co-infections. Those bacteria belonged to enterobacterial and bacterial orders that include hydrogen producers.

Gastrointestinal Tract

The gastrointestinal tract houses most of the microbes in our body, including a rich diversity of archaea. Predominant members of the gastrointestinal archaeome include *M. smithii* and *Candidatus* M. intestini, constituting >90% of the gut archaeome (*4*,*5*). Additional noteworthy members encompass *M. stadtmanae*, *M. oralis*, Methanosarcinales, Methanomassiliicoccales, and Haloarchaea (*33*–*35*).

Methanogenic archaea are known for performing methanogenesis, converting bacterial end products (hydrogen and carbon dioxide) into methane and adenosine triphosphate (*1*,*36*). Methane travels through the gut and is expelled through flatus or enters the blood to eventually be excreted through the lungs; it is detectable in human breath (*37*). High methane breath levels (>5 ppm) were shown to correlate with a thousandfold increase in *Methanobrevibacter* abundance in the gut (*6*). Therefore, methane production serves as a reliable biomarker for the presence of methanogens in the gut. Varied breath methane levels (and corresponding methanogen abundances) have been associated with diverse health conditions, including small intestinal bacterial overgrowth (SIBO) (*4*).

SIBO

SIBO is characterized by an overgrowth of bacteria, surpassing normal levels (>10^5 colony-forming units), in the small intestine (*38*). Usually, this overgrowth is caused by gram-negative anaerobic bacteria, manifesting by a hydrogen-positive breath test. In a substantial (30%) number of cases, the overgrowth of archaea was reported (as methane-dominant SIBO or intestinal methanogen overgrowth), recognized by the production of methane, instead of H_2. Of note, SIBO is more prevalent in patients with inflammatory bowel syndrome than in healthy controls; a link with methanogen presence and constipation-type IBS has been established (*39*).

Madigan et al. suggested differing symptoms between SIBO caused by methanogens and that caused by hydrogen-producing bacteria (*40*). Methane-producing SIBO, especially prevalent in older persons, is linked to a reduced incidence of vitamin B12 (cobalamin) deficiency (*38*,*41*). Methanogens, which are able to produce cobalamin themselves (*42*), could help to make up for such a deficiency, which is in line with a previous study that showed that reduced vitamin B12 uptake was associated with a high methanogen load in the gastrointestinal tract (*6*,*40*). Conversely, hydrogenic SIBO is associated with higher occurrences of symptoms like diarrhea, cholecystectomy, diabetes, and Roux-en-Y gastric bypass surgery. Those distinctions may arise from varying sensitivities of archaeal physiology to host factors, including gut anatomy, motility, luminal bile acid concentration, and the capacity to synthesize or salvage cobalamin from neighboring microbiota or diet (*40*).

Urogenital Tract

The urogenital tract encompasses a system of organs integral to urinary and reproductive functions. This system comprises the kidneys, ureters, bladder, and urethra to form, transport, and eliminate urine. Furthermore, it incorporates reproductive organs such as testes in male persons and the ovaries, uterus, and vagina in females (*43*). The urogenital microbiota contribute to the maintenance of homeostasis in the urinary tract by influencing the immune response; alterations of the microbial communities are documented to be related to various diseases (*44*). The close proximity of the urinary tract, vagina, and gastrointestinal tract enables the transmission of microorganisms, including archaea, from feces to those regions, which

may contribute to infectious diseases such as urinary tract infections and vaginosis.

Urinary Tract Infections

Traditionally, urine was believed to be sterile; however, current understanding acknowledges the presence of a microbiome in the urogenital tract. This microbiome plays a crucial role in the pathophysiology of urinary tract infections (UTIs) and the maintenance of urinary tract health (*44*,*45*). UTIs commonly arise when microbes from the rectal area enter the urethra, migrating upward into the bladder or other areas of the urinary tract (*46*).

Various factors, including sexual activity, urinary tract abnormalities, a weakened immune system, catheter use, and hormonal changes, can elevate the risk of a UTI developing (*48*). Bacteria are typically associated with UTIs; however, *M. smithii* has also been identified as a component of the urinary microbial community. Urine samples containing *M. smithii* have exhibited the presence of hydrogen-producing enterobacteria, including *Escherichia coli* and *Klebsiella pneumoniae*. The consistent co-occurrence suggests a potential role of *M. smithii* in supporting the dysbiosis by promoting the growth of enterobacteria, which are recognized agents of UTIs (*45*,*46*).

Vaginosis

Vaginosis refers to an imbalance in the vaginal microbiota, leading to discomfort and noticeable symptoms (*48*). The vagina typically hosts microbiota with lower diversity, predominantly consisting of lactobacilli. Vaginosis can arise as a result of changes in vaginal pH or transfer of fecal microbes from the gastrointestinal tract to the vagina (*48*). Of note, *M. smithii* has been identified in patients with vaginosis, and its presence has been proposed as a potential biomarker for this condition (*48*). This association is plausible, considering that *M. smithii* is the most prevalent archaea found in the gastrointestinal tract (*4*). Some studies have faced challenges in detecting archaea in samples from both healthy and infected women (*49*). It has been suggested that methanogens contribute to vaginal health (C.J. Neumann et al., unpub. data, https://www.biorxiv.org/content/10.1101/2023.08.31.555744v1).

Methanogenesis by archaea is believed to play a role in maintaining the pH balance of the vaginal microbiome. Moreover, it helps prevent the accumulation of acidic conditions that could disrupt the vaginal microbiome (*50*). Although *M. smithii* might be among the usual vaginal microbiota, its specific connection to vaginosis requires further investigations for a comprehensive understanding.

Conclusions

The literature demonstrates that archaea constitute active components within the human microbiome and are prevalent across a range of different body sites (*2*). Associations with various infectious diseases, such as periodontitis and endodontic infections within the oral cavity, SIBO in the gastrointestinal tract, and infections of the urogenital tract, have been reported (*1*,*4*). Although many of those reports are preliminary and do not fully resolve the archaeal components taxonomically, the genus *Methanobrevibacter* emerges as the most commonly observed archaea possibly linked to these infectious diseases (Figure 2; Appendix, https://wwwnc.cdc.gov/EID/article/30/8/24-0181-App1.pdf).

Understanding the complexities of detoxifying microbial metabolic products, particularly in the context of methanogenesis, carries substantial implications for both pathogen growth and disease onset. The interaction between archaea and bacteria in syntrophic relationships offers valuable insights into the dynamics within microbial communities. It is essential to conduct a thorough investigation to reveal the complex mechanisms behind these connections, which could play a role in shifting the microbiome toward a diseased state. Those experiments not only would shed light on potential disease mechanisms but also could open up paths for novel therapeutic approaches to address microbial dysbiosis linked to conditions such as periodontitis and other diseases (*50*).

The extent to which interactions with archaea are beneficial, neutral, or pathogenic is not well understood. Furthermore, advancing research in human health demands an increased focus on clinical studies that consider the inflammatory potential of archaea. In addition, such studies should explore the influence of archaeal metabolisms and their products, including the effects of methane on the human body (*1*). Although archaea are generally considered nonpathogenic, they could have the potential prerequisites for pathogenesis. Various hypotheses, such as the not-yet-been-discovered, metabolism, gene-absence, and virus hypotheses, are proposed to explain the apparent absence of archaeal pathogens (*8*,*10*,*11*,*16*). However, because of limited knowledge, challenges in gene annotation, and the complex nature of archaeal behavior in host environments, those hypotheses have not been proven. Although some pathogenic traits overlap between bacteria and archaea, the discussion of potential pathogenic action of archaea is ongoing and emphasizes the need for further research to understand their role in disease.

To gain a more comprehensive understanding of the role of archaea in health and disease requires additional initiatives aimed at effectively characterizing host-associated and disease-associated archaea. Despite the use of molecular biologic techniques in studying the archaeome, detecting archaea presents challenges primarily because standard protocols in research and diagnostics that are optimized for bacteria prove suboptimal for archaea because of their diverse cell structure, physiology, and metabolic activity. Those distinctive features, coupled with inappropriate protocols for sampling, DNA extraction, and PCR primer selection, create obstacles in visualizing, culturing, or analyzing archaea. Moreover, the absence of extensive reference databases hinders a thorough evaluation of the acquired data. Compounding this challenge is the presence of a robust bacterial or host background, further complicating the detection and analysis of archaea (*8*).

The limited availability of archaeal cultures hinders in-depth, mechanistic, physiologic and comprehensive analyses, including multiomics and interaction studies that could deepen our comprehension of archaea's role in health and disease (Figure 3). According to the Global Catalog of Microorganisms (https://gcm.wdcm.org/species?taxonid=2173), only a handful of host-associated archaeal isolates are publicly accessible in culture. Those isolates include 3 strains of *M. oralis* from the human oral cavity and subgingival plaque, along with 4 strains of *M. smithii* isolated from human feces and the large intestine. The limited availability of cultures presents a substantial hindrance to conducting thorough research. Publications do exist describing the successful isolation of various archaea from patients with diverse health conditions (*5*), but there is currently no comprehensive culture collection for archaea. Establishing such a collection would be pivotal for advancing research on the archaeome; we have established a cultivation pipeline for the enrichment and cultivation of methanogenic archaea in a highly efficient way (J. Duller, et al., unpub. data, https://doi.org/10.1101/2024.04.10.588852).

Expanding our collection of human-derived isolates is crucial for gaining deeper insights into the functions and roles of archaea, enabling functional analyses in disease models, and determining the

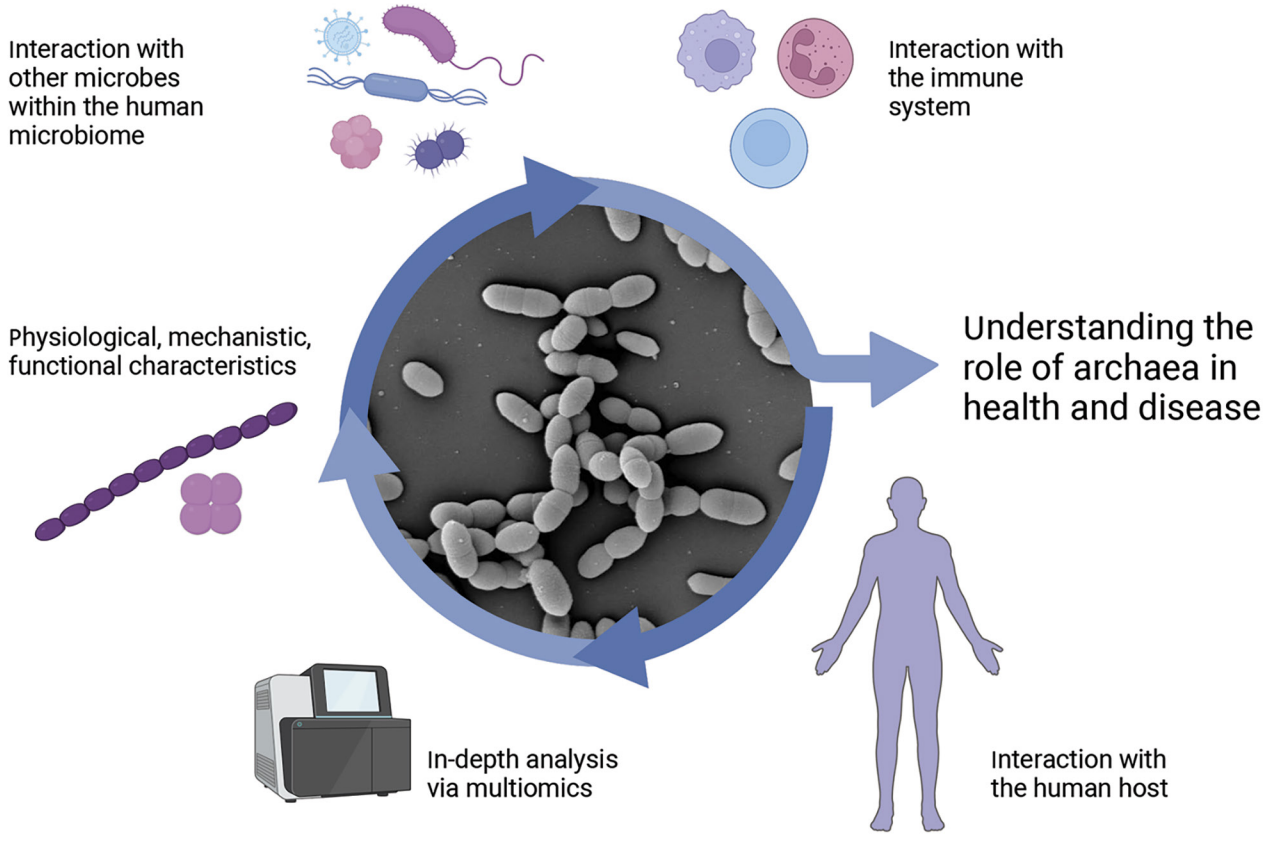

Figure 3. Exploration of analytical potentials using archaeal isolates to enhance understanding of the role of archaea in health and disease. Figure created with BioRender (https://www.biorender.com).

effects of their structural elements and metabolites. Microorganisms within a microbiome network engage in various interactions that affect each other and the health of the host. Understanding of such microbial interactions beyond the bacterial sphere is essential for a more comprehensive grasp of disease mechanisms and the search for new diagnostic, preventive, and therapeutic strategies.

This research was funded in whole or in part by the Austrian Science Fund (FWF) (grants P 32697, P 30796, SFB F-83, COE 7, given to C.M.E.). S.D. was supported by the local PhD program MolMed.

About the Author

Stefanie Duller is a PhD candidate in molecular medicine at the Medical University of Graz. Her research interests include investigating microbial community dynamics, microbe-microbe interactions, and the role of archaea in health and disease.

References

1. Borrel G, Brugère JF, Gribaldo S, Schmitz RA, Moissl-Eichinger C. The host-associated archaeome. Nat Rev Microbiol. 2020;18:622–36. https://doi.org/10.1038/s41579-020-0407-y
2. Bang C, Schmitz RA. Archaea associated with human surfaces: not to be underestimated. FEMS Microbiol Rev. 2015;39:631–48. https://doi.org/10.1093/femsre/fuv010
3. Koskinen K, Pausan MR, Perras AK, Beck M, Bang C, Mora M, et al. First insights into the diverse human archaeome: specific detection of Archaea in the gastrointestinal tract, lung, and nose and on skin. MBio. 2017;8:e00824-17. https://doi.org/10.1128/mBio.00824-17
4. Mohammadzadeh R, Mahnert A, Duller S, Moissl-Eichinger C. Archaeal key-residents within the human microbiome: characteristics, interactions and involvement in health and disease. Curr Opin Microbiol. 2022;67:102146. https://doi.org/10.1016/j.mib.2022.102146
5. Chibani CM, Mahnert A, Borrel G, Almeida A, Werner A, Brugère JF, et al. A catalogue of 1,167 genomes from the human gut archaeome. Nat Microbiol. 2021;7:48–61. https://doi.org/10.1038/s41564-021-01020-9
6. Kumpitsch C, Fischmeister FPS, Mahnert A, Lackner S, Wilding M, Sturm C, et al. Reduced B12 uptake and increased gastrointestinal formate are associated with archaeome-mediated breath methane emission in humans. Microbiome. 2021;9:193. https://doi.org/10.1186/s40168-021-01130-w
7. Sun Y, Liu Y, Pan J, Wang F, Li M. Perspectives on cultivation strategies of archaea. Microb Ecol. 2020;79:770–84. https://doi.org/10.1007/s00248-019-01422-7
8. Mahnert A, Blohs M, Pausan MR, Moissl-Eichinger C. The human archaeome: methodological pitfalls and knowledge gaps. Emerg Top Life Sci. 2018;2:469–82. https://doi.org/10.1042/ETLS20180037
9. Bartlett A, Padfield D, Lear L, Bendall R, Vos M. A comprehensive list of bacterial pathogens infecting humans. Microbiology (Reading). 2022;168. https://doi.org/10.1099/mic.0.001269
10. Gill EE, Brinkman FSL. The proportional lack of archaeal pathogens: do viruses/phages hold the key? BioEssays. 2011;33:248–54. https://doi.org/10.1002/bies.201000091
11. Cavicchioli R, Curmi PMG, Saunders N, Thomas T. Pathogenic archaea: do they exist? BioEssays. 2003;25:1119–28. https://doi.org/10.1002/bies.10354
12. Conway de Macario E, Macario AJL. Methanogenic archaea in health and disease: a novel paradigm of microbial pathogenesis. Int J Med Microbiol. 2009;299:99–108. https://doi.org/10.1016/j.ijmm.2008.06.011
13. Lurie-Weinberger MN, Gophna U. Archaea in and on the human body: health implications and future directions. PLoS Pathog. 2015;11:e1004833. https://doi.org/10.1371/journal.ppat.1004833
14. Martin W, Cavicchioli R, Curmi P. Pathogenic archaebacteria: do they not exist because archaebacteria use different vitamins? BioEssays. 2004;26:592–3. https://doi.org/10.1002/bies.20044
15. Valentine DL. Adaptations to energy stress dictate the ecology and evolution of the Archaea. Nat Rev Microbiol. 2007;5:316–23. https://doi.org/10.1038/nrmicro1619
16. Ezepchuk YV. Biological concept of bacterial pathogenicity (theoretical review). Adv Microbiol. 2017;07:535–44. https://doi.org/10.4236/aim.2017.77042
17. Vierbuchen T, Bang C, Rosigkeit H, Schmitz RA, Heine H. The human-associated archaeon *Methanosphaera stadtmanae* is recognized through its RNA and induces Tlr8-dependent nlrP3 inflammasome activation. Front Immunol. 2017;8:1535. https://doi.org/10.3389/fimmu.2017.01535
18. Pausan MR, Blohs M, Mahnert A, Moissl-Eichinger C. The sanitary indoor environment—a potential source for intact human-associated anaerobes. NPJ Biofilms Microbiomes. 2022;8:44. https://doi.org/10.1038/s41522-022-00305-z
19. Hajishengallis G, Darveau RP, Curtis MA. The keystone-pathogen hypothesis. Nat Rev Microbiol. 2012;10:717–25. https://doi.org/10.1038/nrmicro2873
20. Volmer JG, McRae H, Morrison M. The evolving role of methanogenic archaea in mammalian microbiomes. Front Microbiol. 2023;14:1268451. https://doi.org/10.3389/fmicb.2023.1268451
21. Kuehnast T, Kumpitsch C, Mohammadzadeh R, Weichhart T, Moissl-Eichinger C, Heine H. Exploring the human archaeome: its relevance for health and disease, and its complex interplay with the human immune system. FEBS J. 2024;febs.17123. https://doi.org/10.1111/febs.17123
22. Probst AJ, Auerbach AK, Moissl-Eichinger C. Archaea on human skin. PLoS One. 2013;8:e65388. https://doi.org/10.1371/journal.pone.0065388
23. Frencken JE, Sharma P, Stenhouse L, Green D, Laverty D, Dietrich T. Global epidemiology of dental caries and severe periodontitis—a comprehensive review. J Clin Periodontol. 2017;44(Suppl 18):S94–105. https://doi.org/10.1111/jcpe.12677
24. Chen C, Hemme C, Beleno J, Shi ZJ, Ning D, Qin Y, et al. Oral microbiota of periodontal health and disease and their changes after nonsurgical periodontal therapy. ISME J. 2018;12:1210–24. https://doi.org/10.1038/s41396-017-0037-1
25. Vianna ME, Holtgraewe S, Seyfarth I, Conrads G, Horz HP. Quantitative analysis of three hydrogenotrophic microbial groups, methanogenic archaea, sulfate-reducing bacteria, and acetogenic bacteria, within plaque biofilms associated with human periodontal disease. J Bacteriol. 2008;190:3779–85. https://doi.org/10.1128/JB.01861-07
26. Huynh HTT, Pignoly M, Drancourt M, Aboudharam G. A new methanogen "*Methanobrevibacter massiliense*" isolated in a case of severe periodontitis. BMC Res Notes. 2017;10:657. https://doi.org/10.1186/s13104-017-2980-3

27. Pilliol V, Beye M, Terlier L, Balmelle J, Kacel I, Lan R, et al. *Methanobrevibacter massiliense* and *Pyramidobacter piscolens* co-culture illustrates transkingdom symbiosis. Microorganisms. 2024;12:215. https://doi.org/10.3390/microorganisms12010215
28. Bringuier A, Khelaifia S, Richet H, Aboudharam G, Drancourt M. Real-time PCR quantification of *Methanobrevibacter oralis* in periodontitis. J Clin Microbiol. 2013;51:993–4. https://doi.org/10.1128/JCM.02863-12
29. Lepp P W PW, Brinig MM, Ouverney CC, Palm K, Armitage GC, Relman DA. Methanogenic archaea and human periodontal disease. Proc Natl Acad Sci U S A. 2004;101:6176–81.
30. Efenberger M, Agier J, Pawłowska E, Brzezińska-Błaszczyk E. Archaea prevalence in inflamed pulp tissues. Cent Eur J Immunol. 2015;40:194–200. https://doi.org/10.5114/ceji.2015.51358
31. Drancourt M, Nkamga VD, Lakhe NA, Régis JM, Dufour H, Fournier PE, et al. Evidence of archaeal methanogens in brain abscess. Clin Infect Dis. 2017;65:1–5. https://doi.org/10.1093/cid/cix286
32. Djemai K, Gouriet F, Michel J, Radulesco T, Drancourt M, Grine G. *Methanobrevibacter smithii* tonsillar phlegmon: a case report. New Microbes New Infect. 2021;42:100891. https://doi.org/10.1016/j.nmni.2021.100891
33. Kim JY, Whon TW, Lim MY, Kim YB, Kim N, Kwon MS, et al. The human gut archaeome: identification of diverse haloarchaea in Korean subjects. Microbiome. 2020;8:114. https://doi.org/10.1186/s40168-020-00894-x
34. Scanlan PD, Shanahan F, Marchesi JR. Human methanogen diversity and incidence in healthy and diseased colonic groups using mcrA gene analysis. BMC Microbiol. 2008;8:79. https://doi.org/10.1186/1471-2180-8-79
35. Borrel G, McCann A, Deane J, Neto MC, Lynch DB, Brugère JF, et al. Genomics and metagenomics of trimethylamine-utilizing Archaea in the human gut microbiome. ISME J. 2017;11:2059–74. https://doi.org/10.1038/ismej.2017.72
36. Polag D, Keppler F. Global methane emissions from the human body: past, present and future. Atmos Environ. 2019;214:116823. https://doi.org/10.1016/j.atmosenv.2019.116823
37. Hudson MJ, Tomkins AM, Wiggins HS, Drasar BS. Breath methane excretion and intestinal methanogenesis in children and adults in rural Nigeria. Scand J Gastroenterol. 1993;28:993–8. https://doi.org/10.3109/00365529309098298
38. Hoegenauer C, Hammer HF, Mahnert A, Moissl-Eichinger C. Methanogenic archaea in the human gastrointestinal tract. Nat Rev Gastroenterol Hepatol. 2022;19:805–13. https://doi.org/10.1038/s41575-022-00673-z
39. O'Dwyer D. Homemade elemental diet to treat intestinal methanogen overgrowth: a case report. Integr Med (Encinitas). 2021;20:32–41.
40. Madigan KE, Bundy R, Weinberg RB. Distinctive clinical correlates of small intestinal bacterial overgrowth with methanogens. Clin Gastroenterol Hepatol. 2022;20:1598–1605.e2. https://doi.org/10.1016/j.cgh.2021.09.035
41. Pimentel M, Saad RJ, Long MD, Rao SSC. ACG Clinical guideline: small intestinal bacterial overgrowth. Am J Gastroenterol. 2020;115:165–78. https://doi.org/10.14309/ajg.0000000000000501
42. Jiang Q, Lin L, Xie F, Jin W, Zhu W, Wang M, et al. Metagenomic insights into the microbe-mediated B and K_2 vitamin biosynthesis in the gastrointestinal microbiome of ruminants. Microbiome. 2022;10:109. https://doi.org/10.1186/s40168-022-01298-9
43. Neugent ML, Hulyalkar NV, Nguyen VH, Zimmern PE, De Nisco NJ. Advances in understanding the human urinary microbiome and its potential role in urinary tract infection. MBio. 2020;11:e00218-20. https://doi.org/10.1128/mBio.00218-20
44. Kim YB, Whon TW, Kim JY, Kim J, Kim Y, Lee SH, et al. In-depth metataxonomic investigation reveals low richness, high intervariability, and diverse phylotype candidates of archaea in the human urogenital tract. Sci Rep. 2023;13:11746. https://doi.org/10.1038/s41598-023-38710-9
45. Grine G, Lotte R, Chirio D, Chevalier A, Raoult D, Drancourt M, et al. Co-culture of *Methanobrevibacter smithii* with enterobacteria during urinary infection. EBioMedicine. 2019;43:333–7. PubMed https://doi.org/10.1016/j.ebiom.2019.04.037
46. Flores-Mireles AL, Walker JN, Caparon M, Hultgren SJ. Urinary tract infections: epidemiology, mechanisms of infection and treatment options. Nat Rev Microbiol. 2015;13:269–84. https://doi.org/10.1038/nrmicro3432
47. Vasudevan R. Urinary tract infection: an overview of the infection and the associated risk factors. J Microbiol Exp. 2014. https://doi.org/10.15406/jmen.2014.01.00008
48. Grine G, Drouet H, Fenollar F, Bretelle F, Raoult D, Drancourt M. Detection of *Methanobrevibacter smithii* in vaginal samples collected from women diagnosed with bacterial vaginosis. Eur J Clin Microbiol Infect Dis. 2019;38:1643–9. https://doi.org/10.1007/s10096-019-03592-1
49. Belay N, Mukhopadhyay B, Conway de Macario E, Galask R, Daniels L. Methanogenic bacteria in human vaginal samples. J Clin Microbiol 1990;28:1666–68. https://doi.org/10.1128/jcm.28.7.1666-1668.1990
50. Guerra A. Human associated Archaea: a neglected microbiome worth investigating. World J Microbiol Biotechnol. 2024;40:60. https://doi.org/10.1007/s11274-023-03842-7

Address for correspondence: Christine Moissl-Eichinger, Neue Stiftingtalstraße 6, 8010 Graz, Austria; email: christine.moissl-eichinger@medunigraz.at

Outbreak of Intermediate Species *Leptospira venezuelensis* Spread by Rodents to Cows and Humans in *L. interrogans*–Endemic Region, Venezuela

Lizeth Caraballo, Yaritza Rangel, Armando Reyna-Bello,[1] Mariana Muñoz, Roque Figueroa-Espinosa,[2] Carlos E. Sanz-Rodriquez,[3] Elba Guerrero, Carmen Luisa Loureiro, Qingyun Liu,[4] Howard E. Takiff

Leptospirosis is a common but underdiagnosed zoonosis. We conducted a 1-year prospective study in La Guaira State, Venezuela, analyzing 71 hospitalized patients who had possible leptospirosis and sampling local rodents and dairy cows. *Leptospira rrs* gene PCR test results were positive in blood or urine samples from 37/71 patients. *Leptospira* spp. were isolated from cultured blood or urine samples of 36/71 patients; 29 had *L. interrogans*, 3 *L. noguchii*, and 4 *L. venezuelensis*. Conjunctival suffusion was the most distinguishing clinical sign, many patients had liver involvement, and 8/30 patients with *L. interrogans* infections died. The *Leptospira* spp. found in humans were also isolated from local rodents; *L. interrogans* and *L. venezuelensis* were isolated from cows on a nearby, rodent-infested farm. Phylogenetic clustering of *L. venezuelensis* isolates suggested a recently expanded outbreak strain spread by rodents. Increased awareness of leptospirosis prevalence and rapid diagnostic tests are needed to improve patient outcomes.

Leptospirosis, one of the most common zoonoses worldwide, (*1*,*2*) is caused by *Leptospira* spp. In humans, its most severe, multiorgan, potentially fatal form is known as Weil's disease (*3*). *Leptospira* can also infect animals, such as cattle, sheep, cats, and dogs. Rodents are the reservoir for most *Leptospira* spp.; rodent kidneys can become colonized with *Leptospira* and chronically shed the bacteria in urine. Except for occupational or recreational exposure, leptospirosis generally occurs in residents of marginal, rodent-infested areas, often in coastal regions of tropical countries (*3*).

According to their ability to cause human disease, *Leptospira* bacteria were originally divided into fully pathogenic (P1), intermediate pathogenic (P2), and saprophytic or nonpathogenic (S1 and S2) subclades; this phylogenetic separation is confirmed by genome sequencing (*4*,*5*). The pathogenic species, most commonly *L. interrogans*, can cause leptospirosis and Weil's disease, but the role of intermediate species in human illness is unclear (*5*). Intermediate *Leptospira* spp. have been discovered by environmental sampling of soil and water (*5*), but they have also been found in animals and humans, where they are thought to cause only mild, self-limited illness without liver, kidney, or pulmonary involvement (*5*).

Leptospira infections are classically diagnosed by using the microscopic agglutination test (MAT) to detect *Leptospira*-specific antibodies, but diagnosis often requires comparing titers of acute and convalescent serum samples. Culturing *Leptospira* for a definitive bacteriologic diagnosis is difficult and takes weeks

Author affiliations: Instituto Venezolano de Investigaciones Científicas, Caracas, Venezuela (L. Caraballo, Y. Rangel, M. Muñoz, R. Figueroa-Espinosa, C.E. Sanz-Rodriquez, E.Guerrero, C.L. Loureiro, H.E. Takiff); Universidad Nacional Experimental Simón Rodríguez, Caracas (A. Reyna-Bello) Harvard T.H. Chan School of Public Health, Boston, Massachusetts, USA (Q. Liu)

DOI: https://doi.org/10.3201/eid3008.231562

[1]Current affiliation: Universidad de las Fuerzas Armadas ESPE, Santo Domingo, Ecuador.

[2]Current affiliation: Universidad de Buenos Aires, Buenos Aires, Argentina.

[3]Current affiliation: Institut Pasteur de Montevideo, Montevideo, Uruguay.

[4]Current affiliation: The University of North Carolina, Chapel Hill, North Carolina, USA.

to months. Therefore, *Leptospira* bacteria are usually detected by PCR of blood or urine samples and identified by sequencing the amplified genes and comparing those sequences to known *Leptospira* spp. (*6*).

Venezuela is considered a moderate-incidence country for leptospirosis (*7*), but the true incidence is unknown because of a lack of clinical recognition of the disease and difficulties in laboratory diagnosis. To determine the presence of *Leptospira* spp., identify local strains, and evaluate leptospirosis incidence in Venezuela, we performed a prospective study in La Guaira, a small state on Venezuela's Caribbean coast. Although the study was conducted in 2010–2011 and reporting delayed because of Venezuela's economic situation, we believe the clinical leptospirosis data and epigenomic study of an intermediate *Leptospira* sp. outbreak remain relevant.

Methods

Ethics Approval

The Bioethics Commission of the Instituto Venezolano de Investigaciones Científicas, Caracas, Venezuela, approved the human study. The National Office of Biologic Diversity within the Venezuela Ministry for the Environment (Document 0264) and the Instituto Venezolano de Investigaciones Científicas Commission on Animal Bioethics approved the capture of rodents.

Study Area

We included patients with possible leptospirosis in La Guaira State, located on the northern Caribbean coast of Venezuela. La Guaira contains a shipping port and the nation's principal airport and has a population of ≈353,000. It is a beach resort for residents of Caracas but also contains low socioeconomic urban and rural areas. In the 1999 Vargas tragedy, mudslides destroyed much of the infrastructure of La Guaira (formerly Vargas State), causing thousands of fatalities.

Patient Selection

We visited Dr. José María Vargas Hospital during March 2010–March 2011 and Dr. Rafael Medina Jiménez Hospital during March–July 2010 and February–March 2011; visits were ≥2 times per week each. We reviewed diagnoses of new patients at admission and questioned hospital staff about new patients who had clinical symptoms suggestive of leptospirosis. Inclusion criteria were residence or place of work in La Guaira and an initial evaluation that included ≥1 sign or symptom of leptospirosis as described by the World Health Organization (*8*): fever >38°C with unknown etiology for ≤21 days, fever with renal failure (anuria, oligouria, or elevated creatinine), abdominal or muscle pain, icterus, conjunctival suffusion, hypokalemia or hyponatremia, hemoptysis or pulmonary hemorrhage, or an initial diagnosis of hepatitis or dengue. After patients voluntarily signed an informed consent form, we interviewed those patients and collected their clinical histories and places of residence. We also consulted the physician's notes. We excluded patients who were unable to complete the interview or provide adequate data. We enrolled a total of 71 patients from whom blood and urine specimens were obtained. Of those 71 patients, 38 had serologic tests for dengue and 39 for hepatitis A or B. Frozen serum samples from some patients were subsequently tested for hepatitis viruses A and B by PCR (Appendix Table 1, https://wwwnc.cdc.gov/EID/article/30/8/23-1562-App1.pdf).

Leptospira Cultures

Leptospira were cultured at 28–30°C in liquid or semisolid Ellinghausen-McCullough-Johnson-Harris (EMJH) medium with 10% supplement and 50–100 mg/mL of 5-fluorouracil for initial cultures (Appendix). All solutions and media were prepared according to the World Health Organization technical manual (*8*).

Rodent Capture

We set up Sherman aluminum traps in urban areas close to the residences of patients who were PCR positive for *Leptospira* (Appendix). The species of captured rodents were determined by amplifying and sequencing a subunit of the cytochrome c oxidase gene (*9*).

Cow Samples

We collected blood with and without EDTA anticoagulant from the caudal vein of 16 crossbred *Bos taurus* × *Bos indicus* (predominantly *Bos taurus*) dairy cows. Cows were 3–10 years of age and located on a farm in Miranda State, Venezuela, ≈30 km from La Guaira State (Appendix). We collected urine samples from the same cows after intramuscular injection of the diuretic furosemide (1 mg/kg). We cultured blood and urine samples and performed PCR for the *Leptospira* genes *rrs* (16S rDNA) and *lipL32*.

Passaging of Isolates in Hamsters

We intraperitoneally injected *Leptospira* isolates from second to fourth passages of liquid culture into 4-week-old male Syrian golden hamsters (*Mesocricetus auratus*). Sixteen days after injection, we euthanized the hamsters and removed and macerated the kidneys. We placed the kidney tissue into EMJH medium to sediment and then inoculated culture medium with the supernatant.

Molecular Detection of *Leptospira*

We amplified *lipL32* (*10*) and regions V3–V6 of the *rrs* gene from isolated DNA by using PCR (*11*) (Appendix Table 1). We purified the *rrs* gene amplification products (QIAGEN, https://www.qiagen.com), which were then sequenced by Macrogen (https://www.macrogen.com). We also sequenced the *lig* gene from a few specimens (*12*). We used the *L. interrogans* genes *pntA*, *sucA*, *pfkB*, *tpiA*, *mreA*, *glmU*, and *caiB* (*13*,*14*) for multilocus sequence typing (MLST). We performed variable-number tandem-repeat (VNTR) analysis of *L. interrogans* isolates as previously described (*15*).

MAT of Bovine Serum Samples

MATs were performed in the bacteriology laboratory of the Instituto Nacional de Investigaciones Agricolas according to 2003 Pan American Health Organization standards (https://www.paho.org/es/documentos/leptospirosis-humana-guia-para-diagnostico-vigilancia-control). MATs were considered positive when ≥50% of *Leptospira* bacteria were agglutinated.

Phylogenetic Reconstruction of *L. venezuelensis* Isolates

We used Velvet (*16*) for de novo assembly of genome contigs from sequencing reads of *L. venezuelensis* isolates. We used cow isolate 201502610 (GenBank Biosample accession no. SAMEA5168082) as a reference to map reads from the other *L. venezuelensis* isolates (Appendix).

Statistics

We performed statistical analyses of patient signs and symptoms and clinical test values by using Stata 13 (StataCorp LLC, https://www.stata.com). We did not adjust p values for multiple statistical testing.

Results

PCR and Cultures of Patient Specimens

Through twice-weekly visits to the 2 hospitals in La Guaira state over a 1-year period, we identified 71 patients who met the inclusion criteria (Appendix Tables 2, 3). We PCR amplified the *Leptospira rrs* gene from blood samples of 17, urine samples of 22, and both blood and urine samples of 2 patients. We also cultured *Leptospira* bacteria from blood samples from 13, urine samples from 20, and both blood and urine samples from 3 patients (Appendix Table 4). Using PCR amplification of *Leptospira rrs* in either blood or urine samples as confirmation of leptospirosis, the sensitivity of the *rrs* gene for diagnosing leptospirosis was 46% for blood and 59% for urine specimens; both sample types had 100% specificity. For *lipL32* PCR amplification, sensitivity was 41% for blood, 35% for urine, and 70% when both blood and urine samples were tested; all samples had 100% specificity. For blood cultures, sensitivity was 43%, and specificity was 100%; for urine cultures, sensitivity was 59%, and specificity was 97%; for either positive blood or urine cultures, sensitivity was 95%, and specificity was 97% (Table 1; Appendix Tables 4–6). The *rrs* gene was amplified from 2 patients who had negative *Leptospira* cultures: from a blood specimen of a patient with jaundice and from the urine of a patient who died of severe pulmonary disease.

Initial diagnoses were similar for patients in this study who had positive or negative *Leptospira* PCR and were most commonly dengue, hepatitis, icteric hemorrhagic syndrome, febrile syndrome, or unknown. Leptospirosis was listed as an initial diagnosis for 6 patients from whom *Leptospira* spp. were isolated and for 1 patient who had negative *Leptospira* cultures. Dengue

Table 1. Tests used for leptospirosis diagnoses in study of outbreak of intermediate species *Leptospira venezuelensis* spread by rodents to cows and humans in *L. interrogans*–endemic region, Venezuela*

Diagnostic test†	*rrs* PCR+, n = 37‡	*rrs* PCR–, n = 34‡	% Sensitivity (95% CI)	% Specificity (95% CI)	% PPV (95% CI)	% NPV (95% CI)	% Accuracy (95% CI)
rrs PCR							
Blood, +	17	0	46 (30–63)	100 (90–100)	100 (80–100)	63 (56–70)	72 (60–82)
Blood, –	20	34	NA	NA	NA	NA	NA
Urine, +	22	0	59 (42–75)	100 (90–100)	100 (85–100)	69 (61–77)	79 (68–88)
Urine, –	15	34	NA	NA	NA	NA	NA
Both, +	2	0	NA	NA	NA	NA	NA
Culture							
Blood, +	16	0	43 (27–61)	100 (90–100)	100 (80–100)	62 (55–68)	70 (58–81)
Urine, +	22	1	59 (42–75)	97 (85–100)	96 (76–99)	69 (60–77)	77 (66–87)
Either, +	35	1	95 (82–99)	97 (85–100)	97 (84–100)	94 (81–98)	96 (88–99)
lipL32 PCR							
Blood, +	15	0	41 (25–58)	100 (90–100)	100 (78–100)	61 (54–67)	69 (57–79)
Urine, +	13	0	35 (20–53)	100 (90–100)	100 (75–100)	59 (53–64)	66 (54–77)
Either, +	26	0	70 (53–84)	100 (90–100)	100 (87–100)	76 (65–84)	85 (74–92)

*Diagnostic values were obtained for *Leptospira* cultures and PCR of *Leptospira lipL32* and *Leptospira rrs* (16S rDNA) genes of blood and urine specimens from hospitalized patients. NA, not applicable; NPV, negative predictive value; PPV, positive predictive value; –, negative; +, positive.
†Test results are shown for patients who had *Leptospira* detected in blood, urine, or either blood or urine.
‡Total numbers of study patients who had the *Leptospira rrs* gene detected by PCR of either blood or urine samples.

was diagnosed in 3 patients and hepatitis in 4 patients who had positive *Leptospira* cultures; dengue was diagnosed in 5 patients and hepatitis in 4 patients who had negative cultures. *Leptospira* isolation was not correlated with seasonal variation in precipitation.

We compared PCR sequences of *rrs* with GenBank sequences by using BLAST (*17*). We identified 29 sequences as *L. interrogans*, 3 as *L. noguchii*, and 4 were 99% identical to the intermediate species *L. licerasiae* and *L. wolffi* (Appendix Tables 7, 8); genome sequencing showed those 4 isolates belonged to a novel intermediate species that we then named *L. venezuelensis* (*18*). The *lig* gene (*12*) was amplified by PCR from the urine of the culture-negative patient who died of pulmonary disease and was identified as belonging to *L. interrogans* by using BLAST. Patients who had positive tests for hepatitis or dengue and positive *Leptospira* blood or urine cultures all grew *L. interrogans* and were assumed to be co-infected. Serum samples from *L. venezuelensis*–positive patients were negative for hepatitis viruses A and B (Appendix Table 9).

Clinical Characteristics

Patients who had PCR-amplified *rrs* were more likely to have conjunctival suffusion, dyspnea, cough, hemoptysis, and myalgias (Figure 1; Appendix Tables 10, 11). Eight (27%) of the 30 patients who had *L. interrogans* infections died of their illness, whereas no deaths were recorded among the 34 patients who had no evidence of leptospirosis. Leptospirosis patients who died had more severe infections, with pulmonary and renal involvement, than did those who survived (Figure 2; Appendix Tables 12, 13). Patients who died of leptospirosis had more hemoptysis but less abdominal pain and myalgias and also had higher mean urea and creatinine levels, higher leukocyte counts, higher percentages of neutrophils, and lower percentages of lymphocytes than those who survived.

Cultures from Captured Rodents

To delineate reservoir hosts for *Leptospira*, we captured 45 rodents from 27 communities where patients who had positive cultures resided. We captured 30 *Mus musculus* mice and 11 *Rattus rattus* and 4 *R. norvegicus* rats. We amplified the *rrs* gene by PCR and cultured *Leptospira* from kidney tissue samples from all 45 rodents; 36 (80%) isolates were *L. interrogans*, 4 (9%) were *L. noguchii*, 3 (7%) were the intermediate species *L. fainei*, and 2 (4%) were *L. venezuelensis*. *L. interrogans* was isolated from all 3 rodent species, *L. noguchii* was isolated only from mice, and the intermediate species *L. fainei* and *L. venezuelensis* were only isolated from *R. rattus* rats.

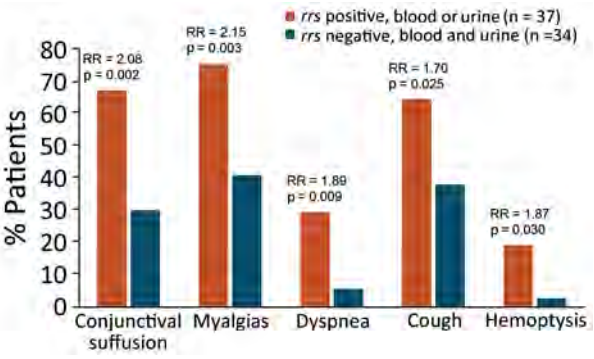

Figure 1. Distinguishing clinical features of hospitalized patients in study of outbreak of intermediate species *Leptospira venezuelensis* spread by rodents to cows and humans in *L. interrogans*–endemic region, Venezuela. The most statistically different clinical symptoms are shown for hospitalized patients considered to have leptospirosis according to positive PCR for the *Leptospria rrs* gene in either blood or urine specimens compared with those without leptospirosis according to negative *rrs* PCR in both blood and urine samples. PCR primers for *rrs* amplify a region of the gene encoding 16S rRNA that is highly conserved in *Leptospira* (Appendix Table 1, https://wwwnc.cdc.gov/EID/article/30/8/23-1562-App1.pdf). One patient whose urine culture grew *L. venezuelensis* was *rrs* PCR negative, and leptospirosis was not diagnosed (Appendix Table 9). Comparisons of all clinical features with 95% CIs were also determined (Appendix Tables 10, 11). RRs and Pearson χ^2 test p values were calculated by using Stata 13 (StataCorp LLC, https://www.stata.com). RR, risk ratio.

Leptospira in Cows on Nearby Farm

Leptospira spp. are known to infect cattle. In a preliminary study, we performed MATs on serum samples from 48 cows on 8 small farms in adjacent Miranda State. We found *Leptospira*-specific antibodies against ≥1 *Leptospira* serovars in 2 animals from a single farm located ≈30 km from where the leptospirosis patients in this study resided. We then obtained blood and urine specimens from 16 cows randomly selected from that single farm and performed MATs against live antigens of 23 *Leptospira* reference strains; 9 samples agglutinated ≥1 serovar (Table 2; Appendix Table 14). Of those 9 cows, 8 had urine positive for *Leptospira rrs* by PCR; 2 urine samples had positive cultures of *L. interrogans*, and 7 had positive cultures of *L. venezuelensis*. The cows that had *L. venezuelensis*–positive urine had MAT titers of 1:400 to 1:800 against reference strain *L. interrogans* serovar Wolffi, serogroup Sejroe. The 2 *L. interrogans*–positive cows had high MAT titers for other serovars: 1:400 for *L. hebdomadis* (cow 5) and 1:400 for *L. mini* (cow 9). Cows 1 and 8 were negative according to MATs and *rrs* PCR of their urine, but their blood samples were *rrs* PCR–positive. Urine of cow 8 grew *L. interrogans*, whereas urine of cow 1 grew *L. venezuelensis* (Table 2; Appendix Table 14). Cow 11 had a MAT titer of 1:1,600 for *L. interrogans* serovar Bataviae and *rrs*-positive urine, but no *Leptospira*

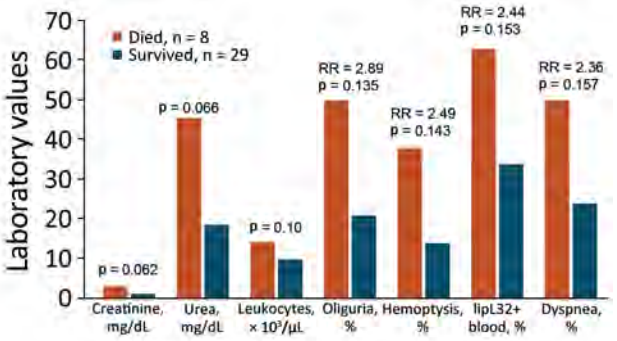

Figure 2. Clinical features most strongly associated with fatal outcomes in study of outbreak of intermediate species *Leptospira venezuelensis* spread by rodents to cows and humans in *L. interrogans*–endemic region, Venezuela. Clinical features are shown for hospitalized patients who had positive PCR tests for the *Leptospira rrs* (16S rDNA) gene in blood or urine and either survived or succumbed to their illness. Laboratory units of measure are indicated on the x axis for each bar. Comparisons of all clinical features with 95% CIs were also determined (Appendix Tables 12, 13, https://wwwnc.cdc.gov/EID/article/30/8/23-1562-App1.pdf). p values comparing creatinine, urea, and number of lymphocytes were obtained from Pearson χ^2 tests. p values comparing percentages of patients with oliguria, hemoptysis, *lipL32*, and dyspnea were obtained from 2-tailed *t*-tests. All statistical calculations were performed by using Stata 13 (StataCorp LLC, https://www.stata.com). RR, risk ratio.

spp. were isolated from either the blood or urine. *L. venezuelensis* isolates did not agglutinate with antiserum to common *L. interrogans* serovars, although antiserum to serovar Wolffi was not included.

Growth in Hamsters

We purified all *Leptospira* isolates by injecting early passage cultures into the peritoneal cavities of Syrian golden hamsters and performing necropsies 16 days after inoculation; 3 hamsters infected with *L. interrogans* and 1 infected with *L. noguchii* died before 16 days. We cultured aliquots of macerated kidney extracts from all inoculated hamsters and performed PCR to detect *Leptospira rrs*. In each case, sequences of *rrs* from the hamster kidney extracts were identical to the sequences from the corresponding original specimens and also the *Leptospira* cultured from those hamster kidney extracts.

Molecular Epidemiology of *L. interrogans*

Among the *L. interrogans* strains isolated from humans or rodents, 3 clusters had 7/7 identical MLST alleles; in each cluster, 2 patients resided in the same residential zone (Table 3). Of the 27 different MLST profiles, only 4 were present in the *Leptospira* PubMLST database (https://pubmlst.org/organisms/leptospira-spp), 2 of which (sequence types 27 and 50) were in clusters that had 7/7 identical alleles. Sequence types 20 and 37 were clustered with strains that had 6/7 identical alleles. VNTR clustering was not concordant with MLST clustering (Appendix Table 15). Two of the 3 *L. interrogans* strains isolated from cows had identical alleles in 4 VNTR loci (Appendix Table 16) but were not analyzed by using MLST.

New Intermediate Species of *Leptospira*

L. venezuelensis, isolated from 4 patients (Appendix Table 9), 2 rodents, and 7 cows, is located on the phylogenetic tree within the *Leptospira* intermediate pathogen or P2 subclade (5). Three of the 4 patients infected with *L. venezuelensis* resided in the same municipality; the fourth patient resided in an adjacent

Table 2. Analysis of blood and urine specimens from cows in study of outbreak of intermediate species *Leptospira venezuelensis* spread by rodents to cows and humans in *L. interrogans*–endemic region, Venezuela*

	rrs PCR		*lipL32* PCR		Serology		Cultures		Sequenced
Cow no.	Blood	Urine	Blood	Urine	MAT titer	Serovar	Blood	Urine	species†
1	+	–	–	–	Negative	NA	+	–	*L. venezuelensis*
2	–	–	–	–	Negative	NA	–	–	NA
3	–	+	–	–	1:800	*L. wolffii*	–	+	*L. venezuelensis*
4	–	–	–	–	Negative	NA	–	–	NA
5	–	+	–	+	1:400	*L. hebdomadis*	–	+	*L. interrogans*
6	–	–	–	–	Negative	NA	–	–	NA
7	–	+	–	–	1:800	*L. wolffii*	–	+	*L. venezuelensis*
8	+	–	+	–	Negative	NA	+	–	*L. interrogans*
9	–	+	–	+	1:400	*L. mini*	–	+	*L. interrogans*
10	–	–	–	–	Negative	NA	–	–	NA
11	–	+	–	–	1:1,600	*L. bataviae*	–	–	NA
12	–	+	–	–	1:800	*L. wolffii*	–	+	*L. venezuelensis*
13	–	+	–	–	1:400	*L. wolffii*	–	+	*L. venezuelensis*
14	–	+	–	–	1:800	*L. wolffii*	–	+	*L. venezuelensis*
15	–	–	–	–	Negative	NA	–	–	NA
16	–	+	–	–	1:400	*L. wolffii*	–	+	*L. venezuelensis*

*Results for MAT serology, cultures, and PCR of the *Leptospira lipL32* and *rrs* (16S rDNA) genes from cultured isolates. MAT, microscopic agglutination test; NA, not applicable; –, negative; +, positive.
†*Leptospira* spp. were determined by sequencing the PCR-amplified *rrs* gene.

Table 3. MLST of *Leptospira interrogans* isolates in study of outbreak of intermediate species *L. venezuelensis* spread by rodents to cows and humans in *L. interrogans*–endemic region, Venezuela*

Isolates†	MLST allele nos.							ST‡
	glmU	*pntA*	*sucA*	*tpiA*	*pfkB*	*mreA*	*caiB*	
Human								
CAB-H41	1	1	2	1	7	7	8	NP*
CAY-U48	1	1	2	1	7	4	3	20
CAB-U03	1	1	2	2	7	4	3	NP
MAC-H04	1	1	2	2	7	4	5	NP
URI-U06	**1**	**1**	**3**	**2**	**7**	**4**	**3**	NP
URI-H01	**1**	**1**	**3**	**2**	**7**	**4**	**3**	NP
CLM-H09	1	1	3	2	4	7	5	NP
CLM-U30	1	3	2	2	4	4	19	NP
MAC-H63	1	3	2	2	7	7	19	NP
CAY-H65	1	3	3	1	4	5	5	NP
SOB-U13	1	12	3	3	10	4	5	NP
MAQ-U18	1	12	3	3	10	5	19	NP
CLM-U22	1	12	2	3	10	6	19	NP
CLM-U28	**1**	**12**	**3**	**3**	**10**	**6**	**19**	27
CLM-H08	**1**	**12**	**3**	**3**	**10**	**6**	**19**	27
GUA-H40	**1**	**12**	**3**	**3**	**10**	**6**	**19**	27
CLM-U45	**3**	**3**	**3**	**2**	**4**	**5**	**5**	NP
CLM-U47	**3**	**3**	**3**	**3**	**4**	**5**	**5**	37
NAG-U02	6	1	3	2	4	7	3	NP
CAY-U49	6	1	3	3	76	7	3	NP
CLM-U46	6	2	3	3	7	7	19	NP
CLM-U24	6	1	3	12	4	5	5	NP
GUA-H52	6	3	2	2	4	4	3	NP
GUA-H64	6	3	2	3	4	7	5	NP
CAB-U11	6	3	3	2	4	5	5	NP
GUA-H21	6	3	3	3	1	7	5	NP
CAO-U23	6	3	3	3	4	5	19	NP
MAQ-H53	**6**	**8**	**2**	**2**	**9**	**7**	**5**	50
MAQ-H60	**6**	**8**	**2**	**2**	**9**	**7**	**5**	50
Rat								
CLM-R09-A	1	1	2	2	7	4	8	NP
CLM-R11-A	1	1	3	3	4	6	19	NP
SOB-R13-B§	1	12	3	3	10	6	19	27

*Bold font indicates isolates that had identical profiles. MLST, multilocus sequence typing; NP, not present in database; ST, sequence type.
†The first 3 letters for each isolate indicate the area of the patient's residence or where the rodent was captured in the state of La Guaira, Venezuela: CAB, Caraballeda; CAO, Caruao; CAY, Carayaca; CLM, Catia La Mar; GUA, La Guaira; MAC, Macuto; MAQ, Maiquetia; NAG, Niguata; SOB, Soublette; or URI, Urimare. The fourth letter is H (isolated from human blood), U (isolated from human urine), or R (isolated from rat tissue).
‡STs found in the *Leptospira* PubMLST database (https://pubmlst.org/organisms/leptospira-spp) (*14*).
§Rat sequence shared an MLST profile for some alleles with human isolates CLM-U28, CLM-H08, and GUA-H40.

district. This municipality was the most frequent residence of leptospirosis patients, home to 10 of 32 patients with other *Leptospira* infections. Of the 2 rats infected with *L. venezuelensis*, 1 was trapped in the same municipality and the other in a nearby district.

Phylogenetic reconstruction of genomes from the 6 sequenced *L. venezuelensis* isolates uncovered limited genetic diversity (Figure 3). The isolates from human, rodent, and bovine hosts all differed by <12 single-nucleotide polymorphisms (SNPs), suggesting a recent outbreak of a *L. venezuelensis* strain that was spread, presumably by rodents, to different host populations. The *L. venezuelensis* genome sequence data have been deposited in GenBank (Biosample accession nos. SAMEA5168082, SAMEA5168083, SAMEA5168130, SAMEA5168133, SAMEA5168318, SAMN06855518, SAMN39993761, SAMN39993762, and SAMN39993763).

Discussion

The true incidence of leptospirosis in La Guaira state has been unknown, likely because it has been difficult or impossible to diagnose and has not been considered by clinicians, even in patients with characteristic signs and symptoms. Our prospective search for leptospirosis cases in La Guaira's 2 hospitals during a 1-year period found *rrs* PCR evidence of *Leptospira* spp. in blood or urine specimens from 37 hospitalized patients, including 8 patients who died. We also cultured *Leptospira* from 36 patient samples. Two patients with positive *rrs* PCR had negative cultures, but 1 of those patients had an *L. interrogans lig* gene fragment amplified from their urine. The population of La Guaira is ≈353,000, corresponding to a borderline high incidence of 10 leptospirosis cases/100,000 population. However, this figure is almost certainly an underestimate because the study only included

patients ill enough to require hospitalization and did not capture patients with less severe illness, who represent up to 90% of leptospirosis cases (*2*).

Leptospira spp. were isolated from the kidneys of all 45 rodents captured in the region. *Leptospira* species distributions were similar in rodents and humans; most isolates were *L. interrogans,* which is globally the species most associated with severe human illness. *L. venezuelensis* was also isolated from 7 cows on a nearby farm, whereas *L. interrogans* was isolated from only 3 cows on the same farm (Table 2; Appendix Table 14).

Leptospirosis is difficult to diagnose in a clinically useful time frame, but *rrs* PCR of both blood and urine samples detected 37 cases. The most discriminative clinical finding in patients was conjunctival suffusion (*19*), but *Leptospira*-positive patients also had more myalgias, dyspnea, cough, and hemoptysis than did hospitalized *Leptospira*-negative patients. *L. interrogans* was recovered from patients with the most severe cases, and 27% (8/30) of *L. interrogans*–infected patients died. However, for patients with mild to moderate disease, the infecting species could not be distinguished by patient signs, symptoms, or laboratory values (Appendix Table 8).

The intermediate species *L. fainei* was isolated from the kidneys of 3/45 captured rodents. *L. fainei* has been reported to cause disease in humans (*20*) but was not isolated from any human patient or bovid in this study. *L. venezuelensis* is phylogenetically closer to other intermediate species reported to cause human illness, such as *L. liceraciae* (*21*) and *L. wolffi* (*22*) and is phylogenetically close to *Leptospira* spp. isolated from environmental samples in Malaysia, Mayotte, and New Caledonia (*5*).

Few studies have been conducted to determine the phylogenetic relatedness of different strains of *Leptospira* spp. isolated from a particular geographic region. *L. interrogans* isolates from this study had many MLST profiles, including clusters of profiles found in the *Leptospira* PubMLST database (Table 3). MATs showed that serum samples from 3 cows each reacted to a different *L. interrogans* serovar, including 2 whose isolates had the same VNTR pattern (Appendix Tables 14, 16). The heterogeneity of *L. interrogans* strains suggests a long-term endemic presence in the local rodent population. In contrast, the genomes of 6 *L. venezuelensis* isolates differed by a maximum of 11 SNPs (Figure 3), suggesting an outbreak strain. Although only 6 of the 13 *L. venezuelensis* isolates were sequenced, they were

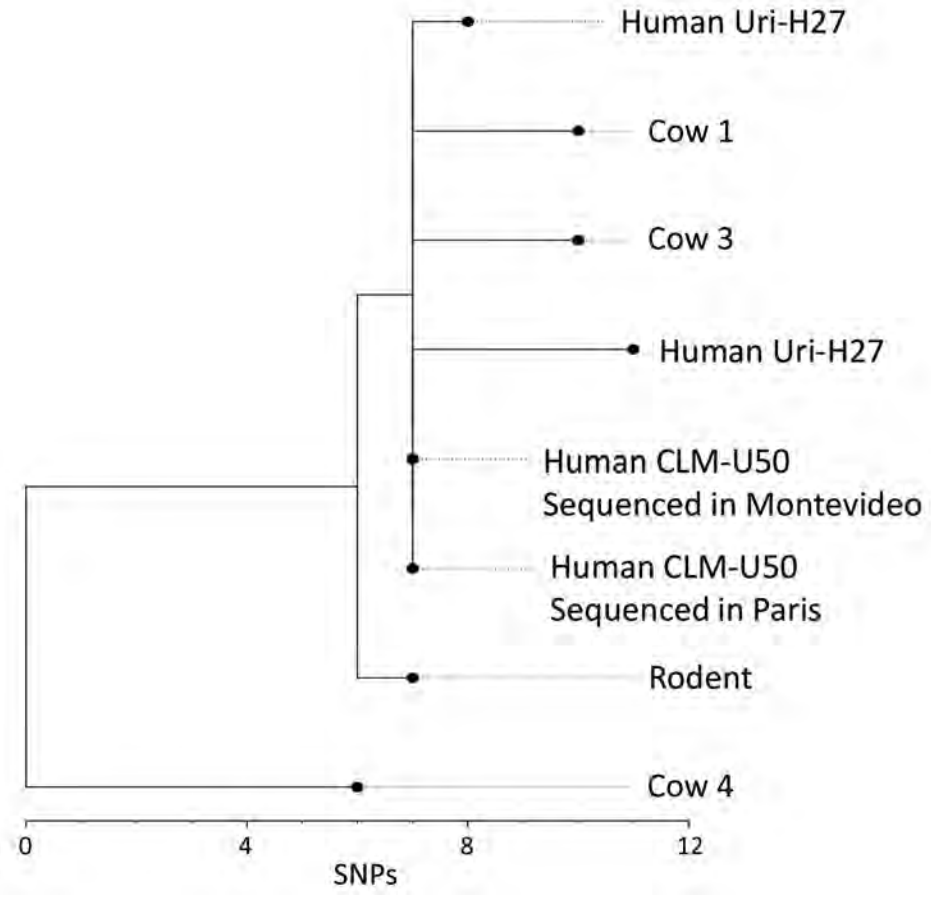

Figure 3. Phylogenetic analysis of *Leptospira venezuelensis* isolates in study of outbreak of intermediate species *L. venezuelensis* spread by rodents to cows and humans in *L. interrogans*–endemic region, Venezuela. Branch length indicates the number of SNPs separating *L. venezuelensis* strains. Phylogenetic tree was reconstructed according to comparisons of whole-genome sequences from 6 *L. venezuelensis* strains isolated from hospitalized leptospirosis patients in La Guaira State on the Caribbean coast of Venezuela, from rodents captured near the residences of hospitalized leptospirosis patients, and from dairy cows on a farm 30 km away from La Guaira State. Human isolate CLM-50 was sequenced at both the Institute Pasteur in Paris, France, and the Institute Pasteur in Montevideo, Uruguay. Human isolate Uri-H27 was sequenced twice at the Institute Pasteur in Paris; the genome of the isolate after many passages in culture contained 3 SNPs that were not present in the same isolate from an earlier passage. Scale bar indicates number of SNPs per site. SNP, single-nucleotide polymorphism.

obtained from a diverse sampling of hospitalized humans, rats captured in La Guaira, and cows on a farm 30 km away from patient residences. Unless *L. venezuelensis* has a mutation rate even slower than slow-mutating *Mycobacterium tuberculosis* (*23*), the low genetic diversity reflects a recently expanded bacteria population. Greater genomic heterogeneity would be expected if *L. venezuelensis* evolved from a local environmental *Leptospira* sp. Instead, the close genomic similarity between isolates suggests a recent introduction of *L. venezuelensis* into the region, perhaps arriving with rats on a ship that docked in the port of La Guaira and then spread within the local rodent population.

Infections with intermediate clade *Leptospira* spp. have only rarely been associated with icteric human illness (*6*), but 3 of 4 patients from whom *L. venezuelensis* was isolated were icteric, had liver aminotransferase values >250 (Appendix Table 9) and negative test results for hepatitis viruses A and B. Only 1 patient with *L. venezuelensis* infection was tested for dengue, but all 4 had platelet levels within reference ranges, which is uncharacteristic for acute dengue.

Although intermediate *Leptospira* spp. are thought to be incapable of surviving in an animal model, infection of rats has been reported for the intermediate species *L. licerasiae* (*24*). We recovered all 13 *L. venezuelensis* isolates from hamster kidneys 16 days after intraperitoneal inoculation of low passage isolates, although later passages of the same isolates could not be recovered from hamsters after high-dose intraperitoneal infections (data not shown). The acquisition of SNPs and loss of virulence during *in vitro* passages of *Leptospira* isolates has been previously described (*25*,*26*).

Leptospira intermediate species are often isolated from environmental samples (*5*), but it seems unlikely that *L. venezuelensis* was an environmental or laboratory contaminant. The *rrs* PCR of the original human, bovine, and rodent specimens; the isolate cultures; and hamster infection studies were all performed separately before sequencing results were available, and the samples containing *L. venezuelensis* were not temporally linked. The MAT titers of serum samples from *L. venezuelensis*–positive bovids all showed the same presumed cross-reaction with *L. interrogans* serovar Wolffi, consistent with genomic evidence of an outbreak strain. Human disease causality could be confirmed by high or rising MAT titers in patient serum samples, but acute serum samples from 2 *L. venezuelensis* and 4 *L. interrogans* patients did not have titers >1:50, and convalescent patient blood samples were not collected.

In Argentina (*27*), *L. wolffii* was isolated from a patient who died of a severe respiratory syndrome, but PCR results suggested an *L. interrogans* co-infection. Similarly, 2 of the 4 *L. venezuelensis*–positive patients in this study had positive *lipL32* PCR results (Appendix Table 9). The *lipL32* primers were designed to amplify *lipL32* from *L. interrogans* or other pathogenic *Leptospira* spp. but not from intermediate species, such as *L. venezuelensis*. Although the amplified *lipL32* fragments were not sequenced, the 2 *lipL32*-positive patients could have been co-infected with *L. venezuelensis* and *L. interrogans.* Another patient from whom *L. venezuelensis* was cultured had negative *rrs* PCR results in both blood and urine. The pathogenicity of this intermediate species could not be confidently evaluated from the 4 *L. venezuelensis*–positive patients in this study.

In conclusion, an *L. venezuelensis* outbreak circulating in rodents appears to have spread to cows in the region and also infected humans, in whom it might have caused febrile illness with hepatic involvement. Our findings indicate the need for increased awareness of leptospirosis prevalence and characteristics in Venezuela and other tropical, rodent infested coastal regions and also indicates an urgent need for rapid point-of-care tests to diagnose leptospirosis and improve patient treatment and outcomes.

Acknowledgments

We thank Albert Ko, Paula Ristow, and the staff of the Centro de Referencia Internacional de Leptospirosis de la Fundación Oswaldo Cruz, Salvador de Bahía, Brazil, for training L.C. and generously providing reference strains; Raphael Puche and the Unidad de Estudios Genéticos y Forenses, Instituto Venezolano de Investigaciones Científica for genomic sequencing and analysis; Benjamin Valencia for help in verifying patient data; Mathieu Picardeau and his laboratory for genomic sequencing, hamster infections, serovar tests, help, and advice; Hans van der Linden and Harry Bannister for help interpreting the MAT results; and Yadira Castillo, Yurimia Oropeza, Rumania Miranda, Alexandra González, Mariela Gómez, Carmen Bogado, and Miguel Damargo for help identifying patients, collecting biological samples, and capturing rodents. Without their kind and generous assistance, this study would not have been possible.

This work was supported by the regular budget allotment of the Instituto Venezolano de Investigaciones Científicas to the Laboratorio de Genética Molecular and Institut Pasteur (project no. PTR 30-17).

About the Author

Ms. Caraballo received her undergraduate degree in biology from the University of Zulia, Venezuela, and is pursuing a PhD in the Laboratorio de Genética Molecular, Centro de Microbiología y Biología Celular, Instituto Venezolano de Investigaciones Científica, Caracas,

Venezuela. Her principal research interest is the molecular epidemiology of human and animal leptospirosis.

References

1. Costa F, Hagan JE, Calcagno J, Kane M, Torgerson P, Martinez-Silveira MS, et al. Global morbidity and mortality of leptospirosis: a systematic review. PLoS Negl Trop Dis. 2015;9:e0003898. https://doi.org/10.1371/journal.pntd.0003898
2. Wang S, Stobart Gallagher MA, Dunn N. Leptospirosis. In: StatPearls. Treasure Island (FL): StatPearls Publishing; 2024.
3. Bharti AR, Nally JE, Ricaldi JN, Matthias MA, Diaz MM, Lovett MA, et al.; Peru–United States Leptospirosis Consortium. Leptospirosis: a zoonotic disease of global importance. Lancet Infect Dis. 2003;3:757–71. https://doi.org/10.1016/S1473-3099(03)00830-2
4. Fouts DE, Matthias MA, Adhikarla H, Adler B, Amorim-Santos L, Berg DE, et al. What makes a bacterial species pathogenic?: comparative genomic analysis of the genus *Leptospira*. PLoS Negl Trop Dis. 2016;10:e0004403. https://doi.org/10.1371/journal.pntd.0004403
5. Vincent AT, Schiettekatte O, Goarant C, Neela VK, Bernet E, Thibeaux R, et al. Revisiting the taxonomy and evolution of pathogenicity of the genus *Leptospira* through the prism of genomics. PLoS Negl Trop Dis. 2019;13:e0007270. https://doi.org/10.1371/journal.pntd.0007270
6. Balamurugan V, Gangadhar NL, Mohandoss N, Thirumalesh SRA, Dhar M, Shome R, et al. Characterization of *Leptospira* isolates from animals and humans: phylogenetic analysis identifies the prevalence of intermediate species in India. Springerplus. 2013;2:362. https://doi.org/10.1186/2193-1801-2-362
7. Pappas G, Papadimitriou P, Siozopoulou V, Christou L, Akritidis N. The globalization of leptospirosis: worldwide incidence trends. Int J Infect Dis. 2008;12:351–7. https://doi.org/10.1016/j.ijid.2007.09.011
8. World Health Organization. Human leptospirosis: guidance for diagnosis, surveillance and control. 2003 [cited 2023 Oct 15]. https://www.who.int/publications/i/item/human-leptospirosis-guidance-for-diagnosis-surveillance-and-control
9. Robins JH, McLenachan PA, Phillips MJ, Craig L, Ross HA, Matisoo-Smith E. Dating of divergences within the *Rattus* genus phylogeny using whole mitochondrial genomes. Mol Phylogenet Evol. 2008;49:460–6. https://doi.org/10.1016/j.ympev.2008.08.001
10. Bomfim MRQ, Koury MC. Evaluation of LSSP-PCR for identification of *Leptospira* spp. in urine samples of cattle with clinical suspicion of leptospirosis. Vet Microbiol. 2006;118:278–88. https://doi.org/10.1016/j.vetmic.2006.07.020
11. Ahmed A, Anthony RM, Hartskeerl RA. A simple and rapid molecular method for *Leptospira* species identification. Infect Genet Evol. 2010;10:955–62. https://doi.org/10.1016/j.meegid.2010.06.002
12. Palaniappan RUM, Chang YF, Chang CF, Pan MJ, Yang CW, Harpending P, et al. Evaluation of *lig*-based conventional and real time PCR for the detection of pathogenic leptospires. Mol Cell Probes. 2005;19:111–7. https://doi.org/10.1016/j.mcp.2004.10.002
13. Thaipadungpanit J, Wuthiekanun V, Chierakul W, Smythe LD, Petkanchanapong W, Limpaiboon R, et al. A dominant clone of *Leptospira interrogans* associated with an outbreak of human leptospirosis in Thailand. PLoS Negl Trop Dis. 2007;1:e56. https://doi.org/10.1371/journal.pntd.0000056
14. Boonsilp S, Thaipadungpanit J, Amornchai P, Wuthiekanun V, Bailey MS, Holden MTG, et al. A single multilocus sequence typing (MLST) scheme for seven pathogenic *Leptospira* species. PLoS Negl Trop Dis. 2013;7:e1954. https://doi.org/10.1371/journal.pntd.0001954
15. Salaün L, Mérien F, Gurianova S, Baranton G, Picardeau M. Application of multilocus variable-number tandem-repeat analysis for molecular typing of the agent of leptospirosis. J Clin Microbiol. 2006;44:3954–62. https://doi.org/10.1128/JCM.00336-06
16. Zerbino DR. Using the Velvet de novo assembler for short-read sequencing technologies. Curr Protoc Bioinformatics. 2010;11:11.5. PubMed https://doi.org/10.1002/0471250953.bi1105s31
17. Altschul SF, Gish W, Miller W, Myers EW, Lipman DJ. Basic local alignment search tool. J Mol Biol. 1990;215:403–10. https://doi.org/10.1016/S0022-2836(05)80360-2
18. Puche R, Ferrés I, Caraballo L, Rangel Y, Picardeau M, Takiff H, et al. *Leptospira venezuelensis* sp. nov., a new member of the intermediate group isolated from rodents, cattle and humans. Int J Syst Evol Microbiol. 2018;68:513–7. https://doi.org/10.1099/ijsem.0.002528
19. Levett PN. Leptospirosis. Clin Microbiol Rev. 2001;14:296–326. https://doi.org/10.1128/CMR.14.2.296-326.2001
20. Arzouni JP, Parola P, La Scola B, Postic D, Brouqui P, Raoult D. Human infection caused by *Leptospira fainei*. Emerg Infect Dis. 2002;8:865–8. https://doi.org/10.3201/eid0808.010445
21. Matthias MA, Ricaldi JN, Cespedes M, Diaz MM, Galloway RL, Saito M, et al. Human leptospirosis caused by a new, antigenically unique *Leptospira* associated with a *Rattus* species reservoir in the Peruvian Amazon. PLoS Negl Trop Dis. 2008;2:e213. https://doi.org/10.1371/journal.pntd.0000213
22. Rahman S, Paul SK, Aung MS, Ahmed S, Haque N, Raisul MNI, et al. Predominance of *Leptospira wolffii* in north-central Bangladesh, 2019. New Microbes New Infect. 2020;38:100765. https://doi.org/10.1016/j.nmni.2020.100765
23. Didelot X, Bowden R, Wilson DJ, Peto TEA, Crook DW. Transforming clinical microbiology with bacterial genome sequencing. Nat Rev Genet. 2012;13:601–12. https://doi.org/10.1038/nrg3226
24. Fernandez C, Lubar AA, Vinetz JM, Matthias MA. Experimental infection of *Rattus norvegicus* by the group II intermediate pathogen, *Leptospira licerasiae.* Am J Trop Med Hyg. 2018;99:275–80. https://doi.org/10.4269/ajtmh.17-0844
25. Picardeau M. Toolbox of molecular techniques for studying *Leptospira* spp. Curr Top Microbiol Immunol. 2018;415:141–62. https://doi.org/10.1007/82_2017_45
26. Lehmann JS, Corey VC, Ricaldi JN, Vinetz JM, Winzeler EA, Matthias MA. Whole genome shotgun sequencing shows selection on *Leptospira* regulatory proteins during in vitro culture attenuation. Am J Trop Med Hyg. 2016;94:302–13. https://doi.org/10.4269/ajtmh.15-0401
27. Chiani Y, Jacob P, Varni V, Landolt N, Schmeling MF, Pujato N, et al. Isolation and clinical sample typing of human leptospirosis cases in Argentina. Infect Genet Evol. 2016;37:245–51. https://doi.org/10.1016/j.meegid.2015.11.033

Address for correspondence: Howard E. Takiff, Laboratorio de Genética Molecular, CMBC, Instituto Venezolano de Investigaciones Científicas, Km11, Carretera Panamericana, Caracas 1020A, Venezuela; email: htakiff@gmail.com

Systematic Review of Prevalence of *Histoplasma* Antigenuria in Persons with HIV in Latin America and Africa

Preethiya Sekar, Gila Hale, Jane Gakuru, David B. Meya, David R. Boulware, Jayne Ellis, Elizabeth Nalintya, Nathan C. Bahr, Radha Rajasingham

Histoplasmosis is a fungal disease associated with substantial mortality rates among persons with advanced HIV disease. Our systematic review synthesized data on the global prevalence of *Histoplasma*-caused antigenuria in persons with HIV. We searched PubMed/Medline, Embase, and Scopus databases on January 3, 2023, to identify cross-sectional and cohort studies evaluating *Histoplasma* antigenuria prevalence among adults with HIV infection. We calculated point estimates and 95% CIs to summarize prevalence. Of 1,294 studies screened, we included 15. We found *Histoplasma* antigenuria among 581/5,096 (11%; 95% CI 11%–12%) persons with HIV and 483/3,789 persons with advanced HIV disease (13%; 95% CI 12%–14%). Among persons with HIV and symptoms consistent with histoplasmosis, *Histoplasma* antigenuria prevalence was 14% (95% CI 13%–15%; 502/3,631 participants). We determined that persons with advanced HIV disease, inpatients, and symptomatic persons might benefit from a systematic approach to early detection of histoplasmosis using urine antigen testing.

Histoplasmosis is an endemic fungal infection caused by *Histoplasma capsulatum*. In immunocompetent persons, histoplasmosis is often asymptomatic or localized to the pulmonary system. However, in immunocompromised persons, histoplasmosis can manifest in a progressive disseminated form that is an AIDS-defining illness. Even with prompt treatment, disseminated histoplasmosis has a high mortality rate (*1*,*2*). Given historically limited awareness of the disease and poor diagnostic capacity, histoplasmosis has been underdiagnosed, and the true global burden remains unknown. Although well documented in much of the Americas, with recent studies showing prevalence rates up to 30% in some areas of Central America (*3*), histoplasmosis is also considered endemic in parts of Africa and Asia, and expanding regions of endemicity have been recognized in the past decade (*4*). Given the potential illness and death from HIV-associated histoplasmosis, a critical need exists for improved diagnostics and treatments.

In persons with HIV, histoplasmosis can be difficult to detect because the signs and symptoms of disseminated histoplasmosis closely mimic those of disseminated tuberculosis (TB), increasing risk of misdiagnosis and undertreatment, especially in regions where both diseases are endemic (*5*). Histopathology and culture provide the most accurate methods for diagnosing histoplasmosis, but resource-limited settings often lack the personnel and laboratory infrastructure to use these methods.

Enzyme immunoassays (EIAs), where available, have bridged this diagnostic gap by enabling detection of *Histoplasma* antigen in both urine and serum samples (*6*). The first EIA test, developed by MiraVista Diagnostics (https://miravistalabs.com), is 95% sensitive in urine samples (*7*), but this test is not a viable option for low- and middle-income countries because samples can be processed only at 1 reference laboratory in Indianapolis, Indiana, USA. Optimum Imaging Diagnostics (https://optimumimaging.com) has also developed a urine histoplasmosis sandwich EIA using rabbit monoclonal antibodies that has

Author affiliations: University of Minnesota, Minneapolis, Minnesota, USA (P. Sekar, D.R. Boulware, N.C. Bahr, R. Rajasingham); Makerere University Infectious Diseases Institute, Kampala, Uganda (G. Hale, J. Gakuru, D.B. Meya, E. Nalintya); London School of Hygiene and Tropical Medicine, London, UK (J. Ellis); University of Kansas, Kansas City, Kansas, USA (N.C. Bahr)

DOI: https://doi.org/10.3201/eid3008.231710

a sensitivity of 92% and a specificity of 32% (*8*). The IMMY Alpha test (https://www.immy.com) is a US Food and Drug Administation–approved polyclonal antibody ELISA that has 62%–81% sensitivity and 96%–97% specificity (*7*,*9*). IMMY subsequently developed the Clarus *Histoplasma* galactomannan assay, a monoclonal antibody test, for use on urine samples; sensitivity is 91% and specificity is 91% (*7*). Advent of urinary EIA screening tests might offer a feasible testing strategy, especially in endemic settings, for earlier detection of active histoplasmosis infection than with other testing strategies (*10*). The historical absence of sufficiently sensitive rapid testing that can be routinely performed in resource-limited settings has led to a dearth of accurate prevalence data on the global burden of histoplasmosis.

By performing this systematic review, we aimed to synthesize current research about the prevalence of *Histoplasma* antigens in urine (antigenuria) among persons living with advanced HIV disease worldwide. Understanding the prevalence and burden of *Histoplasma* antigenuria might aid in developing screening and treatment algorithms to improve clinical outcomes related to HIV-associated histoplasmosis. We registered our study at PROSPERO International prospective register of systematic reviews (study identification CRD42023399523).

Methods

Eligibility Criteria

We included cross-sectional or cohort studies of adults living with HIV in whom *Histoplasma* antigen testing was performed. We included studies conducted in inpatient and outpatient settings that had both asymptomatic and symptomatic participants. We defined symptomatic histoplasmosis as having ≥1 associated clinical signs and symptoms, such as fever, weight loss, night sweats, and respiratory symptoms. We excluded studies involving nonhuman subjects or persons <18 years old, non-*Histoplasma* studies, non–English-language studies, conference abstracts, reviews, case reports, and commentaries.

Search Strategy

We conducted a systematic search of PubMed/Medline, Embase, and Scopus databases using PRISMA (Preferred Reporting Items for Systematic Reviews and Meta-Analyses; https://www.prisma-statement.org) guidelines for studies published during January 1, 1947–January 3, 2023 (Figure 1). Search terms included combinations of histoplasmosis, antigen detection, and HIV or advanced HIV. We updated the search on July 20, 2023 (Appendix Table 1, https://wwwnc.cdc.gov/EID/article/30/8/23-1710-App1.pdf).

Data Collection

Three systematic review team members independently assessed abstracts to select articles for full-text review based on specified criteria using Rayyan (https://www.rayyan.ai) and resolved disagreements through discussion. For the full-text review, we used a Qualtrics form (https://www.qualtrics.com) to abstract data. Three reviewers independently completed the form, and a fourth adjudicated discrepancies. Data abstracted were journal name and publication date, article title, first author name, study design, geographic location, setting (inpatient or outpatient), clinical phenotype (i.e., screening among asymptomatic or symptomatic persons according to study author definitions), age range, sex, percentage of participants on antiretroviral therapy, median CD4 count, active TB infection (presumed versus confirmed), type of *Histoplasma* antigen testing kit, other *Histoplasma* diagnostics employed, sample size, number of positive *Histoplasma* cases, percentage of participants with *Histoplasma* detected, and 95% CIs. We also reviewed treatment provided, prophylaxis, and clinical outcomes, but that information was not consistently available across studies.

Outcome Measures

We assessed *Histoplasma* antigen prevalence among subgroups, including persons with HIV regardless of CD4 count, persons with advanced HIV disease (CD4 <200 or World Health Organization stage 3 or 4), inpatients, outpatients, patients with symptoms of histoplasmosis (i.e., fevers, weight loss, night sweats, respiratory symptoms), and asymptomatic patients.

Risk of Bias Assessment

We determined the risk for bias for cross-sectional studies using the Agency for Healthcare Research and Quality Methodology Checklist (Appendix Table 2) and for cohort studies using the modified criteria of the Risk of Bias Assessment Tool for Nonrandomized Studies (Appendix Table 3). The cross-sectional studies checklist assesses the presence, absence, or undetermined status of 11 items: sources of data, inclusion/exclusion criteria, time period, study population selection, blinding, quality assurance of testing, reason for patient exclusion, missing data, confounding, completeness of data collection, and follow-up for missing data (Appendix Table 5). The cohort study assessment tool rates risk for bias as low, high,

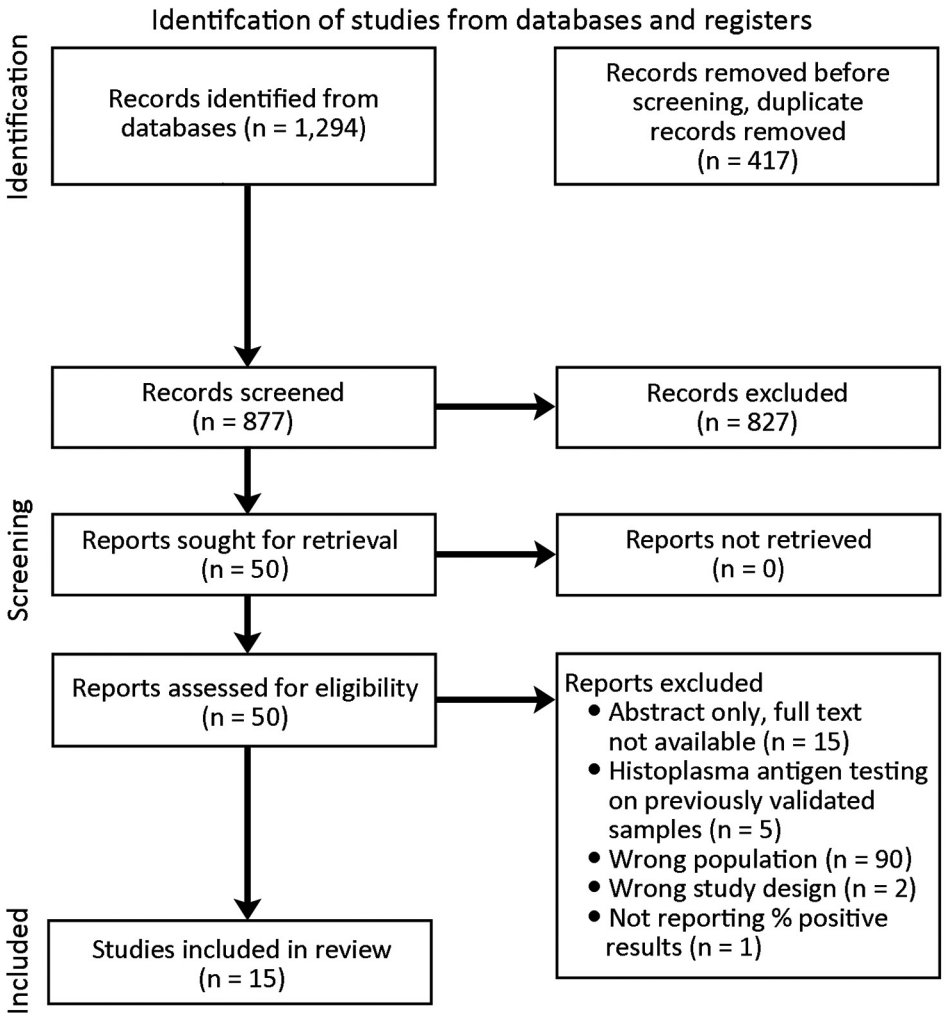

Figure 1. PRISMA (Preferred Reporting Items for Systematic Reviews and Meta-Analyses) flow diagram for systematic review of prevalence of *Histoplasma* antigenuria in persons with HIV in Latin America and Africa.

or unclear in 6 different domains: participant selections, confounding variables, measurement of exposures, blinding of outcome assessments, incomplete outcome data, and selective outcome reporting. Three reviewers independently determined the risk for bias in each domain for each eligible study; a fourth reviewer identified and resolved any disagreements. We classified included studies at low risk of bias if ≥4 of 6 domains were determined to be low. We classified remaining studies at high risk of bias.

Effect Measures and Synthesis Methods

We calculated point estimates and 95% CIs for each of the study outcomes. We also stratified studies selected for full review and data extraction for subgroup analyses on the basis of attributes (e.g., inpatient cohort vs. symptomatic cohort). If inpatient versus outpatient setting was not specified in an article, or if disaggregated data were not provided, we excluded those studies from the setting subgroup analysis. We included studies in the symptomatic cohort if they described participants with ≥1 clinical signs: fever, weight loss, night sweats, or respiratory symptoms. We grouped participants without any signs or symptoms at time of screening in the asymptomatic cohort. If cohorts included a mixture of symptomatic and asymptomatic participants, only those studies that provided disaggregated prevalence results stratified by symptom status were included in the subgroup analysis. We pooled estimates with 95% CIs based on subgroups for forest plots and summary tables. We used Microsoft Excel 2019 version 16.7 (https://www.microsoft.com) when conducting analyses. We used the GRADE (Grading of Recommendations, Assessment, Development, and Evaluations) approach to assess the certainty of evidence by considering risk of bias, inconsistency, indirectness, imprecision, and publication bias (*11*). Four levels of certainty ratings were possible: very low, low, moderate, and high.

Results

Study Selection

Through our database search we identified 1,294 titles. After deduplication, 877 titles remained for abstract review. Of the 877 abstracts reviewed, we excluded 827 because they were not published in English (n = 9), were case reports (n = 416) or systematic reviews (n = 38), did not have a study population with confirmed HIV infection status (n = 36), did not use *Histoplasma* antigen testing (n = 129), or did not report the percentage of the cohort that was *Histoplasma* antigen positive (n = 199). Of the remaining 50 publications available for full-text review, we excluded 35 (Figure 1).

Study Characteristics

We included 15 articles published during 2012–2023 covering 5,096 HIV-positive adults (cohort sizes 35–4,453) undergoing urinary *Histoplasma* antigen testing. Eleven studies (n = 4,057/5,096 participants) were cross-sectional and the other 4 were prospective cohort studies (Table 1). Nine cross-sectional studies (2,753/5,096 participants) took place in sub-Saharan Africa; the remaining 2 were performed in Central or South America (2,343/5,096 participants) (Figure 2). No studies evaluated *Histoplasma* antigenuria prevalence in Asia, Europe, Australia, or North America. Ten of 15 studies (3,789/5,096 participants) focused specifically on populations with advanced HIV disease, whereas 5 studies included all persons with HIV, regardless of CD4 count or World Health Organization disease stage. Eight studies (3,631/5,096 participants) described persons who initially sought treatment with symptoms, and 7 studies (1465/5096 participants) focused on asymptomatic screening cohorts. Most studies were conducted in the outpatient setting, but 8 recruited hospitalized patients (3,286/5,096 participants). The 15 included studies used a mixture of tools to identify *Histoplasma* antigenuria: 2 used MiraVista *Histoplasma* Quantitative EIA test, 4 used IMMY Alpha *Histoplasma* EIA, 7 used IMMY GM *Histoplasma* EIA, 1 used Optimum

Table. Characteristics of Histoplasma urine antigen prevalence studies included in systematic review of prevalence of Histoplasma antigenuria in persons with HIV in Latin America and Africa*

Reference	Country	Study design	Study population†	Clinical status	Setting	Test type‡	No. participants	No. samples tested	HUA positivity, %
(*14*)	Tanzania	Cross-sectional	All HIV and non-HIV	Symptomatic	Inpatient	MV EIA	628	628	1.1
(*15*)	Uganda	Cohort	Advanced HIV	Asymptomatic	Outpatient	IMMY GM EIA	388	388	1.0
(*16*)	Uganda	Cohort	Advanced HIV/meningitis	Symptomatic	Inpatient	MV EIA	257	257	0.0
(*17*)	South Africa	Cross-sectional	Advanced HIV	Symptomatic	Outpatient	IMMY Alpha EIA	34	17	23.5
(*18*)	South Africa	Cross-sectional	Advanced HIV	Asymptomatic	Inpatient	IMMY GM EIA	189	189	5.8
(*19*)	Cameroon	Cross-sectional	All HIV	Asymptomatic	Outpatient	OIDx EIA	138	138	26.1
(*20*)	Ghana	Cross-sectional	All HIV	Asymptomatic	Outpatient	IMMY GM EIA + OIDx LFA	150	107	5.6
(*21*)	Nigeria	Cross-sectional	Advanced HIV	Symptomatic	Outpatient	IMMY GM EIA	213	41	7.3
(*22*)	Nigeria	Cross-sectional	Advanced HIV	Symptomatic	Inpatient	IMMY GM EIA	988	988	7.7
(*23*)	Mexico	Cohort	Advanced HIV	Symptomatic	Inpatient	IMMY Alpha EIA	288	288	21.5
(*24*)	Brazil	Cohort	Advanced HIV	Asymptomatic	Inpatient	IMMY Alpha EIA	106	106	3.8
(*25*)	Colombia	Cross-sectional	Advanced HIV	Symptomatic	Inpatient	IMMY Alpha EIA	172	172	29.1
(*26*)	Colombia	Cross-sectional	Advanced HIV	Asymptomatic	Outpatient	CDC ELISA	768	154	20.1
(*27*)	Panama, Honduras, Nicaragua	Cross-sectional	All HIV	Symptomatic	Inpatient	IMMY GM EIA	4453	1343	20.0
(*28*)	Trinidad	Cross-sectional	HIV	Asymptomatic	Outpatient	IMMY GM EIA + OIDx LFA	280	280	6.4

*EIA, enzyme immunoessay; GM, galactomannan; HUA, histoplasma urine antigen; LFA, lateral flow assay.
†All HIV refers to participants with HIV who were not stratified by CD4 or limited to CD4 counts <200, such as persons in advanced HIV cohorts.
‡Test manufacturers and types: MV, MiraVista Diagnostics EIA (https://miravistalabs.com); IMMY Alpha and GM EIAs (https://www.immy.com); OIDx, Optimum Imaging Diagnostics LFA (https://optimumimaging.com).

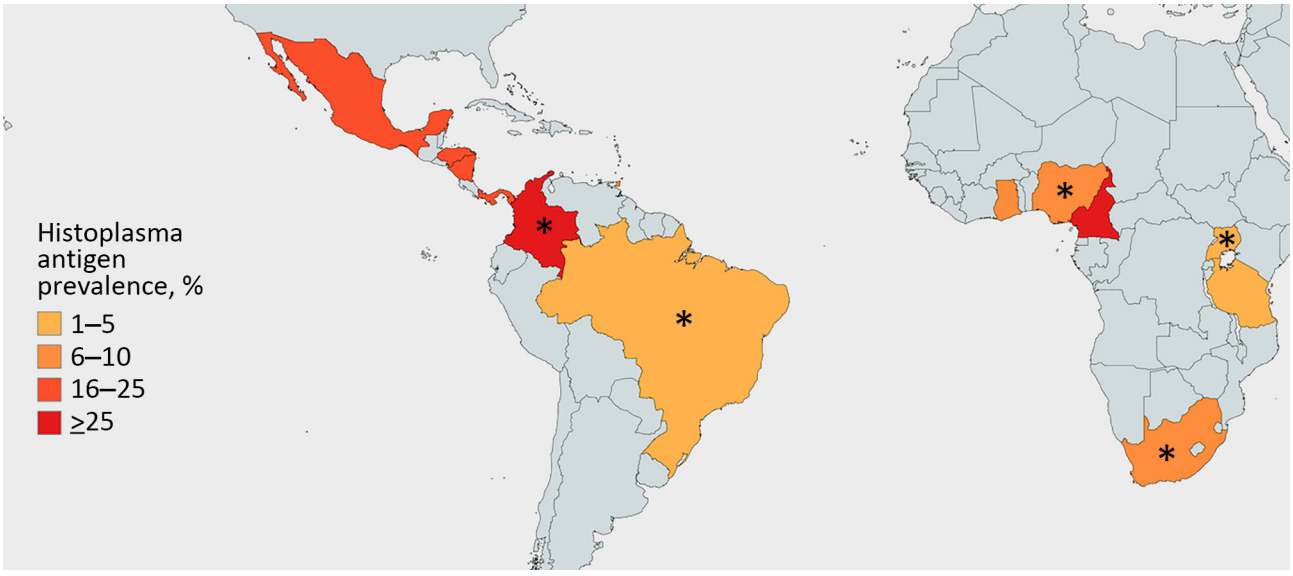

Figure 2. Country-level *Histoplasma* antigenuria prevalence in systematic review of prevalence of *Histoplasma* antigenuria in persons with HIV in Latin America and Africa. Asterisks denote countries with studies that were done in advanced HIV populations, whereas solid colors denote countries with studies of participants with HIV screened for histoplasmosis irrespective of CD4 count.

Imaging Diagnostics *Histoplasma* Sandwich EIA, and 1 used ELISA.

Histoplasma Antigen Prevalence

Of 5,096 persons with HIV tested for *Histoplasma* antigen in their urine from the 15 included studies, 11% (95% CI 11%–12%; n = 581) were antigen positive. Among persons with advanced HIV disease, prevalence of *Histoplasma* antigenuria was 13% (95% CI 12%–14%; n = 483) (Figure 3). Among symptomatic persons with HIV, 14% (95% CI 13%–15%; n = 502) were antigen positive, whereas among asymptomatic persons, 5% (95% CI 4%–7%; n = 79) were *Histoplasma* antigen positive. *Histoplasma* antigen prevalence among inpatients with HIV was 13% (95% CI 12%–14%; 433/3,286) and among outpatients was 7% (95% CI 6%–9%; 111/1,549) ($p<0.05$). We also noted marked geographic variation, with the prevalence of both *Histoplasma* antigenuria and histoplasmosis ranging from 1% in Uganda to 26% in Cameroon (Table; Figure 2).

Risk of Bias in Studies

All of the included studies were observational in nature (Appendix Table 4). In the 2 cohort studies, we found uncertain risk of bias in the selective outcome reporting and low risk throughout all other domains. We determined that all 13 cross-sectional studies defined their information sources, listed inclusion and exclusion criteria for participant selection, indicated at least the start date of the testing period, and specified populations. Two of 13 studies were blinded; the remaining 11 studies did not specify blinding. Six of 13 studies had persons excluded from analyses, often because the participant lacked urine samples. Seven studies addressed confounding variables such as TB or other opportunistic

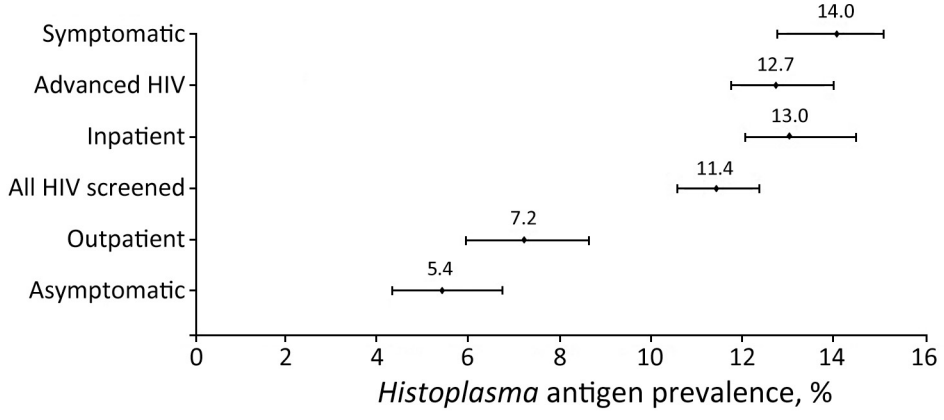

Figure 3. Forest plot of *Histoplasma* antigen prevalence among subgroups of interest in systematic review of prevalence of *Histoplasma* antigenuria in persons with HIV in Latin America and Africa. Error bars indicate 95% CIs.

infections; the remaining 8 studies did not test participants for confounding conditions. Furthermore, thorough analysis of bias risk is consistent with overall low risk of bias, although some categories of risk were unclear in individual studies.

Discussion

From 15 studies that assessed the prevalence of *Histoplasma* antigenuria among 5,096 persons with HIV, we identified 11% (95% CI 11%–12%) *Histoplasma* antigenuria prevalence among all persons with HIV and 13% (95% CI 12%–14%) among persons with advanced HIV disease. Among symptomatic persons with HIV, *Histoplasma* antigenuria prevalence was 14% (95% CI 13%–15%), whereas among asymptomatic persons with HIV, prevalence was 5% (95% CI 4%–7%). Taken together, those data help highlight populations that might benefit from systematic screening for histoplasmosis as part of an HIV package of care. Our analysis suggests that the highest yield screening programs would likely be among persons with advanced HIV disease, histoplasmosis inpatients, and persons who have symptoms consistent with histoplasmosis. Whereas we noted general trends in *Histoplasma* antigenuria prevalence by population characteristics, in some individual studies, those trends did not hold true (e.g., low histoplasmosis prevalence among inpatients with advanced HIV). Various factors aside from inpatient/outpatient status and presence of signs and symptoms might explain this variation, such as geographic location, underlying patient characteristics, and the nonspecific nature of symptoms associated with disseminated histoplasmosis that are shared with other conditions. Therefore, summary data must be considered in the context of the population characteristics of individual studies.

Our systematic review was limited by the modest number of studies available, but the moderate size of our cohorts provided good precision around our prevalence estimates. Included prevalence studies came from just 6 countries in Central and South America and 9 in sub-Saharan Africa, but few studies from Asia, North America, Europe, and Australia have been published. In our analysis, we found only 3 countries (South Africa, Nigeria, and Colombia) in which ≥1 antigen prevalence study had been conducted. Prevalence of histoplasmosis transmission is classically thought to be associated with sources for local exposure, such as bat guano, poultry, caves, housing, construction, and certain occupations, although persons not reporting those classic exposures can also manifest histoplasmosis. This duality underscores the importance of conducting regional prevalence studies to assess fluctuations in histoplasmosis prevalence. Prospective studies are needed to better understand disease prevalence and consider the effects of symptoms, CD4 count, coexisting TB infection, and TB diagnostics on recognizing the disease.

The observational nature of all of the included studies and resulting selection bias limits the generalizability of our findings; inpatient studies might have excluded TB patients before enrollment. For example, in studies of identified *Histoplasma* antigenuria among only symptomatic inpatients, prevalence might have been higher than among inpatients in whom TB had not yet been excluded. In cohort studies, there might be a bias to include persons with confirmed histoplasmosis and consequentially report a higher prevalence of histoplasmosis compared with cross-sectional screening studies. Very few studies included TB diagnostics or consideration of coexisting TB infection. The small number of studies and limited data also prevented any further subgroup analyses of *Histoplasma* antigenuria prevalence (e.g., by antiretroviral therapy status). Prospective clinical studies are needed to identify persons with advanced HIV disease who have asymptomatic *Histoplasma* antigenuria, particularly those from geographic areas not represented by currently available data.

Histoplasma antigenuria prevalence among asymptomatic persons with HIV was 5%. The clinical significance of asymptomatic *Histoplasma* antigenuria among persons with HIV is unknown, and further research is required to investigate whether antifungal therapy is required or a watch-and-wait policy alongside antiretroviral therapy with immune reconstitution is sufficient among persons in that group. Those results could be false positives; they could indicate that patients with a low antigen burden who are undergoing antiretroviral therapy might not require antifungal therapy; or they could represent early dissemination that would progress without antifungal treatment.

Clinical studies and studies on the burden of histoplasmosis disease are hampered by a historical lack of histoplasmosis diagnostics. Although culture and histopathology are the most accurate methods for diagnosis, many resource-limited settings do not have the laboratory capacity or staffing to perform these tests. Furthermore, culture results require several weeks, which is clinically impractical. Antigen detection assays for histoplasmosis have 95% sensitivity (95% CI 94%–97%) and 97% specificity (95% CI 97%–98%) and are found to be most accurate among persons with HIV in whom fungal burden is gen-

erally highest (*12*). Access to point-of-care, rapid antigen assays that do not require laboratory infrastructure would enable better characterization of histoplasmosis burden in limited resource settings, where the burden of advanced HIV disease is highest. Two companies, Optimum Imaging Diagnostics and MiraVista, have now produced lateral flow assays that have European Union CE marks, which indicates that a product has been assessed by the manufacturer and deemed to meet European Union safety, health, and environmental protection requirements; however, those products have not been approved by the US Food and Drug Administration (*7*,*12*,*13*). Another company, IMMY, is developing a lateral flow assay, but it has not yet been tested clinically. Further development and testing of these assays is necessary. Beyond the role of antigen testing to provide updated epidemiologic data, rapid antigen tests have the potential to improve clinical management among persons with advanced HIV disease and symptomatic histoplasmosis. If clinical trials demonstrate survival benefit from histoplasmosis screening and treatment among asymptomatic persons with advanced HIV disease, a rapid, point-of-care assay would be essential for diagnosis of cryptococcal diseases.

G.H., J.G., and P.S. independently assessed abstracts to select articles for full-text review and along with R.R. resolved any disagreements. G.H., J.G., and P.S. independently completed the form and R.R. adjudicated discrepancies. G.H., J.G., and P.S. independently determined the risk of bias in each eligible study in each domain. R.R. identified and resolved any disagreements.

About the Author

Ms. Sekar is a 4th year medical student at the University of Minnesota. During 2022–2023, she completed a Fogarty fellowship and studied advanced HIV disease and opportunistic infections in Kampala, Uganda.

References

1. Adenis AA. AIDS-related histoplasmosis in Latin America [abstract]. Med Mycol. 2018;56(Suppl 2):S7. https://doi.org/10.1093/mmy/myy036
2. Samayoa B, Roy M, Cleveland AA, Medina N, Lau-Bonilla D, Scheel CM, et al. High mortality and coinfection in a prospective cohort of human immunodeficiency virus/acquired immune deficiency syndrome patients with histoplasmosis in Guatemala. Am J Trop Med Hyg. 2017;97:42–8. https://doi.org/10.4269/ajtmh.16-0009
3. Adenis AA, Valdes A, Cropet C, McCotter OZ, Derado G, Couppie P, et al. Burden of HIV-associated histoplasmosis compared with tuberculosis in Latin America: a modelling study. Lancet Infect Dis. 2018;18:1150–9. https://doi.org/10.1016/S1473-3099(18)30354-2
4. Ashraf N, Kubat RC, Poplin V, Adenis AA, Denning DW, Wright L, et al. Re-drawing the maps for endemic mycoses. Mycopathologia. 2020;185:843–65. https://doi.org/10.1007/s11046-020-00431-2
5. Adenis A, Nacher M, Hanf M, Basurko C, Dufour J, Huber F, et al. Tuberculosis and histoplasmosis among human immunodeficiency virus-infected patients: a comparative study. Am J Trop Med Hyg. 2014;90:216–23. https://doi.org/10.4269/ajtmh.13-0084
6. Villareal K, Price A, Pasqualotto AC, Bahr NC. The current and future states of diagnostic tests for histoplasmosis with a focus on people with HIV and disseminated histoplasmosis. J Fungi (Basel). 2023;9:793793. https://doi.org/10.3390/jof9080793
7. Martínez-Gamboa A, Niembro-Ortega MD, Torres-González P, Santiago-Cruz J, Velázquez-Zavala NG, Rangel-Cordero A, et al. Diagnostic accuracy of antigen detection in urine and molecular assays testing in different clinical samples for the diagnosis of progressive disseminated histoplasmosis in patients living with HIV/AIDS: a prospective multicenter study in Mexico. PLoS Negl Trop Dis. 2021;15:e0009215. https://doi.org/10.1371/journal.pntd.0009215
8. Cáceres DH, Gómez BL, Tobón ÁM, Chiller TM, Lindsley MD. Evaluation of OIDx *Histoplasma* urinary antigen EIA. Mycopathologia. 2022;187:129–31. https://doi.org/10.1007/s11046-021-00602-9
9. Torres-González P, Niembro-Ortega MD, Martínez-Gamboa A, Ahumada-Topete VH, Andrade-Villanueva J, Araujo-Meléndez J, et al. Diagnostic accuracy cohort study and clinical value of the *Histoplasma* urine antigen (ALPHA *Histoplasma* EIA) for disseminated histoplasmosis among HIV infected patients: a multicenter study. PLoS Negl Trop Dis. 2018;12:e0006872. https://doi.org/10.1371/journal.pntd.0006872
10. Theel ES, Jespersen DJ, Harring J, Mandrekar J, Binnicker MJ. Evaluation of an enzyme immunoassay for detection of *Histoplasma capsulatum* antigen from urine specimens. J Clin Microbiol. 2013;51:3555–9. https://doi.org/10.1128/JCM.01868-13
11. Goldet G, Howick J. Understanding GRADE: an introduction. J Evid Based Med. 2013;6:50–4. https://doi.org/10.1111/jebm.12018
12. Caceres DH, Knuth M, Derado G, Lindsley MD. Diagnosis of progressive disseminated histoplasmosis in advanced HIV: a meta-analysis of assay analytical performance. J Fungi (Basel). 2019;5:76.
13. Abdallah W, Myint T, LaRue R, Minderman M, Gunn S, Wheat LJ, et al. Diagnosis of histoplasmosis using the MVista *Histoplasma* galactomannan antigen qualitative lateral flow-based immunoassay: a multicenter study. Open Forum Infect Dis. 2021;8:ofab454.
14. Lofgren SM, Kirsch EJ, Maro VP, Morrissey AB, Msuya LJ, Kinabo GD, et al. Histoplasmosis among hospitalized febrile patients in northern Tanzania. Trans R Soc Trop Med Hyg. 2012;106:504–7. https://doi.org/10.1016/j.trstmh.2012.05.009
15. Sekar P, Nalintya E, Kwizera R, Mukashyaka C, Niyonzima G, Namakula LO, et al. Prevalence of *Histoplasma antigenuria* among outpatient cohort with advanced HIV in Kampala, Uganda. J Fungi (Basel). 2023;9:757. https://doi.org/10.3390/jof9070757
16. Bahr NC, Sarosi GA, Meya DB, Bohjanen PR, Richer SM, Swartzentruber S, et al. Seroprevalence of histoplasmosis

in Kampala, Uganda. Med Mycol. 2016;54:295–300. https://doi.org/10.1093/mmy/myv081
17. Schwartz IS, Kenyon C, Lehloenya R, Claasens S, Spengane Z, Prozesky H, et al. AIDS-related endemic mycoses in western Cape, South Africa, and clinical mimics: a cross-sectional study of adults with advanced HIV and recent-onset, widespread skin lesions. Open Forum Infect Dis. 2017;4:ofx186. https://doi.org/10.1093/ofid/ofx186
18. van Schalkwyk E, Mhlanga M, Maphanga TG, Mpembe RS, Shillubane A, Iyaloo S, et al. Screening for invasive fungal disease using non-culture-based assays among inpatients with advanced HIV disease at a large academic hospital in South Africa. Mycoses. 2020;63:478–87. https://doi.org/10.1111/myc.13071
19. Kuate MPN, Nyasa R, Mandengue C, Tendongfor N, Bongomin F, Denning DW. Screening for acute disseminated histoplasmosis in HIV disease using urinary antigen detection enzyme immunoassay: a pilot study in Cameroon. J Microbiol Methods. 2021;185:106226. https://doi.org/10.1016/j.mimet.2021.106226
20. Ocansey BK, Otoo B, Asamoah I, Ganu V, Berko KP, Oladele O, et al. Cryptococcal and *Histoplasma* antigen screening among people with human immunodeficiency virus in Ghana and comparative analysis of OIDx *Histoplasma* lateral flow assay and IMMY *Histoplasma* enzyme immunoassay. Open Forum Infect Dis. 2022;9:ofac277.
21. Ekeng BE, Oladele RO, Emanghe UE, Ochang EA, Mirabeau TY. Prevalence of histoplasmosis and molecular characterization of *Histoplasma* species in patients with presumptive pulmonary tuberculosis in Calabar, Nigeria. Open Forum Infect Dis. 2022;9:ofac368.
22. Oladele RO, Osaigbovo II, Akanmu AS, Adekanmbi OA, Ekeng BE, Mohammed Y, et al. Prevalence of histoplasmosis among persons with advanced HIV disease, Nigeria. Emerg Infect Dis. 2022;28:2261–9. https://doi.org/10.3201/eid2811.220542
23. Torres-González P, Niembro-Ortega MD, Martínez-Gamboa A, Ahumada-Topete VH, Andrade-Villanueva J, Araujo-Meléndez J, et al. Diagnostic accuracy cohort study and clinical value of the *Histoplasma* urine antigen (ALPHA *Histoplasma* EIA) for disseminated histoplasmosis among HIV infected patients: a multicenter study. PLoS Negl Trop Dis. 2018;12:e0006872. https://doi.org/10.1371/journal.pntd.0006872
24. Vidal JE, Werlang PC, Muniz BM, Rego CM, Barbalho RE, Baptista AM, et al. Combining urine antigen and blood polymerase chain reaction for the diagnosis of disseminated histoplasmosis in hospitalized patients with advanced HIV disease. Med Mycol. 2021;59:916–22. https://doi.org/10.1093/mmy/myab022
25. Hoyos Pulgarin JA, Alzate Piedrahita JA, Moreno Gómez GA, Sierra Palacio JF, Ordoñez KM, Arias Ramos D. Closing gaps in histoplasmosis: clinical characteristics and factors associated with probable/histoplasmosis in HIV/AIDS hospitalized patients, a retrospective cross-sectional study in two tertiary centers in Pereira, Colombia. AIDS Res Ther. 2021;18:51. https://doi.org/10.1186/s12981-021-00377-5
26. Caceres DH, Zuluaga A, Arango-Bustamante K, de Bedout C, Tobón ÁM, Restrepo Á, et al. Implementation of a training course increased the diagnosis of histoplasmosis in Colombia. Am J Trop Med Hyg. 2015;93:662–7. https://doi.org/10.4269/ajtmh.15-0108
27. Caceres DH, Arauz AB, Flores C, Santiago E, Montoya S, Saenz C, et al. Implementation of rapid diagnostics assays for detection of histoplasmosis and cryptococcosis in Central American people living with HIV. Mycoses. 2021;64:1396–401. https://pubmed.ncbi.nlm.nih.gov/33966300
28. Edwards RJ, Todd S, Edwards J, Samaroo-Francis W, Lyons N, Boyce G, et al. The incidence of histoplasmosis and cryptococcal antigenemia among patients attending a large HIV clinic in Trinidad. Diagn Microbiol Infect Dis. 2023;106:115952. https://doi.org/10.1016/j.diagmicrobio.2023.115952

Address for correspondence: Radha Rajasingham, University of Minnesota, Minneapolis, 689 SE 23rd Ave, Minneapolis, MN 55455, USA; email: radha@umn.edu

Environmental Hot Spots and Resistance-Associated Application Practices for Azole-Resistant *Aspergillus fumigatus*, Denmark, 2020–2023

Maiken Cavling Arendrup, Rasmus Krøger Hare, Karin Meinike Jørgensen, Ulla E. Bollmann, Tina B. Bech, Cecilie Cetti Hansen, Thies M. Heick, Lise Nistrup Jørgensen

Azole-resistant *Aspergillus fumigatus* (AR*Af*) fungi have been found inconsistently in the environment in Denmark since 2010. During 2018–2020, nationwide surveillance of clinical *A. fumigatus* fungi reported environmental TR_{34}/L98H or TR_{46}/Y121F/T289A resistance mutations in 3.6% of isolates, prompting environmental sampling for AR*Af* and azole fungicides and investigation for selection of AR*Af* in field and microcosmos experiments. AR*Af* was ubiquitous (20% of 366 samples; 16% TR_{34}/L98H- and 4% TR_{46}/Y121F/T289A-related mechanisms), constituting 4.2% of 4,538 *A. fumigatus* isolates. The highest proportions were in flower- and compost-related samples but were not correlated with azole-fungicide application concentrations. Genotyping showed clustering of tandem repeat–related AR*Af* and overlaps with clinical isolates in Denmark. *A. fumigatus* fungi grew poorly in the field experiment with no postapplication change in AR*Af* proportions. However, in microcosmos experiments, a sustained complete (tebuconazole) or partial (prothioconazole) inhibition against wild-type *A. fumigatus* but not AR*Af* indicated that, under some conditions, azole fungicides may favor growth of AR*Af* in soil.

Azole resistance in *Aspergillus fumigatus* fungi has increased during the past 25 years. Increasing evidence documents that selection of azole-resistant *A. fumigatus* (AR*Af*) takes place in the environment (*1*,*2*). Investigations have been performed or initiated in several countries to investigate the relative contributions of various environmental azole fungicide applications to selection for AR*Af* (*3*–*5*).

In Denmark during June–August 2009, AR*Af* was first found in 1/17 *A. fumigatus* isolates from hospital surroundings and 3/21 from a park in Copenhagen (*6*), but subsequent environmental soil and air samples collected during September–October 2013 were negative for AR*Af* (*7*). That finding is somewhat in contrast to findings in clinical samples from Denmark. After the first isolation of TR_{34}/L98H mutants in late 2007 and TR_{46}/Y121F/T289A in 2012 (*7*–*9*), an increasing rate of AR*Af* of environmental origin from 1.5% (2/133) in 2007–2009 to 3.6% (5/137) in 2018 has been found in patients with cystic fibrosis (*8*,*10*). Moreover, during 2018–2020, the nationwide surveillance of AR*Af* revealed a rate of 3.6% environmental AR*Af* among 1,083 patients (*11*).

Which environmental azole fungicide uses are potentially safe and which contribute mostly to the increasing proportion of AR*Af* is not clear. However, because selection of resistance through either emergence of resistance in a susceptible isolate or favored growth of an already existing AR*Af* subpopulation requires *A. fumigatus* multiplication, azole residues in soils or plant debris where *A. fumigatus* fungi thrives are probably the biggest source for dissemination of AR*Af*. Prior studies have suggested that hot spots for AR*Af* include azole-treated flower bulb production (*1*), plant waste piles, and composting heaps (*1*,*12*), whereas cold spots probably include animal manure and grain (*1*,*13*) and arable farming (*14*,*15*), including potato fields (*3*). However, variable findings have

Author affiliations: Rigshospitalet, Copenhagen University, Denmark (M.C. Arendrup); Statens Serum Institut, Copenhagen, Denmark (M.C. Arendrup, R.K. Hare, K.M. Jørgensen); Geological Survey of Denmark and Greenland, Copenhagen (U.E. Bollmann, T.B. Bech, C.C. Hansen); Aarhus University, Flakkebjerg, Slagelse, Denmark (T.M. Heick, L.N. Jørgensen)

DOI: https://doi.org/10.3201/eid3008.240096

been reported for several settings, including greenhouses and strawberry crops (*3*,*5*,*16*).

On the basis of those findings, the Danish Ministry of Environment supported a research project about the presence and selection of AR*Af* in Denmark. The project included extensive environmental sampling with determination of azole-susceptible and -resistant *A. fumigatus* and of azole concentrations; characterization of resistance mechanisms and molecular genotypes to determine if resistant genotypes come from outside (by wind and goods) or multiply and expand in Denmark; and microcosmos and field experiments investigating the potential of various azole fungicides to select for AR*Af*.

Materials and Methods

Environmental Hot Spot and Field-Experiment Sampling

We collected 366 samples (Appendix Table 1, https://wwwnc.cdc.gov/EID/article/30/8/24-0096-App1.pdf): agricultural fields (air and soil; n = 167, including 40 samples obtained before/between/after azole spraying); park and private garden soil (n = 60); flower and potatoes (n = 100); compost soil (from garden waste) and compost heaps from vegetable waste and garden waste (n = 20); animal manure heaps with straw or peat and associated stable bedding (n = 25); and wood paint–associated soil (n = 14). We sampled air (1 m^3/sample) through a gelatin filter by using a Sartorius MD8 Airport Portable Sampler (https://shop.sartorius.com). We placed the gelatin filter on yeast glucose chloramphenicol (YGC) agar and incubated it 1 day at 37°C, 1 day at 50°C, and 1 day at 37°C, inspecting it daily. That procedure favored growth of *A. fumigatus* fungi over other molds, thereby enhancing *A. fumigatus* isolation in a pilot study. Solid samples (e.g., soil top 5 cm [*5*], compost, manure heap) were suspended in sterile water with 0.1% Tween 20 (2.5 mL/g sample), vortexed, and allowed to settle for 10–15 minutes. We transferred ≈10 mL top fluid to a new tube, vortexed it, and cultured 500 µL or 250 µL on YGC and on YGC supplemented with tebuconazole (3 mg/g agar [YGC-Teb]). We centrifuged the remaining fluid (3,000 rpm, ≈1,942 g, 10 minutes), discarded ≈8 mL supernatant, and resuspended the pellet in the remaining liquid followed by plating of 500 µL on YGC and YGC-Teb. For air samples, we incubated all plates as described above.

We isolated *A. fumigatus* fungi (maximum 30 isolates/sample), subcultured, and identified by using macro- and micro-morphology and thermotolerance of 50°C supplemented with matrix-assisted laser desorption/ionization time-of-flight mass spectrometry (Bruker, https://www.bruker.com) and the online available spectrum database mass spectrometry imaging when needed (*17*,*18*). When we identified mixed TR_{34}/L98H and TR_{46}/Y121F/T289A mutations, we attempted isolation from susceptibility plate wells containing voriconazole (favoring TR_{46}/Y121F/T289A) and posaconazole (favoring TR_{34}/L98H).

Susceptibility Testing

Initially, *A. fumigatus* colonies on YGC-Teb underwent azole-resistance screening (EUCAST E.Def 10.1), followed by determination of MICs of itraconazole, posaconazole, isavuconazole, and voriconazole (EUCAST E.Def 9.3) if screening positive. Because of equal performance of YGC-TEB and E.Def 10.1, we subsequently omitted the E.Def 10.1 screening step (*19*,*20*). We compared individual proportions of AR*Af* pairwise by using a χ^2 or Fisher exact test with the GraphPad Prism 9.3.1 program (https://www.graphpad.com).

Extraction and Concentration Determination of Azoles

We analyzed azole content as previously described for soil samples by using sonication/shaking-extraction and high-performance liquid chromatography–tandem mass spectrometry analysis (*21*) with minor modifications: soil samples were sieved (2 mm) and homogenized manually; potted plant soil/root mix and freeze-dried potato peels were homogenized in a blender (Appendix Table 2). We prepared blank and control samples as well as calibration standards in a reference matrix (organically farmed soil or potato peel), extracted, and analyzed together with each set of samples. When no matching reference matrix was available (potted plants, compost), we used standard addition.

Molecular Characterization of Azole Resistance Mechanisms

We sequenced the *cyp51A* gene, including promoter, as previously described for AR*Af* isolates and selected susceptible *A. fumigatus* isolates (*8*,*22*) (Appendix Table 3). Azole-resistant isolates that were *cyp51A* wild-type underwent full-length *hmg1* sequencing as previously reported (*23*), with some modifications (Appendix Table 4). We assembled sequences and compared them with appropriate reference sequences (*cyp51A*, GenBank accession no. AF338659; *hmg1*, GenBank accession no. Afu2g03700) by using CLC Main Workbench versions 22 and 23 (QIAGEN, https://www.qiagen.com). We reported only tandem repeats in the promoter region (*cyp51A* only) and mutations leading to amino acid changes.

Genotyping

We conducted genotyping by using the short tandem repeat *A. fumigatus* (STR*Af*) method with all 9 microsatellite markers as previously described (*24*) (Appendix Table 5). We performed genotype analyses by using BioNumerics versions 7 and 8 (bioMérieux, https://www.biomerieux.com), illustrated as minimum spanning trees with default settings. We compared the genotype to worldwide genotypes from the Czech Republic (n = 1), Australia (n = 2), China (n = 8), the United Kingdom (n = 10), Cuba (n = 14), Switzerland (n = 71), Germany (n = 100), the United States (n = 102), Belgium (n = 108), Norway (n = 209), Spain (n = 219), and the Netherlands (n = 615) (*9*), as well as addition genotypes not previously reported from Finland (n = 1), Austria (n = 3), and Sweden (n = 5).

Microcosmos Selection Experiments

For microcosmos experiments, we placed 4 g dry sterile soil and 1 mL of 2–5 × 10^2 CFU/mL *A. fumigatus* solution (wild type, TR_{34}/L98H, and TR_{46}/Y121F/T289A) in 0.85% NaCl in 25 mL glass vials. We included sandy soil (total organic carbon content 0.92%) and a soil with high organic content (total organic carbon content 5.68%). The soils originated from fields organically farmed for 40 years (Svanholm Gods, Denmark). The microcosmos vials were initially incubated at 10°C, 15°C, and 20°C and consecutively sampled for *A. fumigatus* and AR*Af* quantification (Appendix Figure 1). For selection experiments, we chose incubation at 20°C and added 100 µL azole fungicide solution (tebuconazole [Folicur EW-250, 250 g/L; Bayer]), prothioconazole [Proline EC-250, 250 g/L; Bayer], mefentrifluconazole [Revysol, 100 g/L; BASF, https://agriculture.basf.com], or MilliQ water [control; Sigma Aldrich, https://www.sigmaaldrich.com]) 2 days after inoculation in application concentrations of 2.5–2,500 mg/L and homogenized the content with an inoculation loop. Final wet-weight concentrations were 0.049–49 mg/kg (spike solution concentration × applied volume)/dry weight) (Appendix Table 6).

A. fumigatus and AR*Af* Quantification in Microcosmos by PCR

We extracted DNA from the microcosmos samples (≈250 mg) and the collected soil samples by using DNeasy PowerLyzer PowerSoil Kit (QIAGEN) and 50 µL elution buffer. To quantify, we used quantitative PCR or droplet digital PCR (Appendix Table 7). For the first microcosmos experiments, the target was a multicopy internal transcribed spacer, and for subsequent experiments, we used primers and probes targeting the *cyp51A* promoter able to distinguish TR_{34}/L98H and TR_{46}/Y121F/T289A (Appendix Table 6). We ran controls for the standard curve and samples in triplicate.

Results

Environmental Sampling

Environmental sampling consisted of 366 samples and 4,538 *A. fumigatus* isolates (Table 1). In 2020, AR*Af* harboring TR_{34}/L98H or associated variants (TR_{34}/T-67G/L98H or TR_{34}/L98H/S297T/F495I), specifically, were found in all sample types and years, except 1 potato field. In 2021 and 2022, *A. fumigatus* fungi harboring TR_{46}/Y121F/T289A or associated variants (TR_{46}/Y121F/T289A/S363P/I364V/G448S or TR_{46}[3]/Y121F/M172I/T289A/G448S) were found in samples from fields, flowers/flower beds, compost, and stable bedding.

Agricultural Fields

AR*Af* was less common during 2020 (2.3%–7.7% of soil and air samples and 0.3%–1.7% of isolates) than during 2021–2022 (20%–21.6% of soil and air samples and 2.8%–6.6% of isolates). Most AR*Af* harbored TR_{34}/L98H (25/32, 78%), whereas 1 harbored TR_{46}/Y121F/T289A and 1 harbored TR_{46}/Y121F/T289A/S363P/I364V/G448S (6% of AR*Af*). Air sampling was performed before (15 samples), during (29 samples), and after (19 samples) harvesting. The *A. fumigatus* counts were highest in samples taken during harvest (380 [13.1/sample]), compared with before harvest (28 [1.9/sample)] and after harvest (46 [2.4/sample]). Ten air samples (10/63 [15.9%]) contained AR*Af*, 8 of which were taken during harvest (8/29 [27.6%]). Among 454 *A. fumigatus* air isolates, 4.6% were AR*Af* (including 3.7% TR_{34}/L98H and 0.2% TR_{46}/Y121F/T289A).

Produce

Potatoes from supermarket potatoes (washed and bagged) contained very little *A. fumigatus* and no AR*Af* (Table 1). Potatoes from the farm shop and fields had some soil on the surface. All potato samples were positive for *A. fumigatus* fungi (2.4–15.9/sample), and 25% (4/16) samples contained *ARAf* harboring TR_{34}/L98H (3.1%–10.5% of isolates). Flowerpot soil samples from 3 flower types and nurseries contained high amounts of *A. fumigatus* fungi. AR*Af* was absent in cactus pot soil, whereas 25% (10/40) of samples from poinsettia and campanula contained AR*Af* (2.5%–4.8% of isolates), including TR_{34}/L98H or TR_{34}/L98H/S297T/F495I (21/27 AR*Af* isolates

during 2020–2021) and TR_{46}/Y121F/T289A or TR_{46}/Y121F/T289A/S363P/I364V/G448S (3/14 AR*Af* isolates during 2021). One AR*Af* harbored an F262 deletion within the sterol-sensing domain of Hmg1, which has previously been associated with azole MIC elevation (*23*). Last, air samples from a plant nursery contained few *A. fumigatus* fungi and no AR*Af*.

Flower beds

From flower beds sampled in 3 public parks and 2 private gardens, 59/60 samples contained *A. fumigatus* isolates (mean 24.6 isolates/sample). AR*Af* was found at all sites and in 30% of samples, ranging from 5% (1/20) to 47% (7/15) among public parks and 50% (5/10) of samples from private gardens. TR_{34}/L98H and TR_{34}/T-67G/L98H were found in 85% of AR*Af* isolates and 3% of *A. fumigatus* isolates. TR_{46}/Y121F/T289A, TR_{46}/Y121F/T289A/S363P/I364V/G448S, and TR_{46}[3]/Y121F/M172I/T289A/G448S found in 1 park and both gardens constituted 0.5% of *A. fumigatus* isolates and accounted for most AR*Af* (6/7 AR*Af* isolates) in the 2 private gardens.

Soil

Soil near painted allotment houses/terraces was sampled because runoff water from painted surfaces might contain azoles. All samples contained *A. fumigatus* isolates (mean 25.6 isolates/sample). Two samples were positive for AR*Af* (14.3% samples and 1.1% *A. fumigatus* isolates); 3/4 AR*Af* isolates harbored

Table 1. Overview of *Aspergillus fumigatus* and AR*Af* showing total and TR_{34}/L98H-related [TR_{34}] and TR_{46}/Y121F/T289A-related [TR_{46}] isolates from the environment, Denmark, 2020–2022*

	Samples, no. (%)				Isolates of *Af* and AR*Af*			
Location (samples/sites), date	*A. fumigatus*	AR*Af*	TR_{34}	TR_{46}	*Af*, no. (no./sample)	AR*Af*, no. (%)	TR_{34}, no. (%)	TR_{46}, no. (%)
Field soil (84/7)								
Cereal and potato (44/5), 2020	43 (98)	1 (2.3)	1 (2.3)	2	318 (7.2)	1 (0.3)	1 (0.3)	0
Cereal (40/2), 2022 May–Sep	40	8 (20)	5 (13)	1 (3)	360 (9.0)	10 (2.8)	7 (1.9)	1 (0.3)
Field air (63/3)								
Field air (26/1), 2020	23 (100)	2 (7.7)	2 (7.7)	0	181 (7.0)	3 (1.7)	3 (1.7)	0
Field air (37/2), 2021	35 (95)	8 (21.6)	5 (13.5)	1 (2.7)	273 (7.4)	18 (6.6)	14 (5.1)	1 (0.4)
Vegetables (40/10), 2020								
Potato-supermarkets (24/6)	7 (29)	0	0	0	9 (0.4)	0	0	0
Potato-farm shop (8/2)	8 (100)	2 (25)	2 (25)	0	19 (2.4)	2 (10.5)	2 (10.5)	0
Potato-field (Flakkebjerg) (8/2)	8 (100)	2 (25)	2 (25)	0	127 (15.9)	4 (3.1)	4 (3.1)	0
Flower-producers soil (50/3), 2020 and 2021								
Poinsettia (20/2), Campanula (10/1), 2020	30 (100)	8 (27)	6 (20)	0	516 (17.2)	13 (2.5)	11 (2.1)	0
Cactus (10/1), 2020	10 (100)	0	0	0	200 (20.0)	0	0	0
Poinsettia (10/1), 2021	10 (100)	2 (20)	2 (20)	1 (10)	289 (28.9)	14† (4.8)	10 (3.5)	3 (1.0)
Flower-producers air (10/1), 2021	9 (90)	0	0	0	24 (2.4)	0	0	0
Park & garden flowerbed soil (60/5), 2021	59 (98)	18 (30)	14 (23.3)	4 (6.7)	1,476 (24.6)	52 (3.5)	44 (3.0)	8 (0.5)
Allotment near soil (14/14), 2021								
Allotment houses (14)†	14 (100)	2 (14.3)	2 (14.3)	0	358 (25.6)	4† (1.1)	3 (0.8)	0
Compost related (20/3), 2022								
Recycle soil from garden waste (5)	5 (100)	4 (80)	4 (80)	0	219 (43.8)	6 (2.7)	6 (2.7)	0
Compost heap garden waste (10)	10 (100)‡	5 (NP)	5 (NP)	4 (NP)	12‡ (100)	11 (92)	7 (58)	3 (25)
Compost heap vegetable production (5)	5 (100)	5 (100)	5 (100)	3 (60)	21§ (100)	21 (100)	17 (81)	4 (19)
Manure heaps from horses (12/2), 2022								
Center 1 (7), 2022 Feb	5	3 (43)	3 (43)	0	54 ((7.7)	14 (25.9)	14 (25.9)	0
Center 2 (5), 2022 Nov	3	0	0	0	19 (3.8)	0	0	0
Horse stable and beddings (13/1), 2022								
Stable bedding with wheat (2)	2	0	0	0	8	0	0	0
Stable bedding with barley (3)	3	2	1	1	33 (11)	13 (39)	12 (36)	1 (3)
Stable bedding with peat (2)	1	1	1	0	5 (2.5)	2 (40)	2 (40)	0
Fresh wheat (2)	2	0	0	0	10	0	0	0
Fresh barley (2)	1	0	0	0	5	0	0	0
Fresh peat (2)	1	0	0	0	2	0	0	0
Total (366)	334 (91.0)	73 (20.0)	60 (16.0)	15 (0.04)	4,538 (12.4)	188 (4.2)	157 (3.5)	21 (0.5)

*Darker red indicates increasing percentage. AR*Af*, azole-resistant *A. fumigatus*, NP, not possible to determine exact denominator because of uncountable number of colonies on the plate.
†One AR*Af* from poinsettia harbored an Hmg1 F262-deletion and 1 from painted wood–related soil harbored an Hmg1 E306K alteration within the sterol-sensing domain.
‡Plates were massively overgrown by Mucorales spp. From 5 samples, it was possible to perform *A. fumigatus* PCR and direct target gene sequencing yielding TR_{34}/L98H, TR_{46}/Y121F/T289A, or both.
§Of >200 resistant colonies per sample (growing on tebuconazole containing agars), 21 individual colonies were selected for susceptibility testing and target gene sequencing.

Table 2. Overview of Cyp51A and Hmg1 genotypes of azole-resistant *Aspergillus fumigatus* isolates, sorted by susceptibility classification, Denmark, 2020–2022

Susceptibility classification and *A. fumigatus* protein alterations	No. genotypes
38 azole-susceptible comparator isolates: 20 Cyp51A wild types	37
6 F46Y/M172V/E427K	
1 M172V	
1 I242V	
10 susceptible isolates, no Cyp51A profile, mixed genotypes	
18 azole-nonsusceptible isolates (9.3% of all nonsusceptible isolates);* 18 Cyp51A wild-types	18
11 Hmg1: Wild type	
1 Hmg1: F262-DEL	
1 Hmg1: W272L (and E105K)	
1 Hmg1: E306K	
3 Hmg1: E105K (outside the sterol-sensing domain)	
1 Hmg1: S541G (outside the sterol-sensing domain)	
22 TR_{46} isolates (11.3%)	13
9 TR_{46}/Y121F/T289A	7
10 TR_{46}/Y121F/T289A/S363P/I364V/G448S†	5
3 TR_{46}^{3}/Y121F/M172I/T289A/G448S‡	1
154 TR_{34} isolates (79.4%)	72
137 TR_{34}/L98H	64
14 have a unique variant in the promotor (T-67G)§	3
3 TR_{34}/L98H/S297T/F495I¶	1

*Isolates that were resistant for ≥1 triazoles on ≥1 MIC determination.
†From flower bed in a private garden in 2021, flower pot soil in 2021, green waste and garden waste compost heaps in 2022, and from field soil in 2022.
‡From flower bed in another private garden in 2021.
§From flower bed in a public park 2021, horse manure heap in 2022.
¶From flower pot soil in 2021.

TR_{34}/L98H, and 1 harbored an Hmg1 alteration E306K in the sterol-sensing domain.

Compost

All compost soil samples contained *A. fumigatus* isolates (mean 43.8 isolates/sample), and 4/5 samples contained AR*Af* isolates harboring TR_{34}/L98H (2.7% of isolates). Investigation of garden waste heap samples was complicated by high contents of Mucorales interfering with *A. fumigatus* isolation. Consequently, it was only possible to isolate 12 individual *A. fumigatus* isolates, 11 of which harbored TR_{34}/L98H (n = 7), TR_{46}/Y121F/T289A or TR_{46}/Y121F/T289A/S363P/I364V/G448S (n = 3), or F46Y/M172V/E427K (n = 1) *Cyp51A* alterations. The samples from a vegetable composting heap all grew *A. fumigatus* fungi, AR*Af*, and TR_{34}/L98H; and 3/5 samples also grew TR_{46}/Y121F/T289A or TR_{46}/Y121F/T289A/S363P/I364V/G448S. Moreover, many samples grew >200 colonies/plate. Isolation from voriconazole/posaconazole susceptibility plate wells yielded 21 single AR*Af* isolates, of which 81% harbored TR_{34}/L98H- and 19% TR_{46}/Y121F/T289A-related mechanisms. However, the true number of resistant isolates was probably higher because genotyping suggested mixed genotypes in isolates with a single resistance mechanism.

Manure Heaps and Stable Bedding

Of 12 manure heap samples, 8 contained *A. fumigatus* isolates; the highest isolate numbers were in the 4–5-month-old manure heap at the center 1 (7.7 isolates/sample vs. 3.8 isolates/sample at center 2 with frequent emptying). AR*Af* isolates were found at center 1 (3/5 samples and 25.9% of isolates, all harboring TR_{34}/L98H or TR_{34}/T-67G/L98H) but not at center 2. Sampling of used stable bedding and the same unused material documented AR*Af* (TR_{34}/L98H and TR_{46}/Y121F/T289A) in stable bedding but not in unused straw or peat (Table 1).

Azole Fungicide

Concentrations in environmental samples were determined for 8 azole fungicides (Appendix Table 8). Levels were generally low and without correlation to AR*Af* detection. Hypothesizing, that a selective fungicide concentration should be at least one tenth of the mean MIC against wild-type *A. fumigatus* fungi, we found such concentrations for prothioconazole-desthio in 18 field soil samples (range 9.8–42.9 µg/kg), 1 of which was AR*Af* positive; for metconazole (38.4–135 µg /kg) in 4 potted plant samples, 3 of which contained AR*Af*; and for difenoconazole (367–717 µg /kg) in 4 field samples, none of which contained AR*Af*. In contrast, AR*Af* was found in 4 potato samples, 1 cactus pot soil, 8 flower bed samples, 5 compost, and 2 wood paint–associated samples with no or very low azole fungicide concentrations (*25*).

Molecular Characterization of *A. fumigatus* Isolates

Molecular analyses of the 194 resistant and 38 comparator study isolates demonstrated 139 microsatellite genotypes (Table 2). A total of 103 genotypes were

found among the resistant isolates and 37 genotypes among susceptible isolates. One genotype was shared among a susceptible and a nonsusceptible isolate (both wild-type *cyp51A*).

The TR_{34}/L98H study isolates included 1 main cluster-1 of 34 TR_{34}/L98H identical or closely related isolates from 14 different sampling sites (Figure 1). Other isolate clusters primarily reflect multiple isolates cultured from the same sites. Among the 22 TR_{46}-AR*Af* study isolates, 13 unique genotypes were found. One final comparison introduced 1,468 worldwide genotypes from 16 countries (Figure 2). The genotypes from Denmark were widely distributed, corresponding to the worldwide diversity of genotypes. Most AR*Af* isolates were gathered in the top, except for all cluster-1 AR*Af* isolates, which were placed to the right.

Microcosmos Experiments for AR*Af* Selection

Wild-type *A. fumigatus*, TR_{34}/L98H, and TR_{46}/Y121F/T289A failed to grow at 10°C but grew equally well to a maximum of 10^6–10^7 CFU/g in heat-sterilized organic rich and sandy soil at 15°C and 20°C (Appendix Figures 1, 2). Sustained complete inhibition was found for wild-type *A. fumigatus* fungi but not AR*Af* at the highest tebuconazole concentration (≈49 mg/kg wet weight) (Figure 3). Prothioconazole conferred initial growth inhibition for all strains, but growth appeared on day 5 or 8 after application and reached the levels of the untreated controls for the TR_{34}/L98H and TR_{46}/Y121F/T289A strains but not for the wild type (Appendix Figure 3). In contrast, treatment with mefentrifluconazole inhibited growth during the entire microcosmos experiment except for a single replicate with TR_{34}/L98H day 27 (Appendix Figure 3).

Field Experiment for AR*Af* Selection

Of the prespraying and postspraying samples obtained from untreated and azole-treated field sites (Table 3), all samples contained *A. fumigatus* isolates (n = 360, mean 9 isolates/sample), but for all fields, numbers declined 2-fold over time. Ten (2.8%) AR*Af* isolates were found, 4 in unsprayed soil (4/167 = 2.4%) and 6 in treated soil (6/193 = 3.1%, p = 0.757). Seven harbored TR_{34}/L98H, 4 found in untreated soil and 3 found after the first prothioconazole spraying in Flakkebjerg. One harbored TR_{46}/Y121F/T289A and was found after the third tebuconazole spraying. Two isolates harbored Hmg1 alterations, of which the W272L alteration is situated within the sterol-sensing domain. Those 2 isolates were found after treatment with mefentrifluconazole and prothioconazole. Overall, the resistance percentage increased numerically (p>0.05) from 2.5% before spraying to 6.3% in the first postspraying samples and then declined by 2.5%, 1.9%, and 0 in the remaining postspraying samples. The percentages of AR*Af* harboring tandem repeat mechanisms followed the same pattern.

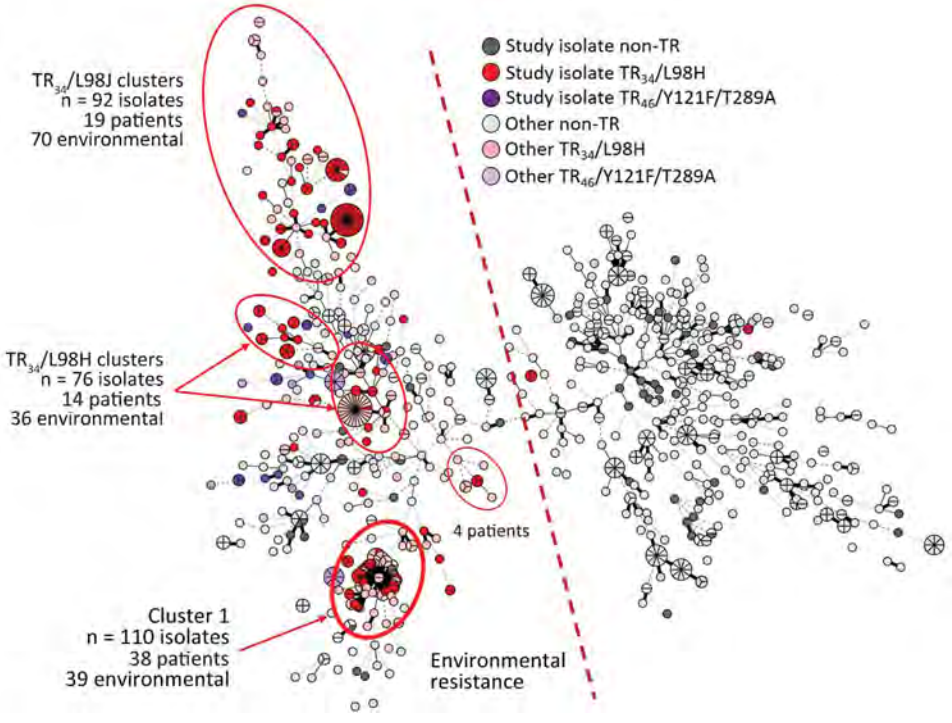

Figure 1. Minimum spanning tree of 232 *Aspergillus fumigatus* genotyped study isolates including 741 Denmark background isolates (627 isolates from 326 patients and 114 isolates from the environment) for study of environmental hot spots and resistance-related application practices for azole-resistant *A. fumigatus*, Denmark, 2020–2022. Colors emphasize isolates with environmental azole resistance mechanisms, TR_{34}/L98H (red) or TR_{46}/Y121F/T289A (purple). With a few exceptions, all TR_{34}/L98H and TR_{46}/Y121F/T289A reside on the left side of the tree. Moreover, several TR_{34}/L98H clusters include patient and environmental isolates, of which cluster 1 displays almost identical genotypes.

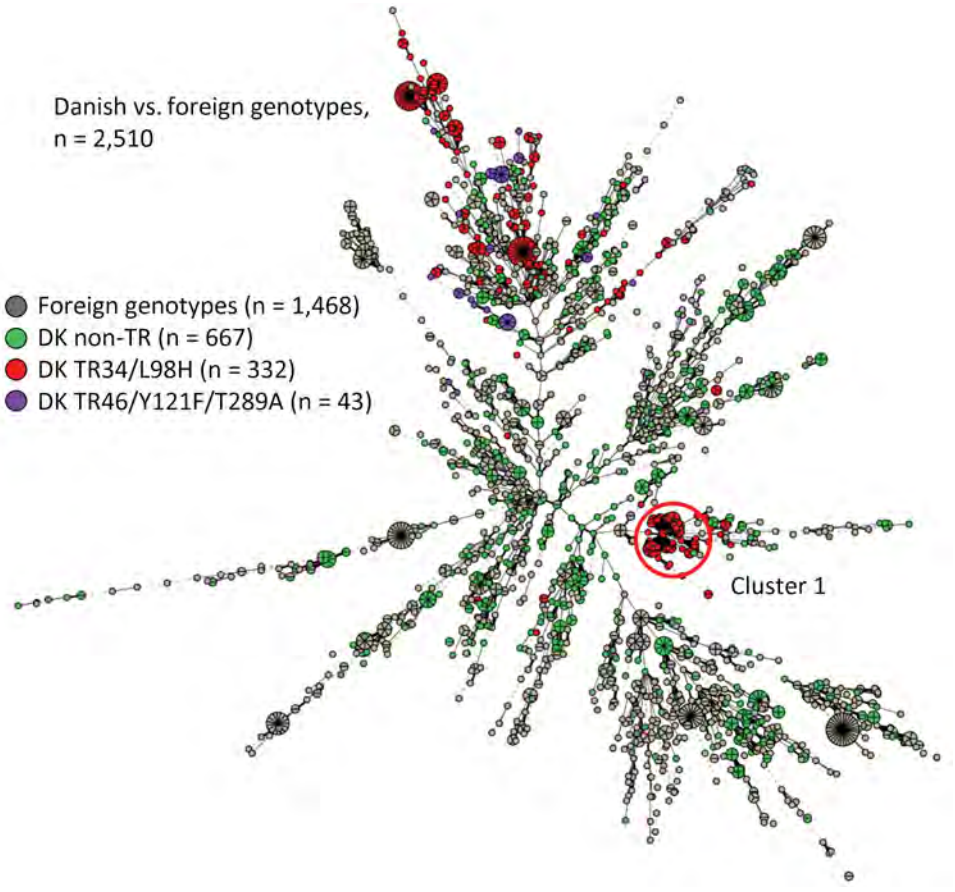

Figure 2. Minimum spanning tree of 1,042 *Aspergillus fumigatus* genotypes from Denmark (green, red, and purple) compared with 1,468 genotypes from other countries (gray) as part of study of environmental hot spots and resistance-related application practices for azole-resistant *A. fumigatus*, Denmark, 2020–2022. The isolates from other countries were mostly azole-resistant *A. fumigatus* and dominated by TR_{34}/L98H (F. Hagen, Westerdijk Fungal Biodiversity Institute, pers. comm., 2024 Apr 28). Numbers of isolates from other countries: the Netherlands, n = 615; Norway, n = 209; Belgium, n = 108; Germany, n = 100; Spain, n = 219; United States, n = 102; other, n = 115).

Discussion

Our study demonstrated that AR*Af* is extensively distributed in the environment in Denmark. AR*Af* was found in 20% of 366 samples, and 4.2% of 4,538 investigated isolates were azole resistant, dominated by TR_{34}/L98H-related and, to a lesser extent, TR_{46}/Y121F/T289A-related mechanisms. Although the study was not designed to capture longitudinal changes, 3 observations suggest that AR*Af* is increasing in Denmark. First, although AR*Af* percentages were relatively low (0.3%–2.8%) among *A. fumigatus* isolates in agricultural soil samples from Denmark, they were higher than in studies conducted in 2010 and 2013, where no AR*Af* was found among 113 *A. fumigatus* isolates from flower beds, potted plants, and conventional and organic fields (*7*). Second, the AR*Af* proportion was higher in field air in 2021 than in 2020 ($p = 0.0202$) and higher in field soil in 2022 than in 2020 ($p = 0.0127$). Third, TR_{46}/Y121F/T289A was found in multiple settings during 2021–2022 but not in 2020, despite a comparable number of samples. Those findings coincide with the first of several isolations of TR_{46}/Y121F/T289A from patients in Denmark in 2021 (M.C. Arendrup, unpub. data) since the initial finding of this genotype in a single patient in 2014 (*7*). Genotyping identified a nationwide cluster of TR_{34}/L98H with wide geographic distribution across Denmark, including clinical and environmental isolates. That particular clone has remained dominant among azole-resistant clinical isolates from Denmark since 2018. Whether that trait of augmented mutation rate is a virulence factor and responsible for the relatively high prevalence among Denmark AR*Af* warrants further investigation, but it aligns with the observed increasing incidence. It is also of interest that that cluster is located quite distant from most other tandem repeat isolates, possibly indicating that that clone has appeared through sexual recombination of unrelated strains.

The AR*Af* isolates were more closely related than the *A. fumigatus*–susceptible isolates. That finding suggests more recent ancestors and that the increasing environmental resistance rates are driven mainly by factors favoring propagation of TR_{34}/L98H and TR_{46}/Y121F/T289A genotypes already present over the susceptible population rather than induction of resistance in susceptible isolates from outside.

Besides characterizing the prevalence of AR*Af* and relevant hot spots in Denmark, it was our intention to investigate potential links between the presence of azoles in the samples and AR*Af*. Azoles were found at low concentrations in most soil samples, indicating persistence of azoles in the soils and a measurable carryover concentration from season to season (data not shown). We saw no association between AR*Af* findings and azole concentration in any specific sample or across sample types, nor did we verify increasing resistance after azole spraying in wheat field trials, potentially because *A. fumigatus* growth was absent. In contrast, our microcosmos experiments suggested that azole fungicides may favor AR*Af* growth over wild-type *A. fumigatus* in soil. Few studies have been able to confirm a link between specific azole use and resistance in *A. fumigatus* (*3*). A study in China indicated a link between use of azoles in paddy rice and resistance development, whereas a recent study in Switzerland found that azole resistance was

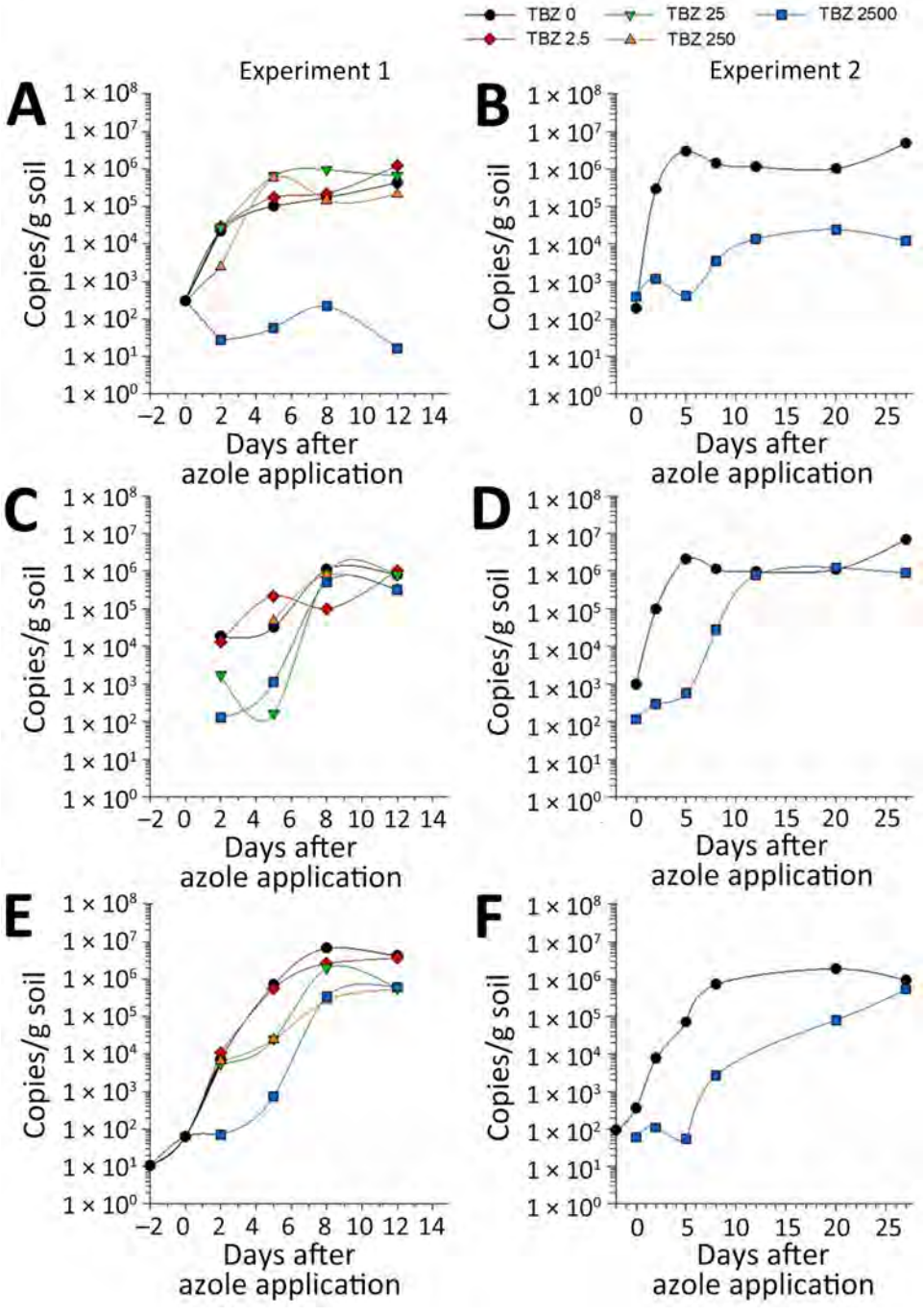

Figure 3. Selective pressure of TBZ on *Aspergillus fumigatus* wild type (A, B), TR_{34}/L98H (TR34) (C, D), and TR_{46}/Y121F/T289A (TR46) (E, F) in sandy soil (n = 1) in 2 independent microcosmos experiments as part of a study of environmental hot spots and resistance-related application practices for azole-resistant *A. fumigatus*, Denmark, 2020–2022. In experiment 1, in which 4 different concentrations of tebuconazole were used to spike the microcosmos: 2.5 mg/L (red line), 25 mg/L (green line), 250 mg/L (orange line), and 2,500 mg/L (blue line), and growth was followed over 14 days. Growth was quantified by measuring copies of the *cyp51A* promoter region by quantitative PCR. Growth was quantified from day −2 after azole application (the day of inoculation) for the untreated samples and from day 2 after azole application for the samples treated with TBZ. In experiment 2, the effect of the 2,500 mg/L treatment was repeated, and growth was followed over 27 days. Growth was quantified from the day of inoculation (2 days before TBZ application) by measuring copies of the *cyp51A* promoter region by droplet digital PCR. The experiment with TR_{46}/Y121F/T289A was in a different microcosmos trial than for wild type and TR_{34}/L98H but followed the same protocol. TBZ, tebuconazole.

Table 3. Azole-resistant *A. fumigatus* isolates found among *A. fumigatus* isolates obtained at each sampling date in 2 winter wheat fields testing different azole-fungicides applied 2 times for control of leaf diseases, Denmark, 2020–2022*

Sample sites and treatments and doses	Sampling related to spraying				
	Before first spray	Before second spray	Week 3 after second spray	Week 6 after second spray	Week 10 after second spray
Flakkebjerg					
Untreated control field	0/8	0/10	0/10†	0/3†	0/2†
Prothioconazole 2 × 0.4 L/ha	0/29	**3**/12	0/16†	0/5†	0/6†
Tebuconazole 2 × 0.5 L/ha	**1**/16	0/11	0/13†	**1**/9†	0/9†
Mefentrifluconazole 2 × 0.75/ha	**1**/11	**1**/13	0/14†	0/5†	0/4†
Fredericia					
Untreated control field	0/12	0/6	**1**/6	0/9	0/3
Prothioconazole 2 × 0.4 L/ha	0/15	0/2	**1**/7	0/4	0/6
Tebuconazole 2 × 0.5 L/ha	**1**/13	0/7	0/3	0/9	0/12
Mefentrifluconazole 2× 0.75 L/ha	0/14	0/2	0/11	0/8	0/5
AR*Af* isolates/*A. fumigatus* (per date)	3/118	4/63	2/80	1/52	0/47
Isolates w. TR_{34} or TR_{46}, no. (%)	3 TR_{34} (2.5)	3 TR_{34} (4.8)	1 TR_{34}(1.3)	1 TR_{46} (1.9)	0
Isolates w. Hmg1 alterations		1 Hmg1 E105K (1.6)	1 Hmg1 E105K/ W272L (1.3)		

*Green indicates findings from untreated sites (before spraying or control sites); gray indicates findings from sprayed sites. Sampling dates in 2020 were May 15, May 30, Jun 20, Jul 11, and Aug 12 for Flakkebjerg and May 12, May 30, Jun 17, Jul 12, and Aug 8 for Fredericia. Boldface indicates resistant isolates. *Af*, *Aspergillus fumigatus*; AR*Af*, azole-resistant *A. fumigatus*.
†Sites that received an additional tebuconazole third spray on June 19, 2022, to stop a rust disease outbreak.

neither associated with any specific agricultural practice nor with the presence of azole fungicides (*26*,*27*). The concentration of azoles in an environmental sample is a snapshot, which fails to provide information about previous exposures, potentially relevant for resistance selection. Other factors may influence selection and presence of AR*Af* at the time of sampling (e.g., soil type, temperature, humidity, competition from the indigenous microbial community, azole application concentration and subsequent kinetics of free and soil bound fractions, liquid manure application, and amount of organic matter). Those factors complicate identification of safe and unsafe procedures, particularly as the annual increase in AR*Af* appears to be well below 1% in Denmark, suggesting a slow and potentially fluctuating increase that is difficult to capture in light of the heterogeneity of environmental samples.

We confirmed that the hot spots for AR*Af* are compost, flower beds, and flower production; but we also found AR*Af* in stables and horse manure heaps (*1*,*3*,*28*). Azoles are not used in parks, gardens, or stables. However, planting azole-treated bulbs and using compost soil based on azole-containing plant material can turn flower beds and garden waste heaps into hot spots (*29*). Of note, the tulip cultivars found in the private gardens were old cultivars and the azole contents were very low, suggesting that the AR*Af* found could reflect the general background AR*Af* population combined with good growth conditions for *A. fumigatus* rather than a direct link to azole-treated bulb planting. In addition, our study findings suggest that it is plausible that use of azole-containing conventional straw for stable bedding similarly can turn stable bedding and manure heaps into hot spots and thus reflect collateral damage associated with azole use elsewhere.

One limitation of our study is that the sensitivity for AR*Af* detection in a given sample and sample type will vary because of the variable number of *A. fumigatus* in the environmental samples. Consequently, we cannot exclude that AR*Af* may be found in negative samples, in which *A. fumigatus* numbers were low. Yet it is plausible that such settings, because of the overall lower *A. fumigatus* prevalence, may contribute less to resistance selection and human exposure. Another limitation is that we did not have funding for whole-genome sequencing. However, microsatellite typing has been widely used and has a high discriminative power, enabling us to compare with already published data.

In conclusion, our study and the available literature strongly suggest that the dual use of azoles in clinical medicine and for crop and material protection has introduced azole resistance in *A. fumigatus*, which challenges patient management. Isolates harboring environmental resistance mechanisms were found in every setting explored and expand the numbers, genotypes, and target gene variants found in earlier studies. Because of a lack of fitness cost (*30*), the AR*Af* variants will remain even if use of azoles active against *A. fumigatus* is terminated. It seems advisable to avoid future dual use of agents used in human medicine, such as drug candidates olorofim and fosmanogepix, which are threatened by new compounds developed for plant protection (*31*). Prioritizing the use of *A. fumigatus* active azole fungicides might potentially slow the rise in rates of resistance.

The study was funded by the Danish Ministry of Environment's Research Program for Pesticides (Journal number 2019-15114).

The authors declare no conflicts of interest related to this study. Outside this study, the authors declare that M.C.A. has over the past 5 years received research grants/contract work (paid to the SSI) from Cidara, F2G, Gilead, and Scynexis and speaker honoraria (personal fee) from Astellas, Chiesi, Gilead, and F2G. She is the current chairman of the EUCAST-AFST. L.N.J has over the past 5 years received research grants/contract work (paid to the AU) from BASF, BAYER CropScience, Syngenta Nordic, Corteva Agriscience, ADAMA, and UPL Limited. and speaker honoraria (personal fee) from BASF, Syngenta, and Corteva. R.K.H. has over the past 5 years received a travel grant and an unrestricted research grant from Gilead.

About the Author

Dr. Arendrup is a professor at Copenhagen University and the head of the national reference laboratory for mycology and the EUCAST development laboratory at the Statens Serum Institute in Copenhagen, Denmark. Her main research interests are the epidemiology, susceptibility, breakpoint development, diagnostics, and treatment of fungal infections.

References

1. Schoustra SE, Debets AJM, Rijs AJMM, Zhang J, Snelders E, Leendertse PC, et al. Environmental hotspots for azole resistance selection of *Aspergillus fumigatus*, the Netherlands. Emerg Infect Dis. 2019;25:1347–53. https://doi.org/10.3201/eid2507.181625
2. Risum M, Hare RK, Arendrup MC. DANMAP 2019: azole resistance in *Aspergillus fumigatus* – nationwide surveillance data from the first 18 months [cited 2024 Mar 15]. https://www.danmap.org/reports/2019
3. Doughty KJ, Sierotzki H, Semar M, Goertz A. Selection and amplification of fungicide resistance in *Aspergillus fumigatus* in relation to DMI fungicide use in agronomic settings: hotspots versus coldspots. Microorganisms. 2021;9:2439. https://doi.org/10.3390/microorganisms9122439
4. Le Pape P, Lavergne R-A, Morio F, Alvarez-Moreno C. Multiple fungicide-driven alterations in azole-resistant *Aspergillus fumigatus*, Colombia, 2015. Emerg Infect Dis. 2016;22:156–7. https://doi.org/10.3201/eid2201.150978
5. Chen Y, Dong F, Zhao J, Fan H, Qin C, Li R, et al. High azole resistance in *Aspergillus fumigatus*, China, 2018. Emerg Infect Dis. 2020;26:81–9. https://doi.org/10.3201/eid2601.190885
6. Mortensen KL, Mellado E, Lass-Flörl C, Rodriguez-Tudela JL, Johansen HK, Arendrup MC. Environmental study of azole-resistant *Aspergillus fumigatus* and other aspergilli in Austria, Denmark, and Spain. Antimicrob Agents Chemother. 2010;54:4545–9. https://doi.org/10.1128/AAC.00692-10
7. Astvad KMT, Jensen RH, Hassan TM, Mathiasen EG, Thomsen GM, Pedersen UG, et al. First detection of TR46/Y121F/T289A and TR34/L98H alterations in *Aspergillus fumigatus* isolates from azole-naive patients in Denmark despite negative findings in the environment. Antimicrob Agents Chemother. 2014;58:5096–101. https://doi.org/10.1128/AAC.02855-14
8. Mortensen KL, Jensen RH, Johansen HK, Skov M, Pressler T, Howard SJ, et al. *Aspergillus* species and other molds in respiratory samples from patients with cystic fibrosis: a laboratory-based study with focus on *Aspergillus fumigatus* azole resistance. J Clin Microbiol. 2011;49:2243–51. https://doi.org/10.1128/JCM.00213-11
9. Jensen RH, Hagen F, Astvad KMT, Tyron A, Meis JF, Arendrup MC. Azole-resistant *Aspergillus fumigatus* in Denmark: a laboratory-based study on resistance mechanisms and genotypes. Clin Microbiol Infect. 2016;22:570.e1–9. https://doi.org/10.1016/j.cmi.2016.04.001
10. Risum M, Hare RK, Gertsen JB, Kristensen L, Johansen HK, Helweg-Larsen J, et al. Azole-resistant *Aspergillus fumigatus* among Danish cystic fibrosis patients: increasing prevalence and dominance of TR_{34}/L98H. Front Microbiol. 2020;11:1850. https://doi.org/10.3389/fmicb.2020.01850
11. Risum M, Hare RK, Gertsen JB, Kristensen L, Rosenvinge FS, Sulim S, et al. Azole resistance in *Aspergillus fumigatus*. The first 2-year's data from the Danish National Surveillance Study, 2018-2020. Mycoses. 2022;65:419–28. https://doi.org/10.1111/myc.13426
12. Zhang J, Snelders E, Zwaan BJ, Schoustra SE, Meis JF, van Dijk K, et al. A novel environmental azole resistance mutation in *Aspergillus fumigatus* and a possible role of sexual reproduction in its emergence [cited 2024 Jun 5]. https://mbio.asm.org/content/8/3/e00791-17
13. Anonymous. Azole resistance selection in *Aspergillus fumigatus* – final report 2015–2017 [cited 2024 Jun 5]. https://www.clm.nl/uploads/pagina-pdfs/Azole-resistance_selection_in_Aspergillus_fumigatus_Final_Report.pdf
14. Fraaije B, Atkins S, Hanley S, Macdonald A, Lucas J. The multi-fungicide resistance status of *Aspergillus fumigatus* European environment. Front Microbiol. 2020;11:599233. https://doi.org/10.3389/fmicb.2020.599233
15. Barber AE, Riedel J, Sae-Ong T, Kang K, Brabetz W, Panagiotou G, et al. Effects of agricultural fungicide use on *Aspergillus fumigatus* abundance, antifungal susceptibility, and population structure. MBio. 2020;11:e02213–20.
16. Alvarez-Moreno C, Lavergne RA, Hagen F, Morio F, Meis JF, Le Pape P. Fungicide-driven alterations in azole-resistant *Aspergillus fumigatus* are related to vegetable crops in Colombia, South America. Mycologia. 2019;111:217–24. https://doi.org/10.1080/00275514.2018.1557796
17. Imbert S, Normand AC, Gabriel F, Cassaing S, Bonnal C, Costa D, et al. Multi-centric evaluation of the online MSI platform for the identification of cryptic and rare species of *Aspergillus* by MALDI-TOF. Med Mycol. 2019;57:962–8. https://doi.org/10.1093/mmy/myz004
18. Normand AC, Becker P, Gabriel F, Cassagne C, Accoceberry I, Gari-Toussaint M, et al. Validation of a new web application for identification of fungi by use of matrix-assisted laser desorption ionization–time of flight mass spectrometry. J Clin Microbiol. 2017;55:2661–70.
19. Arendrup MC, Meletiadis J, Mouton JW, Guinea J, Cuenca-Estrella M, Lagrou K, et al.; Subcommittee on Antifungal Susceptibility Testing (AFST) of the ESCMID European Committee for Antimicrobial Susceptibility Testing (EUCAST). EUCAST technical note on isavuconazole breakpoints for *Aspergillus*, itraconazole breakpoints for *Candida* and updates for the antifungal susceptibility testing method documents. Clin Microbiol Infect. 2016;22:571.e1–4. https://doi.org/10.1016/j.cmi.2016.01.017

20. Guinea J, Verweij PE, Meletiadis J, Mouton JW, Barchiesi F, Arendrup MC, et al.; Subcommittee on Antifungal Susceptibility Testing (AFST) of the ESCMID European Committee for Antimicrobial Susceptibility Testing (EUCAST). How to: EUCAST recommendations on the screening procedure E.Def 10.1 for the detection of azole resistance in *Aspergillus fumigatus* isolates using four-well azole-containing agar plates. Clin Microbiol Infect. 2019;25:681–7. https://doi.org/10.1016/j.cmi.2018.09.008
21. Albers CN, Johnsen AR, Bollmann UE. Urban areas as sources of the groundwater contaminants N,N-dimethylsulfamide (N,N-DMS) and 1,2,4-triazole. Sci Total Environ. 2023;881:163377.
22. Mellado E, Diaz-Guerra TM, Cuenca-Estrella M, Rodriguez-Tudela JL. Identification of two different 14-alpha sterol demethylase-related genes (cyp51A and cyp51B) in *Aspergillus fumigatus* and other *Aspergillus* species. J Clin Microbiol. 2001;39:2431–8. https://doi.org/10.1128/JCM.39.7.2431-2438.2001
23. Rybak JM, Ge W, Wiederhold NP, Parker JE, Kelly SL, Rogers PD, et al. Mutations in hmg1, challenging the paradigm of clinical triazole resistance in *Aspergillus fumigatus*. MBio. 2019;10:e00437–19. 10.1128/mBio.00437-19
24. de Valk HA, Meis JFGM, Curfs IM, Muehlethaler K, Mouton JW, Klaassen CHW. Use of a novel panel of nine short tandem repeats for exact and high-resolution fingerprinting of *Aspergillus fumigatus* isolates. J Clin Microbiol. 2005;43:4112–20. https://doi.org/10.1128/JCM.43.8.4112-4120.2005
25. Jørgensen KM, Helleberg M, Hare RK, Jørgensen LN, Arendrup MC. Dissection of the activity of agricultural fungicides against clinical *Aspergillus* isolates with and without environmentally and medically induced azole resistance. J Fungi (Basel). 2021;7:205. https://doi.org/10.3390/jof7030205
26. Cao D, Wang F, Yu S, Dong S, Wu R, Cui N, et al. Prevalence of azole-resistant *Aspergillus fumigatus* is highly associated with azole fungicide residues in the fields. Environ Sci Technol. 2021;55:3041–9. https://doi.org/10.1021/acs.est.0c03958
27. Schürch S, Gindro K, Schnee S, Dubuis P-H, Codina JM, Wilhelm M, et al. Occurrence of *Aspergillus fumigatus* azole resistance in soils from Switzerland. Med Mycol. 2023;61:1–10. https://doi.org/10.1093/mmy/myad110
28. Rocchi S, Godeau C, Scherer E, Reboux G, Millon L. One year later: the effect of changing azole-treated bulbs for organic tulips bulbs in hospital environment on the azole-resistant *Aspergillus fumigatus* rate. Med Mycol. 2021;59:741–3. https://doi.org/10.1093/mmy/myab007
29. Khan MS, Douglas P, Hansell AL, Simmonds NJ, Piel FB. Assessing the health risk of living near composting facilities on lung health, fungal and bacterial disease in cystic fibrosis: a UK CF Registry study. Environ Health. 2022;21:130. https://doi.org/10.1186/s12940-022-00932-1
30. Verweij PE, Chowdhary A, Melchers WJG, Meis JF. Azole resistance in *Aspergillus fumi*gatus: can we retain the clinical use of mold-active antifungal azoles? Clin Infect Dis. 2016;62:362–8.
31. Verweij PE, Arendrup MC, Alastruey-Izquierdo A, Gold JAW, Lockhart SR, Chiller T, et al. Dual use of antifungals in medicine and agriculture: how do we help prevent resistance developing in human pathogens? Drug Resist Updat. 2022;65:100885. https://doi.org/10.1016/j.drup.2022.100885

Address for correspondence: Maiken Cavling Arendrup, Unit for Mycology Building 43/317, Statens Serum Institut, Artillerivej 5, DK-2300 Copenhagen S, Denmark; email: maca@ssi.dk

Retrospective Study of Infections with *Corynebacterium diphtheriae* Species Complex, French Guiana, 2016–2021

Mélanie Gaillet, Mélanie Hennart, Vincent Sainte Rose, Edgar Badell, Céline Michaud, Romain Blaizot, Magalie Demar, Luisiane Carvalho, Jean François Carod, Audrey Andrieu, Félix Djossou, Julie Toubiana, Loic Epelboin, Sylvain Brisse

Medscape CME Activity

In support of improving patient care, this activity has been planned and implemented by Medscape, LLC and Emerging Infectious Diseases. Medscape, LLC is jointly accredited with commendation by the Accreditation Council for Continuing Medical Education (ACCME), the Accreditation Council for Pharmacy Education (ACPE), and the American Nurses Credentialing Center (ANCC), to provide continuing education for the healthcare team.

Medscape, LLC designates this Journal-based CME activity for a maximum of 1.00 ***AMA PRA Category 1 Credit(s)™***. Physicians should claim only the credit commensurate with the extent of their participation in the activity.

Successful completion of this CME activity, which includes participation in the evaluation component, enables the participant to earn up to 1.0 MOC points in the American Board of Internal Medicine's (ABIM) Maintenance of Certification (MOC) program. Participants will earn MOC points equivalent to the amount of CME credits claimed for the activity. It is the CME activity provider's responsibility to submit participant completion information to ACCME for the purpose of granting ABIM MOC credit.

All other clinicians completing this activity will be issued a certificate of participation. To participate in this journal CME activity: (1) review the learning objectives and author disclosures; (2) study the education content; (3) take the post-test with a 75% minimum passing score and complete the evaluation at https://www.medscape.org/qna/processor/72159?showStandAlone=true&src=prt_jcme_eid_mscpedu; and (4) view/print certificate. For CME questions, see page 1745.

NOTE: It is Medscape's policy to avoid the use of Brand names in accredited activities. However, in an effort to be as clear as possible, trade names are used in this activity to distinguish between the mixtures and different tests. It is not meant to promote any particular product.

Release date: July 16, 2024; Expiration date: July 16, 2025

Learning Objectives

Upon completion of this activity, participants will be able to:

- Analyze the epidemiology of corynebacteria infections
- Assess the clinical presentation of corynebacteria infections
- Distinguish the most common anatomic site for cutaneous *Corynebacterium diphtheriae* infections in the current study
- Evaluate the management of outcomes of corynebacteria infections

CME Editor

Jill Russell, BA, Technical Writer/Editor, Emerging Infectious Diseases. *Disclosure: Jill Russell, BA, has no relevant financial relationships.*

CME Author

Charles P. Vega, MD, Health Sciences Clinical Professor of Family Medicine, University of California, Irvine School of Medicine, Irvine, California. *Disclosure: Charles P. Vega, MD, has the following relevant financial relationships: served as an advisor or consultant for Boehringer Ingelheim; GlaxoSmithKline.*

Authors

Mélanie Gaillet, MPH, MD; Mélanie Hennart, PhD; Vincent Sainte Rose, PharmD; Edgar Badell, PhD; Céline Michaud, MD; Romain Blaizot, MD, PhD, MPH; Magalie Demar, MD, PhD, MPH; Luisiane Carvalho, MPH; Jean François Carod, PharmD; Audrey Andrieux, MPH; Félix Djossou, MD, PhD, MPH; Julie Toubiana, MD, PhD, MPH; Loic Epelboin, MD, PhD, MPH; Sylvain Brisse, PhD.

Human infections with *Corynebacterium diphtheriae* species complex (CdSC) bacteria were rare in French Guiana until 2016, when the number of cases diagnosed increased. We conducted an epidemiologic, multicenter, retrospective study of all human CdSC infections diagnosed in French Guiana during January 1, 2016–December 31, 2021. A total of 64 infectious episodes were observed in 60 patients; 61 infections were caused by *C. diphtheriae* and 3 by *C. ulcerans*. Estimated incidence increased from 0.7 cases/100,000 population in 2016 to 7.7 cases/100,000 population in 2021. The mean patient age was 30.4 (±23.7) years, and male-to-female ratio was 1.7:1 (38/22). Of the 61 *C. diphtheriae* isolates, 5 tested positive for the diphtheria toxin gene, and all results were negative by Elek test; 95% (61/64) of cases were cutaneous, including the *C. ulcerans* cases. The increase in reported human infections underscores the need to raise awareness among frontline healthcare practitioners to improve prevention.

Corynebacterium diphtheriae species complex (CdSC; also called cornyebacteria of the *diphtheriae* species complex) include *Corynebacterium diphtheriae* and *C. ulcerans*, 2 potentially toxigenic and highly pathogenic species for humans (*1*). Human corynebacterial infections can be potentially fatal if left untreated (*2*). Risk for infection is higher among immunocompromised persons and socially disadvantaged persons. Socioeconomic challenges in particular are a major concern in French Guiana, a French overseas territory located in northeastern South America and covered by the Amazon Rain Forest (*3*).

The classical clinical manifestation of diphtheria is a pseudomembrane in the upper respiratory airways (tonsils, pharynx, or larynx) that can cause possible fatal airway obstruction. Cutaneous forms are less severe but have been reported more frequently than respiratory forms in recent studies (*4*); those forms play a key role in the transmission of *C. diphtheriae*. In addition, potentially serious systemic nontoxigenic infections have also been observed (*5*). The zoonotic species *C. ulcerans* can also occur as respiratory or cutaneous forms. The severity of the disease is mainly because of the production by toxigenic strains of the diphtheria toxin, which can cause systemic damages, particularly with cardiac and neurologic involvement (*2*).

In French Guiana, diphtheria infection might be suspected by physicians in the presence of a suggestive clinical picture. Diphtheria infection must be confirmed by a standard bacteriological examination. However, clinical diagnosis is not always easy, particularly in the case of the cutaneous form, because of its nonspecific manifestations (*6*) and the many differential diagnoses that exist, such as leishmaniasis or scabies (*7*). The diagnosis can therefore often be made by chance. In accordance with recommendations in France, all bacteriological diagnoses of CdSC must be supplemented by PCR testing for the diphtheria toxin gene, which is performed at the National Reference Centre (NRC) in Paris and, since 2019, at the Cayenne Hospital Center (CHC) for all of French Guiana. Depending on the clinical manifestations and the species and presence of the toxin, clinical management of diphtheria involves respiratory or wound isolation, antibiotic therapy, and vaccine update, as well as screening and management of contact cases (*8*). If the toxin is present, administering diphtheria antitoxin should be considered rapidly, depending on the symptoms (a supply is available at CHC) (*8*).

However, clinical management is complex in French Guiana because of the challenges in access to care and prevention for populations living in remote areas of the territory (*9*). Furthermore, availability of healthcare services remains inadequate, particularly in those remote areas (*10*). Although 80% of the population lives in the coastal zone, where healthcare services are concentrated (*10*,*11*), ≈60,000 persons live in isolation along the rivers and in areas of the Amazon Rain Forest in the interior of the territory (*3*).

Immunization is the most effective approach to prevent severe infections (*5*). According to available estimates, the diphtheria vaccination coverage rate for persons <18 years of age in French Guiana was 63.4% in 2014. Given the absence of a large-scale vaccination campaign in the territory during 2014–2021 and the delay in vaccination during the COVID-19 pandemic, that rate will likely remain low (*12*,*13*).

Cases of corynebacterial human infections were rare in French Guiana until 2016; only 2 cases, both

Author affiliations: Grenoble University Hospital, Grenoble, France (M. Gaillet); Laboratory TIMC-IMAG, Grenoble Alpes University, Grenoble (M. Gaillet); Cayenne Hospital Center, Cayenne, French Guiana (M. Gaillet, V. Sainte Rose, C. Michaud, R. Blaizot, M. Demar, F. Djossou, L. Epelboin); Institut Pasteur, Université Paris Cité, Paris, France (M. Hennart, E. Badell, J. Toubiana, S. Brisse); National Reference Center for Corynebacteria of the diphtheriae complex, Institut Pasteur, Paris (E. Badell, J. Toubiana, S. Brisse); French Guiana University, Cayenne (R. Blaizot, M. Demar, F. Djossou, L. Epelboin); Public Health France, Cayenne (L. Carvalho); Western Guianese Hospital Center, Saint-Laurent du Maroni, French Guiana (J.F. Carod); Regional Health Agency, Cayenne (A. Andrieu); Necker-enfants malades hospital, Paris (J. Toubiana); INSERM 1424, Cayenne (L. Epelboin)

DOI: https://doi.org/10.3201/eid3008.231671

from nontoxigenic *C. diphtheriae* strains, an unspecified bacteremia form and an endocarditis, were described in this territory (*14*,*15*). Since 2016, however, physicians and laboratories have reported an abnormally high number of these infections compared with previous years. To learn more about this emergence, our main objective was to describe sociodemographic, clinical, and microbiological characteristics of those cases. The secondary objectives were to estimate the annual incidence of cases, to study the resistance phenotypes of the bacterial isolates, and to study the genetic diversity of those isolates and potential links between cases.

Methods

Study Design and Settings

We conducted a retrospective and multicenter study in French Guiana, which covers an area of 83,846 km^2 and neighbors Brazil and Suriname. The private healthcare sector in French Guiana is limited; healthcare services are provided mainly by 3 hospital centers. CHC and Western Guianese Hospital Center (WGHC) are the 2 major healthcare centers (Figure 1). A total of 16 Delocalized Centers for Prevention and Care (DCPCs), which are a hospital department of CHC (i.e., sharing the same medical tools and software), oversee the primary care for persons in the Amazon areas of the territory. All samples collected in the DCPCs were sent to CHC, except samples from the DCPCs of Grand Santi, Apatou, Javouhey, and Awala Yalimapo, which were sent to WGHC by agreement.

Sociodemographic and Clinical Data Collection

We extracted all cases with a bacterial isolate belonging to the CdSC, laboratory diagnosed in CHC or WGHC during January 1, 2016–December 31, 2021, using HEXALIS results-reporting software (AGFA Healthcare). We arbitrarily considered positive samples for the same patient as 2 distinct episodes when they were collected >6 months apart and after clinical cure of the first episode or negative bacteriological control after ≥1 month of well-managed treatment.

We extracted patient sociodemographic and clinical data using the medical monitoring software (Cora Systems) for CHC and WGHC (including DCPC). We excluded patients without any clinical information found. Patients who objected to the use of their medical data in this study were secondarily excluded. We treated patient data that were not available in the medical records as unavailable data. For data describing patient progress, we considered patients who did not attend scheduled consultations as lost to follow-up (and not as unavailable data).

Bacterial Isolation, Identification, and Toxigenicity and Antimicrobial Susceptibility Testing

We identified and cultivated bacteria at CHC and WGHC on Columbia horse blood agar plate (bioMérieux) for 24 hours at 35°C–37°C. We performed bacterial identification by using Bruker matrix-assisted laser desorption/ionization time-of-flight mass spectrometry. We routinely sent all CdSC isolates to the NRC at the Institut Pasteur of Paris for further analysis.

At NRC, isolates were grown and purified on Tinsdale agar and characterized for pyrazinamidase, urease, nitrate reductase, use of maltose, and glycogen fermentation (*16*). We used a 4-plex real-time PCR to detect the diphtheria toxin gene and confirm species (*17*). We assessed the phenotypic production of the toxin using a modified Elek test (*18*). We performed antimicrobial susceptibility testing by disc diffusion (Bio-Rad Laboratories) and used E-test for MIC determination if deemed resistant on the basis of disk diffusion (Appendix, https://wwwnc.cdc.gov/EID/article/30/8/23-1671-App1.pdf).

Genome Sequencing and Phylogenetic Analyses

We performed genomic analyses at NRC using Illumina technology and de novo assembly as previously described (*16*,*19*). We conducted the search for resistance genes and *tox* gene integrity using diphtOscan (*20*). We defined multilocus sequence type (MLST) and core-genome MLST (cgMLST) genotypes using the Institut Pasteur CdSC database (https://bigsdb.pasteur.fr/diphtheria). For *C. diphtheriae* isolates, we defined the sublineages (500 mismatches) and genetic clusters (25 mismatch threshold) groupings as previously proposed (*19*) (Appendix).

Statistical Analysis

We performed statistical analyses using Microsoft Excel and RStudio version 02.3 software. We expressed qualitative variables as numbers and percentages and distribution of quantitative variables as means and SDs. We calculated estimates of annual incidence per 100,000 inhabitants on the basis of demographic data published annually by the French National Institute of Statistics and Economic Studies during 2016–2021 (*21*–*26*) (Appendix).

Ethics Approval

In conformity with French legislation, this retrospective study not involving human persons adheres to the Reference Methodology MR-004, with CHC's compliance commitment dated December 21, 2021. A privacy impact analysis was conducted; a study

summary is available on the Health-Data-Hub (no. F20220825152116). Its legal basis is a public interest mission. Data were sourced from routine care patient medical files and anonymized. Regulatory steps were taken to inform patients and allow refusal (Appendix). This approach was conducted in compliance with regulations in Europe (https://www.cnil.fr/fr/reglement-europeen-protection-donnees).

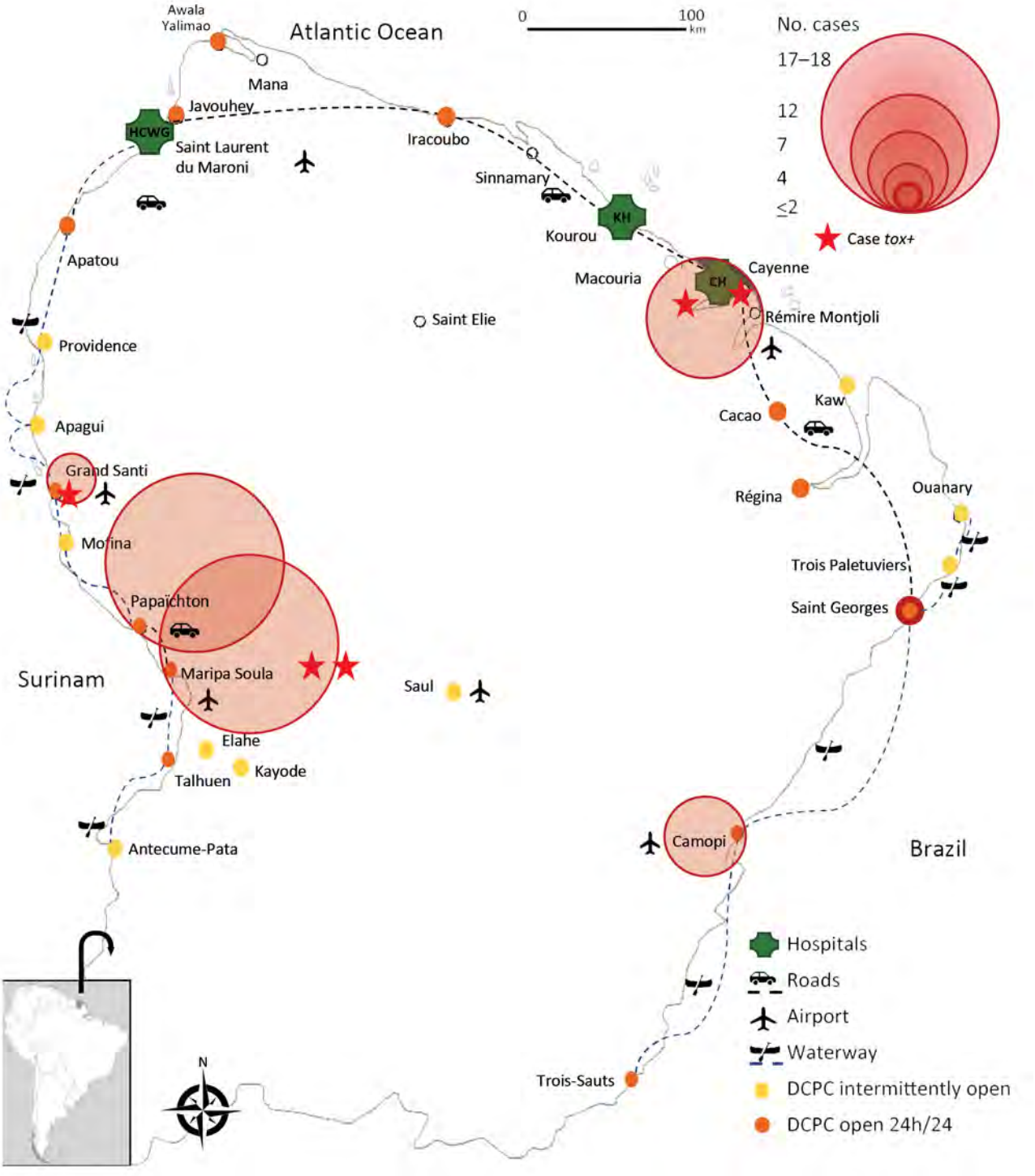

Figure 1. Geographic distribution of 64 cases of *Corynebacterium diphtheriae* species complex infections, French Guiana, 2016–2021. Inset map shows location of French Guiana in South America. DCPC, Delocalized Centers for Prevention and Care.

Results

Included Bacterial Isolates and Associated Clinical Cases

For the study period, we identified 64 cases of bacterial isolates of CdSC isolated from 60 patients. No patients objected to the use of their data for the study, and none were excluded (Figure 2). We found 61 cases of *C. diphtheriae*, corresponding to 58 cutaneous forms and 3 noncutaneous forms (1 superinfection of chronic nasal mucosal disease, 1 respiratory infection, and 1 endocarditis), and 3 cases of *C. ulcerans*, all of which were cutaneous forms. Of the 60 patients, 2 had 2 positive *C. diphtheriae* samples each, corresponding to unrelated cases of cutaneous infection, and 1 patient had 3 positive *C. ulcerans* samples, corresponding to 3 different cases.

A total of 5 *C. diphtheriae* cases were *tox*-positive by quantitative PCR (qPCR) (8%; 5/64). However, they did not produce the diphtheria toxin; they were all negative by Elek's test. Those 5 cases thus correspond to nontoxigenic *tox* gene–bearing isolates.

Evolution of Estimated Incidence during Study Period

The number of annual cases has risen steadily. Only 2 cases were diagnosed in 2016 and 2017, but in 2022, the number of annual cases reached 22. The estimated incidence has risen from 0.7 cases/100,000 inhabitants/year in 2016 to 7.7 cases/100,000 inhabitants/year in 2021 (Figure 3).

Epidemiology, Sociodemographics, and Medical History of Patients

In total, 80% (51/64) of the cases in our study were diagnosed in a DCPC by initial bacteriological sampling, whereas the others were mainly geographically dispersed (Figure 1). Mean patient age was 30.4 (±23.7) years (interquartile range 10.5–49.5) the male-to-female ratio was 1.7:1 (38/22). Of the 55 patients for whom information was available, 19 (35%) did not have social security coverage at the time of care, and 3 (5%) were homeless.

Of 58 patients with available data, 6 (10%) had a history of relative immunosuppression (diabetes, n = 3; alcoholic cirrhosis, n = 2; panhypopituitarism, n = 1). In addition, 10 (17%) were alcoholics, smokers, or polydrug addicts; 3 (5%) had a psychiatric pathology; and 8 (14%) had a chronic skin pathology that predisposed them to wounds or superinfections. Of 44 patients with available vaccination data, 29 (66%) were up-to-date with diphtheria vaccination at the time of infection (in accordance with French Public Health requirements for diphtheria) (*27*).

Clinical Description of Cases Caused by *C. diphtheriae*

Among the 61 cases caused by *C. diphtheriae*, 58 were cutaneous infections and 3 noncutaneous infections. Of the 58 cutaneous infections, the infection occurred on an existing wound in 23 (40%) persons: 6 occurred in a chronic skin lesion (lasting >6 weeks) and 17 occurred in an acute lesion (lasting <6 weeks). The infections mainly involved the lower limbs (62%, 36/58), followed by the head (12%, 7/58), the abdomen (7%, 4/58) and the upper limbs (2%, 1/58); 17% of cases extended to ≥2 areas of the body (10/58). In 57% (33/58) of cases, several lesions were present; in 25 cases, fibrinous involvement was described (56%, 25/45; data were not available for 13 cases). One patient, in whom 2 cases of cutaneous infection were present, had a background of immunosuppression; those 2 cases occurred on a chronic cutaneous lesion.

Data regarding clinical management were available for 52 cases. For 6 (12%) cases, treatment consisted only of simple dressing care. The 46 (88%) other cases were also treated by antibiotics; 40 were treated with amoxicillin (16 for 14 days, 16 for ≤10 days; data were not available for 8 cases), 2 were treated with azithromycin for 3 days, and 4 were treated with ciprofloxacin, pristinamycin, or ceftriaxone. One patient with multiple abscesses underwent surgery. The 5 patients with *tox*-positive isolates had cutaneous infection without toxic manifestations. No patients received diphtheria antitoxin while results of the qPCR were pending because they had no signs of severity attributable to toxin expression. For the 58 patients with *C. diphtheria* cutaneous infections, the outcome was favorable for 22 persons, 4 were lost to follow-up, and information was missing for 25. The clinical outcome was described as unfavorable for 7 patients (i.e., 1 patient died, 2 had a recurrence after 1 month, ulcerations were described as persistent despite well-managed treatment for 2 others, and details were not available for 2 more). For 18 cases (44%, 18/41 with available data among the 58 *C. diphtheriae* cutaneous cases), an investigation was conducted into the case.

For the 3 noncutaneous infections, the first patient (68 years of age) had a lower respiratory infection; *Staphylococcus aureus*, *Pseudomonas aeruginosa*, and *Corynebacterium diphtheriae* were also found in the bronchial aspirate. The patient died of septic shock caused by *Klebsiella pneumoniae*. The second patient, a 2-year-old child with a polymalformative syndrome, had a diagnosis of endocarditis to *C. diphtheriae* (confirmed by blood sample and secondarily confirmed by cardiac biopsy). The third patient (72 years of age) experienced a nasal mucosal form (superinfection of a chronic injury confirmed by mucus sampling). For those last 2 patients, details on the nature

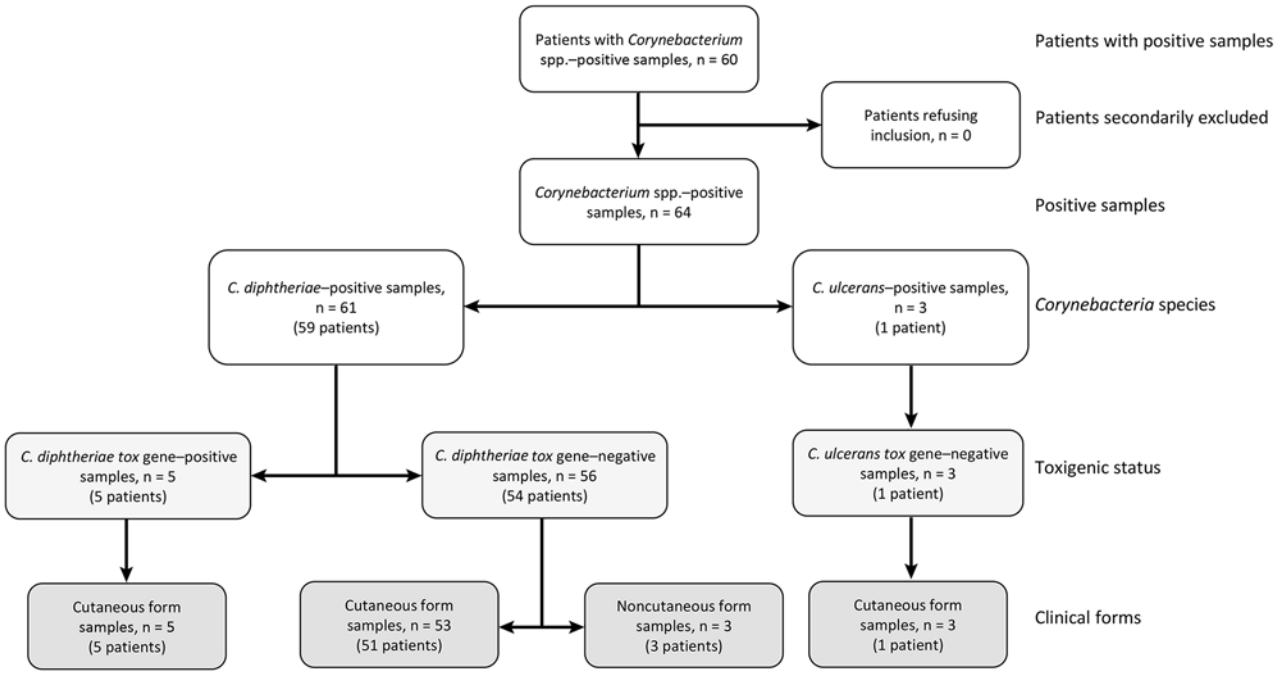

Figure 2. Flowchart of cases included in retrospective study of infections with *Corynebacterium diphtheriae* species complex, French Guiana, 2016–2021.

of the treatment were not available, but the clinical outcome was favorable. The diphtheria vaccination status of those patients was unknown.

Three Cutaneous Cases Caused by *C. ulcerans* in 1 Patient

One patient (74 years of age), who did not live with pets, was up-to-date on diphtheria vaccination, and had an underlying chronic skin wound (lymphatic filariasis sequelae), experienced 3 unrelated cases at 1-year intervals; eradication was monitored by samples collected 2 months after acute and treated cases. He had several lesions with fibrinous involvement located in the lower limbs (2 cases) and in upper limbs (1 case). Treatment consisted of amoxicillin for the first infection (unknown duration) and trimethoprim/sulfamethoxazole (for 10 days) for the second one; treatment for the last infection was not specified. The clinical course was described as good for all infections. Investigation into the case was not documented. The 3 *C. ulcerans* isolates belonged to the same genotype (sequence type [ST] 719) and were almost identical at the genomic sequence level (Appendix Figure).

Description of Coinfections

Of the 64 samples included, 61 (95%) were associated with bacterial co-infections. Among those 61 co-infections, 44 (69%) isolates were associated with a *Streptococcus* sp., 45 (70%) with *S. aureus*, and 31 (48%) with both of those 2 species; 15 (23%) were co-infected with another bacterium. The 3 non–co-infected cases corresponded to a blood culture sample and 2 cutaneous forms.

Genomic Epidemiology of Isolates

We studied the genomic diversity of 63 sequenced isolates (1 *C. diphtheriae* isolate could not be sequenced). The phylogenetic structure of the *C. diphtheriae* isolates from French Guiana formed 2 main lineages (Figure 4); 26 isolates corresponded to biovar Gravis (and its *spuA* marker gene) and 32 corresponded to biovar Mitis (*16*). Two isolates were biovar Belfanti (nitrate negative); for 1 of those, a disruptive mutation on the *narH* gene involved in nitrate reduction was found.

For *C. diphtheriae* isolates, sublineage-level classification showed 16 distinct sublineages (SL; defined using the 500 cgMLST mismatch threshold) (Figure 4). The most frequent SL was SL536 (6.6%, 11/63; all ST536). The other SLs had on average 3.3 isolates (SD 2.1). On the finer classification level, 26 genomic clusters were identified (defined using the 25 cgMLST mismatch threshold). One genomic cluster, GC295, was collected 9 times and belongs to the predominant SL536 (Figure 4). The 5 *tox*-positive isolates (but nontoxigenic because of a stop codon) belonged to

the same sublineage and genomic cluster (ST67, all biovar Mitis).

When reanalyzing 1,350 global *C. diphtheriae* isolates (*20*), we found only 3 sublineages of this study were also observed outside of French Guiana: in metropolitan France, Brazil, or Malaysia. At the genomic cluster level, only 1 French Guiana genotype (GC341) was also observed in metropolitan France, consistent with this patient having recently traveled there. Most isolates (41/63) were susceptible to all antimicrobial drugs tested (Appendix).

Discussion

We investigated 64 human cases of corynebacterial infections in 60 patients observed during 2016–2021 in French Guiana and found none were toxigenic. Most cases were cutaneous, although 1 case of endocarditis was observed. Cases were diagnosed mainly in the DCPCs located throughout the remote Amazon territories, where care can be difficult to perform. The increase in cases during this period raises public health concerns, and several factors should be considered.

Bacteriological techniques for identifying isolates evolved in French Guiana in 2016 with the introduction of matrix-assisted laser desorption/ionization time-of-flight mass spectrometry. This tool has probably contributed to improved identification of corynebacterial infections. In addition, the emergence of cases constituted a health signal. As a result, beginning in late 2018, healthcare professionals in French Guiana were taught by the territory's infectiologists how to diagnose and manage diphtheria, in line with current national recommendations (*8*). That training might have contributed to improved detection of cases by clinicians. However, the increase in cases during 2018 when that additional measure had not yet been deployed argues in favor of an actual increase in incidence.

Several factors suggest that cases were still underdiagnosed and therefore underestimated. First, the aspecific nature of cutaneous forms of infection, as confirmed in this study, means that clinicians might have missed diagnoses (*6*). In addition, national recommendations in France for the management of cutaneous wounds do not recommend bacteriological sampling (*28*), leading to a probable lack of screening for cutaneous forms. Finally, in 2020 and 2021, the COVID-19 pandemic affected access to healthcare in French Guiana because of repeated lockdowns and reorientation of medical care toward health crisis management (*9*). The number of cases was therefore probably underestimated during this period, despite the observed increase in incidence.

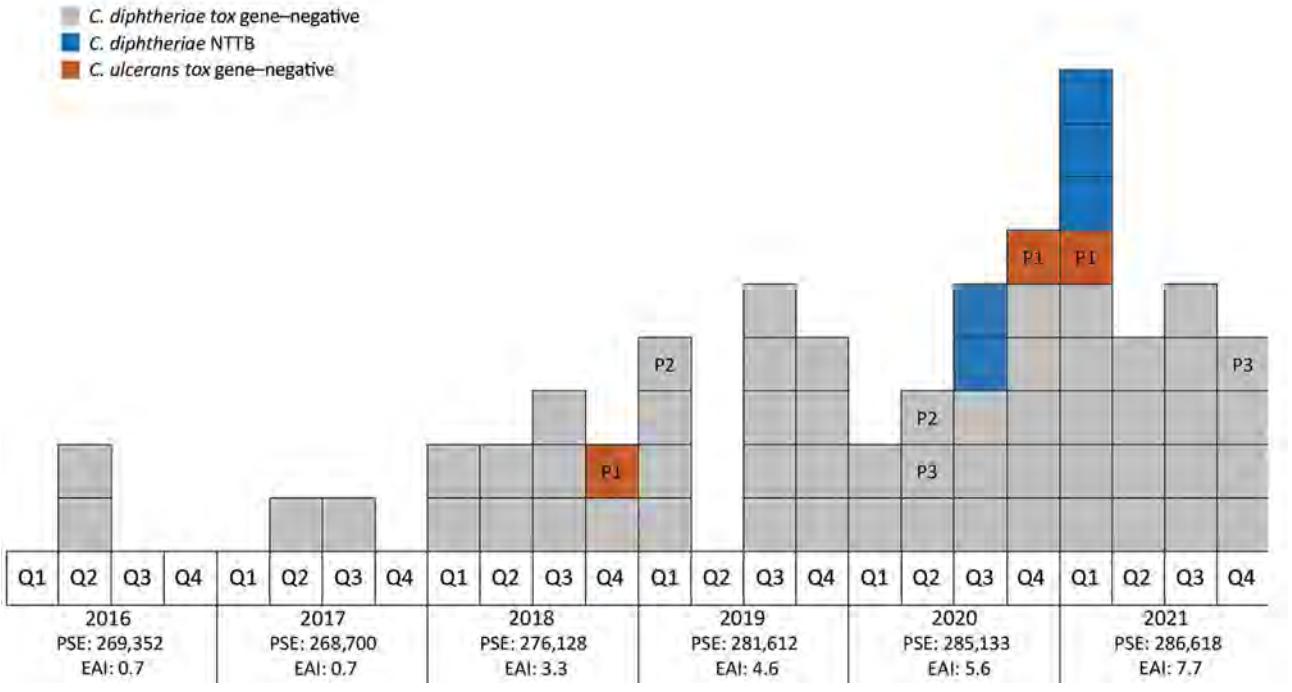

Figure 3. Temporal distribution of isolates corresponding to 64 clinical episodes of infection with *Corynebacterium diphtheriae* species complex in French Guiana, 2016–2021. Each box indicates 1 case; patient number labels (e.g., P1) indicate multiple cases in the same patient. EAI, estimated annual incidence (cases/100,000 population); NTTB, nontoxigenic *tox*-gene–bearing; PSE, population size estimation; Q, quarter.

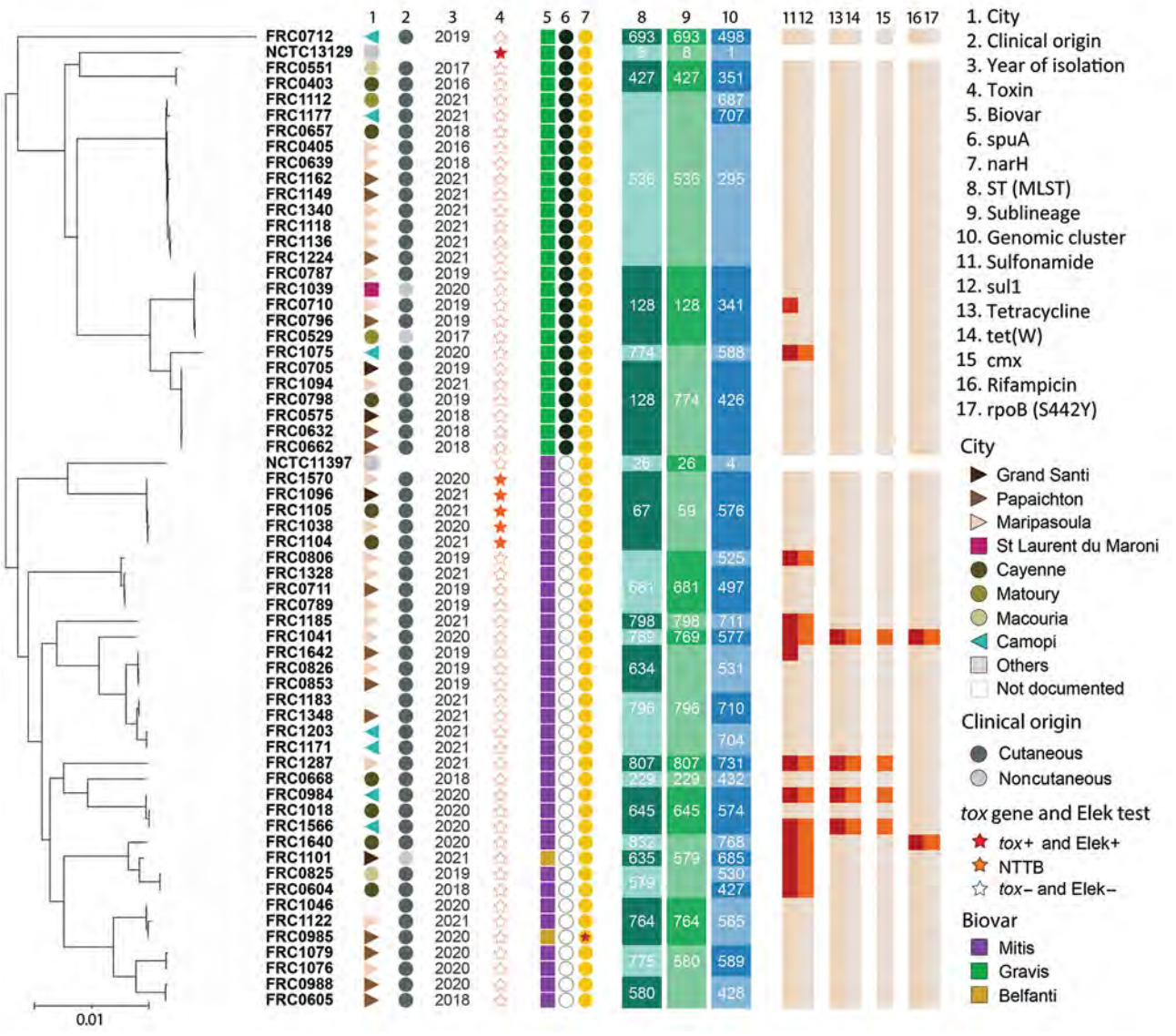

Figure 4. Diversity of *Corynebacterium diphtheriae* isolates in retrospective study of infections with *C. diphtheriae* species complex, French Guiana, 2016–2021. Star in column 7 indicates narH gene was not complete. MLST, multilocus sequence type; ST, sequence type.

As discussed previously, cutaneous forms of CdSC infections can very easily go unnoticed, which raises several questions. The probable antimicrobial therapy recommended for managing skin wounds is a short treatment, usually <7 days, targeting *Staphylococcus* and *Streptococcus* (*28*). The antimicrobial agents used, mainly amoxicillin/clavulanic acid, also correspond to the first-line treatment for diphtheria. However, the duration (7 days vs. 14 days as recommended for diphtheria infections) (*8*) is insufficient to obtain optimal clearance (*29*,*30*). Furthermore, use of an antibiogram is crucial because of emerging antimicrobial resistance (*12*,*16*). We identified 4 multidrug-resistant isolates (including the same genomic context). Therefore, lack of diagnosis and appropriate medical care exposes the risk for inadequate treatment, which can lead to unfavorable wound progression, risk for recurrence, and community spread of the pathogen (*23*). Last, the lack of contact patient screening also likely affected risk for transmission (*12*,*24*,*25*). Here, we observed 20 genomic clusters (with >1 isolate), distributed in time or space, demonstrating active transmission in the population. Furthermore, some inhabitants of French Guiana, particularly those living in remote areas, follow a cross-border lifestyle and are mobile in the territory, which, in addition to making care more complex, can contribute to spread (*26*).

All of those factors call for increased vigilance and a review of recommendations for screening and managing skin wounds, which should be adapted to the specific epidemiologic characteristics of French Guiana. In addition, taking better account of the risk for diphtheria when evaluating upper respiratory and systemic infections in French Guiana is key. Building and maintaining awareness of corynebacterial infections among healthcare providers throughout the territory is essential. In 2019, French Guiana began deploying mobile public health teams within the territory, but that effort was focused on the fight against the pandemic during 2020–2021 and could not fully contribute to the management of diphtheria cases. Those mobile health teams will provide valuable assistance in the management of patients who are farthest from care and will conduct investigations around cases using the go-to approach (i.e., teams going to the patient to provide care). Because of lacking human resources, qPCR cannot always be conducted at the CHC, extending the time taken to obtain results by 3 to 5 days after strains have been sent to Paris. Increasing the capacity of CHC to carry out routine toxin qPCR is therefore necessary. Last, increasing diphtheria vaccination coverage in French Guiana is key to combatting this problem effectively. Insufficient diphtheria vaccination coverage exposes the population at increased risk for circulation of toxigenic strains which could find a favorable niche. There are migratory flows in French Guiana from countries where diphtheria epidemics have been described (Brazil, Haiti, Dominican Republic) and where vaccination coverage is low (*31*). However, *C. diphtheriae* appears to have a phylogeographic structure represented by area-specific variants, and almost all isolates described in French Guiana have not been described elsewhere.

This study's first limitation is that, because of its retrospective nature, a substantial amount of information is lost. Moreover, data collection only concerned the 2 main hospitals in French Guiana and did not include private laboratories or Center Hospital of Kourou, limiting its exhaustiveness and impact estimates, even though no other cases were transmitted to the NRC during the study period.

In conclusion, nontoxigenic corynebacterial cutaneous infections have been increasingly diagnosed in French Guiana since 2016. A few severe forms have been described (i.e., endocarditis, surgical lesion). Given low vaccination coverage and the presumed chains of transmission, toxigenic isolates could find a favorable environment if introduced from other countries. These considerations call for regular training courses to raise awareness among frontline workers. In addition, reinforcing and adapting diagnostic and management recommendations in French Guiana is essential. Infection with members of the CdSC remains a public health issue, and increasing awareness among clinicians worldwide is necessary.

Acknowledgments

We thank the participants of the study, as well as all healthcare providers involved in the management of the patients. The mobile public health teams, the mediators from the DAAC association in Camopi, and Sabrina Walacou provided crucial support throughout this study. Camille Thorey and Cyril Leborgne coordinated data collection. Théo Blaise provided help and advice to complete the regulatory ethical procedures.

The National Reference Center for Corynebacteria of the *diphtheriae* Species Complex is supported financially by the Ministry of Health (Public Health France) and Institut Pasteur. The funding bodies had no role in the study and in the publication process.

M.G. and S.B. designed and conceived the study. M.G. wrote the first version of the manuscript. M.G., M.H., and S.B. contributed to the writing of the manuscript. M.G., V.S.R., L.E., J.F.C., S.B., M.H., E.B.O., J.T., and S.B. collected the data. M.G., M.H., S.B., and E.B.O. analyzed the data. All authors contributed to the latest version of the document and approved the contents of the final manuscript.

About the Author

Dr. Gaillet is an infectious diseases physician involved in public health research in the TIMC-IMAG laboratory of Grenoble Alpes University, France. Her research focuses on the epidemiology of infectious diseases of public health importance, as well as on health promotion.

References

1. Wagner KS, White JM, Crowcroft NS, De Martin S, Mann G, Efstratiou A. Diphtheria in the United Kingdom, 1986–2008: the increasing role of *Corynebacterium ulcerans*. Epidemiol Infect. 2010;138:1519–30. https://doi.org/10.1017/S0950268810001895
2. Hadfield TL, McEvoy P, Polotsky Y, Tzinserling VA, Yakovlev AA. The pathology of diphtheria. J Infect Dis. 2000;181(Suppl 1):S116–20. https://doi.org/10.1086/315551
3. Institut national de la statistique et des études économiques. Complete file, department of French Guiana (973) [in French] [cited 2024 Apr 11]. https://www.insee.fr/fr/statistiques/2011101?geo=DEP-973
4. Gower CM, Scobie A, Fry NK, Litt DJ, Cameron JC, Chand MA, et al. The changing epidemiology of diphtheria in the United Kingdom, 2009 to 2017. Euro Surveill. 2020;25:1900462. https://doi.org/10.2807/1560-7917.ES.2020.25.11.1900462

5. Galazka A. The changing epidemiology of diphtheria in the vaccine era. J Infect Dis. 2000;181(Suppl 1):S2–9. https://doi.org/10.1086/315533
6. Reacher M, Ramsay M, White J, De Zoysa A, Efstratiou A, Mann G, et al. Nontoxigenic *Corynebacterium diphtheriae*: an emerging pathogen in England and Wales? Emerg Infect Dis. 2000;6:640–5. https://doi.org/10.3201/eid0606.000614
7. Malmontet T, Guarmit B, Gaillet M, Michaud C, Garceran N, Chanlin R, et al. Spectrum of skin diseases in Amerindian villages of the Upper Oyapock, French Guiana. Int J Dermatol. 2020;59:599–605. https ://doi.org/10.1111/ijd.14848
8. Haut Conseil de la Santé Publique. What to do when a case of diphtheria develops [in French] [cited 2024 Apr 11]. https://www.pasteur.fr/sites/default/files/hcspr20110304_conduitediphterie.pdf
9. Epelboin L, Succo T, Michaud C, Oberlis M, Bidaud B, Naudion P, et al. COVID-19 epidemic in remote areas of the French Amazon, March 2020 to May 2021: another reality. Rev Soc Bras Med Trop. 2022;55:e02742021. https ://doi.org/10.1590/0037-8682-0274-2021
10. Haut Conseil de Santé Publique. Health inequalities in Guiana: inventory and recommendations [in French] [cited 2024 Apr 11]. https://www.hcsp.fr/explore.cgi/avisrapportsdomaine?clefr=1007
11. Carde E. Discrimination and access to care in French Guiana [in French]. Montreal: Presses de l'universite de Montreal; 2016.
12. Koivogui A, Carbunar A, Lmounga L, Larouade C, Laube S. Vaccination coverage among children and adolescents below 18 years of age in French Guiana: inventory and determinant factors. Public Health. 2018:158:15–24.
13. Santé Publique France. French Guiana public health bulletin April 2018 [in French] [cited 2024 Apr 11]. https://www.santepubliquefrance.fr/regions/guyane/documents/bulletin-regional/2018/bulletin-de-sante-publique-guyane.-avril-2018
14. Schnell D, Beyler C, Lanternier F, Lucron H, Lebeaux D, Bille E, et al. Nontoxinogenic corynebacterium diphtheriae as a rare cause of native endocarditis in childhood. Pediatr Infect Dis J. 2010;29:886–8. https://doi.org/10.1097/INF.0b013e3181de74ee
15. Patey O, Bimet F, Riegel P, Halioua B, Emond JP, Estrangin E, et al.; Coryne Study Group. Clinical and molecular study of *Corynebacterium diphtheriae* systemic infections in France. J Clin Microbiol. 1997;35:441–5. https://doi.org/10.1128/jcm.35.2.441-445.1997
16. Hennart M, Panunzi LG, Rodrigues C, Gaday Q, Baines SL, Barros-Pinkelnig M, et al. Population genomics and antimicrobial resistance in *Corynebacterium diphtheriae*. Genome Med. 2020;12:107. https://doi.org/10.1186/s13073-020-00805-7
17. Badell E, Guillot S, Tulliez M, Pascal M, Panunzi LG, Rose S, et al. Improved quadruplex real-time PCR assay for the diagnosis of diphtheria. J Med Microbiol. 2019;68:1455–65. https://doi.org/10.1099/jmm.0.001070
18. Engler KH, Glushkevich T, Mazurova IK, George RC, Efstratiou A. A modified Elek test for detection of toxigenic corynebacteria in the diagnostic laboratory. J Clin Microbiol. 1997;35:495–8. https://doi.org/10.1128/jcm.35.2.495-498.1997
19. Guglielmini J, Hennart M, Badell E, Toubiana J, Criscuolo A, Brisse S. Genomic epidemiology and strain taxonomy of *Corynebacterium diphtheriae*. J Clin Microbiol. 2021;59:e0158121. https://doi.org/10.1128/JCM.01581-21
20. Hennart M, Crestani C, Bridel S, Armatys N, Brémont S, Carmi-Leroy A, et al. A global *Corynebacterium diphtheriae* genomic framework sheds light on current diphtheria reemergence. Peer Community J. 2023;3:e76. https://doi.org/10.24072/pcjournal.307
21. Raimbaud B. Population census in French Guiana: 269,352 inhabitants on 1 January 2016 [in French] [cited 2024 Apr 11]. https://www.insee.fr/fr/statistiques/3679865
22. Jeanne-Rose M. 268,700 inhabitants on 1 January 2017: population census in French Guiana [in French] [cited 2024 Apr 11]. https://www.insee.fr/fr/statistiques/4271842
23. Reif X, Chanteur B. Population census in French Guiana: 276,128 inhabitants on 1 January 2018 [in French] [cited 2024 Apr 11]. https://www.insee.fr/fr/statistiques/5005684
24. Douriaud C, Reif X. Population census in French Guiana: 281,678 inhabitants on 1 January 2019 [in French] [cited 2024 Apr 11]. https://www.insee.fr/fr/statistiques/6012651
25. Douriaud C. 285,133 inhabitants in French Guiana on 1 January 2020 [in French] [cited 2024 Apr 11]. https://www.insee.fr/fr/statistiques/6681450
26. Douriaud C. 286,618 inhabitants in French Guiana on 1 January 2021 [in French] [cited 2024 Apr 11]. https://www.insee.fr/fr/statistiques/7739154
27. Ministère de la Santé et de la Prévention. Vaccination schedule 2023 [in French] [cited 2024 Apr 11]. https://sante.gouv.fr/prevention-en-sante/preserver-sa-sante/vaccination/calendrier-vaccinal
28. Haute Autorité de Santé. Management of common bacterial skin infections [in French] [cited 2024 Apr 11]. https://www.has-sante.fr/jcms/c_2911550/fr/prise-en-charge-des-infections-cutanees-bacteriennes-courantes
29. Miller LW, Bickham S, Jones WL, Heather CD, Morris RH. Diphtheria carriers and the effect of erythromycin therapy. Antimicrob Agents Chemother. 1974;6:166–9. https://doi.org/10.1128/AAC.6.2.166
30. Sharma NC, Efstratiou A, Mokrousov I, Mutreja A, Das B, Ramamurthy T. Diphtheria. Nat Rev Dis Primer. 2019;5:81. https://doi.org/10.1038/s41572-019-0131-y
31. Pan American Health Organization/World Health Organization. Epidemiological update diphtheria. Washington: The Organizations; 2021.

Address for correspondence: Mélanie Gaillet, SAN, Avenue Lapita, BP01, 98860 Koné, New Caledonia, France; email: gailletmelanie@gmail.com

Emergence of Bluetongue Virus Serotype 3, the Netherlands, September 2023

Melle Holwerda,[1] Inge M.G.A. Santman-Berends,[1] Frank Harders, Marc Engelsma, Rianka P.M. Vloet, Eveline Dijkstra, Rene G.P. van Gennip, Maria H. Mars, Marcel Spierenburg, Lotte Roos, René van den Brom,[1] Piet A. van Rijn[1]

Since 1998, notifiable bluetongue virus (BTV) serotypes 1–4, 6, 8, 9, 11, and 16 have been reported in Europe. In August 2006, a bluetongue (BT) outbreak caused by BTV serotype 8 began in northwestern Europe. The Netherlands was declared BT-free in February 2012, and annual monitoring continued. On September 3, 2023, typical BT clinical manifestations in sheep were notified to the Netherlands Food and Product Safety Consumer Authority. On September 6, we confirmed BTV infection through laboratory diagnosis; notifications of clinical signs in cattle were also reported. We determined the virus was serotype 3 by whole-genome sequencing. Retrospective analysis did not reveal BTV circulation earlier than September. The virus source and introduction route into the Netherlands remains unknown. Continuous monitoring and molecular diagnostic testing of livestock will be needed to determine virus spread, and new prevention strategies will be required to prevent BTV circulation within the Netherlands and Europe.

Bluetongue virus (BTV) is an arthropodborne virus that can cause clinical disease and death in ruminants. All ruminants are susceptible to infection by BTV; infections in New World camelids have also been described (*1*–*3*). Other species, including humans, are not susceptible to infection, indicating that bluetongue (BT) is not a zoonosis.

BTV is transmitted by *Culicoides* spp. biting midges and has been historically present only between latitudes 35°S and 50°N (*4*,*5*). The BTV serogroup consists of >30 serotypes, of which serotypes 1–24 are notifiable to the World Organisation for Animal Health (WOAH). Since 1998, notifiable BTV serotypes 1–4, 6, 8, 9, 11, and 16 and nonnotifiable BTV serotypes 25 and 27 have been found in Europe and the Mediterranean Basin (*6*). In 2006, bluetongue virus serotype 8 (BTV-8) emerged in northwestern Europe, and the Netherlands was the first country where the virus infection was detected (*7*,*8*). After a major BT outbreak caused by BTV-8 in Europe during 2006–2007, an emergency BTV-8 vaccine became available in 2008 (*9*,*10*). Many owners of cattle herds and small ruminant flocks participated in the voluntary vaccination program conducted by the government of the Netherlands (*11*), resulting in a dramatic decline in the number of BTV clinical notifications to the Netherlands Food and Consumer Product Safety Authority (NVWA) in 2008. At the end of 2008, BTV antibodies were found in >80% of the susceptible host populations tested because of either natural infection or vaccination. No new infections were observed after 2009, and, after 3 years of screening for possible BTV circulation, the Netherlands regained its official BT-free status in February 2012. This BT disease–free status has been monitored annually according to European Union (EU) regulation 1108/2008/EC and has been confirmed without interruption up to December 2022. However, because of the risk of introducing BTV-8 from neighboring countries, vaccination has been authorized and, therefore, some farmers still vaccinate their animals for BTV-8.

On September 3, 2023, clinical signs in sheep indicative of BT were notified to authorities in the Netherlands simultaneously by 2 veterinary practices located within the middle of the country. We

Author affiliations: Wageningen Bioveterinary Research, Lelystad, the Netherlands (M. Holwerda, F. Harders, M. Engelsma, R.P.M. Vloet, R.G.P. van Gennip, P.A. van Rijn); Royal GD, Deventer, the Netherlands (I.M.G.A. Santman-Berends, E. Dijkstra, M.H. Mars, L. Roos, R. van den Brom); Netherlands Food and Consumer Product Safety Authority, Utrecht, the Netherlands (M. Spierenburg); North-West University, Potchefstroom, South Africa (P.A. van Rijn)

DOI: https://doi.org/10.3201/eid3008.231331

[1]These authors contributed equally to this article.

describe the questions raised and actions taken during the first 3 weeks after the initial notified clinical case was confirmed as a BTV infection by laboratory diagnostic tests.

Methods

Sheep and Cattle Populations in the Netherlands and Clinical Examination

In 2022, the Netherlands had ≈1,080,631 sheep and ≈1,596,894 dairy cattle >2 years of age, distributed among ≈31,000 sheep farms and 14,000 cattle herds (*12*,*13*). Farms that notified authorities of possible BT were visited by a veterinary team, specializing in small ruminants, who reviewed reported clinical symptoms and collected samples for BT diagnosis. In addition, several farms already confirmed as BTV-positive were visited by Royal GD (formerly the Gezondheidsdienst voor Dieren) personnel, who clinically examined the sheep and cattle on those farms and described clinical signs.

Retrospective Study

We investigated whether the initial BT outbreak started in the area of the 4 BTV serotype 3 (BTV-3)–confirmed sheep farms in central Netherlands or whether the outbreak began earlier than September. We screened bulk tank cow milk samples submitted during August 2023 for routine testing from all over the Netherlands to determine if BTV antibodies were present. Royal GD coordinates a national monitoring program for which ≈12,000 (90%) dairy cattle farmers in the Netherlands submit monthly bulk tank milk samples. A total of 1,000 submitted milk samples were eligible for inclusion in the BTV screening.

We used identification and registration data from the Rijksdienst Voor Ondernemend Nederland (https://www.rvo.nl) to enable selection of dairy herd farms that did not purchase any cattle during the vector-active season (beginning in April 2023 until the start of the outbreak in September 2023) and only housed animals bred in the Netherlands. After applying the selection criteria, we were able to use bulk milk samples from 7,900 dairy herds for the screening. The Netherlands is divided into 20 compartments as proposed in the EU Commission Decision 2005/393/EC. We randomly selected 1,000 bulk milk samples to include all 20 compartments (Appendix Figure 1, https://wwwnc.cdc.gov/EID/article/30/8/23-1331-App1.pdf), resulting in ≈50 sampled herds per compartment and enabling a 14% prevalence estimate with 95% confidence. On September 11, we presented the first preliminary results to the government of the Netherlands. On September 13, additional data on vaccination purchases registered in the MediRund database (https://www.medirund.nl) during 2019 through September 2023 became available, and we combined those data with the results from the bulk milk screening.

BTV Genome Detection by PCR

We performed BTV-specific real-time reverse transcription PCR (RT-PCR) as previously described (*14*). In brief, we extracted virus RNA from 200 μL of EDTA blood by using the Magnapure 96 robotic machine (Roche, https://www.roche.com) and MagnaPure 96 DNA and Viral NA Small Volume Kit (Roche). For RT-PCR, we combined 5 μL eluted RNA and 15 μL LightCycler RNA Master HybProbe kit (Roche) reagent containing enzymes and BTV-specific primers and probe and loaded each reaction mixture per well into a 96-well plate. We amplified the resulting cDNA by using a LightCycler 480 II instrument (Roche) and LightCycler integrated software version 1.5.1, without the external predenaturation step (*14*).

Serologic Analysis using Competitive ELISA

We performed a competitive ELISA by using an ID Screen Bluetongue Competition ELISA kit (Innovative Diagnostics, https://www.innovative-diagnostics.com) according to the manufacturer's protocol. This ELISA has a sensitivity and specificity of 100% for BTV-specific antibodies but cannot detect antibodies generated against the genetically related epizootic hemorrhagic disease virus. We measured optical density at 450 nm by using a Multiskan FC instrument (Thermo Fisher Scientific, https://www.thermofisher.com) and MikroWin software version 5.09 (Labsis, https://labsis.de) and calculated the percentage inhibition by using the positive and negative controls supplied with the ELISA kit.

Whole-Genome Sequencing

We extracted RNA from EDTA blood and amplified BTV genome segments by using a sequence-independent single-primer amplification approach. We performed first-strand cDNA synthesis by combining 5 μL RNA and Superscript III (Thermo Fisher Scientific) according to the manufacturer's protocol and 2 μmol/L of the oligonucleotide 5′-GTTTCCCAGTCACGATA(N9)-3′. We incubated the mixture for 3 minutes at 95°C to denature double-stranded virus RNA, then cooled on ice. We added the remaining reagents and incubated the reaction at 25°C for 5 minutes, 42°C for 50 minutes, and 70°C for 15 minutes, and then stored at 4°C. We performed second-strand synthesis by using Sequenase (Thermo

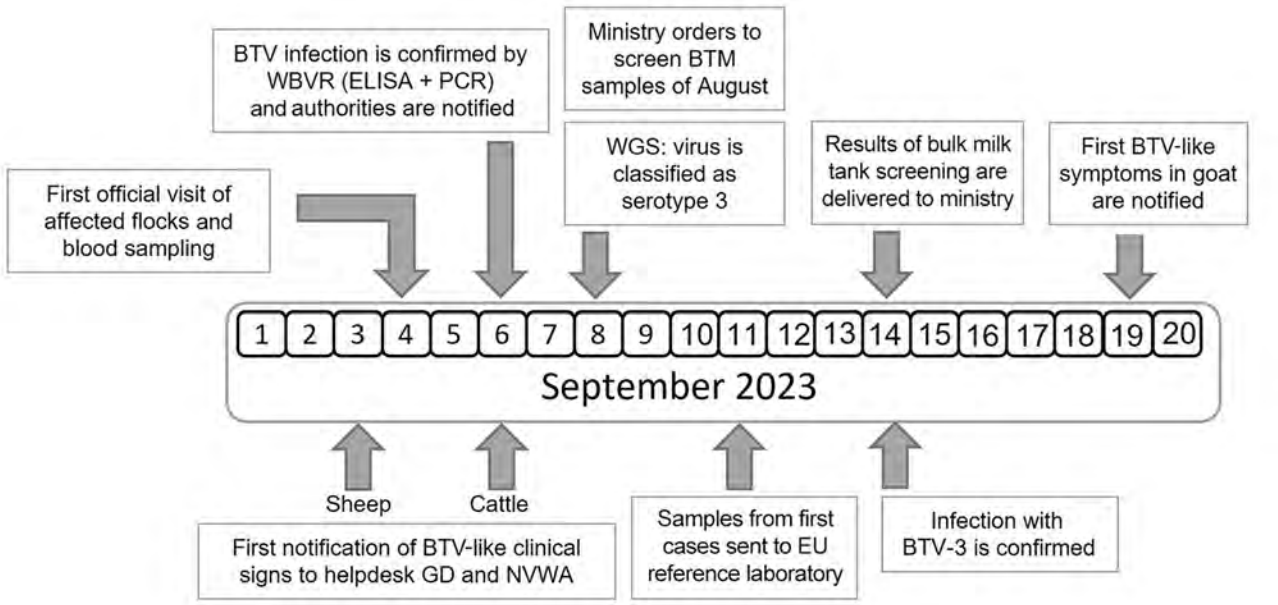

Figure 1. Timeline of the initial bluetongue outbreak caused by BTV-3 in the Netherlands in September 2023. BTV, bluetongue virus; BTV-3, BTV serotype 3; EU, European Union; GD, Gezondheidsdienst voor Dieren; NVWA, Netherlands Food and Consumer Product Safety Authority; WBVR, Wageningen Bioveterinary Research; WGS, whole-genome sequencing.

Fisher Scientific) according to the manufacturer's protocol. We amplified the products by using Q5 high-fidelity DNA polymerase (New England Biolabs, https://www.neb.com) according to the manufacturer's guidelines, 2 μmol/L of oligonucleotide 5′-GTTTCCCAGTCACGATA-3′, and the following cycle conditions: 94°C for 4 minutes; 68°C for 5 minutes; 35 cycles of 94°C for 30 seconds, 50°C for 1 minute, and 68°C for 3 minutes; then 68°C for 5 minutes and cooling at 10°C. To enhance the number of virus sequence reads, we performed a size selection of >200 bp by using SPRIselect beads (Beckman Coulter Life Sciences, https://www.beckman.com) at a ratio of 100 μL sample to 80 μL beads. We barcoded ≈150 ng cDNA from each sample by using the Native Barcoding Kit 96 V14 (Oxford Nanopore Technologies, https://www.nanoporetech.com) according to the manufacturer's protocol and sequenced the cDNA by using a PromethION Flow Cell, R10 M version (Oxford Nanopore Technologies). To align the reads, we applied Minimap 2 version 2.26 (*15*) against a custom BTV reference database to construct a draft genome by using reference-based mapping. We deposited the sequences into GenBank on September 26, 2023 (accession nos. OR603992–4001).

We conducted phylogenetic analysis separately for each genome segment sequence by using BLAST (https://blast.ncbi.nlm.nih.gov) and the alignment results of the top 15 sequences used for the analysis. In addition, we added genome segment (Seg)-2 reference strains and a selected number of closely related BTV-3 strains to the phylogenetic analysis (*16*). We aligned the sequences by using MAFFT version 7.475 (*17*) and reconstructed the phylogeny by using maximum-likelihood analysis in IQ-TREE version 2.0.3 (*18*) and 1,000 ultrafast bootstrap replicates (*19*). We visualized the tree by using the ggtree R package (*20*).

Antibody Detection in Bulk Tank Milk by Indirect ELISA

For the retrospective analysis of BTV antibodies in bulk milk, we used the ID Screen Bluetongue Milk Indirect ELISA (Innovative Diagnostics) according to the manufacturer's protocol; this ELISA uses the recombinant VP7 protein as the antigen and was

Table 1. Average sequence coverage for each genome segment of 3 BTV-3 isolates in study of emergence of BTV-3 in the Netherlands, September 2023*

Sample no.	Ct value	Average no. reads/nucleotide for each genome segment									
		Seg-1	Seg-2	Seg-3	Seg-4	Seg-5	Seg-6	Seg-7	Seg-8	Seg-9	Seg-10
23014055	23.3	431	898	548	1,386	642	2,570	664	4,311	1,905	200
23014071	28.6	72	112	76	149	99	135	107	223	113	30
23014098	25.2	217	313	228	470	192	488	258	630	283	45

*Three blood samples from sheep were collected at 3 unrelated farms; isolated virus was subjected to whole-genome sequencing. All 10 RNA genome segments were sequenced. BTV-3, bluetongue virus serotype 3; Ct, cycle threshold; Seg, genome segment.

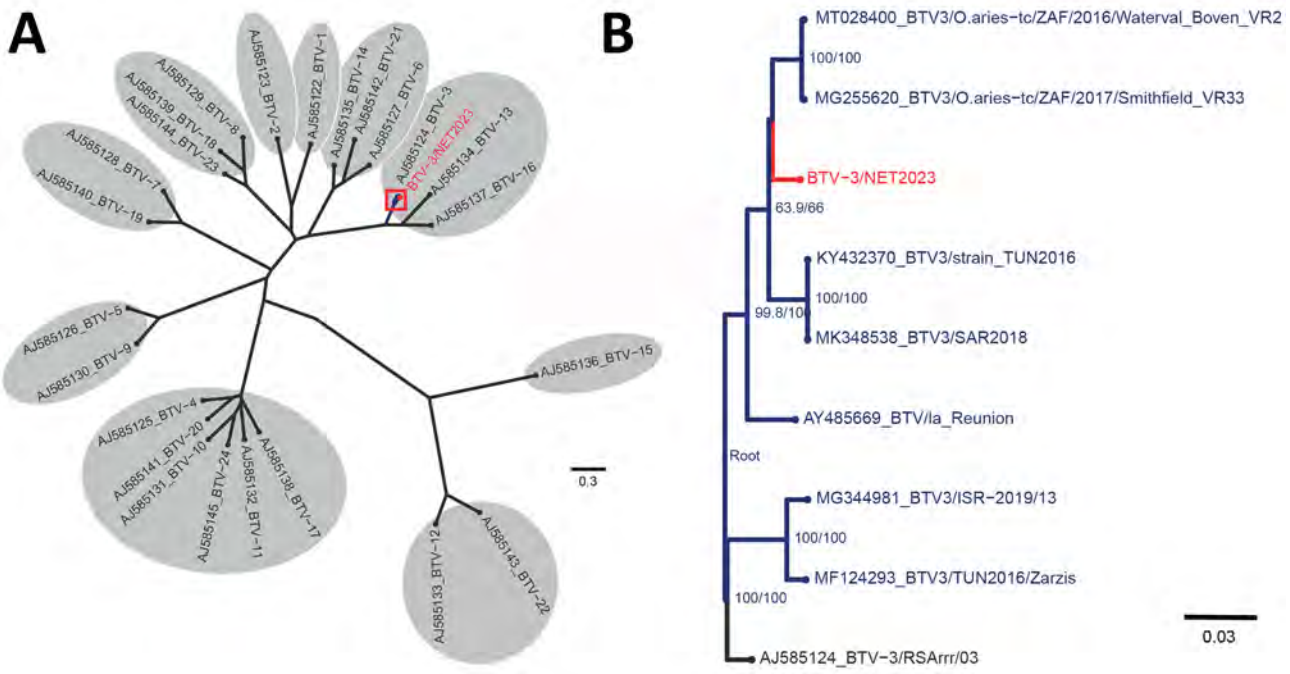

Figure 2. Phylogenetic analysis of BTV-3 variant found in livestock in the Netherlands, September 2023. Trees were obtained by using the maximum-likelihood method. A) Initial phylogenetic comparison of genome segment 2 sequence of the emerging BTV-3/NET2023 variant from the Netherlands with segment 2 sequences from notifiable BTV reference strain serotypes 1–24. B) Available and closely related genome segment 2 sequences from different BTV-3 strains selected for detailed phylogenetic analysis. Unrooted tree branches have bootstrap values indicated at the nodes. GenBank accession numbers are included in sequence names. Scale bars indicate nucleotide substitutions per site. BTV, bluetongue virus; BTV-3, BTV serotype 3.

validated in the Netherlands in 2007 (*21*). To study herd prevalence of BTV-3 infections in 2023, we used the cutoff values described in the ELISA manual: sample/positive control (S/P) values of ≤30% were considered negative, S/P values of >30% to ≤40% were considered potential positives, and S/P values >40% were considered positive. Using those cutoff values, the test had a sensitivity of ≈95% and specificity of 100%.

Geographic Distribution of BTV Clinical Cases

We graphically displayed sheep and cattle densities in thematic maps of the Netherlands according to 2-digit postal codes. We used BTV-confirmed clinical notifications of sheep and cattle cases until September 29, 2023. We generated all maps by using Stata version 17 (StataCorp LLC., https://www.stata.com).

Results

Timeline of Outbreak

On September 3 and 4, 2023, NVWA was notified of clinical signs that were indicative of BTV infections at 5 sheep farms in the central region of the Netherlands near the Loosdrechtse Plassen. Flocks were visited by

Table 2. Percentage homology between BTV-3/NET2023 variant and closest isolates deposited in GenBank in study of emergence of BTV-3 in the Netherlands, September 2023*

Segment	Virus protein	Highest % identity†	Isolate name	GenBank accession no.
Seg-1	VP1	97.69	BTV-8/2020_13	OQ860824.1
Seg-2	VP2	98.09	BTV-3/ZIM2002/01	AJ585179.1
Seg-3	VP3	98.30	BTV-5/O.aries-tc/ZAF/2011/Benoni_01012015	MG255451.1
Seg-4	VP4	98.37	BTV-3/TUN2016/Zarzis	MF124295.1
Seg-5	NS1	98.42	BTV-1/ISR-2050/19	OM502356.1
Seg-6	VP5	97.50	BTV-3/O.aries-tc/ZAF/2017/Smithfield_VR33	MG255623.1
Seg-7	VP7	98.27	BTV-3/O.aries-tc/ZAF/2016/Waterval_Boven_VR22	MT028405.1
Seg-8	NS2	97.69	BTV-2/O.aries-tc/ZAF/2017/Queenstown_VR18	MG255577.1
Seg-9	VP6/NS4	97.43	BTV-4/SPA2003/03	KP821911.1
Seg-10	NS3/NS3a	98.42	BTV-18/BT32/76	JX272448.1

*BTV-3/NET2023 variant was isolated from sheep in the Netherlands in September 2023 and genome segments were compared with those of BTV isolates deposited in GenBank. BTV-3, bluetongue virus serotype 3; NS, nonstructural protein; Seg, genome segment; VP, virus protein.
†Highest % identity (>97%) compared with BTV-3/NET2023.

Figure 3. Clinical manifestations of bluetongue caused by bluetongue virus serotype 3 (BTV-3) variant infections in sheep and cattle in study of emergence of BTV-3 in the Netherlands, September 2023. A–C) Hypersalivation (A), erosion of the oral mucous membranes (B), and bleeding of the lips (C) were observed in sheep infected with the BTV-3 variant. D–F) Ulceration of the oral mucous membrane (D), crust formation at the nostrils (E), and necrosis of the teats (F) were detected in cattle infected with the BTV-3 variant.

a team of veterinary specialists, and serum and EDTA blood samples were collected from the sheep and sent to the Netherlands National Veterinary Reference Laboratory for BTV at Wageningen Bioveterinary Research (WBVR).

On September 6, we confirmed BTV infections by real-time RT-PCR and competitive ELISAs (Figure 1). Of the 7 blood samples taken from 5 sheep farms, 6 samples from 4 different farms had BTV-positive RT-PCR results; cycle threshold values were 23–31. BTV antibodies were found in blood samples from 5 of the 6 PCR-positive sheep; blocking was >90% in competitive ELISAs. We immediately reported the findings to the Ministry of Agriculture, Nature and Food Quality of the Netherlands, and requested new samples for confirmation and shipment to the EU Reference Laboratory for BTV, Center for Animal Health Research, National Center for Agricultural and Food Research and Technology, in Madrid, Spain. In addition, using nanopore technology, WBVR conducted whole-genome sequencing on the RT-PCR–positive samples. The first suspicion of BTV in cattle was also notified to the NVWA on September 6.

On September 8, three blood samples from sheep sampled at 3 unrelated farms showed sufficient sequence coverage per nucleotide (range 30–2,570 reads) (Table 1) to reliably determine contig sequences for all 10 genome segments for those 3 samples. Contig sequences derived from individual samples were 100% identical. Contigs represented full-length sequences of Seg-1–Seg-9, including the 5′ and 3′ termini. Contigs of Seg-10 were incomplete and were completed by using Sanger sequencing, except for the ultimate 22 nt at the 3′ end, corresponding to the amplification primer. Phylogenetic analysis of Seg-2, which encodes the serotype-dominant VP2 protein, along with prototypic isolates of WOAH-notifiable BTV serotypes 1–24 identified the causative BT agent as BTV-3, which was designated as variant BTV-3/NET2023. Phylogenetic clustering of sequences was also observed with serotypes 13 and 16, confirming previous genetic analysis (Figure 2, panel A) (22). On the basis of the phylogenetic tree, WBVR announced that genotyping revealed the BT outbreak was caused by BTV-3 because of the high homology with known serotype 3 isolates. Detailed phylogenetic analysis showed a close relationship with Seg-2 from BTV-3 isolates from Italy and Tunisia (Figure 2, panel B). Phylogenetic analyses of other genome segments of BTV-3/

NET2023 did not indicate a particular ancestor but had close identity (>97%) to genome segments of various other sequenced BTV isolates deposited in GenBank (Table 2).

On September 11, WBVR confirmed BTV in newly collected serum and EDTA blood samples from all 4 initially infected sheep farms and sent the samples to the EU Reference Laboratory for confirmation and serotyping by serotype-specific real-time RT-PCR. On September 14, the EU Reference Laboratory confirmed the results by using the WOAH-recommended RT-PCR test targeting Seg-10. RT-PCR specific for serotypes 3, 4, and 8 clearly confirmed serotype 3, and the results were immediately forwarded to the Ministry of Agriculture, Nature and Food Quality of the Netherlands and NVWA.

On September 19, the first suspicion of BTV in a goat was notified to the NVWA; specimens collected from 1 goat were positive for BTV by real-time RT-PCR. In addition, BTV-3/NET2023 isolation from sheep EDTA blood from the initial 4 farms was successful by using *Culicoides*-derived KC cells (*23*).

Clinical Manifestations in Sheep, Cattle, and Goats

BTV-3–infected sheep showed signs of fever, lethargy, hypersalivation, ulcerations and erosions of the oral and nasal mucous membranes, facial edema, lesions of the coronary band, lameness, and death (Figure 3). Several days after the initial outbreak confirmation in sheep, clinical signs were also reported in cattle. Clinical signs observed in cattle were fever, apathy, conjunctivitis, nasal discharge, erosions and crust formation on lips and nostrils, ulcerations and erosions of oral mucosa, edema of the nose, coronitis, and superficial necrosis of teats. The goat reported on September 19 showed signs of edema of the lips and fever (Appendix Figure 2).

After the outbreak began, the number of notifications increased rapidly for both sheep flocks and cattle herds (Figure 4). The initial cases included 4 sheep farms. One week later (calendar week 36), a total of 25 sheep flock and 12 cattle herd notifications were confirmed as BTV-3–positive by RT-PCR. In the second week (calendar week 37), the total number of positive suspicions increased to 18 sheep flocks and 55 cattle herds. In the third week (calendar week 38), the total

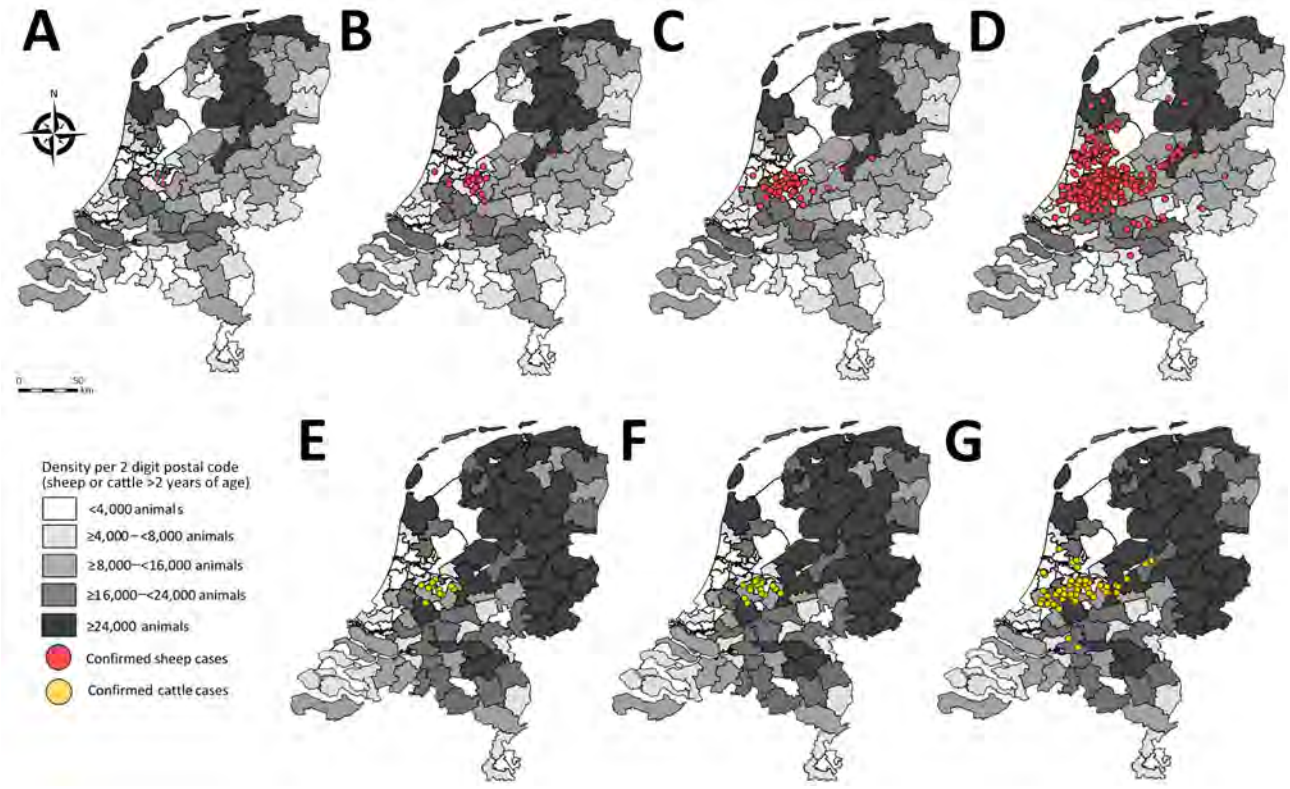

Figure 4. Density of sheep or cattle per 2-digit postal code and number of confirmed cases of bluetongue virus serotype (BTV-3)–positive flocks or herds in the Netherlands, September 2023. Gray shading indicates the density of animals. A–D) Distribution of sheep flocks infected with BTV-3. A) Initial 4 cases of BTV-3–infected sheep flocks notified on September 3, 2023. Confirmed sheep cases during calendar week 36 (B), calendar week 37 (C), and calendar week 38 (D). E–G) Distribution of cattle herds infected with BTV-3. Confirmed cases of infected cattle herds during calendar week 36 (E), calendar week 37 (F), and calendar week 38 (G).

Table 3. Herd-level BTV antibody results for 991 cow bulk milk samples collected in August 2023 in study of emergence of BTV-3, the Netherlands*

Compartment	No. dairy herds	No. herds tested	No. negative bulk milk samples	No. milk samples with potentially positive or positive result			Antibody-positive milk samples, % (95% CI)†
				Total	Evidence of BTV vaccination	No evidence of BTV vaccination	
1	1,669	49	49	0	0	0	0 (0–5.9)
2	678	49	49	0	0	0	0 (0–5.9)
3	880	51	51	0	0	0	0 (0–5.7)
4	1,040	49	48	1	0	1	2.0 (0.1–10.9)
5	963	47	45	2	2	0	0 (0–6.4)
6	352	49	49	0	0	0	0 (0–5.9)
7	562	52	52	0	0	0	0 (0–5.6)
8	1,332	50	49	1	1	0	0 (0–5.9)
9	610	51	51	0	0	0	0 (0–5.7)
10	546	48	47	1	0	1	2.1 (0.1–11.1)
11	1,412	48	46	2	1	1	2.1 (0.1–11.3)
12	942	50	49	1	0	1	2.0 (0.1–10.6)
13	464	53	52	1	1	0	0 (0–5.6)
14	162	48	44	4	2	2	4.3 (0.1–14.8)
15	96	50	50	0	0	0	0 (0–5.8)
16	457	47	46	1	1	0	0 (0–6.3)
17	293	52	43	9	7	2	4.4 (0.1–15.1)
18	778	52	47	5	5	0	0 (0–6.2)
19	361	48	43	5	3	2	4.4 (0.1–15.1)
20	145	48	45	3	1	2	4.3 (0.1–14.5)
Total	13,742	991	955	36	24	12	1.2 (0.1–2.2)

*Bulk milk samples were collected from dairy cattle herds in 20 compartments of the Netherlands in August 2023 and retrospectively analyzed to determine if BTV infections occurred before the detection of BTV-3 in sheep in September. BTV, bluetongue virus.
†Determined for cows that had no evidence of vaccination against BTV.

number of PCR-positive BTV-3–diagnosed flocks or herds increased to 324 sheep flocks, 61 cattle herds, and 1 goat herd.

Retrospective Study

To investigate whether the BT outbreak began at the 4 initially-infected sheep farms, we screened bulk tank milk samples submitted in August from cattle farms for routine BTV antibody testing. Of the 991 bulk tank milk samples, 955 tested negative, 8 tested potentially positive, and 28 tested positive for BTV antibodies; antibody prevalence was 2.8% (95% CI 1.9%–4.1%) (Table 3). However, 24 of 36 bulk tank milk samples showing potentially positive or positive results (67%) were from farms that had a proven history of animal vaccination against BTV-8. BTV antibodies that could not be linked to a recorded history of BTV vaccination were found in 12 of 991 bulk tank milk samples. However, the 12 antibody-positive herds were not clustered, and 7 of those 12 herds were located near the borders with Belgium and Germany, suggesting a high likelihood that those farms in the Netherlands might have vaccinated their animals because of the presence of BTV-8 in Belgium and Germany (Figure 5). Altogether, no area in the Netherlands had a high seroprevalence for BTV antibodies in August 2023 according to cow milk sampling, and no BTV-specific antibodies were found in the region where the initial BTV notifications were made. Therefore, the 4 BT index cases occurred in the 4 initially affected sheep farms.

Discussion

We describe the actions taken after a novel BTV-3 strain emerged in sheep and cattle in the Netherlands. Initially, sheep from 4 farms showed clinical signs of fever, lethargy, hypersalivation, ulcerations, erosions of the oral and nasal mucous membranes, or sudden death. The sheep were positive for BTV by real-time RT-PCR, and all but 1 showed seroconversion by using a competition ELISA. Whole-genome sequencing using nanopore technology showed the full virus genome sequence could be characterized quickly, and the generated nucleotide sequence of Seg-2 aligned with other BTV-3 sequences. We investigated BTV epidemiology during the month before the first cases were reported in sheep by retrospectively testing bulk tank cow milk; however, either no high seroprevalence was observed or seropositive samples were found within the region where the initial cases were detected. A very low number of antibody-positive bulk milk samples (n = 12) were found that could not be linked to previous vaccination. It is possible that the cows from those herds were still vaccinated, but that possibility could not be substantiated on the basis of available data. In addition, those findings might have been false positives despite the high specificity of the ELISA (*21*). We concluded that a massive

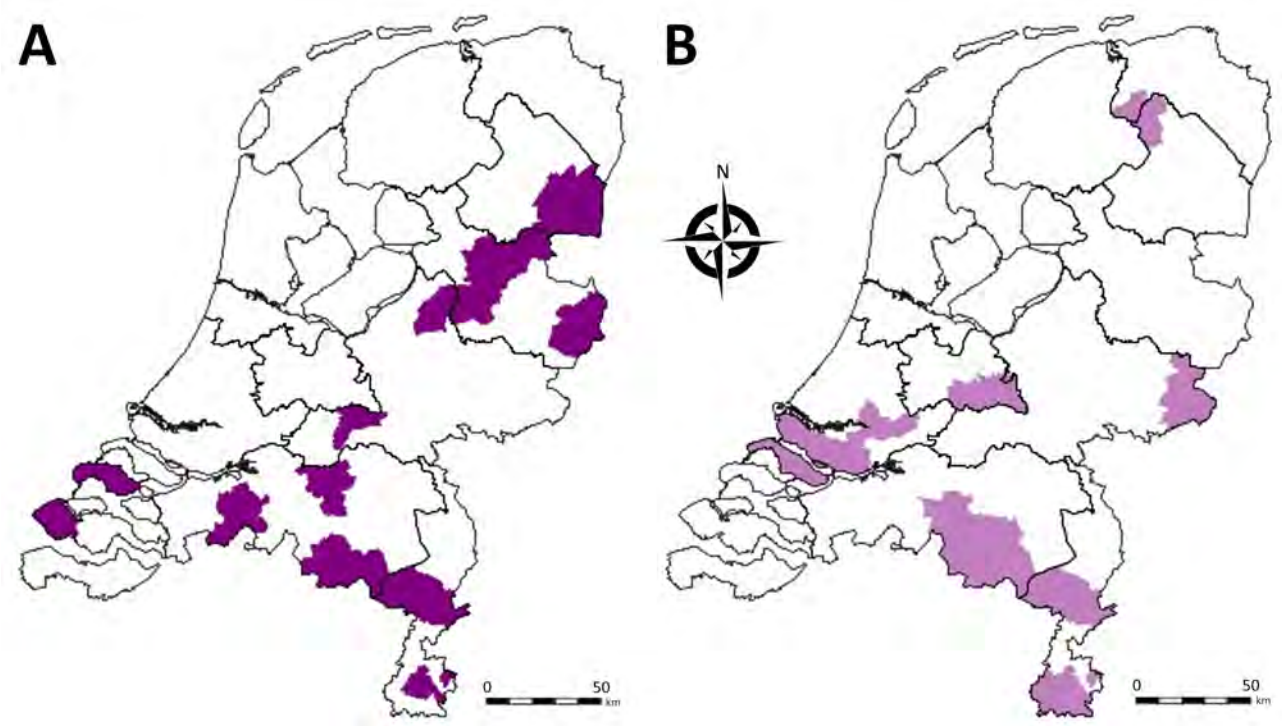

Figure 5. Geographic distribution of bulk milk samples in the Netherlands tested for bluetongue virus (BTV) antibodies in study of emergence of BTV serotype 3 in September 2023. Milk samples were collected in August 2023. Purple shading indicates locations of dairy cattle herds that had animals considered potential positive or positive for BTV-specific antibodies by using ELISA. A) Herds having evidence of vaccination in the previous 5 years. B) Herds having no evidence of vaccination in the previous 5 years.

spread of BTV did not occur before the first detection of BTV-3 in the sheep farms, which agrees with the findings of a retrospective analysis of 1,003 sheep serum samples from 89 flocks that indicated a 3.4% BTV herd prevalence in August (I.M.G.A. Santman-Berends et al., unpub. data). As of March 12, 2024, animals from a total of 4,371 farms or holdings have been confirmed as BTV-3 positive by real-time PCR.

Early detection of diseases by clinical diagnosis remains challenging, especially for unpredicted non-endemic diseases. BT displays a wide and nonspecific spectrum of clinical manifestations in ruminants, such as fever, hypersalivation, lameness, edema, and sudden death. BT disease severity in sheep and cattle overlaps with several other endemic infections, such as orf, dermatophilosis, haemonchosis, pasteurellosis, strawberry footrot, and photosensitization, which are relevant, differentially diagnosed endemic conditions in sheep. Malignant catarrhal fever and photosensitization can cause signs similar to BT in cattle (*24*,*25*). Awareness of BTV-like symptoms by veterinarians is also of great importance for other notifiable diseases, such as foot-and-mouth disease, peste des petits ruminants, sheep and goat pox, and epizootic hemorrhagic disease, and should be notified to the official authorities when suspected.

During a BT outbreak, communication creates increased awareness among veterinarians and farmers, which might lead to an increase in false BT notifications because of nonspecific clinical signs. Therefore, education and training of veterinarians and livestock farmers about the clinical manifestations of BT and other diseases remains critical, especially for notifiable diseases that have not occurred for an extended time, because many veterinarians might not have seen the clinical symptoms in their practice. Only a laboratory diagnosis can and should rapidly differentiate between notifiable diseases to support a clinical diagnosis. Nevertheless, in the outbreak described in this study, the emerging BT disease was detected successfully at an early stage.

The rapid spread of BTV after the initial emergence shows that indigenous *Culicoides* spp. midges in the Netherlands are competent vectors for transmitting BTV-3/NET2023. The BTV vector, the *C. imicola* midge, found predominantly in Africa and Asia, is not found in northwestern Europe, and BTV-6 introduction in the Netherlands in 2008 showed that the outbreak dies out when indigenous *Culicoides* spp. midges are unable to effectively transmit the virus (*26*). BTV-3/NET2023 is the second BTV variant, after BTV-8/NET2006, that has been successfully transmitted

by indigenous biting midge species in northwestern Europe (*27*). BTV-8/NET2006 is transmitted by indigenous biting midge species of the *C. obsoletus* complex, including *C. obsoletus*, *C. scoticus*, *C. dewulfi*, and *C. chiopterus* (*28*–*30*). Entomologic research is needed to identify the biting midge species involved in BTV-3/NET2023 transmission.

The geographic origin and route of introduction of BTV-3/NET2023 into the Netherlands are unknown. Phylogenetic analysis of Seg-2 shows clustering with other BTV-3 Seg-2 sequences, including geographically close BTV-3 variants. However, BTV-3 has only been described in Europe in Sicily and Sardinia, Italy, and the few sequences available from those virus isolates show a relatively high variation compared with BTV-3/NET2023 sequences from the Netherlands. In addition, other genome segment sequences did not show high homology with sequences from different BTV-3 variants. Therefore, tracing the origin of BTV-3/NET2023 has been difficult. The segmented genome of BTV enables reassortment, also known as antigenic shift, between variants, which further hampers unravelling the geographic source of BTV-3/NET2023. The virus was likely introduced into the Netherlands from a distant source because the neighboring countries Belgium and Germany have had BT-free status since June 2023. Although the source and route of BTV-3/NET2023 is unclear, yearly monitoring and the findings from this retrospective study indicate that virus circulation began in September 2023 within the Netherlands.

In conclusion, after a decade of having BT-free status, the Netherlands saw BTV-3 emerge in 2023, causing clinical signs and death in sheep and cattle. The causative virus strain is designated BTV-3/NET2023. The source, geographic origin, and introduction route of BTV-3/NET2023 are unknown, but virus circulation has rapidly expanded. BTV-3/NET2023 is transmitted by indigenous biting midges, but the vector-competent midge species has not yet been identified. Continuous monitoring and molecular diagnostic testing of sheep, cattle, and goats will be needed to determine virus spread, and new vaccination and other prevention strategies will be required to prevent BTV circulation within the Netherlands and Europe.

Acknowledgments

We thank the veterinary practitioners from Dierenartsenpraktijk Gorter and Dierenkliniek Amstel in Vecht en Venen, all the laboratory personnel at WBVR and Royal GD, and all veterinarians who conducted the herd visits for their laborious work and for providing photographs.

This study was supported by the Netherlands Ministry of Agriculture, Nature and Food Quality (project no. 1600002757 VZVD).

About the Author

Dr. Holwerda is head of the national reference laboratory for viral veterinary vectorborne diseases at Wageningen Bioveterinary Research. His research interests focus on the diagnosis and pathogenesis of veterinary virus infections.

References

1. Henrich M, Reinacher M, Hamann HP. Lethal bluetongue virus infection in an alpaca. Vet Rec. 2007;161:764. https://doi.org/10.1136/vr.161.22.764
2. Meyer G, Lacroux C, Léger S, Top S, Goyeau K, Deplanche M, et al. Lethal bluetongue virus serotype 1 infection in llamas. Emerg Infect Dis. 2009;15:608–10. https://doi.org/10.3201/eid1504.081514
3. Ortega J, Crossley B, Dechant JE, Drew CP, Maclachlan NJ. Fatal bluetongue virus infection in an alpaca (*Vicugna pacos*) in California. J Vet Diagn Invest. 2010;22:134–6. https://doi.org/10.1177/104063871002200129
4. Zhang N, MacLachlan NJ, Bonneau KR, Zhu J, Li Z, Zhang K, et al. Identification of seven serotypes of bluetongue virus from the People's Republic of China. Vet Rec. 1999;145:427–9. https://doi.org/10.1136/vr.145.15.427
5. Mellor PS, Carpenter S, Harrup L, Baylis M, Mertens PPC. Bluetongue in Europe and the Mediterranean Basin: history of occurrence prior to 2006. Prev Vet Med. 2008;87:4–20. https://doi.org/10.1016/j.prevetmed.2008.06.002
6. Lundervold M, Milner-Gulland EJ, O'Callaghan CJ, Hamblin C. First evidence of bluetongue virus in Kazakhstan. Vet Microbiol. 2003;92:281–7. https://doi.org/10.1016/S0378-1135(02)00365-6
7. van Wuijckhuise L, Dercksen D, Muskens J, de Bruijn J, Scheepers M, Vrouenraets R. Bluetongue in The Netherlands; description of the first clinical cases and differential diagnosis. Common symptoms just a little different and in too many herds [in Dutch]. Tijdschr Diergeneeskd. 2006;131:649–54.
8. Elbers ARW, Backx A, Meroc E, Gerbier G, Staubach C, Hendrickx G, et al. Field observations during the bluetongue serotype 8 epidemic in 2006. I. Detection of first outbreaks and clinical signs in sheep and cattle in Belgium, France and the Netherlands. Prev Vet Med. 2008;87:21–30. https://doi.org/10.1016/j.prevetmed.2008.06.004
9. Wäckerlin R, Eschbaumer M, König P, Hoffmann B, Beer M. Evaluation of humoral response and protective efficacy of three inactivated vaccines against bluetongue virus serotype 8 one year after vaccination of sheep and cattle. Vaccine. 2010;28:4348–55. https://doi.org/10.1016/j.vaccine.2010.04.055
10. Oura CAL, Edwards L, Batten CA. Evaluation of the humoral immune response in adult dairy cattle three years after vaccination with a bluetongue serotype 8 inactivated vaccine. Vaccine. 2012;30:112–5. https://doi.org/10.1016/j.vaccine.2011.10.100
11. Elbers ARW, de Koeijer AA, Scolamacchia F, van Rijn PA. Questionnaire survey about the motives of commercial livestock farmers and hobby holders to vaccinate their animals against bluetongue virus serotype 8 in 2008–2009 in

the Netherlands. Vaccine. 2010;28:2473–81. https://doi.org/10.1016/j.vaccine.2010.01.047
12. Dijkstra E, Vellema P, Peterson K, Bogt-Kappert CT, Dijkman R, Harkema L, et al. Monitoring and surveillance of small ruminant health in the Netherlands. Pathogens. 2022;11:635. https://doi.org/10.3390/pathogens11060635
13. Santman-Berends IMGA, Brouwer-Middelesch H, Van Wuijckhuise L, de Bont-Smolenaars AJG, Van Schaik G. Surveillance of cattle health in the Netherlands: monitoring trends and developments using routinely collected cattle census data. Prev Vet Med. 2016;134:103–12. https://doi.org/10.1016/j.prevetmed.2016.10.002
14. van Rijn PA, Heutink RG, Boonstra J, Kramps HA, van Gennip RGP. Sustained high-throughput polymerase chain reaction diagnostics during the European epidemic of bluetongue virus serotype 8. J Vet Diagn Invest. 2012;24:469–78. https://doi.org/10.1177/1040638712440986
15. Li H. Minimap2: pairwise alignment for nucleotide sequences. Bioinformatics. 2018;34:3094–100. https://doi.org/10.1093/bioinformatics/bty191
16. Maan S, Maan NS, Samuel AR, Rao S, Attoui H, Mertens PPC. Analysis and phylogenetic comparisons of full-length VP2 genes of the 24 bluetongue virus serotypes. J Gen Virol. 2007;88:621–30. https://doi.org/10.1099/vir.0.82456-0
17. Katoh K, Standley DM. MAFFT multiple sequence alignment software version 7: improvements in performance and usability. Mol Biol Evol. 2013;30:772–80. https://doi.org/10.1093/molbev/mst010
18. Nguyen LT, Schmidt HA, von Haeseler A, Minh BQ. IQ-TREE: a fast and effective stochastic algorithm for estimating maximum-likelihood phylogenies. Mol Biol Evol. 2015;32:268–74. https://doi.org/10.1093/molbev/msu300
19. Hoang DT, Chernomor O, von Haeseler A, Minh BQ, Vinh LS. UFBoot2: improving the ultrafast bootstrap approximation. Mol Biol Evol. 2018;35:518–22. https://doi.org/10.1093/molbev/msx281
20. Yu G, Smith DK, Zhu H, Guan Y, Lam TTY. GGTREE: an R package for visualization and annotation of phylogenetic trees with their covariates and other associated data. Methods Ecol Evol. 2017;8:28–36. https://doi.org/10.1111/2041-210X.12628
21. Mars MH, van Maanen C, Vellema P, Kramps JA, van Rijn PA. Evaluation of an indirect ELISA for detection of antibodies in bulk milk against bluetongue virus infections in the Netherlands. Vet Microbiol. 2010;146:209–14. https://doi.org/10.1016/j.vetmic.2010.05.009
22. van Rijn PA. Prospects of next-generation vaccines for bluetongue. Front Vet Sci. 2019;6:407. https://doi.org/10.3389/fvets.2019.00407
23. Wechsler SJ, McHolland LE, Wilson WC. A RNA virus in cells from *Culicoides variipennis*. J Invertebr Pathol. 1991;57:200–5. https://doi.org/10.1016/0022-2011(91)90117-9
24. Williamson S, Woodger N, Darpel K. Differential diagnosis of bluetongue in cattle and sheep. In Pract. 2008;30:242–51. https://doi.org/10.1136/inpract.30.5.242
25. Dercksen D, Lewis C. Bluetongue virus serotype 8 in sheep and cattle: a clinical update. In Pract. 2007;29:314–8. https://doi.org/10.1136/inpract.29.6.314
26. van Rijn PA, Geurts Y, van der Spek AN, Veldman D, van Gennip RGP. Bluetongue virus serotype 6 in Europe in 2008—emergence and disappearance of an unexpected non-virulent BTV. Vet Microbiol. 2012;158:23-32. https://doi.org/10.1016/j.vetmic.2012.01.022
27. Mellor PS, Boorman J, Baylis M. *Culicoides* biting midges: their role as arbovirus vectors. Annu. Rev. Entomol. 2000;45:307–40. https://doi.org/10.1146/annurev.ento.45.1.307
28. Mehlhorn H, Walldorf V, Klimpel S, Jahn B, Jaeger F, Eschweiler J, et al. First occurrence of *Culicoides obsoletus*–transmitted bluetongue virus epidemic in Central Europe. Parasitol Res. 2007;101:219–28. https://doi.org/10.1007/s00436-007-0519-6
29. Meiswinkel R, van Rijn P, Leijs P, Goffredo M. Potential new *Culicoides* vector of bluetongue virus in northern Europe. Vet Rec. 2007;161:564–5. https://doi.org/10.1136/vr.161.16.564
30. Dijkstra E, van der Ven IJK, Meiswinkel R, Hölzel DR, Van Rijn PA, Meiswinkel R. *Culicoides chiopterus* as a potential vector of bluetongue virus in Europe. Vet Rec. 2008;162:422. https://doi.org/10.1136/vr.162.13.422-a

Address for correspondence: Melle Holwerda, Wageningen Bioveterinary Research (WBVR), Department of Virology, PO Box 65, 8200 AB Lelystad, the Netherlands; email: melle.holwerda@wur.nl

Phylogeographic Analysis of *Mycobacterium kansasii* Isolates from Patients with *M. kansasii* Lung Disease in Industrialized City, Taiwan

Patrick George Tobias Cudahy, Po-Chen Liu, Joshua L. Warren, Benjamin Sobkowiak, Chongguang Yang, Thomas R. Ioerger, Chieh-Yin Wu, Po-Liang Lu, Jann-Yuan Wang, Hsiao-Han Chang, Hung-Ling Huang, Ted Cohen, Hsien-Ho Lin

Little is known about environmental transmission of *Mycobacterium kansasii*. We retrospectively investigated potential environmental acquisition, primarily water sources, of *M. kansasii* among 216 patients with pulmonary disease from an industrial city in Taiwan during 2015–2017. We analyzed sputum mycobacterial cultures using whole-genome sequencing and used hierarchical Bayesian spatial network methods to evaluate risk factors for genetic relatedness of *M. kansasii* strains. The mean age of participants was 67 years; 24.1% had previously had tuberculosis. We found that persons from districts served by 2 water purification plants were at higher risk of being infected with genetically related *M. kansasii* isolates. The adjusted odds ratios were 1.81 (1.25–2.60) for the Weng Park plant and 1.39 (1.12–1.71) for the Fongshan plant. Those findings unveiled the association between water purification plants and *M. kansasii* pulmonary disease, highlighting the need for further environmental investigations to evaluate the risk for *M. kansasii* transmission.

Mycobacterium kansasii, a slow-growing nontuberculous mycobacteria (NTM), can cause destructive pulmonary diseases in humans that cause similar clinical manifestations to those of *M. tuberculosis* pulmonary disease (*1*). In recent years, *M. kansasii* has become one of the most frequently reported NTMs in the world (*2*), but whether increasing notifications in some countries (*3*) reflects true increases in the incidence of *M. kansasii* disease or improvements in laboratory identification is not well understood.

Infection with *M. kansasii* has been predominantly reported in urban settings, in high-density and low-income communities, and among gold miners (*4*). Despite recent reports of potential human-to-human transmission for other NTMs (*5*), *M. kansasii* lung disease has been generally assumed to be acquired from environmental sources (*6*). Nonetheless, the precise route of transmission is yet to be characterized. *M. kansasii* is ubiquitous in the environment; tap water is reported as a major reservoir (*6*). The waterborne acquisition of *M. kansasii* is enabled by its intrinsic resistance to disinfectants, acid, and heat (*7*); its ability to survive in oligotrophic water; and its ability to form pipe surface biofilms (*8*). In previous studies, *M. kansasii* has been isolated from the water distribution system in the same communities in which cases with *M. kansasii* disease arise (*9*). However, evidence on environmental acquisition on the basis of genotyping of clinical or environmental isolates has been limited.

We investigated the environmental acquisition of *M. kansasii* in the industrial city of Kaohsiung, located in southern Taiwan. Our earlier multicenter study revealed that the number of patients with *M. kansasii*

Author affiliations: Yale School of Medicine, New Haven, Connecticut, USA (P.G.T. Cudahy); National Taiwan University, Taipei, Taiwan (P.-C. Liu, C.-Y. Wu, J.-Y. Wang, H.-H. Lin); Yale School of Public Health, New Haven (J.L. Warren, B. Sobkowiak, T. Cohen); Sun Yat-Sen University School of Public Health, Guangzhou, China (C. Yang); Texas A&M University, College Station, Texas, USA (T.R. Ioerger); Kaohsiung Medical University, Kaohsiung, Taiwan (P.-L. Lu, H.-L. Huang); Kaohsiung Medical University Hospital, Kaohsiung (P.-L. Lu, H.-L. Huang); National Tsing Hua University, Hsinchu, Taiwan (H.-H. Chang); Kaohsiung Municipal Ta-Tung Hospital, Kaohsiung,(H.-L. Huang)

DOI: https://doi.org/10.3201/eid3008.240021

pulmonary infection was nearly 5-fold higher in Kaohsiung than in Taipei in northern Taiwan (*10*). Higher humidity levels, warmer temperatures, and industrial areas with greater air pollution in Kaohsiung might explain this difference. We previously identified 2 spatial hotspots of high risk for *M. kansasii* infection in Kaohsiung by using clinical data collected from patients in all tertiary medical centers of the city (*11*). We hypothesized that specific water supplies or heavy industrial areas might be associated with the risk for *M. kansasii* infection. In this study, we extended the previous spatial analysis to include whole-genome sequencing (WGS) data of clinical *M. kansasii* isolates along with geographic information from patients, area-level industrialization, and water supply systems to comprehensively assess the risk and drivers of *M. kansasii* in Kaohsiung.

Methods

Study Participants

We included 302 patients >20 years of age who had newly diagnosed *M. kansasii* lung disease, consistent with American Thoracic Society/Infectious Diseases Society of America guidelines (*12*) from 1 tertiary medical center and its affiliated regional hospitals in Kaohsiung during 2015–2017. We conducted chart reviews to collect clinical and demographic data from eligible persons.

Mycobacterial WGS

Of the 302 patients, we performed WGS on mycobacterial isolates from 243 patients with high-quality culture samples from pretreatment sputum or bronchoalveolar lavage fluid. We performed sequencing in the Laboratory of Genomics and Bioinformatics Service at Texas A&M AgriLife (College Station, TX, USA) and constructed libraries by using the NEXTFLEX Rapid XP DNA-Seq Kit (Revvity, https://www.revvity.com). We performed paired-end sequencing using the NovaSeq 6000 Sequencing System (Illumina, https://www.illumina.com) with a read length of 150 bp and anticipated minimum mean depth of coverage of 100×. We removed 22 samples with most reads from a species other than *M. kansasii* from analysis. One additional sample had a large degree of nonmycobacterial reads, and 4 samples were from participants missing clinical or residential data. We excluded those from analysis, leaving 216 samples for our primary analysis.

Environmental Exposure Data

Our primary environmental exposure of interest was the water sources. We collected information on the service areas of water purification plants in Kaohsiung through the official website of Taiwan Water Corporation (*13*). In total, 5 water purification plants provide service to most households in Kaohsiung. Among those, Pingding is the largest by volume (44% of the total water supply from the 5 plants), followed by Chengcing (29%), Kaotan (12%), Fongshan (10%), and Weng Park (4%) (*13*). The water supply networks of those purification plants overlap; a single district often receives service from >1 water plant (Figure 1). We identified areas of heavy industrial zoning in Kaohsiung and used a probabilistic approach to identify participants who had a high probability of working in 1 of those zones (Appendix, https://wwwnc.cdc.gov/EID/article/30/8/24-0021-App1.pdf).

Data Analysis

We classified and filtered raw fastq reads using kraken2 (*14*) with a custom database, bracken (*15*), and ntm-profiler (*16*) (Appendix). We used Shovill (*17*) for de novo assembly using SPAdes (*18*). We aligned assemblies using ska (S.R. Harris, unpub. data, https://www.biorxiv.org/content/10.1101/453142v1) to the *M. kansasii* strain ATCC 12478, and all had >90% genomic coverage of the reference. We identified and masked regions of horizontal sequence transfer using Gubbins (*19*) and constructed a recombination-masked pairwise single-nucleotide polymorphism (SNP) distance matrix with snp-dists (*20*). We used this structure to create a phylogenetic tree with RAxML-NG (*21*) using the *M. kansasii* strain FDA-ARGOS 1615 as an outgroup, a generalized time reversible with gamma model of rate heterogeneity, and 50 starting trees (25 random and 25 parsimony) and calculated the transfer bootstrap expectation metric. To assess the association between genetic clade and water purification plant, we used Pearson χ^2 tests.

To assess the sensitivity of our phylogenetic analysis, we repeated the analysis with the addition of genomic sequences obtained from public sources and identified as obtained from outside of Taiwan. We used a list of available isolates (*9*) to download short-read sequences of 22 specimens from the National Center for Biotechnology Information Sequence Read Archive database. We speciated and filtered the sequences with the same analysis pipeline as our samples from Taiwan and repeated phylogenetic analyses using a tree constructed from the combined sample sets.

To analyze factors affecting the genetic relatedness of *M. kansasii* strains between pairs of persons from the study sample, we used hierarchical Bayesian spatial network methods implemented in the R package

GenePair (22). As opposed to standard regression modeling, GenePair methods are designed to account for correlation observed in dyadic data given that the same person is represented across multiple pairs (i.e., network dependence), spatial correlation between paired outcomes because of unmeasured transmission dynamics, and specific distributional features of genetic relatedness outcomes (23).

We modeled 2 outcomes of genetic relatedness: a binary outcome in which we classified pairs of strains as clustered or not based on a threshold SNP distance and a continuous measure of SNP distance between pairs of strains. For the binary outcome, the bimodal distribution of observed SNP distances between strains (Appendix Figure 1) suggested a threshold of ≤45 SNPs to classify pairs of strains as being within a cluster. In a sensitivity analysis, we also investigated a more conservative cutoff of ≤32 SNPs. We fit all models using Markov chain Monte Carlo sampling techniques and assessed convergence using trace plots and Geweke's diagnostic for all relevant model parameters. When making statistical inference, we reported posterior means and 95% equal-tailed quantile-based credible intervals.

Independent variables included the time between the date of each participant's sputum collection in

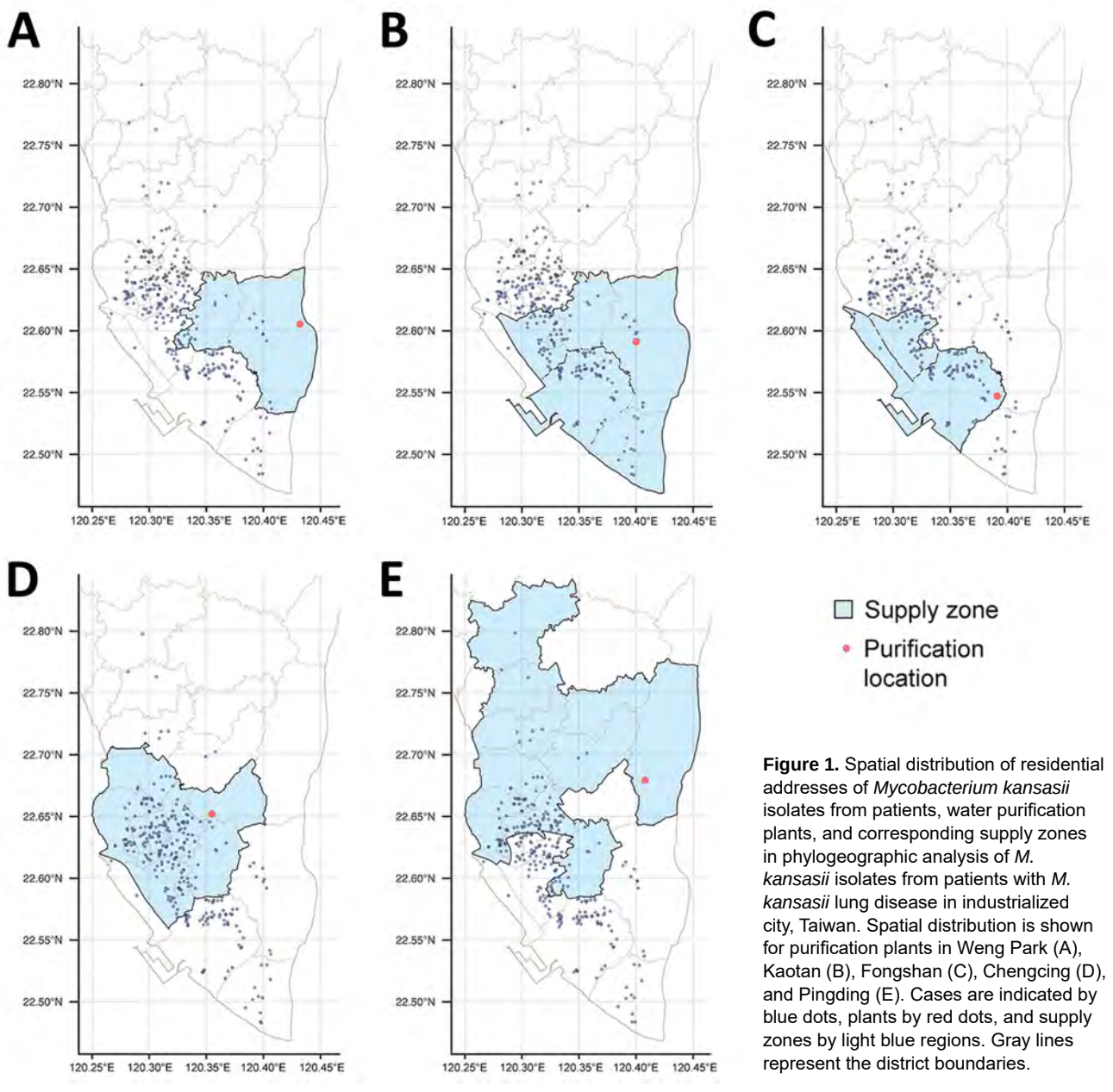

Figure 1. Spatial distribution of residential addresses of *Mycobacterium kansasii* isolates from patients, water purification plants, and corresponding supply zones in phylogeographic analysis of *M. kansasii* isolates from patients with *M. kansasii* lung disease in industrialized city, Taiwan. Spatial distribution is shown for purification plants in Weng Park (A), Kaotan (B), Fongshan (C), Chengcing (D), and Pingding (E). Cases are indicated by blue dots, plants by red dots, and supply zones by light blue regions. Gray lines represent the district boundaries.

days, the combined age of both participants in years, the age difference between pairs of participants in years, whether both were male or female, whether either person in the pair had cavitary disease on chest radiograph, geographic distance between participant households in kilometers, whether participant households were both supplied by the same water purification plants, whether both participants resided in villages with a high degree of linkage to the 4 heavy industrial zones, and whether the patients had received their diagnosis and been treated in the same hospital. We chose demographic and clinical variables included in the models a priori on the basis of clinical relevance.

The study was approved by the institutional ethics committees of the participating hospitals (KMUHIRB-F(I)-20210173, KMUHIRB-E(I)-20210380). The study funders had no role in the design and conduct of the study, the analysis and interpretation of data, or in the preparation, review, or approval of the manuscript.

Results

Demographics

Of the 216 cases with complete information, the mean patient age was 67 years (SD 17.6); 146 (67.6%) were men and 70 (32.4%) women (Table). Mean body mass index was 21 (SD 4.1). Of the 216 case-patients, 46 (21.3%) were current smokers, 45 (20.8%) were ex-smokers, and 125 (57.9%) had never smoked. On chest radiograph, 42 (20.1%) persons had consolidation, 37 (17.1%) had fibrocavitary disease, 81 (38.8%) had nodular bronchiectasis, 3 (1.4%) had nodules, 1 (0.5%) had fibrosis, and 52 (24.1%) had mixed image patterns. Tuberculosis had been diagnosed previously in 52 (24.1%) persons.

Sources of Residential Water Purification

Participant households were served by a median of 2 (maximum 3) of 8 different water purification plants. Chengcinghu supplied 128 (59.3%) of participant households, Pingding supplied 84 (38.9%), Kaotan supplied 99 (45.8%), Fongshan supplied 70 (32.4%), Weng Park supplied 22 (10.2%), Lingkou supplied 4 (1.9%), and Baolai and Lujhu each supplied 1 (0.5%) (Table; Figure 1).

Factors Associated with Genetic Relatedness between Pairs of Participants

Before analyzing genetic relatedness of *M. kansasii* strains, we masked areas of horizontal sequence transfer as previously described. This process reduced the median number of SNPs per strain from 23 (interquartile range [IQR] 537) to 13 (IQR 14.25). We constructed hierarchical Bayesian models to evaluate factors associated with being part of a genetic cluster (i.e., *M. kansasii* SNP distance between isolates of <45) as well as factors associated with continuous SNP distance. The model results (Figure 2) indicated that for each pair of participants, if both participant residences were supplied by the Weng Park water purification plant, their *M. kansasii* isolates had increased likelihood of being genetically clustered (odds ratio [OR] 1.81, 95% credible interval [CrI] 1.25–2.60), after adjusting for the other relevant factors. This finding was mirrored in the SNP model, where the SNP distances between the *M. kansasii* isolates of those pairs of persons were ≈12% smaller on average (risk ratio [RR] 0.88, 95% CrI 0.85–0.92). With a clustered model and a more conservative cutoff of 32 SNPs, the magnitude of the association was similar but not statistically significant (OR 1.54, 95% CrI 0.96–2.45) (Appendix Figure 2). We found a lower magnitude of association for the Fongshan water purification plant with a clustering OR of 1.39 (95% CrI 1.12−1.71) and a RR of SNP distance of 0.96 (0.94–0.98). We observed an inverse but statistically insignificant association between linear spatial distance and odds of clustering; adjusted OR was 0.77 (95% CrI 0.20–2.88) for every 1 km increase in spatial distance. Having a linkage to the same heavy industrial zone and sharing the same healthcare facility were not significantly associated with genetic relatedness, nor did they significantly alter the effect sizes for other variables in the model. Therefore, we removed those 2 variables from the final multivariable models for parsimony.

The statistical models also provided an estimate of a spatially referenced random effect parameter for each person that described the participants' residual (after adjustment for other factors) risk of being infected with an *M. kansasii* isolate that was genetically similar to other participants in the study. We mapped posterior mean estimates for those parameters (Appendix Figure 3). From visual inspection, we noted no obvious areas of increased residual risk.

Tree Structure of *M. kansasii* Population

We created a maximum-likelihood phylogram that showed 3 main clades (Figure 3). Participants with residential water supplied by the Weng Park water purification plant were more likely to be in clade A. Of the 73 persons in clade A, 14 (19.2%) were supplied by Weng Park. Of 58 participants in clade B, 3 (5.2%) had water purified by Weng Park; 5 (6.1%) of 82 participants in clade C had water purified by Weng Park ($p = 0.008$ for the association between genetic clade

and Weng Park). Participants supplied by the Fongshan water purification plant were more likely to be in clade B. Of the 58 participants in clade B, 27 (46.6%) were supplied by Fongshan. Of 73 participants in clade A, 15 (20.5%) were supplied by Fongshan; 27 (32.9%) of 82 in clade C were supplied by Fongshan (p = 0.006 for the association between genetic clade and Fongshan). We conducted a sensitivity analysis that included an additional 22 publicly available *M. kansasii* isolates from outside Taiwan in the phylogenetic analysis. The resulting phylogeny revealed the 3 major clades, which contained the same Taiwan samples as in the main analysis (Appendix Figure 4). Similarly, when we constructed a phylogeny of our samples from Taiwan without masking recombinant regions, the same clades were identified with identical members in clades A and B. Clade C in the phylogeny constructed without recombination masking contained all of the samples seen in the primary analysis but also overlapped with 59 samples from clade B.

Table. Demographics of included population in study of phylogeographic analysis of *Mycobacterium kansasii* isolates from patients with *M. kansasii* lung disease in industrialized city, Taiwan*

Characteristic	Value
Total no. participants	216
Mean age, y (SD)	67.29 (17.59)
Sex	
F	70 (32.4)
M	146 (67.6)
Mean body mass index (SD)	20.98 (4.14)
Smoking status	
Current smoker	46 (21.3)
Ex-smoker	45 (20.8)
Never smoked	125 (57.9)
Chest radiograph findings	
Consolidation	42 (20.1)
Fibrocavitary disease	37 (17.1)
Fibrosis	1 (0.5)
Nodular bronchiectasis	81 (38.8)
Nodule	3 (1.4)
Other†	52 (24.1)
Prior tuberculosis	52 (24.1)
Chronic obstructive disease	51 (23.6)
Pulmonary disease	
Bronchiectasis	35 (16.2)
Asthma	19 (8.8)
Pneumoconiosis	4 (1.9)
Lung cancer	9 (4.2)
Inhaled corticosteroid use	19 (8.8)
Residential water purification plant‡	
Baolai	1 (0.5)
Weng Park	22 (10.2)
Lingkou	4 (1.9)
Lujhu	1 (0.5)
Kaotan	99 (45.8)
Fongshan	70 (32.4)
Chengcinghu	128 (59.3)
Pingding	84 (38.9)

*Values are no. (%) except as indicated.
†Other patterns included mixtures of the aforementioned patterns.
‡Participant residences may be supplied by >1 water purification plant.

Discussion

Using densely sampled cases of *M. kansasii* infection from a tropical metropolitan city in southern Taiwan, we investigated environmental factors associated with genetic relatedness using WGS data. We found that pairs of persons with *M. kansasii* lung disease living in a district served by specific water purification plants (Weng Park and Fongshan) were at greater risk of being infected with genetically similar *M. kansasii* isolates. The association of smaller spatial distances between pairs of persons had a statistically significant trend toward more genetically similar *M. kansasii* strains.

We previously conducted a spatial analysis of 537 *M. kansasii* cases from 4 major tertiary hospitals in Kaohsiung and identified 2 suspicious spatial clusters (*11*). In this analysis, we found that the Weng Park and Fongshan water purification plants, both near 1 of the previously identified spatial hotspots, were associated with increased genetic relatedness among case pairs.

Weng Park, the water purification plant with the strongest signal of genetic relatedness (adjusted OR 1.81, 95% CrI 1.25–2.60) among *M. kansasii* cases, accounted for only 4% of the total water supply in the study area but was associated with 22 (10%) of the total 216 cases. We also observed that Weng Park was significantly associated with 1 major *M. kansasii* clade in our phylogenic analysis. Because water from different water plants mixed in underground water pipes, determining the source of supply for a particular household was difficult. Given the relatively low number of households supplied by Weng Park, the cases and households labeled as Weng Park might have also received their supply from other water plants, such as Kaotan and Pingding (Figure 1). The misclassification of water purification plants at the household level would lead us to underestimate the association between Weng Park and genetic relatedness of *M. kansasii* among case pairs.

This study does not provide a mechanism for the association between Weng Park and Fongshan water plants and the genetic clustering of *M. kansasii*–infected cases. Each water plant applied different methods of water purification, resulting in differences in pH value or organic matter content that might affect the risk for contamination and growth of *M. kansasii* (*6*). Different sources of raw water might also potentially influence the microbiological ecology; a 2003 analysis found that water from Weng Park had substantially higher general hardness than other water plants, suggesting a higher contribution from underground water as the source (*13*). The presence of more sediment accumulation in pipelines from underground water than from surface water might accelerate biofilm development (*24*). As

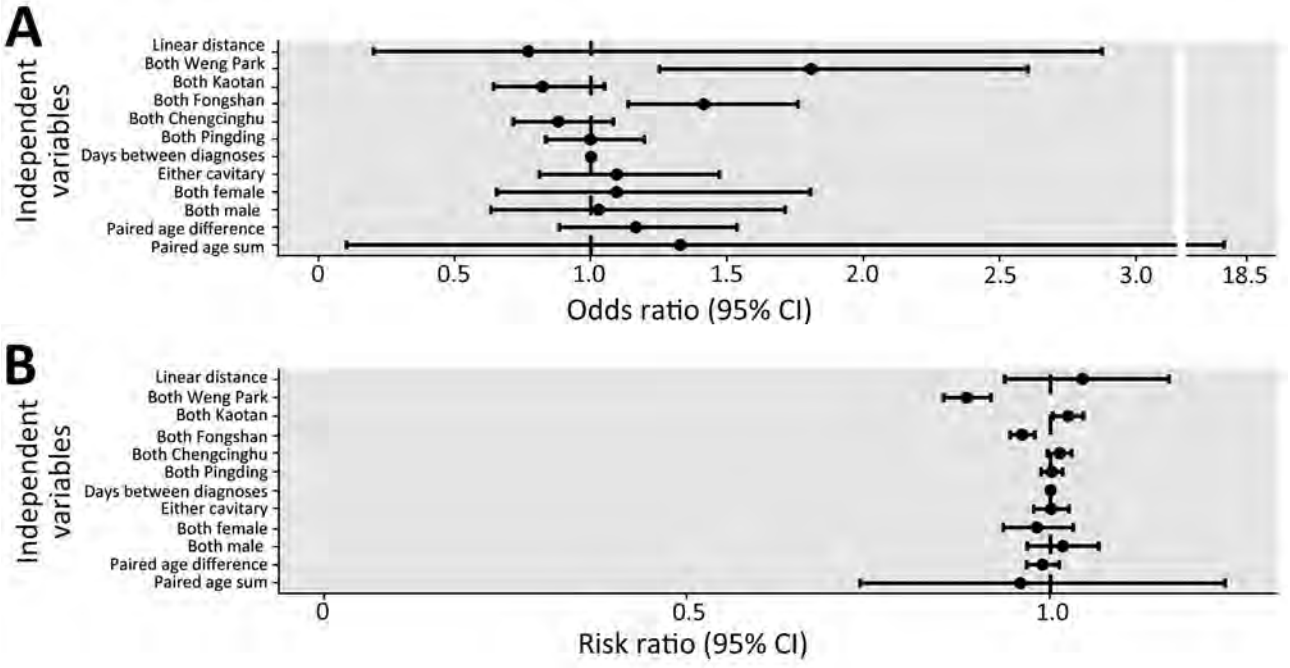

Figure 2. Associations of environmental and clinical risk factors with genetic relatedness based on pair-level data using hierarchical Bayesian regression models in phylogeographic analysis of *Mycobacterium kansasii* isolates from patients with *M. kansasii* lung disease in industrialized city, Taiwan. A) Odds ratios for pairs of *M. kansasii* isolates to be in a genetic cluster (using the single-nucleotide polymorphism [SNP] cutoff of 45). An odds ratio of >1 suggests that the risk factor was associated with genetic clustering. B) Risk ratios for increase in SNP distance between pairs of isolates. A risk ratio of <1 suggests that the risk factor was associated with a shorter pairwise SNP distance. The 3 smaller water purification plants (Lingkou, Baolai, and Lujhu) were not considered in the analysis as they together only provided service to 6 participants.

an example of the effect of the water treatment and distribution system on NTM abundance, a previous study in the United States reported low NTM relative abundances in Mississippi River water, a source for the drinking water system, but high relative abundances in the distribution system and tap water (*25*). Further environmental samplings should be conducted to examine the distribution of *M. kansasii* isolates in different water sources and plants, particularly Weng Park and Fongshan water plants.

Recent analyses of *M. abscessus*, another pathogenic NTM, have suggested that transmission might occur from person-to-person, especially in cystic fibrosis patients who might attend the same clinic (*5*). Our study did not find a potential link between shared clinic visits and the genetic clustering of *M. kansasii* in the investigated cases by analyzing pairs of persons' strains treated at the same hospital.

Although WGS has been widely applied to understand the transmission dynamics of *M. tuberculosis*, its application for studying NTM transmission including *M. kansasii* is still limited (*9*,*26*,*27*). The population structure and genomic diversity of *M. kansasii* on a global scale have been previously reported (*28*), but the genomic diversity over a well-defined geography has not been characterized. We used the cutoff of 45 and 32 SNPs to define genetic relatedness on the basis of the empirical SNP distribution in our population, but the relationship between those measures of genetic distance and transmission remains uncertain. A major difference between *M. tuberculosis* and *M. kansasii* is that genomic recombination occurs frequently in *M. kansasii* through distributive conjugal transfer (*28*). A recent study using 60 samples of *M. kansasii* from different provinces of China revealed that the pairwise SNP distance (after masking recombinant regions) of those isolates were all within 20 SNPs and suggested a threshold of 4 SNPs to define clustering (*29*). Both that study and ours excluded recombinant regions using the same methods, further complicating the interpretation of our analysis in terms of transmission inference. In addition, selecting an effective threshold to cluster cases with a potential shared exposure site might be dependent on the local epidemiology and genetic diversity of the tested population. Along with this study, 2 other large analyses of clinical *M. kansasii* whole-genome sequences (*9*,*29*) showed that, after masking recombinant regions, the resulting sequences appeared to belong to homogeneous clusters with maximum SNP distances on the

order of 100 SNPs. The largest analysis to date created a phylogeny that estimated the most recent common ancestor of a global collection of clinical isolates to be timed to the early 1900s (*9*).

A major strength of this study is the combination of WGS and detailed spatial information on the environmental determinants of interest, including the water supply and heavy industrial zoning. The novel Bayesian hierarchical modeling approach correctly accounts for the correlation of pairwise spatial-genetic data and the simultaneous adjustment for potential confounders. Previous studies on the transmission of *M. kansasii* have mostly applied conventional genotyping methodologies (e.g., restriction fragment length polymorphism or targeted PCR analysis) (*30*,*31*).

The first limitation of this study is that the *M. kansasii* isolates came from 1 major tertiary medical center and its affiliated hospitals (accounting for 56% of all *M. kansasii* isolates from all major medical centers in Kaohsiung during the same period) (*11*). *M. kansasii* infection is not a notifiable disease in Kaohsiung, and thus the population coverage of this

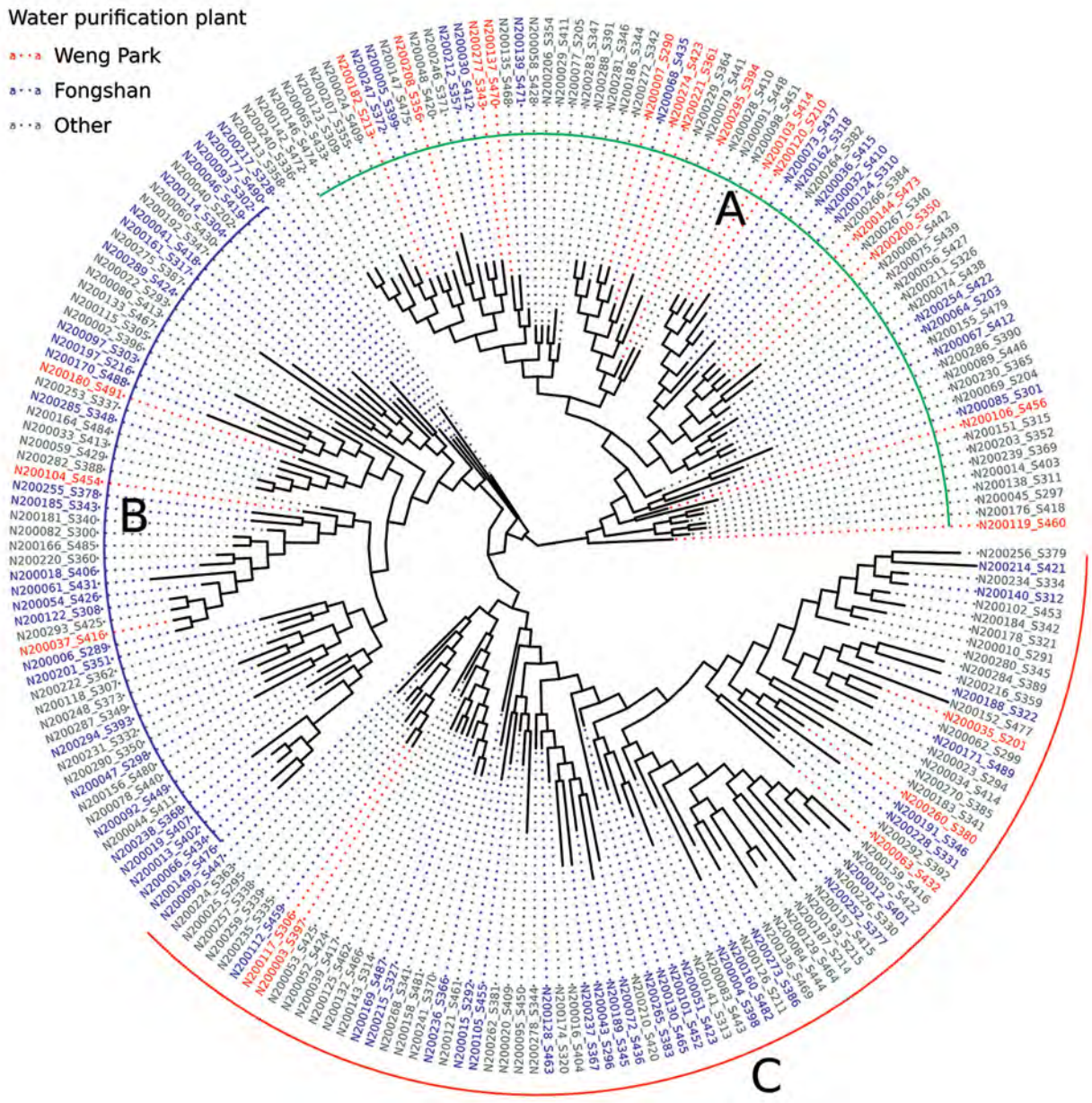

Figure 3. Maximum-likelihood phylogram of clinical *Mycobacterium kansasii* isolates from patients with *M. kansasii* lung disease in industrialized city, Taiwan. Phylogeny with major clades are labeled as A, B, and C; colored text indicates source of water for patient households.

analysis is not comprehensive. The suboptimal population coverage posed a challenge in identifying environmental exposures. Second, our analysis revealed an association between certain water purification plants (Weng Park and Fongshan) and genetic relatedness, but the route of transmission cannot be confirmed without environmental sampling. Weng Park only accounted for 10% of total cases and Fongshan accounted for 32% of cases. Environmental determinants of most *M. kansasii* cases remain to be elucidated. Third, we only have crude (district-level) spatial coverage of the water purification plants, and misclassification of water supply at the household level might well occur. Last, we used the residential address as the proxy for exposure assessment, and we were not able to obtain definitive workplace exposures.

In conclusion, our novel spatial phylogenetic analysis in a densely sampled, well-defined geography revealed an independent association between certain water purification plants and the genetic relatedness of *M. kansasii* isolates. Our approach demonstrated the utility of combining WGS sequencing and readily available clinical and environmental information to obtain useful insights into the transmission of *M. kansasii* to trigger further environmental investigation and control measures.

Acknowledgments

We thank laboratory members Mo-Hua Li and Yu-Wei Chen for helping with mycobacterial culture and DNA extraction of *M. kansasii* isolates.

Funding for this study was provided by Taiwan Ministry of Science and Technology (MOST 111-2628-B-002-045, MOST 112-2314-B-037 −073 -MY3), Kaohsiung Municipal Ta-Tung Hospital (KMTTH-111-039, KMTTH-112-R002), and National Health Research Institutes (NHRI-EX108-10805PI). P.G.T.C. was funded by a career development grant from the Fogarty International Center of the National Institutes of Health (5K01TW011194).

All genomes are shared through the US National Center for Biotechnology Information Sequence Read Archive.

P.G.T.C., P.C.L., H.L.H., T.C., and H.H.L. conceptualized the study. P.G.T.C., J.L.W., and T.C. did the genomic and statistical analyses. B.S., C.Y., and T.I. contributed to the genomic analyses. P.C.L. contributed to the spatial analysis. P.L.L. provided isolates for analyses. P.G.T.C., P.C.L., H.L.H., T.C., and H.H.L. wrote the initial draft of the manuscript. All authors edited and reviewed the final manuscript. All authors had full access to all the data in the study and had final responsibility for the decision to submit for publication.

About the Author

Dr. Cudahy is an infectious disease specialist and assistant professor at Yale School of Medicine. His primary research interest is mycobacterial infection outcomes and epidemiology.

References

1. Huang HL, Lu PL, Lee CH, Chong IW. Treatment of pulmonary disease caused by *Mycobacterium kansasii*. J Formos Med Assoc. 2020;119(Suppl 1):S51–7. https://doi.org/10.1016/j.jfma.2020.05.018
2. Martín-Casabona N, Bahrmand AR, Bennedsen J, Thomsen VO, Curcio M, Fauville-Dufaux M, et al.; Spanish Group for Non-Tuberculosis Mycobacteria. Non-tuberculous mycobacteria: patterns of isolation. A multi-country retrospective survey. Int J Tuberc Lung Dis. 2004;8:1186–93.
3. Marras TK, Chedore P, Ying AM, Jamieson F. Isolation prevalence of pulmonary non-tuberculous mycobacteria in Ontario, 1997–2003. Thorax. 2007;62:661–6. https://doi.org/10.1136/thx.2006.070797
4. Corbett EL, Hay M, Churchyard GJ, Herselman P, Clayton T, Williams BG, et al. *Mycobacterium kansasii* and *M. scrofulaceum* isolates from HIV-negative South African gold miners: incidence, clinical significance and radiology. Int J Tuberc Lung Dis. 1999;3:501–7.
5. Bolden N, Mell JC, Logan JB, Planet PJ. Phylogenomics of nontuberculous mycobacteria respiratory infections in people with cystic fibrosis. Paediatr Respir Rev. 2023;46:63–70.
6. Vaerewijck MJM, Huys G, Palomino JC, Swings J, Portaels F. Mycobacteria in drinking water distribution systems: ecology and significance for human health. FEMS Microbiol Rev. 2005;29:911–34. https://doi.org/10.1016/j.femsre.2005.02.001
7. Blanc SM, Robinson D, Fahrenfeld NL. Potential for nontuberculous mycobacteria proliferation in natural and engineered water systems due to climate change: a literature review. City Environ Interact. 2021;11:100070. https://doi.org/10.1016/j.cacint.2021.100070
8. Gan Y, Rahmatika I, Kurisu F, et al. The fate and risk of nontuberculous mycobacteria in the water supply system: a review. H2Open J. 2022;5:180–197.
9. Luo T, Xu P, Zhang Y, Porter JL, Ghanem M, Liu Q, et al. Population genomics provides insights into the evolution and adaptation to humans of the waterborne pathogen *Mycobacterium kansasii*. Nat Commun. 2021;12:2491. https://doi.org/10.1038/s41467-021-22760-6
10. Huang HL, Cheng MH, Lu PL, Shu CC, Wang JY, Wang JT, et al. Epidemiology and predictors of NTM pulmonary infection in Taiwan—a retrospective, five-year multicenter study. Sci Rep. 2017;7:16300. https://doi.org/10.1038/s41598-017-16559-z
11. Liu BC, Huang HL, Chan TC, Lee SJ, Lin JN, Lee CH, et al. Spatial cluster analysis of *Mycobacterium kansasii* infection in Kaohsiung, Taiwan. Taiwan J Public Health. 2021;40:713–23.
12. Daley CL, Iaccarino JM, Lange C, Cambau E, Wallace RJ Jr, Andrejak C, et al. Treatment of nontuberculous mycobacterial pulmonary disease: an official ATS/ERS/ESCMID/IDSA clinical practice guideline. Clin Infect Dis. 2020;71:e1–36. https://doi.org/10.1093/cid/ciaa241
13. Kuo J, Chen Y. Statistical analysis and exploration of drinking water quality in Kaohsiung City. Kaohsiung City Government; 2007 [cited 2022 Sep 16]. https://ksepb.kcg.gov.tw/FileDownLoad/FileUpload/20191027122705617901.odt

14. Wood DE, Lu J, Langmead B. Improved metagenomic analysis with Kraken 2. Genome Biol. 2019;20:257. https://doi.org/10.1186/s13059-019-1891-0
15. Lu J, Breitwieser FP, Thielen P, Salzberg SL. Bracken: estimating species abundance in metagenomics data. PeerJ Comput Sci. 2017;3:e104. https://doi.org/10.7717/peerj-cs.104
16. Phelan J. NTM-profiler [cited 2022 Sep 14]. https://zenodo.org/records/10851060
17. Seemann T. Shovill [cited 2022 Sep 14]. https://github.com/tseemann/shovill
18. Prjibelski A, Antipov D, Meleshko D, Lapidus A, Korobeynikov A. Using SPAdes de novo assembler. Curr Protoc Bioinformatics. 2020;70:e102. https://doi.org/10.1002/cpbi.102
19. Croucher NJ, Page AJ, Connor TR, Delaney AJ, Keane JA, Bentley SD, et al. Rapid phylogenetic analysis of large samples of recombinant bacterial whole genome sequences using Gubbins. Nucleic Acids Res. 2015;43:e15–15. https://doi.org/10.1093/nar/gku1196
20. Seemann T. snp-dists [cited 2022 Sep 14]. https://github.com/tseemann/snp-dists
21. Kozlov AM, Darriba D, Flouri T, Morel B, Stamatakis A. RAxML-NG: a fast, scalable and user-friendly tool for maximum likelihood phylogenetic inference. Bioinformatics. 2019;35:4453–5. https://doi.org/10.1093/bioinformatics/btz305
22. Warren JL, Chitwood MH, Sobkowiak B, Colijn C, Cohen T. Spatial modeling of Mycobacterium tuberculosis transmission with dyadic genetic relatedness data. Biometrics. 2023;79:3650–63. https://doi.org/10.1111/biom.13836
23. Hoff PD. Random effect models for network data. In: Dynamic social network modeling and analysis: workshop summary and papers. Washington: The National Academies Press; 2003. p. 303–12.
24. Learbuch KLG, Smidt H, van der Wielen PWJJ. Water and biofilm in drinking water distribution systems in the Netherlands. Sci Total Environ. 2022;831:154940. https://doi.org/10.1016/j.scitotenv.2022.154940
25. Hull NM, Holinger EP, Ross KA, Robertson CE, Harris JK, Stevens MJ, et al. Longitudinal and source-to-tap New Orleans, LA, U.S.A. drinking water microbiology. Environ Sci Technol. 2017;51:4220–9. https://doi.org/10.1021/acs.est.6b06064
26. Bryant JM, Grogono DM, Rodriguez-Rincon D, Everall I, Brown KP, Moreno P, et al. Emergence and spread of a human-transmissible multidrug-resistant nontuberculous mycobacterium. Science. 2016;354:751–7. https://doi.org/10.1126/science.aaf8156
27. Nikolayevskyy V, Niemann S, Anthony R, van Soolingen D, Tagliani E, Ködmön C, et al. Role and value of whole genome sequencing in studying tuberculosis transmission. Clin Microbiol Infect. 2019;25:1377–82. https://doi.org/10.1016/j.cmi.2019.03.022
28. Tagini F, Pillonel T, Bertelli C, Jaton K, Greub G. Pathogenic determinants of the *Mycobacterium kansasii* complex: an unsuspected role for distributive conjugal transfer. Microorganisms. 2021;9:348. https://doi.org/10.3390/microorganisms9020348
29. Guo Y, Cao Y, Liu H, Yang J, Wang W, Wang B, et al. Clinical and microbiological characteristics of *Mycobacterium kansasii* pulmonary infections in China. Microbiol Spectr. 2022;10:e0147521. https://doi.org/10.1128/spectrum.01475-21
30. Picardeau M, Prod'Hom G, Raskine L, LePennec MP, Vincent V. Genotypic characterization of five subspecies of *Mycobacterium kansasii*. J Clin Microbiol. 1997;35:25–32. https://doi.org/10.1128/jcm.35.1.25-32.1997
31. Kwenda G, Churchyard GJ, Thorrold C, Heron I, Stevenson K, Duse AG, et al. Molecular characterisation of clinical and environmental isolates of *Mycobacterium kansasii* isolates from South African gold mines. J Water Health. 2015;13:190–202. https://doi.org/10.2166/wh.2014.161

Address for correspondence: Hsien-Ho Lin, Institute of Epidemiology and Preventive Medicine, College of Public Health, National Taiwan University, Taipei 100, Taiwan; email: hsienho@ntu.edu.tw; Hung-Ling Huang, Department of Internal Medicine, Kaohsiung Medical University Hospital, Kaohsiung 807, Taiwan; email: 990325kmuh@gmail.com

Potential of Pan-Tuberculosis Treatment to Drive Emergence of Novel Resistance

C. Finn McQuaid, Theresa S. Ryckman, Nicolas A. Menzies, Richard G. White, Ted Cohen, Emily A. Kendall

New tuberculosis (TB) drugs with little existing antimicrobial resistance enable a pan-TB treatment regimen, intended for universal use without prior drug-susceptibility testing. However, widespread use of such a regimen could contribute to an increasing prevalence of antimicrobial resistance, potentially rendering the pan-TB regimen ineffective or driving clinically problematic patterns of resistance. We developed a model of multiple sequential TB patient cohorts to compare treatment outcomes between continued use of current standards of care (guided by rifampin-susceptibility testing) and a hypothetical pan-TB approach. A pan-TB regimen that met current target profiles was likely to initially outperform the standard of care; however, a rising prevalence of transmitted resistance to component drugs could make underperformance likely among subsequent cohorts. Although the pan-TB approach led to an increased prevalence of resistance to novel drugs, it was unlikely to cause accumulation of concurrent resistance to novel drugs and current first-line drugs.

Rifampin-resistant tuberculosis (RR-TB) is a key contributor to global antimicrobial resistance; >400,000 persons had RR-TB in 2020, nearly 40% of whom probably died as a result (*1*). More than 57% of those who have RR-TB disease are not enrolled in RR-TB treatment, including those who are not treated for tuberculosis (TB) at all and those who are inappropriately given treatments for rifampin-susceptible TB (RS-TB) (*1*). For those who are enrolled in RR-TB treatment, recent advances, including 6-month oral regimens (*2*), have improved tolerability and increased cure rates to >80%, but the need to identify drug resistance and direct patients with RR-TB down a second-line treatment pathway still complicates the diagnosis and treatment of TB.

Although tailored treatment remains a key pillar in preventing antimicrobial-resistance in general, a lack of access to rapid drug-susceptibility testing (DST) for TB represents a critical issue in reducing inappropriate treatment, in which drugs for TB treatment are almost solely used for TB. The growing availability of novel drugs and drug candidates with low or no resistance (*3*,*4*) has enabled a pan-TB treatment approach, offering 1 universal treatment regimen and no requirement for DST before initiating treatment. The World Health Organization (WHO) target profile for a pan-TB regimen also calls for short duration and improved tolerability and forgiveness (i.e., ability to withstand nonadherence without negative consequences) compared with the current standard of care (*5*). Such a regimen has the potential to remove barriers to initiation of appropriate treatment, improve treatment outcomes, and be effective and cost-effective (*6*). Although the regimen could be highly effective, the pan-TB approach requires that resistance to its component drugs is rare.

One concern about such a regimen is that widespread use of new drugs could exert a selective pressure that favors increases in resistance. Testing for both phenotypic and genotypic resistance to novel drugs remains limited and, because of technical difficulties, is likely to remain so in the near future (*7*). In the context of emerging resistance to a pan-TB regimen's component drugs, continued use of the regimen without routine susceptibility testing could lead to resistance to multiple drugs in the regimen and poor clinical outcomes. In addition, use of current first-line drugs such as rifampin to retreat those with resistance to the pan-TB regimen could lead to the

Author affiliations: London School of Hygiene and Tropical Medicine, London, UK (C.F. McQuaid, R.G. White); Johns Hopkins University School of Medicine, Baltimore, Maryland, USA (T.S. Ryckman, E.A. Kendall); Harvard T.H. Chan School of Public Health, Boston, Massachusetts, USA (N.A. Menzies); Yale School of Public Health, New Haven, Connecticut, USA (T. Cohen)

DOI: https://doi.org/10.3201/eid3008.240541

development of TB strains simultaneously resistant to both pan-TB drugs and current first-line drugs, leaving limited treatment options for affected persons.

Those resistance-related risks warrant particularly careful consideration given that leading candidate regimens in development for the pan-TB indication share newer drugs such as bedaquiline and pretomanid with the regimens currently recommended for treating RR-TB (clinical trial nos. NCT05971602 [https://www.clinicaltrials.gov/study/NCT05971602] and NCT06114628 [https://www.clinicaltrials.gov/study/NCT06114628]) (*8*–*11*). Although most TB, including most RR-TB, remains susceptible to these new drugs, resistance has emerged quickly in some patient populations for whom they have been used. For example, in South Africa, an early adopter of bedaquiline for RR-TB treatment, as much as 8% of the 2017 RR-TB cohort also had bedaquiline resistance (*12*). Those data suggest that resistance to some pan-TB regimen components might be prevalent among patients with RR-TB by the time a pan-TB regimen becomes available and that similar emergence could occur among RS-TB if pan-TB regimens are not designed to guard against emergent resistance.

Evidence is limited on the pace of emerging resistance or its effects on treatment outcomes, but an urgent need exists to anticipate pathways by which resistance could emerge. We used a modeling approach to explore the circumstances under which use of a pan-TB regimen could contribute to increasing resistance prevalence to new and existing drugs, posing resistance-related risks that could compromise the overall health benefit of a pan-TB strategy.

Methods

We developed a cohort model to evaluate clinical and drug-resistance outcomes over multiple successive cohorts of patients (Appendix Table 1, https://wwwnc.cdc.gov/EID/article/30/8/24-0541-App1.pdf) (Figure 1). We followed each cohort from the time of initial TB diagnosis, comparing a pan-TB strategy with current standards of care.

Modeling of Drugs, Regimens, and Drug Resistance

We explicitly modeled 3 drug classes as components of treatment regimens and drug-susceptibility phenotypes: rifamycins including rifampin (R), diarylquinolines including bedaquiline (B), and an additional unspecified novel drug (X) that is a

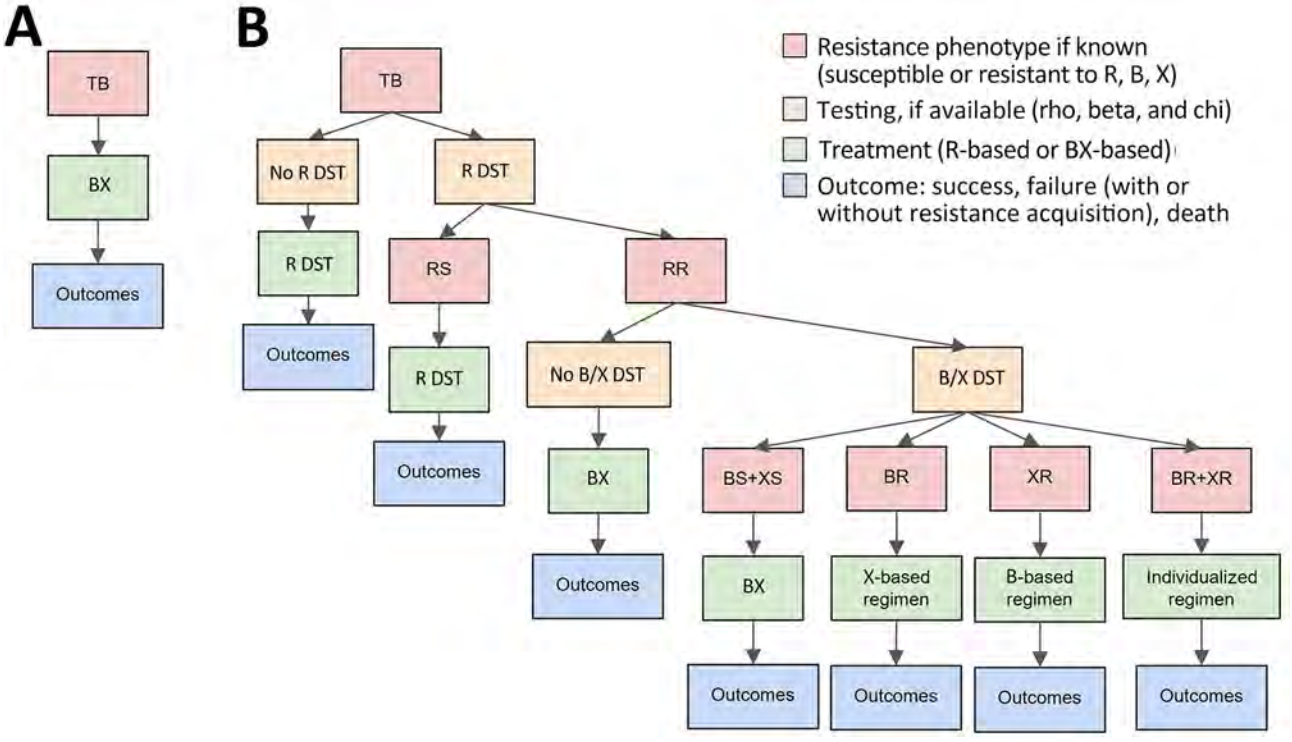

Figure 1. Treatment pathways for new TB patients in study of potential of pan-TB treatment to drive emergence of novel resistance, comparing a pan-TB treatment scenario (A) with the standard-of-care scenario (B). Retreatment pathways are shown in Appendix Figure 1 (https://wwwnc.cdc.gov/EID/article/30/8/24-0541-App1.pdf). BR-TB, diarylquinoline-resistant TB; RR-TB, rifampin-resistant TB; RS-TB, rifampin-susceptible TB; TB, tuberculosis; XR-TB, TB resistant to additional novel drug X; R DST, rifampin drug-susceptibility testing; B DST, diarylquinoline susceptibility testing; X DST, other novel drug (or drugs) susceptibility testing.

component of RR-TB and pan-TB regimens. X was modeled on bedaquiline in its propensity to develop drug-resistance and the effects of that drug resistance on treatment outcome. The standard-of-care regimen for treatment of RS-TB is denoted R but implicitly includes additional drugs such as isoniazid, and the B- and X- containing regimen (BX) implicitly includes ≥1 additional novel drugs.

Phenotypes resistant to R, B, and X are shown as RR-TB, BR-TB, and XR-TB, respectively. Those phenotypic categories enable resistance to additional drugs whose resistance was not explicitly modeled; for example, RR-TB is usually isoniazid-resistant and may be fluoroquinolone-resistant, and XR-TB may be resistant to ≥1 components of the pan-TB regimen. We modeled resistance to each drug in simplified binary fashion, corresponding to accepted breakpoints for phenotypic resistance to rifampin and bedaquiline. We defined concurrent resistance both to R and to either B, X, or both B and X as complex resistance in our model. We combined DST coverage and sensitivity to detect RR, BR, and XR phenotypes into probability-of-resistance-detection parameters.

Initial Treatment Pathways

In the standard-of-care scenario, R was used to treat RS-TB. We assumed current levels of DST coverage for rifampin. BX was used for treatment of RR-TB, reflecting current WHO guidelines recommending BPaL(M) (*13*), and we assumed that future improvements to the efficacy or safety of this regimen's component classes would be incorporated into future RR-TB regimens. We assumed that only a fraction of patients would undergo DST for B and X before RR-TB treatment, estimated based on current fluoroquinolone DST coverage. For patients with detected resistance to rifamycins and ≥1 novel drugs (B or X), we assumed that an individualized second-line regimen would be constructed, with inclusion of either B or X (i.e., an X-based or B-based individualized regimen) if susceptibility to 1 of these drugs was retained and a conventional second-line regimen otherwise.

In the pan-TB scenario, we assumed use of the BX regimen for all new TB patients. In addition, no DST was conducted for any drugs before initial treatment.

Treatment Outcomes

We modeled 4 possible outcomes of TB treatment: durable cure, non-cure (i.e., treatment failure or relapse) without acquisition of new resistance, non-cure with acquisition of new resistance to some component of the treatment regimen, and death. Probabilities of cure accounted for nonadherence, the possibility of early treatment discontinuation, and the effects of any preexisting resistance (Appendix Table 2); we separately estimated the likely outcome for each possible combination of regimen and pretreatment resistance phenotype (Appendix Table 3). Differences between regimens in terms of efficacy, duration of treatment, tolerability, and forgiveness correspond to a pan-TB target product profile developed by WHO (*5*), and we implicitly represented these factors as determinants of the proportion of patients durably cured on the basis of a previous study (*14*). For example, we implicitly represented the effect of poor treatment adherence attributable to low tolerability through a decreased probability of durable cure, dependent on regimen forgiveness. We assumed the same programmatic support across all regimens and did not explicitly consider regimen cost (including monitoring for side effects and other programmatic support) or ease of access to drugs, although those factors might be expected to have a differential effect on regimen use. We did not model rare acquisition of resistance to multiple regimen components during 1 treatment course.

Retreatment Pathways

For patients who did not recover or who relapsed after a first round of treatment, the selection of retreatment regimens took into account the previous treatment regimen, any previously known drug resistance and, potentially, the results of additional or repeat DST (Appendix Figure 1). In the standard-of-care scenario, the mapping between known drug resistance and selected regimen was the same for retreatment as for initial treatment, but DST coverage for R (among patients not already known to have RR-TB) and for B and X (among patients with RR-TB) was higher in retreatment. In the pan-TB scenario, R was used as a retreatment regimen for patients with confirmed rifampin susceptibility, but BX continued to be the default regimen in retreatment for patients with no DST results. DST coverage for retreatment patients in the pan-TB scenario was the same as for new patients in the standard-of-care scenario. We also performed a sensitivity analysis where DST was performed at these levels for R but not for B or X and where DST coverage for R was 100%.

Time Approximation

To simulate the accumulation of resistance and its effect on outcomes over time, we extended the cohort model over multiple treatment cohorts representing successive generations of transmitted TB. Our representation captured the number of generations of

transmission but ignored the (large variation in) calendar time per generation. In estimating how transmission from earlier cohorts contributed to a future cohort of new TB patients, we assumed that cohort sizes remained the same over time (i.e., an effective reproduction number of 1 in all scenarios). The distribution of resistance in each cohort (but not the absolute size of the cohort) assumed that patients who had been unsuccessfully treated in previous cohorts had generated on average as much transmission after their initial diagnosis as before. Therefore, the initial drug-resistance composition of a given treatment cohort was a weighted average of the immediately preceding cohort at 3 different timepoints (at the start of treatment, after initial treatment, and after retreatment) weighted by the proportion of the cohort still with TB at each of those timepoints. We modeled 10 generations of new treatment cohorts.

Although our results can be loosely translated into calendar time (assuming, for example, that 1 cohort generation of transmission corresponds to a serial interval of 1–2 years on average [*15*]), our estimation of timescales does not take into account the distributions of times to secondary case generation or to diagnosis, both of which can be highly varied and setting-dependent for TB (*16*–*18*). Overinterpretation of the generation time is inadvisable.

We assumed that 4% of cases in the first cohort were RR-TB (*1*), of which 2% were also resistant to B, on the basis of recent clinical data on bedaquiline resistance (*12*,*19*–*21*). Simultaneously, 0.2% of RS-TB cases had resistance to B, also assumed on the basis of clinical trial and surveillance data for bedaquiline (*22*,*23*). We assumed that initial prevalence of resistance to X was zero. A sensitivity analysis considered higher baseline prevalence of BR (by the same relative factor among both RS-TB and RR-TB cases) to account for the possible accumulation of resistance between the present day and when pan-TB may become available in the future.

Parameter Uncertainty

Many of our parameter values had little data to inform them. As such, we selected wide uncertainty ranges on the basis of the range of estimates available in the literature. We assumed β distributions for all parameter values except the risk ratio describing the effect of existing resistance on further resistance acquisition (Appendix Table 1), for which we assumed a uniform distribution because of the extremely high uncertainty and a desire to explore extreme values. To propagate uncertainty through the analysis, we created 1,000 parameter sets simultaneously, independently sampling from the distributions of all uncertain parameters, and we reestimated the model with each of these parameter sets. We explored parameter extremes through 1- and 2-way sensitivity analyses.

Results

Model Approach

Over multiple cohorts of patients in both scenarios, the proportion of TB that was resistant to ≥1 modeled drug was projected to increase (i.e., the proportion of cases that was DS was projected to decrease) (Figure 2). The change was estimated to be slightly faster in

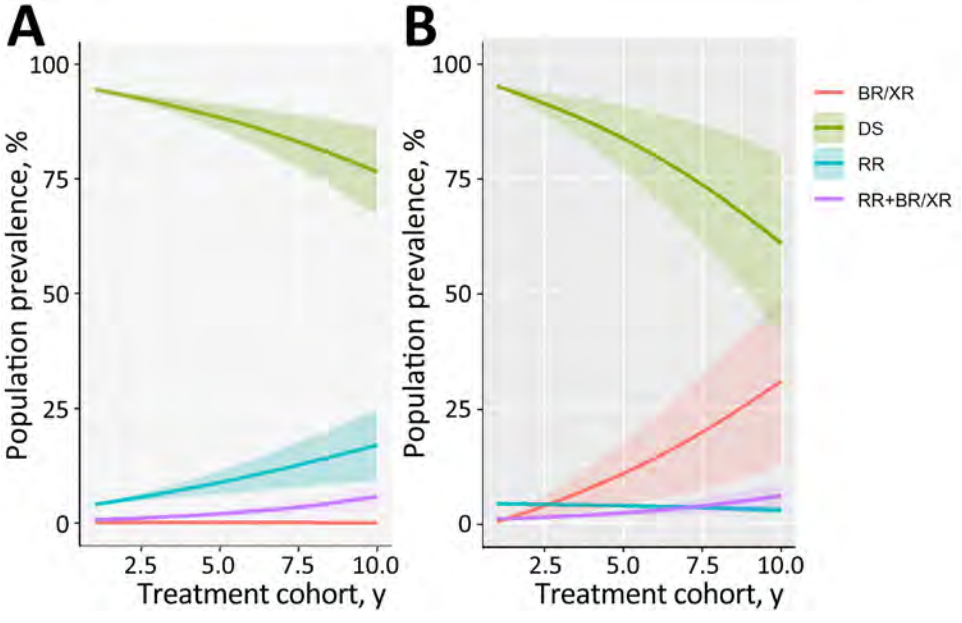

Figure 2. Prevalence of resistance phenotypes over multiple cohorts of TB treatment in study of potential of pan-TB treatment to drive emergence of novel resistance for standard-of-care (A) and pan-TB (B) treatment scenarios. Shaded areas indicate 95% CIs. x-axis indicates scale indicates treatment generations. BR/XR, TB resistant to a diarylquinoline or novel drug X or both only; DS, drug-susceptible TB; RR, rifampin-resistant TB; RR+BR/XR, TB resistant both to rifampin and to either a diarylquinoline, novel drug X, or both; TB, tuberculosis.

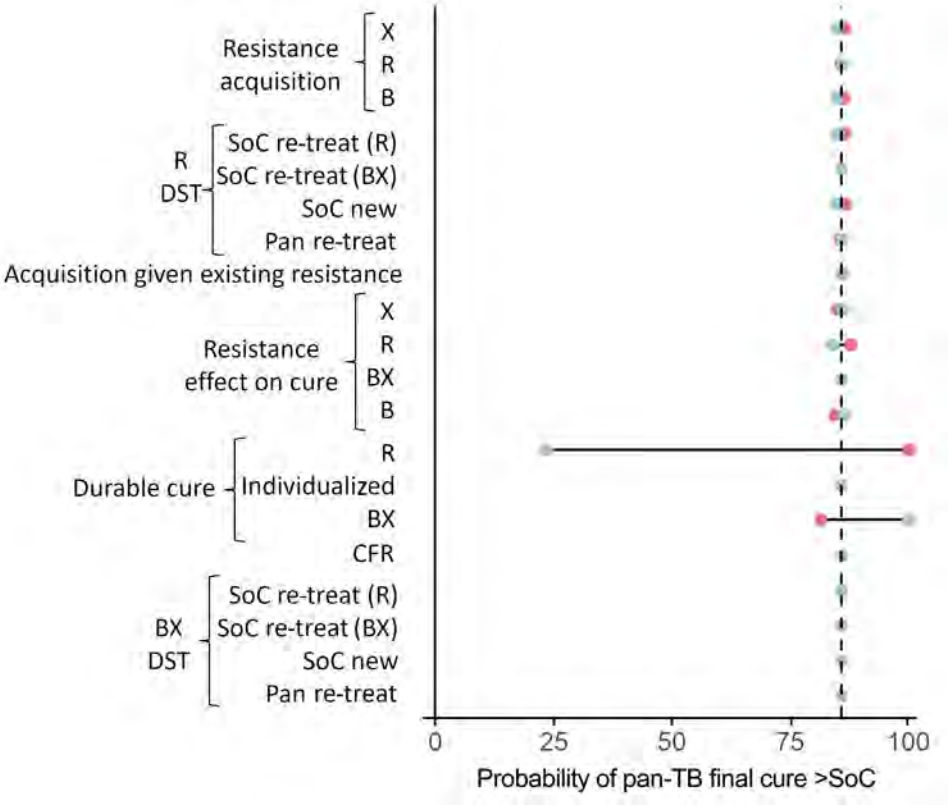

Figure 3. Univariate sensitivity analysis for initial TB treatment regimen comparison in study of potential of pan-TB treatment to drive emergence of novel resistance. Parameter sets are sampled with 1 parameter fixed at the extremes of its 95% CI. The outcome is the proportion of samples that result in more patients durably cured in the pan-TB scenario than the SoC scenario, within the first cohort of patients treated, and at current prevalence of resistance. Blue circles indicate use of upper bound of the parameter's 95% CI; red circles indicate the lower bound. B, diarylquinolines; BX, diarylquinoline- and novel drug X–containing regimen; CFR, case-fatality ratio; DST, drug-susceptibility testing; R, rifamycins; re-treat, patients with previously treated TB; SoC, standard of care; X, additional novel drug X.

the pan-TB scenario, such that by the 10th generation, only 61.0% (95% CI 42.3%–79.7%) of patients had no drug resistance under the pan-TB scenario, compared with 76.7% (95% CI 67.3%–86.0%) under the standard of care. However, those are proportion-based results and do not show changes in absolute TB incidence or drug-resistant TB incidence that may result from improved regimens.

The drug resistance that initially emerged under the pan-TB scenario was primarily B or X mono-resistance (mirroring the continued selection of R resistance in the standard-of-care scenario), but over time, with DST-free use of the pan-TB regimen, simultaneous resistance to both B and X became more common (30.8% [95% CI 12.6%–48.9%] of all TB cases after 10 cohorts of treatment) (Figure 2). We examined the routes by which patients with different resistance phenotypes arrive at their final treatment outcomes (Appendix Figure 2).

Performance of Pan-TB versus Standard of Care

For a single cohort of patients, when sampling our uncertainty distributions for all parameters (including initial prevalences of resistance) simultaneously, pan-TB was highly (85.9%) likely to result in more patients cured than the standard of care (Figure 3). In univariate analysis (fixing 1 parameter at an extreme of its uncertainty range while varying all others), the probability of standard of care outperforming pan-TB was observed to depend most heavily on the relative effectiveness of the pan-TB regimen compared with the standard of care in achieving durable cure among patients with DS-TB. The outperformance of the pan-TB regimen compared with the standard of care, in an initial cohort of patients, was robust to variation in any single resistance-related parameter and to simultaneous variation in the prevalence of both R and B resistance (Appendix Figure 3); however, assuming a higher prevalence of B resistance increased the sensitivity to other uncertain parameters (Appendix Figure 4).

Pan-TB Viability over Time

In addition to modeling the treatment outcomes of a single cohort with current levels of initial drug resistance (Figure 3), we assessed how the effects of uncertain model parameters can compound over multiple generations of transmission and treatment by comparing multiple generations of the standard of care to multiple generations of the pan-TB approach for each sampled set of parameters (Figure 4). We estimated that the probability of pan-TB outperforming the standard of care in a patient cohort would drop to 38% within 10 generations (Figure 4, panel A) compared with 86% in the initial patient cohort (Figure 3).

In sensitivity analyses that propagated uncertainty through multiple patient cohorts, the comparison between regimen outcomes in later cohorts remained sensitive to the regimens' relative effectiveness for DS-TB, but resistance-related parameters also increased in importance. The probability that the pan-TB regimen remained superior to the standard of care after 10 generations could vary from 11% to 68% as a result of varying the per-treatment risk for acquired B resistance and from 22% to 48% when varying the effects of that B resistance on efficacy. The durability of the pan-TB approach was even more certain to be short when these 2 parameters were varied simultaneously (Figure 4, panel B), when the corresponding parameters for both B and novel drug X were varied simultaneously (Appendix Figure 5), or when the rate of acquisition of resistance to novel drugs was increased (by extending the upper bound of the 95% CIs to 8%, as has been reported among RR-TB cohorts treated with bedaquiline, for example [*13*,*24*], and under programmatic conditions for earlier regimens [*25*]) (Appendix Figure 6).

Emergence of Complex Resistance

The prevalence of concurrent, complex resistance both to R and to a novel drug (B, X, or both) increased at a similarly slow pace in both scenarios. The prevalence of complex resistance reached 6.0% (95% 2.3%–9.8%) of all TB in the 10th treatment generation of the pan-TB scenario and 5.9% (95% CI 2.9%–9.0%) in the 10th generation under the standard of care (Figure 5, panel A). These trends in complex resistance were largely unaffected by the availability of R DST and B or X DST for retreatment patients in the pan-TB scenario (Appendix Figure 7). The pan-TB scenario led to a higher prevalence of complex resistance than the standard of care when the acquisition rate of resistance to novel drugs was low (such that much of the B resistance reflected selection among RR-TB before introduction of the pan-TB regimen) and the effect of that resistance on cure was high (Figure 5, panel B; Appendix Figure 8).

Discussion

Assuming that a pan-TB regimen was similarly efficacious against pan-susceptible TB as the current rifampin-susceptible TB regimen (leading to noninferiority under optimal trial conditions) and also had a shorter duration and improved adherence (resulting in high effectiveness under real-world conditions), we found that the pan-TB approach was very

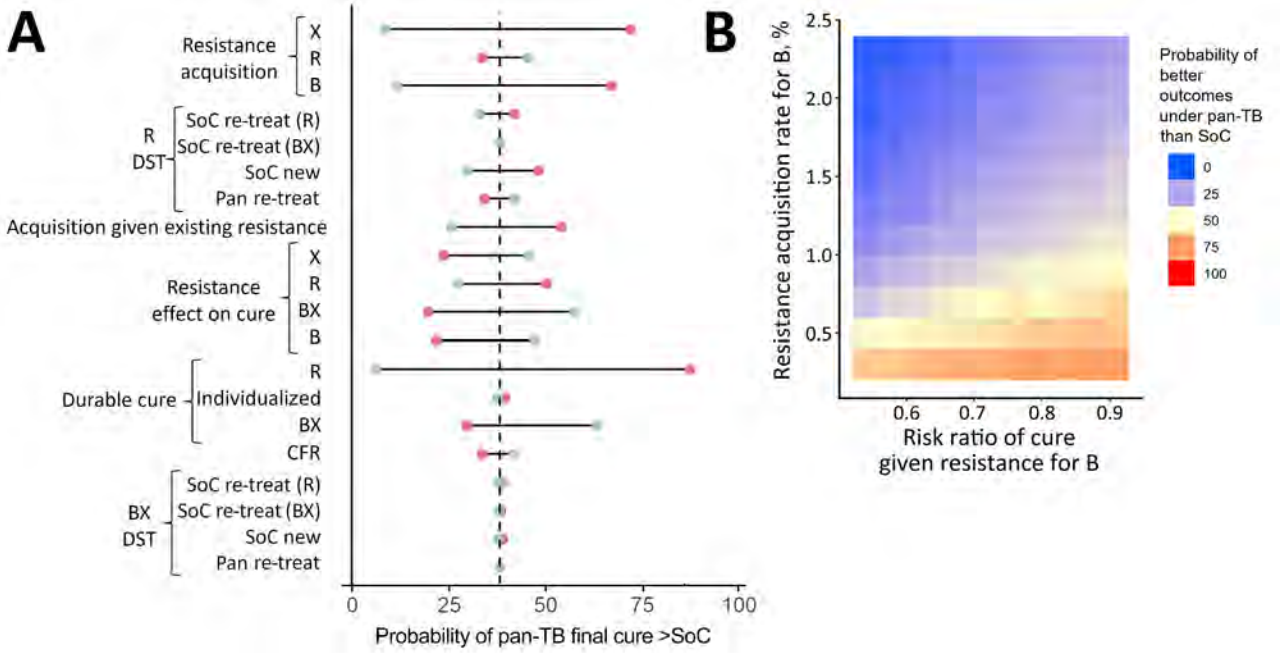

Figure 4. Sensitivity analysis for TB treatment regimen comparison after use in multiple patient cohorts in study of potential of pan-TB treatment to drive emergence of novel resistance. Comparison shows an outcome of proportion of patients durably cured in the 10th cohort when using either the pan-TB or the SoC approach for 10 cohorts. A) Univariate sensitivity analysis, sampling parameter sets with 1 parameter fixed at an extreme of its 95% CI, where blue circles indicate high parameter values and red circles low parameter values. B) Multivariate sensitivity analysis varying 2 resistance-related parameters simultaneously, where red indicates when pan-TB TB regimen performs better and blue when SoC regimen performs better. B, diarylquinolines; BX, diarylquinoline- and novel drug X–containing regimen; CFR, case-fatality ratio; DST, drug susceptibility testing; R, rifamycins; re-treat, those with previously treated TB; SoC, standard of care; X, additional novel drug X.

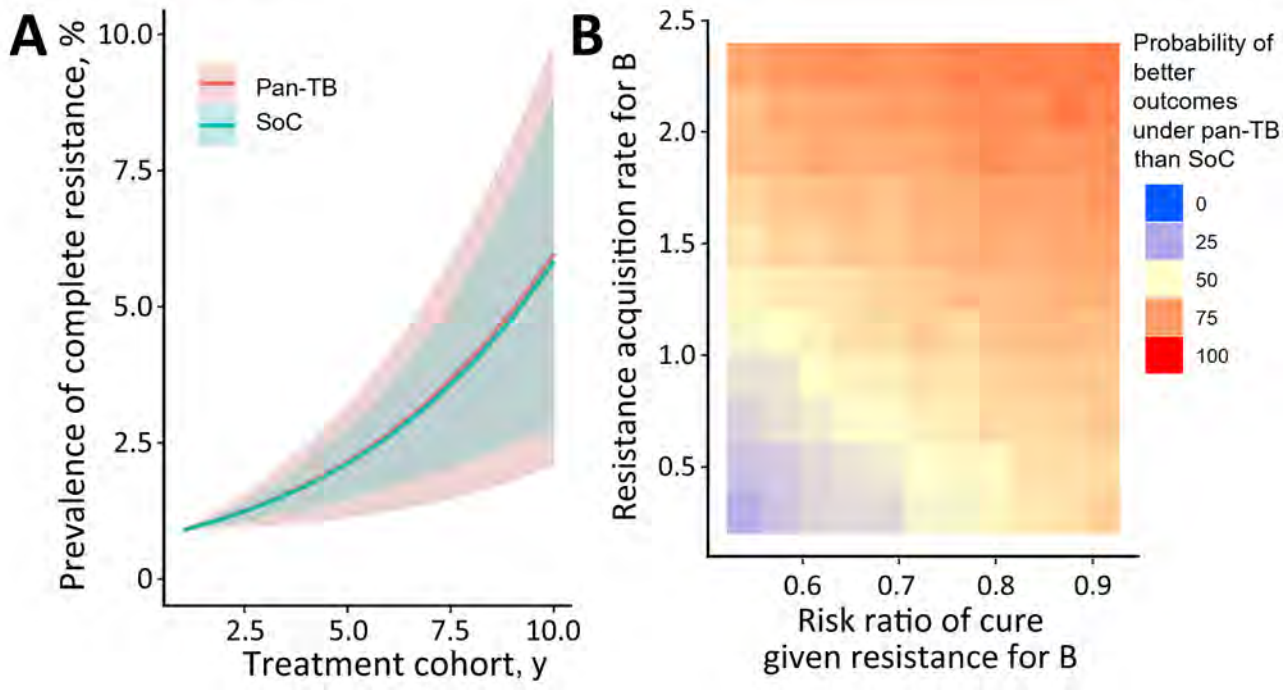

Figure 5. Prevalence of complex resistance to both R and a pan-TB treatment regimen component (B, X, or both) resulting from the pan-TB compared with standard-of-care scenario in study of potential of pan-TB treatment to drive emergence of novel resistance. A) Prevalence over treatment generations; B) probability that the pan-TB scenario leads to higher prevalence of complex resistance as a proportion of all TB after 10 cohorts. Red indicates when pan-TB regimen performs better (<50% probability of higher prevalence of complex resistance) and blue when SoC regimen performs better. B, diarylquinolines; SoC, standard of care; TB, tuberculosis.

likely to outperform the standard of care when initially introduced, even with high levels of bedaquiline resistance in the population. As resistance to the pan-TB regimen accumulated (including resistance to multiple component novel drugs), the probability of outperformance declined rapidly. Still, the pan-TB approach was unlikely to cause accumulation of concurrent resistance to both novel and current drugs.

Our results affirm that introduction of a pan-TB regimen meeting current regimen-development targets is highly likely to initially improve population-wide treatment outcomes, primarily as a result of improved outcomes for patients with DS-TB. However, our results also demonstrate the likelihood that, after several cycles of transmission, continued use of a single pan-TB regimen will no longer be viable because of emerging resistance, including resistance to multiple components of the pan-TB regimen. Some combination of regimen improvements and DST reintroduction would be needed to maintain the improved health outcomes that the pan-TB regimen had initially offered. Given a pipeline of more potent diarylquinolines and novel drug classes (4), updating a pan-TB regimen to counteract this decline might be possible; however, further work is needed to compare the timescales of this emergence of resistance to those of regimen development and TB elimination and to understand the most effective responses to emerging resistance and their optimal timing.

Another potential concern about using novel drugs such as bedaquiline in all patients is that the broader population scale of acquired resistance might leave many patients without effective treatment options. We did not identify any clinical pathways by which this scenario was likely to occur. In our model, RR-TB was treated similarly in both scenarios (dependent on DST coverage) and showed high enough rates of durable cure to cause preexisting RR-TB to decrease over time in the pan-TB scenario. Meanwhile, although we modeled retreatment with a rifamycin-based regimen for a substantial proportion of RS-TB cases that were not cured with initial pan-TB regimen treatment (some of which had resistance to B, X, or both), we projected similar levels of complex resistance with this approach as with continued use of a rifamycin-based first-line regimen followed by use of novel drugs after selection of rifampin resistance. This finding suggests that, even as resistance accumulated to components of a pan-TB regimen, most patients for whom the pan-TB regimen was ineffective would (once identified by DST) have existing rifamycin-based regimens as back-ups.

In reality, many of the characteristics of future pan-TB regimens are unknown. Although the pan-TB target regimen profile seeks to improve regimen duration, tolerability, and pharmacologic forgiveness, the effects of those improvements on adherence and ultimately effectiveness may be unpredictable and setting-dependent. Our model suggests that if the difference in effectiveness is small between a pan-TB regimen and the rifamycin-based alternative for treating RS-TB, then the health advantages of the pan-TB regimen will be smaller and contingent on maintaining a low prevalence of resistance to drugs in the pan-TB regimen. Moreover, even for a pan-TB regimen much more effective than the standard of care, unfavorable resistance-related regimen characteristics could eventually threaten that effectiveness. For a pan-TB regimen to continue to achieve high rates of cure in the long term, it needs to be constructed to guard against acquisition of resistance to all of its components or to ensure that regimen efficacy remains high in the presence of any forms of resistance that are likely to emerge.

Our results are limited by a lack of data on elements of the pan-TB regimen, in particular around the acquisition and effect of resistance. Those data are limited for current novel drugs such as bedaquiline and are based entirely on assumptions for other drugs that may compose future pan-TB regimens. We also approximated as zero the probability of acquiring resistance to multiple regimen components during 1 treatment course; however, there may be scenarios in which multiple drugs share resistance pathways and simultaneous acquisition is common. Further, our approach could be improved by the use of a transmission model, both for estimating the timescales of temporal trends and for estimating changes in absolute TB incidence as a result of more effective regimens. Our focus on cycles of transmission and proportions of patients with resistance could have led to an overestimate in the absolute prevalence of resistance generated by the pan-TB regimen, given that we did not fully account for reductions in transmission or potential disproportionate removal of DS-TB because of successful cure. Furthermore, our results are based on target regimen profiles, which assume that pan-TB regimens will be more effective than existing DS-TB regimens. We assume that if such regimens were available, they would be used at a minimum for patients with RR-TB, which leads to the counterintuitive standard-of-care scenario, where treatment outcomes for patients with RR-TB are better than for those with DS-TB.

Overall, we found that a pan-TB regimen adhering to the current target regimen profile is unlikely to drive an increase in complex resistance to both novel and older TB drugs. However, pan-TB regimens that are associated with both frequent acquisition of resistance and large associated reductions in efficacy, as well as pan-TB regimens that only marginally outperform the existing standard of care when introduced, could have short-lived viability as pan-TB regimens, requiring either regimen replacement or reintroduction of DST to maintain the improved health outcomes that a pan-TB regimen would initially offer. As new regimens are scaled up, TB programs will need to ensure effective support for adherence and regimen completion, implement systems to identify and effectively treat patients who experience treatment failure or TB recurrence and conduct ongoing surveillance to track any rise in resistance to the new regimens.

C.F.M., T.S.R., and E.A.K. were funded for this work by the Bill and Melinda Gates Foundation (project no. INV-059518). C.F.M. was funded for other work by the Bill and Melinda Gates Foundation (grant no. TB MAC OPP1135288), the US National Institutes of Health (grant no. R-202309-71190), and Unitaid (grant no. 20193–3-ASCENT). T.S.R. reports other relevant funding from the World Health Organization. R.G.W. was funded for other work by the Wellcome Trust (grant no. 218261/Z/19/Z), the US National Institutes of Health (grant no. 1R01AI147321-01), the European and Developing Countries Clinical Trials Partnership (grant no. RIA208D-2505B), the UK Medical Research Council (grant CCF 17-7779 through the Bloomsbury SET [Science, Economics, Technology] Knowledge Exchange), the UK Economic and Social Research Council (grant no. ES/P008011/1), the Bill and Melinda Gates Foundation (grant nos. OPP1084276, OPP1135288, and INV-001754), and WHO. The funders had no role in the decision to submit the paper for publication. All authors declare no conflicts of interest.

Model code is available at https://github.com/cfmcquaid/panTB_acquisition.

Author contributions: C.F.M., T.S.R., T.C., N.A.M., and E.A.K. conceived and designed the study. C.F.M. did the modelling. C.F.M. and E.A.K. wrote a first draft of the article. All authors designed the methodology, critiqued the results, and contributed to editing the final draft.

References

1. World Health Organization. Global tuberculosis report 2023. 2023 [cited 2024 Apr 12]. https://www.who.int/teams/global-tuberculosis-programme/tb-reports/global-tuberculosis-report-2023
2. Nyang'wa BT, Berry C, Kazounis E, Motta I, Parpieva N, Tigay Z, et al.; TB-PRACTECAL team. Short oral regimens for pulmonary rifampicin-resistant tuberculosis

(TB-PRACTECAL): an open-label, randomised, controlled, phase 2B-3, multi-arm, multicentre, non-inferiority trial. Lancet Respir Med. 2024;12:117–28. https://doi.org/10.1016/S2213-2600(23)00389-2
3. Nuermberger EL, Chaisson RE. Restocking the tuberculosis drug arsenal. Nat Med. 2024;30:642–3. https://doi.org/10.1038/s41591-024-02840-y
4. Treatment Action Group. Pipeline report 2023: tuberculosis treatment. 2023 [cited 2024 Apr 12]. https://www.treatmentactiongroup.org/wp-content/uploads/2024/03/pipeline_TB_Treatment_2023_final.pdf
5. World Health Organization. Target regimen profiles for tuberculosis treatment, 2023 update. 2023 [cited 2024 Apr 14]. https://www.who.int/publications/i/item/9789240081512
6. Arinaminpathy N, Gomez GB, Sachdeva KS, Rao R, Parmar M, Nair SA, et al. The potential deployment of a pan-tuberculosis drug regimen in India: a modelling analysis. PLoS One. 2020;15:e0230808. https://doi.org/10.1371/journal.pone.0230808
7. Saluzzo F, Maria Cirillo D. Mind the gap. Rolling out new drug resistant tuberculosis regimens with limited diagnostic tools. J Clin Tuberc Other Mycobact Dis. 2023;32:100350. https://doi.org/10.1016/j.jctube.2023.100350
8. Conradie F, Bagdasaryan TR, Borisov S, Howell P, Mikiashvili L, Ngubane N, et al.; ZeNix Trial Team. Bedaquiline-pretomanid-linezolid regimens for drug-resistant tuberculosis. N Engl J Med. 2022;387:810–23. https://doi.org/10.1056/NEJMoa2119430
9. Nyang'wa BT, Berry C, Kazounis E, Motta I, Parpieva N, Tigay Z, et al.; TB-PRACTECAL Study Collaborators. A 24-week, all-oral regimen for rifampin-resistant tuberculosis. N Engl J Med. 2022;387:2331–43. https://doi.org/10.1056/NEJMoa2117166
10. Foundation for the National Institutes of Health. PAN-TB, Project to Accelerate New Treatments for Tuberculosis. 2023 [cited 2024 Apr 11]. https://fnih.org/our-programs/pan-tb-project-to-accelerate-new-treatments-for-tuberculosis
11. TB Alliance. TB Alliance launches five-country phase 2 clinical trial evaluating next-generation tb drug. 2023 [cited 2024 Apr 11]. https://www.tballiance.org/news/tb-alliance-launches-five-country-phase-2-clinical-trial-evaluating-next-generation-tb-drug-0#:~:text=%E2%80%9CA%20'universal'%20TB%20medicine,and%20CEO%20of%20TB%20Alliance
12. Derendinger B, Dippenaar A, de Vos M, Huo S, Alberts R, Tadokera R, et al. Bedaquiline resistance in patients with drug-resistant tuberculosis in Cape Town, South Africa: a retrospective longitudinal cohort study. Lancet Microbe. 2023;4:e972–82. https://doi.org/10.1016/S2666-5247(23)00172-6
13. World Health Organization. WHO consolidated guidelines on tuberculosis. Module 4: treatment— drug-resistant tuberculosis treatment, 2022 update [cited 2024 Apr 8]. https://www.who.int/publications/i/item/9789240063129
14. Ryckman TS, Schumacher SG, Lienhardt C, Sweeney S, Dowdy DW, Mirzayev F, et al. Economic implications of novel regimens for tuberculosis treatment in three high-burden countries: a modelling analysis. Lancet Glob Health. 2024;12:e995–1004. https://doi.org/10.1016/S2214-109X(24)00088-3
15. Borgdorff MW, Sebek M, Geskus RB, Kremer K, Kalisvaart N, van Soolingen D. The incubation period distribution of tuberculosis estimated with a molecular epidemiological approach. Int J Epidemiol. 2011;40:964–70. https://doi.org/10.1093/ije/dyr058
16. Law I, Floyd K, African TB; African TB Prevalence Survey Group. National tuberculosis prevalence surveys in Africa, 2008–2016: an overview of results and lessons learned. Trop Med Int Health. 2020;25:1308–27. https://doi.org/10.1111/tmi.13485
17. Onozaki I, Law I, Sismanidis C, Zignol M, Glaziou P, Floyd K. National tuberculosis prevalence surveys in Asia, 1990–2012: an overview of results and lessons learned. Trop Med Int Health. 2015;20:1128–45. https://doi.org/10.1111/tmi.12534
18. Horton KC, Richards AS, Emery JC, Esmail H, Houben RMGJ. Reevaluating progression and pathways following *Mycobacterium tuberculosis* infection within the spectrum of tuberculosis. Proc Natl Acad Sci U S A. 2023;120:e2221186120. https://doi.org/10.1073/pnas.2221186120
19. Ismail NA, Aono A, Borroni E, Cirillo DM, Desmaretz C, Hasan R, et al. A multimethod, multicountry evaluation of breakpoints for bedaquiline resistance determination. Antimicrob Agents Chemother. 2020;64:e00479–20. https://doi.org/10.1128/AAC.00479-20
20. Liu Y, Gao M, Du J, Wang L, Gao J, Shu W, et al. Reduced susceptibility of *Mycobacterium tuberculosis* to bedaquiline during antituberculosis treatment and its correlation with clinical outcomes in China. Clin Infect Dis. 2021;73:e3391–7. https://doi.org/10.1093/cid/ciaa1002
21. Perumal R, Bionghi N, Nimmo C, Letsoalo M, Cummings MJ, Hopson M, et al. Baseline and treatment-emergent bedaquiline resistance in drug-resistant tuberculosis: a systematic review and meta-analysis. Eur Respir J. 2023;62:2300639. https://doi.org/10.1183/13993003.00639-2023
22. Timm J, Bateson A, Solanki P, Paleckyte A, Witney AA, Rofael SAD, et al. Baseline and acquired resistance to bedaquiline, linezolid and pretomanid, and impact on treatment outcomes in four tuberculosis clinical trials containing pretomanid. PLOS Glob Public Health. 2023;3:e0002283. https://doi.org/10.1371/journal.pgph.0002283
23. Li S, Tan Y, Deng Y, Bai G, Huang M, Shang Y, et al. The emerging threat of fluroquinolone-, bedaquiline-, and linezolid-resistant *Mycobacterium tuberculosis* in China: observations on surveillance data. J Infect Public Health. 2024;17:137–42. https://doi.org/10.1016/j.jiph.2023.11.018
24. Chesov E, Chesov D, Maurer FP, Andres S, Utpatel C, Barilar I, et al. Emergence of bedaquiline resistance in a high tuberculosis burden country. Eur Respir J. 2022;59:2100621. https://doi.org/10.1183/13993003.00621-2021
25. Cegielski JP, Dalton T, Yagui M, Wattanaamornkiet W, Volchenkov GV, Via LE, et al.; Global Preserving Effective TB Treatment Study (PETTS) Investigators. Extensive drug resistance acquired during treatment of multidrug-resistant tuberculosis. Clin Infect Dis. 2014;59:1049–63. https://doi.org/10.1093/cid/ciu572

Address for correspondence: C. Finn McQuaid, London School of Hygiene and Tropical Medicine, Keppel St, London WC1E 7HT, UK; email: finn.mcquaid@lshtm.ac.uk

Wastewater Surveillance to Confirm Differences in Influenza A Infection between Michigan, USA, and Ontario, Canada, September 2022–March 2023

Ryland Corchis-Scott, Mackenzie Beach, Qiudi Geng, Ana Podadera, Owen Corchis-Scott, John Norton, Andrea Busch, Russell A. Faust, Stacey McFarlane, Scott Withington, Bridget Irwin, Mehdi Aloosh, Kenneth K.S. Ng, R. Michael McKay

Wastewater surveillance is an effective way to track the prevalence of infectious agents within a community and, potentially, the spread of pathogens between jurisdictions. We conducted a retrospective wastewater surveillance study of the 2022–23 influenza season in 2 communities, Detroit, Michigan, USA, and Windsor-Essex, Ontario, Canada, that form North America's largest cross-border conurbation. We observed a positive relationship between influenza-related hospitalizations and the influenza A virus (IAV) wastewater signal in Windsor-Essex ($\rho = 0.785$; $p<0.001$) and an association between influenza-related hospitalizations in Michigan and the IAV wastewater signal for Detroit ($\rho = 0.769$; $p<0.001$). Time-lagged cross correlation and qualitative examination of wastewater signal in the monitored sewersheds showed the peak of the IAV season in Detroit was delayed behind Windsor-Essex by 3 weeks. Wastewater surveillance for IAV reflects regional differences in infection dynamics which may be influenced by many factors, including the timing of vaccine administration between jurisdictions.

The SARS-CoV-2 pandemic reasserted the importance of epidemic preparedness and surveillance systems for infectious diseases (*1*). Informed responses to public health challenges require that data be available to decision-makers in a timely manner for early interventions (*1*). However, traditional clinical based measures of disease incidence have limited use in providing early warnings. Relying on influenza-like illness data is problematic because of difficulty distinguishing between infections ascribed to influenza A virus (IAV), influenza B virus, SARS-CoV-2, or respiratory syncytial virus (*2*). Virologic surveillance enables respiratory illness to be classified on the basis of etiologic agent. However, results are often slow, and interpretation must account for factors such as test-seeking behavior, accessibility of healthcare services, severity of infection, diagnostic practices of healthcare providers, and hospital protocols. In addition, laboratory capacity may be exceeded, and testing is expensive (*3*,*4*).

Wastewater surveillance (WS) is shown to be a practical approach for disease surveillance at various spatial scales, offering effectiveness and economic advantage (*5*,*6*). WS for SARS-CoV-2 relies on quantifying viral RNA shed in feces and has substantially increased in use since its implementation to track infections during the COVID-19 pandemic. Studies have found the concentration of SARS-CoV-2 RNA in municipal sewage covaries with the levels of disease circulating within the community served and can predict trends in clinical cases and hospitalizations (*7*,*8*). In addition, WS has the potential to be rapid; sample

Author affiliations: University of Windsor, Windsor, Ontario, Canada (R. Corchis-Scott, M. Beach, Q. Geng, A. Podadera, O. Corchis-Scott, K.K.S. Ng, R.M. McKay); Great Lakes Water Authority, Detroit, Michigan, USA (J. Norton, A. Busch); Oakland County Health Division, Oakland, Michigan, USA (R.A. Faust); Macomb County Health Department, Macomb, Michigan, USA (S. McFarlane); Detroit Health Department, Detroit (S. Withington);Windsor-Essex County Health Unit, Windsor (B. Irwin, M. Aloosh); McMaster University, Hamilton, Ontario (M. Aloosh)

DOI: https://doi.org/10.3201/eid3008.240225

processing, measurement, analysis, and dissemination of results took <6 hours in Windsor-Essex, Ontario, Canada. Calls have been made to expand the scope of WS to include monitoring of IAV and other endemic respiratory pathogens that are underreported (*9*,*10*). Similar to SARS-CoV-2, IAV can be shed in feces (*11*), and recent studies have used WS to track IAV (*12*–*14*). However, more work needs to be done to validate WS compared with traditional surveillance metrics. WS can be useful in measuring regional differences in infection dynamics and understanding how IAV and other pathogens spread across jurisdictional boundaries.

The Detroit-Windsor metropolitan area, encompassing the cities of Detroit, Michigan USA, and Windsor-Essex, Ontario, Canada, is North America's largest transborder conurbation and is the busiest cross-border region for trade between the United States and Canada, handling 42% of commercial traffic between Ontario and Michigan and accounting for ≈25% of total daily commercial traffic between the United States and Canada (*15*). The region is a major entry point for visitors, including >5,000 commuters from Windsor-Essex who cross the border daily for work (*15*,*16*). Detroit and Windsor-Essex represent government structures and public health jurisdictions that adopted fundamentally different vaccination and mitigation strategies during the COVID-19 pandemic. The cessation of COVID-19 pandemic mitigation strategies, such as masking and social distancing, affected the circulation of respiratory pathogens other than SARS-CoV-2, such as IAV. The end of those mitigation strategies resulted in a delayed start to the 2021–22 influenza season in Windsor-Essex, which coincided with the removal of mask mandates in Ontario in March 2022, and may have had a role in unusual patterns of influenza incidence during the 2022–23 influenza season in Canada (*17*,*18*). Similarly, the 2021–22 influenza season in Michigan was mild, with an increase in influenza activity observed in November, followed by a decline in January 2022 and a subsequent rise in activity in March 2022. Trends in Michigan were similar to national trends; levels of influenza activity remained elevated through mid-June 2022 (*19*,*20*). Those unusual patterns of influenza prompted this retrospective investigation comparing the incidence of influenza in Windsor-Essex with the incidence of influenza in Detroit. Our goal is to understand how jurisdictional differences in pandemic mitigation strategies and public health policy influenced the timing of influenza seasons.

The initial investigation into influenza hospitalization data for Windsor-Essex and Michigan through a visual inspection of the data showed a delay in the onset and peak of the 2022–23 influenza season in Michigan compared with Windsor-Essex. Because influenza incidence data (including hospitalizations) specific to Detroit are not publicly available and influenza is an underreported disease, the trend observed through examination of clinical data may not be sufficient to claim a delayed onset in the influenza season. Because WS is based on the aggregated waste of an entire community, it is anonymous and reflects population level trends that could produce a more sensitive and non-biased measure of influenza incidence to confirm trends in clinical data. Analysis of WS data, coupled with traditional measures of disease incidence, will enable a more complete understanding of how differences in public health approaches in a divided, yet contiguous, metropolitan area influenced the trajectory of the influenza season after COVID-19 mitigation policy removal.

Methods

Sample Collection

During September 1, 2022–March 31, 2023, we collected composite (24-h) wastewater samples 3–5 days/week from 2 different wastewater treatment plants that serve a resident population of ≈270,000 persons, ≈50% of the regional population, located in Windsor-Essex. In parallel, we collected composite samples 1 day/week from the 3 interceptors terminating at the Water Resource Recovery Facility (WRRF) operated by the Great Lakes Water Authority (GLWA), located in Detroit (*21*) (Appendix, https://wwwnc.cdc.gov/EID/article/30/8/24-0225-App1.pdf). The WRRF serves the entire city of Detroit and treats the waste of ≈3 million people, 88% of the residents in the greater Detroit metropolitan area and approximately one third the population of Michigan (*22*).

Sample Processing

We concentrated composite samples of raw wastewater by using filtration, then extracted RNA from the filters (Appendix). We used quantitative reverse transcription PCR (qRT-PCR) to measure the concentration of IAV in wastewater samples (Appendix). The assay targeted RNA coding for the matrix protein 1 (M1) of IAV by using primers and probes developed by the Centers for Disease Control and Prevention (*23*). We used a synthetic influenza H3N2 RNA (Twist Bioscience, https://www.twistbioscience.com) as a standard for comparison. We conducted qRT-PCR to measure the levels of pepper mild mottle virus (PMMoV) within the wastewater (Appendix); PMMoV

can indicate the presence of human fecal matter and is used to account for variability in wastewater flow or other physicochemical parameters influencing viral RNA concentration (*24*). We sequenced select IAV amplicons produced through qRT-PCR of RNA extracted from wastewater to validate the identity of the target (Appendix).

Clinical Data

We obtained influenza hospitalization data for Windsor-Essex through collaboration with the Windsor-Essex County health unit. Using IntelliHealth (https://intellihealth.moh.gov.on.ca) on April 17, 2024, we extracted data from the discharge abstract database and included hospitalization data from September 2022–March 2023. Influenza hospitalizations included hospital admissions where the main diagnoses had a code of J09, J100, J101, J108, J110, J111, or J118 from the International Classification of Diseases, 10th Revision. Windsor-Essex hospitalization data captured all local hospitalizations and included hospitalizations among all residents of Windsor-Essex County, regardless of where the hospitalization occurred. We aggregated influenza hospitalizations by epidemiologic week of initial admission and used hospitalizations per 100,000 persons in subsequent analysis.

We collected influenza-related hospitalization data for Michigan from the Centers for Disease Control and Prevention's influenza hospitalization surveillance network (FluSurv-NET), which records laboratory-confirmed influenza-associated hospitalizations during the influenza season as cases per 100,000 persons. We defined influenza-related hospitalization rates as the number of hospitalized persons who tested positive for influenza, of any subtype, through laboratory testing within the 14 days before or during hospitalization (*25*). Hospitalization data were available beginning in October 2022. Although hospitalization data were only available for Clinton, Eaton, Genesee, Ingham, and Washtenaw counties, those data are considered a statewide assessment of influenza for Michigan. Because the WRRF serves approximately one third of the state population, influenza-related hospitalization trends are likely to be reflected in IAV RNA concentrations at the WRRF.

Data Analysis and Visualization

We used R version 4.3.2 (The R Foundation for Statistical Computing, https://www.r-project.org) for data analysis, including the calculations of Kendall rank correlation coefficient (τ), Spearman rank correlation coefficient (ρ), nonparametric measures of correlation, and nonparametric time lagged cross correlation (TLCC) by using the ccf_boot function in the R package funtimes (Functions for Time Series Analysis, https://cran.r-project.org/web/packages/funtimes). We used Veusz version 3.6.2 (https://veusz.github.io) for data visualization. By using a population-weighted mean, we combined IAV and PMMoV RNA concentration measurements from Windsor-Essex wastewater treatment facilities. We then used downsampling through blockwise averaging to condense the data into a single measurement for each epidemiologic week; this process produced equally spaced data and enabled comparison with hospitalization data available in weekly reports (*26*). Blockwise averaging was not possible for IAV and PMMoV RNA concentration measurements of samples collected from the GLWA-WRRF because samples were collected weekly. No samples were collected from GLWA-WRRF interceptors during epidemiologic week 40 (October 2–8, 2022) and 48 (November 27–December 3, 2022). We filled in the data from epidemiologic weeks 40 and 48 by using linear interpolation before analysis. We used a population-weighted mean to combine the IAV and PMMoV signal for the 3 interceptors that discharge to the GLWA-WRRF, which produced 31 measurements of IAV RNA and 31 measurements of PMMoV RNA concentration for Detroit. All gene concentrations are reported as gene copies (gc) per liter. We produced normalized values for the IAV signal by taking the ratio of IAV M1 gene concentration to the concentration of PMMoV.

We used TLCC with Spearman rank correlations to determine if IAV wastewater signals were leading or lagging indicators of influenza-associated hospitalizations in Windsor-Essex and Michigan. TLCC relies on correlations between data series shifted relative to each other in time and can identify peak synchrony. We determined peak synchrony by the shift that produced the highest Spearman rank correlation coefficient between the 2 timeseries. We also used TLCC to compare the IAV wastewater signal in Windsor-Essex to the IAV wastewater signal in Detroit. We verified the nonnormal data by examining the quantile-quantile plots. We used nonparametric means of correlation, including Kendall rank correlation coefficient and Spearman rank correlation coefficient, to quantify the association between the IAV signal in the wastewater and influenza hospitalizations in both Windsor and Detroit. Correlations between influenza-related hospitalizations and wastewater signal in Detroit were based on 26 weeks of data because hospitalization data were not available until October 2022.

Results

IAV M1 Gene Concentrations in Windsor-Essex

Trends in IAV M1 gene concentrations at the monitored plants visually matched trends in influenza-associated hospitalizations in Windsor-Essex for September 2022–March 2023 (Figure). The TLCC for Windsor-Essex showed that wastewater signal lagged new hospital admissions on an epidemiologic week basis (Table 1) and therefore did not provide lead-time. We observed a strong positive relationship between influenza-associated hospitalizations and the population-weighted mean IAV M1 gene concentration ($\tau = 0.650$, $p<0.001$; $\rho = 0.785$, $p<0.001$) (Table 2). Signal normalization with PMMoV RNA concentrations did not improve the association between wastewater signal and influenza-associated hospitalizations ($\tau = 0.754$, $p<0.001$; $\rho = 0.630$, $p<0.001$) or change peak synchrony (Tables 1, 2).

IAV M1 Gene Concentrations in Detroit

IAV M1 gene concentrations for metro Detroit closely matched the number of new influenza-related hospitalizations in Michigan from October 2022–March 2023 (Figure). We observed a strong positive relationship between influenza-related hospitalizations and the population-weighted mean IAV M1 gene concentration for Detroit ($\tau = 0.616$, $p<0.001$; $\rho = 0.769$, $p<0.001$) (Table 3). The nonparametric TLCC results showed the IAV wastewater signal from Detroit neither lagged nor led influenza-related hospitalizations in the state of Michigan, suggesting the IAV wastewater signal is concordant with influenza-related hospitalizations (Table 1; Figure). Normalization of IAV M1 gene concentrations with PMMoV RNA concentrations did not change the degree of association between the wastewater signal and influenza-related hospitalizations for Michigan ($\tau = 0.559$, $p<0.001$; $\rho = 0.708$, $p<0.001$) or change peak synchrony (Tables 1, 3).

Cross-Border Comparison of WS for IAV

The onset and peak of the 2022–23 IAV wastewater signal in Windsor-Essex was observed before the onset and peak of the IAV wastewater signal in Detroit (Figure). TLCC using Spearman rank correlations between the population-weighted weekly average of M1 gene concentrations in Detroit and Windsor-Essex showed the 2022–23 IAV wastewater signal in Detroit lagged the corresponding IAV wastewater signal in Windsor by ≈3 weeks (Table 1). Further comparison by using PMMoV-normalized, population-weighted, weekly averages of the wastewater signal corroborated the lag of ≈3 weeks between Windsor-Essex and Detroit (Table 1).

Discussion

Our study builds on a growing body of evidence that WS for IAV is highly concordant with the results of other disease incidence measures (*13*,*28*). During the 31-week period of retrospective analysis, influenza-related hospitalizations within Windsor-Essex and Michigan covaried with the concentration of IAV RNA measured in wastewater. However, the IAV signal was not a leading indicator of influenza incidence in

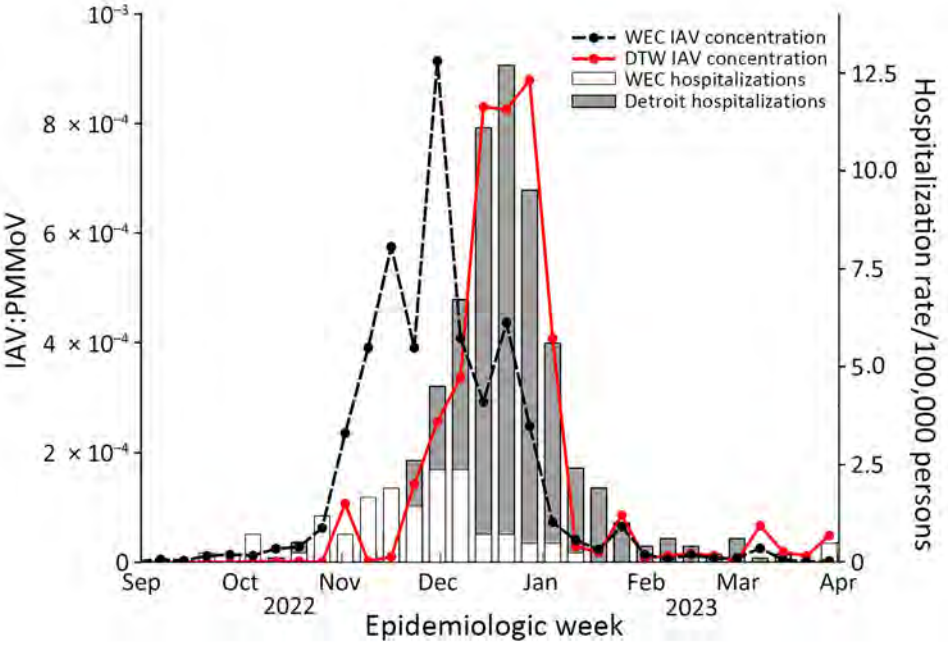

Figure. Influenza-associated hospitalization rates and aggregate population-weighted wastewater concentrations for influenza A virus, by epidemiologic week, in Windsor-Essex, Ontario, Canada, and Detroit, Michigan, USA, September 2022–March 2023. The population-weighted PMMoV normalized IAV concentration (lines) is superimposed over the rate of influenza-related hospitalizations (bars). DTW, Detroit wastewater; IAV, influenza A virus; PMMoV, pepper mild mottle virus; WEC, Windsor-Essex County wastewater.

Table 1. Temporal shift at which peak synchrony was found between concentrations of influenza A in wastewater and influenza-associated hospitalizations for Windsor-Essex, Ontario, Canada (September 2022–March 2023), and Detroit, Michigan, USA (October 2022–March 2023)*

Associations†	Peak synchrony, wk	Spearman ρ
WEC M1:PMMoV and influenza-associated hospitalizations	1	0.797
WEC M1 and influenza-associated hospitalization	1	0.841
DTW M1:PMMoV and influenza-associated hospitalizations	0	0.708
DTW M1 and influenza-associated hospitalizations	0	0.769
WEC M1:PMMoV and DTW M1:PMMoV	−3	0.642
WEC M1 and DTW M1	−3	0.695

*Peak synchrony was also found between Windsor-Essex and Detroit influenza A wastewater signals during September 2022–March 2023. Wastewater signals were shifted, and clinical metrics remained stationary. Positive values indicate a lagging wastewater signal and negative values indicate a leading wastewater signal. DTW, Detroit wastewater; M1, matrix 1 gene: PMMoV, pepper mottle mild virus; WEC, Windor-Essex County wastewater.
†DTW M1, aggregate concentration of influenza A M1 gene (genome copies/mL) in DTW; DTW M1:PMMoV, concentration of influenza A M1 gene in DTW normalized to PMMoV (unitless); WEC M1, aggregate concentration of influenza A M1 gene in WEC (gc/L); WEC M1:PMMoV, concentration of influenza A M1 gene in WEC normalized to PMMoV concentration (unitless).

either community when analyzed on an epidemiologic week basis; wastewater signal either lagged or was synchronous with hospitalization data. Observation of synchronous or delayed wastewater signal is not without precedent. Recent surveillance efforts have noted lagging wastewater signals (*29*). Other studies have cited the predictive ability of WS in the context of influenza monitoring (*13*,*14*,*30*). In our study, application of blockwise averaging to produce average concentrations of IAV RNA by epidemiologic week could have masked lead time within the data.

Viral load in influenza patients may peak 1–2 days after symptom onset on the basis of nose and throat swab testing results, and shedding may last 6–7 days (*31*). A meta-analysis of challenge studies examining respiratory tract shedding found shedding lasts an average of 4.8 days, and peak shedding rates occur 2 days after exposure (*32*). A clinical study reported that 41% of IAV-positive patients produced detectable levels of IAV RNA in their feces (*11*). Another study of hospitalized patients found that 47% of people infected with IAV shed IAV RNA in their feces (*33*). Because only some people shed IAV RNA in feces, incubation periods are short, and viral loads rapidly peak, WS loses its ability to predict influenza-associated hospitalizations when the temporal granularity of incidence data is limited. However, producing meaningful data through clinical testing takes longer than results from WS. Case data obtained through laboratory-based virology are released weeks after testing occurs and are often subject to revision because results may reflect data compiled from multiple laboratories. WS can provide more timely measures of incidence because sample processing, RNA quantification, data analysis, and reporting are often completed the same day as sample collection in Windsor-Essex. WS can be considered de facto lead-time because data may be disseminated to public health officials well in advance of case data.

The utility of WS is not restricted to predictive ability. WS is an independent and sensitive measure of disease prevalence (*34*), enabling it to be used as an additional metric for trend comparison across jurisdictional boundaries, and it may be helpful when testing conventions and public health policies differ. Unlike WS, influenza cases and hospitalizations likely represent only the most severe cases of influenza in which people sought medical testing and treatment, and they do not necessarily represent population-wide trends. WS has the potential to aid in accurately tracking infection dynamics when testing capacity is limited or few patients seek medical care.

In the case of Windsor-Essex and Detroit, the cross-border movement of persons and goods is vital to the region because of strong economy integration (*35*). Many people, such as healthcare and automotive workers, commute across the border daily to work in Michigan while living in Ontario (*16*). Almost 18,000 people crossed into Windsor-Essex from Detroit daily over the course of our study, which suggests

Table 2. Unshifted correlations between influenza-associated hospitalizations and the aggregate population-weighted wastewater concentrations for influenza A virus in Windsor-Essex, Ontario, Canada, September 2022–March 2023*

Associations†	Statistical test results		2-tailed 95% CI‡	2-tailed p value
	Kendall τ	Spearman ρ		
WEC M1 and influenza-associated hospitalization	0.650		0.482–0.772	<0.001
WEC M1:PMMoV and influenza-associated hospitalizations	0.630		0.456–0.758	<0.001
WEC M1 and influenza-associated hospitalization		0.785	0.589–0. 893	<0.001
WEC M1:PMMoV and influenza-associated hospitalizations		0.754	0.538–0.877	<0.001

*M1, matrix 1 gene: PMMoV, pepper mottle mild virus; WEC, Windor-Essex County wastewater.
†WEC M1, aggregate concentration of influenza A M1 gene in WEC (gc/L); WEC M1:PMMoV, concentration of influenza A M1 gene in WEC normalized to PMMoV concentration (unitless).
‡Estimation is based on Fisher r-to-z transformation; estimation of SE is based on the formula proposed by Fieller, Hartley, and Pearson (*27*).

Table 3. Unshifted correlations between influenza-associated hospitalizations in Michigan, USA, and the aggregate population-weighted wastewater concentrations for influenza A virus in Detroit, MI, USA from October 2022–March 23*

Associations†	Statistical test results		2-tailed 95% CI‡		2-tailed p value
	Kendall τ	Spearman ρ			
DTW M1 and influenza-associated hospitalizations	0.616		0.415	0.759	<0.001
DTW M1:PMMoV and influenza-associated hospitalizations	0.559		0.341	0720	<0.001
DTW M1 and influenza-associated hospitalizations		0.769	0.535	0.893	<0.001
DTW M1:PMMoV and influenza-associated hospitalizations		0.708	0. 433	0.863	<0.001

*DTW, Detroit wastewater; M1, matrix 1 gene: PMMoV, pepper mottle mild virus.
†DTW M1, aggregate concentration of influenza A M1 gene (genome copies/mL) in DTW; DTW M1:PMMoV, concentration of influenza A M1 gene in DTW normalized to PMMoV (unitless).
‡Estimation is based on Fisher r-to-z transformation; estimation of SE is based on the formula proposed by Fieller, Hartley, and Pearson (*27*).

the communities could have concurrent influenza seasons (Appendix Figure 1). Contrary to this expectation, we observed the peak and onset of the 2022–23 IAV wastewater signal in Detroit was delayed by ≈3 weeks when compared with Windsor-Essex. An explanation for this discrepancy could be the lingering effect of travel restrictions implemented during the COVID-19 pandemic, which limited travel between these interconnected cities (Appendix Figure 1). There was no restriction on trade or the commutes of essential workers, and testing requirements for cross-border travel ended in April 2022. The remaining COVID-19 related travel restrictions were lifted at the start of October 2022, before the onset of the influenza season. Despite the removal of restrictions, the number of people crossing into Windsor-Essex each day during the second half of 2022 was ≈25% less than the number of people crossing prior to the COVID-19 pandemic (17,867 vs. 24,260) (Appendix Figure 2). The residual effect of border restrictions, evidenced by the suppressed cross-border traffic in the leadup to the 2022–23 respiratory season, shows that border restrictions could have played a role in the observed discrepancies between Windsor-Essex and Detroit.

Another potential cause of the timing difference in the influenza seasons between Detroit and Windsor-Essex could be pandemic mitigation strategies, such as mask mandates and social distancing guidance. Ontario was slower to implement a mask mandate but kept the mandate in place much longer than Michigan did. Michigan lifted all masking requirements on June 22, 2021, whereas Ontario ended its mask mandate 272 days later, on March 21, 2022 (*36*,*37*). Michigan ending the mask mandate early could have enabled the circulation of influenza in Detroit before the 2022–23 respiratory season, increasing levels of natural immunity in Michigan. However, clinical data and wastewater surveillance in Windsor-Essex show that influenza was circulating in Windsor-Essex in spring 2022 (Appendix Figure 3).

Differences in influenza immunization campaigns might also explain the differences in influenza season onset between Detroit and Windsor-Essex. Influenza vaccines could have played a role in determining the effective reproduction number for IAV in the 2022–23 season. Preliminary research showed the vaccine effectiveness (VE) in Canada against IAV subtype H3N2 was 54% for people <65 years of age (*17*). H3N2 was the dominant IAV subtype, representing ≈95% of cases (*17*), in contrast with the limited sequencing results of a selection of amplicons (Appendix Figure 4). Similar estimates of VE for this cohort were produced for Wisconsin (60%) (*38*) and across the United States (51%) (*39*). Michigan and Ontario use similar vaccines, with a focus on administering quadrivalent-inactivated influenza vaccines to the population (*40*,*41*). Although inoculation with some vaccine types, such as live attenuated vaccines, is associated with viral shedding, it is unlikely to contribute to wastewater signals (*42*). Because VE and vaccine type were similar between Michigan and Ontario, the differentiating factor could be inoculation timing. Influenza vaccine distribution in Michigan typically begins earlier than Ontario, with inoculations happening as early as July. By November 2022, a total of 2,632,430 Michigan residents were vaccinated (≈25% of the population) (*43*). Inoculation efforts in Ontario began later, and vaccines were not made available to all residents until November (*44*). Mass influenza inoculation efforts in Ontario began after IAV RNA concentration started increasing in the wastewater, signaling the start of the influenza season. Vaccination campaigns were already well under way in Michigan when the IAV RNA concentration began to increase in wastewater. We speculate that people from Ontario were less likely to have vaccine-induced immunity than those from Michigan early in the season, potentially contributing to the earlier peak in Windsor-Essex wastewater IAV signal. However, it is unclear if the timing of vaccine campaigns contributed to the observed difference between the Michigan and Ontario influenza seasons. Additional factors, including socio-economic status (*45*), access to healthcare, racial demographics (*46*), population age structure (*47*), and virus–virus interactions (*48*) could have contributed to the differences. Population-level administration schedules for

seasonal influenza vaccines merit further investigation; those schedules help determine when herd immunity is reached and if herd immunity is reached before the spread of illness within a community.

The first limitation of our study is that WRRF does not serve the Michigan counties where FluSurv-NET–participating hospitals are located. However, both the hospitalization data garnered from FluSurv-Net and wastewater data can be considered a proxy for statewide incidence. All influenza-associated hospitalizations were included in this dataset, for both Michigan and Windsor-Essex, even though the WS focused only on IAV. Our analysis could have been affected by focus on IAV, despite its dominance in the 2022–23 influenza season (*17*). Not all hospitalizations recorded in the Windsor-Essex data were laboratory confirmed cases of influenza. The temporal resolution of sample collection at the WRRF was limited, and weekly sampling might have failed to capture variability in the wastewater signal. Finally, the wastewater treatment plants monitored in both Windsor-Essex and Detroit, although serving representative populations, do not encompass all the residents and could have failed to capture variability in IAV wastewater signal.

In conclusion, our study demonstrates how wastewater surveillance can shed light on regional differences that may have otherwise gone unnoticed, or remain unvalidated, because of the inherent limitations of traditional metrics to capture population-wide trends. Future studies investigating influenza vaccine administration schedules should incorporate WS as an independent metric of disease incidence. WS can potentially provide more timely measures of incidence, rather than waiting for the release of laboratory testing. The utility of WS as a predictive metric, and as a metric for trend comparison across jurisdictional boundaries with different approaches to vaccination and collecting disease incidence metrics, demonstrates its usefulness when testing conventions and public health policies differ.

Acknowledgments

We thank the employees and management of the following wastewater treatment facilities for their collaboration: Wastewater Resource Recovery Facility, Great Lakes Water Authority; Pollution Control, City of Windsor.

Funding was provided by the Ontario Ministry of Environment, Conservation, and Parks, the Government of Canada's New Frontiers in Research Fund (grant no. NFRFR-2022-00416), the Canada Biomedical Research Fund (grant no. CBRF2-2023-00008), and Ontario Genomics.

About the Author

Mr. Corchis-Scott is a PhD candidate in environmental science at the Great Lakes Institute for Environmental Research at the University of Windsor. His research interests include wastewater-based surveillance of respiratory pathogens, antimicrobial resistance genes, conservation genetics, and a One Health approach to advancing human health.

References

1. Fauci AS, Folkers GK. Pandemic preparedness and response: lessons from COVID-19. J Infect Dis. 2023;228:422–5. https://doi.org/10.1093/infdis/jiad095
2. Havasi A, Visan S, Cainap C, Cainap SS, Mihaila AA, Pop LA. Influenza A, influenza B, and SARS-CoV-2 similarities and differences—a focus on diagnosis. Front Microbiol. 2022;13:908525. https://doi.org/10.3389/fmicb.2022.908525
3. Yuan P, Aruffo E, Tan Y, Yang L, Ogden NH, Fazil A, et al. Projections of the transmission of the omicron variant for Toronto, Ontario, and Canada using surveillance data following recent changes in testing policies. Infect Dis Model. 2022;7:83–93. https://doi.org/10.1016/j.idm.2022.03.004
4. Koplan JP, Butler-Jones D, Tsang T, Yu W. Public health lessons from severe acute respiratory syndrome a decade later. Emerg Infect Dis. 2013;19:861–3. https://doi.org/10.3201/eid1906.121426
5. Wright J, Driver EM, Bowes DA, Johnston B, Halden RU. Comparison of high-frequency in-pipe SARS-CoV-2 wastewater-based surveillance to concurrent COVID-19 random clinical testing on a public U.S. university campus. Sci Total Environ. 2022;820:152877. https://doi.org/10.1016/j.scitotenv.2021.152877
6. Yoo BK, Iwamoto R, Chung U, Sasaki T, Kitajima M. Economic evaluation of wastewater surveillance combined with clinical COVID-19 screening tests, Japan. Emerg Infect Dis. 2023;29:1608–17. https://doi.org/10.3201/eid2908.221775
7. D'Aoust PM, Graber TE, Mercier E, Montpetit D, Alexandrov I, Neault N, et al. Catching a resurgence: increase in SARS-CoV-2 viral RNA identified in wastewater 48 h before COVID-19 clinical tests and 96 h before hospitalizations. Sci Total Environ. 2021;770:145319. https://doi.org/10.1016/j.scitotenv.2021.145319
8. Ahmed W, Tscharke B, Bertsch PM, Bibby K, Bivins A, Choi P, et al. SARS-CoV-2 RNA monitoring in wastewater as a potential early warning system for COVID-19 transmission in the community: a temporal case study. Sci Total Environ. 2021;761:144216. https://doi.org/10.1016/j.scitotenv.2020.144216
9. Diamond MB, Keshaviah A, Bento AI, Conroy-Ben O, Driver EM, Ensor KB, et al. Wastewater surveillance of pathogens can inform public health responses. Nat Med. 2022;28:1992–5. https://doi.org/10.1038/s41591-022-01940-x
10. Rolfes MA, Foppa IM, Garg S, Flannery B, Brammer L, Singleton JA, et al. Annual estimates of the burden of seasonal influenza in the United States: a tool for strengthening influenza surveillance and preparedness. Influenza Other Respir Viruses. 2018;12:132–7. https://doi.org/10.1111/irv.12486
11. Al Khatib HA, Coyle PV, Al Maslamani MA, Al Thani AA, Pathan SA, Yassine HM. Molecular and biological characterization of influenza A viruses isolated from human

fecal samples. Infect Genet Evol. 2021;93:104972. https://doi.org/10.1016/j.meegid.2021.104972
12. Toribio-Avedillo D, Gómez-Gómez C, Sala-Comorera L, Rodríguez-Rubio L, Carcereny A, García-Pedemonte D, et al. Monitoring influenza and respiratory syncytial virus in wastewater. Beyond COVID-19. Sci Total Environ. 2023; 892:164495. https://doi.org/10.1016/j.scitotenv.2023.164495
13. Mercier E, D'Aoust PM, Thakali O, Hegazy N, Jia JJ, Zhang Z, et al. Municipal and neighbourhood level wastewater surveillance and subtyping of an influenza virus outbreak. Sci Rep. 2022;12:15777. https://doi.org/10.1038/s41598-022-20076-z
14. Ahmed W, Bivins A, Stephens M, Metcalfe S, Smith WJM, Sirikanchana K, et al. Occurrence of multiple respiratory viruses in wastewater in Queensland, Australia: potential for community disease surveillance. Sci Total Environ. 2023; 864:161023. https://doi.org/10.1016/j.scitotenv.2022.161023
15. Maoh H, Dimatulac T, Khan S, Litwin M. Studying border crossing choice behavior of trucks moving between Ontario, Canada and the United States. J Transp Geogr. 2021;91:102992. https://doi.org/10.1016/j.jtrangeo.2021.102992
16. Dunphy S. Cross-border labour mobility in the Windsor-Detroit region: the case of nurses. The Estey Centre Journal of International Law and Trade Policy. 2015;16:14–38.
17. Skowronski DM, Chuang ES, Sabaiduc S, Kaweski SE, Kim S, Dickinson JA, et al. Vaccine effectiveness estimates from an early-season influenza A(H3N2) epidemic, including unique genetic diversity with reassortment, Canada, 2022/23. Euro Surveill. 2023;28:2300043. https://doi.org/10.2807/1560-7917.ES.2023.28.5.2300043
18. Kim S, Chuang ES, Sabaiduc S, Olsha R, Kaweski SE, Zelyas N, et al. Influenza vaccine effectiveness against A(H3N2) during the delayed 2021/22 epidemic in Canada. Euro Surveill. 2022;27:2200720. https://doi.org/10.2807/1560-7917.ES.2022.27.38.2200720
19. Centers for Disease Control and Prevention. Preliminary flu burden estimates, 2021–22 season. 2023 [cited 2024 Apr 11]. https://www.cdc.gov/flu/about/burden/2021-2022.htm
20. Michigan Department of Health & Human Services. Past Michigan flu focus reports [cited 2023 Sep 28]. https://www.michigan.gov/flu/surveillance/past-michigan-flu-focus-surveillance-reports
21. Zhao L, Geng Q, Corchis-Scott R, McKay RM, Norton J, Xagoraraki I. Targeting a free viral fraction enhances the early alert potential of wastewater surveillance for SARS-CoV-2: a methods comparison spanning the transition between delta and omicron variants in a large urban center. Front Public Health. 2023;11:1140441. https://doi.org/10.3389/fpubh.2023.1140441
22. CDM Smith. Great Lakes Water Authority wastewater master plan. 2020 Jun [cited 2024 Apr 23]. https://www.glwater.org/wp-content/uploads/2020/12/Full_WWMP_Report_Final_June-2020.pdf
23. Centers for Disease Control and Prevention. CDC's influenza SARS-CoV-2 multiplex assay. 2020 [cited 2023 Sep 20]. https://www.cdc.gov/coronavirus/2019-ncov/lab/multiplex.html
24. Rosario K, Symonds EM, Sinigalliano C, Stewart J, Breitbart M. Pepper mild mottle virus as an indicator of fecal pollution. Appl Environ Microbiol. 2009;75:7261–7. https://doi.org/10.1128/AEM.00410-09
25. Centers for Disease Control and Prevention. Influenza Hospitalization Surveillance Network. 2024 [cited 2024 Apr 11]. https://www.cdc.gov/flu/weekly/influenza-hospitalization-surveillance.htm
26. Rauch W, Schenk H, Insam H, Markt R, Kreuzinger N. Data modelling recipes for SARS-CoV-2 wastewater-based epidemiology. Environ Res. 2022;214:113809. https://doi.org/10.1016/j.envres.2022.113809
27. Fieller EC, Hartley HO, Pearson ES. Tests for rank correlation coefficients. I. Biometrika. 1957;44:470–81. https://doi.org/10.1093/biomet/44.3-4.470
28. DeJonge PM, Adams C, Pray I, Schussman MK, Fahney RB, Shafer M, et al. Wastewater surveillance data as a complement to emergency department visit data for tracking incidence of influenza A and respiratory syncytial virus — Wisconsin, August 2022–March 2023. MMWR Morb Mortal Wkly Rep. 2023;72:1005–9. https://doi.org/10.15585/mmwr.mm7237a2
29. Faherty EAG, Yuce D, Korban C, Bemis K, Kowalski R, Gretsch S, et al. Correlation of wastewater surveillance data with traditional influenza surveillance measures in Cook County, Illinois, October 2022-April 2023. Sci Total Environ. 2024;912:169551. https://doi.org/10.1016/j.scitotenv.2023.169551
30. Schoen ME, Bidwell AL, Wolfe MK, Boehm AB. United States influenza 2022–2023 season characteristics as inferred from wastewater solids, influenza hospitalization, and syndromic data. Environ Sci Technol. 2023;57:20542–50. https://doi.org/10.1021/acs.est.3c07526
31 Ip DKM, Lau LLH, Chan KH, Fang VJ, Leung GM, Peiris MJS, et al. The dynamic relationship between clinical symptomatology and viral shedding in naturally acquired seasonal and pandemic influenza virus infections. Clin Infect Dis. 2016;62:431–7.
32. Carrat F, Vergu E, Ferguson NM, Lemaitre M, Cauchemez S, Leach S, et al. Time lines of infection and disease in human influenza: a review of volunteer challenge studies. Am J Epidemiol. 2008;167:775–85. https://doi.org/10.1093/aje/kwm375
33. Chan MCW, Lee N, Chan PKS, To KF, Wong RYK, Ho WS, et al. Seasonal influenza A virus in feces of hospitalized adults. Emerg Infect Dis. 2011;17:2038–42. https://doi.org/10.3201/eid1711.110205
34. Mattei M, Pintó RM, Guix S, Bosch A, Arenas A. Analysis of SARS-CoV-2 in wastewater for prevalence estimation and investigating clinical diagnostic test biases. Water Res. 2023;242:120223. https://doi.org/10.1016/j.watres.2023.120223
35. Brunet-Jailly E. Cross-border cooperation: a global overview. Alternatives (Boulder). 2022;47:3–17. https://doi.org/10.1177/03043754211073463
36. Jabakhanji S, Knope J. Ontario to drop most mask mandates on March 21, remaining pandemic rules to lift by end of April. 2022 [cited 2023 Sep 28]. https://www.cbc.ca/news/canada/toronto/covid19-ontario-march-9-mask-mandates-1.6378148
37. Boucher D. Michigan ends most COVID-19 restrictions today: what it means for you [cited 2023 Nov 23]. https://www.freep.com/story/news/local/michigan/2021/06/22/covid-updates-michigan-restrictions-mask-mandate/7774556002/
38. McLean HQ, Petrie JG, Hanson KE, Meece JK, Rolfes MA, Sylvester GC, et al. Interim estimates of 2022-23 seasonal influenza vaccine effectiveness — Wisconsin, October 2022–February 2023. MMWR Morb Mortal Wkly Rep. 2023;72:201–5 https://doi.org/10.15585/mmwr.mm7208a1
39. Centers for Disease Control and Prevention. Preliminary flu vaccine effectiveness (VE) data for 2022–2023. 2023 [cited 2023 Oct 26]. https://www.cdc.gov/flu/vaccines-work/2022-2023.html

40. Public Health Sudbury & Districts. Influenza vaccine availability for the 2022/2023 season [cited 2023 Sep 28]. https://www.phsd.ca/professionals/health-professionals/advisory-alerts-health-care-professionals/influenza-vaccine-availability-for-the-2022-2023-season
41. Michigan Department of Health and Human Services, Division of Immunization. Seasonal influenza vaccines 2023–2024. 2023. [cited 2023 Sep 28]. https://www.michigan.gov/flu/-/media/Project/Websites/flu/Flu-Presentation-Chart-23-24_FINAL.pdf
42. Armas F, Chandra F, Lee WL, Gu X, Chen H, Xiao A, et al. Contextualizing wastewater-based surveillance in the COVID-19 vaccination era. Environ Int. 2023;171:107718. https://doi.org/10.1016/j.envint.2022.107718
43. Michigan Department of Health & Human Services. Flu dashboard [cited 2023 Sep 28]. https://www.michigan.gov/flu/flu-dashboard
44. Moore KM. Ontario's universal influenza immunization program (UIIP)–2022/2023. 2022 [cited 2023 Sep 28]. https://www.wechu.org/sites/default/files/pdf/2022-23_UIIP_CMOH_letter_to_HCPs_EN.pdf
45. Mamelund SE, Shelley-Egan C, Rogeberg O. The association between socioeconomic status and pandemic influenza: systematic review and meta-analysis. PLoS One. 2021;16:e0244346. https://doi.org/10.1371/journal.pone.0244346
46. Kurupati R, Kossenkov A, Haut L, Kannan S, Xiang Z, Li Y, et al. Race-related differences in antibody responses to the inactivated influenza vaccine are linked to distinct pre-vaccination gene expression profiles in blood. Oncotarget. 2016;7:62898–911. https://doi.org/10.18632/oncotarget.11704
47. Jayasundara K, Soobiah C, Thommes E, Tricco AC, Chit A. Natural attack rate of influenza in unvaccinated children and adults: a meta-regression analysis. BMC Infect Dis. 2014;14:670. https://doi.org/10.1186/s12879-014-0670-5
48. Pinky L, Dobrovolny HM. Epidemiological consequences of viral interference: a mathematical modeling study of two interacting viruses. Front Microbiol. 2022;13:830423. https://doi.org/10.3389/fmicb.2022.830423

Address for correspondence: Ryland Corchis-Scott, Great Lakes Institute for Environmental Research, University of Windsor, 401 Sunset Ave, Windsor, ON N9B 3P4, Canada; email: corchisr@uwindsor.ca

etymologia revisited

Malaria
[mə-lar'e-ə]

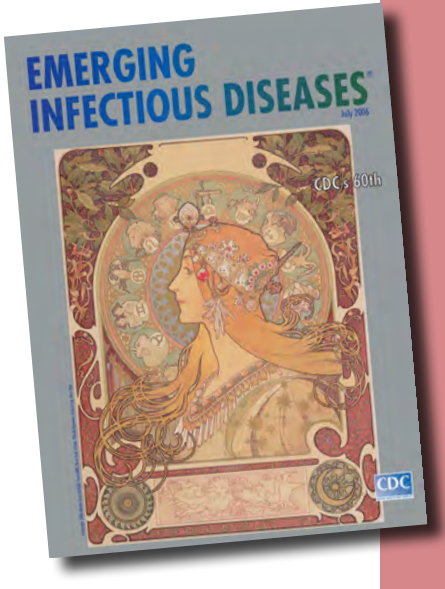

Originally published in July 2006

Malaria, "bad air" in Italian, was blamed for the deaths of >1,000 workers digging the Erie Canal in 1819. Work on the canal continued in winter, when the swamp was frozen over (and, although the vector was not known at the time, mosquitoes were dormant). Malaria, caused by parasites of the genus *Plasmodium* and usually transmitted by the bite of infected *Anopheles* mosquitoes, is endemic in many warm regions. Charles Louis Alphonse Laveran discovered the protozoan cause of malaria in 1880. The Office of Malaria Control in War Areas, which was established in 1942 to control malaria and other vectorborne diseases in the southern United States, evolved into what is today the Centers for Disease Control and Prevention.

Source:
Dorland's illustrated medical dictionary. 30th ed. Philadelphia: Saunders; 2003; cdc.gov; and wikipedia.org

https://wwwnc.cdc.gov/eid/article/12/7/ET-1207_article

Fatal SARS-CoV-2 Infection among Children, Japan, January–September 2022[1]

Shingo Mitsushima,[2] Yuichiro Yahata,[2] Yuuki Tsuchihashi, Chiaki Ikenoue, Munehisa Fukusumi, Shogo Otake, Tomoe Shimada, Takuya Yamagishi, Hajime Kamiya, Yusuke Kobayashi, Hitomi Kurosu, Mai Okuyama, Saeko Morino, Miho Shibamura, Sayaka Takanashi, Taro Kamigaki, Kanako Otani, Manami Nakashita, Hanae Ito, Ayako Miyazaki, Masaya Koshiko, Masanao Harakuni, Megumi Onuma, Hiroko Chiba, Maki Masutani, Natsu Sudani, Yuka Satsuki, Taketoshi Takara, Akira Oka, Tomohiro Katsuta, Naoki Shimizu, Akihiko Saitoh, Tetsuya Sakamoto, Motoi Suzuki, Tomimasa Sunagawa; COVID-19 Fatal Pediatric Cases Database Group[3]

To determine the characteristics of pediatric patients 0–19 years of age who died after onset of SARS-CoV-2 infection in Japan during January 1–September 30, 2022, we reviewed multiple sources. We identified 62 cases, collected detailed information from medical records and death certificates, and conducted interviews, resulting in 53 patients with detailed information for our study. Among 46 patients with internal causes of death (i.e., not external causes such as trauma), 15% were <1 year of age, 59% had no underlying disease, and 88% eligible for vaccination were unvaccinated. Nonrespiratory symptoms were more common than respiratory symptoms. Out-of-hospital cardiac arrest affected 46% of patients, and time from symptom onset to death was <7 days for 77%. Main suspected causes of death were central nervous system abnormalities (35%) and cardiac abnormalities (20%). We recommend careful follow-up of pediatric patients after SARS-CoV-2 infection during the first week after symptom onset, regardless of underlying diseases.

COVID-19 has spread worldwide since December 2019. Among the mutated variants, some were designated by the World Health Organization as variants of concern because of their transmissibility or virulence (*1*). On November 26, 2021, the Omicron variant was designated as one such variant of concern (*2*). The first case caused by the Omicron variant was detected in November 2021 in South Africa, and the variant quickly spread worldwide, including to Japan (*3*). In Japan, the proportion of the Omicron variant among detected in SARS-CoV-2 isolates rose sharply in late December 2021, reached almost 100% in January 2022, and remained almost 100% throughout our study period (*4*).

In Japan, public health centers and hospitals mandatorily registered the number of COVID-19 cases and the characteristics of those cases at diagnosis (e.g., date of symptom onset and severity) on the Health Center Real-time Information-sharing System on COVID-19 (HER-SYS), a national surveillance system. Public health centers next conducted epidemiologic investigations based on information in HER-SYS. HER-SYS did not require mandatory follow-up of the details of the clinical course (e.g., medical intervention, hospitalization, and death) and therefore

Author affiliations: National Institute of Infectious Diseases, Tokyo, Japan (S. Mitsushima, Y. Yahata, Y. Tsuchihashi, C. Ikenoue, M. Fukusumi, S. Otake, T. Shimada, T. Yamagishi, H. Kamiya, Y. Kobayashi, H. Kurosu, M. Okuyama, S. Morino, M. Shibamura, S. Takanashi, T. Kamigaki, K. Otani, M. Nakashita, H. Ito, A. Miyazaki, M. Koshiko, M. Harakuni, M. Onuma, H. Chiba, M. Masutani, N. Sudani, Y. Satsuki, T. Takara, M. Suzuki, T. Sunagawa); Saitama Children's Medical Center, Saitama, Japan (A. Oka); St. Marianna University School of Medicine, Kanagawa, Japan (T. Katsuta, N. Shimizu); Niigata University Graduate School of Medical and Dental Sciences, Niigata, Japan (A. Saitoh); Teikyo University School of Medicine, Tokyo (T. Sakamoto)

DOI: https://doi.org/10.3201/eid3008.240031

[1]Preliminary results from this study were presented in Japanese as a government surveillance report at https://www.niid.go.jp/niid/ja/2019-ncov/2559-cfeir/11727-20.html.

[2]These first authors contributed equally to this article.

[3]Members of the COVID-19 Fatal Pediatric Cases Database Group who contributed data are listed at the end of this article.

could not collect accurate information about severe or fatal cases.

After the Omicron variant was first detected, in 2022, the number of pediatric COVID-19 patients increased dramatically. According to national data, by December 2021 the number of SARS-CoV-2–positive patients 0–19 years of age was 240,000 (0–9 years, 84,000; 10–19 years, 156,000); during January–September 2022 (the Omicron variant period), the number increased to 4.8 million (0–9 years, 2.4 million; 10–19 years, 2.4 million) (*5*). The trend of increasing pediatric patients, including those hospitalized as Omicron began to spread, was also observed in South Africa (*6*,*7*). Although the number of reported deaths among patients 0–19 years of age was only 3 in 2020–2021, starting in January 2022 the number increased as the number SARS-CoV-2–positive patients 0–19 years of age increased (*5*).

In general, SARS-CoV-2 infections in children are considered to be less severe than those in adults, and deaths among children are rare (*8*). Few studies have reported the details of fatal cases in children after SARS-CoV-2 infection, such as clinical courses leading to death and causes of death, especially during the Omicron variant period. Therefore, we aimed to determine the characteristics of fatal cases in children after SARS-CoV-2 infection during that period. However, we could not determine the exact number or the details, including cause of death (COD), based on the national surveillance system. Thus, we identified fatal cases in children through multiple sources and describe the overall characteristics and clinical courses, categorized by suspected COD, for pediatric patients after SARS-CoV-2 infection during the Omicron variant period. Our field investigation was conducted under the stipulations of the Infectious Diseases Control Law; therefore, ethics approval was not needed for our study.

Materials and Methods

In Japan, the Ministry of Health, Labour and Welfare (MHLW) and the National Institute of Infectious Diseases conducted an enhanced epidemiologic investigation in cooperation with academic societies (Japan Pediatric Society, The Japanese Society of Intensive Care Medicine, and the Japanese Association for Acute Medicine). They investigated fatal cases after SARS-CoV-2 infection in patients 0–19 years of age (fatal pediatric cases) under the Act on the Prevention of Infectious Diseases and Medical Care for Patients with Infectious Diseases (Infectious Diseases Control Law).

To determine the actual number and characteristics of the cases, we collected information on fatal pediatric cases from the MHLW, local governments, public health centers, HER-SYS, academic societies, and the media. A case was defined as a fatal case occurring after SARS-CoV-2 infection in a young patient 0–19 years of age whose date of symptom onset or death was during January 1–September 30, 2022. The diagnosis of SARS-CoV-2 infection was based on PCR or antigen test results. Because our study was based on a public health response requiring rapid results, the study period was set until the end of September 2022. We collected cases without considering the duration from day of symptom onset to day of death because we assessed patients, including those with a long-time course, from symptom onset to death.

During August–December 2022, the research staff of the National Institute of Infectious Diseases collected epidemiologic data from local health authorities, and 2 or 3 staff members, including at least 1 pediatrician, visited the hospitals where the patients died (field investigation). We also obtained descriptions of epidemiologic investigations conducted by the public health centers. We collected data on the characteristics of the patients from medical records and death certificates of the hospital where the patients died and from records of epidemiologic investigations conducted by the public health centers. We collected information on patient age, sex, body weight, height, gestational age, physical handicap, SARS-CoV-2 vaccination history of parents and patients, underlying diseases, clinical courses comprising data on the diagnostic examination, date of symptom onset, date of admission, date of first consultation, date of cardiopulmonary arrest, date of death, symptoms/findings, out-of-hospital cardiac arrest, suspected infection source, pathogen detected in blood culture, imaging findings, treatment, and suspected COD. We did not perform additional testing to determine the suspected COD, which we classified as internal or external; we defined internal COD as death caused by disease excluding trauma and external COD as death caused by trauma. Our classification was intended to distinguish between internal and external COD for which the association with SARS-CoV-2 infection was considered low (e.g., death caused by incidental trauma after SARS-CoV-2 infection). We also divided the internal COD into central nervous system (CNS) abnormalities, cardiac abnormalities, respiratory abnormalities, other, and unknown. We determined those categorizations by comprehensively reviewing medical records, death certificates, and our physician interviews. Next, we conducted descriptive epidemiology of the characteristics of the patients and calculated the median and interquartile range (IQR) for the number of days from symptom onset to cardiopulmonary

arrest and for the number of days from symptom onset to death. To test for goodness of fit in selected variables, we performed χ^2 or Fisher exact tests. To compare intervals between symptom onset and first consultation, cardiopulmonary arrest, or death among different initial CODs, we next performed the log-rank test. For all statistical tests we used R 4.3.1 (The R Foundation for Statistical Computing, https://www.r-project.org). For some cases, we could not describe the details of patients because of privacy reasons.

Results

We identified 62 cases. Symptom onset or diagnosis of the first fatal pediatric case occurred in epidemiologic week 1 of 2022 (January 3–9), and subsequent cases occurred continuously (Figure 1). The number of cases increased on week 28 (July 11–17) and peaked during week 33 (August 15–21). The number of fatal cases seemed to be in line with the reported number of COVID-19 patients of all ages (*9*).

Of the 62 cases, we could not conduct field investigations for 5 (8%) and were unable to obtain permission to publish data from the hospital for 4 (6%). We thus describe the remaining 53 cases. Among suspected CODs, 46 (87%) were internal and 7 (13%) were external. The 46 internal COD cases were further divided (Figure 2).

Fatal Pediatric Cases with Internal CODs

Among the 46 patients with internal COD, most were 5–11 years of age, but deaths per 100,000 persons were highest among those <1 year of age (Appendix Table, https://wwwnc.cdc.gov/EID/article/30/8/24-0031-App1.pdf). Seven patients were <1 year of age (3 were <6 months of age), which was the highest number by age. No underlying diseases were noted for 27 patients, whereas some underlying diseases were noted for 19 patients. At the time of investigation, 24 (52%) patients were eligible for vaccination against SARS-CoV-2 because they were ≥5 years of age. Among them, 21 (88%) had received no vaccination, but the other 3 (13%) patients who were ≥12 years of age had received first and second vaccine doses, and their dates of symptom onset were >3 months after the date of their last vaccination. The suspected source of infection for 21 (46%) patients was within the family.

Before hospital admission, nonrespiratory symptoms were more common than respiratory symptoms (Figure 3). The most frequent suspected CODs were CNS abnormalities (e.g., acute encephalopathy), followed by cardiac abnormalities (e.g., acute myocarditis) and respiratory abnormalities (e.g., acute pneumonia). We did not find any instances of multisystem inflammatory syndrome in children. Among patients without underlying disease, the most common suspected COD was CNS abnormalities for 11, followed by cardiac abnormalities for 5; there were no cases of respiratory abnormalities. The number of deaths confirmed in the emergency department before the patient could be admitted to hospital was 19, and the number after admission

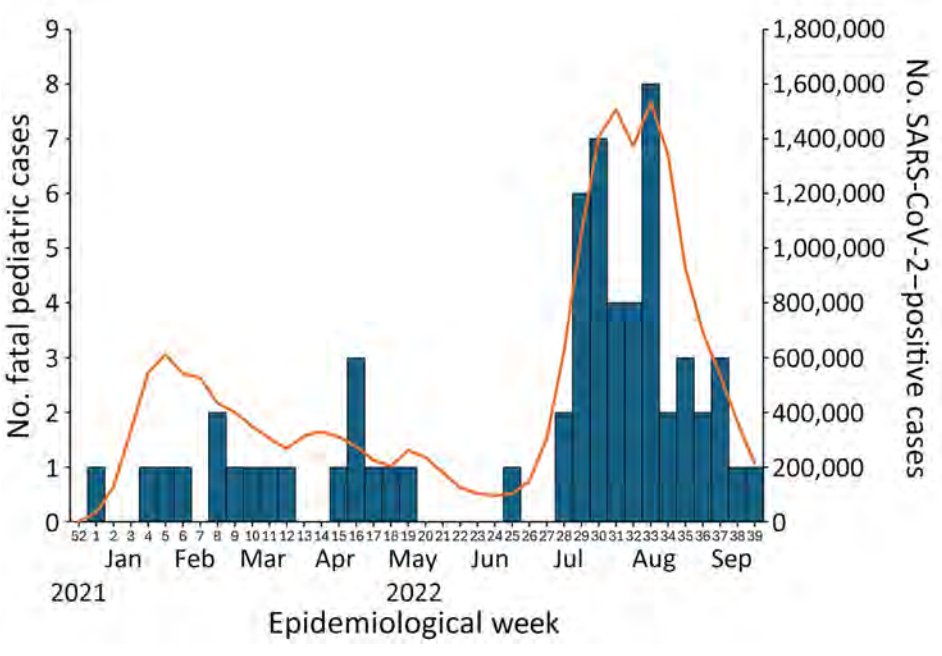

Figure 1. Number of reported fatal cases after COVID-19 among 61 children 0–19 years of age, by week of symptom onset or diagnosis, Japan, January–September 2022, and number of reported COVID-19 cases among patients of all ages. Excludes 1 patient for whom date of symptom onset and date of diagnosis of COVID-19 were unknown. Date of symptom onset for the 61 pediatric patients was January 1, 2022 (epidemiologic week 52, 2021) through September 30, 2022 (epidemiologic week 39, 2022). Bars denote the number of reported fatal pediatric cases (left axis); line denotes the numbers of COVID-19 patients of all ages reported by the Ministry of Health, Labour and Welfare (right axis). Scales for the y-axes differ substantially to underscore patterns but do not permit direct comparisons.

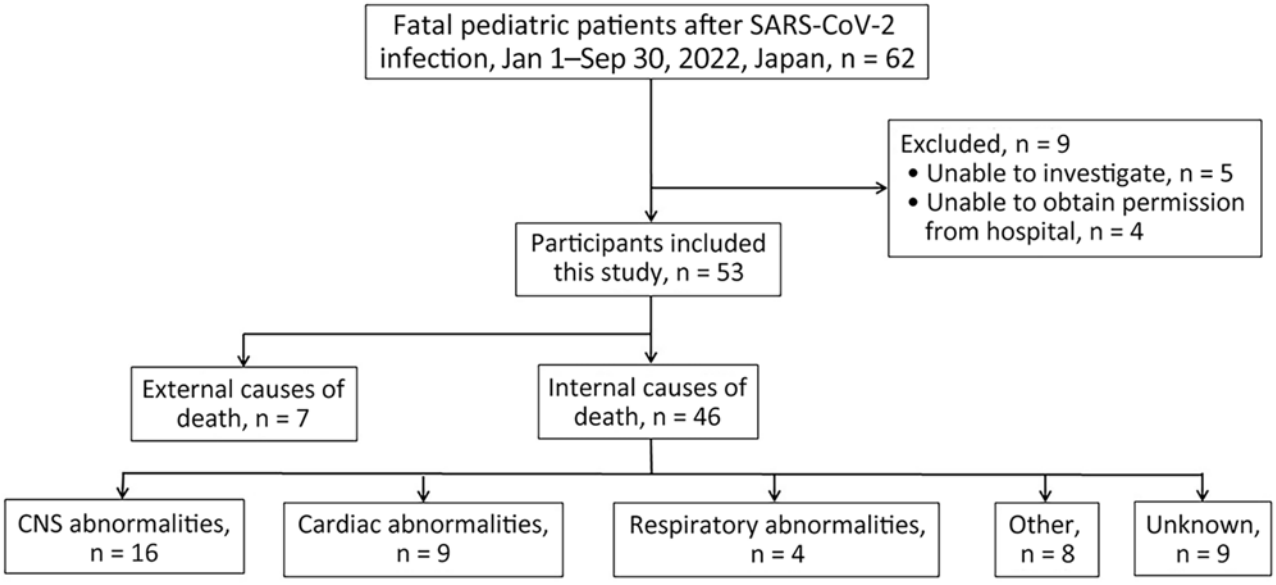

Figure 2. Patient selection in study of fatal SARS-CoV-2 infection among children, Japan, January–September 2022. CNS, central nervous system.

was 27. Forty-six percent of patients died of out-of-hospital cardiac arrest. The proportion of out-of-hospital cardiac arrest caused by CNS abnormalities was significantly lower than that not caused by CNS abnormalities ($p = 0.02$), whereas the proportion of out-of-hospital cardiac arrest caused by cardiac abnormalities did not differ significantly from that not caused by cardiac abnormalities ($p = 0.26$).

We collected data on blood examinations, drugs, and treatment for 27 hospitalized patients (Tables 1, 2). We excluded patients with external COD, those who died before they could be admitted, and those with out-of-hospital cardiac arrest (because the results of blood examinations in patients with cardiopulmonary arrest were extreme and reflected cardiac arrest and not a disease condition). D-dimer levels were high. Among patients for whom blood cultures were positive, we determined that for 1 patient, the pathogen detected from blood culture potentially contributed to death, whereas for the remaining patients, it was difficult to evaluate whether the pathogen affected death. Autopsies were performed for 7 patients, of which 2 showed no abnormalities, 2 showed evidence of pathology, and 3 showed inconclusive evidence.

CNS Abnormalities

Of the 16 cases, CNS abnormalities were observed most often among patients 5–11 years of age, whereas none were observed in patients <1 year of age (Table 3). The most frequent clinical sign/symptom was fever, followed by disturbance of consciousness, seizure, nausea or vomiting, and headache, which are typically associated with acute encephalopathy. Digestive symptoms (e.g., stomachache and diarrhea) developed in a few patients. Acute encephalopathy affected 12 (75%) patients, intracranial hemorrhage in 1 (6%), and other conditions in 3 (19%). Among the 12 patients with acute encephalopathy, hemorrhagic shock and encephalopathy syndrome (HSES) was suspected for 5 (42%), encephalopathy with acute fulminant cerebral edema was present in 1 (8%), and unclassifiable encephalopathy was present in 6 (50%).

Among 11 patients for whom time from symptom onset to cardiopulmonary arrest was <5 days, 6 (55%) had cerebral edema and 3 (27%) had rapidly progressing cerebral herniation. Of the 5 patients for whom the interval was ≥10 days, 4 (80%) showed a flat electroencephalogram in the first 4 days after symptom onset. Of the 16 patients who died of CNS abnormalities, 2 died before and 14 died after hospitalization.

Cardiac Abnormalities

The most frequent symptom was fever, followed by nausea or vomiting, loss of appetite, consciousness disturbance, and cough (Table 4). Out-of-hospital cardiac arrest affected 67% of the 9 patients with cardiac abnormality, higher than the 19% of patients for which the suspected COD was CNS abnormalities, although no significant difference was noted in the number of days from symptom onset to first consultation between the patients who died of cardiac abnormalities versus CNS abnormalities ($p = 0.1$). The

number of days from symptom onset to cardiopulmonary arrest and death for all patients was <7 days, whereas no difference in intervals was noted between CNS abnormalities (p = 0.6) and cardiac abnormalities (p = 0.1). Clinical acute myocarditis was detected in 8 of the 9 patients.

Fatal Pediatric Cases with External Causes of Death

Of the 7 patients with an external COD, 2 were <5 years of age and 5 were ≥5 years of age. External CODs included unexpected accidents such as drowning and suffocation but not traffic accidents, fires, poisoning, or disasters. Some patients were suspected of experiencing consciousness disturbance before the external COD.

Discussion

In our descriptive study, to present the overall characteristics and clinical course after SARS-CoV-2 infection, we investigated not only internal CODs but external CODs. Our study included 62 fatal pediatric cases for which dates of symptom onset and death were January 1–September 2022. The most common patient age was <1 year, similar to the trend reported for a prior study in the United States (*10*). More than half of the patients whose COD was internal had no underlying disease, and most were unvaccinated. CNS abnormalities comprised the highest number of suspected CODs, followed by cardiac abnormalities. We observed that nearly 80% of the patients died and 85% had cardiopulmonary arrest within 7 days of first symptoms, regardless of the suspected COD. That finding was consistent with that of a previous survey of deaths among children and young persons

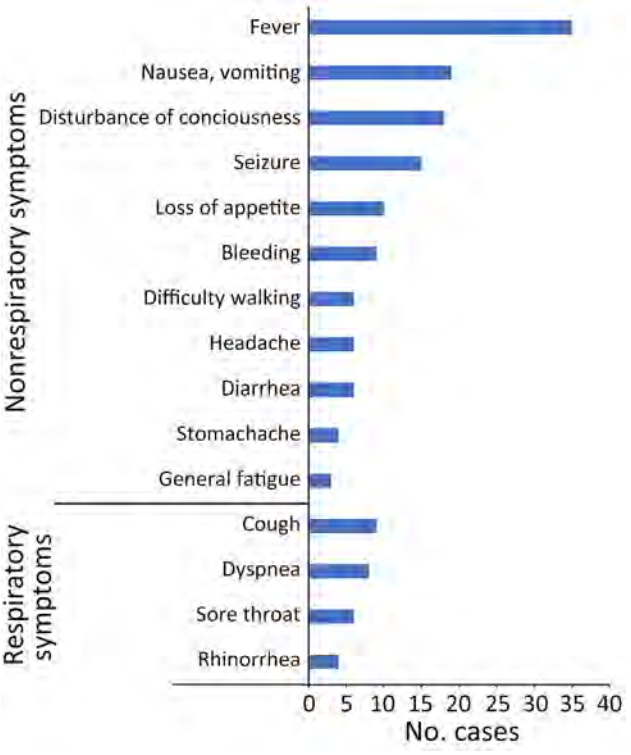

Figure 3. Distribution of symptoms before admission or death in outpatient settings in study of fatal SARS-CoV-2 infection among children, Japan, January–September 2022 (n = 46). Data account for multiple symptoms in some patients.

Table 1. Results of blood examinations, drugs, and treatments after hospitalization for 27 patients in study of fatal SARS-CoV-2 infection among patients 0–19 years of age, Japan, January–September 2022*

Blood examinations at admission†	No. patients	Median (IQR)	Reference range
Leukocytes, no./μL	12	9,200 (6,270–14,450)	4,100–16,300
Neutrophils, %	11	65.7 (32.6–76.0)	18–94
Lymphocytes, %	11	27.0 (11.4–32.3)	18–82
Hemoglobin, g/dL	12	13.4 (12.8–14.5)	11.5–14.4
Hematocrit, %	12	41.2 (38.9–44.6)	34.5–43.0
Platelets, 10^4/μL	12	19.4 (15.0–25.7)	18.0–51.0
PT-INR	5	1.32 (1.23–1.60)	0.75–1.15
Fibrinogen, mg/dL	6	186 (144–244)	200–400
D-dimer, ng/dL	5	39.3 (27.3–79.7)	0.15–1.0
Albumin, g/dL	10	4.6 (4.1–4.8)	3.6–4.7
Total bilirubin, mg/dL	7	0.31 (0.30–0.80)	0.3–0.9
Alanine aminotransferase, U/L	12	47 (25.5–274.5)	9–28
Aspartate aminotransferase, U/L	12	61 (42–322)	24–38
Lactate dehydrogenase, U/L	11	397 (254–738)	175–320
Creatine kinase, U/L	10	83.5 (62–201)	46–230
C-reactive protein, mg/dL	12	0.31 (0.11–0.47)	0.0–0.3
Sodium, mmol/L	12	137 (135–142)	137–144
Potassium, mmol	12	4.5 (3.7–5.3)	3.6–4.7
Glucose, mg/dL	9	171 (138–236)	70–200
Blood urea nitrogen, mg/dL	12	15.9 (13.8–19.5)	6.6–19.6
Creatinine, mg/dL	12	0.61 (0.42–1.38)	0.25–0.34
Lactate, mmol/L	9	4.8 (4.2–9.7)	0.5–2.0

*Reference ranges are for persons 6 years of age. IQR, interquartile range; PT-INR, prothrombin time international normalized ratio.
†Excludes patients who died before admission to the hospital and those with out-of-hospital cardiac arrest.

Table 2. Results of examinations, drugs, and treatments after hospitalization for 27 patients in study of fatal SARS-CoV-2 infection among patients 0–19 years of age, Japan, January–September 2022*

Result	No. (%) patients
Pathogen detected in blood culture†	
Streptococcus spp.	2 (7)
Escherichia spp.	1 (4)
Fusobacterium spp.	1 (4)
Chest CT findings‡	
Ground-glass opacity	5 (21)
Consolidation	5 (21)
Pleural effusion	1 (4)
Brain CT findings§	
Cerebral edema	14 (40)
Loss of gray-white matter differentiation	7 (20)
Intracranial hemorrhage	3 (9)
Hydrocephalus	3 (9)
Congenital abnormalities	3 (9)
Drug†	
Inotrope	16 (59)
Steroid	14 (52)
Antiviral	12 (44)
Treatment†	
Mechanical ventilation	23 (85)
Extracorporeal membrane oxygenation	5 (19)
Targeted temperature management	4 (15)
Blood transfusion	13 (48)
Immune globulin	4 (15)
Dialysis	3 (11)
Plasmapheresis	1 (4)

*CT, computed tomography.
†Includes multiple pathogens, drugs, and treatments.
‡Includes multiple findings; 24 cases involving chest CT are included.
§Includes multiple findings; 35 cases involving head CT are included.

in England after SARS-CoV-2 infection during March 2020–February 2021, which reported that the time interval between a positive SARS-CoV-2 test and death in 84% for those dying of COVID-19 was within 7 days (*11*). Several patients in our study were transferred to the hospital soon after rapid illness progression and received intensive care but did not recover. Follow-up of pediatric cases in an out-of-hospital setting is crucial for the first 7 days after symptom onset.

We found more patients without than with underlying disease. Earlier reports, before the advent of the Omicron variant, indicated that deaths caused by COVID-19 tend to occur in those with underlying disease (*11*,*12*). A study conducted in South Korea, which included the Omicron variant period, showed that more than half of the patients ≤18 years of age who died had no underlying disease, which was similar to our finding (*13*). In addition, the proportion of nonrespiratory symptoms was higher than that of respiratory symptoms (Figure 3). The COVID-19 registry survey conducted by the Japan Pediatric Society during the very early Omicron variant phase (January 1–February 20, 2022) reported that among 1,058 pediatric patients with COVID-19, respiratory symptoms such as cough and runny nose were common (*14*), which differed from our findings, possibly because of differences in illness severity or in the study period and population. Our study showed the value of considering nonrespiratory symptoms (e.g., neurologic and digestive) as critical signs during the Omicron variant period.

Regarding vaccination, among the 46 case-patients with internal COD, 52% of the patients in our study were eligible for vaccination; among them, 13% had received 2 doses of vaccine. All vaccinated patients were ≥12 years of age. In Japan, vaccination against SARS-CoV-2 for those ≥12 years of age started in June 2021, that for children 5–11 years of age started in February 2022, and that for those 6 months to 4 years of age started in October 2022. Thus, in our study, patients ≥5 years of age were eligible for vaccination before disease onset. The percentage of children 5–11 years of age who had received ≥1 vaccine was 22.5% as of September 30, 2022, which was higher than the 13% of children in our study who had undergone vaccinations (*15*). Prior studies showed that COVID-19 vaccines for children 5–11 years of age could prevent severe COVID-19, including that caused by the Omicron variant (*16*–*18*). Although the lower proportion of persons vaccinated in our study population compared with the general population might have affected their deaths, we could not evaluate the effect of vaccination because we collected data on fatal cases only. Furthermore, caution is necessary when applying the results

of our study to the general population because of the low proportion of vaccinated patients.

Among the 16 patients with CNS abnormalities, we collected data for 12 with acute encephalopathy. Among them, 5 patients had HSES, and 1 had encephalopathy with acute fulminant cerebral edema, which might be remarkable. In general, the most common type of encephalopathy is acute encephalopathy with biphasic seizures and late reduced diffusion, followed by clinically mild encephalitis/encephalopathy with a reversible splenial lesion and HSES (*19*,*20*). HSES is a rare type of encephalopathy with a high mortality rate. It is associated with cytokine storms with disseminated intravascular coagulation and multiple organ failure at the time of initial examination (*21*,*22*). In a prior study, encephalopathy with acute fulminant cerebral edema was reported to be relatively common among COVID-19 patients, and a type of encephalopathy in which initial examinations (e.g., blood tests and computed tomography of the head) showed only minor abnormalities and then rapid progression was reported (*21*,*23*). Other reports, which might include this particular encephalopathy, suggested that encephalopathy results in severe sequelae or fatal outcomes (*23*–*26*). The Japanese Society of Child Neurology and the Research Committee on Acute Encephalopathy conducted an epidemiologic investigation that suggested that acute encephalopathy associated with COVID-19 had a poor clinical outcome and was more severe than acute encephalopathy associated with other viruses (*23*,*27*). In our study, frequency of out-of-hospital cardiac arrest was significantly lower among patients who died of CNS abnormalities than among those who died of causes other than CNS abnormalities, whereas the intervals between symptom onset and cardiopulmonary arrest or death did not differ between patients who died of cardiac abnormalities or CNS abnormalities. Illness of pediatric patients who died of CNS abnormalities was assessed as less severe at the time of arrival, but both conditions worsened rapidly. For some patients, electroencephalogram was flat,

Table 3. Characteristics of 16 patients for whom central nervous system abnormalities were suspected of causing death in study of fatal SARS-CoV-2 infection among patients 0–19 years of age, Japan, January–September 2022*

Characteristics	Value
Age group, y	
0	0
1–4	5 (31)
5–11	9 (56)
12–19	2 (13)
Sex	
M	8 (50)
F	8 (50)
Underlying disease	
Yes	5 (31)
No	11 (69)
Vaccination	
None	11 (69)
Ineligible	5 (31)
Symptoms/signs	
Fever	14 (88)
Disturbance of consciousness	13 (81)
Seizure	11 (69)
Nausea/vomiting	8 (50)
Headache	6 (38)
OHCA	
Yes	3 (19)
No	13 (81)
Days from symptom onset to first consultation	
0–2	16 (100)
≥3	0
Median (IQR)	0.5 (0–1.0)
Days from symptom onset to cardiopulmonary arrest	
0–4	11 (69)
5–9	0
≥10	5 (31)
Median (IQR)	2.0 (1.0–12.0)
Days from symptom onset to death	
0–4	9 (56)
5–9	0
≥10	7 (44)
Median (IQR)	3.5 (2.0–14.5)

*Values are no. (%) patients except as indicated. OHCA, out-of-hospital cardiac arrest; IQR, interquartile range.

Table 4. Characteristics of 9 patients for whom cardiac abnormalities were suspected as cause of death in study of fatal SARS-CoV-2 infection among patients 0–19 years of age, Japan, January–September 2022*

Characteristic	Value
Sex	
M	2 (44)
F	7 (56)
Underlying disease	
Yes	4 (44)
No	5 (56)
Vaccination	
None	4 (44)
2 doses	1 (11)
Ineligible	4 (44)
Symptoms/signs	
Fever	7 (78)
Nausea/vomiting	4 (44)
Loss of appetite	3 (33)
Disturbance of consciousness	2 (22)
Cough	2 (22)
OHCA	
Yes	6 (67)
No	3 (33)
Days from symptom onset to first consultation	
0–2	7 (78)
3–6	2 (22)
≥7	0
Median (IQR)	1.0 (0–2.0)
Days from symptom onset to cardiopulmonary arrest	
0–2	4 (44)
3–6	5 (56)
≥7	0
Median (IQR)	4.0 (2.0–4.0)
Days from symptom onset to death	
0–2	4 (44)
3–6	5 (56)
≥7	0
Median (IQR)	4.0 (2.0–5.0)

*Values are no. (%) except as indicated. Age distribution could not be shown because it could lead to the identification of specific persons. OHCA, out-of-hospital cardiac arrest; IQR, interquartile range.

which meant irreversible neurologic damage, within a few days after symptom onset. The irreversible neurologic damage might be one of the reasons why patients with neurologic complications are at risk of dying. Therefore, clinicians should be aware that COVID-19 may cause acute encephalopathy that leads to irreversible neurologic damage and that acute encephalopathy can rapidly progress to death even if the patient receives intensive care.

Among the strengths of our study is that we detected fatal pediatric cases for which outcomes were not reported to HER-SYS because we could collect cases from multiple sources. In addition, we could describe the details of the cases by suspected COD, which were not collected by HER-SYS. The insights provided by our study differ greatly from those that would be obtained from a database study.

The first limitation of our study was that we might not have captured all characteristics during the Omicron variant period because it concluded while the epidemic was still ongoing. Second, we did not examine the causal relationship between SARS-CoV-2 infection and death. Through review of medical records, death certificates, and our physician interviews by pediatricians, we were able to determine whether SARS-CoV-2 infection was an underlying COD. We determined that SARS-CoV-2 infection contributed to most of the deaths. However, there were a few cases in which underlying disease potentially contributed more to death than did SARS-CoV-2 infection. It was difficult to accurately evaluate the extent to which SARS-CoV-2 infection affected death in cases for which autopsies or examinations such as imaging and blood examinations could not be performed. Therefore, determining whether SARS-CoV-2 infection was the underlying COD was challenging. Third, cases might have been underreported because case detection was based on voluntary reporting. If a physician determined that there was no association between SARS-CoV-2 infection and death, the case might not have been reported. Encephalopathy or carditis might be more likely to have been reported, whereas reporting of deaths caused by trauma or exacerbation of underlying diseases after SARS-CoV-2 infection might be less

likely. However, the study conducted in Korea showed similar epidemiologic trends, such as in the number of deaths and the age of patients, which support the results of our study (*13*). Fourth, collection of all data was not always possible because of missing data. Last, diagnosis, examination, and treatment might differ because they were conducted at different hospitals.

In conclusion, the most common COD among fatal pediatric SARS-CoV-2 cases in this study was CNS abnormalities, followed by cardiac abnormalities. For pediatric patients, clinicians should pay attention not only to respiratory signs/symptoms but also to nonrespiratory signs/symptoms. In addition to addressing signs/symptoms, clinicians should carefully observe pediatric patients during at least the first 7 days from onset of COVID-19 regardless of underlying diseases because most pediatric patients who died rapidly progressed to death within that period.

Members of the COVID-19 Fatal Pediatric Cases Database Group: Hiroshi Komatsu (National Hospital Organization Maizuru Medical Center, Kyoto, Japan), Hiroyuki Matsuura (Toho University Omori Medical Center, Tokyo), Ryosuke Fukushima (Fujisawa City Hospital, Kanagawa, Japan), Daisuke Tamura (Jichi Medical University, Tochigi, Japan), Masao Murabayashi (Numazu City Hospital, Shizuoka, Japan), Hironobu Yamaga (Naga Municipal Hospital, Wakayama, Japan), Kotoko Matsui (Juntendo University Faculty of Medicine, Tokyo), Hideki Kawamura (Kagoshima University Hospital, Kagoshima, Japan), Hidetoshi Igari (Chiba University Hospital, Chiba, Japan), Masashi Kasai (Hyogo Prefectural Kobe Children's Hospital, Hyogo, Japan), Cho Yoshiaki (Okinawa Prefectural Nanbu Medical Center & Children's Medical Center, Okinawa, Japan), Meiwa Shibata (Tokyo Metropolitan Children's Medical Center, Tokyo), Kenji Dohi (Showa University, Tokyo), Mineji Hayakawa (Hokkaido University Hospital, Hokkaido, Japan), Hiroshi Imai (Mie University Hospital, Mie, Japan), Hijiri Watanabe (Kumamoto Rosai Hospital, Kumamoto, Japan), Kazuma Yamakawa (Osaka Medical and Pharmaceutical University, Osaka, Japan), Hiroaki Takada (National Hospital Organization Disaster Medical Center, Tokyo), Takayuki Yamanaka (Niigata City General Hospital, Niigata, Japan), Atsumi Uemura (National Hospital Organization Nishibeppu National Hospital, Oita, Japan), Kenta Ito (Aichi Children's Health and Medical Center, Aichi, Japan), Kentaro Ide (National Center for Child Health and Development, Tokyo), Kiyoko Amo (Osaka City General Hospital, Osaka), Akira Watase (National Hospital Organization Tokyo Medical Center, Tokyo), Makoto Shinba (Shinshiro Municipal Hospital, Aichi), Yoshiyuki Sugishita (Tokyo Metropolitan Government, Tokyo).

Acknowledgments

We express our sincere gratitude to the Japan Pediatric Society, the Japanese Society of Intensive Care Medicine, the Japanese Association for Acute Medicine, local governments, public health centers, the Japan MHLW, Kazuhiro Muramatsu, Hiroshi Kurosawa, Shinsuke Mizuno, Hiroaki Kise, Eiju Hasegawa, Shotaro Matsumoto, Hyogo Prefectural Amagasaki General Medical Center, Iwate Medical University Hospital, Okayama University Hospital, Yamagata Prefectural Shinjo Hospital, and St. Luke's International Hospital for their cooperation with this investigation.

The availability of data is restricted for privacy reasons. The data were used under the stipulations of the Infectious Diseases Control Law and therefore are not available to the public.

A.O. reports a relationship with Nobelpharma Co., Ltd., that includes speaking and lecture fees, a relationship with Nippon Shinyaku Co., Ltd., which includes speaking and lecture fees, and a relationship with Eisai Co., Ltd., which includes speaking and lecture fees. T.K. reports a relationship with Merck Sharp & Dohme Corp., which includes speaking and lecture fees.

About the Author

Dr. Mitsushima is a pediatrician and researcher at the Center for Field Epidemic Intelligence, Research and Professional Development of the National Institute of Infectious Diseases. His specialty is the epidemiology of infectious diseases.

References

1. World Health Organization. Tracking SARS-CoV-2 variants [cited 2024 Jan 4]. https://www.who.int/activities/tracking-SARS-CoV-2-variants
2. World Health Organization. Classification of Omicron (B.1.1.529): SARS-CoV-2 Variant of Concern [cited 2024 Jan 4]. https://www.who.int/news/item/26-11-2021-classification-of-omicron-(b.1.1.529)-sars-cov-2-variant-of-concern
3. Meo SA, Meo AS, Al-Jassir FF, Klonoff DC. Omicron SARS-CoV-2 new variant: global prevalence and biological and clinical characteristics. Eur Rev Med Pharmacol Sci. 2021;25:8012–8.
4. National Institute of Infectious Diseases. Mutated strains of SARS-CoV-2 [in Japanese] [cited 2024 Jan 4]. https://www.niid.go.jp/niid/ja/from-lab/488-flu/12054-flu2-1-2.html
5. Ministry of Health, Labour and Welfare. Visualizing the data: the data on SARS-CoV-2 infection [cited 2024 Jan 4]. https://covid19.mhlw.go.jp
6. Cloete J, Kruger A, Masha M, du Plessis NM, Mawela D, Tshukudu M, et al. Paediatric hospitalisations due to COVID-19 during the first SARS-CoV-2 Omicron (B.1.1.529) variant wave in South Africa: a multicentre observational study. Lancet Child Adolesc Health. 2022;6:294–302. https://doi.org/10.1016/S2352-4642(22)00027-X

7. Chiwandire N, Jassat W, Groome M, Kufa T, Walaza S, Wolter N, et al. Changing epidemiology of COVID-19 in children and adolescents over four successive epidemic waves in South Africa, 2020–2022. J Pediatric Infect Dis Soc. 2023; 12:128–34. PubMed https://doi.org/10.1093/jpids/piad002
8. Pierce CA, Herold KC, Herold BC, Chou J, Randolph A, Kane B, et al. COVID-19 and children. Science. 2022;377:1144–9. PubMed https://doi.org/10.1126/science.ade1675
9. Ministry of Health, Labour and Welfare. Published database on the number of patients diagnosed as COVID-19 [in Japanese] [cited 2024 Jan 4]. https://www.mhlw.go.jp/stf/covid-19/open-data.html
10. Flaxman S, Whittaker C, Semenova E, Rashid T, Parks RM, Blenkinsop A, et al. Assessment of COVID-19 as the underlying cause of death among children and young people aged 0 to 19 years in the US. JAMA Netw Open. 2023;6:e2253590. https://doi.org/10.1001/jamanetworkopen.2022.53590
11. Smith C, Odd D, Harwood R, Ward J, Linney M, Clark M, et al. Deaths in children and young people in England after SARS-CoV-2 infection during the first pandemic year. Nat Med. 2022;28:185–92. https://doi.org/10.1038/s41591-021-01578-1
12. Bertran M, Amin-Chowdhury Z, Davies HG, Allen H, Clare T, Davison C, et al. COVID-19 deaths in children and young people in England, March 2020 to December 2021: an active prospective national surveillance study. PLoS Med. 2022;19:e1004118. https://doi.org/10.1371/journal.pmed.1004118
13. Shin E, Choe YJ, Ryu B, Kim NY, Lee HJ, Kim DH, et al. Pediatric deaths associated with coronavirus disease 2019 (COVID-19) in Korea. J Korean Med Sci. 2023;38:e21. https://doi.org/10.3346/jkms.2023.38.e21
14. Japan Pediatric Society. Interium report of a survey of the clinical course of pediatric coronavirus disease 2019 (COVID-19) cases using the database in Japan: third report, 28 March, 2022 [in Japanese] [cited 2024 Jan 4]. http://www.jpeds.or.jp/uploads/files/20220328_tyukan_hokoku3.pdf
15. Cabinet Secretariat. The reports vaccination against SARS-CoV-2. 2023 [in Japanese] [cited 2024 Jan 4]. https://www.kantei.go.jp/jp/headline/kansensho/vaccine.html
16. Jang EJ, Choe YJ, Kim RK, Park YJ. BNT162b2 vaccine effectiveness against the SARS-CoV-2 Omicron variant in children aged 5 to 11 years. JAMA Pediatr. 2023;177:319–20. https://doi.org/10.1001/jamapediatrics.2022.5221
17. Cohen-Stavi CJ, Magen O, Barda N, Yaron S, Peretz A, Netzer D, et al. BNT162b2 vaccine effectiveness against Omicron in children 5 to 11 years of age. N Engl J Med. 2022;387:227–36. https://doi.org/10.1056/NEJMoa2205011
18. Piechotta V, Siemens W, Thielemann I, Toews M, Koch J, Vygen-Bonnet S, et al. Safety and effectiveness of vaccines against COVID-19 in children aged 5–11 years: a systematic review and meta-analysis. Lancet Child Adolesc Health. 2023;7:379–91. PubMed https://doi.org/10.1016/S2352-4642(23)00078-0
19. Hoshino A, Saitoh M, Oka A, Okumura A, Kubota M, Saito Y, et al. Epidemiology of acute encephalopathy in Japan, with emphasis on the association of viruses and syndromes. Brain Dev. 2012;34:337–43. https://doi.org/10.1016/j.braindev.2011.07.012
20. The Japanese Society of Child Neurology. Guidelines for the treatment of pediatric acute encephalopathy 2016 [in Japanese]. Tokyo: Shindan to Chiryo-sha; 2016.
21. Nukui M, Kawawaki H, Inoue T, Kuki I, Okazaki S, Amo K, et al. Clinical characteristics of acute encephalopathy with acute brain swelling: a peculiar type of acute encephalopathy. Brain Dev. 2018;40:792–8. https://doi.org/10.1016/j.braindev.2018.05.004
22. Levin M, Pincott JR, Hjelm M, Taylor F, Kay J, Holzel H, et al. Hemorrhagic shock and encephalopathy: clinical, pathologic, and biochemical features. J Pediatr. 1989; 114:194–203. PubMed https://doi.org/10.1016/S0022-3476(89)80783-8
23. Sakuma H, Takanashi JI, Muramatsu K, Kondo H, Shiihara T, Suzuki M, et al.; Japanese Pediatric Neuro-COVID-19 Study Group. Severe pediatric acute encephalopathy syndromes related to SARS-CoV-2. Front Neurosci. 2023;17:1085082. https://doi.org/10.3389/fnins.2023.1085082
24. Lan SY, Lin JJ, Hsia SH, Wang HS, Chiu CH, Lin KL; CHEESE Study Group. Analysis of fulminant cerebral edema in acute pediatric encephalitis. Pediatr Neonatol. 2016;57:402–7. PubMed https://doi.org/10.1016/j.pedneo.2015.11.002
25. Glaser CA, Honarmand S, Anderson LJ, Schnurr DP, Forghani B, Cossen CK, et al. Beyond viruses: clinical profiles and etiologies associated with encephalitis. Clin Infect Dis. 2006;43:1565–77. https://doi.org/10.1086/509330
26. Krishnan P, Glenn OA, Samuel MC, Sheriff H, Foster-Barber A, Sejvar JJ, et al. Acute fulminant cerebral edema: a newly recognized phenotype in children with suspected encephalitis. J Pediatric Infect Dis Soc. 2021;10:289–94. https://doi.org/10.1093/jpids/piaa063
27. Kasai M, Shibata A, Hoshino A, Maegaki Y, Yamanouchi H, Takanashi JI, et al. Epidemiological changes of acute encephalopathy in Japan based on national surveillance for 2014–2017. Brain Dev. 2020;42:508–14. https://doi.org/10.1016/j.braindev.2020.04.006

Address for correspondence: Yuuki Tsuchihashi, Center for Field Epidemic Intelligence, Research and Professional Development, National Institute of Infectious Diseases, 1-23-1 Toyama, Shinjuku-ku, Tokyo 162-8640, Japan; email: yuuki@niid.go.jp

Metagenomic Detection of Bacterial Zoonotic Pathogens among Febrile Patients, Tanzania, 2007–2009[1]

Robert J. Rolfe, Sarah W. Sheldon, Luke C. Kingry, Jeannine M. Petersen, Venance P. Maro, Grace D. Kinabo, Wilbrod Saganda, Michael J. Maze, Jo E.B. Halliday, William L. Nicholson, Renee L. Galloway, Matthew P. Rubach, John A. Crump

Bacterial zoonoses are established causes of severe febrile illness in East Africa. Within a fever etiology study, we applied a high-throughput 16S rRNA metagenomic assay validated for detecting bacterial zoonotic pathogens. We enrolled febrile patients admitted to 2 referral hospitals in Moshi, Tanzania, during September 2007–April 2009. Among 788 participants, median age was 20 (interquartile range 2–38) years. We performed PCR amplification of V1–V2 variable region 16S rRNA on cell pellet DNA, then metagenomic deep-sequencing and pathogenic taxonomic identification. We detected bacterial zoonotic pathogens in 10 (1.3%) samples: 3 with *Rickettsia typhi*, 1 *R. conorii*, 2 *Bartonella quintana*, 2 pathogenic *Leptospira* spp., and 1 *Coxiella burnetii*. One other sample had reads matching a *Neoerhlichia* spp. previously identified in a patient from South Africa. Our findings indicate that targeted 16S metagenomics can identify bacterial zoonotic pathogens causing severe febrile illness in humans, including potential novel agents.

Bacterial zoonoses cause severe febrile illness in East Africa (*1*). Patients with bacterial zoonotic diseases can have nonspecific febrile illnesses that are difficult to diagnose clinically or in the laboratory because many of the pathogens are fastidious or nonculturable. Previous studies have used serologic or molecular methods to confirm leptospirosis, Q fever, spotted fever group rickettsioses (SFGR), and typhus group rickettsioses (TGR) among febrile participants at hospitals in East Africa (*2*–*5*). We previously evaluated participants from 2 cohort studies of febrile inpatients in northern Tanzania by using paired microscopic agglutination test (MAT) and PCR for leptospirosis, and by using paired immunofluorescence antibody (IFA) test for SFGR, TGR, and Q fever (*6*–*9*). In those cohort studies from 2007–2008 and 2012–2014, the estimated prevalence of acute leptospirosis was 8.8% (2007–2008) and 1.8% (2012–2014), acute SFGR prevalence 8.8% (2007–2008) and 8.9% (2012–2014), and acute Q fever prevalence 4.7% (2007–2008) and 8.1% (2012–2014) (*7*,*8*). Acute TGR was evaluated in 1 of the cohorts, and 2 confirmed infections were identified among 450 febrile participants (*6*).

PCR on acute samples and serologic testing of acute and convalescent samples are currently the most common methods to confirm diagnosis of several bacterial zoonoses (*10*). However, PCR and serology both target known pathogens and neither can identify potential novel pathogens. To characterize novel tickborne pathogens, the Bacterial Diseases Branch,

Author affiliations: Duke University Department of Medicine Division of Infectious Diseases and International Health, Durham, North Carolina, USA (R.J. Rolfe, M.P. Rubach, J.A. Crump); Centers for Disease Control and Prevention, Fort Collins, Colorado, USA (S.W. Sheldon, L.C. Kingry, J.M. Petersen); Kilimanjaro Christian Medical Centre, Moshi, Tanzania (V.P. Maro, G.D. Kinabo, M.P. Rubach, J.A. Crump); Kilimanjaro Christian Medical University College, Moshi (V.P. Maro, G.D. Kinabo, J.A. Crump); Mawenzi Regional Referral Hospital, Moshi (W. Saganda); University of Otago Department of Medicine, Christchurch, New Zealand (M.J. Maze); University of Glasgow School of Biodiversity, One Health and Veterinary Medicine, Glasgow, Scotland, UK (J.E.B. Halliday); Centers for Disease Control and Prevention, Atlanta, Georgia, USA (W.L. Nicholson, R.L. Galloway); Duke-National University of Singapore Programme in Emerging Infectious Diseases, Singapore (M.P. Rubach); Duke University Global Health Institute, Durham (M.P. Rubach, J.A. Crump); Centre for International Health, University of Otago, Dunedin, New Zealand (J.A. Crump)

DOI: https://doi.org/10.3201/eid3008.240529

[1]Preliminary results of this study were presented at the 72nd American Society of Tropical Medicine and Hygiene Annual Meeting; October 18–22, 2023; Chicago, Illinois, USA.

Division of Vector-Borne Diseases, National Center for Emerging and Zoonotic Infectious Diseases, Centers for Disease Control and Prevention (CDC; Fort Collins, CO, USA), developed a 16S rRNA metagenomics assay to evaluate samples for known and novel tickborne and other zoonotic pathogens (*11*). The assay accurately differentiated and identified *Anaplasma*, *Bartonella*, *Borrelia*, *Coxiella*, *Ehrlichia*, *Leptospira*, and *Rickettsia* bacteria (*11*). CDC tested spiked healthy human blood and water specimens, and the assay readily identified zoonotic pathogens among commensal and background organisms commonly amplified when targeting 16S (*11*). In spiked blood specimens, the assay demonstrated equivalent analytic sensitivity to reverse transcription PCR (RT-PCR) but showed some loss of sensitivity when specimens were spiked with multiple pathogenic species (*11*).

In this study, we leveraged that high-throughput 16S rRNA metagenomic assay to interrogate venous blood cell pellets for a broad range of bacterial zoonotic pathogens in a febrile patient study cohort. We assessed whether 16S interrogation could provide insights into causes of febrile illness by detecting novel or under-appreciated pathogens or by genotypic characterization of pathogens already known to cause disease in the study area, such as SFGR and TGR.

Methods

Study Procedures and Participants

We performed a prospective cohort study that enrolled pediatric and adult medical patients admitted with fever to 2 referral hospitals in Moshi, Tanzania, duing September 2007–April 2009 (*4*–*6*,*12*,*13*). In brief, infants and children ≥2 months and <13 years of age admitted to the pediatric ward were eligible if they had a history of fever in the previous 48 hours, an axillary temperature ≥37.5°C, or a rectal temperature of ≥38.0°C. Adolescents and adults ≥13 years of age who were admitted to the adult medicine ward were eligible to participate if they had an oral temperature ≥38.0°C.

A clinical officer performed a standardized clinical history and physical examination and recorded vital signs. Collected demographic and clinical information included sex, age, and rural or urban residence.

We drew venous blood samples in EDTA tubes within 24 hours of hospital admission and fractionated samples by centrifugation into plasma and cell pellets. We fractionated blood collected into red top plain tubes into serum, first by gravity on the bench top, then by centrifugation. We performed complete blood counts by using Cell-Dyn 3500 automated hematology analyzer (Abbott Laboratories, https://www.abbott.com). We asked participants to return 4–6 weeks after enrollment to provide a convalescent serum sample. We stored the resulting serum, plasma, and cell pellets at −70°C. We shipped cell pellets on dry ice to CDC for 16S metagenomic analysis. The pellets remained frozen at −70°C after collection and did not go through freeze–thaw cycles until testing. CDC performed testing in 3 different sequencing runs during August 5–December 20, 2021.

We used serology and PCR testing to determine patients' HIV status. We performed serologic testing by using 2 rapid antibody tests on whole blood, Capillus HIV-1/HIV-2 (Trinity Biotech PLC, https://www.trinitybiotech.com) and Determine HIV-1/2 Ag/AB Combo (Abbott Laboratories). After March 4, 2008, we replaced the Capillus test with the SD Bioline HIV 1/2 Test version 3.0 (Abbott Laboratories). When rapid test results were discordant, we tested the sample by using Vironostika Uni-Form HIV II plus O Ab ELISA (bioMérieux, https://www.biomerieux.com). If the ELISA was positive, we used Genetic Systems HIV-1 Western blot kit (Bio-Rad Laboratories, https://www.bio-rad.com) as a confirmatory test. We obtained HIV-1 RNA by using the Abbott m2000 System RealTime HIV-1 assay (Abbott Laboratories) to diagnose acute HIV infection in seronegative adults and for early HIV diagnosis in infants (*6*,*12*).

As described previously (*4*,*6*–*9*), we shipped serum and plasma on dry ice to CDC's Bacterial Special Pathogens Branch, Division of High-Consequence Pathogens and Pathology, for MAT for pathogens that cause leptospirosis. We shipped samples to CDC's Rickettsial Zoonoses Branch, Division of Vector-Borne Diseases, for IFA serologic analyses for pathogens that cause Q fever, SFGR, and TGR.

CDC performed *Leptospira* real-time PCR on samples from participants with serologically confirmed or probable leptospirosis and on participants who died before providing a convalescent serum sample (*9*). In that population of febrile participants, cases of confirmed acute leptospirosis were defined by a ≥4-fold increase in MAT titer or detection by real-time PCR; cases of probable leptospirosis had a reciprocal MAT titer ≥800 and evidence of exposure to pathogenic leptospires as a reciprocal MAT titer ≥100 (*5*). For seropositive cases, we defined the predominant reactive serogroup as the serovar with the highest MAT titer.

We defined cases of confirmed acute Q fever as active fever and a ≥4-fold increase in reciprocal IFA titer to the *C. burnetii* phase II antigen. We defined serologic

evidence of Q fever exposure as a case with an IFA titer ≥1,000 to phase I antigen; for patients who did not meet the case definition of a serologic diagnosis, we considered ≥64 to phase II antigen in either acute or convalescent sample as confirmed acute Q fever (*4*).

We defined confirmed acute SFGR and TGR cases as presence of fever and ≥4-fold rise in IFA titer to *R. conorii* for SFGR or *R. typhi* for TGR. For patients who did not meet the case definition for confirmed acute SFGR or TGR, we defined an IFA titer ≥64 for *R. conorii* as exposure for SFGR and titer of ≥64 for *R. typhi* as exposure for TGR (*4*).

16S rRNA Metagenomic Assay

We performed metagenomic 16S rRNA testing by using previously outlined methods (*1*). In brief, we extracted DNA from cell pellets by using the MagNA Pure 96 instrument (Roche, https://www.roche.com) and the DNA and Viral NA Small-Volume kit with the associated DNA Blood SV 3.1 extraction protocol (Roche) using input and elution volumes of 100 μL. To perform multiplex sequencing on the 788 samples, we amplified the V1–V2 region of the 16S rRNA and added dual Nextera XT indices by using the XT Index Kit v2, sets A–D (Illumina, https://www.illumina.com) to the V1–V2 amplicons. We quantified, normalized to a final concentration of 4 nM, and pooled resulting libraries to enable sequencing of 384 samples in each Illumina MiSeq run. We also included DNA extraction controls, PCR controls, and internal sequencing controls in each run (*8*). Pooled libraries had a final contration of 12.5 pM with 12.5 pM PhiX (10%), which we then sequenced by using MiSeq v2 (500 cycle) reagent kit and MiSeq sequencer (Illumina).

Bioinformatic Analysis, Taxonomic Prediction, and Phylogenetic Analysis

We performed bioinformatic data processing as previously described (*11*). We demultiplexed sequence reads into individual samples, then used internal MiSeq software to remove the adaptor and indices. We used Kraken 0.10.5 (*14*) and the MiniKraken database (https://ccb.jhu.edu/software/kraken) to assign taxonomic predictions to quality-trimmed, merged reads. We mapped reads from samples with a MiniKraken taxonomic prediction of *Anaplasma*, *Bartonella*, *Coxiella*, *Ehrlichia*, *Leptospira*, or *Rickettsia* to reference sequences by using CLC Genomics Workbench (QIAGEN, https://www.qiagen.com), and tested by BLASTn (https://blast.ncbi.nlm.nih.gov). We did not perform further analyses for reads with taxonomic predictions to other genera, including commensal and background organisms identified in control specimens (i.e., Enterobacterales). We constructed phylogenetic trees in MEGA version 10.0.5 (*15*) by using the maximum-likelihood method and Kimura 2-parameter model with 1,000 bootstrap replicates.

Statistical Analyses

We performed descriptive data analysis in proportions. We described continuous variables as median and interquartile range (IQR). We performed statistical analyses in R version 4.0.1 (The R Foundation for Statistical Computing, https://www.r-project.org) using the tableone and tidyverse packages (*16*,*17*). We predicated sample size on participant accrual during the parent study enrollment period (*12*,*13*).

Ethics Considerations

This study was approved by the Kilimanjaro Christian Medical University College Heath Research Ethics Committee (clearance certificates 133 and 138), the Tanzania National Institute for Medical Research Ethics Coordinating Committee (clearance certificates NIMR/HQ/R.8a/Vol.IX/439 and NIMR/HQ/R.8a/Vol.IX/473), and the Institutional Review Board at Duke University Medical Center (protocol nos. 8397 and 8400). CDC acknowledged the study protocol through deferral to the Duke University Medical Center Institutional Review Board.

Written informed consent was obtained from all participants. A parent or legal guardian provided consent for participants <18 years of age. In addition to consent for study participation, which included permission for future not yet determined analyses on stored blood for HIV research, written informed consent was also obtained from participants for a data and sample repository for future, unspecified research.

Results

Among 788 febrile illness participants who had a cell pellet available for testing and available sociodemographic data, the median age was 20 (IQR 2–38) years, 239/744 (32.1%) were HIV-infected, 384/766 (50.1%) were male and 382/766 (49.9%) female, and 314/664 (47.3%) lived in an urban setting. Ten (1.3%) participants had 100% sequence identity match in BLASTn for a bacterial zoonotic pathogen detected in cell pellets via 16S metagenomic sequencing: 3 *R. typhi* matched accession no. NC_017066.1, one *R. conorii* matched accession no. NC_003103.1, two *Bartonella quintana* matched accession no. AP019773.1, one *Leptospira borgpetersenii* matched accession no. NZ_CP026671.1, one *L. kirschneri* matched accession no. CP092660.1, and

one *C. burnetii* matched accession no. CP014563.1; one sample had reads matching an uncultured and unnamed *Neoehrlichia* sp. previously identified in a patient from South Africa (*18*). Of the 10 participants with a detected bacterial zoonotic pathogen, 5 (50.0%) were male and 5 (50.0%) female; median age was 41 (IQR 32–56) years. One of the 2 participants with detected *B. quintana* was HIV-infected (Table 1). Symptom onset varied from 3–40 days before enrollment, and 7 (70%) patients had symptoms for ≤7 days. For the 10 samples with detected bacterial zoonotic pathogens, we used BLASTn for taxonomic prediction, read counts, and abundance relative to all other bacterial taxa detected by 16S in clinical samples (Table 2).

We created a phylogenetic tree for the identified *Candidatus* Neoehrlichia spp. (Figure 1). A 1,467-bp 16S sequence amplified from a bone marrow aspirate from a patient from South Africa (GenBank accession no. OP208838) matched 100% over the 296-bp V1–V2 target sequence amplified in this study (*18*).

Table 1. Organisms and patient characteristics in a study of metagenomic detection of bacterial zoonotic pathogens among febrile patients, Tanzania, 2007–2009*

Organism detected	Patient age, y/sex	Rural res.	Illness onset, d	Symptoms	Cell count, × 10^3/μL			Serologic testing			Results
					WBC†	Plat.	ALC	*Leptospira* MAT	Q fever IFA	*Rickettsia* IFA	
Bartonella quintana	10/M	Y	4	Fever, dyspnea, convulsions	11.9	89	2.59	Acute and convalescent	ELISA screen negative	Acute and convalescent	Probable acute leptospirosis‡
B. quintana	47/M§	N	40	Fever, cough, hemoptysis, dyspnea, weight loss	18.4	124	1.55	ND	ND	ND	NA
Coxiella burnetii	22/M	Y	2	Fever, rigors	4.6	93	1.92	Acute only	ND	Acute only	Probable acute leptospirosis‡
Leptospira borgpetersenii	43/F	Y	4	Fever, rigors, emesis, headache	4.2	85	0.33	Acute and convalescent	ELISA screen negative	Acute and convalescent	Confirmed acute leptospirosis‡
L. kirschneri	60/F	N	3	Fever, emesis, headache	5.4	114	0.52	Acute only	ND	Acute only	NA
Rickettsia conorii	70/M	Y	7	Fever, rigors, dyspnea, diarrhea, headache	15.1	118	1.77	ND	ND	ND	NA
Rickettsia typhi	36/M	Y	14	Fever, rigors, headache, nuchal rigidity, dysuria	6.6	52	0.92	Acute only	ND	Acute only	Exposure to SFG *Rickettsia* and typhus group *Rickettsia*
R. typhi	77/F	N	3	Fever, rigors	4.5	97	0.35	Acute and convalescent	ELISA screen negative	Acute and convalescent	Confirmed acute SFGR
R. typhi	31/F	Y	30	Fever, rigors, emesis, headache	7.2	148	0.66	Acute and convalescent	ELISA screen negative	Acute and convalescent	Confirmed acute SFGR; exposure to typhus group *Rickettsia*
Neoehrlichia spp.	40/F	N	3	Fever, rigors, hemoptysis, diarrhea, emesis, headache	3.0	25	0.65	ND	ND	ND	NA

*Most patients were HIV-negative; 1 patient with *B. quintana* was HIV-infected. ALC, absolute lymphocyte count; IFA, immunofluorescence assay; MAT, microscopic agglutination testing; NA, not applicable; ND, not done; Plat., platelets; res., resident; SFG, spotted fever group; SFGR, spotted fever group rickettsioses; WBC, white blood cells (leukocytes).
†Based on MAT results.
‡*Leptospira* PCR was not performed for this sample.
§HIV-positive patient.

Table 2. Metagenomic sequencing results used for detection of bacterial zoonotic pathogens among febrile patients, Tanzania, 2007–2009*

Organism	V1–V2 sufficient for species ID	MiniKraken taxonomic prediction†	BLASTn taxonomic prediction (% identity)‡	Sequence in database	Read count	% Abundance
Bartonella quintana	Y	*B. quintana*	*B. quintana* AP019773.1 (100)	Y	4,730	98.21
B. quintana	Y	*B. quintana*	*B. quintana* AP019773.1 (100)	Y	3,568	38.60
Coxiella burnetii	Y	*C. burnetii*	*C. burnetii* CP014563.1 (100)	Y	1,795	47.97
Leptospira borgpetersenii	Y	*L. borgpetersenii*	*L. borgpetersenii* CP047520.1 (100)	Y	18,903	94.41
L. kirschneri	Y	*Leptospira* spp.	*L. kirschneri* CP092660.1 (100)	N	28,008	99.32
Rickettsia conorii	Y	*Rickettsia* spp.	*R. conorii* MG564258.1 (100)	N	159	28.29
R. typhi	Y	*Rickettsia typhi*	*R. typhi* LS992663.1 (100)	Y	429	47.72
R. typhi	Y	*Rickettsia typhi*	*R. typhi* LS992663.1 (100)	Y	7,274	82.02
R. typhi	Y	*Rickettsia typhi*	*R. typhi* LS992663.1 (100)	Y	9,527	83.16
Candidatus Neoehrlichia spp.	Y	Anaplasmataceae, *Ehrlichia ruminantium*, *Ehrlichia*	Uncultured *Candidatus* Neoehrlichia sp. SA1 OP208838.1 (100)	N	40,238	98.56

*ID, identification; V1–V2, variable regions 1 and 2.
†Johns Hopkins University Center for Computational Biology (https://ccb.jhu.edu/software/kraken).
‡National Center for Biotechnology Information taxonomy and accession nos. from BLASTn (https://blast.ncbi.nlm.nih.gov).

We created a phylogenetic tree to compare the 16S V1–V2 of the *Rickettsia* sequences from this cohort to sequences from closely related *Rickettsia* species (Figure 2). The sequence from the study sample with *R. conorii* aligned 100% with *R. conorii* strain Malish (GenBank accession no. NC_003103.1) and was distinct from *R. africae* (accession no. NC_012633.1). The 3 *R. typhi* sequences all aligned 100% with *R. typhi* (accession no. NC_017066.1) and were distinct from *R. prowazekii* (accession no. NC_017049.1). The V1–V2

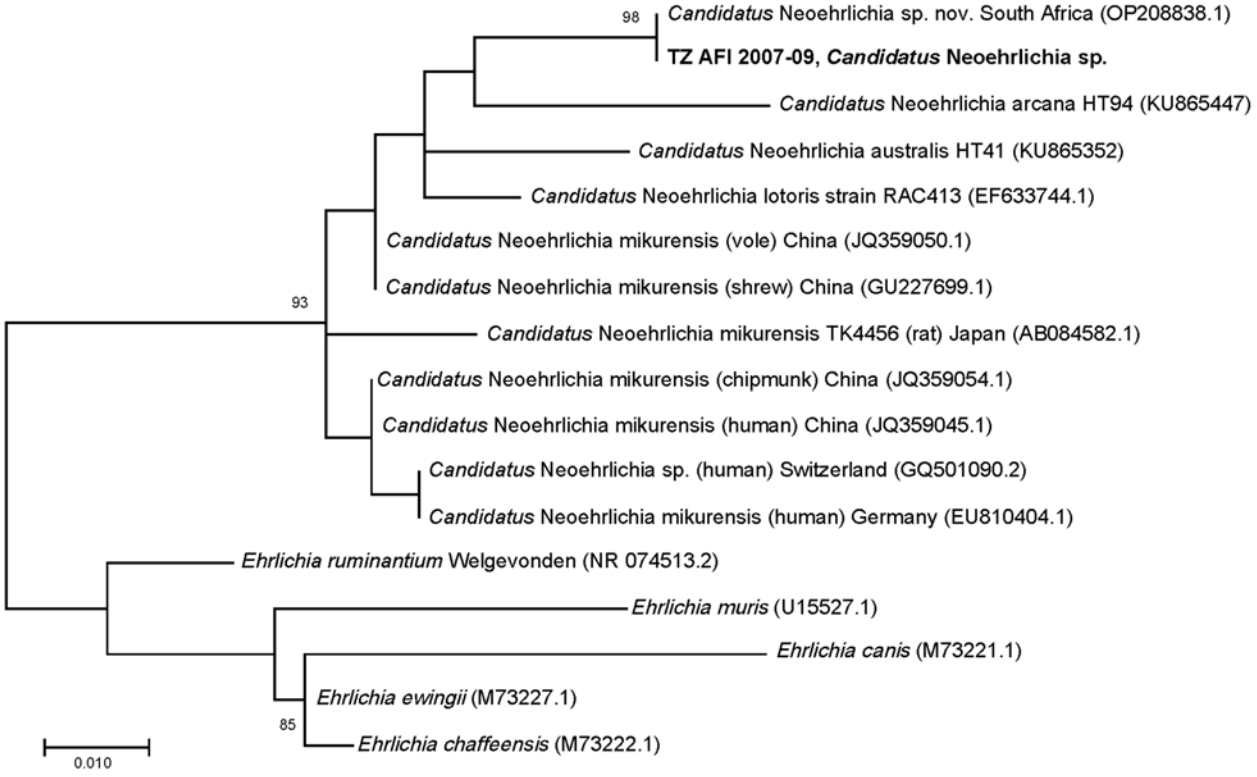

Figure 1. Phylogenetic tree for *Candidatus* Neoehrlichia spp. identified during metagenomic detection of bacterial zoonotic pathogens among febrile patients, Tanzania, 2007–2009. Bold text indicates the sequence from this study. Numbers in parentheses indicate GenBank accession numbers. A 1,467-bp 16S sequence amplified from a bone marrow aspirate from a patient from South Africa (GenBank accession no. OP208838) matched 100% over the 296-bp variable regions 1 and 2 target sequence amplified in this study (*18*). Scale bar indicates nucleotide substitutions per site.

16S target is not sufficient to differentiate between *R. conorii* subspecies *heilogjiangensis* and *R. japonica*, nor among *R. rickettsia*, *R. peacockii*, *R. philipii*, and *R. slovaca*. However, that target is sufficient to differentiate between *R. conorii* and *R. africae* because 2 single-nucleotide differences are expected between those strains and *R. africae* has a TTT insertion.

We detected *Leptospira* from 2 patients in the cohort. The phylogenetic tree comparing the 16S V1–V2 of the *Leptospira* sequences from this cohort to sequences from closely related species showed 1 *L. kirshneri* detection related to GenBank accession no. CP092660.1 and 1 *L. borgpetersenii* detection related to accession no. NZ_CP026671.1 (Figure 3).

We compiled serologic and PCR results of the 10 participants with bacterial zoonotic pathogen–positive samples (Table 1). Of those participants, 5 did not have serologic testing performed for the pathogen

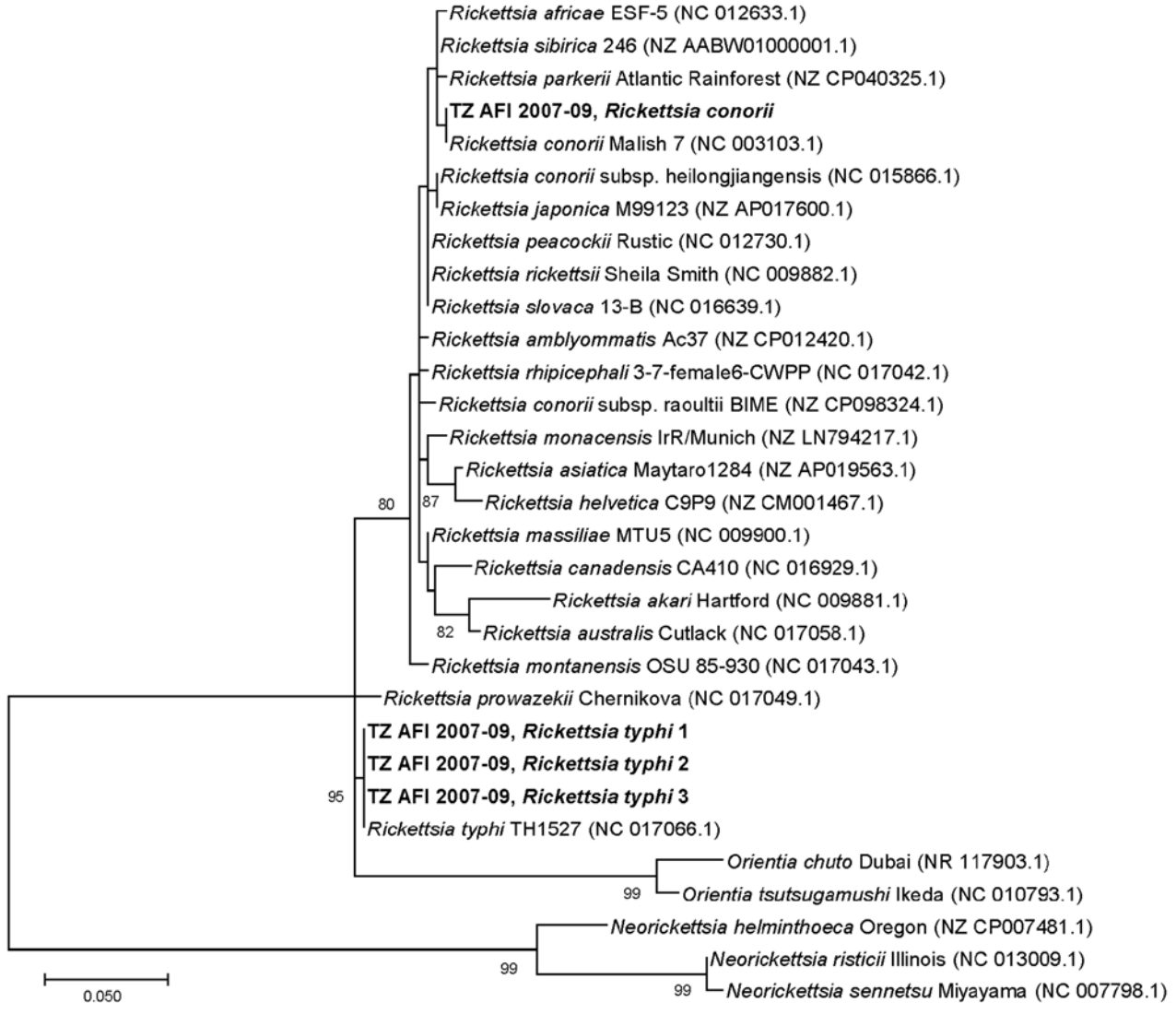

Figure 2. Phylogenetic tree of *Rickettsia* spp. sequences detected in metagenomic analysis of bacterial zoonotic pathogens among febrile patients, Tanzania, 2007–2009. The tree compares sequences from the 16S variable regions 1 and 2 (V1–V2) of the *Rickettsia* cohort from this study (bold text) to sequences from closely related *Rickettsia* species. Numbers in parentheses indicate GenBank accession numbers. The sequence from the study sample with *R. conorii* aligned 100% *R. conorii* strain Malish (accession no. NC003103.1) and was distinct from *R. africae* (accession no. NC012633.1). All 3 *R. typhi* strains from this study aligned 100% with *R. typhi* reference strain (accession no. NC017066.1) and were distinct from *R. prowazekii* (accession no. NC017049.1). The V1–V2 16S target is not sufficient to differentiate between *R. conorii* subsp. *heilogjiangensis* and *R. japonica*, or between *R. rickettsia*, *R. peacockii*, *R. philipii*, and *R. slovaca*. However, the V1–V2 16S target is sufficient to differentiate between *R. conorii conorii* and *R. africae* because 2 single-neucleotide differences would be expected between *R. conorii conorii* and *R. africae* and a TTT insertion in *R. africae*. Scale bar indicates nucleotide subsitutions per site.

identified by 16S; 1 participant with detected *B. quintana* had serologic testing consistent with probable acute leptospirosis. The participant with *L. borgpetersenii* 16S detection had serologic testing consistent with acute leptospirosis and seroconverted to serogroup Mini, represented in the MAT panel by serovar Georgia. Real-time PCR *Leptospira* testing was not performed on samples from either of those participant. Two participants with *R. typhi* 16S detection had serologic evidence of exposure to typhus group *Rickettsia*, and 1 had serologic evidence of exposure to both spotted fever group *Rickettsia* and typhus group *Rickettsia* (Table 1).

Discussion

Metagenomic sequencing on venous blood cell pellets from patients admitted with febrile illness in Tanzania

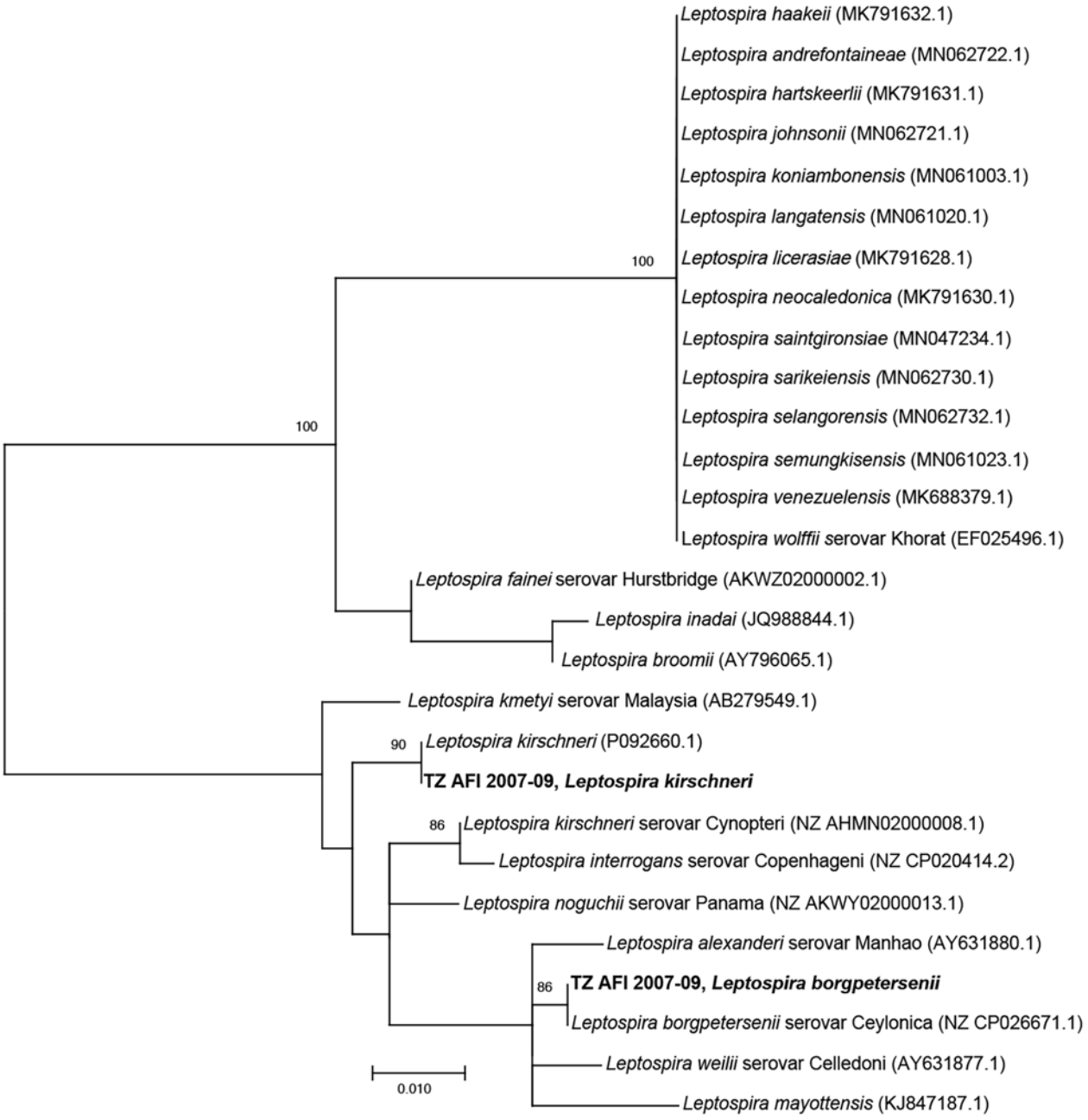

Figure 3. Phylogenetic tree of *Leptospira* sequences detected in metagenomic analysis of bacterial zoonotic pathogens among febrile patients, Tanzania, 2007–2009. The tree compares sequences from the 16S V1–V2 of the *L. kerchnerii* and *L. borgpetersenii* cohort from this study (bold text) to sequences from closely related *Leptospira* species. Numbers in parentheses indicate GenBank accession numbers. Scale bar indicates nucleotide subsitutions per site.

generated several noteworthy findings, including detection of fleaborne or louseborne zoonotic pathogens, *B. quintana* and *R. typhi*; genetic confirmation of *R. conorii* in a febrile human from Tanzania, where spotted fever group *Rickettsia* is a common cause of febrile illness; and description of a potentially novel agent of neoehrlichiosis.

Identification of *B. quintana* and *R. typhi*, both considered reemerging pathogens (*19*), are notable for northern Tanzania. In a study on *Rickettsia*, *Bartonella*, and *Yersinia* detected in fleas in 3 countries in Africa, *R. typhi* DNA was detected in 2 (2%) of 94 fleas collected in Tanzania, but *Bartonella* was not detected (*20*). However, multiple *Bartonella* species have been detected in fleas and small mammal samples in northern Tanzania (*21*). Despite those documented detections in fleas in Tanzania, the body louse is considered the primary vector for *B. quintana* (*22*). Consistent with the established clinical epidemiology of bartonellosis caused by *B. quintana*, 1 of the 2 *B. quintana* cases detected in our cohort occurred in an HIV-infected participant.

Detection of *R. conorii* in this cohort are a substantial public health finding because SFGR is a common cause of severe febrile illness in East Africa. Serologic testing is unable to distinguish among SFGR pathogens, including between *R. conorii* and *R. africae* (*23*). In a previous report, *R. africae* was detected from a patient with an eschar after travel to Tanzania (*24*). However, after comprehensive literature searches in multiple databases, extensive gray literature searching, and consultation with a reference librarian, we found no other examples of molecular detection of *R. conorii* in Tanzania. Genomic detection of *R. conorii*, the causative agent of Mediterranean spotted fever, is notable because *R. conorii* causes a more severe disease than *R. africae* and sometimes is fatal (*25*). Detection of *R. conorii* as a causative agent of SFGR in Tanzania is consistent with detections elsewhere in East Africa, including an *R. conorii* detection by PCR in a traveler returning to Japan from Kenya (*26*) and a report of fatal SFGR infection in Kenya in which the *Rickettsia* species was not identified (*27*). SFGR caused by *R. conorii* in East Africa is also supported by a domestic animal sampling study in which *R. conorii* subsp. *israelensis* was identified in domestic animals in Kenya and in ticks at slaughterhouses in Nairobi and Mombasa (*28*). Previous research in northern Tanzania has shown that SFGR is endemic (*4*,*8*). The identification of *R. conorii* as one of the agents of SFGR increases the severity profile of this disease in Tanzania and supports the need for advances in diagnostic testing for SFGR. In addition to the implications for SFGR disease burden due to severity and potential death, this finding also has implications for targeting disease prevention measures because *R. conorii* transmission would likely occur via *Rhipicephalus* ticks that infest canines, but *R. africae* transmission to humans would likely occur via *Amblyomma* ticks that infest cattle or other livestock (*29*,*30*).

The specimen with MiniKraken taxonomic predictions of Anaplasmataceae, *Ehrlichia ruminantium*, and *Ehrlichia* (Table 2) showed 100% sequence identity to a recently published novel *Candidatus* Neoehrlichia sp. sequence derived from a case of febrile illness in an immunocompetent child from South Africa who lived on a farm but had no reported tick bite (*18*). The 16S sequence from the patient from South Africa showed 100% identity to a 345-bp partial V3-V4 16S sequence (GenBank accession no. KT895260) derived from the blood culture of an patient from Austria with travel history to Tanzania who did not recall a tick bite during her trip but did have skin contact exposure to a prosimian (*31*). Those 2 *Candidatus* Neoehrlichia species infections and ours highlight the organism as a potential cause of a febrile illness in Africa. Further research is needed to determine illness severity, potential reservoirs, and geographic distribution.

Detection of pathogenic *Leptospira* spp. and *C. burnetii* is consistent with our prior work describing leptospirosis and acute Q fever as relatively common causes of febrile illness in northern Tanzania (*4*,*5*). Genetic characterization of both *Leptospira* spp. and *C. burnetii* associated with severe febrile illness in northern Tanzania are nonetheless notable findings and could aid in future studies investigating source attribution via genomic methods.

The participant with *L. borgpetersenii* seroconverted to serogroup Mini represented by serovar Georgia in the MAT panel. Few human leptospirosis infections in Tanzania have been genotypically characterized as *Leptospira* and our case had a combination of species and serogroup conversion (*32*). *L. kirschneri* was also detected from a febrile participant recruited in northern Tanzania during a 2012–2014 study. That participant seroconverted to serogroup Sejroe (*9*). Combined molecular and serologic data indicate multiple circulating *Leptospira* serovars in a small number of positive samples over 2 time periods. *Leptospira* diversity likely indicates complex transmission ecology in Tanzania with multiple serovars co-circulating in diverse hosts and circulating serovars changing over time (*33*).

One limitation of our study is that sensitivity of V1–V2 16S metagenomics was previously determined

to be equivalent to that of RT-PCR in whole blood (*11*). However, the blood cell pellets used in this study represent a fraction of whole blood, a specific specimen type that has not been previously evaluated. In addition, although the overall percentage of samples positive by 16S metagenomics low (1.2%), that value was higher than the percentage (0.6%) of positive samples reported in a previous study that screened >10,000 specimens submitted for tickborne illness in the United States (*11*). Both studies relied on screening residual specimens; thus, the proportion of participants in whom bacterial sequencing detected a zoonotic pathogen does not give accurate indicators of disease prevalence.

In conclusion, by using targeted V1–V2 16S metagenomic testing among participants with febrile illness in Tanzania, we detected genera and some species of bacterial zoonoses that are of clinical and public health concern in northern Tanzania. The genetic confirmation of *R. conorii* detected here more broadly expands our understanding of the species responsible for SFGR in Tanzania and East Africa. 16S rRNA metagenomics also confirmed typhus group *Rickettsia*, *Leptospira*, and *C. burnetii* as causes of severe febrile illness in northern Tanzania. The assay also detected *Bartonella* and identified a potentially novel agent of neoehrlichiosis in sub-Saharan Africa. We demonstrated that metagenomic approaches can improve the etiologic and epidemiologic understanding of febrile illness. Although the overall low number of detections might preclude the 16S rRNA platform from being a standalone surveillance approach, our study highlights that this sequence-based approach provides genetic epidemiologic insights that can inform and optimize disease surveillance and prevention strategies.

Acknowledgments

We thank Anne B. Morrissey for laboratory support; Ahaz T. Kulanga for providing administrative support; and Pilli M. Chambo, Beata V. Kyara, Beatus A. Massawe, Anna D. Mtei, Godfrey S. Mushi, Lillian E. Ngowi, Flora M. Nkya, and Winfrida H. Shirima for reviewing and enrolling study participants. We also thank Paul S. Mead and Ronald Rosenberg, who were instrumental in facilitating this collaboration.

This research was supported by an International Studies on AIDS Associated Co-infections (ISAAC) award, a US National Institutes of Health (NIH)–funded program (no. U01 AI062563). Investigator support was received from NIH ISAAC awards (to J.A.C., A.B.M., V.P.M., and G.D.K.); AIDS International Training and Research Program (award no. D43 PA-03-018 to J.A.C., V.P.M., and G.D.K.); the Duke Clinical Trials Unit and Clinical Research Sites (award no. U01 AI069484 to J.A.C., V.P.M., and G.D.K.); the Center for HIV/AIDS Vaccine Immunology (award no. U01 AI067854 to J.A.C.); the joint NIH–National Science Foundation Ecology of Infectious Disease program, the UK Economic and Social Research Council, and UK Biotechnology and Biological Sciences Research Council (award no. R01TW009237 to J.A.C., V.P.M., and W.S.), and Research Career Development Award (award no. K23 AI116869 to M.P.R.).

About the Author

Dr. Rolfe is an infectious diseases physician at Duke University in Durham, North Carolina, USA. His main research interests are the utility of diagnostic platforms in describing the epidemiology of bacterial zoonoses.

References

1. Prasad N, Murdoch DR, Reyburn H, Crump JA. Etiology of severe febrile illness in low- and middle-income countries: a systematic review. PLoS One. 2015;10:e0127962. https://doi.org/10.1371/journal.pone.0127962
2. Maina AN, Farris CM, Odhiambo A, Jiang J, Laktabai J, Armstrong J, et al. Q fever, scrub typhus, and rickettsial diseases in children, Kenya, 2011–2012. Emerg Infect Dis. 2016;22:883–6. https://doi.org/10.3201/eid2205.150953
3. Dreyfus A, Dyal JW, Pearson R, Kankya C, Kajura C, Alinaitwe L, et al. Leptospira seroprevalence and risk factors in health centre patients in Hoima District, Western Uganda. PLoS Negl Trop Dis. 2016;10:e0004858. https://doi.org/10.1371/journal.pntd.0004858
4. Prabhu M, Nicholson WL, Roche AJ, Kersh GJ, Fitzpatrick KA, Oliver LD, et al. Q fever, spotted fever group, and typhus group rickettsioses among hospitalized febrile patients in northern Tanzania. Clin Infect Dis. 2011;53:e8–15. https://doi.org/10.1093/cid/cir411
5. Biggs HM, Bui DM, Galloway RL, Stoddard RA, Shadomy SV, Morrissey AB, et al. Leptospirosis among hospitalized febrile patients in northern Tanzania. Am J Trop Med Hyg. 2011;85:275–81. https://doi.org/10.4269/ajtmh.2011.11-0176
6. Crump JA, Morrissey AB, Nicholson WL, Massung RF, Stoddard RA, Galloway RL, et al. Etiology of severe non-malaria febrile illness in northern Tanzania: a prospective cohort study. PLoS Negl Trop Dis. 2013;7:e2324. https://doi.org/10.1371/journal.pntd.0002324
7. Maze MJ, Cash-Goldwasser S, Rubach MP, Biggs HM, Galloway RL, Sharples KJ, et al. Risk factors for human acute leptospirosis in northern Tanzania. PLoS Negl Trop Dis. 2018;12:e0006372. https://doi.org/10.1371/journal.pntd.0006372
8. Pisharody S, Rubach MP, Carugati M, Nicholson WL, Perniciaro JL, Biggs HM, et al. Incidence estimates of acute Q fever and spotted fever group rickettsioses, Kilimanjaro, Tanzania, from 2007 to 2008 and from 2012 to 2014. Am J Trop Med Hyg. 2022;106:494–503. https://doi.org/10.4269/ajtmh.20-1036
9. Allan KJ, Maze MJ, Galloway RL, Rubach MP, Biggs HM, Halliday JEB, et al. Molecular detection and typing of pathogenic *Leptospira* in febrile patients and phylogenetic comparison with *Leptospira* detected among animals in

Tanzania. Am J Trop Med Hyg. 2020;103:1427–34. https://doi.org/10.4269/ajtmh.19-0703
10. Carugati M, Kilonzo KG, Crump JA. Fever, bacterial zoonoses, and One Health in sub-Saharan Africa. Clin Med (Lond). 2019;19:375–80. https://doi.org/10.7861/clinmed.2019-0180
11. Kingry L, Sheldon S, Oatman S, Pritt B, Anacker M, Bjork J, et al. Targeted metagenomics for clinical detection and discovery of bacterial tick-borne pathogens. J Clin Microbiol. 2020;58:e00147-20. https://doi.org/10.1128/JCM.00147-20
12. Crump JA, Ramadhani HO, Morrissey AB, Msuya LJ, Yang LY, Chow SC, et al. Invasive bacterial and fungal infections among hospitalized HIV-infected and HIV-uninfected children and infants in northern Tanzania. Trop Med Int Health. 2011;16:830–7. https://doi.org/10.1111/j.1365-3156.2011.02774.x
13. Crump JA, Ramadhani HO, Morrissey AB, Saganda W, Mwako MS, Yang LY, et al. Invasive bacterial and fungal infections among hospitalized HIV-infected and HIV-uninfected adults and adolescents in northern Tanzania. Clin Infect Dis. 2011;52:341–8. https://doi.org/10.1093/cid/ciq103
14. Wood DE, Salzberg SL. Kraken: ultrafast metagenomic sequence classification using exact alignments. Genome Biol. 2014;15:R46. https://doi.org/10.1186/gb-2014-15-3-r46
15. Kumar S, Stecher G, Li M, Knyaz C, Tamura K. MEGA X: Molecular Evolutionary Genetics Analysis across computing platforms. Mol Biol Evol. 2018;35:1547–9. https://doi.org/10.1093/molbev/msy096
16. Yoshida K, Bartel A, Chipman JJ, Bohn J, D'Augustino McGowan C, Barrett M, et al. tableone: create 'Table 1' to describe baseline characteristics with or without propensity score weights [cited 2023 Dec 13]. https://cloud.r-project.org/web/packages/tableone/tableone.pdf
17. Wickham H, Averick M, Bryan J, Chang W, McGowan LDA, François R, et al. Welcome to the tidyverse. J Open Source Softw. 2019;4:1686. https://doi.org/10.21105/joss.01686
18. Bamford C, Blumberg LH, Bosman M, Frean J, Hoek KGP, Miles J, et al. Neoehrlichiosis in symptomatic immunocompetent child, South Africa. Emerg Infect Dis. 2023;29:407–10. https://doi.org/10.3201/eid2902.221451
19. Bitam I, Dittmar K, Parola P, Whiting MF, Raoult D. Fleas and flea-borne diseases. Int J Infect Dis. 2010;14:e667–76. https://doi.org/10.1016/j.ijid.2009.11.011
20. Leulmi H, Socolovschi C, Laudisoit A, Houemenou G, Davoust B, Bitam I, et al. Detection of *Rickettsia felis*, *Rickettsia typhi*, *Bartonella* species and *Yersinia pestis* in fleas (Siphonaptera) from Africa. PLoS Negl Trop Dis. 2014;8:e3152. https://doi.org/10.1371/journal.pntd.0003152
21. Theonest NO, Carter RW, Amani N, Doherty SL, Hugho E, Keyyu JD, et al. Molecular detection and genetic characterization of *Bartonell*a species from rodents and their associated ectoparasites from northern Tanzania. PLoS One. 2019;14:e0223667. https://doi.org/10.1371/journal.pone.0223667
22. Badiaga S, Brouqui P. Human louse-transmitted infectious diseases. Clin Microbiol Infect. 2012;18:332–7. https://doi.org/10.1111/j.1469-0691.2012.03778.x
23. Fournier PE, Jensenius M, Laferl H, Vene S, Raoult D. Kinetics of antibody responses in *Rickettsia africae* and *Rickettsia conorii* infections. Clin Diagn Lab Immunol. 2002;9:324–8.
24. Harrison N, Burgmann H, Forstner C, Ramharter M, Széll M, Schötta AM, et al. Molecular diagnosis of African tick bite fever using eschar swabs in a traveller returning from Tanzania. Wien Klin Wochenschr. 2016;128:602–5. https://doi.org/10.1007/s00508-016-1047-0
25. Ericsson CD, Jensenius M, Fournier P-E, Raoult D. Rickettsioses and the international traveler. Clin Infect Dis. 2004;39:1493–9. https://doi.org/10.1086/425365
26. Yoshikawa H, Kimura M, Ogawa M, Rolain J-M, Raoult D. Laboratory-confirmed Mediterranean spotted fever in a Japanese traveler to Kenya. Am J Trop Med Hyg. 2005;73:1086–9. https://doi.org/10.4269/ajtmh.2005.73.1086
27. Rutherford JS, Macaluso KR, Smith N, Zaki SR, Paddock CD, Davis J, et al. Fatal spotted fever rickettsiosis, Kenya. Emerg Infect Dis. 2004;10:910–3. https://doi.org/10.3201/eid1005.030537
28. Mutai BK, Wainaina JM, Magiri CG, Nganga JK, Ithondeka PM, Njagi ON, et al. Zoonotic surveillance for rickettsiae in domestic animals in Kenya. Vector Borne Zoonotic Dis. 2013;13:360–6. https://doi.org/10.1089/vbz.2012.0977
29. Zemtsova GE, Apanaskevich DA, Reeves WK, Hahn M, Snellgrove A, Levin ML. Phylogeography of *Rhipicephalus sanguineus* sensu lato and its relationships with climatic factors. Exp Appl Acarol. 2016;69:191–203. https://doi.org/10.1007/s10493-016-0035-4
30. Lynen G, Zeman P, Bakuname C, Di Giulio G, Mtui P, Sanka P, et al. Cattle ticks of the genera *Rhipicephalus* and *Amblyomma* of economic importance in Tanzania: distribution assessed with GIS based on an extensive field survey. Exp Appl Acarol. 2007;43:303–19. https://doi.org/10.1007/s10493-007-9123-9
31. Schwameis M, Auer J, Mitteregger D, Simonitsch-Klupp I, Ramharter M, Burgmann H, et al. Anaplasmataceae-specific PCR for diagnosis and therapeutic guidance for symptomatic neoehrlichiosis in immunocompetent host. Emerg Infect Dis. 2016;22:281–4. https://doi.org/10.3201/eid2202.141762
32. Motto SK, Shirima GM, de Clare Bronsvoort BM, Cook EAJ. Epidemiology of leptospirosis in Tanzania: a review of the current status, serogroup diversity and reservoirs. PLoS Negl Trop Dis. 2021;15:e0009918. https://doi.org/10.1371/journal.pntd.0009918
33. Hagedoorn NN, Maze MJ, Carugati M, Cash-Goldwasser S, Allan KJ, Chen K, et al. Global distribution of *Leptospira* serovar isolations and detections from animal host species: a systematic review and online database. Trop Med Int Health. 2024;29:161–72. https://doi.org/10.1111/tmi.13965

Address for correspondence: John A. Crump, Centre for International Health, University of Otago, PO Box 56, Dunedin 9054, New Zealand; email: john.crump@otago.ac.nz

SARS-CoV-2 Seropositivity in Urban Population of Wild Fallow Deer, Dublin, Ireland, 2020–2022

Kevin Purves,[1] Hannah Brown,[1] Ruth Haverty, Andrew Ryan, Laura L. Griffin, Janet McCormack, Sophie O′Reilly, Patrick W. Mallon, Virginie Gautier, Joseph P. Cassidy, Aurelie Fabre, Michael J. Carr, Gabriel Gonzalez, Simone Ciuti, Nicola F. Fletcher

SARS-CoV-2 can infect wildlife, and SARS-CoV-2 variants of concern might expand into novel animal reservoirs, potentially by reverse zoonosis. White-tailed deer and mule deer of North America are the only deer species in which SARS-CoV-2 has been documented, raising the question of whether other reservoir species exist. We report cases of SARS-CoV-2 seropositivity in a fallow deer population located in Dublin, Ireland. Sampled deer were seronegative in 2020 when the Alpha variant was circulating in humans, 1 deer was seropositive for the Delta variant in 2021, and 12/21 (57%) sampled deer were seropositive for the Omicron variant in 2022, suggesting host tropism expansion as new variants emerged in humans. Omicron BA.1 was capable of infecting fallow deer lung type-2 pneumocytes and type-1–like pneumocytes or endothelial cells ex vivo. Ongoing surveillance to identify novel SARS-CoV-2 reservoirs is needed to prevent public health risks during human–animal interactions in periurban settings.

SARS-CoV-2, a member of the family Coronaviridae, is a positive-sense, single-stranded RNA (ssRNA) virus that has an ≈30-kb genome (*1*). During the COVID-19 pandemic, SARS-CoV-2 has caused ≈7 million deaths (*2*) and infected multiple mammalian species (*3*). Concerns have arisen regarding reverse zoonosis, during which the virus spills back from humans to animals, potentially leading to emerging new variants (*3*). High SARS-CoV-2 seroprevalence rates have been reported in white-tailed deer (*Odocoileus virginianus*) in the United States and Canada (*4*–*7*). Infected deer shed virus and transmit it to other deer; several lineages have been found to be similar to human SARS-CoV-2 genomes, raising the possibility of reverse zoonosis (*6*,*7*). This finding highlights the need to monitor wildlife, including deer, to understand whether those animals might serve as reservoirs for SARS-CoV-2 and pose a risk for transmission to other species (*8*).

Limited data exist on deer susceptibility to SARS-CoV-2 infection in Europe. As of 2021, surveillance reports from the United Kingdom, Austria, and Germany have not found evidence of SARS-CoV-2 exposure in fallow deer (*Dama dama*), red deer (*Cervus elaphus*), roe deer (*Capreolus capreolus*), or sika deer (*C. nippon*) (*9*,*10*). Whether infections are rare or nonexistent in those deer species remains uncertain. Although interactions between wild deer and humans might be low, angiotensin converting enzyme 2 (ACE2), a receptor for SARS-CoV-2, is expressed in bronchiolar epithelium of several deer species (*11*), suggesting that those species might be susceptible to SARS-CoV-2 infection (*12*). We conducted a SARS-CoV-2 surveillance study on a wild, free-ranging population of fallow deer in Europe's largest urban park in Dublin, Ireland, during 2020–2022. We used quantitative reverse transcription PCR (qRT-PCR) and neutralization assays to detect SARS-CoV-2 virus in deer tissue and serum samples; in addition, we assessed the ability of ancestral and Omicron variants to infect fallow deer lung tissue and tracheal explants.

Methods

Study Area and Population

The study population of fallow deer is located in Phoenix Park, a 707-hectare urban park in Dublin

Author affiliations: University College Dublin, Dublin, Ireland (K. Purves, H. Brown, R. Haverty, A. Ryan, L.L. Griffin, J. McCormack, S. O′Reilly, P.W. Mallon, V. Gautier, J.P. Cassidy, A. Fabre, M.J. Carr, G. Gonzalez, S. Ciuti, N.F. Fletcher); St Vincent's University Hospital, Dublin (P.W. Mallon, A. Fabre); Hokkaido University, Sapporo, Japan (M.J. Carr, G. Gonzalez)

DOI: https://doi.org/10.3201/eid3008.231056

[1]These authors contributed equally to this article.

(data from the Ireland Office of Public Works, https://www.gov.ie/en/organisation/office-of-public-works); a resident population of ≈600 free-ranging fallow deer exists in the park (*13*). The park receives up to 10 million visitors per year, and, since 2013, visitors have repeatedly been documented hand-feeding the deer population (*13*). The number of park visitors observed within 250 meters of deer herds during weekend observations was always >10 persons per deer group during 2019–2022: mean 19.7 (SD 14.7) persons in summer 2019, mean 21.9 (SD 22.8) in summer 2020, mean 15.7 (SD 18.0) in summer 2021, and mean 11.67 (SD 9.24) in summer 2022 (*13*). Phoenix Park is a critical site for biodiversity, supporting 50% of the wild mammal species found in Ireland and ≈40% of bird species (data from the Ireland Office of Public Works); mammals include badgers (*Meles meles*) and red foxes (*Vulpes vulpes*). Park visitors can bring their dogs into the park grounds, in most cases leashed, although unleashed dogs are permitted except during the deer fawning season.

The behavior of the deer and their interactions with humans have been extensively characterized, and >80% of the population has been identified by using ear tags (*14*). Areas of the park accessible to the public are used by 86% of the deer; of those, 24% have a high contact rate with humans that includes taking food (consistent beggars), 68% display intermediate deer–human contact rates (occasional beggars), and 8% systematically avoid any interactions with humans despite living in areas open to the public (rare beggars). The remaining 14% (avoiders) avoid areas of the park accessible to humans (*13*,*15*). The interaction categories are defined on the basis of begging rank, which is a scale of most to least likely to beg according to previously generated models of begging behavior (Appendix 1, https://wwwnc.cdc.gov/EID/article/30/8/23-1056-App1.pdf) (*13*). Deer are culled annually by professional deer stalkers over the winter period; the deer stalkers aim to maintain a population that mimics a natural structure.

Sample Collection and Storage

Culling of fallow deer occurred on November 2 and 25, 2021, and February 16, 2022; in addition, we collected archived serum samples from November 2020 (Appendix 2 Table 1, https://wwwnc.cdc.gov/EID/article/30/8/23-1056-App2.xlsx). We collected retropharyngeal lymph nodes, palatine tonsil, nasopharyngeal mucosa and cecal content within 1 hour after death and blood samples immediately after death. We chose the sampling strategy according to the highest viral loads reported from experimental infection of white-tailed deer (*7*). We did not collect nasopharyngeal swab samples from the deer; we elected to directly sample nasopharyngeal mucosal tissues postmortem. We stored tissue samples and cecal content at −80°C before RNA extraction and serum samples at −20°C.

SARS-CoV-2 Surrogate Virus Neutralization Test

We performed SARS-CoV-2 surrogate virus neutralization tests (sVNTs) on deer serum samples by using the Genscript cPass SARS-CoV-2 sVNT Kit (Genescript, https://www.genscript.com) according to the manufacturer's instructions (Appendix 1). We screened serum samples in duplicate within each assay and performed 2 independent assays, expressing results as percent neutralization.

Nucleic Acid Extraction and SARS-CoV-2 qRT-PCR

We isolated total RNA from tissues by homogenizing in TRIzol, extracting the aqueous layer, and then using the RNeasy Mini Kit (QIAGEN, https://www.qiagen.com)

Table. Profiles and SARS-CoV-2 PCR status of seropositive fallow deer in study of SARS-CoV-2 seropositivity in urban population of wild fallow deer, Dublin, Ireland, 2020–2022*

Animal code	Sample date	Age, y/sex	Neutralization, %†	Tissue PCR	Cecal content PCR	Begging category‡
18_B_2021	2021 Nov 25	4/M	30	ND	ND	Unranked
4_C_2022	2022 Feb 16	1/M	39	ND	ND	Occasional
5_C_2022	2022 Feb 16	6/F	33	ND	ND	Occasional
6_C_2022	2022 Feb 16	<1/M	32	ND	ND	Unranked
7_C_2022	2022 Feb 16	1/M	42	ND	ND	Occasional
10_C_2022	2022 Feb 16	8/F	34	ND	ND	Occasional
12_C_2022	2022 Feb 16	2/M	34	ND	ND	Unranked
15_C_2022	2022 Feb 16	3/F	31	ND	ND	Occasional
16_C_2022	2022 Feb 16	3/M	34	ND	ND	Consistent
19_C_2022	2022 Feb 16	7/M	34	ND	ND	Unranked
21_C_2022	2022 Feb 16	5/M	34	ND	ND	Consistent
23_C_2022	2022 Feb 16	5/M	34	ND	ND	Unranked
31_C_2022	2022 Feb 16	1/M	32	ND	ND	Unranked

*SARS-CoV-2 seropositive fallow deer sampled in February 2022 (n = 21) were PCR negative for the SARS-CoV-2 envelope gene in all samples tested (retropharyngeal lymph nodes, nasopharyngeal mucosa, palatine tonsil, and cecal content). ND, not detected.
†SARS-CoV-2 surrogate virus neutralization test was used to determine % neutralizing antibodies in deer serum samples.
‡Begging ranks were occasional or consistent beggars or unranked. Unranked indicates the deer were untagged.

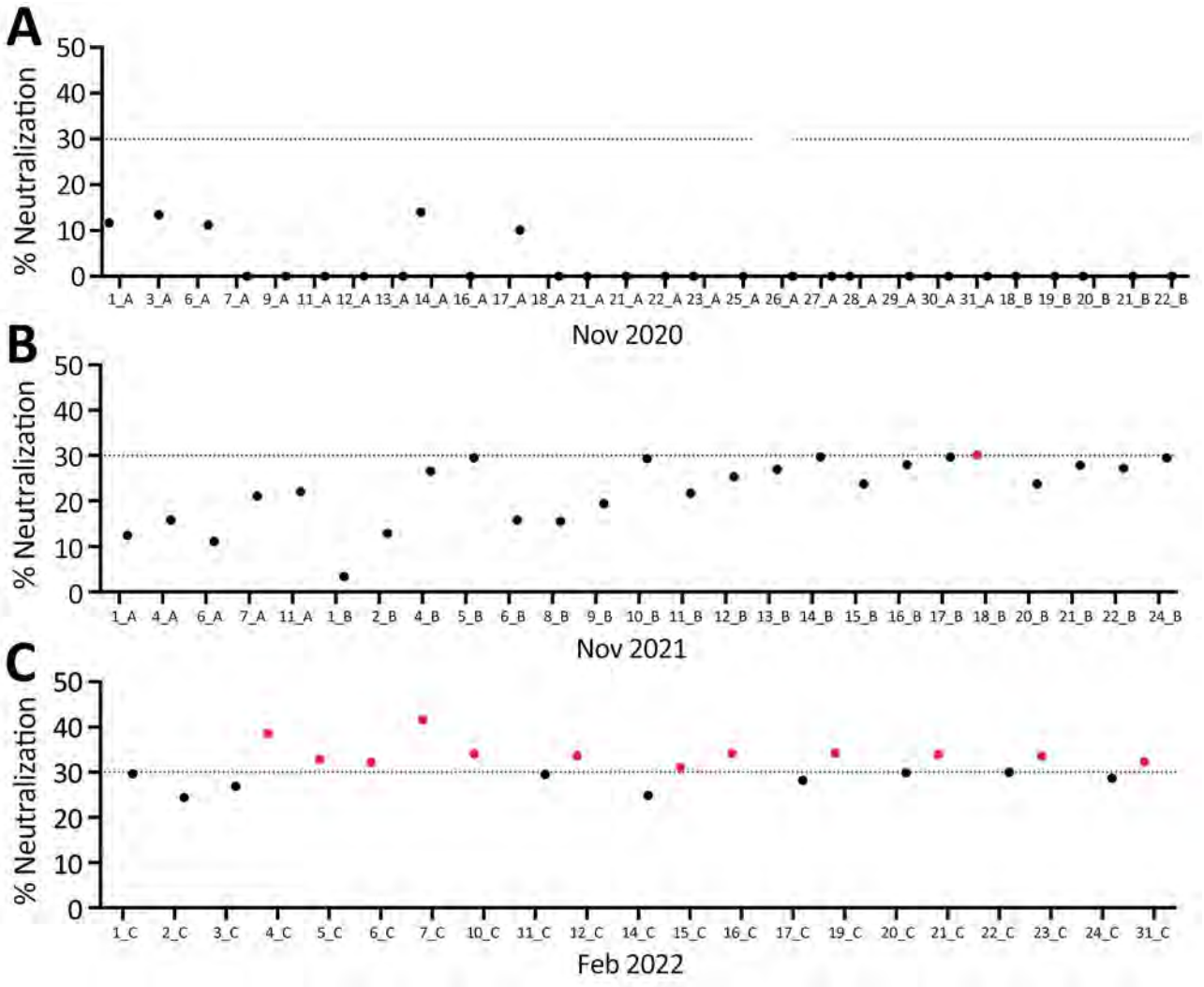

Figure 1. SARS-CoV-2 neutralizing antibodies found in serum samples from fallow deer in an urban deer population located in Dublin, Ireland, 2020–2022. A) Serum samples collected in November 2020 (n = 28); B) samples from November 2021 (n = 25); C) samples from February 2022 (n = 21). Serum samples were collected from wild fallow deer and screened in duplicate for SARS-CoV-2 neutralizing antibodies by using the Genscript cPass SARS-CoV-2 surrogate virus neutralization test (Genescript, https://www.genscript.com). Deer identification numbers are shown on the x axes for each year. Dotted lines indicate a cutoff of 30% neutralization. Red dots indicate serum samples that had ≥30% neutralization and were considered seropositive for SARS-CoV-2. Data are presented as mean percent neutralization calculated from duplicate wells from 2 independent assays.

according to the manufacturer's instructions. We spiked the tissue RNA samples with 1 µg MS2 bacteriophage RNA as an extraction control. We isolated RNA from cecal content samples as previously described (Appendix 1) (*16*) and spiked those samples with 100 µL of murine hepatitis virus (4.22×10^7 50% tissue culture infectious dose [$TCID_{50}$]/mL) as extraction controls. We performed qRT-PCR on an ABI 7500 Real-Time PCR System (Thermo Fisher Scientific, https://www.thermofisher.com) by using Taqman Fast Virus 1-Step Master Mix (Thermo Fisher Scientific) and specific oligonucleotide primer and probe sequences and thermocycling conditions (Appendix 1 Table). We used EURM-019, a synthetic SARS-CoV-2 ssRNA obtained from the European Commission Joint Research Centre (https://joint-research-centre.ec.europa.eu), as a standard for SARS-CoV-2 envelope (E) gene quantification. We analyzed all samples and controls in triplicate.

Cell Culture, SARS-CoV-2 Pseudovirus, and Infectious Virus Neutralization Test

We propagated untransfected Vero E6 cells (American Type Culture Collection, https://www.atcc.org) and Vero E6 cells transiently expressing an untagged transmembrane protease, serine 2 (TMPRSS2) cDNA

expression vector (Sino Biological, https://www.sinobiological.com) as previously described (*17*). We generated SARS-CoV-2 pseudoviruses bearing spike proteins from Alpha, Delta, Omicron BA.1, and Omicron BA.2 variants (InvivoGen, https://www.invivogen.com) as previously described (*18*). In brief, we co-transfected 293T cells with plasmids encoding an HIV-1 provirus expressing luciferase (pNL4-3-Luc-R-E; National Institute for Biologic Standards and Control, https://nibsc.org) and either vesicular stomatitis virus glycoprotein, SARS-CoV-2 spike protein, or a no E control. We harvested supernatants 48 and 72 hours after transfection, filtered them through a 0.45-μm filter, and stored them at −80°C.

We propagated SARS-CoV-2 strain 2019-nCoV/Italy-INMI1 (European Virus Archive Global, https://www.european-virus-archive.com; GenBank accession no. MT077125.1) in Vero E6 cells as previously described (*17*). We performed $TCID_{50}$ assays of Vero E6 cells in quadruplicate and determined infectious titers as previously described (*19*). We isolated SARS-CoV-2 Omicron BA.1 (GenBank accession no. ON350968, passage 2) from a SARS-CoV-2–positive nasopharyngeal swab sample obtained during the All Ireland Infectious Disease Cohort Study (P.W.G. Mallon et al., unpub. data, https://doi.org/10.1101/2021.02.09.21251402) and amplified the virus on Vero E6/TMPRSS2–expressing cells obtained from the Centre For AIDS Reagents at the National Institute for Biologic Standards and Control (*20*).

We incubated individual pseudoviruses or infectious viruses with deer serum samples at a 1:1 ratio for 1 hour at 37°C and then titrated the viruses on Vero E6/TMPRSS2 cells. For pseudovirus infections, we lysed the cells after 48 hours by using Passive

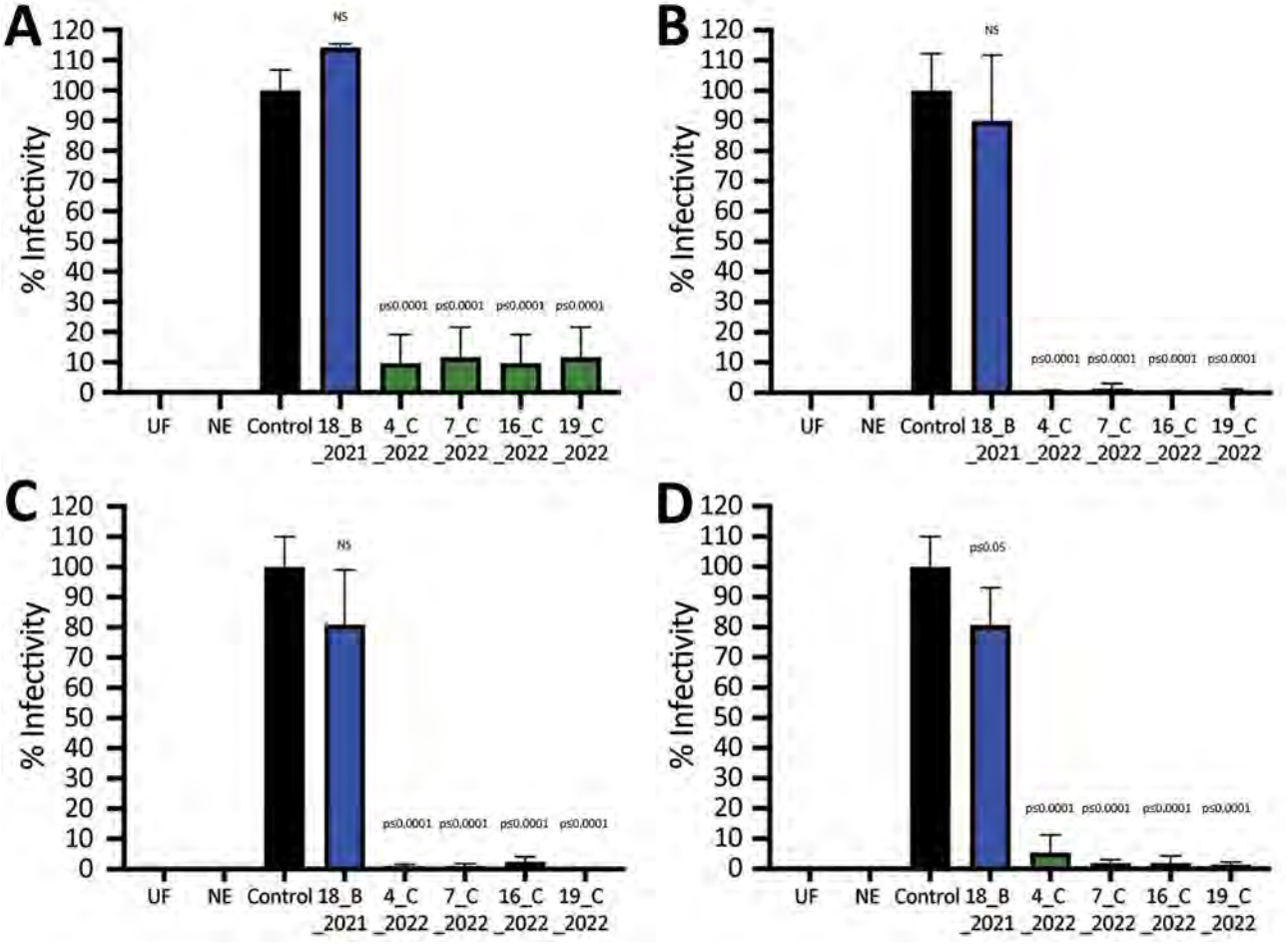

Figure 2. Infectivity of SARS-CoV-2 pseudoviruses after incubation with SARS-CoV-2–positive serum samples from wild fallow deer, Dublin, Ireland, 2020–2022. Spike proteins were from Alpha (A), Delta (B), Omicron BA.1 (C), and Omicron BA.2 (D) variants of concern. SARS-CoV-2 pseudoviruses bearing spike proteins from different variants of concern were incubated with 5 deer serum samples at a 1:1 ratio in triplicate and then used to infect Vero E6/TMPRSS2 cells. Identification numbers of deer are indicated. Controls were virus incubated in triplicate at a 1:1 ratio with culture medium. Relative light units from a luciferase reporter were used to calculate percentage infectivity relative to the untreated control virus. Data are from 2 independent experiments with 3 biologic replicates per experiment. Error bars indicate SDs. NE, no envelope naked pseudovirus control; NS, not significant; UF, uninfected cells.

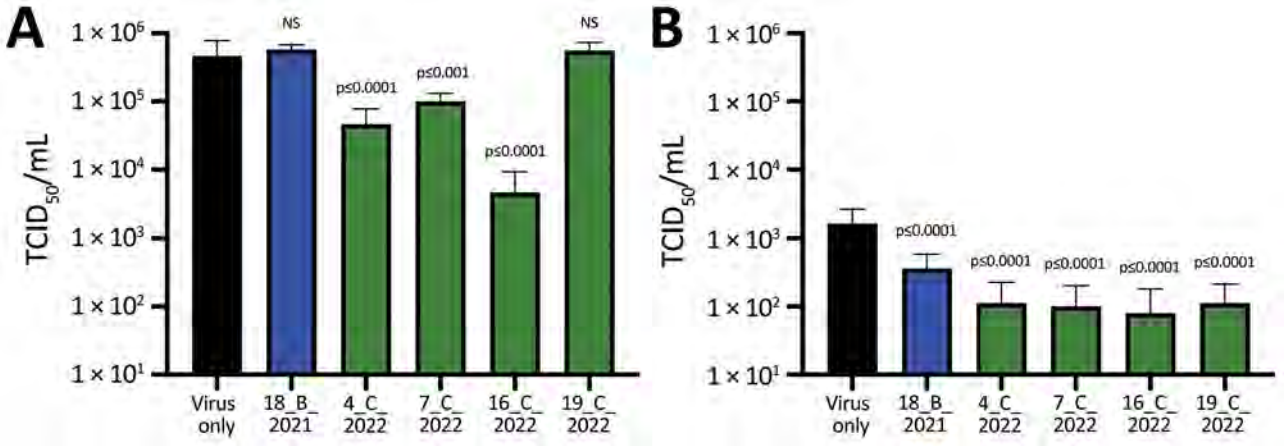

Figure 3. Infectivity of SARS-CoV-2 infectious viruses after incubation with SARS-CoV-2–positive serum samples from wild fallow deer, Dublin, Ireland, 2020–2022. Deer serum samples were incubated with infectious SARS-CoV-2 ancestral strain Italy_INMI1 (A) or Omicron BA.1 (B) and then used to infect Vero E6/TMPRSS2 cells. Identification numbers of deer are indicated. Cytopathic effect was calculated as $TCID_{50}$, as previously described (*19*). Data are from 2 independent experiments with 8 biologic replicates per experiment. p values were calculated by using 1-way analysis of variance (Appendix 2 Tables 2, 3, https://wwwnc.cdc.gov/EID/article/30/8/23-1056-App2.xlsx). Error bars indicate SDs. NS, not significant; $TCID_{50}$, 50% tissue culture infectious dose.

Lysis Buffer (Promega, https://www.promega.com) and quantified luciferase activity by using a TriStar² LB 942 Multimode Reader (Berthold Technologies, https://www.berthold.com). We expressed infectivity as relative light units, minus the no-E control signal, relative to the virus only control. For infectious virus assays, we scored the cytopathic effect 48 hours after infection and calculated $TCID_{50}$ (*19*). To differentiate between cytopathic effect and cytotoxicity following incubation with serum samples, we titrated each serum sample alone on Vero E6/TMPRSS2 cells and scored cytotoxicity 48 hours after inoculation; we only scored dilutions that had no visible cytotoxic effect (i.e., rounded or detached cells) in $TCID_{50}$ assays.

SARS-CoV-2 Superlineages Circulating during Sampling Months

We performed SARS-CoV-2 whole-genome sequencing of human clinical samples collected in Ireland as described previously (*21*), covering 1-month periods concurrent with the deer culling dates; human sequences were downloaded from GISAID (https://www.gisaid.org). We assigned lineages by using the Pangolin application version 4.3 and Pangolin data version 1.20 (https://github.com/cov-lineages/pangolin) and assigned superlineages by using the most recent common ancestors of SARS-CoV-2 variants B.1, B.1.177, B.1.1.7 (Alpha), P.2 (Zeta), B.1.617.2 (Delta), B.1.1.529.1 (Omicron BA.1), B.1.1.529.2 (Omicron BA.2), and B.1.1.529.3 (Omicron BA.3). For graphical representations, we sampled 108 genomes proportionally to their superlineage frequencies from all 3 sampling periods.

We aligned multiple sequences of the SARS-CoV-2 genome sequences from humans with a GenBank reference sequence (accession no. MN908947) by using the MAFFT program and FFT-NS-I algorithm (*22*). We inferred a phylogenetic tree by aligning sequences (n = 109) by using the program RAxML (https://antonellilab.github.io/raxmlGUI) and a general time-reversible substitution model and estimated branch support by using 100 bootstrap replicates.

SARS-CoV-2 Infection of Tracheal Explants and Precision Cut Lung Slices

We generated precision cut lung slices (PCLSs) and tracheal explants from 2 SARS-CoV-2–seronegative fallow deer and inoculated the tissues with either SARS-CoV-2 Italy-INMI-1 (ancestral virus) or Omicron BA.1 strains (Appendix 1). For tracheal infections, we added 100 µL virus (Italy-INMI-1 titer, 3.9×10^5 $TCID_{50}$/mL; Omicron BA.1 titer, 1.3×10^3 $TCID_{50}$/mL) to the epithelial surface of tracheal tissue; for PCLS infections, we added 500 µL virus and 500 µL culture medium to each well containing lung tissue. We infected tissue with each virus variant in triplicate. We removed virus 24 hours after inoculation, washed the tissue in phosphate-buffered saline, replenished the culture medium, and cultured the tissue for another 48 hours. Then, we fixed tissue with 10% neutral-buffered formalin.

Immunohistochemistry to Detect SARS-CoV-2 Antigen

To evaluate SARS-CoV-2 expression profiles, we immunohistochemically stained formalin-fixed, paraffin-embedded tissue sections (Appendix 1) by using

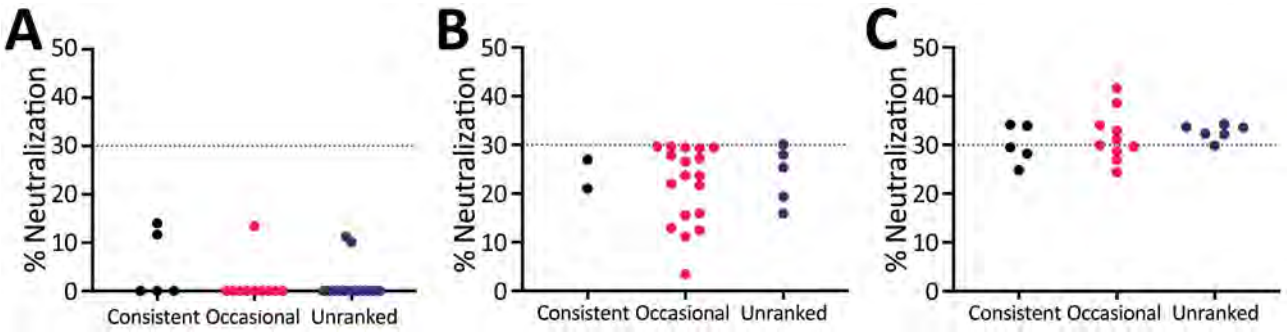

Figure 4. Begging behavior of deer sampled to detect SARS-CoV-2 neutralizing antibodies in study of SARS-CoV-2 seropositivity in urban population of wild fallow deer, Dublin, Ireland, 2020–2022. A) November 2020; B) November 2021; C) February 2022. Dotted lines indicate a cutoff of 30% neutralization of SARS-CoV-2 by serum antibodies; ≥30% neutralization was considered SARS-CoV-2 seropositive. Red dots indicate occasional beggars; most deer were either consistent or occasional beggars.

mouse monoclonal IgG1 antibody against SARS-CoV-2 spike protein (GeneTex, https://www.genetex.com) and the EnVision Flex kit (Agilent Technologies Inc., https://www.agilent.com). We scanned the slides by using the Aperio AT2 digital slide scanner and reviewed images by using Aperio ImageScope 12.4 software (both Leica Biosystems, https://www.leicabiosystems.com).

Statistical Analyses

We expressed in vitro results as means ±SD, except as indicated, and analyzed data by using 1-way analysis of variance in Prism 9.0 (GraphPad, https://www.graphpad.com). We estimated individual begging behavior as previously described (Appendix 1) (*13*).

Results

SARS-CoV-2–Seropositive Fallow Deer

Using an sVNT specific for SARS-CoV-2, we screened serum samples from fallow deer culled in November 2020 (n = 28), November 2021 (n = 25), and February 2022 (n = 21) for SARS-CoV-2 neutralizing antibodies. All deer culled in November 2020 had sVNT neutralization cutoff values of <30% and were considered seronegative. All deer, except 1 from the November 2021 cull, were also seronegative. Deer no. 18_B_2021, culled on November 25, 2021, had an sVNT neutralization value of 30% and was considered seropositive. Twelve of 21 (57%) deer culled in February 2022 had neutralization values >30% and were considered seropositive for SARS-CoV-2 (Table; Figure 1). SARS-CoV-2 seropositive animals ranged from <1 (fawn) to 8 years of age and were from various subherds within the park (Table). Of the 13 seropositive deer, 10 (77%) were male and 3 (23%) female (Table).

SARS-CoV-2 Pseudovirus and Infectious Virus Neutralization

To confirm the ability of sVNT-positive deer serum samples to neutralize SARS-CoV-2 pseudovirus and infectious virus, we selected 4 serum samples with the highest sVNT neutralization titers from the February 2022 cull together with a seropositive sample from the November 2021 cull (deer no. 18_B_2021). All SARS-CoV-2–seropositive serum samples from 2022 neutralized pseudoviruses bearing Alpha, Delta, Omicron BA.1, and BA.2 spike proteins, whereas the sample from deer no. 18_B_2021 only significantly inhibited pseudovirus containing the BA.2 spike protein (Figure 2). None of the 5 serum samples neutralized vesicular stomatitis virus glycoprotein from an unrelated pseudovirus construct. Using infectious ancestral SARS-CoV-2 (Italy-INMI1) and Omicron BA.1 viruses, we observed significant inhibition of the ancestral virus by 3 of 5 serum samples and Omicron

Figure 5. Example of fallow deer–human interaction in study of SARS-CoV-2 seropositivity in urban population of wild fallow deer, Dublin, Ireland, 2020–2022. Photograph by Bawan Amin, University College Dublin, July 2018.

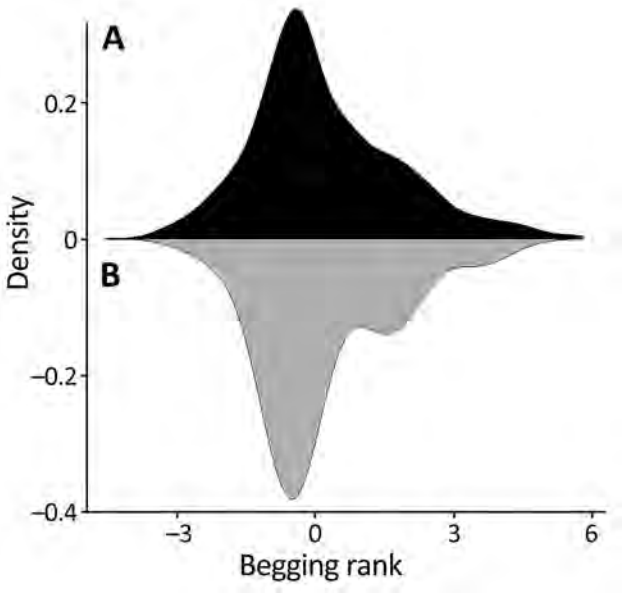

Figure 6. Deer begging rank distributions in study of SARS-CoV-2 seropositivity in urban population of wild fallow deer, Dublin, Ireland, 2020–2022. Mirror density plot was generated to compare begging rank distributions (Appendix 1, https://wwwnc.cdc.gov/EID/article/30/8/23-1056-App1.pdf) for the whole deer population (black shading) and sampled deer (gray shading).

BA.1 by all 5 serum samples tested (Figure 3; Appendix 2 Tables 2, 3).

Fallow Deer qRT-PCR Negative for SARS-CoV-2

All animals were PCR negative for the SARS-CoV-2 E gene in tissues collected during November 2021 and February 2022, regardless of serum status (Table; Appendix 1 Table). SARS-CoV-2 ssRNA controls were amplified in all assays, indicating the qRT-PCR amplified the SARS-CoV-2 E gene correctly.

Begging Behavior of SARS-CoV-2 Seropositive Deer

Most sampled deer were consistent or occasional beggars (Figure 4) (*13*). Of the seropositive animals sampled during February 2022, 7/12 (58%) were consistent or occasional beggars; the remaining 6 seropositive deer from both 2021 and 2022 were unranked, indicating they were either not tagged or tagged without an assigned rank, as in the case of a fawn (deer no. 6_C_2022). However, the fawn's mother is a documented consistent beggar; therefore, it is possible that this fawn came in contact with humans while following its mother. Beggars took various foodstuffs from humans (Figure 5) (*13*). The sampled deer represented the entire fallow deer population in terms of begging rank (Figure 6), begging category (Figure 7), and age and sex classes (Figure 8). We attempted to link begging rank to serum status by using a regression model that had the year of study and begging rank as predictors and serum status as the response variable. Although we observed a positive relationship between the variables, not enough power was achieved for a significant p value, because many seropositive animals were untagged.

SARS-CoV-2 Superlineages Circulating in Human Population

The SARS-CoV-2 genome sequences (n = 5,012) from human clinical samples obtained during November 2020 (n = 224), November 2021 (n = 2,883), and February 2022 (n = 1,905) enabled the examination of variants circulating in the human population during the fallow deer cull periods (Figure 9). The genome sequences from clinical samples showed a clear demarcation between different variant waves and nonoverlapping phylogenetic relationships among the lineages identified during the 3 deer sampling periods. During the first sampling period (November 2020), B.1 and B.1.177 were the main lineages circulating among the population in Ireland; Alpha and Zeta variants were detected during this month, and the Alpha variant was predominant during the following months (P.W.G. Mallon,

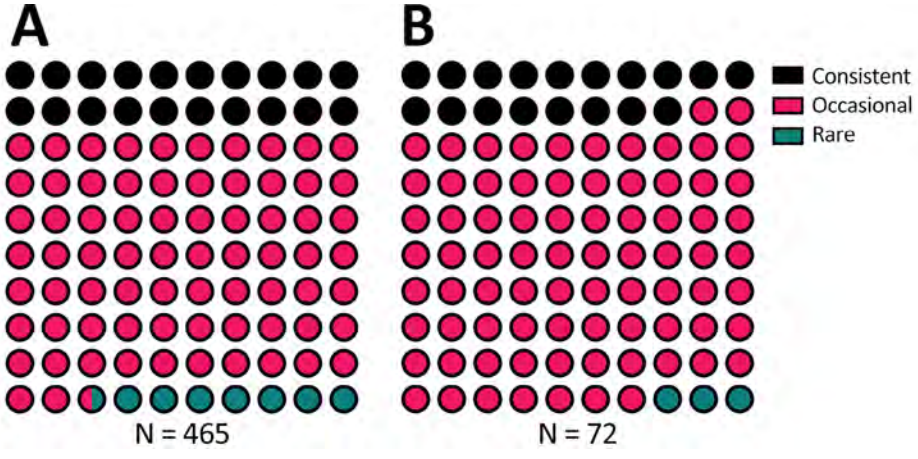

Figure 7. Begging category proportions in study of SARS-CoV-2 seropositivity in urban population of wild fallow deer, Dublin, Ireland, 2020–2022. A) Total fallow deer population; B) fallow deer sampled for SARS-CoV-2 serum antibodies.

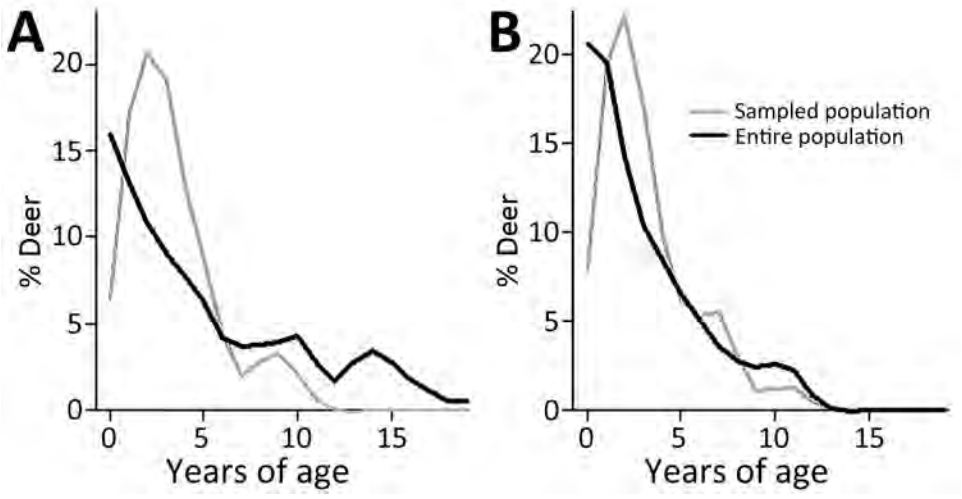

Figure 8. Deer age and sex structure in study of SARS-CoV-2 seropositivity in urban population of wild fallow deer, Dublin, Ireland, 2020–2022. A) Female deer; B) male deer.

et al., unpub. data). During November 2021, the Delta variant was the main circulating variant for the entire month, whereas in February 2022, Omicron variants BA.1 and BA.2 were the main variants detected; Omicron BA.3 was detected at the end of February 2022.

Fallow Deer Trachea and Lung Tissues Infected by SARS-CoV-2

Two board-certified pathologists (J.P.C. and A.F.) reviewed the tissue slides without having prior knowledge of sample treatment and assessed the presence or absence of SARS-CoV-2 staining and the likely

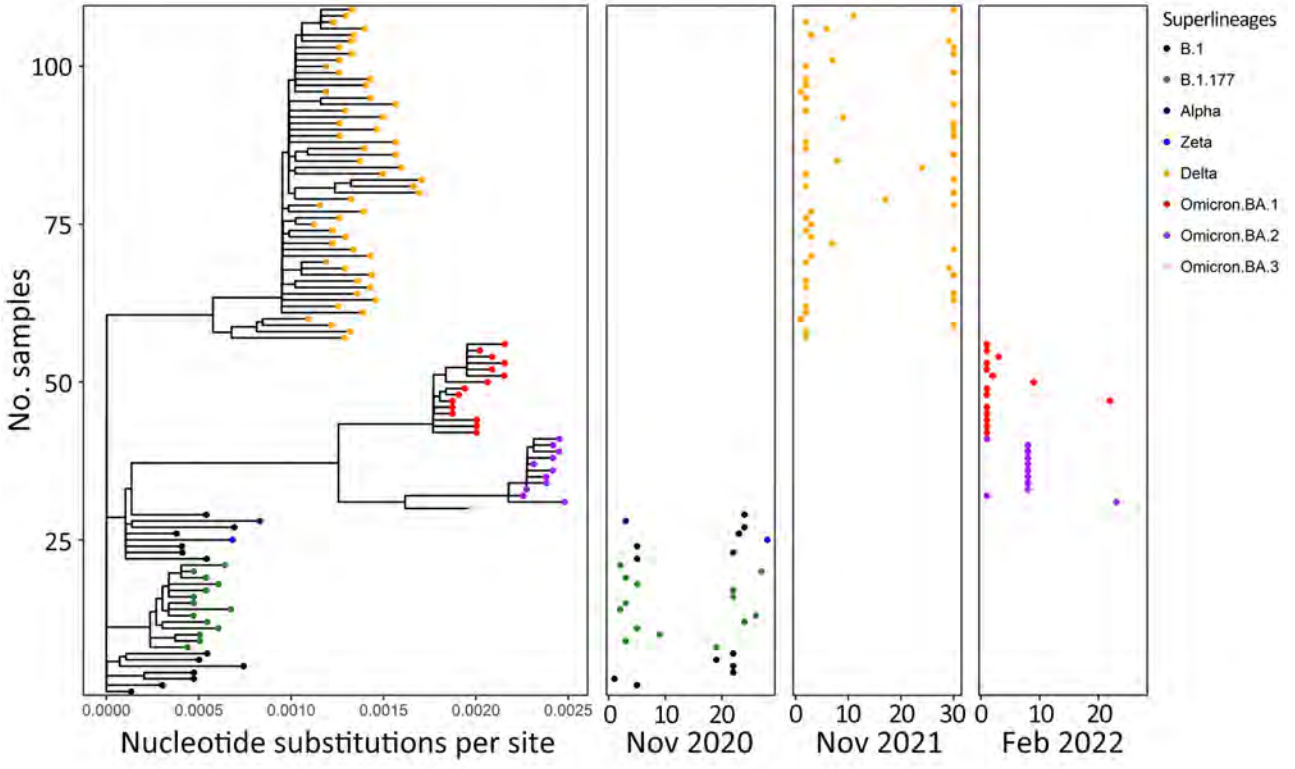

Figure 9. Phylogenetic analysis of SARS-CoV-2 superlineages circulating in humans during deer sampling months in study of SARS-CoV-2 seropositivity in wild fallow deer, Dublin, Ireland, 2020–2022. We analyzed SARS-CoV-2 whole-genome sequences from human clinical samples collected in Ireland covering months corresponding to the deer culling dates (November 2020, November 2021, and February 2022). Branch lengths in the phylogenetic tree (left panel) show the number of base substitutions per site. Colors indicate different SARS-CoV-2 variants. Pangolin lineages are shown with corresponding major circulating variants for each cull month. Location of dots shown for each cull month (right 3 panels) corresponds to the sampling date in each month (horizontal axis) and the phylogenetic position within the tree panel (vertical axis).

cells showing immunoreactivity. Tracheal epithelium inoculated with Italy-INMI1 (ancestral SARS-CoV-2), but not Omicron, was antigen-positive in 2 of 3 experimental replicates from 1 deer (Figure 10). In contrast, in lung tissue, cells morphologically consistent with type 2 pneumocytes and elongated cells representing type 1 pneumocytes or endothelial cells were immunoreactive in all 3 replicates from animals inoculated with Omicron BA.1, but not Italy-INMI1 (Figure 11). No immunoreactivity was observed in tracheal or lung tissue stained with the IgG control or in mock-infected tissue (Figure 11). We attempted to confirm infection by using qRT-PCR for the SARS-CoV-2 E gene 24–72 hours postinfection but were unable to distinguish between residual input virus and de novo virus released from infected PCLSs.

Discussion

The World Health Organization, World Organisation for Animal Health, and Food and Agriculture Organization of the United Nations have emphasized the need to monitor SARS-CoV-2 in wildlife because of the potential establishment of animal reservoirs and possible generation of novel variants (*23*). Minimizing transmission between humans and wildlife has also been emphasized, including educating the public about the risks of contact with wild animals (*24*).

White-tailed deer and mule deer are the only deer species reported to be susceptible to SARS-CoV-2 infection (*5*,*24*). White-tailed deer shed infectious virus, leading to deer-to-deer and deer-to-human transmission (*7*,*25*). Other mammal species capable of transmitting SARS-CoV-2 are mink, raccoons, dogs, cats, ferrets, hamsters, mice, Egyptian fruit bats, and deer mice (*3*). In contrast to white-tailed and mule deer, fallow deer (both *Dama dama* and *D. mesopotamica*) are a monophyletic clade within Old World deer (*26*). Human interactions with the fallow deer population in Phoenix Park have increased since 2013 because of higher social media visibility of the deer in the Park and the animals' willingness to take food from humans (*13*). During the COVID-19 pandemic, human–deer interactions rose in 2020 because of increased park usage for recreation during lockdown, but interactions returned to prepandemic levels by summer 2021 (*27*).

We identified 13 seropositive deer that showed 34% mean SARS-CoV-2 neutralization in the sVNT; the highest neutralization was 42%. Although this sVNT has not been specifically validated for deer species, the same sVNT has been used to report neutralization levels approaching 80%–90% for white-tailed deer (*4*), and the assay has been assessed in other species susceptible to SARS-CoV-2 infection, such as hamsters, mink, ferrets, and cats (*28*). In this study, SARS-CoV-2 neutralization levels using pseudoviruses were higher than those from the Genescript sVNT assays used for serum samples from February 2022 and the positive serum sample from November 2021 (deer 18_B_2021). The serum sample from deer 18_B_2021 significantly inhibited the BA.2 pseudovirus. All serum samples were capable of neutralizing infectious Omicron BA.1, but only 3 of 5 significantly neutralized infectious virus strain Italy_INMI1.

Because the sVNT uses the SARS-CoV-2 spike protein from the ancestral virus, it is possible that more seropositive serum samples might have been detected if the sVNT had incorporated later mutated variants (*29*). This sVNT result, together with other studies, suggests the sVNT should be interpreted qualitatively rather than quantitatively (*28*). The sVNT specifically detects SARS-CoV-2 neutralizing antibodies and has no cross-reactivity with other human coronaviruses or

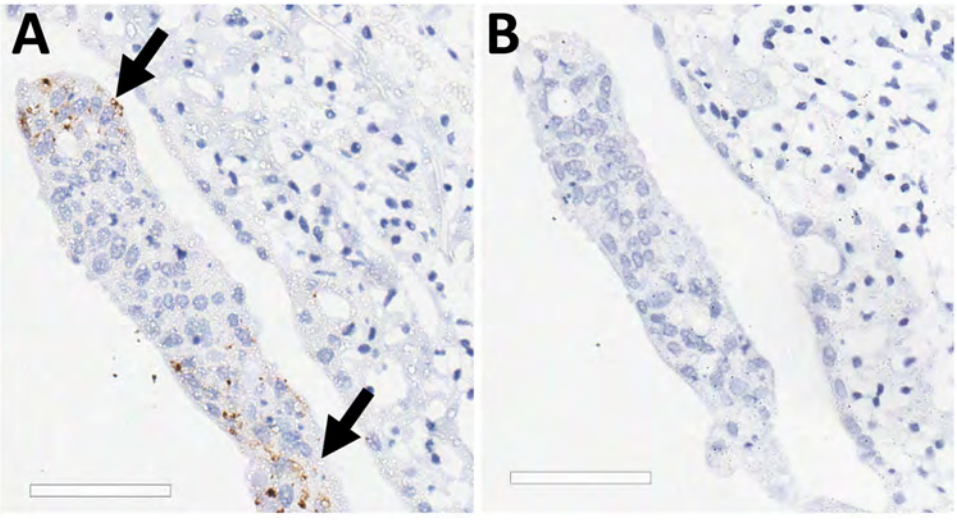

Figure 10. SARS-CoV-2 infection of tracheal explant in study of SARS-CoV-2 seropositivity in urban population of wild fallow deer, Dublin, Ireland, 2020–2022. Tracheal explants from 2 SARS-CoV-2–seronegative deer were inoculated with SARS-CoV-2 Italy-INMI1 and stained by using immunohistochemistry. Control sections were stained with IgG only or mock infected. A) Arrows indicate SARS-CoV-2 Italy-INMI1 antigen immunoreactivity in tracheal epithelium; B) no immunoreactivity was observed after staining with the IgG control. Scale bars indicate 60 μm.

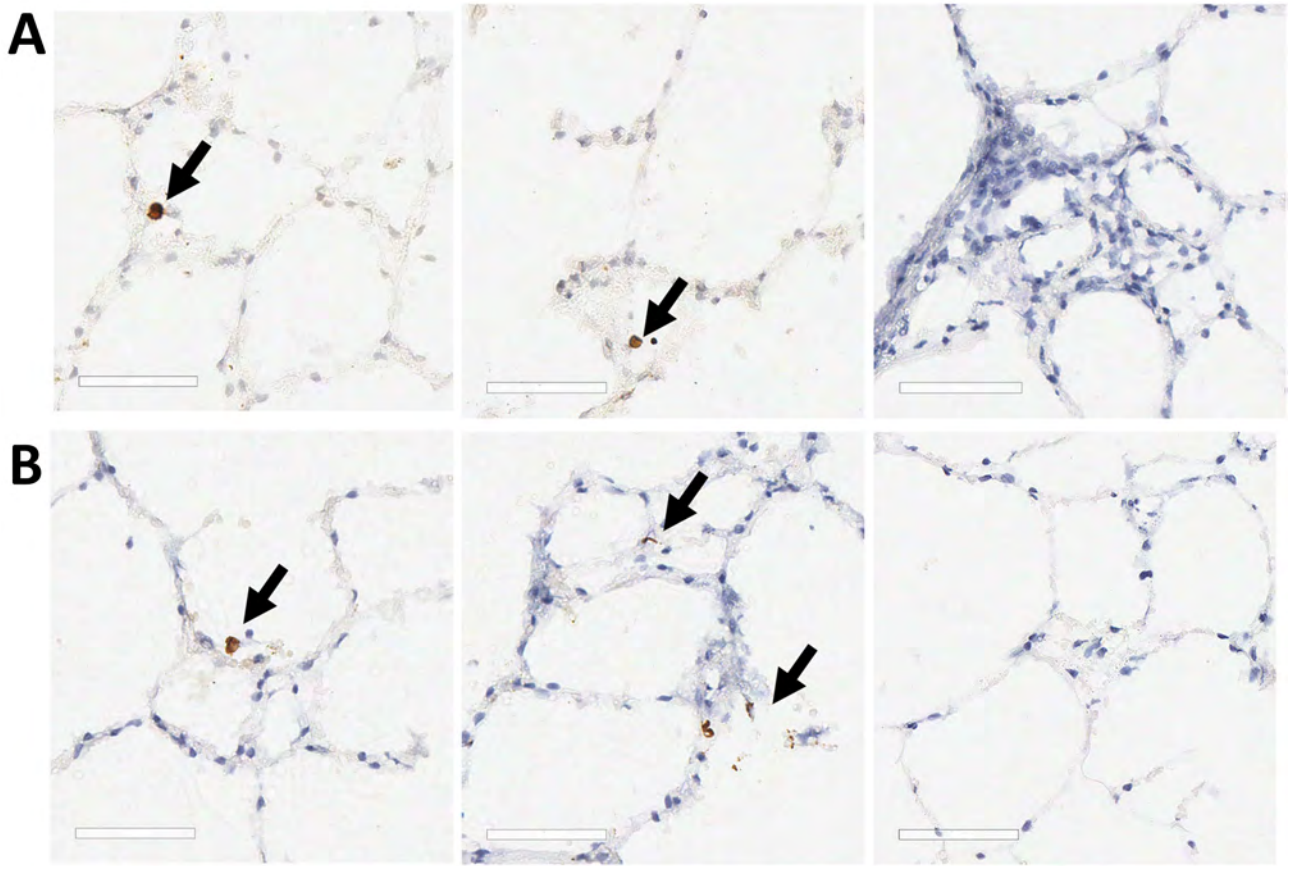

Figure 11. SARS-CoV-2 Omicron BA.1 infection of ex vivo lung tissue in study of SARS-CoV-2 seropositivity in urban population of wild fallow deer, Dublin, Ireland, 2020–2022. Precision cut lung slices were collected from 2 SARS-CoV-2–seronegative deer and inoculated with SARS-CoV-2 Omicron BA.1; sections were stained by using immunohistochemistry. Control sections were stained with IgG only or mock infected. A) Deer 1; B) deer 2. Arrows in first and middle panels indicate Omicron BA.1 immunoreactivity in cells morphologically consistent with type 2 pneumocytes. Third panel indicates no immunoreactivity after staining with the IgG control. No immunoreactivity was observed in the mock-infected tissues for either animal. Scale bars indicate 60 μm.

respiratory viruses or Middle East respiratory syndrome coronavirus (*28*) except SARS-CoV, which is closely related antigenically to SARS-CoV-2, according to cPass SARS-CoV-2 sVNT Kit documentation (Genescript). During the fallow deer sampling period, no evidence of SARS-CoV circulation existed in Ireland. However, although respiratory disease was not observed in the study population, cross-reactivity with other animal coronaviruses in the sVNT, including bovine coronavirus, is possible but has not been evaluated. It is unclear whether bovine coronavirus is circulating in this population (*30*), but other respiratory viruses have a low seroprevalence in deer in Ireland (*31*).

SARS-CoV-2–seropositive deer in this study were mainly occasional beggars, which reflected the begging category distribution of the entire deer population (*13*). We only sampled 2 rare beggars or avoiders in this study, likely because of their contact avoidance with humans and, therefore, their lower likelihood of being culled, which agrees with previous studies that shyer animals evade observation and trapping (*13*,*32*). Overall, 77% of seropositive deer were male, consistent with the hypothesis of anthroponosis, because male deer are more likely to beg for food (*13*).

During the 3 sampling periods, diverse SARS-CoV-2 variants circulated in the human population (*22*; A.M. Rice et al., unpub. data, https://doi.org/10.1101/2023.05.11.23289783). Because of the high frequency of interactions with humans, it is likely that the fallow deer population was exposed to SARS-CoV-2 through human contact. Although the February 2022 deer sampling period coincided with circulation of the Omicron variant within the human population, it is not possible to definitively state to which subvariant the seropositive deer in this study were exposed or whether SARS-CoV-2 transmission occurred between deer. SARS-CoV-2 surveillance studies in Europe have not sampled animals after 2021 or studied deer that had

defined interactions with humans (*9*,*10*). Our study highlights the need for ongoing SARS-CoV-2 surveillance in animals, particularly as novel variants of concern are still emerging (*23*).

We showed that fallow deer PCLS tissue supported SARS-CoV-2 infection with Omicron BA.1 but not the ancestral virus. Omicron-positive cells were observed in PCLS tissue 72 hours after infection, and those cells expressed ACE2 (*11*). Whether other receptors, such as TMPRSS2, are necessary for SARS-CoV-2 infection in fallow deer remains unknown. Infected cells were observed in tracheal epithelium from 1 of 2 animals inoculated with ancestral SARS-CoV-2 but not Omicron. The reasons for differences in tissue distribution are unclear, and further studies will be needed to determine tissue distribution at different timepoints after infection (*33*,*34*).

None of the deer sampled in this study were PCR positive for SARS-CoV-2, and no clinical signs were observed. However, because of the short duration of viral replication compared with the extended persistence of antibodies in white-tailed deer (>13 months), we were more likely to detect seropositive animals than those shedding virus (*35*). Although an annotated fallow deer genome is not available, ACE2 residues binding SARS-CoV-2 spike protein are conserved across cervids and have high homology to human ACE2 (*36*). Moreover, deer species for which ACE2 sequences are not available, including *D. dama*, are also likely to have conserved key ACE2 residues (*36*). Our findings suggests that the SARS-CoV-2 Omicron variant might infect fallow deer lung tissue in contrast to ancestral SARS-CoV-2, highlighting the importance of ongoing deer surveillance.

In conclusion, we report SARS-CoV-2 seropositivity in fallow deer in Ireland. In February 2022, Omicron was the dominant variant in humans, and 57% of fallow deer were also seropositive for SARS-CoV-2. Ongoing surveillance to identify novel reservoirs of SARS-CoV-2 and other zoonotic pathogens is needed to prevent ecologic public health risks for human–animal interactions in periurban settings.

Acknowledgments

We thank the University College Dublin Veterinary Medicine Containment Level 3 Laboratory and its managers, Stephen Gordon, John Browne, and Bridget Hogg, for assisting with this study; Marc Farrelly, Tiffany Morey, and Christopher Evans for technical assistance; Jane Fauli for providing visitor numbers to the Phoenix Park; Bawan Amin for the use of the photograph in Figure 3; and the Office of Public Works, Ireland, for providing access to the Phoenix Park deer.

This study was funded by a Wellcome Trust Institutional Strategic Support Fund Grant through the University College Dublin (grant no. R22631). S.O.R. is the recipient of an Irish Research Council, Government of Ireland postgraduate scholarship (no. GOIPG/2019/4432).

About the Author

Dr. Purves is a postdoctoral research assistant in the Veterinary Sciences Centre at the University College Dublin. His research interests focus on virus persistence in the environment and animal reservoirs and on One Health research approaches.

References

1. V'kovski P, Kratzel A, Steiner S, Stalder H, Thiel V. Coronavirus biology and replication: implications for SARS-CoV-2. Nat Rev Microbiol. 2021;19:155–70. https://doi.org/10.1038/s41579-020-00468-6
2. World Health Organization. WHO COVID-19 dashboard [cited 2023 Jul 21]. https://covid19.who.int
3. European Centre for Disease Prevention and Control. SARS-CoV-2 in animals: susceptibility of animal species, risk for animal and public health, monitoring, prevention and control. February 28, 2023 [cited 2023 Jul 21]. https://www.ecdc.europa.eu/en/publications-data/sars-cov-2-animals-susceptibility-animal-species-risk-animal-and-public-health
4. Chandler JC, Bevins SN, Ellis JW, Linder TJ, Tell RM, Jenkins-Moore M, et al. SARS-CoV-2 exposure in wild white-tailed deer (*Odocoileus virginianus*). Proc Natl Acad Sci USA. 2021;118:e2114828118. https://doi.org/10.1073/pnas.2114828118
5. Hale VL, Dennis PM, McBride DS, Nolting JM, Madden C, Huey D, et al. SARS-CoV-2 infection in free-ranging white-tailed deer. Nature. 2022;602:481–6. https://doi.org/10.1038/s41586-021-04353-x
6. Martins M, Boggiatto PM, Buckley A, Cassmann ED, Falkenberg S, Caserta LC, et al. From deer-to-deer: SARS-CoV-2 is efficiently transmitted and presents broad tissue tropism and replication sites in white-tailed deer. PLoS Pathog. 2022;18:e1010197. https://doi.org/10.1371/journal.ppat.1010197
7. Palmer MV, Martins M, Falkenberg S, Buckley A, Caserta LC, Mitchell PK, et al. Susceptibility of white-tailed deer (*Odocoileus virginianus*) to SARS-CoV-2. J Virol. 2021;95:e00083-21. https://doi.org/10.1128/JVI.00083-21
8. World Organisation for Animal Health. OIE statement on monitoring white-tailed deer for SARS-CoV-2. December 3, 2021 [cited 2023 Jul 21]. https://www.woah.org/en/oie-statement-on-monitoring-white-tailed-deer-for-sars-cov-2
9. Holding M, Otter AD, Dowall S, Takumi K, Hicks B, Coleman T, et al. Screening of wild deer populations for exposure to SARS-CoV-2 in the United Kingdom, 2020–2021. Transbound Emerg Dis. 2022;69:e3244–9. https://doi.org/10.1111/tbed.14534
10. Moreira-Soto A, Walzer C, Czirják GÁ, Richter MH, Marino SF, Posautz A, et al. Serological evidence that SARS-CoV-2 has not emerged in deer in Germany or Austria during the COVID-19 pandemic. Microorganisms. 2022;10:748. https://doi.org/10.3390/microorganisms10040748

11. Lean FZX, Cox R, Madslien K, Spiro S, Nymo IH, Bröjer C, et al. Tissue distribution of angiotensin-converting enzyme 2 (ACE2) receptor in wild animals with a focus on artiodactyls, mustelids and phocids. One Health. 2023;16:100492. https://doi.org/10.1016/j.onehlt.2023.100492
12. Zhang Y, Wei M, Wu Y, Wang J, Hong Y, Huang Y, et al. Cross-species tropism and antigenic landscapes of circulating SARS-CoV-2 variants. Cell Rep. 2022;38:110558. https://doi.org/10.1016/j.celrep.2022.110558
13. Griffin LL, Haigh A, Amin B, Faull J, Norman A, Ciuti S. Artificial selection in human–wildlife feeding interactions. J Anim Ecol. 2022;91:1892–905. https://doi.org/10.1111/1365-2656.13771
14. Amin B, Jennings DJ, Smith AF, Quinn M, Chari S, Haigh A, et al. In utero accumulated steroids predict neonate anti-predator response in a wild mammal. Funct Ecol. 2021;35:1255–67. https://doi.org/10.1111/1365-2435.13790
15. Griffin LL, Haigh A, Conteddu K, Andaloc M, McDonnell P, Ciuti S. Reducing risky interactions: identifying barriers to the successful management of human–wildlife conflict in an urban parkland. People Nat. 2022;4:918–30. https://doi.org/10.1002/pan3.10338
16. Grierson SS, McGowan S, Cook C, Steinbach F, Choudhury B. Molecular and in vitro characterisation of hepatitis E virus from UK pigs. Virology. 2019;527:116–21. https://doi.org/10.1016/j.virol.2018.10.018
17. Purves K, Haverty R, O'Neill T, Folan D, O'Reilly S, Baird AW, et al. A novel antiviral formulation containing caprylic acid inhibits SARS-CoV-2 infection of a human bronchial epithelial cell model. J Gen Virol. 2023;104:001821. PubMed https://doi.org/10.1099/jgv.0.001821
18. Fletcher NF, Meredith LW, Tidswell EL, Bryden SR, Gonçalves-Carneiro D, Chaudhry Y, et al. A novel antiviral formulation inhibits a range of enveloped viruses. J Gen Virol. 2020;101:1090–102. https://doi.org/10.1099/jgv.0.001472
19. Reed LJ, Muench H. A simple method of estimating fifty percent endpoints. Am J Hyg. 1938;27:493–7. https://doi.org/10.1093/oxfordjournals.aje.a118408
20. Matsuyama S, Nao N, Shirato K, Kawase M, Saito S, Takayama I, et al. Enhanced isolation of SARS-CoV-2 by TMPRSS2-expressing cells. Proc Natl Acad Sci USA. 2020;117:7001–3. https://doi.org/10.1073/pnas.2002589117
21. Reynolds LJ, Gonzalez G, Sala-Comorera L, Martin NA, Byrne A, Fennema S, et al. SARS-CoV-2 variant trends in Ireland: wastewater-based epidemiology and clinical surveillance. Sci Total Environ. 2022;838:155828. https://doi.org/10.1016/j.scitotenv.2022.155828
22. Katoh K, Rozewicki J, Yamada KD. MAFFT online service: multiple sequence alignment, interactive sequence choice and visualization. Brief Bioinform. 2019;20:1160–6. https://doi.org/10.1093/bib/bbx108
23. World Health Organization. Joint statement on the prioritization of monitoring SARS-CoV-2 infection in wildlife and preventing the formation of animal reservoirs. March 7, 2022 [cited 2023 Jul 21]. https://www.who.int/news/item/07-03-2022-joint-statement-on-the-prioritization-of-monitoring-sars-cov-2-infection-in-wildlife-and-preventing-the-formation-of-animal-reservoirs
24. World Organisation for Animal Health. SARS-COV-2 in animals—situation report 11. March 31, 2022 [cited 2023 Jul 21]. https://www.woah.org/app/uploads/2022/04/sars-cov-2-situation-report-11.pdf
25. Pickering B, Lung O, Maguire F, Kruczkiewicz P, Kotwa JD, Buchanan T, et al. Divergent SARS-CoV-2 variant emerges in white-tailed deer with deer-to-human transmission. Nat Microbiol. 2022;7:2011–24. https://doi.org/10.1038/s41564-022-01268-9
26. Pitra C, Fickel J, Meijaard E, Groves PC. Evolution and phylogeny of old world deer. Mol Phylogenet Evol. 2004;33:880–95. https://doi.org/10.1016/j.ympev.2004.07.013
27. Griffin LL, Nolan G, Haigh A, Condon H, O'Hagan H, McDonnell P, et al. How can we tackle interruptions to human–wildlife feeding management? Adding media campaigns to the wildlife manager's toolbox. People Nat. 2023;5:1299–315. https://doi.org/10.1002/pan3.10499
28. Embregts CWE, Verstrepen B, Langermans JAM, Böszörményi KP, Sikkema RS, de Vries RD, et al. Evaluation of a multi-species SARS-CoV-2 surrogate virus neutralization test. One Health. 2021;13:100313. https://doi.org/10.1016/j.onehlt.2021.100313
29. Tan CW, Chia WN, Zhu F, Young BE, Chantasrisawad N, Hwa SH, et al. SARS-CoV-2 Omicron variant emerged under immune selection. Nat Microbiol. 2022;7:1756–61. https://doi.org/10.1038/s41564-022-01246-1
30. Dastjerdi A, Floyd T, Swinson V, Davies H, Barber A, Wight A. Parainfluenza and corona viruses in a fallow deer (*Dama dama*) with fatal respiratory disease. Front Vet Sci. 2022;9:1059681. https://doi.org/10.3389/fvets.2022.1059681
31. Graham DA, Gallagher C, Carden RF, Lozano JM, Moriarty J, O'Neill R. A survey of free-ranging deer in Ireland for serological evidence of exposure to bovine viral diarrhoea virus, bovine herpes virus-1, bluetongue virus and Schmallenberg virus. Ir Vet J. 2017;70:13. https://doi.org/10.1186/s13620-017-0091-z
32. Biro PA, Dingemanse NJ. Sampling bias resulting from animal personality. Trends Ecol Evol. 2009;24:66–7. https://doi.org/10.1016/j.tree.2008.11.001
33. Bagato O, Balkema-Buschmann A, Todt D, Weber S, Gömer A, Qu B, et al. Spatiotemporal analysis of SARS-CoV-2 infection reveals an expansive wave of monocyte-derived macrophages associated with vascular damage and virus clearance in hamster lungs. Microbiol Spectr. 2024;12:e0246923. https://doi.org/10.1128/spectrum.02469-23
34. Lean FZX, Lamers MM, Smith SP, Shipley R, Schipper D, Temperton N, et al. Development of immunohistochemistry and in situ hybridisation for the detection of SARS-CoV and SARS-CoV-2 in formalin-fixed paraffin-embedded specimens. Sci Rep. 2020;10:21894. https://doi.org/10.1038/s41598-020-78949-0
35. Hamer SA, Nunez C, Roundy CM, Tang W, Thomas L, Richison J, et al. Persistence of SARS-CoV-2 neutralizing antibodies longer than 13 months in naturally infected, captive white-tailed deer (*Odocoileus virginianus*), Texas. Emerg Microbes Infect. 2022;11:2112–5. https://doi.org/10.1080/22221751.2022.2112913
36. Lopes LR. Cervids ACE2 residues that bind the spike protein can provide susceptibility to SARS-CoV-2. EcoHealth. 2023;20:9–17. https://doi.org/10.1007/s10393-023-01632-z

Address for correspondence: Nicola F. Fletcher, Rm 228, Veterinary Sciences Centre, University College Dublin, Belfield, Dublin D04 W6F6, Ireland; email: nicola.fletcher@ucd.ie

Detection of Nucleocapsid Antibodies Associated with Primary SARS-CoV-2 Infection in Unvaccinated and Vaccinated Blood Donors

Eduard Grebe,[1] Mars Stone,[1] Bryan R. Spencer, Akintunde Akinseye, David J. Wright, Clara Di Germanio, Roberta Bruhn, Karla G. Zurita, Paul Contestable, Valerie Green, Marion C. Lanteri, Paula Saa, Brad J. Biggerstaff, Melissa M. Coughlin, Steve Kleinman, Brian Custer, Jefferson M. Jones, Michael P. Busch

Nucleocapsid antibody assays can be used to estimate SARS-CoV-2 infection prevalence in regions implementing spike-based COVID-19 vaccines. However, poor sensitivity of nucleocapsid antibody assays in detecting infection after vaccination has been reported. We derived a lower cutoff for identifying previous infections in a large blood donor cohort (N = 142,599) by using the Ortho VITROS Anti-SARS-CoV-2 Total-N Antibody assay, improving sensitivity while maintaining specificity >98%. We validated sensitivity in samples donated after self-reported swab-confirmed infection diagnoses. Sensitivity for first infections in unvaccinated donors was 98.1% (95% CI 98.0–98.2) and for infection after vaccination was 95.6% (95% CI 95.6–95.7) based on the standard cutoff. Regression analysis showed sensitivity was reduced in the Delta compared with Omicron period, in older donors, in asymptomatic infections, ≤30 days after infection, and for infection after vaccination. The standard Ortho N antibody threshold demonstrated good sensitivity, which was modestly improved with the revised cutoff.

In the United States, as in many countries, convenience sample serosurveillance studies (e.g., in blood donors) have demonstrated that most of the population has SARS-CoV-2 antibodies from vaccination, infection, or both (*1*–*3*). Therefore, continued surveillance using serologic tests requires robust detection of first infections in vaccinated persons (infection after vaccination) and reinfections to yield meaningful estimates of infection incidence. Serologic detection of nucleocapsid antibodies has been a critical tool to detect previous SARS-CoV-2 infection and discriminate between vaccine- and infection-induced antibody reactivity in the context of spike-based vaccines.

The National Blood Donor Cohort (NBDC), a longitudinal study sponsored by the Centers for Disease Control and Prevention (CDC), was conducted in partnership with the 2 largest US blood collectors (Vitalant and the American Red Cross) and their central testing laboratory Creative Testing Solutions (M. Stone et al., unpub. data). We classified participating donors into 4 groups on the basis of infection and vaccination status as of mid-2021: not previously infected or vaccinated, previously infected, previously vaccinated, or both previously infected and vaccinated. An earlier iteration of this program (the National Blood Donor Serosurvey) conducted serial monthly cross-sectional

Author affiliations: Vitalant Research Institute, San Francisco, California, USA (E. Grebe, M. Stone, C. Di Germanio, R. Bruhn, K.G. Zurita, B. Custer, M.P. Busch); University of California, San Francisco (M. Stone, R. Bruhn, M.C. Lanteri, B. Custer, M.P. Busch); American Red Cross, Rockville, Maryland, USA (B.R. Spencer, P. Saa); Westat, Rockville (A. Akinseye, D. Wright); QuidelOrtho, Rochester, New York, USA (P. Contestable); Creative Testing Solutions, Tempe, Arizona, USA (V. Green, M.C. Lanteri); Centers for Disease Control and Prevention, Fort Collins, Colorado, USA (B.J. Biggerstaff); Centers for Disease Control and Prevention, Atlanta, Georgia, USA (M.M. Coughlin, J.M. Jones); University of British Columbia, Vancouver, British Columbia, Canada (S. Kleinman)

DOI: https://doi.org/10.3201/eid3008.240659

[1]These first authors contributed equally to this article.

serosurveys during July 2020–December 2021 (*4*–*6*) to provide population-weighted seroprevalence estimates. However, because vaccination rates increased in 2021, the percentage of donations with vaccine-induced, infection-induced, or both vaccine-induced and infection-induced spike antibody reactivity approached 95%, and rates of infection-induced N antibody reactivity exceeded 75% in the United States by the end of 2022 (*1*,*7*), thus diminishing the value of cross-sectional serosurveillance. Important objectives of the NBDC included continued monitoring of SARS-CoV-2 infection incidence and vaccine- and infection-induced seroprevalence in the context of endemic SARS-CoV-2 transmission and increasing frequency of infection after vaccination and reinfections (M. Stone et al., unpub. data).

Several studies have suggested that the sensitivity of nucleocapsid antibody serologic tests for detecting previous SARS-CoV-2 infection is reduced in vaccinated persons compared with unvaccinated persons (*8*–*10*; H.J. Whitaker et al., unpub. data, https://doi.org/10.1101/2021.10.25.21264964). Significantly reduced nucleocapsid antibody reactivity has been reported in previously vaccinated persons with PCR-confirmed infections compared with infections in unvaccinated persons (H.J. Whitaker et al., unpub. data). Moderna mRNA vaccine trial data showed lower rates of nucleocapsid antibody seropositivity after PCR-confirmed infection among vaccine recipients compared with placebo recipients (40.4% vs. 93.4%) (*8*). A blunted nucleocapsid antibody response for infection after vaccination, and consequently reduced sensitivity of nucleocapsid antibody serology, may result from suppression of viral replication attributable to existing spike antibodies and an associated anamnestic response (*11*). In addition, studies relying on nucleocapsid IgG detection (*12*) may be confounded by rapidly waning antibodies below the limit of detection (i.e., seroreversion) (*13*–*16*).

We previously demonstrated good performance of the Ortho VITROS Anti-SARS-CoV-2 Total N Antibody (Ortho nucleocapsid antibody) assay (Quidel Ortho, https://www.quidelortho.com) and Roche Elecsys NC Anti-SARS-CoV-2 (Roche nucleocapsid antibody) assay (Roche, https://www.roche.com) for serosurveillance applications, without differentiating infections in vaccinated and unvaccinated persons (*17*). In this study, to increase sensitivity while maintaining high specificity for serologic detection of infection after vaccination, we derived a revised reactive versus nonreactive cutoff for those assays. In addition, for the Ortho nucleocapsid antibody assay we sought to validate the sensitivity of both the manufacturer's recommended and our revised cutoff for identifying first infections in vaccinated and unvaccinated donors who self-reported swab-confirmed infections. We then assessed factors influencing detection of nucleocapsid antibodies and assessed the durability of antibody detection after primary infection.

Materials and Methods

Study Population

We identified repeat blood donors from 2 national blood collection organizations (Vitalant and American Red Cross) who had known prior SARS-CoV-2 infection and COVID-19 vaccination status determined during June 2020–July 2021, when all donations were tested for SARS-CoV-2 antibodies and donors reported vaccination status at the time of donation. Eligible donors were those presenting ≥2× during the screening period and meeting all blood donor eligibility criteria. The NBDC includes 142,599 repeat blood donors. We based eligibility screening on donations tested with Ortho VITROS Anti-SARS-CoV-2 (spike) antibody assay and Roche nucleocapsid antibody assay, and we retained all spike antibody–reactive samples (*5*,*6*,*18*,*19*). During follow-up from July 2021 through December 2022, we identified donation specimens in real time and stored them frozen at –20°C. In 2022, we tested 1 donation specimen per donor per quarter by using the Ortho VITROS Anti-SARS-CoV-2 IgG Quantitative Test and the Ortho nucleocapsid antibody assay at Creative Testing Solutions and Vitalant Research Institute. We captured self-reported vaccination status at each donation as part of routine donation procedures. We invited all cohort donors to respond to electronic surveys on vaccination history, infection history, and clinical outcomes of infections; the overall response rate was 46.5%. NBDC seroprevalence estimates have been published (*1*).

Analysis and Statistical Methods

We conducted all analyses by using the SAS System version 9.4 (SAS Institute, https://www.sas.com). In total, we conducted 6 specific statistical analyses.

Derivation of Revised Nonreactive versus Reactive Cutoff for Ortho Nucleocapsid Antibody Assay

To detect infections serologically with optimal sensitivity, we derived a revised cutoff by using receiver operating characteristic (ROC) curve analysis (Appendix, https://wwwnc.cdc.gov/EID/article/30/8/24-0659-App1.pdf). We consequently defined gray zone reactivity as reactivity above the revised threshold and below the standard threshold (0.395≤signal-to-cutoff ratio [S/CO]<1.0).

Effect of Vaccination Status on Nucleocapsid Antibody Reactivity

To assess whether first infections after vaccination were associated with reduced postinfection nucleocapsid antibody reactivity compared with first infections in unvaccinated donors, we evaluated Ortho nucleocapsid antibody assay reactivity distributions after infection in 2 groups: serologically identified putative first infections, defined as the first donation sample for each donor in which nucleocapsid antibody reactivity was above the revised cutoff, among all donors in the NBDC; and first survey-reported swab-confirmed infections. For the first group, we based vaccination status on self-report at the time of donation. For the second group, we defined swab-confirmed infections as infections confirmed by viral antigen or PCR testing or by physician diagnosis (presumed positive swab-based test) and vaccination status at the time of infection on survey-reported vaccinations. For both groups, we stratified donation samples by vaccination status (vaccinated vs. unvaccinated) at the time of infection and by period (the Delta variant era, July–December 2021, vs. the Omicron era, January–December 2022 [*20*]) and stratified them further by quarter. We calculated the proportions of donation samples with reactivity in the gray zone for each group.

Sensitivity of Manufacturer's Recommended and Revised Cutoffs for Detection of First Infections

To validate sensitivity, we identified survey-reported swab-confirmed first SARS-CoV-2 infections. We classified an infection as occurring in an unvaccinated donor if the donor had not reported any vaccination before the date of diagnosed infection, and we defined an infection as infection after vaccination if it occurred ≥14 days after completion of an approved primary vaccination series (1 dose of the J&J/Janssen vaccine [https://www.jnj.com] or 2 doses of either the Pfizer-BioNtech [https://www.pfizer.com] or Moderna [https://www.modernatx.com] mRNA vaccines). For cases to be included in this analysis, ≥1 donation sample had to have been collected 14–180 days after diagnosis with no prior nucleocapsid antibody reactivity above the standard cutoff. We identified a total of 2,751 swab-confirmed first infections in unvaccinated donors and 8,187 swab-confirmed first infections that were infection after vaccination. For a secondary, more restrictive analysis, we only included infection after vaccination if a postvaccination spike antibody–reactive, nucleocapsid antibody–nonreactive sample had been collected before infection, demonstrating vaccine-induced spike antibodies seroconversion in the absence of infection-induced nucleocapsid antibodies. We excluded infections occurring after only 1 mRNA vaccination dose or <14 days after completion of a vaccination series. We identified 5,079 infection after vaccination cases for this analysis. We included only 1 postinfection sample per case in either analysis.

We estimated the sensitivity of both the manufacturer's recommended and our revised cutoffs on the Ortho nucleocapsid antibody assay in first donation samples after swab-confirmed infection, stratified by vaccination status of the donor at the time of infection. In addition, we stratified infections according to the variant era (Delta period vs. Omicron period), donor age (<65 years vs. ≥65 years), and whether the infection was associated with ≥1 self-reported symptom. We defined sensitivity as the proportion of samples that were reactive and calculated 95% CIs by using the Wilson score method. We assessed differences in sensitivity for different strata by using the binomial exact test. We assessed differences in sensitivity associated with different cutoffs computed on the same stratum by computing a p value for the difference in the Youden's J statistic associated with each cutoff.

Factors Associated with Nucleocapsid Antibody Seroconversion after Swab-Confirmed Infection

We performed bivariate and multivariable logistic regression to assess the effect of vaccination status, timing of sample collection relative to infection, donor demographics (age and sex), presence of symptoms, and variant era on nucleocapsid antibody detection. We included samples collected <14 days or >180 days after swab-confirmed infection because the model adjusted for time from infection to sample collection. We computed unadjusted odds ratios (ORs) and adjusted odds ratios (aORs) from logistic regression. After assessing ORs, we combined the vaccination status and timing variables for the multivariable regression.

Durability of Nucleocapsid Antibody Detection

We assessed durability of nucleocapsid antibody detection after primary infection in unvaccinated and vaccinated donors by examining the proportion of primary infections detectable by time from swab-confirmed infection to sample collection (0–13, 14–30, 31–60, 61–90, 91–180, 181–365, and >365 days). To account for multiple observations per time bin per donor, we weighted observations so that donors were equally weighted within each time bin, regardless of the number of observations. We computed 95% CIs by using the Wilson score method.

Effect of Adjustment for Nucleocapsid Antibody Sensitivity on Seroprevalence Estimates

To assess the potential effect of imperfect sensitivity and specificity on estimates of infection rates among vaccinated persons, we compared adjusted and unadjusted estimates of the proportion of vaccinated donors (not previously infected) who experienced infection after vaccination during 3 periods in the NBDC: quarter (Q) 2 2021–Q1 2022, Q1–Q2 2022, and Q2–Q3 2022. We cannot estimate the proportion of infections that were asymptomatic from survey data because diagnostic testing is largely driven by the presence of symptoms; therefore, for the purposes of this model, we used an estimated proportion of infections after vaccination that are asymptomatic of 32.4% (*21*). We then adjusted for a weighted average of symptomatic- and asymptomatic-specific sensitivity estimates and for specificity estimated using prepandemic samples. We computed the adjusted proportion of persons infected during each period by using the estimator derived by Rogan and Gladen (*22*), and we based 95% CIs on parametric bootstrapping (10,000 iterations) of the proportion of tests that were reactive, sensitivity, and specificity (treated as binomially distributed and incorporating the uncertainty arising from limited sample size).

Ethics Considerations

All blood donors consented to use of deidentified, residual specimens for further research purposes. Consistent with the policies and guidance of the University of California–San Francisco Institutional Review Board, Vitalant Research Institute self-certified the use of deidentified donations in this study as not meeting the criteria for human subjects research. CDC investigators reviewed and relied on this determination as consistent with applicable federal law and CDC policy. The donor surveys conducted by Vitalant Research Institute and American Red Cross were conducted under protocols supervised and approved by the Advarra and American Red Cross institutional review boards, respectively, and linked to biospecimens in deidentified form.

Results

Revised Cutoff for Detecting Previous Infection with Ortho Nucleocapsid Antibody Assay

The nonreactive versus reactive threshold on the Roche nucleocapsid antibody cutoff index that maximized Youden's J statistic was ≥0.205, and this optimized cutoff was used in defining cases for the Ortho ROC curve analysis. The ROC-optimized threshold on the Ortho nucleocapsid antibody assay was S/CO ≥0.395, which had a sensitivity of 98.7% and a specificity of 98.7% in the Ortho optimization sample set. The area under the ROC curve was 0.994 (Appendix).

Effect of Vaccination Status on Nucleocapsid Antibody Reactivity

We calculated distributions of Ortho nucleocapsid antibody assay S/COs in first longitudinal samples with reactivity above the revised cutoff (S/CO ≥0.395 [i.e., putative first infections]) from previously uninfected donors (based on negative Ortho nucleocapsid antibody results [S/CO <0.395] in all previous longitudinal samples), by vaccination status and variant era (Figure 1).

During the Delta era, 35.2% of serologically identified infections after vaccination showed gray zone reactivity (0.395≤S/CO< 1.0) compared with 7.5% of serologically identified primary infections in unvaccinated donors, declining to 3.8% for infections after vaccination and 2.7% for primary infections in unvaccinated donors by Q4 2022 (Omicron period Q4) (Figure 1, panel A). Among survey respondents with swab-confirmation infection, we did not observe a similar increased proportion of gray zone nucleocapsid antibody reactivity in the Delta period; most had reactivity above the standard cutoff (Figure 1, panel B). The donation specimens (Figure 1, panel B) correspond to the specimens used in assessing sensitivity for the 2 cutoffs.

Sensitivity for Detection of Swab-Confirmed Primary Infections

Overall sensitivity of the Ortho nucleocapsid antibody assay manufacturer's cutoff was 98.1% (95% CI 98.0%–98.2%) for detection of first infections in unvaccinated donors and 95.6% (95% CI 95.6%–95.7%) for detection of first infections after vaccination (Table). Sensitivity was increased when using the revised cutoff, to 98.4% (95% CI 98.4%–98.5%) in unvaccinated donors and to 97.0% (95% CI 96.9%–97.0%) for infections after vaccination. Although sensitivity is necessarily increased by reducing the cutoff from the manufacturer's suggestion, Youden's J index is not statistically improved by the reduced cutoff ($p = 0.13$ based on a 1-tailed test). Sensitivity for detection of infection after vaccination using the standard cutoff was higher during the Omicron era (96.0% [95% CI 95.9%–96.0%) than the Delta era (93.9% [95% CI 93.5%–95.4%]; $p = 0.001$) and was higher for detecting symptomatic than asymptomatic infections after vaccination (96.2% [95% CI 96.1%–96.2%] vs. 90.1% [95% CI 88.5%–91.7%]; $p<0.0001$). A secondary

Table. Sensitivity of SARS-CoV-2 nucleocapsid antibody assay for detection of first infections in unvaccinated and vaccinated donors, United States, July 2021–December 2022*

Characteristic	Sensitivity for detection of first infections in unvaccinated donors			Sensitivity for detection of first infections in vaccinated donors		
	No. donors	Manufacturer's cutoff,† % (95% CI)	Revised cutoff,‡ % (95% CI)	No. donors	Manufacturer's cutoff,† % (95% CI)	Revised cutoff,‡ % (95% CI)
Overall	2,751	98.1 (98.0–98.2)	98.4 (98.4–98.5)	8,187	95.6 (95.6–95.7)	97.0 (96.9–97.0)
Delta: Jul–Dec 2021	1,343	98.4 (98.2–98.5)	98.5 (98.4–98.6)	1,349	93.9 (93.5–94.4)	95.3 (94.9–95.6)
Omicron: Jan–Dec 2022	1,408	97.9 (97.7–98.0)	98.4 (98.3–98.5)	6,838	96.0 (95.9–96.0)	97.3 (97.3–97.4)
Age <65 y	2,225	98.2 (98.1–98.2)	98.4 (98.4–98.5)	5,194	96.2 (96.1–96.3)	97.3 (97.2–97.3)
Age ≥65 y	526	97.9 (97.5–98.3)	98.5 (98.2–98.8)	2,993	94.7 (94.5–94.9)	96.5 (96.4–96.6)
Symptomatic§	2,430	98.4 (98.3–98.4)	98.7 (98.7–98.8)	7,416	96.2 (96.1–96.2)	97.5 (97.5–97.6)
Asymptomatic§	208	96.6 (95.0–98.3)	96.6 (95.0–98.3)	627	90.1 (88.5–91.7)	91.2 (89.8–92.6)

*Proportion reactive in the first sample collected after reported swab-confirmed infection, collected 14 to 180 days postinfection.
†Signal-to-cutoff ratio ≥1.000.
‡Signal-to-cutoff ratio >0.395.
§Symptomatic or asymptomatic status could not be ascertained for all infections because of incomplete survey responses.

sensitivity analysis using a more restrictive case definition of infection after vaccination, which required spike antibody seroconversion after vaccination, showed similar patterns (Appendix Table 1).

Factors Associated with Nucleocapsid Antibody Seroconversion after Swab-Confirmed Infection

On first samples collected after first swab-confirmed infection, bivariate logistic regression showed that infection during the Delta era, age <65 years, female sex, symptomatic infection, being unvaccinated at the time of infection, longer time between vaccination and infection, and longer intervals between infection and sample collection were all statistically significantly associated with increased probability of detection (Figure 2; Appendix Table 2). Of note, the percentage detected in all time to sample categories, other than donation samples collected <14 days postinfection (dpi) (48.9%), ranged from 87.7% to 98.1%.

In multivariable logistic regression, infection during the Delta period (vs. Omicron period) remained statistically significant, but the direction of effect changed to reduced detection (aOR 0.80 [95% CI 0.66–0.98]) from increased detection in bivariate analysis (OR 1.51 [95% CI 1.28–1.78]), possibly because variant era (calendar time) is also strongly associated with vaccination status. Younger age groups had higher odds of detection than donors ≥65 years of age, whereas donor sex was not significantly associated with detection in the multivariable analysis. Asymptomatic infection was significantly associated with reduced detection (aOR 0.46, 95% CI 0.37–0.57). Being vaccinated at the time of infection significantly reduced detection compared with being unvaccinated (aORs <1), with the exception of primary vaccination ≤30 days before infection, which was not statistically significant. Vaccination reduced detection compared with no vaccination, and more recent receipt of either a primary vaccination series (31–180 days before infection) or a booster vaccination (≤30 days or 31–180 days before infection) was associated with reduced odds of detection than when infections occurred >180 days since the most recent vaccine. Compared with sample collection 31–90 dpi, sample collection <14 days (aOR 0.04 [95% CI 0.03–0.05]) and 14–30 days (aOR 0.34 [95% CI 0.28–0.40]) after infection were associated with greatly reduced detection, whereas sample collection 3–6 months (aOR 1.79 [95% CI 1.40–2.28]) or ≥7 months (aOR 2.19 [95% CI 1.44–3.35]) after infection were associated with increased detection (Figure 2; Appendix Table 2).

Durability of Nucleocapsid Antibody Detection

Nucleocapsid antibody reactivity was detected in less than half of specimens collected <14 dpi, >80% of specimens collected 14–30 dpi, and >90% of specimens collected >90 dpi in donors who were vaccinated and unvaccinated at the time of infection. We observed no decline in percentage detected in later time bins, including >1 year postinfection. The proportion detected was slightly lower in vaccinated donors and for asymptomatic infections at all times after infection (Figure 3).

Effect of Adjustment for Nucleocapsid Antibody Sensitivity on Seroprevalence Estimates

Estimates of the proportion of vaccinated donors who had become infected in each time period (using the nucleocapsid antibody test), adjusted for sensitivity and specificity, and assuming that 32.4% of infections were asymptomatic, differed little from unadjusted estimates. Adjusted estimated infection rates increased in each period by 0.2–0.9 percentage points, or proportionally by 1.5%–4.0% (Appendix Table 3).

Discussion

Despite reports of sensitivity as low as 40% for serologic detection of infection after vaccination (*8*),

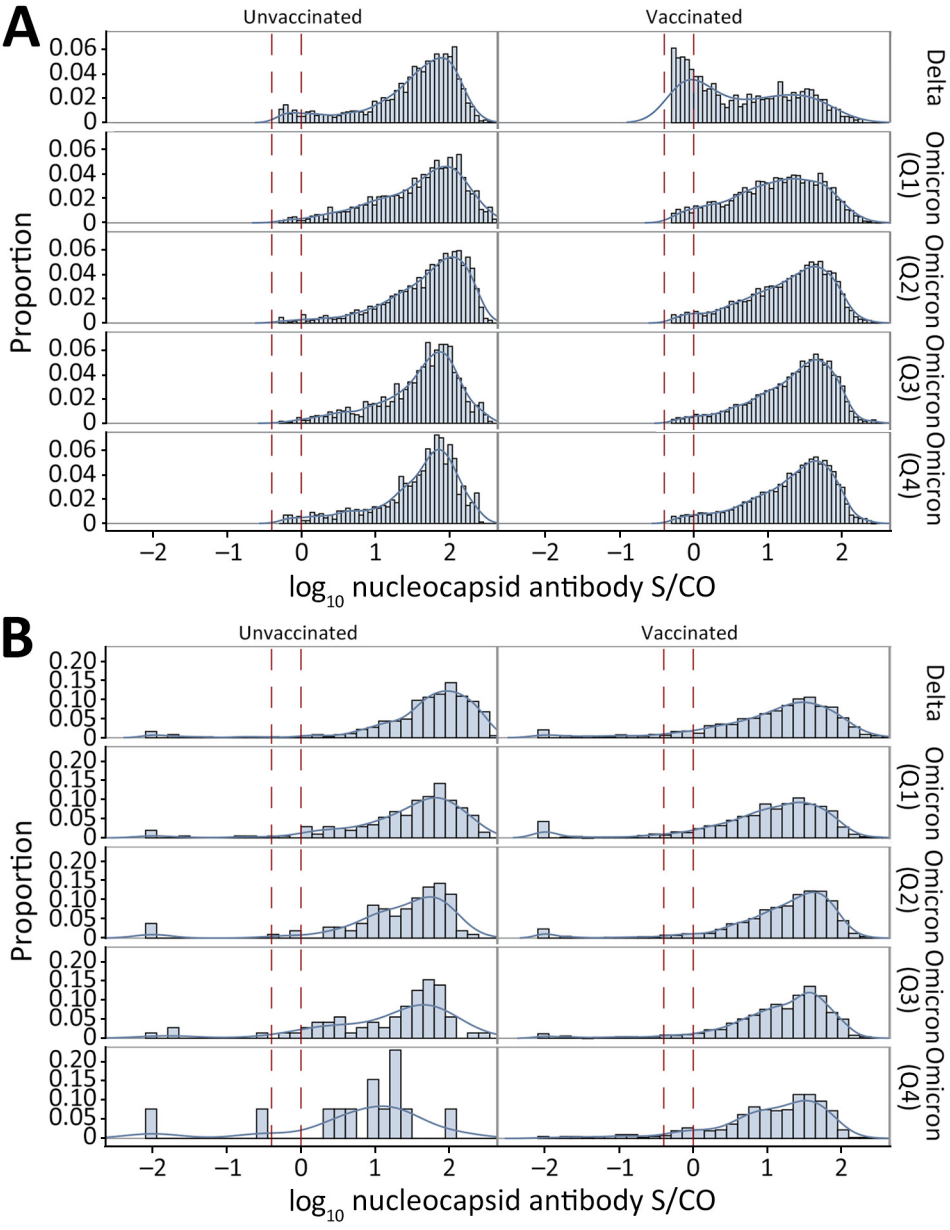

Figure 1. Nucleocapsid antibody signal intensity distributions observed in vaccinated and unvaccinated blood donors after primary SARS-CoV-2 infection, United States, July 2021–December 2022. A) Reactivity of putative serologically identified infections at the first longitudinal sample showing reactivity above the reduced cutoff (gray zone reactivity, S/CO ratio≥0.395≤1), by vaccination status and variant era (6,555 unvaccinated donors [left] and 22,217 vaccinated donors [right]). B) Reactivity at the first sample collected after self-reported swab-confirmed infection (14–80 days postinfection), by vaccination status and variant era (2,751 unvaccinated donors [left] and 8,187 vaccinated donors [right]). Vertical dashed lines indicate the gray zone of nucleocapsid antibodies. Q1, January–March 2022; Q2, April–June 2022; Q3, July–September 2022; Q4, October–December 2022. S/CO, signal-to-cutoff ratio.

our findings demonstrate sensitivity for detection of swab-confirmed first infections >98% among unvaccinated persons and >95% among vaccinated persons and supports use of the manufacturer's recommended cutoff for identifying previous infections in vaccinated and unvaccinated persons. Timing of sample collection after infection affected sensitivity (we observed poorer sensitivity <30 dpi); thus, timing of sample collection must be considered when interpreting previous reports.

In our validation of sensitivity for detection of first infections, the number of infections in vaccinated donors greatly exceeded those in unvaccinated donors in the study period, a function of high donor vaccination rates. This finding demonstrates the importance of sensitive detection of infection after vaccination in SARS-CoV-2 serosurveillance programs.

The revised cutoff for the Ortho nucleocapsid antibody assay offered minimal improvement in sensitivity to detect infection after vaccination compared with the manufacturer's cutoff. Our ROC analysis equally weighted sensitivity and specificity, an approach appropriate for surveillance applications, but potentially less appropriate for clinical applications prioritizing specificity. The revised cutoff was not associated with a statistical improvement in Youden's J statistic and only minimally increased sensitivity. The effect of adjusting seroprevalence estimates in vaccinated NBDC

donors for sensitivity and specificity was modest (Appendix Table 3), not exceeding a proportional effect of 4% on point estimates. This finding indicates that the standard assay cutoff for infection after vaccination detection performed sufficiently.

Recent receipt of primary or booster vaccinations reduced the likelihood of nucleocapsid antibody seroconversion after infection. Multivariable regression showed that recent receipt of an additional vaccine (booster) dose was associated with reduced detection, but the timing of primary vaccination relative to infection affected detection less. A study in Japan showed similar results, indicating reduced sensitivity to detect infection within 1–2 months of a third mRNA COVID-19 vaccine dose (sensitivity 78%) but high sensitivity for infections occurring >3 months after the second or >4 months after the third dose (*23*). The Moderna vaccine trial data (*8*) were selected for infections after vaccination occurring soon after vaccination and were collected relatively soon after infection, likely contributing to poor sensitivity in that study (*8*). Our data confirmed relatively poor sensitivity in specimens collected within 1 month of infection.

Because much of the lack of detection observed in our study occurred at times soon after infection, a longitudinal cohort study probably would detect many of the infections missed at the first postinfection specimen at later timepoints using specimens from those persons. Despite some waning of nucleocapsid antibody levels after infection, longer-term durability of antibody detection >1 year after infection confirmed earlier findings by our group of robust durability of detection using nucleocapsid direct antigen sandwich

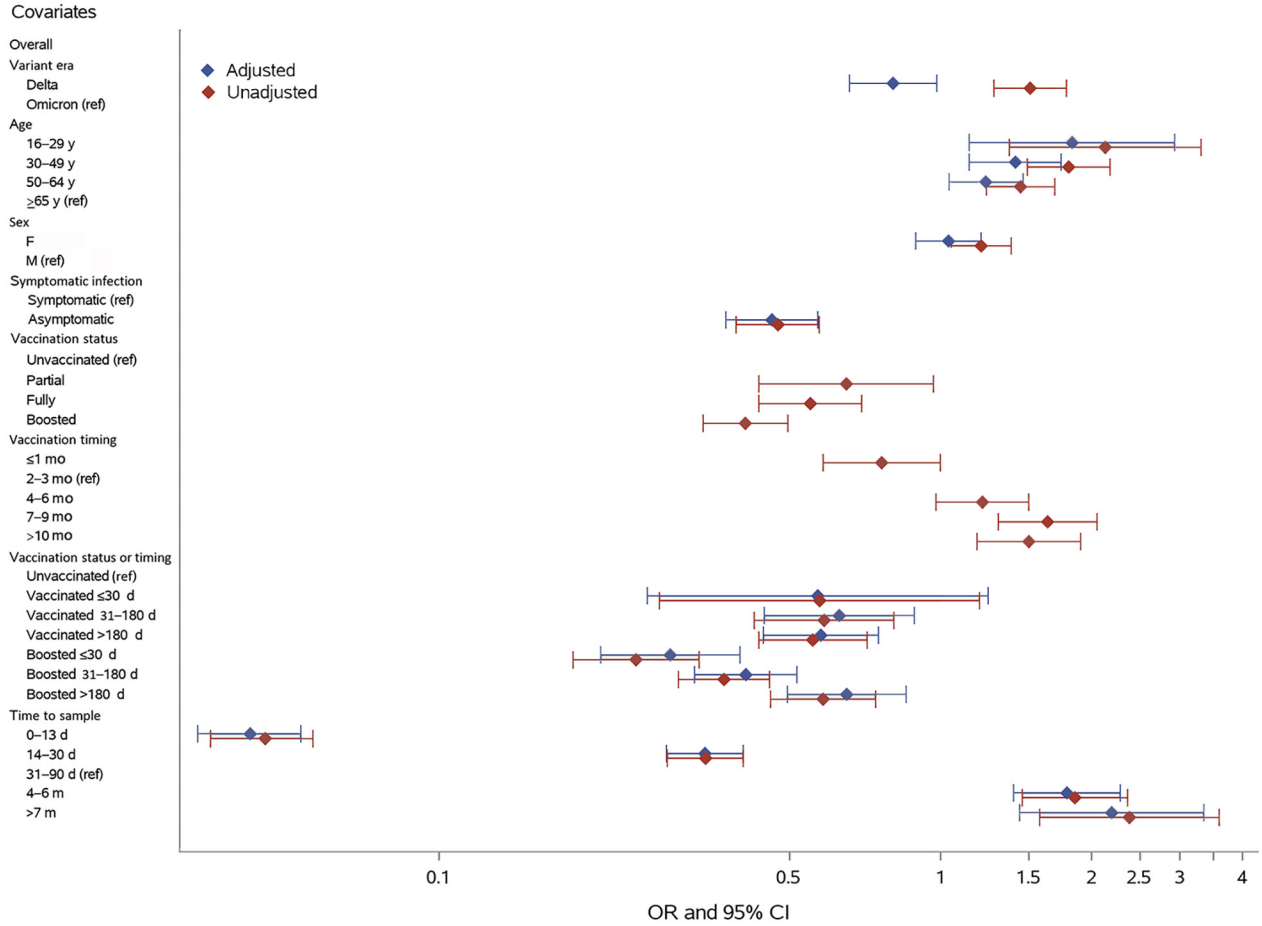

Figure 2. Factors influencing nucleocapsid antibody seroconversion after swab-confirmed first SARS-CoV-2 infections among vaccinated and unvaccinated blood donors, United States, July 2021–December 2022. ORs and 95% CIs from logistic regression are shown. In the multivariable regression model (adjusted ORs), the categories for certain variables have been grouped together; the vaccination status at the time of infection and timing of most recent vaccine before infection were combined in the vaccination status or timing variable, and in the variable for time from infection to tested sample, the groups for samples collected 7–12 months and >1 year postinfection were combined. Number of samples in each group, the proportion of nucleocapsid antibody–reactive samples, and ORs are shown in Appendix Table 2 (https://wwwnc.cdc.gov/EID/article/30/8/24-0659-App1.pdf). OR, odds ratio; ref, referent.

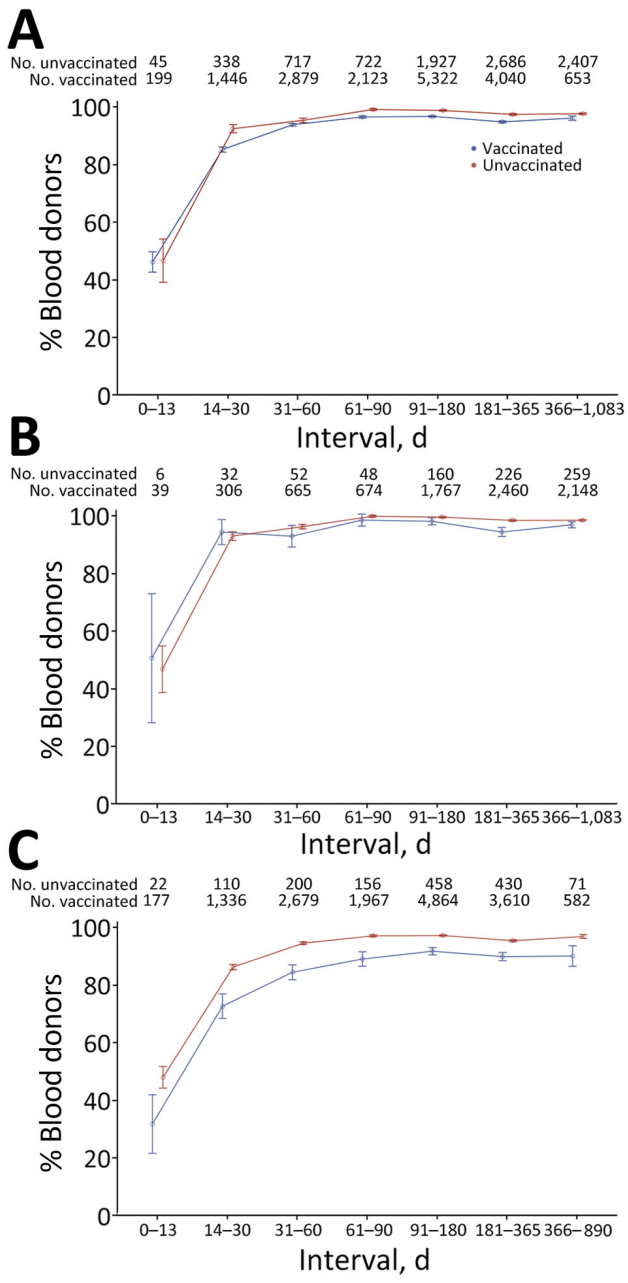

Figure 3. Sensitivity of nucleocapsid antibody serologic tests by time from swab-confirmed infection to sample collection in vaccinated and unvaccinated blood donors, using the manufacturer's recommended cutoff, United States, July 2021–December 2022. The percentage of donors showing reactivity in first or subsequent samples after swab-confirmed infection is shown. A) Reactive proportions stratified by vaccination status at the time of infection. B) Infections in unvaccinated donors stratified by reported symptoms. C) Reactive proportions in unvaccinated donors with swab-confirmed infections stratified by reported symptoms. To account for multiple observations per time bin, observations were weighted so that donors were equally weighted within each time bin, regardless of the number of observations. Error bars indicate median and maximum durations of follow-up for each group.

assays(*13*).We observed substantially reduced detection in the first month after infection, especially during the first 14 days, when <50% of recently infected persons demonstrated nucleocapsid antibody seroconversion but observed very good detection at later timepoints. Nucleocapsid IgG assays used in numerous serosurveillance studies (*14*, *24*–*28*) show more rapid waning in antibody signal than nucleocapsid total Ig assays (*13*) and thus require adjustments for seroreversion in estimating cumulative incidence (*14*). So-called direct immunoassays (i.e., antigen sandwich format total Ig assays), are more sensitive to increasing antibody affinity than IgG assays, which probably explains the more durable reactivity associated with antibody maturation and persistence postinfection despite waning in IgG concentrations (*29*). Although rapidly waning IgG assays may be less appropriate for serosurveillance aimed at documenting cumulative incidence than total Ig assays, they may have advantages for detecting reinfections based on antibody boosting and as correlates of protection (*30*).

A limitation of this study was that the case definition of infection in the validation data was based on self-reported diagnosed infection, without active surveillance of the cohort for asymptomatic infection. As a result, most of survey-reported swab-confirmed infections in the validation set were associated with COVID-19 symptoms (92%). In contrast, a meta-analysis of Omicron infections estimated that 32.4% of infections were asymptomatic (*31*). This limitation may result in a slight upward bias in our overall sensitivity estimates. However, we found that adjusting for sensitivity to detect symptomatic and asymptomatic infection after vaccination had a modest effect on seroprevalence estimates. A further limitation is that blood donors are not fully representative of the general population; they generally are healthier and more likely to be vaccinated and to receive additional doses (*1*,*32*). Furthermore, vaccination and infection history were self-reported in donor surveys and not confirmed by healthcare records; only 46.5% of cohort participants responded to surveys and could be included in this study, which may have resulted in a biased sample.

Our study demonstrates that detection of first SARS-CoV-2 infections using the Ortho nucleocapsid total Ig antibody assay was robust in vaccinated and unvaccinated donors, indicating overall sensitivities >95%. We also found good durability of nucleocapsid antibody detection for up to >1 year after infection. Seroprevalence studies using this assay can accurately estimate the proportion of persons who have been infected with SARS-CoV-2 ≥1 times. Several factors affect the likelihood of nucleocapsid antibody

seroconversion after first infection, including receipt of primary and additional vaccinations, sampling shortly after infection, and asymptomatic infection, although the effect of these factors was relatively small. Revising the cutoff improved sensitivity only modestly; therefore, use of the manufacturer's recommended cutoff is likely appropriate for most serosurveillance studies.

This article was preprinted at https://www.medrxiv.org/content/10.1101/2024.05.23.24307822v1.

Acknowledgments

The authors gratefully acknowledge CDC reviewers, whose comments greatly improved the manuscript. The contributions of numerous laboratory and data management staff, including Hasan Sulaeman, Brendan Balasko, Jahnavi Bhaskar, Patricia Villaflor, Kaya Duncan, Zhanna Kaidarova, Anh (Paul) Nguyen, Marjorie D. Bravo, Edward P. Notari, James Haynes, Jamel Groves, Gary Holley, Rebecca Fink, Athena Nguyen, Dave Kovach, Chloe Byrne, Daishia Hall, Tatum Fenner, and Melissa Briggs-Hagen, are also acknowledged with gratitude.

This work was supported by a research contract from the CDC (contract no. 75D30120C08170).

Vitalant Research Institute receives research funding from QuidelOrtho. The authors have no other conflicts of interest to declare.

About the Authors

Dr. Grebe is an epidemiologist and affiliate investigator at Vitalant Research Institute. His work is focused on infectious diseases surveillance, blood safety, and assay evaluation. Dr. Stone is a virologist and senior director of laboratory cores at Vitalant Research Institute. Her work is focused on transfusion-transmissible infectious diseases, assay evaluation, and public health serosurveillance.

References

1. Jones JM, Manrique IM, Stone MS, Grebe E, Saa P, Germanio CD, et al. Estimates of SARS-CoV-2 seroprevalence and incidence of primary SARS-CoV-2 infections among blood donors, by COVID-19 vaccination status—United States, April 2021–September 2022. MMWR Morb Mortal Wkly Rep. 2023;72:601–5. https://doi.org/10.15585/mmwr.mm7222a3
2. Busch MP, Stone M. Serosurveillance for severe acute respiratory syndrome coronavirus 2 (SARS-CoV-2) incidence using global blood donor populations. Clin Infect Dis. 2021;72:254–6. https://doi.org/10.1093/cid/ciaa1116
3. O'Brien SF, Lieshout-Krikke RW, Lewin A, Erikstrup C, Steele WR, Uzicanin S, et al.; Surveillance, Risk Assessment, Policy Sub-group of the ISBT Transfusion Transmitted Infectious Diseases Working Party. Research initiatives of blood services worldwide in response to the covid-19 pandemic. Vox Sang. 2021;116:296–304. https://doi.org/10.1111/vox.12995
4. Stone M, Di Germanio C, Wright DJ, Sulaeman H, Dave H, Fink RV, et al.; NHLBI Recipient Epidemiology and Donor Evaluation Study-IV-Pediatric (REDS-IV-P). Use of US blood donors for national serosurveillance of severe acute respiratory syndrome coronavirus 2 antibodies: basis for an expanded national donor serosurveillance program. Clin Infect Dis. 2022;74:871–81. https://doi.org/10.1093/cid/ciab537
5. Jones JM, Stone M, Sulaeman H, Fink RV, Dave H, Levy ME, et al. Estimated US infection- and vaccine-induced SARS-CoV-2 seroprevalence based on blood donations, July 2020–May 2021. JAMA. 2021;326:1400–9. https://doi.org/10.1001/jama.2021.15161
6. Jones JM, Opsomer JD, Stone M, Benoit T, Ferg RA, Stramer SL, et al. Updated US infection- and vaccine-induced SARS-CoV-2 seroprevalence estimates based on blood donations, July 2020–December 2021. JAMA. 2022;328:298–301. https://doi.org/10.1001/jama.2022.9745
7. Centers for Disease Control and Prevention. 2022 nationwide COVID-19 infection- and vaccination-induced antibody seroprevalence (blood donations). 2023 [cited 2023 Dec 23]. https://covid.cdc.gov/covid-data-tracker/#nationwide-blood-donor-seroprevalence-2022
8. Follmann D, Janes HE, Buhule OD, Zhou H, Girard B, Marks K, et al. Antinucleocapsid antibodies after SARS-CoV-2 infection in the blinded phase of the randomized, placebo-controlled mRNA-1273 COVID-19 vaccine efficacy clinical trial. Ann Intern Med. 2022;175:1258–65. https://doi.org/10.7326/M22-1300
9. Dhakal S, Yu T, Yin A, Pisanic N, Demko ZO, Antar AAR, et al. Reconsideration of anti-nucleocapsid IgG antibody as a marker of SARS-CoV-2 infection post-vaccination for mild COVID-19 patients. Open Forum Infect Dis. 2022;10:c677. https://doi.org/10.1093/ofid/ofac677
10. Dalai SC, Dines JN, Snyder TM, Gittelman RM, Eerkes T, Vaney P, et al. Clinical validation of a novel T-cell receptor sequencing assay for identification of recent or prior severe acute respiratory syndrome coronavirus 2 infection. Clin Infect Dis. 2022;75:2079–87. https://doi.org/10.1093/cid/ciac353
11. Zuo J, Dowell AC, Pearce H, Verma K, Long HM, Begum J, et al. Robust SARS-CoV-2-specific T cell immunity is maintained at 6 months following primary infection. Nat Immunol. 2021;22:620–6. https://doi.org/10.1038/s41590-021-00902-8
12. Anderson M, Stec M, Gosha A, Mohammad T, Boler M, Tojo Suarez R, et al. Longitudinal severe acute respiratory syndrome coronavirus 2 vaccine antibody responses and identification of vaccine breakthrough infections among healthcare workers using nucleocapsid immunoglobulin G. J Infect Dis. 2022;226:1934–42. https://doi.org/10.1093/infdis/jiac420
13. Stone M, Grebe E, Sulaeman H, Di Germanio C, Dave H, Kelly K, et al. Evaluation of commercially available high-throughput SARS-CoV-2 serologic assays for serosurveillance and related applications. Emerg Infect Dis. 2022;28:672–83. https://doi.org/10.3201/eid2803.211885
14. Buss LF, Prete CA Jr, Abrahim CMM, Mendrone A Jr, Salomon T, de Almeida-Neto C, et al. Three-quarters attack rate of SARS-CoV-2 in the Brazilian Amazon during a largely unmitigated epidemic. Science. 2021;371:288–92. https://doi.org/10.1126/science.abe9728
15. Erikstrup C, Laksafoss AD, Gladov J, Kaspersen KA, Mikkelsen S, Hindhede L, et al. Seroprevalence and

infection fatality rate of the SARS-CoV-2 Omicron variant in Denmark: a nationwide serosurveillance study. Lancet Reg Health Eur. 2022;21:100479. https://doi.org/10.1016/j.lanepe.2022.100479
16. Hønge BL, Hindhede L, Kaspersen KA, Harritshøj LH, Mikkelsen S, Holm DK, et al. Long-term detection of SARS-CoV-2 antibodies after infection and risk of re-infection. Int J Infect Dis. 2022;116:289–92. https://doi.org/10.1016/j.ijid.2022.01.041
17. Sulaeman H, Grebe E, Dave H, McCann L, Di Germanio C, Sanghavi A, et al. Evaluation of Ortho VITROS and Roche Elecsys S and NC immunoassays for SARS-CoV-2 serosurveillance applications. Microbiol Spectr. 2023; 11:e0323422. https://doi.org/10.1128/spectrum.03234-22
18. Fink RV, Fisher L, Sulaeman H, Dave H, Levy ME, McCann L, et al. How do we…form and coordinate a national serosurvey of SARS-CoV-2 within the blood collection industry? Transfusion. 2022;62:1321–33. https://doi.org/10.1111/trf.16943
19. Busch MP, Stramer SL, Stone M, Yu EA, Grebe E, Notari E, et al. Population-weighted seroprevalence from severe acute respiratory syndrome coronavirus 2 (SARS-CoV-2) infection, vaccination, and hybrid immunity among US blood donations from January to December 2021. Clin Infect Dis. 2022;75(Suppl 2):S254–63. https://doi.org/10.1093/cid/ciac470
20. Lambrou AS, Shirk P, Steele MK, Paul P, Paden CR, Cadwell B, et al.; Strain Surveillance and Emerging Variants Bioinformatic Working Group; Strain Surveillance and Emerging Variants NS3 Working Group. Genomic Surveillance for SARS-CoV-2 variants: predominance of the Delta (B.1.617.2) and Omicron (B.1.1.529) variants—United States, June 2021–January 2022. MMWR Morb Mortal Wkly Rep. 2022;71:206–11. https://doi.org/10.15585/mmwr.mm7106a4
21. Shang W, Kang L, Cao G, Wang Y, Gao P, Liu J, et al. Percentage of asymptomatic infections among SARS-CoV-2 Omicron variant-positive individuals: a systematic review and meta-analysis. Vaccines (Basel). 2022;10:1049. https://doi.org/10.3390/vaccines10071049
22. Rogan WJ, Gladen B. Estimating prevalence from the results of a screening test. Am J Epidemiol. 1978;107:71–6. https://doi.org/10.1093/oxfordjournals.aje.a112510
23. Mizoue T, Yamamoto S, Konishi M, Oshiro Y, Inamura N, Nemoto T, et al. Sensitivity of anti-SARS-CoV-2 nucleocapsid protein antibody for breakthrough infections during the epidemic of the Omicron variants. J Infect. 2022;85:573–607. https://doi.org/10.1016/j.jinf.2022.08.015
24. Buss LF, Sabino EC. Intense SARS-CoV-2 transmission among affluent Manaus residents preceded the second wave of the epidemic in Brazil. Lancet Glob Health. 2021;9:e1475–6. https://doi.org/10.1016/S2214-109X(21)00396-X
25. Bloch EM, Kyeyune D, White JL, Ddungu H, Ashokkumar S, Habtehyimer F, et al. SARS-CoV-2 seroprevalence among blood donors in Uganda: 2019–2022. Transfusion. 2023;63:1354–65. https://doi.org/10.1111/trf.17449
26. He Z, Ren L, Yang J, Guo L, Feng L, Ma C, et al. Seroprevalence and humoral immune durability of anti-SARS-CoV-2 antibodies in Wuhan, China: a longitudinal, population-level, cross-sectional study. Lancet. 2021; 397:1075–84. https://doi.org/10.1016/S0140-6736(21)00238-5
27. Murhekar MV, Bhatnagar T, Thangaraj JWV, Saravanakumar V, Santhosh Kumar M, Selvaraju S, et al.; ICMR serosurveillance group. Seroprevalence of IgG antibodies against SARS-CoV-2 among the general population and healthcare workers in India, June–July 2021: a population-based cross-sectional study. PLoS Med. 2021;18:e1003877. https://doi.org/10.1371/journal.pmed.1003877
28. Renaud C, Lewin A, Gregoire Y, Simard N, Vallières É, Paquette M, et al. SARS-CoV-2 immunoassays in a predominantly vaccinated population: performances and qualitative agreements obtained with two analytical approaches and four immunoassays. Vox Sang. 2024 Apr 5 [Epub ahead of print]. https://doi.org/10.1111/vox.13625 PMID:
29. Macdonald PJ, Ruan Q, Grieshaber JL, Swift KM, Taylor RE, Prostko JC, et al. Affinity of anti-spike antibodies in SARS-CoV-2 patient plasma and its effect on COVID-19 antibody assays. EBioMedicine. 2022;75:103796. https://doi.org/10.1016/j.ebiom.2021.103796
30. Prete CA Jr, Buss LF, Buccheri R, Abrahim CMM, Salomon T, Crispim MAE, et al. Reinfection by the SARS-CoV-2 Gamma variant in blood donors in Manaus, Brazil. BMC Infect Dis. 2022;22:127. https://doi.org/10.1186/s12879-022-07094-y
31. Von Bartheld CS, Wang L. An explanation for reports of increased prevalence of olfactory dysfunction with Omicron: asymptomatic infections. J Infect Dis. 2023.
32. Whitaker BI, Walderhaug M, Hinkins S, Steele WR, Custer B, Kessler D, et al. Use of a rapid electronic survey methodology to estimate blood donors' potential exposure to emerging infectious diseases: application of a statistically representative sampling methodology to assess risk in US blood centers. Transfusion. 2020;60:1987–97. https://doi.org/10.1111/trf.15941

Address for correspondence: Eduard Grebe, Vitalant Research Institute, 360 Spear St, San Francisco, CA 94105, USA; email: egrebe@vitalant.org

Standardized Phylogenetic Classification of Human Respiratory Syncytial Virus below the Subgroup Level

Stephanie Goya,[1] Christopher Ruis,[2] Richard A. Neher,[2] Adam Meijer, Ammar Aziz, Angie S. Hinrichs, Anne von Gottberg, Cornelius Roemer, Daniel G. Amoako,[3] Dolores Acuña, Jakob McBroome, James R. Otieno, Jinal N. Bhiman, Josie Everatt, Juan C. Muñoz-Escalante, Kaat Ramaekers,[4] Kate Duggan, Lance D. Presser, Laura Urbanska, Marietjie Venter, Nicole Wolter, Teresa C.T. Peret, Vahid Salimi, Varsha Potdar, Vítor Borges, Mariana Viegas[1]

A globally implemented unified phylogenetic classification for human respiratory syncytial virus (HRSV) below the subgroup level remains elusive. We formulated global consensus of HRSV classification on the basis of the challenges and limitations of our previous proposals and the future of genomic surveillance. From a high-quality curated dataset of 1,480 HRSV-A and 1,385 HRSV-B genomes submitted to GenBank and GISAID (https://www.gisaid.org) public sequence databases through March 2023, we categorized HRSV-A/B sequences into lineages based on phylogenetic clades and amino acid markers. We defined 24 lineages within HRSV-A and 16 within HRSV-B and provided guidelines for defining prospective lineages. Our classification demonstrated robustness in its applicability to both complete and partial genomes. We envision that this unified HRSV classification proposal will strengthen HRSV molecular epidemiology on a global scale.

Human respiratory syncytial virus (HRSV) is a leading cause of acute lower respiratory tract infection in children, elderly, and immunocompromised persons. In 2023, the US Food and Drug Administration and the European Medicines Agency approved the first HRSV vaccines (*1*,*2*). Simultaneously, a monoclonal antibody was approved for widespread use in infants and not limited to high-risk and premature children (*3*). The availability of HRSV immunization highlights the role of molecular epidemiology

Author affiliations: University of Washington, Seattle, Washington, USA (S. Goya); University of Cambridge, Cambridge, UK (C. Ruis); University of Basel and SIB, Basel, Switzerland (R.A. Neher, C. Roemer, L. Urbanska); National Institute for Public Health and the Environment, Bilthoven, the Netherlands (A. Meijer, L.D. Presser); World Health Organization Collaborating Centre for Reference and Research on Influenza, Melbourne, Victoria, Australia (A. Aziz); University of California Santa Cruz, Santa Cruz, California, USA (A.S. Hinrichs, J. McBroome); National Institute for Communicable Diseases of the National Health Laboratory Service, Johannesburg, South Africa (A. von Gottberg, J.N. Bhiman, J. Everatt, N. Wolter); University of Witwatersrand, Johannesburg, South Africa (A. von Gottberg, J.N. Bhiman, N. Wolter); University of KwaZulu-Natal, Durban, South Africa (D.G. Amoako); Universidad Nacional de La Plata, Buenos Aires, Argentina (D. Acuña, M. Viegas); National Scientific and Technical Research Council, Buenos Aires, Argentina (D. Acuña, M. Viegas); Theiagen Genomics, Highlands Ranch, Colorado, USA (J.R. Otieno); Autonomous University of San Luis Potosí, San Luis Potosí, Mexico (J.C. Muñoz-Escalante); Rega Institute for Medical Research, Leuven, Belgium (K. Ramaekers); University of Edinburgh, Edinburgh, Scotland, UK (K. Duggan); University of Pretoria, Pretoria, South Africa (M. Venter); University of Texas Medical Branch, Galveston, Texas, USA (T.C.T. Peret); Tehran University of Medical Sciences, Tehran, Iran (V. Salimi); ICMR National Institute of Virology, Pune, India (V. Potdar); National Institute of Health Doutor Ricardo Jorge, Lisbon, Portugal (V. Borges)

DOI: http://doi.org/10.3201/eid3008.240209

[1]These authors were co–principal investigators.

[2]These authors contributed equally to this article.

[3]Current affiliation: Department of Pathobiology, University of Guelph, Guelph, Ontario, Canada.

[4]Current affiliation: Sciensano, Infectious Diseases in Humans, Unit (Re)-Emerging Viruses, Brussels, Belgium.

as a tool to monitor their efficacy. Standards for HRSV nomenclature for sharing of viral isolates and sequences in databases have been published (*4*). Nevertheless, a standardized HRSV phylogenetic classification system has yet to be defined and implemented.

In 2022, HRSV was designated as *Orthopneumovirus hominis* species within the Pneumoviridae family. Below species level are 2 antigenic groups, known as HRSV subgroup A (HRSV-A) and B (HRSV-B), that were previously referred to as subtypes (*4*–*6*). Within each subgroup, genotypes were initially defined based on statistically supported phylogenetic clades inferred with the second hypervariable region of the G gene (Figure 1, panels A, B) (*7*). The G gene, encoding the attachment glycoprotein, exhibits the highest genetic and antigenic variability. Of note, the gene has undergone a duplication of a 72-nt fragment in HRSV-A and 60-nt fragment in HRSV-B (Figure 1, panel B) (*8*,*9*).

To identify emerging genotypes, researchers have used genetic distances between phylogenetic clades and distinctive genetic features, accompanied by variable nomenclature based on the gene (GA1–GA7 in HRSV-A and GB1–GB4 in HRSV-B), country and subgroup (SAB1–SAB4 for South African genotypes in HRSV-B), or city and province (NA1–NA2 [Niigata] and ON1 [Ontario] in HRSV-A, BA1–BA9 [Buenos Aires] in HRSV-B) (*7*–*16*). Since 2020, alternative phylogenetic reclassifications have been proposed; Goya et al. established a hierarchical classification system for HRSV phylogenies, comprising genotypes, subgenotypes, and lineages, using the G gene (*17*). That framework enabled laboratories without capacity for whole-genome sequencing to conduct molecular epidemiology studies. Independently, Ramaekers et al. (*18*) proposed reclassifications into lineages and Chen et al. (*19*) into genotypes using complete HRSV genomes. Those approaches support comprehensive monitoring of viral evolution across all genes, including the F gene encoding the fusion protein, a crucial target for monoclonal antibodies and the foundation of approved HRSV vaccines (Figure 1, panel A). Of note, challenges in HRSV molecular epidemiology persisted within the reclassification-defined categories because of reliance on genetic or patristic distances between tree tips or nodes.

The milestones achieved in HRSV interventions have renewed interest in addressing the challenge of

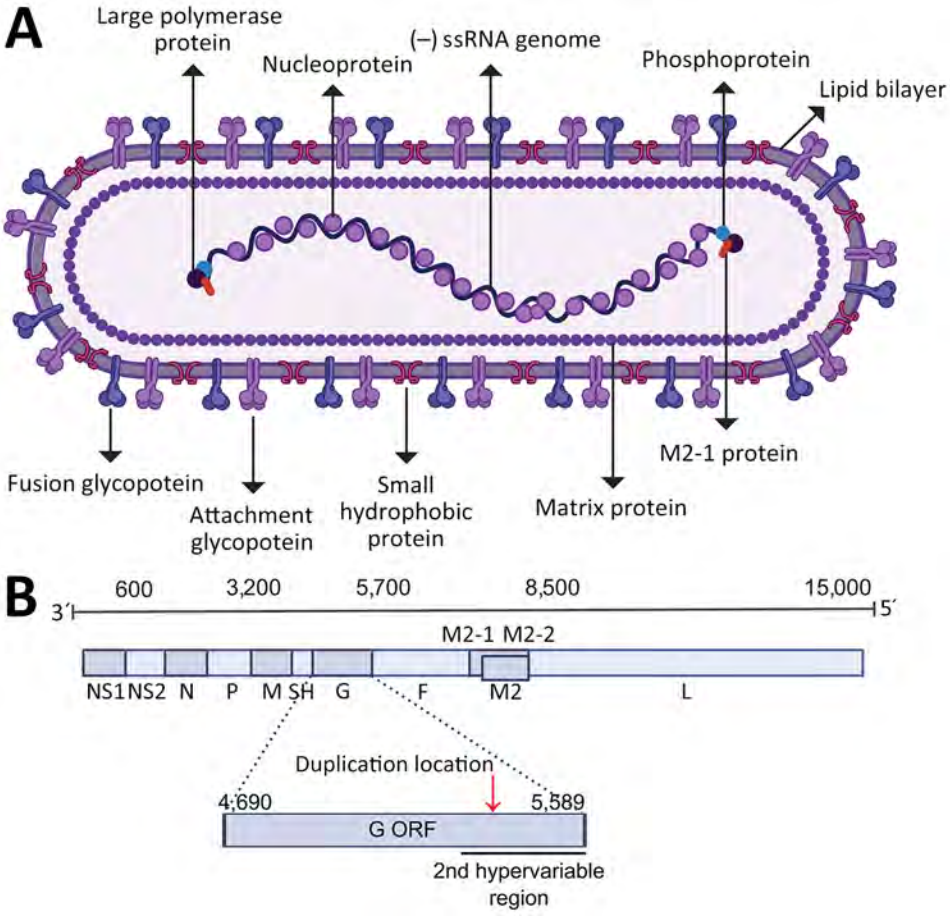

Figure 1. The structure and genome of human respiratory syncytial virus (HRSV). A) Schematic of the HRSV virion structure detailing the location of structural proteins. B) Schematic of the HRSV genome organization with the approximated location of genes highlighted; the exact location slightly differs between subgroups and strains. The location of the second hypervariable region in the G gene, used originally for molecular epidemiology classification, is detailed. Red arrow in panel B indicates location of the G gene 72-nt duplication in HRSV-A and 60-nt duplication in HRSV-B. Figure created with BioRender (https://www.biorender.com). F, fusion glycoprotein; G, attachment glycoprotein; L, large polymerase protein; M, matrix protein; M2, M2 protein; N, nucleocapsid; NS, nonstructural protein; ORF, open reading frame; P, phosphoprotein; SH, small hydrophobic protein.

classifying HRSV below the subgroup level. Those advances prompted establishment of the HRSV Genotyping Consensus Consortium (RGCC), formed by HRSV and virus evolution experts aiming to provide standardized criteria for harmonizing global HRSV molecular surveillance efforts. We present a novel framework for HRSV classification below the subgroup level, based on current knowledge of HRSV diversity and evolution, focused on practical implementation for molecular epidemiology.

Methods

HRSV Sequences Dataset

We downloaded HRSV complete genomes from the National Center for Biotechnology Information Virus (https://www.ncbi.nlm.nih.gov/labs/virus) and GISAID EpiRSV (https://www.gisaid.org) databases through March 11, 2023, using a filter for sequence length >14,000 nt, obtained from human hosts and including the year and country of the sample collection (Appendix 1 Figure 1, https://wwwnc.cdc.gov/EID/article/30/8/24-0209-App1.pdf). We reserved sequences containing nucleotide ambiguities, indicating inadequate sequencing depth, for epidemiologic analysis but excluded them from formal lineage definition (Appendix 1).

We aligned sequences with MAFFT version 7.490, and inspected and corrected alignment artifacts with Aliview version 1.28 (https://ormbunkar.se/aliview), mainly in the G gene (*20*,*21*). We trimmed alignment ends to encompass complete genomes from the first codon of the first gene (NS1) to the last codon of the last gene (L). We considered partial genomes if the lack of sequence was within 50 nt of the genome ends. We used RSVsurver (https://rsvsurver.bii.a-star.edu.sg) to identify and remove genomes with nucleotide insertions or deletions causing frameshift in any open reading frame. After alignment trimming, detection of identical sequences prompted redundancy removal using BBmap (https://jgi.doe.gov/data-and-tools/software-tools/bbtools), resulting in the final set of 1,538 HRSV-A and 1,387 HRSV-B genomes (Appendix 1 Figure 1).

Phylogenetic Analysis

We constructed maximum-likelihood phylogenetic trees with IQ-TREE version 2.2.0 (http://www.iqtree.org) (Appendix 1). We considered monophyletic clades statistically supported when SH-aLRT value was ≥80% and UFBoot2 value was ≥90% (*22*,*23*) (Appendix 1). We assessed temporal signal with TempEst version 1.5.3 (http://tree.bio.ed.ac.uk/software/tempest), and we inferred molecular-clock phylogenies with TreeTime (https://github.com/neherlab/treetime) (*24*).

We inferred the ancestral sequence reconstruction using Augur bioinformatic toolkit version 23.1.0 (https://docs.nextstrain.org/projects/augur/en/23.1.0) (*25*). We assessed recombination events by alignment-based method using RDP4 (http://web.cbio.uct.ac.za/~darren/rdp.html) and phylogenetic-based TreeKnit (https://pierrebarrat.github.io/TreeKnit.jl) (Appendix 1). We inferred the amino acid substitutions linked to the clades in the tree using Augur and automated the initial screening of lineages with Autolin (*26*). We manually curated amino acid comparison among monophyletic clusters to rectify conflicts arising from internal (nested) lineages and the confirmation of the lineage-defining amino acids in >90% of the clade's sequences. Results are available at https://github.com/rsv-lineages/Classification_proposal.

Results

Baseline Agreements on the HRSV Classification Definition

Our proposed classification establishes HRSV lineages for viruses below subgroup level. Studies have shown that HRSV phylogenetic trees constructed with complete genomes exhibit superior resolution (*17*–*19*). Therefore, we defined a classification system based on maximum-likelihood phylogenetic trees inferred from complete HRSV genomes. The maximum-likelihood algorithm formulates hypotheses about the evolutionary relationships among sequences; the implementation within IQ-TREE dealing with large datasets makes it particularly well suited to assert HRSV genomic phylogeny including sequences collected >50 years ago (*22*). We defined complete HRSV genomes to the nucleotide sequences spanning from the first codon of the first gene (NS1) to the last codon of the last gene (L). We considered almost-complete genomes if the sequence information gaps were within a 50-nt window at the genome ends. To define lineages, we only used genomes without nucleotide ambiguities (in accordance with the IUPAC code for nucleotide degeneracy).

Genomic Dataset Used for Lineages Definition

Applying the established baseline agreements, we gathered 1,538 HRSV-A and 1,387 HRSV-B high-quality genomes from public databases. The dataset revealed a limited global HRSV genomic surveillance; <20 genomes deposited annually through 2007 (Figure 2, panel A; Appendix 1 Figure 2). Since 2008, the

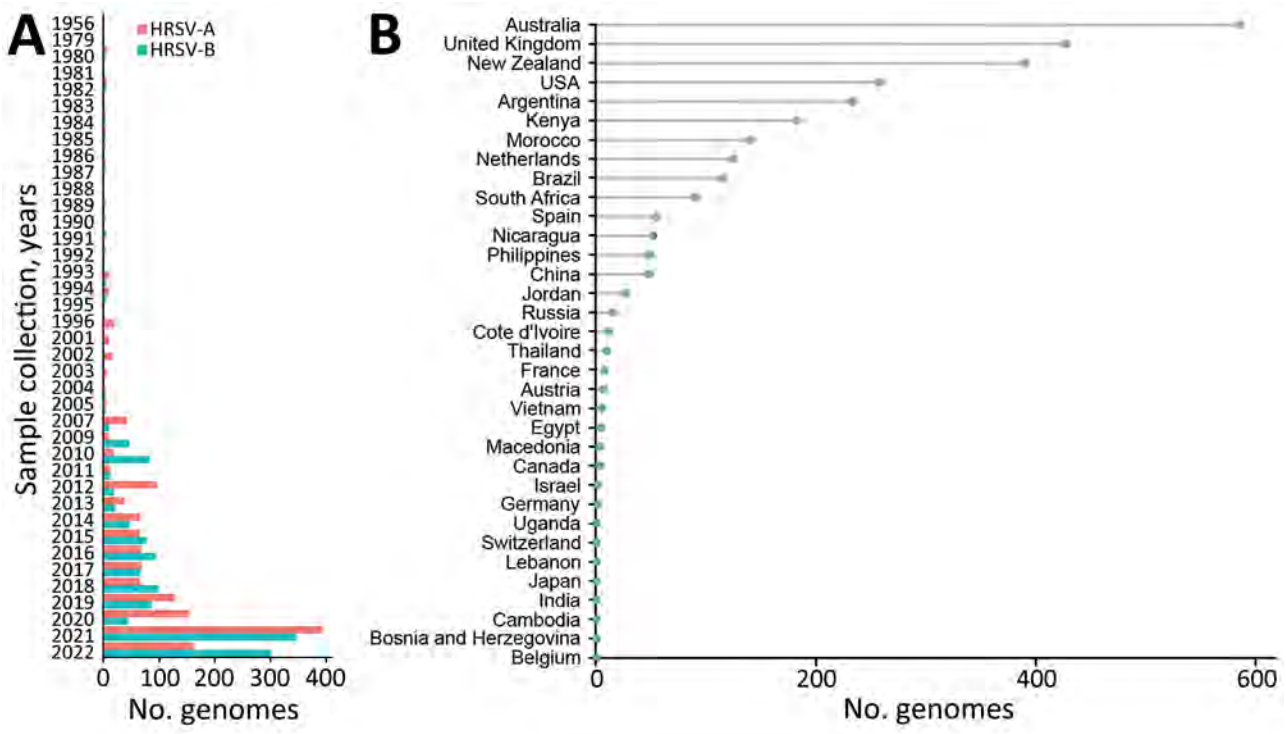

Figure 2. The global HRSV genomics surveillance landscape. HRSV genomes from GenBank and GISAID (https://www.gisaid.org) databases through March 11, 2023, that met inclusion criteria used for classification are shown by year of sample collection and subgroup (A) and by country of origin (B). HRSV, human respiratory syncytial virus.

number of genomes and representation of countries improved; a surge occurred after 2021, probably driven by expansion of viral genomics since the SARS-CoV-2 pandemic and the approval of the HRSV prophylactic treatments (Figure 2, panel A; Appendix 1 Figure 2). Considering delays in genome deposition in public databases, the number of genomes in 2022 may be higher than those used in this study. Regarding geographic representation, 9 countries (Australia, United Kingdom, New Zealand, United States, Argentina, Kenya, Morocco, Netherlands, and Brazil) submitted >100 genomes; only the United Kingdom achieved uninterrupted surveillance since 2008, but Australia deposited the most genomes globally (Figure 2, panel B).

Accurate Root Placement in HRSV Phylogenetic Trees

We reconstructed maximum-likelihood phylogenetic trees for the HRSV-A and HRSV-B datasets. We used 2 approaches to root the trees: the use of an outgroup, a conventional method for inferring the tree root using sequences known to be evolutionarily distant; and phylodynamic analysis, integrating temporal and phylogenetic patterns in virus evolution (Appendix 1). Both approaches consistently identified the same root for each subgroup cluster (Appendix 1 Figure 3). Phylodynamic analysis also identified 58 outlier sequences for HRSV-A and 2 for HRSV-B that were excluded from lineage designation. The final dataset considered for lineage designation comprised 1,480 HRSV-A and 1,385 HRSV-B genomes (Appendix 2 Table, https://wwwnc.cdc.gov/EID/article/30/8/24-0209-App2.xlsx).

HRSV Lineage Definition

We defined HRSV lineage as a statistically supported monophyletic cluster comprising ≥10 sequences and characterized by ≥5 aa substitutions, compared to the parental lineage. The lineage-defining amino acids, present in ≥90% of the sequences within the clade, may be found in any of the viral proteins.

Phylogenetic classifications vary among viral species aiming to define clusters reflecting the heterogeneity of the viral population, considering each virus unique evolutionary characteristics and using arbitrary thresholds for long-term applicability (*27*–*29*). Inherent bias exists in any classification system because of availability and spatiotemporal representation sequences. Therefore, our HRSV lineage definition did not include criteria of sequences from different outbreaks or countries to enable early detection of novel lineages. However, we propose establishing a threshold of ≥10

genomes for defining a lineage to monitor HRSV strains circulating within communities.

We observed the presence of distinctive signature amino acids shared by sequences of a phylogenetic clade in comparison to the parental lineage is a simple method to identify a new lineage. Methods (i.e., average nucleotide genetic distances, average patristic distances, or patristic distances between nodes) need phylogenies with complete datasets to define new categories, becoming complex with rapid increases of available sequences (*16*–*19*). In our proposal, we initially screened different amino acid thresholds in an automated manner, ranging from 1–10 lineage-defining amino acids (Appendix 1). The number of small lineages decreased as the number of lineage-defining amino acids increased, and 5 amino acids resulted in an intermediate complexity of lineages defined for both HRSV subgroups. Furthermore, we proposed that the lineage-defining amino acids should be conserved in ≥90% of the genomes within a clade, considering the potential reversion in some of the genomes within highly mutated hotspot sites. We acknowledged that other numbers of genomes or amino acids thresholds could be useful, but we emphasized that the key to establishing a global consensus is clear operational guidelines and a robust classification, 2 aspects that our proposal fulfills.

HRSV Lineage Nomenclature

We defined the lineage nomenclature integrating the HRSV subgroup letter and ascending ordinal numbers, separated by dots to represent nested lineages (Figure 3, panels A, B; Figure 4, panels A, B). Furthermore, we assigned a distinct nomenclature to the 72-nt (24-aa) G-gene duplication within HRSV-A and 60-nt (20-aa) G-gene duplication within HRSV-B. Those genetic events are epidemiologically relevant, because only viruses with G-gene duplication have been detected since 2017 (*30*–*33*). To track those viruses, we used the alias D, specifically A.D (historically, ON1 genotype) for HRSV-A and B.D (historically, BA genotype), for HRSV-B and nested lineages with increasing ordinal numbers. In summary, letters A and B indicate the HRSV subgroup at the beginning of the lineage name, C is unused, and D serves as an alias for 72-nt and 60-nt duplication within the G gene. In addition, aliases starting from E are limited to 3 numerical levels of nested lineages, preventing indefinite accumulation of numbers. For example, B.D.4.1.1 lineage has descendant lineages named B.D.E.1–B.D.E.4 instead of B.D.4.1.1.1–B.D.4.1.1.4, where E represents 4.1.1 (Figure 4, panels A, B). The nomenclature is based on the tree topology, reflecting the order of the nodes from the root to the tips, but it is unrelated to the sequence collection date or date of the most recent common ancestor of the lineage.

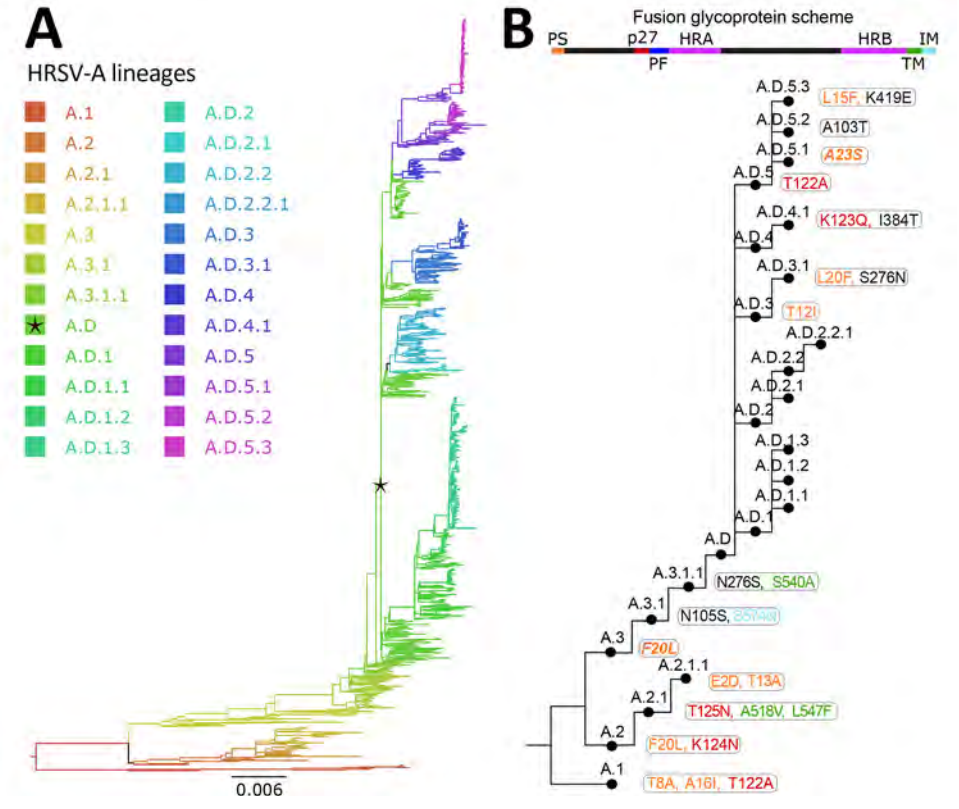

Figure 3. Human respiratory syncytial virus A lineage classification. A) HRSV-A maximum-likelihood phylogenetic tree (1,480 sequences), colored by lineage classification. Black star indicates A.D lineage, defined by the 72-nt duplication in the G gene. Scale bar indicates substitutions per site. B) Simplified scheme of the lineage designation to highlight the presence of nested lineages. The amino acid changes in the F glycoprotein are listed next to lineage name and colored according to their location in the fusion protein.

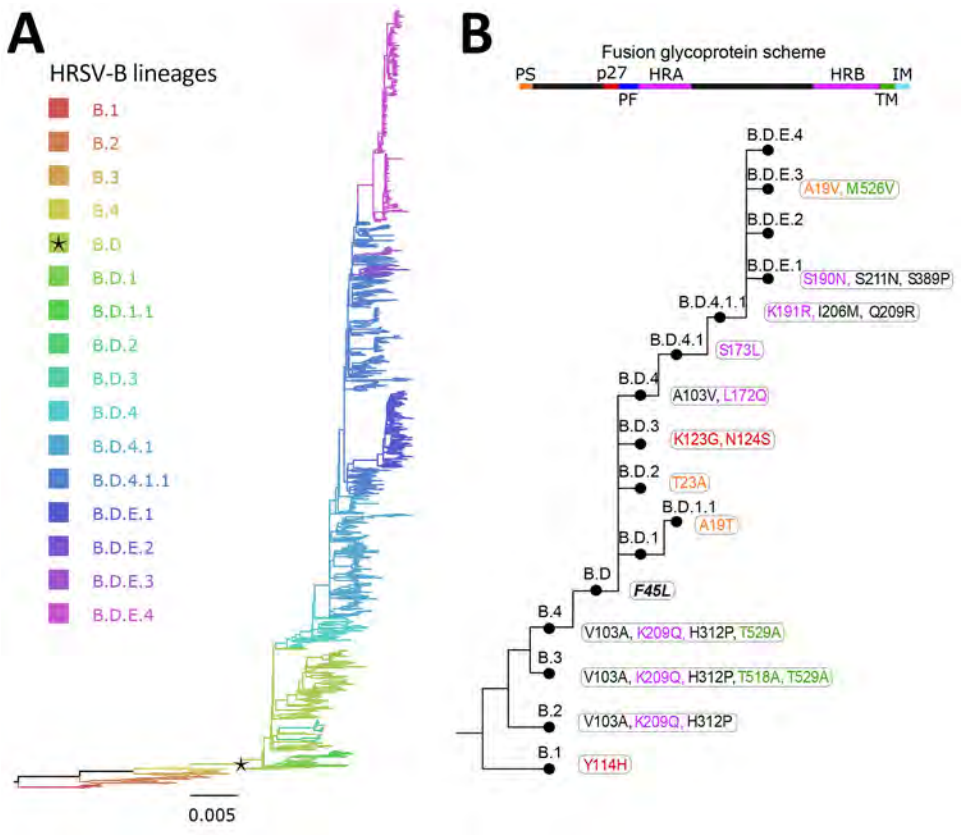

Figure 4. Human respiratory syncytial virus B lineages classification. A) HRSV-B maximum-likelihood phylogenetic tree (1,385 sequences), colored according to lineage classification. Black star indicates B.D lineage, defined by the 60-nt duplication in the G gene. Scale bar indicates substitutions per site. B) Simplified scheme of the lineage designation to highlight the presence of nested lineages. The amino acid changes in the F glycoprotein are listed next to lineage name and colored according to their location in the fusion protein.

To remain functional, a nomenclature system requires periodic updates as new lineages emerge. Therefore, we have established 2 open repositories on GitHub containing definitions of each lineage, signature mutations, and representative sequences. The repositories are available at https://github.com/rsv-lineages/lineage-designation-A and https://github.com/rsv-lineages/lineage-designation-B; they are intended to provide up-to-date definitions and serve as a platform for discussion and designation of novel lineages.

Lineages within the HRSV-A and HRSV-B Rooted Trees

We reconstructed ancestral sequences at the root of the phylogenetic trees. Although the sequences are not biologically real, they served as surrogate parental lineages during initial classification. Identifying monophyletic clusters with ≥10 sequences and ≥5 aa changes compared with the reconstructed root sequence, we defined 3 HRSV-A lineages (A.1–A.3) and 4 HRSV-B lineages (B.1–B.4). We were unable to classify 2 sequences, EPI-ISL-15771600_USA_1956 (GISAID) and MG642074_USA_1980 (GenBank), perhaps because they belong to underrepresented extinct lineages.

We further analyzed the first lineages in an iterative manner to identify nested lineages; as a result, we identified a total of 24 lineages within HRSV-A, and 16 within HRSV-B (Figures 3, 4). Close to the root of the HRSV-B tree, extinct lineages were underrepresented, comprising <10 sequences but featuring >5 distinct amino acids (B.1, B.3, B.4). Despite the low number of sequences, we included them as lineages to trace evolutionary branches that gave rise to currently circulating lineages. In addition, A.D.2 is slightly below the sequence threshold; nonetheless, we kept the lineage category to emphasize the common ancestor among A.D.2.1 and A.D.2.2.

We scrutinized the presence and absence of the duplication in the G gene across each tree. Although patterns were mostly as expected with a single historical duplication event, some genomes within the clade with the duplication in G lacked the duplication. The dispersed association of these sequences in the phylogenetic tree, rather than the monophyletic cluster we expected, suggests the virus did not lose the nucleotide duplication (Appendix 1 Figure 4). Instead, similar read length to the duplication region of certain short-read next-generation sequencing technologies potentially masked the presence of the duplication when used in the consensus genome assembly with reference sequences that do not possess the nucleotide duplication. Therefore, we recommend

using such data with quality filtered reads of a length >150 nt to avoid this problem.

Lineage-defining amino acids were present in all HRSV proteins, primarily identified within the G protein (Tables 1, 2). Also, the lineage-defining amino acids at polymerase L protein were noteworthy, contributing to the distinction of 21 of 24 HRSV-A lineages and 15 of 16 HRSV-B lineages (Tables 1, 2). Of interest, the F protein contributed to define 14 lineages in HRSV-A and 13 in HRSV-B (Figure 3, panel B; Figure 4, panel B). The G and F surface glycoproteins are likely under selection pressure from antibody-mediated immunity and exhibit a robust phylogenetic signal (*18*,*31*). Whereas the G protein displays substantial nucleotide and amino acid sequence plasticity, the F protein experiences strong negative selection, likely attributed to functional or structural constraints (*34*). For instance, the fusion peptide is the only region in F without lineage-defining amino acids (Figure 3, panel B; Figure 4, panel B). Although the low diversity of the F protein is promising for HRSV interventions, monitoring the F protein during global implementation is essential to estimate the antigenic impact of amino acid substitutions.

Using G and F Sequences with the HRSV Lineage Classification System

The main challenge for global expansion of HRSV genomics is the absence of a cost-effective, globally standardized and validated methodology for sequencing, in contrast to SARS-CoV-2 or influenza virus (*35*,*36*). In addition, limited funding and infrastructure cause some laboratories to prefer sequencing the G gene only (*37*–*39*). Although we highly recommend using complete genomes for HRSV lineage assignment to ensure the maximum accuracy of the classification and monitor the amino acid changes in all viral proteins, partial genomes covering the G and F genes can be used because overall they reproduce the topology of the HRSV tree (*17*,*18*). We do not recommend the use of smaller G gene regions such as the second hypervariable region (250-nt length at the 3′ gene end) (Figure 1) that was used historically for molecular epidemiology because previous reports showed a decreased phylogenetic signal (*17*). The use of G, F, or both genes for lineage classification should rely on phylogenetic associations with reference sequences. Of note, using only G and F genes is inadequate for defining novel lineages because of the inability to detect lineage-defining amino acids across all viral proteins. Our analysis showed minimal misclassification (1.2%) in HRSV-A and none in HRSV-B when using only the G gene (Appendix 1 Figure 5). However, the G ectodomain alone resulted in an 18.86% misclassification rate for HRSV-A and none for HRSV-B. The F gene alone had misclassification rates of 38.18% for HRSV-A and 1.23% for HRSV-B because of polytomies affecting lineage assignments within A.D.1 and A.D.5. Combining G and F gene fragments reduced misclassification to 0.07% for HRSV-A and none for HRSV-B, indicating that this approach provides optimal resolution for both subgroups (Appendix 1 Figure 5).

Prospective HRSV Lineage Assignment and Definition

Assigning sequences to the existing lineages can be automated using online tools such as NextClade (https://clades.nextstrain.org) (*40*), ReSVidex (https://cacciabue.shinyapps.io/resvidex_wg), INSaFLU (https://insaflu.insa.pt) (*41*), or UShER (https://usher.bio) (*42*). However, to define a novel lineage, we encourage users to follow our guidelines (Appendix 1), available on GitHub (https://github.com/orgs/rsv-lineages/repositories). We anticipate new lineages of HRSV-A/B will continue to emerge, and we envision updating our proposed nomenclature to incorporate new lineages. We encourage reporting of new HRSV lineages at the RGCC GitHub page as an issue within the corresponding repository for HRSV-A/B. The RGCC study group will evaluate the newly proposed lineage and update reference alignments if confirmed.

Importantly, assigning the lineage of a query sequence does not require the use of complete genomes or the absence of nucleotide ambiguities; rather, it requires a supported association within a phylogenetic clade. However, defining a new lineage requires the use of complete genomes without ambiguities, because amino acid characterization of all viral proteins is essential.

Molecular Epidemiology of HRSV with Proposed Classification

We described the HRSV molecular epidemiology including all available genomes, even those previously discarded during the dataset curation. We analyzed the seasonality of lineages using a dataset comprising 2,277 HRSV-A and 2,058 HRSV-B genomes, revealing notable co-circulation and lineage replacement over time (Figure 5). In HRSV-A, A.1 and A.2 lineages are extinct: the last detected sequences of A.1 were collected in 1995 and of A.2 in 2015. Since 2011, A.D and nested lineages continue to circulate; A.D.2.2 and A.D.4 were detected in 2013, indicating rapid divergence of the HRSV-A viruses with the 72-nt duplication in G gene. In HRSV-B, lineages B.1, B.2, B.3, and B.4 exhibited

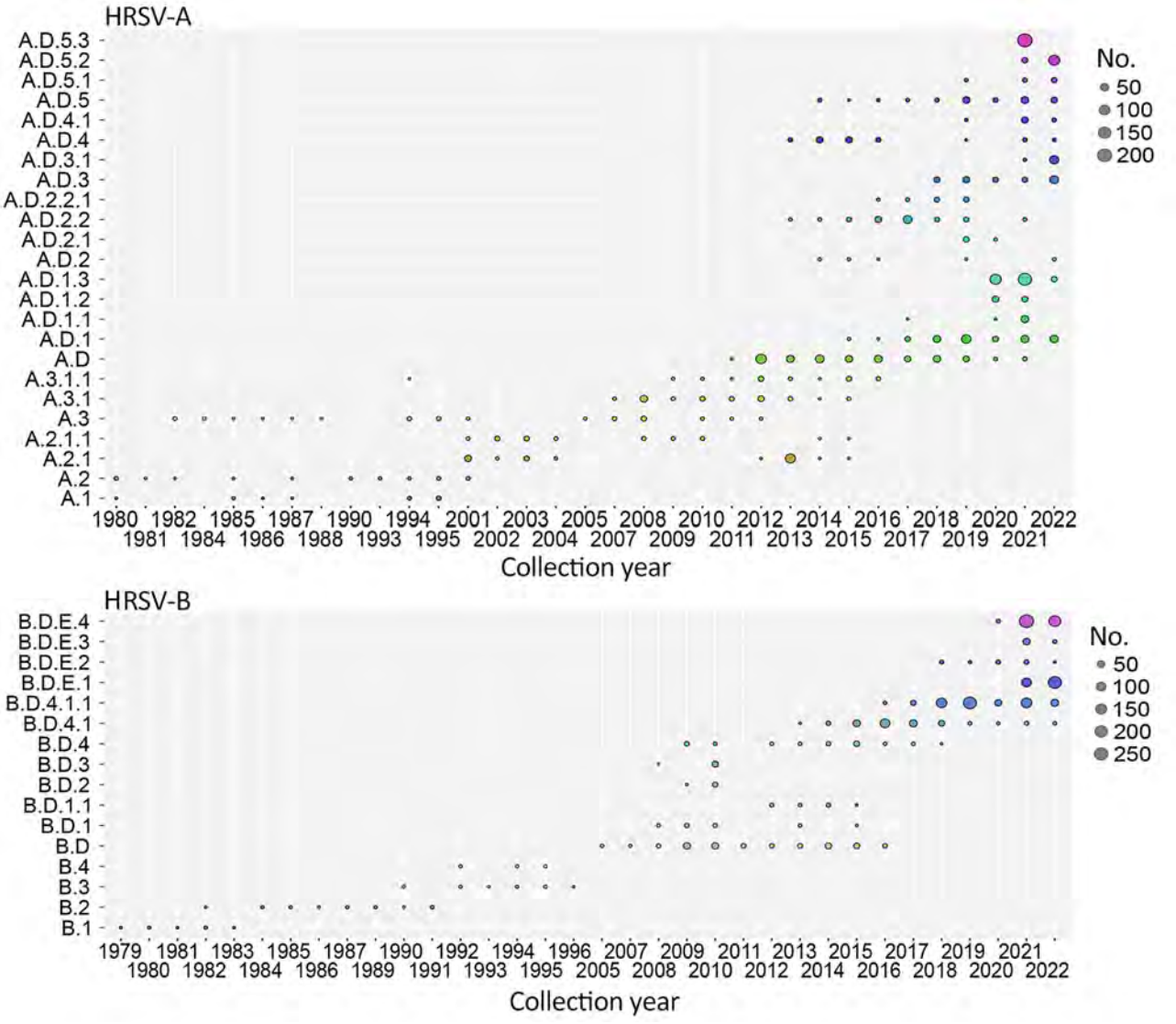

Figure 5. Temporal distribution of HRSV-A and HRSV-B lineages. A total of 2,744 HRSV-A genomes and 2,443 HRSV-B genomes available in public databases through March 2023 were included. HRSV, human respiratory syncytial virus.

strong lineage replacement (Figure 5). Although the B.D lineage with a 60-nt duplication in the G gene (B.D lineage) was detected in 1999, complete genomes became available in 2005 (*8*). By 2009, only B.D and nested lineages were detected, and since 2017, only B.D.4 and nested lineages have been observed.

HRSV lineages may have been underrepresented before the COVID-19 pandemic because of limited genomic surveillance. However, our classification system allows for updates if prepandemic genomes meeting lineage criteria are shared. Some lineages, such as A.D.3.1, A.D.5.2, and A.D.5.3 in HRSV-A and B.D.E.1 and B.D.E.3 in HRSV-B, appear to be exclusive to the postpandemic period, although most of their lineage-defining amino acid were present in parental prepandemic strains. For instance, A.D.5.2 was recognized as a distinct lineage with the emergence of the C26Y substitution in M2–2, whereas other signature amino acids were present in a 2019 parental lineage genome (GenBank accession no. MZ515825). Detection of postpandemic lineages does not contradict studies reporting no new post-pandemic genotypes because those studies relied on earlier classification systems (*43*–*46*). The possibility that these new lineages circulated before the pandemic depends on the deposition of genomes.

Some of the lineages were detected in specific countries (Appendix 1 Figure 6). For example, A.D.1 descendant lineages, A.D.5.3 and most of B.D.E.4 cases were identified in Australia or New Zealand.

Contemporary lineages such as B.D.4.1.1 and descendants B.D.E.1 and B.D.E.3, predominantly consisted of sequences from the United Kingdom. Global genomic surveillance bias presents a major confounding factor in lineage geodetection; for instance, most of the earliest lineages were detected in the United States, the principal contributor of HRSV genomes until 2007 (Appendix 1 Figures 2, 6).

Discussion

Consensus classification of HRSV below the subgroup level has been a challenge for multiple decades. Collaboratively, the HRSV molecular evolution research community, along with experts in the evolution of other respiratory viruses, have worked toward establishing a unified global classification system in the initiative HRSV Genotyping Consensus Consortium (RGCC). Our proposal categorizes HRSV-A/B sequences into lineages based on phylogenetic associations and amino acid markers, relying on complete genomes. Partial or low-quality genomes can be assigned to the existing lineages, emphasizing the robustness of this system. We developed standard guidelines for lineage definition and assignment and created online resources for updates, ensuring long-term utility. Defining a viral category below species through a phylogenetic-based classification is challenging; the system must exhibit reproducibility, balance complexity, and be updatable to capture the level of heterogeneity useful for viral surveillance. Our proposal addresses those requirements comprehensively.

HRSV is not an emerging virus; it generates annual outbreaks with co-circulation and replacement in the prevalence of its antigenic subgroups. Although some HRSV genomes were collected from clinical samples >50 years ago, the largest increase in the number of genomes has occurred since 2021. A limitation of our definition is the uncertainty of the antigenic effect of individual amino acid substitutions on lineages. Hence, whole-genome surveillance together with the study of lineage-phenotype association are essential, as observed in genetic and antigenic characterization in influenza to estimate the effectiveness of immunization (*47*). In 2023, recombinant F protein vaccines were approved; as their implementation progresses, we will learn how the vaccines affect viral evolution. We expect our unification proposal for the phylogenetic classification of HRSV to support spatiotemporal comparative lineage surveillance and detection of emerging lineages. In addition, we anticipate studies of association between lineages and the severity of HRSV disease, as well as associations of particular lineages with patients' demographic characteristics.

This article was preprinted at https://www.medrxiv.org/content/10.1101/2024.02.13.24302237v1.

Acknowledgments

We acknowledge the authors who have shared HRSV genomes on the public databases National Center for Biotechnology Information Virus, GenBank, European Nucleotide Archive, DDBJ, and GISAID EpiRSV. We thank the researchers and public health scientists who provided valuable comments during the initial stages of the RSV Genotyping Consensus Consortium's work.

Authors from second to last are listed alphabetically.

R.A.N. consults for Moderna on matter in virus evolution. N.W. has received grant funding from the Bill and Melinda Gates Foundation and Sanofi. The authors received no financial support for the research, authorship, or publication of this article.

About the Author

Dr. Goya is a postdoctoral researcher in the Department Laboratory of Medicine and Pathology at the University of Washington. Her work focuses on respiratory virus evolution and interactions with the immune system.

References

1. European Medicine Agency. Arexvy. 2023 [cited 2024 Jun 28]. https://www.ema.europa.eu/en/medicines/human/EPAR/arexvy
2. US Food and Drug Administration. Abrysvo. 2023 [cited 2024 Jun 28]. https://www.fda.gov/vaccines-blood-biologics/abrysvo
3. US Food and Drug Administration. Nirsevimab. 2023 [cited 2023 Nov 12]. https://www.fda.gov/news-events/press-announcements/fda-approves-new-drug-prevent-rsv-babies-and-toddlers
4. Salimi V, Viegas M, Trento A, Agoti CN, Anderson LJ, Avadhanula V, et al. Proposal for human respiratory syncytial virus nomenclature below the species level. Emerg Infect Dis. 2021;27:1–9. https://doi.org/10.3201/eid2706.204608
5. Anderson LJ, Hierholzer JC, Tsou C, Hendry RM, Fernie BF, Stone Y, et al. Antigenic characterization of respiratory syncytial virus strains with monoclonal antibodies. J Infect Dis. 1985;151:626–33. https://doi.org/10.1093/infdis/151.4.626
6. Tian D, Battles MB, Moin SM, Chen M, Modjarrad K, Kumar A, et al. Structural basis of respiratory syncytial virus subtype-dependent neutralization by an antibody targeting the fusion glycoprotein. Nat Commun. 2017;8:1877. https://doi.org/10.1038/s41467-017-01858-w
7. Peret TCT, Hall CB, Schnabel KC, Golub JA, Anderson LJ. Circulation patterns of genetically distinct group A and B strains of human respiratory syncytial virus in a community. J Gen Virol. 1998;79:2221–9. https://doi.org/10.1099/0022-1317-79-9-2221
8. Trento A, Galiano M, Videla C, Carballal G, García-Barreno B, Melero JA, et al. Major changes in the

G protein of human respiratory syncytial virus isolates introduced by a duplication of 60 nucleotides. J Gen Virol. 2003;84:3115–20. https://doi.org/10.1099/vir.0.19357-0
9. Eshaghi A, Duvvuri VR, Lai R, Nadarajah JT, Li A, Patel SN, et al. Genetic variability of human respiratory syncytial virus A strains circulating in Ontario: a novel genotype with a 72 nucleotide G gene duplication. PLoS One. 2012;7:e32807. https://doi.org/10.1371/journal.pone.0032807
10. Venter M, Madhi SA, Tiemessen CT, Schoub BD. Genetic diversity and molecular epidemiology of respiratory syncytial virus over four consecutive seasons in South Africa: identification of new subgroup A and B genotypes. J Gen Virol. 2001;82:2117–24. https://doi.org/10.1099/0022-1317-82-9-2117
11. Cui G, Zhu R, Qian Y, Deng J, Zhao L, Sun Y, et al. Genetic variation in attachment glycoprotein genes of human respiratory syncytial virus subgroups a and B in children in recent five consecutive years. PLoS One. 2013;8:e75020. https://doi.org/10.1371/journal.pone.0075020
12. Hirano E, Kobayashi M, Tsukagoshi H, Yoshida LM, Kuroda M, Noda M, et al. Molecular evolution of human respiratory syncytial virus attachment glycoprotein (G) gene of new genotype ON1 and ancestor NA1. Infect Genet Evol. 2014;28:183–91. https://doi.org/10.1016/j.meegid.2014.09.030
13. Blanc A, Delfraro A, Frabasile S, Arbiza J. Genotypes of respiratory syncytial virus group B identified in Uruguay. Arch Virol. 2005;150:603–9. https://doi.org/10.1007/s00705-004-0412-x
14. Dapat IC, Shobugawa Y, Sano Y, Saito R, Sasaki A, Suzuki Y, et al. New genotypes within respiratory syncytial virus group B genotype BA in Niigata, Japan. J Clin Microbiol. 2010;48:3423–7. https://doi.org/10.1128/JCM.00646-10
15. Shobugawa Y, Saito R, Sano Y, Zaraket H, Suzuki Y, Kumaki A, et al. Emerging genotypes of human respiratory syncytial virus subgroup A among patients in Japan. J Clin Microbiol. 2009;47:2475–82. https://doi.org/10.1128/JCM.00115-09
16. Muñoz-Escalante JC, Comas-García A, Bernal-Silva S, Robles-Espinoza CD, Gómez-Leal G, Noyola DE. Respiratory syncytial virus A genotype classification based on systematic intergenotypic and intragenotypic sequence analysis. Sci Rep. 2019;9:20097. https://doi.org/10.1038/s41598-019-56552-2
17. Goya S, Galiano M, Nauwelaers I, Trento A, Openshaw PJ, Mistchenko AS, et al. Toward unified molecular surveillance of RSV: a proposal for genotype definition. Influenza Other Respir Viruses. 2020;14:274–85. https://doi.org/10.1111/irv.12715
18. Ramaekers K, Rector A, Cuypers L, Lemey P, Keyaerts E, Van Ranst M. Towards a unified classification for human respiratory syncytial virus genotypes. Virus Evol. 2020;6:veaa052. https://doi.org/10.1093/ve/veaa052 https://doi.org/10.1093/ve/veaa052
19. Chen J, Qiu X, Avadhanula V, Shepard SS, Kim DK, Hixson J, et al. Novel and extendable genotyping system for human respiratory syncytial virus based on whole-genome sequence analysis. Influenza Other Respir Viruses. 2022;16:492–500. https://doi.org/10.1111/irv.12936
20. Katoh K, Misawa K, Kuma K, Miyata T. MAFFT: a novel method for rapid multiple sequence alignment based on fast Fourier transform. Nucleic Acids Res. 2002;30:3059–66. https://doi.org/10.1093/nar/gkf436
21. Larsson A. AliView: a fast and lightweight alignment viewer and editor for large datasets. Bioinformatics. 2014;30:3276–8. https://doi.org/10.1093/bioinformatics/btu531
22. Minh BQ, Schmidt HA, Chernomor O, Schrempf D, Woodhams MD, von Haeseler A, et al. IQ-TREE 2: new models and efficient methods for phylogenetic inference in the genomic era. Mol Biol Evol. 2020;37:1530–4. https://doi.org/10.1093/molbev/msaa015
23. Hoang DT, Chernomor O, von Haeseler A, Minh BQ, Vinh LS. UFBoot2: improving the ultrafast bootstrap approximation. Mol Biol Evol. 2018;35:518–22. https://doi.org/10.1093/molbev/msx281
24. Sagulenko P, Puller V, Neher RA. TreeTime: maximum-likelihood phylodynamic analysis. Virus Evol. 2018;4:vex042. https://doi.org/10.1093/ve/vex042
25. Huddleston J, Hadfield J, Sibley TR, Lee J, Fay K, Ilcisin M, et al. Augur: a bioinformatics toolkit for phylogenetic analyses of human pathogens. J Open Source Softw. 2021;6:2906. https://doi.org/10.21105/joss.02906
26. McBroome J, de Bernardi Schneider A, Roemer C, Wolfinger MT, Hinrichs AS, O'Toole AN, et al. A framework for automated scalable designation of viral pathogen lineages from genomic data. Nat Microbiol. 2024;9,550–60. https://doi.org/10.1038/s41564-023-01587-5
27. O'Toole Á, Scher E, Underwood A, Jackson B, Hill V, McCrone JT, et al. Assignment of epidemiological lineages in an emerging pandemic using the pangolin tool. Virus Evol. 2021;7:veab064.
28. World Health Organization/World Organisation for Animal Health/Food and Agriculture Organization (WHO/OIE/FAO) H5N1 Evolution Working Group. Revised and updated nomenclature for highly pathogenic avian influenza A (H5N1) viruses. Influenza Other Respir Viruses. 2014;8:384–8. https://doi.org/10.1111/irv.12230
29. Hassan AS, Pybus OG, Sanders EJ, Albert J, Esbjörnsson J. Defining HIV-1 transmission clusters based on sequence data. AIDS. 2017;31:1211–22. https://doi.org/10.1097/QAD.0000000000001470
30. Streng A, Goettler D, Haerlein M, Lehmann L, Ulrich K, Prifert C, et al. Spread and clinical severity of respiratory syncytial virus A genotype ON1 in Germany, 2011–2017. BMC Infect Dis. 2019;19:613. https://doi.org/10.1186/s12879-019-4266-y
31. Goya S, Lucion MF, Shilts MH, Juárez MDV, Gentile A, Mistchenko AS, et al. Evolutionary dynamics of respiratory syncytial virus in Buenos Aires: viral diversity, migration, and subgroup replacement. Virus Evol. 2023;9:vead006.
32. Liang X, Liu DH, Chen D, Guo L, Yang H, Shi YS, et al. Gradual replacement of all previously circulating respiratory syncytial virus A strain with the novel ON1 genotype in Lanzhou from 2010 to 2017. Medicine (Baltimore). 2019;98:e15542. https://doi.org/10.1097/MD.0000000000015542
33. van Niekerk S, Venter M. Replacement of previously circulating respiratory syncytial virus subtype B strains with the BA genotype in South Africa. J Virol. 2011;85:8789–97. https://doi.org/10.1128/JVI.02623-10
34. Hause AM, Henke DM, Avadhanula V, Shaw CA, Tapia LI, Piedra PA. Sequence variability of the respiratory syncytial virus (RSV) fusion gene among contemporary and historical genotypes of RSV/A and RSV/B. PLoS One. 2017; 12:e0175792. https://doi.org/10.1371/journal.pone.0175792
35. Quick J. nCoV-2019 sequencing protocol v1. 2020 Jan [cited 2023 Nov 12]. https://www.protocols.click/view/ncov-2019-sequencing-protocol-bbmuik6w
36. Zhou B, Wentworth DE. Influenza A virus molecular virology techniques. In: Kawaoka Y, Neumann G, editors. Influenza virus: methods and protocols. Totowa, NJ:

Humana Press; 2012. p. 175–92 [cited 2023 Nov 12]. https://doi.org/10.1007/978-1-61779-621-0_11
37. Dong X, Deng YM, Aziz A, Whitney P, Clark J, Harris P, et al. A simplified, amplicon-based method for whole genome sequencing of human respiratory syncytial viruses. J Clin Virol. 2023;161:105423. https://doi.org/10.1016/j.jcv.2023.105423
38. Wang L, Ng TFF, Castro CJ, Marine RL, Magaña LC, Esona M, et al. Next-generation sequencing of human respiratory syncytial virus subgroups A and B genomes. J Virol Methods. 2022;299:114335. https://doi.org/10.1016/j.jviromet.2021.114335
39. Presser LD, van den Akker WMR, Meijer A, for PROMISE investigators. Respiratory Syncytial Virus European Laboratory Network 2022 survey: need for harmonization and enhanced molecular surveillance. J Infect Dis. 2023 Aug 14;jiad341.
40. Aksamentov I, Roemer C, Hodcroft EB, Neher RA. Nextclade: clade assignment, mutation calling and quality control for viral genomes. J Open Source Softw. 2021;6:3773. https://doi.org/10.21105/joss.03773
41. Borges V, Pinheiro M, Pechirra P, Guiomar R, Gomes JP. INSaFLU: an automated open web-based bioinformatics suite "from-reads" for influenza whole-genome-sequencing-based surveillance. Genome Med. 2018;10:46. https://doi.org/10.1186/s13073-018-0555-0
42. Turakhia Y, Thornlow B, Hinrichs AS, De Maio N, Gozashti L, Lanfear R, et al. Ultrafast Sample placement on Existing tRees (USHER) enables real-time phylogenetics for the SARS-CoV-2 pandemic. Nat Genet. 2021;53:809–16. https://doi.org/10.1038/s41588-021-00862-7
43. Redlberger-Fritz M, Springer DN, Aberle SW, Camp JV, Aberle JH. Respiratory syncytial virus surge in 2022 caused by lineages already present before the COVID-19 pandemic. J Med Virol. 2023;95:e28830. https://doi.org/10.1002/jmv.28830
44. Goya S, Sereewit J, Pfalmer D, Nguyen TV, Bakhash SAKM, Sobolik EB, et al. Genomic characterization of respiratory syncytial virus during 2022–23 outbreak, Washington, USA. Emerg Infect Dis. 2023;29:865–8. https://doi.org/10.3201/eid2904.221834
45. Adams G, Moreno GK, Petros BA, Uddin R, Levine Z, Kotzen B, et al. Viral lineages in the 2022 RSV surge in the United States. N Engl J Med. 2023;388:1335–7. https://doi.org/10.1056/NEJMc2216153
46. Dolores A, Stephanie G, Mercedes S NJ, Érica G, Mistchenko AS, Mariana V. RSV reemergence in Argentina since the SARS-CoV-2 pandemic. J Clin Virol. 2022;149:105126. https://doi.org/10.1016/j.jcv.2022.105126
47. van Roekel C, Poukka E, Turunen T, Nohynek H, Presser L, Meijer A, et al. Effectiveness of immunisation products against medically attended respiratory syncytial virus infection: generic protocol for a test-negative case-control study. J Infect Dis. 2023;229(Supplement_1):S92–9. https://doi.org/10.1093/infdis/jiad483 https://doi.org/10.1093/infdis/jiad483

Address for correspondence: Stephanie Goya, Department of Laboratory Medicine and Pathology, University of Washington Medical Center, 850 Republican St, Seattle, WA 98109, USA; email: sgoya@uw.edu

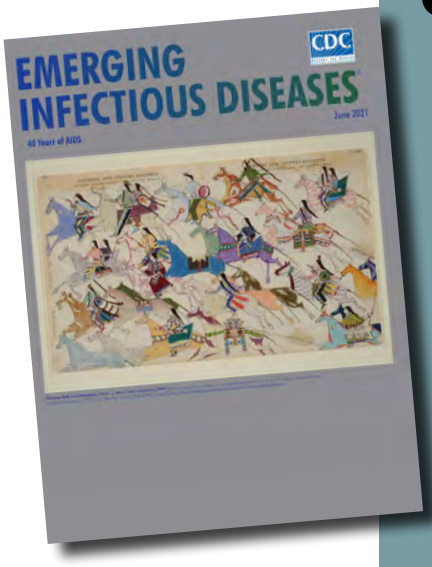

Originally published in June 2021

etymologia revisited

Enterocytozoon bieneusi

[ˈentərəˌsaitəˈʒu:ən bɪəˈnəʊsɪ]

From the Greek *en'tĕr-ō-sī'tōn* (intestine), *kútos* (vessel, cell), and *zō'on* (animal), and the surname Bieneus, in memory of the first infected patient whose case was reported in Haiti during 1985. *Enterocytozoon bieneusi*, a member of the wide-ranging phylum Microsporidia, is the only species of this genus known to infect humans. Microsporidia are unicellular intracellular parasites closely related to fungi, although the nature of the relationship is not clear.

E. bieneusi, a spore-forming, obligate intracellular eukaryote, was discovered during the HIV/AIDS pandemic and is the main species responsible for intestinal microsporidiosis, a lethal disease before widespread use of antiretroviral therapies. More than 500 genotypes are described, which are divided into different host-specific or zoonotic groups. This pathogen is an emerging issue in solid organ transplantation, especially in renal transplant recipients.

Sources

1. Desportes I, Le Charpentier Y, Galian A, Bernard F, Cochand-Priollet B, Lavergne A, et al. Occurrence of a new microsporidan: *Enterocytozoon bieneusi* n.g., n. sp., in the enterocytes of a human patient with AIDS. J Protozool. 1985;32:250–4. https://doi.org/10.1111/j.1550-7408.1985.tb03046.x
2. Didier ES, Weiss LM. Microsporidiosis: not just in AIDS patients. Curr Opin Infect Dis. 2011;24:490–5. https://doi.org/10.1097/QCO.0b013e32834aa152
3. Han B, Weiss LM. Microsporidia: obligate intracellular pathogens within the fungal kingdom. Microbiol Spectr. 2017;5:97–113. https://doi.org/10.1128/microbiolspec.FUNK-0018-2016
4. Moniot M, Nourrisson C, Faure C, Delbac F, Favennec L, Dalle F, et al. Assessment of a multiplex PCR for the simultaneous diagnosis of intestinal cryptosporidiosis and microsporidiosis: epidemiologic report from a French prospective study. J Mol Diagn. 2021;23:417–23. https://doi.org/10.1016/j.jmoldx.2020.12.005

https//wwwnc.cdc.gov/eid/article/27/6/et2706_article

Geographic Distribution of Rabies Virus and Genomic Sequence Alignment of Wild and Vaccine Strains, Kenya

Evalyne N. Wambugu, Gathii Kimita, Sarah N. Kituyi, Michael A. Washington, Clement Masakhwe, Lucy M. Mutunga, Gurdeep Jaswant, S.M. Thumbi, Brian C. Schaefer, John N. Waitumbi

Rabies, a viral disease that causes lethal encephalitis, kills ≈59,000 persons worldwide annually, despite availability of effective countermeasures. Rabies is endemic in Kenya and is mainly transmitted to humans through bites from rabid domestic dogs. We analyzed 164 brain stems collected from rabid animals in western and eastern Kenya and evaluated the phylogenetic relationships of rabies virus (RABV) from the 2 regions. We also analyzed RABV genomes for potential amino acid changes in the vaccine antigenic sites of nucleoprotein and glycoprotein compared with RABV vaccine strains commonly used in Kenya. We found that RABV genomes from eastern Kenya overwhelmingly clustered with the Africa-1b subclade and RABV from western Kenya clustered with Africa-1a. We noted minimal amino acid variances between the wild and vaccine virus strains. These data confirm minimal viral migration between the 2 regions and that rabies endemicity is the result of limited vaccine coverage rather than limited efficacy.

Rabies, a viral disease that causes encephalitis, is consistently deadly in exposed humans who are not vaccinated or promptly treated with postexposure prophylaxis (PEP). Rabies was recognized in Egypt around 2300 BCE (*1*), and a written account of the disease was included in the Laws of Eshnunna in Mesopotamia (2). From that region, rabies spread to Europe and then to Africa, following patterns of human colonization (*3*). In 1768, rabies was described in the Americas, occurring as an epizootic in Boston (E.C. Ramsey, honors thesis, Macalester College, 2017, https://digitalcommons.macalester.edu/cgi/viewcontent.cgi).

Rabies virus (RABV) is transmitted through the bite of an infected animal, which inoculates the virus at the bite site. The virus travels from the inoculation site to the central nervous system (CNS), where it multiplies and migrates to the salivary glands, after which another animal or human can be inoculated through a bite. RABV modifies the behavior of its host, which becomes exceptionally aggressive, thus increasing the odds of conflict and biting (*4*). Once clinical signs appear in an infected host, fatality is nearly always certain (*5*). The primary mechanism of lethality involves direct targeting of the CNS via mechanisms that remain poorly defined (*6*).

RABV belongs to the genus *Lyssavirus*, which also includes Lagos bat virus, Mokola virus, Duvenhage virus, European bat virus 1 and 2, and Australian bat lyssavirus, among others (*7*). The primary viral reservoirs are members of the orders Carnivora (e.g., dogs) and Chiroptera (bats), whereas humans are dead-end hosts (*8*). Compared with other lyssaviruses, RABV is by far the most commonly reported (*9*), causing ≈59,000 human deaths annually (*10*), >99% of which are associated with dog-mediated transmissions (*9*). In rare human cases, rabies has been transmitted through non–bite-associated processes, such as organ transplants and laboratory exposures (*11*,*12*).

Rabies has 2 major epidemiologic cycles: the urban cycle, in which dogs are the major reservoirs, and the sylvatic cycle, in which wild animals are the

Author affiliations: Walter Reed Army Institute of Research–Africa, Kenya Medical Research Institute, Kisumu, Kenya (E.N. Wambugu, G. Kimita, C. Masakhwe, J.N. Waitumbi); University of Embu, Embu, Kenya (E.N. Wambugu, S.N. Kituyi); Dwight D. Eisenhower Army Medical Center, Augusta, Georgia, USA (M.A. Washington); National Institutes of Health, Bethesda, Maryland, USA (M.A. Washington); University of Nairobi, Nairobi, Kenya (L.M. Mutunga, G. Jaswant, S.M. Thumbi); Washington State University, Pullman, Washington, USA (S.M. Thumbi); Uniformed Services University, Bethesda (B.C. Schaefer)

DOI: https://doi.org/10.3201/eid3008.230876

primary reservoirs (*13*). The urban cycle predominates in Africa, Asia, and Central and South America (*13*). The United States and some countries in Europe have used oral rabies vaccine programs to substantially reduce the sylvatic cycle (*14*). Nonetheless, rabies remains a global public health and veterinary challenge, particularly in developing countries (*15*).

RABV can be categorized into 2 major phylogenetic groups: bat-related and dog-related. Bat-related RABV is confined to the New World, but dog-related RABV is globally distributed (*16*–*18*). The dog-related group segregates into 6 distinct clades, which are designated as Africa-2, Asian, Africa-3, Arctic-related, Cosmopolitan, and Indian subcontinent (*19*). Three of those clades, Cosmopolitan (Africa-1 and Africa-4 subclades), Africa-2, and Africa-3, are found in Africa (*2*,*20*). The Cosmopolitan clade has >22 subclades that are widely distributed in >100 countries (*9*). The grouping of those clades is greatly affected by physical barriers that restrict gene flow (*21*). The Africa-1a subclade dominates in northern and eastern Africa, and Africa-1b predominates in central, eastern, and southern Africa. Africa-1c circulates in Madagascar, and Africa-4 was recently discovered in northern Africa (*22*). The Africa-2 clade predominantly circulates in West Africa, but the Africa-3 clade is sustained through a sylvatic cycle in South Africa (*19*,*22*).

Kenya has a >100-year history of rabies; the first case was reported in 1912 (*23*). Despite successful control efforts in the past, the disease has remained endemic because of challenges in sustaining vaccination programs (*24*,*25*). The number of human deaths attributable to rabies in Kenya is unknown (*23*), but some studies report estimates of >2,000 per year and others as low as 523 (*26*,*27*); the highest incidences have been reported in western and eastern Kenya (*23*). The main source of human rabies is the domestic dog (*28*). However, those human deaths are unjustifiable considering the availability of effective mass dog vaccination and therapeutic PEP for persons bitten by rabid animals (*25*,*29*). Kenya has an ambitious plan to end human rabies deaths by 2030; that plan combines mass dog vaccination and prompt provision of PEP to affected humans (*26*). Unfortunately, only 5% of health facilities have PEP, and mass dog vaccination has fallen short of the target (*25*,*26*).

RABV, a negative-stranded RNA virus with a genome size of ≈12 kilobases, encodes 5 proteins: nucleoprotein (N), matrix protein (M), phosphoprotein (P), glycoprotein (G), and large (L) protein or polymerase (*30*,*31*). The N, P, and L proteins comprise the ribonucleoprotein (RNP) complex and the M and G proteins are involved in virus assembly and budding (*32*). The N gene is responsible for transcription and replication and shows antigenic variation that is used for strain discrimination (*7*,*33*,*34*–*36*). Since the 1880s, when Louis Pasteur developed a RABV vaccine (*37*), vaccination has played a crucial role in controlling rabies through production of neutralizing antibodies against the RNP and G antigens (*38*,*39*). G and N are crucial components for rabies vaccine effectiveness (*38*,*39*), and monitoring antigenic variations between vaccine strains and the G and N genes of circulating wild strains can help determine whether the existing vaccine strains remain effective (*33*,*40*). We assessed genetic diversity of wild RABV strains collected from 2 rabies hotspots in Kenya to inform current and future vaccination and PEP efforts.

Methods

Study Areas and Sample Cohort

Veterinary technicians collected postmortem brain stems from suspected rabid animals in Kenya's Siaya County, in the western region, and Makueni County, in the eastern region (Figure 1). Sample collection was approved by the Kenya Medical Research Institute's Scientific and Ethical Research Unit under a rabies surveillance protocol (no. KEMRI/SERU/CGHR 046/3268).

We used Anigen Rapid Rabies Ag Kits (BioNote Inc., https://www.bionote.co.kr) to confirm RABV at the collection sites. That assay has a sensitivity of 92% (95% CI 85.9%–95.6%) and specificity of 100% (95% CI 93.4%–100%) compared with the reference standard fluorescent antibody test and is recommended for confirming clinical rabies cases in animals (*41*). We collected a total of 164 RABV-positive brain stems. We transported brainstems to the laboratory in liquid nitrogen and stored at −80°C until we performed nucleic acid purification.

Nucleic Acid Isolation

We used the Bullet Blender (Next Advance, https://www.nextadvance.com) to homogenize ≈20 mg brainstem with 3-mm ceramic beads in TRIzol reagent (Thermo Fisher Scientific, https://www.thermofisher.com). We cooled samples at room temperature before centrifuging at 12,000 × *g* for 3 minutes at 4°C. We used 200 µL of the aqueous phase to extract nucleic acids by using MagMAX CORE Purification Kit (ThermoFisher Scientific), then eluted extracted nucleic acids in a total volume of 60 µL.

Molecular Detection of RABV by qRT-PCR

We used quantitative reverse transcription PCR (qRT-PCR) to screen nucleic acids for RABV by targeting the large (L) gene using forward

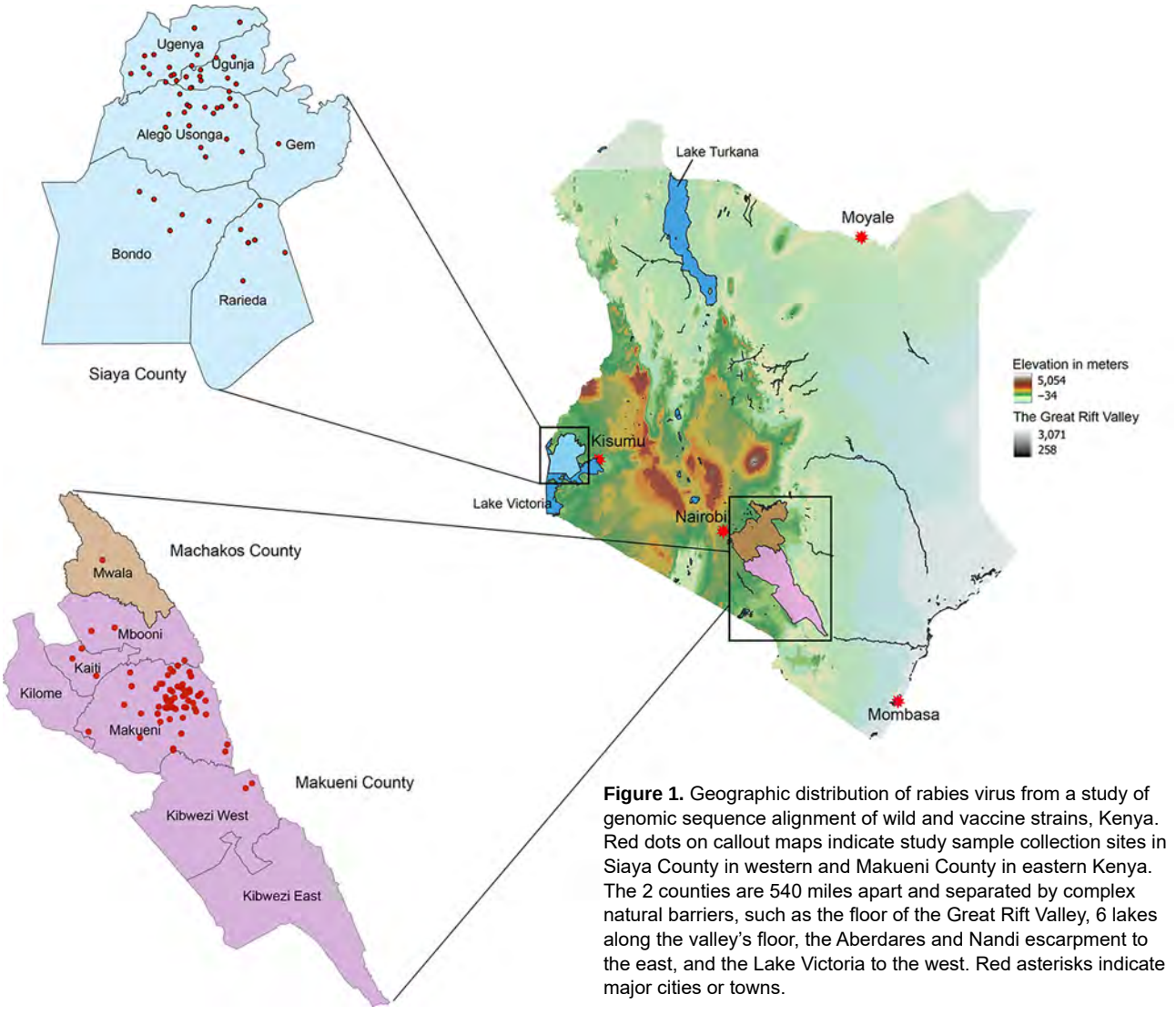

Figure 1. Geographic distribution of rabies virus from a study of genomic sequence alignment of wild and vaccine strains, Kenya. Red dots on callout maps indicate study sample collection sites in Siaya County in western and Makueni County in eastern Kenya. The 2 counties are 540 miles apart and separated by complex natural barriers, such as the floor of the Great Rift Valley, 6 lakes along the valley's floor, the Aberdares and Nandi escarpment to the east, and the Lake Victoria to the west. Red asterisks indicate major cities or towns.

primer 5′-GGTTTCCGGDGCYGTDCCTC-3′, reverse primer 5′-CCTAGGGGAGACYTTGCCRT-3′ primer, and a 6FAM-CCCGTCAYATAGGGT CRGCT-CARGGGC–BBQ probe. The qRT-PCR reaction comprised 4 μL of the nucleic acid, 10 μL of 2x SensiFAST Master mix (Meridian Bioscience, https://www.meridianbioscience.com), 0.8 μL forward and reverse primer mix at a concentration of 10 μM each, 0.4 μL of TaqMan QSY probe (Applied Biosystems/Thermo Fisher Scientific) at a concentration of 10 μM, 3.4 μL of nuclease-free water, 0.4 μL RiboSafe RNase inhibitor (Thermo Fisher Scientific), and 0.2 μL reverse transcriptase. We used an ABI 7500 (Applied Biosystems) for amplification using a reverse transcription cycle at 45°C for 10 minutes and 95°C for 3 minutes to inactivate the reverse transcriptase, followed by 40 cycles of 95°C for 30 seconds and 60°C for 1 minute. Each reaction included a positive control of a known RABV-positive sample and PCR water as a nontemplate negative control.

Whole-Genome Sequencing

We used the TURBO DNase kit (ThermoFisher Scientific) to deplete extracted nucleic acids of host genomic DNA. We used sequence-independent, single-primer amplification to amplify viral RNA as previously described (*42*), with subsequent modifications (*43*). We then reversed transcribed the first cDNA strand by using the LunaScript RT SuperMix kit (New England Biolabs, https://www.neb.com) and the JH17N8 primer (5′-GTTTCCCAGTAGGTCTCNNNNNNNN-3′), which contained a degenerate 8-mer sequence at the 3′ end. We generated the second cDNA strand by amplification using NEB Next Ultra II Q5 master mix (New England Biolabs)

with 10 μM of a specific primer JHP21 (5′-GTTTC-CAGTAGGTCTC-3′) and the following thermal cycling regimen: 1 cycle of 94°C for 3 minutes, 25°C for 30 seconds, 72°C for 1 minute, followed by 35 cycles of 94°C for 30 seconds, 55°C for 30 seconds, and 72°C for 1 minute. We included a final extension step of 72°C for 1 minute, followed by cooling to 4°C. We purified the synthesized dsDNA by using Agencourt AMPure XP beads (Beckman Coulter, https://www.beckmancoulter.com), which we then used to prepare sequence libraries using the Colibri ES DNA Library preparation kit (ThermoFisher Scientific). We quantified libraries by using a Qubit dsDNA HS Assay kit (Invitrogen/Thermo Fisher Scientific) and measured the average library size on the 4200 TapeStation System (Agilent Technologies, https://www.agilent.com). We adjusted the pooled library to 4 nM concentration and then denatured with 0.2 normal sodium hydroxide and further diluted to 9.5 pM. We spiked 5% of PhiX v3 Control Library (Illumina, https://www.illumina.com) into the pool and sequenced the library in pairs using 600 cycles v3 on the Miseq or P3 reagents on the NextSeq 2000 platform (Illumina).

Genome Assembly, Clade Classification, and Phylogenetic Reconstruction

We assessed the quality of the raw sequences in FastQC v0.12.1 (https://github.com/s-andrews/FastQC/releases) and then processed by using the ngs_mapper pipeline (https://github.com/VDBWRAIR/ngs_mapper), which removes low-quality reads (<Q20), failed reads, sequencing adapters, and short reads (<50 nt) by using trimmomatic v0.35 (https://github.com/usadellab/Trimmomatic/releases) and cutadapt v1.9.1 (https://gensoft.pasteur.fr/docs/cutadapt/1.9.1/index.html). We then mapped the filtered reads against a RABV genome from Tanzania (GenBank accession no. KY210291) that had the closest homology to our sample sequences by using bwa v0.7.12 (https://github.com/lh3/bwa/releases). We used Samtools v0.1.19 (https://sourceforge.net/projects/samtools/files/samtools/0.1.19) to create pileups from the read alignments and the consensus genome and generated a variant call format file and coverage visualizations by using several Python scripts (Python Software Foundation, https://www.python.org) housed within the pipeline.

To determine whether the generated whole genomes add value to genomes generated from the N and G genes, we used the RABV-GLUE tool (http://rabv-glue.cvr.gla.ac.uk) to assign the RABV to major and minor clades. Further classification of the whole genomes into lineages was performed using MADDOG (*44*).

To establish the phylogenetic relationships between RABV from Kenya in the context of Africa, we obtained a comprehensive subset of curated, annotated, and published RABV datasets from Africa from the Bacterial and Viral Bioinformatics Resource Center (BV-BRC; https://www.bv-brc.org). We aligned the complete RABV polyprotein, the entire N protein, and the entire G protein of the study genomes and context samples in CLC Genomics workbench version 8.5.1 and the Muscle plugin (QIAGEN, https://www.qiagen.com). To avoid using sequences from recombinations, we ran the aligned sequences in GARD software (Datamonkey, https://www.datamonkey.org) by using the Hyphy package (Datamonkey). We performed phylogenetic inference by using the maximum-likelihood method in IQ-TREE version 2.2.0 (http://www.iqtree.org) and nucleotide substitution models built into ModelFinder in IQ-TREE. We evaluated node support with a combination of approximate likelihood tests and ultrafast bootstraps with 1,000 replicates, each computed in IQ-TREE (*45*). We visualized and annotated the resulting phylogenetic trees by using FigTree version 1.4.2 (http://tree.bio.ed.ac.uk/software/Figtree).

Analysis of Amino Acid Variation at RABV Vaccine Target Sites

To identify amino acid variations at the N and G vaccine target sites of the study genomes and the vaccine strains, we performed sequence alignment of the G (n = 142) and N (n = 144) proteins by using CLC Genomics Main Workbench (QIAGEN). We aligned study sample sequences to 3 commonly used RABV vaccine strains: Pitman-Moore (PM; GenBank accession no. DQ099525), Pasteur virus (PV; GenBank accession no. M13215), and challenge virus standard (CVS; accession no. AF406696 for N and AF406694 for G).

Results

Study Sample Demographics

Domestic dogs contributed most (65%) study samples, followed by cows (18%), and goats (14%). Other species accounted for only 1% of samples (Appendix 1 Table 1, https://wwwnc.cdc.gov/EID/article/30/8/23-0876-App1.xlsx)

RABV Geographic Restriction in Kenya

Of the 164 brainstems collected, 144 samples with genome lengths ranging from 10,024 to 11,923 nt

were used for whole-genome analysis. From whole-genome sequences, we also extracted 142 N and 144 G genes for single-gene analysis. By RABV-GLUE, all genomes belonged to the Cosmopolitan clade, either Africa-1a (71/144) or Africa-1b (73/144) subclades. Further interrogation of the clades using the MAADOG lineage typing tool revealed 14 distinct lineages, 8 in western Kenya and 6 in eastern Kenya, including 1 unclassified lineage in eastern Kenya (Figure 2).

We accessed the BV-BRC database on November 18, 2022, and retrieved 378 RABV polyproteins, 1,500 N, and 130 G sequences that met our inclusion criteria. We used RABV sequences from the study strains and strains subsampled from Africa to construct whole-genome phylogenetic trees (Appendix 2 Figures

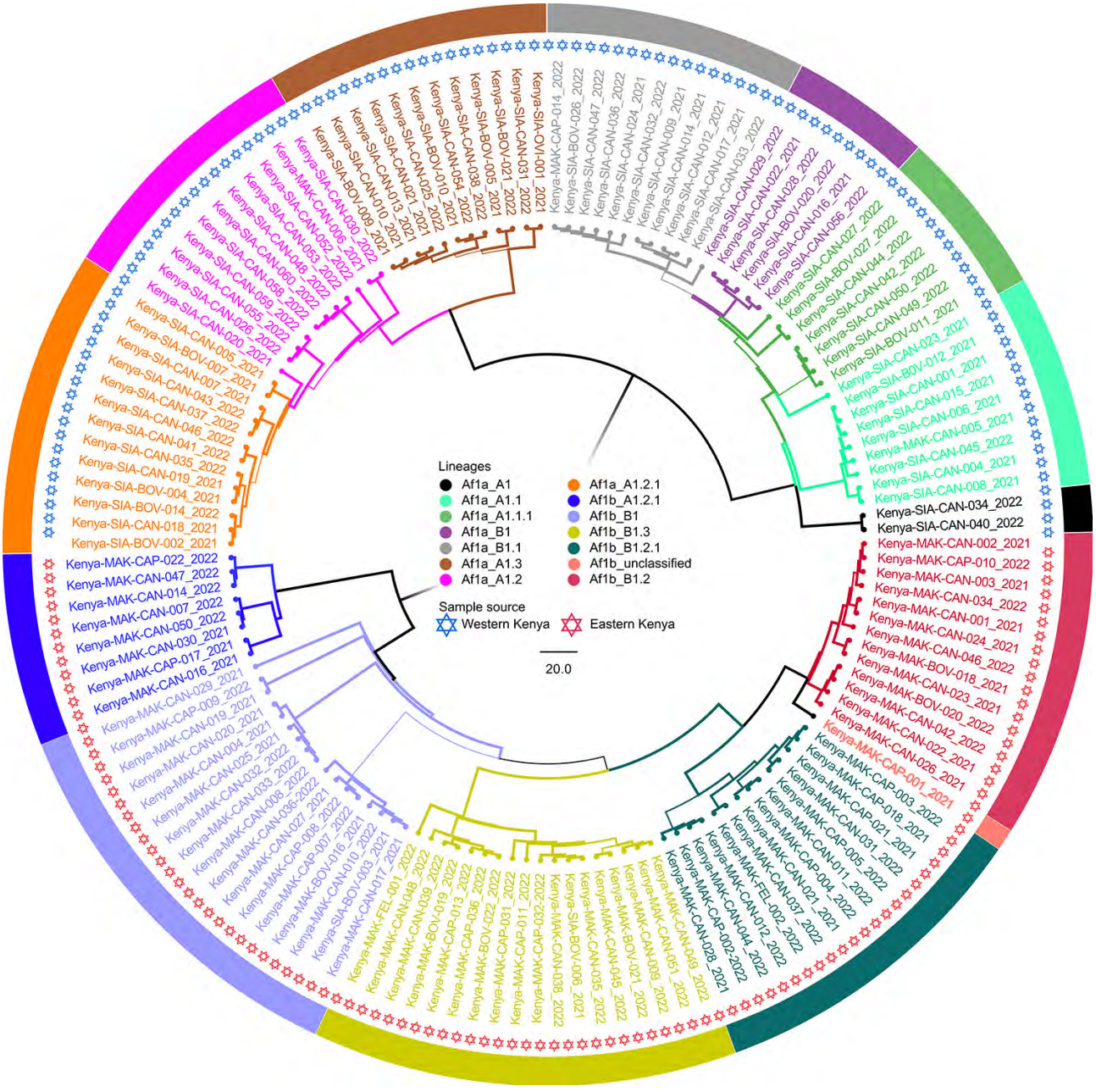

Figure 2. Phylogenetic tree of virus genomes from a study of geographic distribution of rabies virus and genomic sequence alignment of wild and vaccine strains, Kenya. The tree was constructed from whole-genome sequences by using MAD DOG (*44*). All genomes were of Cosmopolitan clade, subclades Africa-1a or Africa-1b, and were further delineated into a total of 14 distinct lineages, 8 from western Kenya and 5 in eastern Kenya. One lineage from eastern Kenya was unclassified. Scale bar indicates nucleotide substitutions per site.

1–3, https://wwwnc.cdc.gov/EID/article/30/8/23-0876-App2.pdf) and individual G and N gene trees (Appendix 2 Figures 4, 5). We compared the phylogenetic trees constructed using a relatively new method of whole-genome sequencing (has only few sequences in literature) with those generated from the old method of individual G and N genes analysis that has been the basis of RABV phylogeography. Both methods identified only the Cosmopolitan clade in our study genomes (Appendix 2 Figures 2, 4, 5). In addition, western Kenya samples (97.2%) branched with the Cosmopolitan Africa-1a subclade, and eastern Kenya samples (95.7%) branched with Cosmopolitan Africa-1b subclade (Appendix 2 Figures 2, 4, 5). Only 2 western Kenya genomes clustered with the Africa-1b subclade (Appendix 2 Figure 1) and only 3 eastern Kenya genomes clustered with the Africa-1a subclade (Appendix 2 Figure 3).

Within the Africa-1b subclade, the eastern Kenya samples appeared to have 2 distinct clusters, 1 major (n = 63) and 1 minor (n = 8) (Appendix 2 Figure 1). In both clusters, the study samples branched with Tanzania genomes. The western Kenya genomes (n = 69) were more homogeneous (Appendix 2 Figure 3). We deposited raw sequence data from this study in the National Center for Biotechnology Information (NCBI; https://www.ncbi.nlm.nih.gov) Sequence Read Archive (BioProject nos. OR256801 and OR270967–1061).

Comparison of Circulating Wild RABV and Vaccine Strains

Compared with sequences of the commonly used RABV vaccine strains in Kenya (PM, PV, and CVS), we noted no amino acid substitutions at the antigenic sites of the G gene, located between amino acids 20–439 (Appendix 1 Table 2). However, sequence homology outside the antigenic sites varied from 92.2% for PM to 93.3% for CVS and 93.0% for PV. In contrast, 2 study samples, Kenya/SIA-CAN-018/2021 and Kenya/SIA-BOV-007/202, were variant at antigenic site II of the N gene, in which alanine was substituted by valine at position 315 (A315V), but the 3 vaccine strains and all the other study samples had alanine in that position. In addition, although all the study samples, PM, and CVS had valine at position 379 of antigenic site III, PV was variant with alanine (V379A). Outside the antigenic sites of the N gene, sequence homology ranged from 98.45% to 99.11% for PM, 97.78% to 98.67% for CVS, and 97.56% to 98.23% for PV.

Discussion

In this study, we used samples collected from 2 geographically isolated counties, Siaya in western Kenya and Makueni in eastern Kenya. We chose those 2 counties because they continuously report the highest rabies incidences in humans (*23*). Of the 164 brainstem study samples, 107 were from domestic dogs (Appendix 1 Table 1). Moreover, the other 57 samples came from animals with a history of having been bitten by a rabid dog, underscoring the role domestic dogs play in rabies transmission.

Previous phylogenetic studies, performed using single G and N genes, have indicated that RABV in Africa falls into several regional groups and that viruses from eastern Africa are genetically distinct from those in the western, central, and southern parts of the continent (*21*). Before this study, NCBI included 43 RABV sequences from Kenya (*46*–*48*). In a previous study (*46*), N and G genes from RABV samples obtained during an outbreak of rabies in African wild dogs in Kenya and Tanzania appeared to be identical. The authors concluded that the outbreak was most likely caused by a viral variant frequently found in domestic dogs in Kenya and Tanzania. A subsequent study that used N and G gene sequences reported existence of 2 Cosmopolitan subclades (*47*), namely Africa-1a and Africa-1b. Subsequent research revealed predominance of Africa-1a in western Kenya, but Africa-1b was more commonly observed in the eastern part of the country (*48*).

We added 144 whole-genome sequences from this study to the NCBI Sequence Read Archive. We used those genomes to further characterize the diversity of RABV from eastern and western Kenya. We also determined whether available rabies vaccines would confer protection. Our study confirms the inferences of previous research that shows an apparent geographic isolation between the RABV strains in eastern and western Kenya (*48*). Of the 3 major clades of RABV found in Africa, only the Cosmopolitan clade was detected by whole genomes (Appendix 2 Figures 1–3) and individual N and G genes (Appendix 2 Figures 4, 5). Predominantly, RABV from eastern Kenya clustered with the Africa-1b subclade, whereas RABV from western Kenya clustered with the Africa-1a subclade. That geographic isolation is probably because of the multiple landscape features that would restrict free movement of animals between the regions (Figure 1), thus promoting localized viral evolution. Similar geographic restriction has also been observed in raccoon-mediated rabies in the eastern United States (*49*). Outlier Africa-1b genomes that were in western Kenya (n = 2), and Africa-1a genomes (n = 3) that were in eastern Kenya indicate that geographic isolation is not absolute in the country (Appendix 2 Figures 1–3).

We found that RABV strains in western Kenya were closely related to each other and dissimilar from other Africa-1a subclade members in neighboring countries (Appendix 2 Figures 1–3). For example, the closest genome that was clearly distinct from the Kenya 1a subclade was from Sudan. Those observations suggest that the members of the Africa-1a circulating in Kenya have evolved separately, most likely from northern, central, and western regions of Africa. The other likely explanation is undersampling given that our study samples were collected in 2021 and 2022, but the other Africa-1a subgenomes were collected during 1986–2015. The Africa-1b genomes from Kenya were less homogeneous and branched into 2 groups: a major group of 63 genomes that clustered together and a minor group of 8 genomes that clustered with genomes that had been collected previously from Kericho and Nakuru, Kenya. However, using the MADDOG lineage typing tool, the western Kenya 1a subclade that was apparently homogeneous revealed 8 lineages, and the eastern Kenya subclade 1b segregated into 5 lineages (Figure 2), indicating that RABV accumulates mutations through the course of transmission. The finding of Africa-1b in Nakuru and Kericho, locales that are close to western Kenya, indicates an ongoing encroachment of the 1b subclade into western Kenya.

Several strains of RABV are used to manufacture vaccines (*38*). The choice of vaccine strain for use in a geographic region is informed by factors such as the circulating wild variants and species of animals being vaccinated (*50*). Live attenuated vaccines are given orally and are used in wild carnivores. Inactivated vaccines are used in humans and domestic animals, including dogs and cats. From the RABV genomes in our study, we evaluated whether the currently used RABV vaccines would confer protection (Appendix 1 Tables 2, 3). In Kenya, the available vaccines are derived from the PM, CVS, and PV RABV strains. An amino acid sequence alignment and comparison of the G sequences of the study genomes and the vaccine strains revealed 100% homology to the vaccine antigenic sites (Appendix 1 Table 2). A similar alignment and comparison using the N gene revealed a V315A replacement at antigenic site II in only 2 study samples. In addition, all the study samples and PM and CVS strains had valine at position 379 of antigenic site III, but the PV was variant with V379A (Appendix 1 Table 3). Although those replacements are too infrequent to effect vaccine efficacy, they raise concerns of potential cumulative changes that could eventually alter vaccine efficacy and underscore the need for continued monitoring of such changes.

In conclusion, we used whole-genome sequencing to define the genetic diversity of RABV in Kenya. Our data demonstrated the presence of localized viral lineages and limited viral migration between the 2 study regions. In addition, obtained data suggest that rabies endemicity is due to limited vaccine use because the sequences of the study strains do not greatly diverge from current vaccine strains. Moving forward, similar studies should expand to the other regions of Kenya to determine the generalizability of our findings. Nonetheless, the viral migration across the regions, though limited, reinforces the need for cross-county rabies surveillance systems in Kenya.

Acknowledgments

We are grateful to the veterinary team that worked hard to trace rabid animals. We thank Rachel Githii for generating the map shown in Figure 1.

Research support was provided by Uniformed Services University grant HU00011920118 to B.C.S.

Material has been reviewed by the Walter Reed Army Institute of Research. There is no objection to its publication. The opinions or assertions contained herein are the private views of the author, and they are not to be construed as official, or as reflecting true views of the Department of the Army or the Department of Defense.

Author contributions: E.W. performed all the assays, performed genome sequencing and associated bioinformatics analysis and interpretation, wrote the first draft, reviewed and edited the manuscript. K.G. assisted E.W. in sequencing, supervised the bioinformatics analysis and interpretation. S.K. assisted E.W. in data analysis and interpretation, reviewed and edited the manuscript. M.A.W. reviewed multiple drafts of the manuscripts, made suggestions in data presentation. C.M. was in charge of maintaining sample inventory, assisted E.W. in nucleic acids extraction and qRT-PCR quality assurance and quality control. L.M. and G.J. supervised field collection and shipping logistic to Kisumu Basic Science Laboratory. T.S.M. was the PI for the protocol that provided the rabies virus for the current study. He revised and edited the manuscript. B.C.S conceived the study and obtained funding that supported the study in Kenya. J.W. was Kenya's principal investigator, supervised all aspects of the study, and worked with E.W. on the multiple versions of the manuscript.

About the Author

Ms. Wambugu is an MS student at the University of Embu. She has broad interests in whole-genome sequencing and bioinformatics.

References

1. Steele JH, Fernandez PJ. History of rabies and global aspects. In: Baer GM, editor. The natural history of rabies. Boca Raton (FL): CRC Press; 2017. p. 1–24.
2. Dunlop RH, Williams DJ. Veterinary medicine: an illustrated history. St. Louis (MO): Mosby-Year Book, Inc.; 1996.
3. Talbi C, Holmes EC, de Benedictis P, Faye O, Nakouné E, Gamatié D, et al. Evolutionary history and dynamics of dog rabies virus in western and central Africa. J Gen Virol. 2009;90:783–91. https://doi.org/10.1099/vir.0.007765-0
4. Schnell MJ, McGettigan JP, Wirblich C, Papaneri A. The cell biology of rabies virus: using stealth to reach the brain. Nat Rev Microbiol. 2010;8:51–61. https://doi.org/10.1038/nrmicro2260
5. Yousaf MZ, Qasim M, Zia S, Rehman Khan M, Ashfaq UA, Khan S. Rabies molecular virology, diagnosis, prevention and treatment. Virol J. 2012;9:50. https://doi.org/10.1186/1743-422X-9-50
6. Fisher CR, Streicker DG, Schnell MJ. The spread and evolution of rabies virus: conquering new frontiers. Nat Rev Microbiol. 2018;16:241–55. https://doi.org/10.1038/nrmicro.2018.11
7. Walker PJ, Freitas-Astúa F, Bejerman N, Blasdell KR, Breyta R, Dietzgen RG, et al. ICTV virus taxonomy profile: *Rhabdoviridae* 2022. J Gen Virol. 2022;103:001689. https://doi.org/10.1099/jgv.0.001689
8. Müller T, Freuling CM. Rabies in terrestrial animals. In: Fooks AR, Jackson AC, editors. Rabies: scientific basis of the disease and its management, 4th edition. London: Elsevier Academic Press; 2020. p. 195–230.
9. Shipley R, Wright E, Lean FZX, Selden D, Horton DL, Fooks AR, et al. Assessing rabies vaccine protection against a novel lyssavirus, Kotalahti bat lyssavirus. Viruses. 2021;13:947. https://doi.org/10.3390/v13050947
10. World Health Organization. WHO expert consultation on rabies. WHO technical report series no. 931. Geneva: The Organization; 2005.
11. Scott TP, Nel LH. Lyssaviruses and the fatal encephalitic disease rabies. Front Immunol. 2021;12:786953. https://doi.org/10.3389/fimmu.2021.786953
12. Singh R, Singh KP, Cherian S, Saminathan M, Kapoor S, Manjunatha Reddy GB, et al. Rabies—epidemiology, pathogenesis, public health concerns and advances in diagnosis and control: a comprehensive review. Vet Q. 2017;37:212–51. https://doi.org/10.1080/01652176.2017.1343516
13. Meske M, Fanelli A, Rocha F, Awada L, Soto PC, Mapitse N, et al. Evolution of rabies in South America and inter-species dynamics (2009–2018). Trop Med Infect Dis. 2021;6:98.
14. Slate D, Allego TP, Nelson KM, Chipman RB, Donovan D, Blanton JD, et al. Oral rabies vaccination in North America: opportunities, complexities, and challenges. PLoS Negl Trop Dis. 2009;3:e549. https://doi.org/10.1371/journal.pntd.0000549
15. World Health Organization. WHO expert consultation on rabies. Second report. World Health Organ Tech Rep Ser. 2013;982:1–139.
16. Zhou M, Zhou Z, Kia GSN, Gnanadurai CW, Leyson CM, Umoh JU, et al. Complete genome sequence of a street rabies virus isolated from a dog in Nigeria. Genome Announc. 2013;1:e00214-12. https://doi.org/10.1128/genomeA.00214-12
17. Kuzmin IV, Shi M, Orciari LA, Yager PA, Velasco-Villa A, Kuzmina NA, et al. Molecular inferences suggest multiple host shifts of rabies viruses from bats to mesocarnivores in Arizona during 2001–2009. PLoS Pathog. 2012;8:e1002786. https://doi.org/10.1371/journal.ppat.1002786
18. Caraballo DA, Lema C, Novaro L, Gury-Dohmen F, Russo S, Beltrán FJ, et al. A novel terrestrial rabies virus lineage occurring in South America: origin, diversification, and evidence of contact between wild and domestic cycles. Viruses. 2021;13:2484. https://doi.org/10.3390/v13122484
19. Troupin C, Dacheux L, Tanguy M, Sabeta C, Blanc H, Bouchier C, et al. Large-scale phylogenomic analysis reveals the complex evolutionary history of rabies virus in multiple carnivore hosts. PLoS Pathog. 2016;12:e1006041. https://doi.org/10.1371/journal.ppat.1006041
20. Bourhy H, Reynes J-M, Dunham EJ, Dacheux L, Larrous F, Huong VTQ, et al. The origin and phylogeography of dog rabies virus. J Gen Virol. 2008;89:2673–81. https://doi.org/10.1099/vir.0.2008/003913-0
21. Brunker K, Hampson K, Horton DL, Biek R. Integrating the landscape epidemiology and genetics of RNA viruses: rabies in domestic dogs as a model. Parasitology. 2012;139:1899–913. https://doi.org/10.1017/S003118201200090X
22. Sadeuh-Mba SA, Momo JB, Besong L, Loul S, Njouom R. Molecular characterization and phylogenetic relatedness of dog-derived rabies viruses circulating in Cameroon between 2010 and 2016. PLoS Negl Trop Dis. 2017;11:e0006041. https://doi.org/10.1371/journal.pntd.0006041
23. Bitek AO, Osoro E, Munyua PM, Nanyingi M, Muthiani Y, Kiambi S, et al. A hundred years of rabies in Kenya and the strategy for eliminating dog-mediated rabies by 2030. AAS Open Res. 2019;1:23.
24. McDermott JJ, Kitala PM. The epidemiology of rabies in Machakos District, Kenya. Nairobi: University of Nairobi College of Agriculture and Veterinary Studies; 2003.
25. Chuchu VM, Kitala PM, Bichanga P, Ksee D, Muturi M, Mwatondo A, et al. Rabies elimination in rural Kenya: need for improved availability of human vaccines, awareness and knowledge on rabies and its management among healthcare workers. Front Public Health. 2022;10:769898. https://doi.org/10.3389/fpubh.2022.769898
26. Republic of Kenya, Ministry of Health and Ministry of Agriculture, Livestock and Fisheries. Strategic plan for the elimination of human rabies in Kenya 2014–2030. Nairobi: The Republic; 2014.
27. Hampson K, Coudeville L, Lembo T, Sambo M, Kieffer A, Attlan M, et al.; Global Alliance for Rabies Control Partners for Rabies Prevention. Estimating the global burden of endemic canine rabies. PLoS Negl Trop Dis. 2015;9:e0003709. https://doi.org/10.1371/journal.pntd.0003709
28. World Health Organization. WHO Expert Consultation on Rabies, WHO technical report series, no. 1012. Geneva: The Organization; 2018.
29. World Health Organization. Rabies vaccines: WHO position paper, April 2018—recommendations. Vaccine. 2018;36:5500–3. https://doi.org/10.1016/j.vaccine.2018.06.061
30. Luo Y, Zhang Y, Liu X, Yang Y, Yang X, Zhang D, et al. Complete genome sequence of a highly virulent rabies virus isolated from a rabid pig in south China. J Virol. 2012;86:12454–5. https://doi.org/10.1128/JVI.02234-12
31. Zhang G, Fu ZF. Complete genome sequence of a street rabies virus from Mexico. J Virol. 2012;86:10892–3. https://doi.org/10.1128/JVI.01778-12
32. Wunner WH, Conzelmann K-K. Rabies virus. In: Fooks AR, Jackson AC, editors. Rabies: scientific basis of the disease and its management, 4th edition. London: Elsevier Academic Press; 2020. p. 43–81.
33. Wang W, Ma J, Nie J, Li J, Cao S, Wang L, et al. Antigenic variations of recent street rabies virus. Emerg Microbes Infect. 2019;8:1584–92. https://doi.org/10.1080/22221751.2019.1683436

34. Morimoto K, Hooper DC, Carbaugh H, Fu ZF, Koprowski H, Dietzschold B. Rabies virus quasispecies: implications for pathogenesis. Proc Natl Acad Sci U S A. 1998;95:3152–6. https://doi.org/10.1073/pnas.95.6.3152
35. de Almeida GL, Cargnelutti JF, Ries AS, Ferreira JC, Rosa JCA, Batista HBCR, et al. Sequence analysis of nucleoprotein gene reveals the co-circulation of lineages and sublineages of rabies virus in herbivorous in Rio Grande do Sul state, Brazil. Braz J Microbiol. 2020;51:837–46. https://doi.org/10.1007/s42770-020-00226-z
36. Zandi F, Goshadrou F, Meyfour A, Vaziri B. Rabies infection: an overview of lyssavirus–host protein interactions. Iran Biomed J. 2021;25:226–42. https://doi.org/10.52547/ibj.25.4.226
37. Brightman C. Rabies: an acute viral infection. Trends Urol Men's Heal. 2012;3:31–3. https://doi.org/10.1002/tre.287
38. Ajorloo M, Mirzaei H, Sadeghi Y, Tarban N, Soltani S, Mohammadi FS, et al. Evaluation and phylogenetic analysis of regular rabies virus vaccine strains. Arch Iran Med. 2018;21:101–10.
39. Kim H-H, Yang D-K, Nah J-J, Song J-Y, Cho I-S. Comparison of the protective efficacy between single and combination of recombinant adenoviruses expressing complete and truncated glycoprotein, and nucleoprotein of the pathogenic street rabies virus in mice. Virol J. 2017;14:122. https://doi.org/10.1186/s12985-017-0789-2
40. Zhang G, Wang H, Mahmood F, Fu ZF. Rabies virus glycoprotein is an important determinant for the induction of innate immune responses and the pathogenic mechanisms. Vet Microbiol. 2013;162:601–13. https://doi.org/10.1016/j.vetmic.2012.11.031
41. Tenzin T, Lhamo K, Rai PB, Tshering D, Jamtsho P, Namgyal J, et al. Evaluation of a rapid immunochromatographic test kit to the gold standard fluorescent antibody test for diagnosis of rabies in animals in Bhutan. BMC Vet Res. 2020;16:183. https://doi.org/10.1186/s12917-020-02405-4
42. Bohlander SK, Espinosa R III, Le Beau MM, Rowley JD, Díaz MO. A method for the rapid sequence-independent amplification of microdissected chromosomal material. Genomics. 1992;13:1322–4. https://doi.org/10.1016/0888-7543(92)90057-Y
43. Wang D, Coscoy L, Zylberberg M, Avila PC, Boushey HA, Ganem D, et al. Microarray-based detection and genotyping of viral pathogens. Proc Natl Acad Sci U S A. 2002;99:15687–92. https://doi.org/10.1073/pnas.242579699
44. Campbell K, Gifford RJ, Singer J, Hill V, O'Toole A, Rambaut A, et al. Making genomic surveillance deliver: a lineage classification and nomenclature system to inform rabies elimination. PLoS Pathog. 2022;18:e1010023. https://doi.org/10.1371/journal.ppat.1010023
45. Minh BQ, Schmidt HA, Chernomor O, Schrempf D, Woodhams MD, von Haeseler A, et al. IQ-TREE 2: new models and efficient methods for phylogenetic inference in the genomic ea. Mol Biol Evol. 2020;37:1530–4. https://doi.org/10.1093/molbev/msaa015
46. Kat PW, Alexander KA, Smith JS, Munson L. Rabies and African wild dogs in Kenya. Proc Biol Sci. 1995;262:229–33. https://doi.org/10.1098/rspb.1995.0200
47. Brunker K, Jaswant G, Thumbi SM, Lushasi K, Lugelo A, Czupryna AM, et al. Rapid in-country sequencing of whole virus genomes to inform rabies elimination programmes. Wellcome Open Res. 2020;5:3. https://doi.org/10.12688/wellcomeopenres.15518.1
48. Gigante CM, Yale G, Condori RE, Costa NC, Long NV, Minh PQ, et al. Portable rabies virus sequencing in canine rabies endemic countries using the Oxford Nanopore MinION. Viruses. 2020;12:1255. https://doi.org/10.3390/v12111255
49. Wheeler DC, Waller LA. Mountains, valleys, and rivers: The transmission of raccoon rabies over a heterogeneous landscape. J Agric Biol Environ Stat. 2008;13:388–406. https://doi.org/10.1198/108571108X383483
50. Metlin A, Paulin L, Suomalainen S, Neuvonen E, Rybakov S, Mikhalishin V, et al. Characterization of Russian rabies virus vaccine strain RV-97. Virus Res. 2008;132:242–7. https://doi.org/10.1016/j.virusres.2007.11.016

Address for correspondence: John N. Waitumbi, WRAIR-Africa, Kenya Medical Research Institute, Basic Science Laboratory, PO Box 54, Kisumu 40100, Kenya; email: john.waitumbi@usamru-k.org

Scrapie versus Chronic Wasting Disease in White-Tailed Deer

Zoe J. Lambert,[1] Jifeng Bian, Eric D. Cassmann, M. Heather West Greenlee, Justin J. Greenlee

White-tailed deer are susceptible to scrapie (WTD scrapie) after oronasal inoculation with the classical scrapie agent from sheep. Deer affected by WTD scrapie are difficult to differentiate from deer infected with chronic wasting disease (CWD). To assess the transmissibility of the WTD scrapie agent and tissue phenotypes when further passaged in white-tailed deer, we oronasally inoculated wild-type white-tailed deer with WTD scrapie agent. We found that WTD scrapie and CWD agents were generally similar, although some differences were noted. The greatest differences were seen in bioassays of cervidized mice that exhibited significantly longer survival periods when inoculated with WTD scrapie agent than those inoculated with CWD agent. Our findings establish that white-tailed deer are susceptible to WTD scrapie and that the presence of WTD scrapie agent in the lymphoreticular system suggests the handling of suspected cases should be consistent with current CWD guidelines because environmental shedding may occur.

Prion diseases, or transmissible spongiform encephalopathies, result from the misfolding of a host's endogenous prion protein and the accumulation of the misfolded form of the prion protein (PrP^{Sc}) (*1*). Accumulation of PrP^{Sc} is associated with neurodegeneration and spongiform lesions that invariably kill the host (*1*). Prion diseases affect mammals: scrapie in sheep, chronic wasting disease (CWD) in cervids, bovine spongiform encephalopathy in cattle, and Creutzfeldt-Jakob disease in humans (*2*). The hallmark of transmissible spongiform encephalopathies is that the misfolded protein itself, devoid of the nucleic acid that drives viruses and bacteria (*1*), is able to transmit prion disease between animals (*3*).

Author affiliations: Oak Ridge Institute for Science and Education, Oak Ridge, Tennessee, USA (Z.J. Lambert); US Department of Agriculture, Ames, Iowa, USA (Z.J. Lambert, J. Bian, E.D. Cassmann, J.J. Greenlee); Iowa State University, Ames (Z.J. Lambert, M.H. West Greenlee)

DOI: https://doi.org/10.3201/eid3008.240007

CWD was first identified in mule deer and black-tailed deer in 1967 (*4*). CWD has spread in cervids across North America and has been detected internationally (*5*). Within a species, prion diseases can occur as strains. Phenotypic features that can be used to differentiate strains may include host susceptibility based on prion protein sequence, incubation periods, age at clinical onset, tissue tropism, histologic patterns of PrP^{Sc} accumulation, biochemical and biological properties of PrP^{Sc}, and range of susceptible species (*6*–*9*). Strain properties can be further differentiated by using rodent models (*10*). Although species outside the cervid family are susceptible to CWD (*11*–*17*), there is no evidence that the disease has been transmitted to humans (*18*).

Speculation about the origin of CWD has often implicated the classical scrapie agent of sheep (*19*–*22*), which is effectively transmitted to white-tailed deer intracranially and oronasally (*23*–*25*). That experimental disease, hereafter referred to as WTD scrapie, is lymphotropic (*23*,*24*), which means it is associated with environmental contamination and horizontal transmission (*26*–*28*) and could enable spread of the WTD scrapie agent in the cervid population (*29*–*31*).

Our purpose with this study was to examine the potential for white-tailed deer to transmit the WTD scrapie agent to other deer via oronasal exposure and to compare the disease phenotype to that of the CWD agent. We discovered that although differences exist between the WTD scrapie agent and the CWD agent in white-tailed deer, the presence of lymphoid involvement suggests that environmental contamination is highly likely. As the geographic distribution and disease incidence of CWD in white-tailed deer increases, information about the potential role of scrapie in the burgeoning CWD epidemic could assist in mitigation efforts. Our animal experiment was approved by the National Animal Disease Center Institutional Animal Care and Use Committee.

[1]Current affiliation: Des Moines University, Des Moines, Iowa, USA.

Materials and Methods

Our study population comprised 3 white-tailed deer that were homozygous for glutamine at codon 95 and glycine at codon 96 (QQ95/GG96) of the *PRNP* gene. To enable comparison of WTD scrapie with CWD by the assays used in this study, we used samples from a deer experimentally inoculated with the CWD agent (National Animal Disease Center [NADC] identification [ID] 1548); the deer was of the same genotype and inoculated by the same route as the 3 deer in our study population.

We oronasally inoculated deer with 1 mL of a 10% wt/vol brainstem homogenate in phosphate-buffered saline (PBS) from a white-tailed deer (NADC ID 18, publication ID 9 [*23*]) in which classical scrapie had developed (isolate no. 13-7 ARQ/ARQ [*32*]) after oronasal inoculation. We conducted antemortem rectal biopsies 17 months after inoculation. Animal caretakers observed the deer daily and euthanized them when they exhibited clinical signs (e.g., weight loss, hair loss, excessive salivation, diarrhea, and progressive weakness). We performed necropsies on the euthanized deer and collected the following samples: whole brain, cerebrospinal fluid, brainstem, spinal cord (cervical, thoracic, and lumbar segments), dorsal root ganglia, eyes, turbinate, nerves (optic, trigeminal, sciatic), lymph nodes (retropharyngeal, prescapular, mesenteric, popliteal), thymus, thyroid gland, trachea, esophagus, foregut (rumen, reticulum, omasum, abomasum), jejunum, ileum, cecum, recto-anal mucosa–associated lymphoid tissue, kidney, adrenal gland, liver, urine, spleen, lung, skin, and muscles (tongue, masseter, heart, diaphragm, triceps brachii, biceps femoris, psoas major, bladder). We collected 2 sets of tissue samples, froze 1 set, and collected the other in 10% formalin and embedded it in paraffin wax. We stained or immunolabelled embedded samples for microscopy and immunohistochemistry. Frozen samples of brainstem and retropharyngeal lymph node underwent enzyme immunoassay. We performed Western blots on brainstem, retropharyngeal lymph node, and cerebrum samples and further evaluated brainstem samples by dot blot PrP^{Sc} conformational stability assay and mouse bioassay.

For genotyping of the white-tailed deer, we extracted DNA before conducting PCR. We combined the DNA samples with PCR mix (5× buffer, deoxynucleotide triphosphates, primer #1, primer #2, dimethyl sulfoxide, Herculase II Fusion DNA polymerase [https://www.agilent.com], and double-distilled water) in a thermal cycler (Applied Biosystems, https://www.thermofisher.com) as previously described (*33*). We modified the program slightly from those previously described: 95°C for 5 minutes, 40 cycles of 95°C for 20 seconds, 54°C for 20 seconds, 72°C for 1 minutes, followed by 72°C for 7 minutes, and held at 4°C until samples were removed. We purified the PCR products by using Amicon Ultra Filters (30 kDa) (Sigma Aldrich, https://www.sigmaaldrich.com) according to manufacturer instructions. We ran the samples on an agarose gel (1%) and DNA sequenced them.

The enzyme immunoassay kit that we used is commercially available (HerdChek, IDEXX Laboratories Inc., https://www.idexx.com), and we followed manufacturer instructions to screen for PrP^{Sc} in the cerebrum, brainstem, retina, and retropharyngeal lymph nodes. We determined the negative cutoff threshold by using the negative control provided in the kit. We considered values above the optical density threshold positive. We quantified the misfolded prion protein in brainstem samples by making 2-fold dilutions to compare relative prion loads for cervidized mouse bioassays (Table 1).

We processed frozen tissues as 20% wt/vol protein homogenates by using PBS for Western blotting in a Bead Mill 24 homogenizer (Fisher Scientific; https://www.fishersci.com). Samples were digested by proteinase K (PK; 1 mg/mL) (Invitrogen, https://www.thermofisher.com) for 1 hour at 37°C with agitation (500 rpm), followed by reaction neutralization with Pefabloc (100 mg/mL) (Roche Diagnostics GmbH, https://www.roche.de) and incubation for 20 minutes at room temperature. We completed immunodetection of the misfolded prion protein on the cerebrum (frontal cortex), cervical spinal cord, retina, and retropharyngeal lymph nodes. Because of lack of tissue availability of the brainstem at the obex, we used cervical spinal cord. We prepared samples with lithium dodecyl sulfate sample buffer and 2-mercaptoethanol before loading them onto commercial-grade 12% SDS-PAGE (sodium dodecyl sulfate–polyacrylamide gel electrophoresis) gel and running for 45 minutes at 200 V in MOPS SDS running buffer (Invitrogen) with Nu PageTM Antioxidant (Invitrogen) in the center chamber. We then transferred the gel to a polyvinylidene difluoride membrane and blocked with 3% bovine serum albumin in Tris-buffered saline with 0.05% Tween 20. We then probed blots with mouse monoclonal antibodies against the prion protein: 6H4, SHA31, 12B2, and P4, all at 1:10,000 dilution (0.1 μg/mL). The C-terminal antibody 6H4 recognizes amino acids PrP-Ov 148-156/PrP-Bov 155-163 (Prionics, https://www.prionics.com), and the SHA31 C-terminal antibody recognizes amino acids 144–155 (Bertin Bioreagent, https://www.bertin-bioreagent.com) of the prion protein. On

the N-terminal of the prion protein, antibody 12B2 targets amino acids PrP-Ov 89-107/PrP-Bov 97-115 (Wageningen Bioveterinary Research, https://www.wur.nl) and antibody P4 targets amino acids PrP-Ov 93-99 (R-Biopharm AG, https://r-biopharm.com). We used an antimouse biotinylated sheep secondary antibody at a 1:400 dilution (Cytiva, https://www.cytivalifesciences.com) and a conjugated streptavidin-horseradish peroxidase at a 1:10,000 dilution (Cytiva) for amplification and signal detection. We incubated primary antibodies overnight in 4°C and the subsequent antibodies for 1 hour each at room temperature. Visualization was achieved by using electrochemiluminescence (Thermo Fisher Scientific, https://www.thermofisher.com and an iBright 1500 (Invitrogen). We used Page Ruler Plus prestained protein ladder (Thermo Fisher Scientific) to demark relative weights.

For immunohistochemistry, we used 4-micrometer paraffin-embedded tissue sections, stained the tissues with hematoxylin and eosin, and used an automated Ventana Discovery XT staining machine (Roche Diagnostics, https://diagnostics.roche.com) for microscopic analysis of misfolded prion protein staining. After deparaffinization and rehydration, we treated samples with 98% formic acid for 5 minutes and then performed antigen retrieval at 121°C for 20 minutes by using Diva Decloaker (Biocare Medical, https://biocare.net). We then probed tissue sections with the primary antibody F99/97 and took images with a Nikon Eclipse 55i microscope (https://www.nikonusa.com) by using Infinity Analyze software (Lumera, https://www.lumenera.com).

We completed bioassays in cervidized mice (Tg12 [34]) that received inoculum from the brainstem of deer 1 (WTD scrapie P2; n = 15). For comparison, we inoculated brainstem from first-passage WTD scrapie agent into cervidized mice and derived from the same deer used for inoculation in this study (WTD scrapie P1; n = 25). We inoculated another group of cervidized mice with brainstem from a white-tailed deer with CWD (WTD CWD, n = 9); the mice were anesthetized and intracranially inoculated with 20 µL of 1% wt/vol brainstem homogenate in PBS. After inoculation, we monitored the mice for clinical signs, then euthanized and necropsied them until study completion.

We conducted a conformational stability assay of the misfolded prion protein by using 96-well plates and 5–50 µg of tissue homogenates from white-tailed deer. We denatured tissue homogenates in 0–5.5 M guanidine hydrochloride G7294 (GdnHCl) (Sigma Aldrich, https://www.sigmaaldrich.com) at room temperature for 1 hour. We then filtered the samples on Amersham Protran nitrocellulose membrane (Cytiva) with a Bio-Dot Microfiltration apparatus (Bio-Rad Laboratories, https://www.bio-rad.com), followed by 2 PBS washes and air drying of the membrane for 1 hour. We then incubated them with

Table 1. Two-fold dilutions of brainstem inoculum in cervidized mice inoculated with WTD deer scrapie agent, passage 1 or 2, compared with WTD CWD agent*

Weight/ volume, %	WTD CWD	WTD scrapie agent	
		Passage 1	Passage 2
10	3.847	3.758	4
5	3.721	3.395	4
1	3.657	1.973	3.784
0.50	3.828	1.363	3.291
0.25	3.643	0.674	2.74
0.125	3.224	0.432	1.808
0.0625	2.354	0.244	1
0.031	1.345	0.138	0.439

*The optical density of brainstem samples after 2-fold dilutions to compare relative load of misfolded prion protein in the inoculum (1% wt/vol) of cervidized mice (Tg12). CWD, chronic wasting disease; WTD, white-tailed deer.

Table 2. Misfolded prion protein presence and accumulation in multiple tissues from 3 white-tailed deer with white-tailed deer scrapie*

Identification	Deer 1	Deer 2	Deer 3
Animal data			
Genotype (95/96)†	QQ/GG	QQ/GG	QQ/GG
Incubation period, mo after inoculation	25.6	21	25.8
EIA OD			
Brainstem	4	3.26	1.79
Cerebrum	4	Not detected	Not detected
Retina	4	Not detected	Not detected
Retropharyngeal lymph nodes	4	4	4
Spongiform lesion on brainstem	+	+	+
Immunohistochemistry			
Antemortem rectal biopsy (17 mpi)	+	Insufficient	+
Brainstem	+	+	+
Cerebrum	+	Not detected	Not detected
Retina	+	+	+
Retropharyngeal lymph nodes	+	+	+
Palatine tonsil	+	+	+

*EIA OD, enzyme immunoassay optical density.
†Homozygous for glutamine at codon 95 and glycine at codon 96 (QQ95/GG96) of the *PRNP* gene.

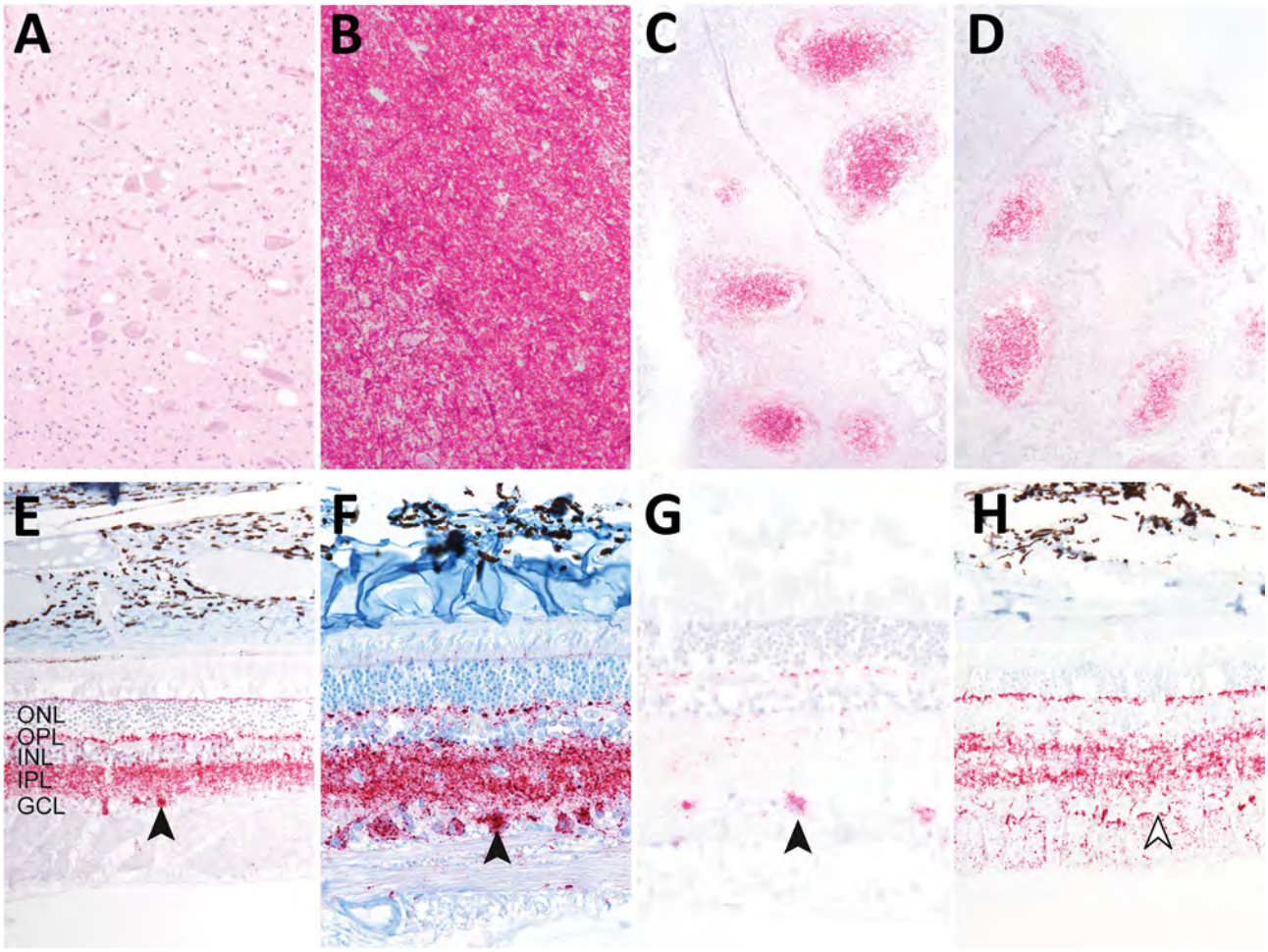

Figure 1. Immunohistochemistry demonstrating misfolded prion protein in white-tailed deer oronasally inoculated with white-tailed deer scrapie (WTD scrapie) agent in study of scrapie versus chronic wasting disease (CWD) in white-tailed deer. A) Vacuolation in the dorsal motor nucleus of the vagus in the brain stem at the level of the obex of each deer. B–D) Misfolded prion protein in the dorsal motor nucleus of the vagus in the brain stem at the level of the obex (B), palatine tonsil (C), and retropharyngeal lymph node (D) of each deer. E–H) Neurotropism of the scrapie form of the prion protein for retinal ganglion cells with scrapie agent (closed arrowheads) and not CWD (open arrowhead). E) Sheep scrapie retina; F) WTD scrapie, passage 1, retina; G) WTD scrapie, passage 2, retina; H) WTD CWD, retina. Hematoxylin and eosin staining; original magnification ×10 for panels A–D, ×20 for panels E–H. GCL, ganglion cell layer; INL, inner nuclear layer; IPL, inner plexiform layer; ONL, outer nuclear layer; OPL, outer plexiform layer.

PK (5 μg/mL) in cell lysis buffer (50 mM Tris-HCl, pH 8.0, 150 mM NaCl, 0.5% sodium deoxycholate, 0.5% Igepal CA-630 [https://www.sigmaaldrich.com]) for 1 hour at 37°C. We inactivated digestion with PK with 2 mM phenylmethylsulfonyl fluoride. Denaturation of the membrane took 10 minutes in 3 M guanidine thiocyanate in Tris-HCl (pH 7.8) at room temperature. After 4 PBS washes, we blocked membranes with 5% nonfat milk in in Tris-buffered saline with 0.05% TWEEN 20 for 1 hour, then probed at 4°C overnight with SHA31 (Bertin Technologies, https://www.bertin-technologies.fr) diluted 1:5,000, followed by horseradish peroxidase–conjugated goat antimouse IgG secondary antibody. We used ECL Plus (Pierce ECL Plus Western Blotting Substrate [Thermo Fisher Scientific]) to develop the membranes, a ChemiDoc imager (Bio-Rad) to take the images, and AzureSpot Pro analysis software (Azure Biosystems, https://azurebiosystems.com) to complete the signal analysis. We completed analysis on 3 biological replicates. We normalized absolute densitometric values by defining the smallest mean of each sample as 0 and largest mean as 1. To produce denaturation curves, we plotted relative levels of the undenatured PrP^{Sc}, referred to as F*app* (apparent fractional change of unfolded PrP^{Sc}), as a function of GdnHCl concentration. We used a nonlinear least-square 4-parameter sigmoidal dose-response regression with the half maximal denaturation concentration, $[GdnHCl]_{1/2}$, calculated by

using Graphpad Prism software (https://www.graphpad.com). We used the Student *t*-test to assess the statistical significance of $[GdnHCl]_{1/2}$.

Results

Of the 3 wild-type (QQ95/GG96) white-tailed deer oronasally inoculated with brainstem homogenate from a deer that succumbed to no. 13-7 classical scrapie, all either exhibited clinical signs (excessive salivation, hair loss, and weight loss) and were euthanized or found dead 21–25.8 months after inoculation (Table 2). Enzyme immunoassays performed on central nervous and lymphoreticular system tissues (Table 2) indicated that all 3 deer were positive for PrP^{Sc} in the brainstem. Deer 1 (optical density [OD] 4.00) and 2 (OD 3.26) had relatively more PrP^{Sc}, indicated by greater optical density than in deer 3 (OD 1.79) in the brainstem. Regardless, all white-tailed deer had 4.0 PrP^{Sc} in the retropharyngeal lymph nodes. Only deer 1 was positive in the cerebrum and retina (OD 4.00).

Immunohistochemistry indicated spongiform lesions and misfolded prion protein accumulation in the dorsal motor nucleus of the vagus in the brainstem at the level of the obex in all 3 white-tailed deer inoculated with WTD scrapie (Figure 1, panels A, B). PrP^{Sc} accumulation was also detected in the palatine tonsils and retropharyngeal lymph nodes of each deer (Figure 1, panels C, D). Only deer 1 exhibited strong immunolabelling for misfolded prion protein in the retina (Figure 1, panel G). That deer also had the greatest level of spongiform lesions and misfolded prion protein accumulation in the dorsal motor nucleus of the vagus in

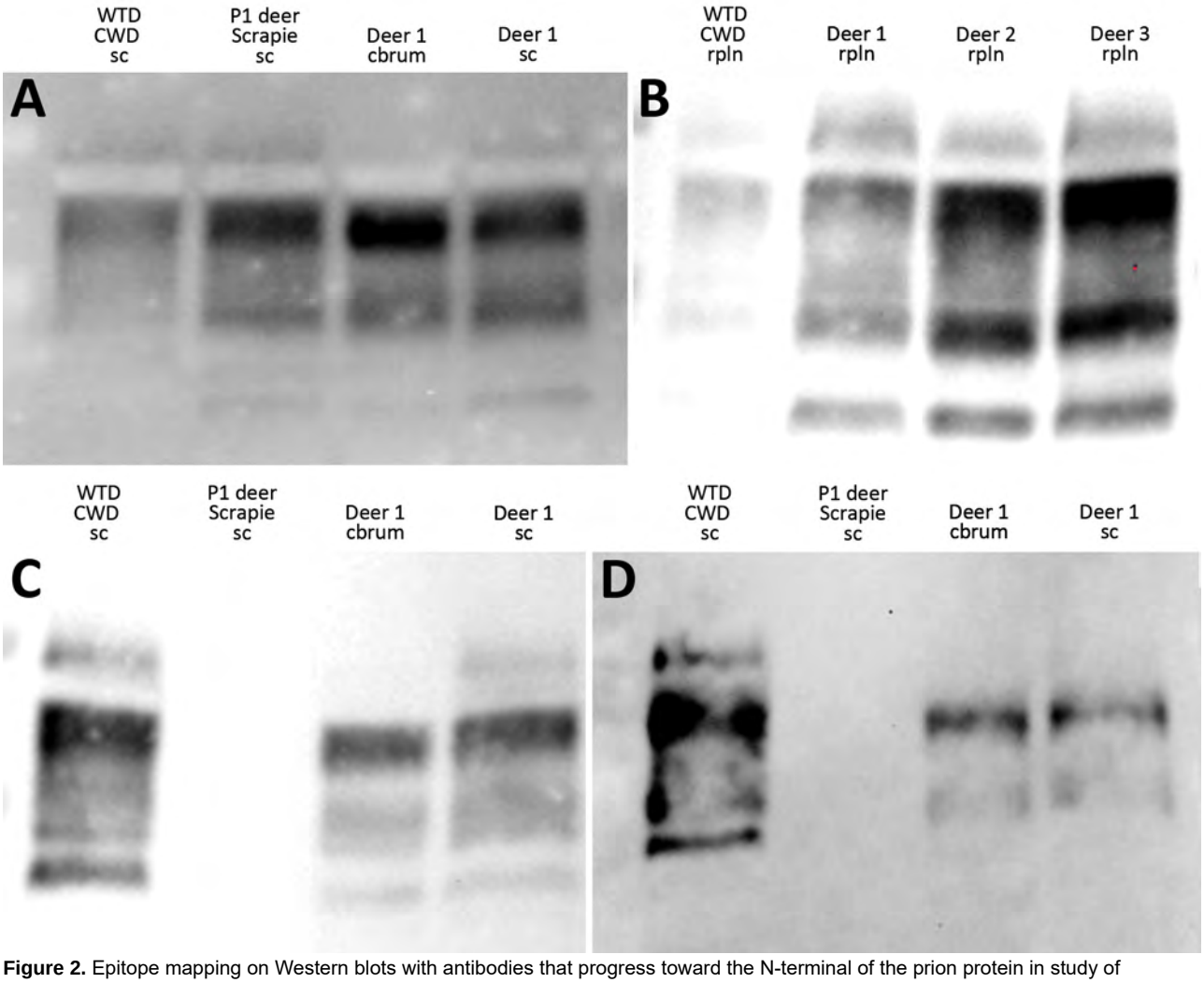

Figure 2. Epitope mapping on Western blots with antibodies that progress toward the N-terminal of the prion protein in study of scrapie versus CWD in white-tailed deer. C-terminal antibodies 6H4 (A) and SHA31 (B) were used to probe brain and lymphoid tissue (representative samples). C) Material from the second passage of WTD scrapie and CWD, both responsive to probing by the N-terminal antibody 12B2. D) WTD scrapie material showing no or low affinity to the N-terminal antibody P4. Cbrum, cerebrum; CWD, chronic wasting disease; P1, first passage; rpln, retropharyngeal lymph node; sc, cervical spinal cord; WTD, white-tailed deer.

the brainstem at the level of the obex. The PrP^{Sc} in the retina of deer 1 was abundant in the retinal ganglion cells (Figure 1, panel G), similar to that in the retinas of white-tailed deer (Figure 1, panel F) and sheep (Figure 1, panel E) inoculated with the no. 13-7 classical scrapie isolate from sheep. That finding differs from that of white-tailed deer with CWD, in which the retinal ganglion cells generally lack that type of accumulation (Figure 1, panel H). Deer 2 and 3 exhibited minimal immunolabelling for PrP^{Sc} in the retina (Table 2). Because staining was limited to the optic disk and plexiform layers in those deer, evaluation of retinal ganglion cells for PrP^{Sc} could not be completed.

Molecular profile differences were reported for tissues from white-tailed deer with first-passage WTD scrapie because brainstem was CWD-like (relatively higher kDa) and cerebrum was scrapie-like (relatively lower kDa) (*23*). Western blots were performed to evaluate whether the molecular profile differences would persist. Epitope mapping using different antibodies enabled assessment of approximate PK cleavage sites. When we used C-terminal antibodies (6H4 or SHA31), the molecular profile of the tissues from second-passage WTD scrapie was similar to that of the inoculum as well as tissues from white-tailed deer with CWD (Figure 2, panels A, B). When we used N-terminal antibody 12B2, the inoculum was nonreactive, but CWD and second-passage WTD scrapie isolates appeared similarly reactive (Figure 2, panel C). However, antibody P4 recognized an epitope further toward the N-terminal than 12B2, enough to distinguish between CWD and second-passage WTD scrapie isolates. Although the signal from white-tailed deer CWD cervical spinal cord remained strong, signals from WTD scrapie isolates were either greatly reduced or completely absent when probed with P4 (Figure 2, panel D).

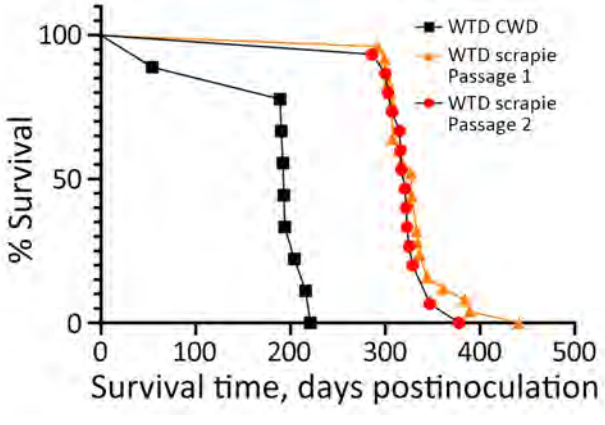

Figure 3. Survival curves for cervidized mice (Tg12) inoculated with brain material from white-tailed deer with CWD, passage 1 WTD scrapie agent, and passage 2 WTD scrapie agent in study of scrapie versus CWD in white-tailed deer. Incubation periods of mice inoculated with WTD scrapie agent were similar, whereas those inoculated with CWD were significantly shorter. CWD, chronic wasting disease; WTD, white-tailed deer.

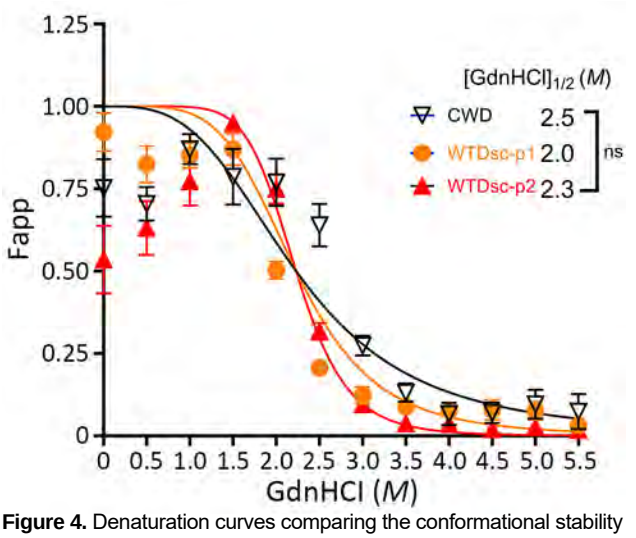

Figure 4. Denaturation curves comparing the conformational stability of scrapie (misfolded) form of prion protein (PrP^{Sc}) in the cervical spinal cords of white-tailed deer with passage 2 WTD scrapie agent, passage 1 WTD scrapie agent, and CWD agent in study of scrapie versus CWD in white-tailed deer. The PrP^{Sc} conformational stability of like tissues did not differ significantly. CWD, chronic wasting disease; F*app*, apparent fractional change of unfolded PrP^{Sc}; GdnHCl, guanidine hydrochloride; M, molar; WTDsc-p1, passage 1 WTD scrapie; WTDsc-p2, passage 2 WTD scrapie.

To identify potential strain differences, we inoculated cervidized mice (Tg12) with brainstem material (Table 1). We compared incubation periods of Tg12 mice inoculated with second-passage WTD scrapie agent (WTD scrapie P2; n = 15) with incubation periods of those inoculated with brainstem material from first-passage WTD scrapie agent (WTD scrapie P1; n = 25) and CWD agent. The incubation period in mice inoculated with brainstem from deer 1 (WTD scrapie P2) was similar to that in mice inoculated with WTD scrapie P1 (Figure 3). The average incubation time in mice inoculated with WTD scrapie P2 was 322 days after inoculation and did not differ significantly from that in mice inoculated with WTD scrapie P1 (340 days after inoculation). The incubation periods in mice inoculated with either WTD scrapie P1 or P2 differed significantly ($p<0.0001$) from those in mice inoculated with CWD agent, for which average incubation period was 199 days after inoculation (WTD CWD, n = 9). Attack rates for the 3 cohorts of mice were high (94%–100%). We performed conformational stability assays to determine if phenotypic differences between WTD scrapie passages and CWD were associated with differences in resistance of PrP^{Sc} to increasing concentrations of denaturant. After denaturation by guanidine hydrochloride, there was no difference in

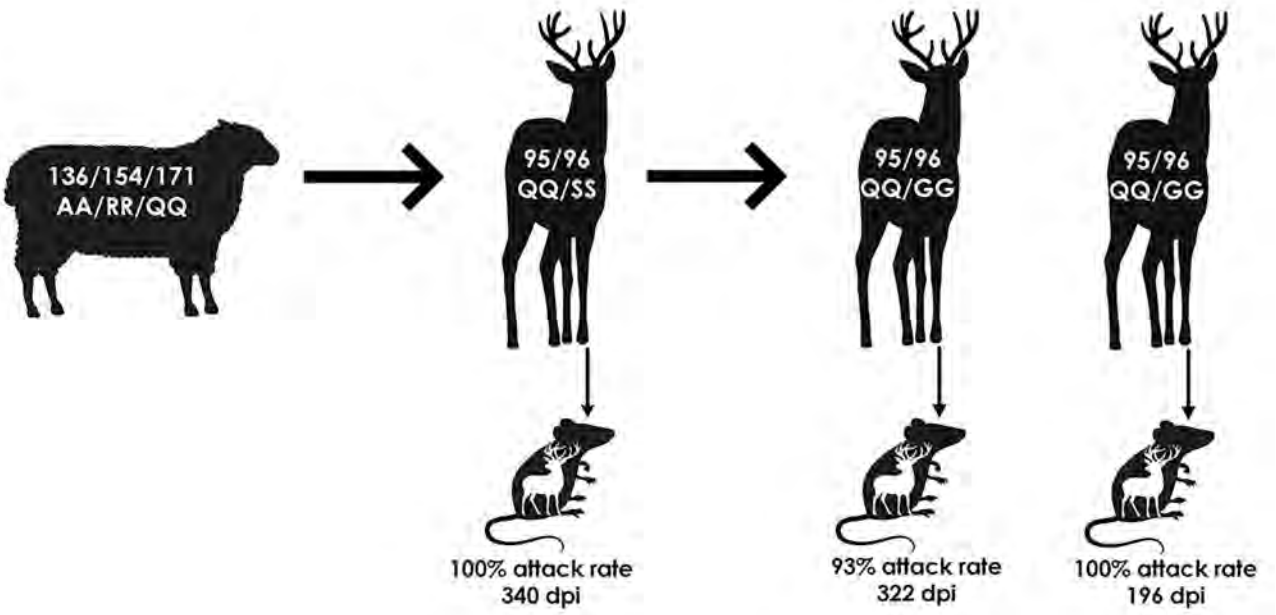

Figure 5. Summary of inoculum data, corresponding attack rates, and cervidized mice bioassays in study of scrapie versus chronic wasting disease in white-tailed deer. A, alanine; dpi, days postinoculation; G, glycine; Q, glutamine; R, arginine; S, serine.

the conformational stability of the misfolded prion protein from the cervical spinal cords of white-tailed deer with second-passage WTD scrapie, first-passage WTD scrapie, or CWD (Figure 4). Therefore, molecular and mouse bioassay differences are not associated with differences in the conformational stability of PrP^{Sc}.

Discussion

Our study demonstrates that the WTD scrapie agent can be efficiently transmitted to wild-type white-tailed deer (Figure 5). After oronasal inoculation with the WTD scrapie agent, all 3 wild-type (QQ95/GG96) white-tailed deer displayed clinical signs and were positive for PrP^{Sc} in multiple nervous and lymphoreticular tissues (100% attack rate). Spongiform lesions, PrP^{Sc} accumulation, and molecular phenotypes of second-passage WTD scrapie were similar to those of the WTD scrapie inoculum. White-tailed deer are susceptible to infection with scrapie agents from various sources (*23*–*25*,*35*). Even when white-tailed deer at the lowest risk for CWD infection (SS96) (*33*,*36*,*37*) were exposed to classical sheep scrapie, they all succumbed to the disease (*23*–*25*). Unlike the initial passage of WTD scrapie agent in white-tailed deer (*23*), all brain tissues from our study exhibited a consistent molecular profile, probably because of the WTD scrapie agent stabilizing on the white-tailed deer PrP and differential neural prion selection (*38*). Further studies are needed to investigate the role that *PRNP* polymorphisms play in the disease progression of WTD scrapie in white-tailed deer (*8*,*39*,*40*).

WTD scrapie remains different from CWD on second passage in white-tailed deer. WTD scrapie differs from CWD in that WTD scrapie PrP^{Sc} accumulates in the retinal ganglion cells (Figure 1, panels E–G), has a shorter PK-resistant core (Figure 2, panels C, D), and has longer incubation periods in mice (Figure 3). Those differences did not result from differences in genotype (*41*), PrP^{Sc} conformational stability (Figure 4), or relative quantity of PrP^{Sc} in the inoculum (Table 1, 1% wt/vol) (*42*). Although many CWD strains in cervids have been characterized (*5*), none are able to address the longstanding hypothesis that classical sheep scrapie may be the origin of CWD in cervids (*43*). Our evidence suggests that WTD scrapie differs from CWD in white-tailed deer. Nevertheless, our evidence is limited to 2 experimental passages and the genotypes of deer used for those passages because genotype can affect prion transmission characteristics (*7*,*8*,*25*,*44*). Evaluating how the scrapie agent evolves in white-tailed deer requires subsequent passages in white-tailed deer of varying genotypes.

WTD scrapie has not been detected in wild or farmed cervids. If WTD scrapie were to be detected in cervids, management would remain consistent with current measures for CWD. WTD scrapie, like CWD, is lymphotropic. Lymphotropism occurs early in disease progression before neuroinvasion and indicates that the animal is shedding PrP^{Sc} into its environment and contaminating it (*26*–*28*). Although the WTD scrapie agent propagates effectively on white-tailed deer PrP, the only reported cases have been through experimental

exposure. Because of the National Scrapie Eradication Program in 2001, cases of classical scrapie in farmed sheep have dramatically dropped and no case of classical scrapie has detected in the United States since January 2021 (https://www.aphis.usda.gov/sites/default/files/scrapie-quarterly-report-june-2024.pdf). The potential for zoonoses of cervid-derived PrP^{Sc} is still not well understood (*6*,*18*,*45*–*47*); however, interspecies transmission can increase host range and zoonotic potential (*48*–*50*). Therefore, to protect herds and the food supply, suspected cases of WTD scrapie should be handled the same as cases of CWD.

This research was supported in part by an appointment to the Agricultural Research Service Research Participation Program administered by the Oak Ridge Institute for Science and Education (ORISE) through an interagency agreement between the US Department of Energy (DOE) and the US Department of Agriculture. ORISE is managed by Oak Ridge Associated Universities (ORAU) under DOE contract no. DE-SC0014664. All opinions expressed in this paper are the authors' and do not necessarily reflect the policies and views of the US Department of Agriculture, DOE, or ORAU/ORISE.

About the Author

Dr. Lambert is an assistant professor at Des Moines University. Her main research interest is prion disease.

References

1. Prusiner SB. Prions. Proc Natl Acad Sci U S A. 1998;95:13363–83. https://doi.org/10.1073/pnas.95.23.13363
2. Lambert ZJ, Greenlee JJ, Cassmann ED, West Greenlee MH. Differential accumulation of misfolded prion strains in natural hosts of prion diseases. Viruses. 2021;13:2453. https://doi.org/10.3390/v13122453
3. Miller MW, Wild MA. Epidemiology of chronic wasting disease in captive white-tailed and mule deer. J Wildl Dis. 2004;40:320–7. https://doi.org/10.7589/0090-3558-40.2.320
4. Williams ES, Young S. Chronic wasting disease of captive mule deer: a spongiform encephalopathy. J Wildl Dis. 1980;16:89–98. https://doi.org/10.7589/0090-3558-16.1.89
5. Otero A, Duque Velasquez C, McKenzie D, Aiken J. Emergence of CWD strains. Cell Tissue Res. 2023;392:135–48. https://doi.org/10.1007/s00441-022-03688-9
6. Pritzkow S, et al. North American and Norwegian chronic wasting disease prions exhibit different potential for interspecies transmission and zoonotic risk. J Infect Dis. 2021.
7. Otero A, Duque Velásquez C, Johnson C, Herbst A, Bolea R, Badiola JJ, et al. Prion protein polymorphisms associated with reduced CWD susceptibility limit peripheral PrP^{CWD} deposition in orally infected white-tailed deer. BMC Vet Res. 2019;15:50. https://doi.org/10.1186/s12917-019-1794-z
8. Johnson CJ, Herbst A, Duque-Velasquez C, Vanderloo JP, Bochsler P, Chappell R, et al. Prion protein polymorphisms affect chronic wasting disease progression. PLoS One. 2011;6:e17450. https://doi.org/10.1371/journal.pone.0017450
9. Moore J, Tatum T, Hwang S, Vrentas C, West Greenlee MH, Kong Q, et al. Novel strain of the chronic wasting disease agent isolated from experimentally inoculated elk with LL132 prion protein. Sci Rep. 2020;10:3148. https://doi.org/10.1038/s41598-020-59819-1
10. Fraser H, Dickinson AG. Scrapie in mice. Agent-strain differences in the distribution and intensity of grey matter vacuolation. J Comp Pathol. 1973;83:29–40. https://doi.org/10.1016/0021-9975(73)90024-8
11. Cassmann ED, Frese RD, Greenlee JJ. Second passage of chronic wasting disease of mule deer to sheep by intracranial inoculation compared to classical scrapie. J Vet Diagn Invest. 2021;33:711–20. https://doi.org/10.1177/10406387211017615
12. Bartz JC, Marsh RF, McKenzie DI, Aiken JM. The host range of chronic wasting disease is altered on passage in ferrets. Virology. 1998;251:297–301. https://doi.org/10.1006/viro.1998.9427
13. Moore SJ, West Greenlee MH, Kondru N, Manne S, Smith JD, Kunkle RA, et al. Experimental transmission of the chronic wasting disease agent to swine after oral or intracranial inoculation. J Virol. 2017;91:e00926-17. https://doi.org/10.1128/JVI.00926-17
14. Greenlee JJ, Nicholson EM, Smith JD, Kunkle RA, Hamir AN. Susceptibility of cattle to the agent of chronic wasting disease from elk after intracranial inoculation. J Vet Diagn Invest. 2012;24:1087–93. https://doi.org/10.1177/1040638712461249
15. Hamir AN, Miller JM, Kunkle RA, Hall SM, Richt JA. Susceptibility of cattle to first-passage intracerebral inoculation with chronic wasting disease agent from white-tailed deer. Vet Pathol. 2007;44:487–93. https://doi.org/10.1354/vp.44-4-487
16. Hamir AN, Kunkle RA, Miller JM, Greenlee JJ, Richt JA. Experimental second passage of chronic wasting disease ($CWD^{mule\ deer}$) agent to cattle. J Comp Pathol. 2006;134:63–9. https://doi.org/10.1016/j.jcpa.2005.07.001
17. Race B, Meade-White KD, Phillips K, Striebel J, Race R, Chesebro B. Chronic wasting disease agents in nonhuman primates. Emerg Infect Dis. 2014;20:833–7. https://doi.org/10.3201/eid2005.130778
18. Zink RM. Genetic and evolutionary considerations of the chronic wasting disease—human species barrier. Infect Genet Evol. 2020;84:104484. https://doi.org/10.1016/j.meegid.2020.104484
19. Williams ES. Chronic wasting disease. Vet Pathol. 2005;42:530–49. https://doi.org/10.1354/vp.42-5-530
20. LaFauci G, Carp RI, Meeker HC, Ye X, Kim JI, Natelli M, et al. Passage of chronic wasting disease prion into transgenic mice expressing Rocky Mountain elk (*Cervus elaphus nelsoni*) PrPC. J Gen Virol. 2006;87:3773–80. https://doi.org/10.1099/vir.0.82137-0
21. Meyerett-Reid C, Wyckoff AC, Spraker T, Pulford B, Bender H, Zabel MD. *De novo* generation of a unique cervid prion strain using protein misfolding cyclic amplification. MSphere. 2017;2:e00372-16. https://doi.org/10.1128/mSphere.00372-16
22. Tamgüney G, Miller MW, Giles K, Lemus A, Glidden DV, DeArmond SJ, et al. Transmission of scrapie and sheep-passaged bovine spongiform encephalopathy prions to transgenic mice expressing elk prion protein. J Gen Virol. 2009;90:1035–47. https://doi.org/10.1099/vir.0.007500-0
23. Greenlee JJ, Moore SJ, Cassmann ED, Lambert ZJ, Kokemuller RD, Smith JD, et al. White-tailed deer are susceptible to the agent of classical sheep scrapie after experimental oronasal exposure. J Infect Dis. 2023;227:1386–95.

24. Greenlee JJ, Smith JD, Kunkle RA. White-tailed deer are susceptible to the agent of sheep scrapie by intracerebral inoculation. Vet Res (Faisalabad). 2011;42:107. https://doi.org/10.1186/1297-9716-42-107
25. Angers R, Christiansen J, Nalls AV, Kang HE, Hunter N, Hoover E, et al. Structural effects of PrP polymorphisms on intra- and interspecies prion transmission. Proc Natl Acad Sci U S A. 2014;111:11169–74. https://doi.org/10.1073/pnas.1404739111
26. John TR, Schätzl HM, Gilch S. Early detection of chronic wasting disease prions in urine of pre-symptomatic deer by real-time quaking-induced conversion assay. Prion. 2013;7:253–8. https://doi.org/10.4161/pri.24430
27. Henderson DM, Denkers ND, Hoover CE, McNulty EE, Cooper SK, Bracchi LA, et al. Progression of chronic wasting disease in white-tailed deer analyzed by serial biopsy RT-QuIC and immunohistochemistry. PLoS One. 2020; 15:e0228327. https://doi.org/10.1371/journal.pone.0228327
28. Davenport KA, Christiansen JR, Bian J, Young M, Gallegos J, Kim S, et al. Comparative analysis of prions in nervous and lymphoid tissues of chronic wasting disease-infected cervids. J Gen Virol. 2018;99:753–8. https://doi.org/10.1099/jgv.0.001053
29. Henderson DM, Denkers ND, Hoover CE, Garbino N, Mathiason CK, Hoover EA. Longitudinal detection of prion shedding in saliva and urine by chronic wasting disease-infected deer by real-time quaking-induced conversion. J Virol. 2015;89:9338–47. https://doi.org/10.1128/JVI.01118-15
30. Tennant JM, Li M, Henderson DM, Tyer ML, Denkers ND, Haley NJ, et al. Shedding and stability of CWD prion seeding activity in cervid feces. PLoS One. 2020;15:e0227094. https://doi.org/10.1371/journal.pone.0227094
31. Mammadova N, Cassmann E, Greenlee JJ. Successful transmission of the chronic wasting disease (CWD) agent to white-tailed deer by intravenous blood transfusion. Res Vet Sci. 2020;133:304–6. https://doi.org/10.1016/j.rvsc.2020.10.009
32. Moore SJ, Smith JD, Greenlee MH, Nicholson EM, Richt JA, Greenlee JJ. Comparison of two US sheep scrapie isolates supports identification as separate strains. Vet Pathol. 2016;53:1187–96. https://doi.org/10.1177/0300985816629712
33. Haley N, Donner R, Merrett K, Miller M, Senior K. Selective breeding for disease-resistant *PRNP* variants to manage chronic wasting disease in farmed whitetail deer. Genes (Basel). 2021;12:1396. https://doi.org/10.3390/genes12091396
34. Kong Q, Huang S, Zou W, Vanegas D, Wang M, Wu D, et al. Chronic wasting disease of elk: transmissibility to humans examined by transgenic mouse models. J Neurosci. 2005;25:7944–9. https://doi.org/10.1523/JNEUROSCI.2467-05.2005
35. Madsen-Bouterse SA, Schneider DA, Zhuang D, Dassanayake RP, Balachandran A, Mitchell GB, et al. Primary transmission of chronic wasting disease versus scrapie prions from small ruminants to transgenic mice expressing ovine or cervid prion protein. J Gen Virol. 2016;97:2451–60. https://doi.org/10.1099/jgv.0.000539
36. Haley NJ, Merrett K, Buros Stein A, Simpson D, Carlson A, Mitchell G, et al. Estimating relative CWD susceptibility and disease progression in farmed white-tailed deer with rare PRNP alleles. PLoS One. 2019;14:e0224342. https://doi.org/10.1371/journal.pone.0224342
37. Seabury CM, Lockwood MA, Nichols TA. Genotype by environment interactions for chronic wasting disease in farmed US white-tailed deer. G3 (Bethesda). 2022;12:jkac109. https://doi.org/10.1093/g3journal/jkac109
38. Wagner K, Pierce R, Gordon E, Hay A, Lessard A, Telling GC, et al. Tissue-specific biochemical differences between chronic wasting disease prions isolated from free-ranging white-tailed deer (*Odocoileus virginianus*). J Biol Chem. 2022;298:101834. https://doi.org/10.1016/j.jbc.2022.101834
39. Hwang S, Greenlee JJ, Vance NM, Nicholson EM. Source genotype influence on cross species transmission of transmissible spongiform encephalopathies evaluated by RT-QuIC. PLoS One. 2018;13:e0209106. https://doi.org/10.1371/journal.pone.0209106
40. Johnson C, Johnson J, Vanderloo JP, Keane D, Aiken JM, McKenzie D. Prion protein polymorphisms in white-tailed deer influence susceptibility to chronic wasting disease. J Gen Virol. 2006;87:2109–14. https://doi.org/10.1099/vir.0.81615-0
41. Duque Velásquez C, Kim C, Haldiman T, Kim C, Herbst A, Aiken J, et al. Chronic wasting disease (CWD) prion strains evolve via adaptive diversification of conformers in hosts expressing prion protein polymorphisms. J Biol Chem. 2020;295:4985–5001. https://doi.org/10.1074/jbc.RA120.012546
42. Cassmann ED, Brown QL, Frese AJ, Lambert ZJ, Greenlee MHW, Greenlee JJ. Effect of inoculation with prion dilutions within the dynamic range of ELISA absorbance on prion incubation period. Vet Res Commun. 2022;46:1377–80. https://doi.org/10.1007/s11259-022-10013-w
43. Ness A, Aiken J, McKenzie D. Sheep scrapie and deer rabies in England prior to 1800. Prion. 2023;17:7–15. https://doi.org/10.1080/19336896.2023.2166749
44. Duque Velásquez C, Kim C, Herbst A, Daude N, Garza MC, Wille H, et al. Deer prion proteins modulate the emergence and adaptation of chronic wasting disease strains. J Virol. 2015;89:12362–73. https://doi.org/10.1128/JVI.02010-15
45. Wang Z, Qin K, Camacho MV, Cali I, Yuan J, Shen P, et al. Generation of human chronic wasting disease in transgenic mice. Acta Neuropathol Commun. 2021;9:158. https://doi.org/10.1186/s40478-021-01262-y
46. Hannaoui S, Zemlyankina I, Chang SC, Arifin MI, Béringue V, McKenzie D, et al. Transmission of cervid prions to humanized mice demonstrates the zoonotic potential of CWD. Acta Neuropathol. 2022;144:767–84. https://doi.org/10.1007/s00401-022-02482-9
47. Race B, Baune C, Williams K, Striebel JF, Hughson AG, Chesebro B. Second passage experiments of chronic wasting disease in transgenic mice overexpressing human prion protein. Vet Res (Faisalabad). 2022;53:111. https://doi.org/10.1186/s13567-022-01130-0
48. Padilla D, Béringue V, Espinosa JC, Andreoletti O, Jaumain E, Reine F, et al. Sheep and goat BSE propagate more efficiently than cattle BSE in human PrP transgenic mice. PLoS Pathog. 2011;7:e1001319. https://doi.org/10.1371/journal.ppat.1001319
49. Joiner S, Asante EA, Linehan JM, Brock L, Brandner S, Bellworthy SJ, et al. Experimental sheep BSE prions generate the vCJD phenotype when serially passaged in transgenic mice expressing human prion protein. J Neurol Sci. 2018;386:4–11. https://doi.org/10.1016/j.jns.2017.12.038
50. Herbst A, Velásquez CD, Triscott E, Aiken JM, McKenzie D. Chronic wasting disease prion strain emergence and host range expansion. Emerg Infect Dis. 2017;23:1598–600. https://doi.org/10.3201/eid2309.161474

Address for correspondence: Justin J. Greenlee, National Animal Disease Center, ARS, USDA, 1920 Dayton Ave, PO Box 70, Ames, IA 50010, USA; email: justin.greenlee@usda.gov

Highly Pathogenic Avian Influenza Virus A(H5N1) Clade 2.3.4.4b Infection in Free-Ranging Polar Bear, Alaska, USA

Raphaela Stimmelmayr,[1] David Rotstein,[1] Mia Kim Torchetti, Robert Gerlach

We report a natural infection with a Eurasian highly pathogenic avian influenza A(H5N1) clade 2.3.4.4b virus in a free-ranging juvenile polar bear (*Ursus maritimus*) found dead in North Slope Borough, Alaska, USA. Continued community and hunter-based participation in wildlife health surveillance is key to detecting emerging pathogens in the Arctic.

Since its emergence in Europe during October 2020, highly pathogenic avian influenza (HPAI) A(H5N1) clade 2.3.4.4b virus has frequently spilled over into diverse mammal hosts globally. In North America, natural H5N1 infections have occurred in several bear species, including American black bears (*Ursus americanus*), Asiatic black bears (*U. thibetanus)*, grizzly bears (*U. arctos horribilis*), and Kodiak brown bears (*U. a. middendorffi*) (*1*). Infections with influenza A(H1N1) viruses have been reported in captive sloth bears (*Melursus ursinus*) and Asiatic black bears (*2*,*3*) and in giant pandas (*Ailuropoda melanoleuca*) (*4*). Detection of hemagglutination inhibition antibodies against H3 and H6 subtype influenza viruses also suggested previous natural exposure to influenza viruses of avian origin (*4*). Seroconversion after natural exposure to bird influenza viruses has been documented in the Barent Sea polar bear subpopulation (2010–2011) (*5*) and brown bears in Alaska (2013–2016) (*6*) but not in the southern Beaufort Sea polar bear subpopulation (2013–2016) (*7*). Polar bears are a threatened species under the US Endangered Species Act. We report and describe an infection by HPAI H5N1 virus in a free-ranging polar bear found dead in Alaska, USA, during 2023.

The Study

The North Slope Borough Department of Wildlife Management (NSB DWM) in Alaska conducts wildlife health research and maintains community-based harvest monitoring programs for marine mammals, including polar bears. The Alaska Office of the State Veterinarian conducts surveillance for notifiable infectious diseases in wildlife. After detecting HPAI H5N1 in birds of prey and a red fox (*Vulpes vulpes*) in April 2022, the Office of the State Veterinarian initiated collaborative surveillance testing with NSB DWM for avian influenza in birds and other wildlife. In August 2023, community members reported a dead polar bear without obvious external injuries near Point Barrow, Alaska (71°23′N, 156°28′W). At the NSB DWM laboratory in Utqiagvik, Alaska, we conducted a postmortem examination of the bear. The bear was young and male, 120 cm in body length, and in moderate to advanced decomposition. Body condition was fair to poor, with no back or visceral fat. Gross findings were multiple 1–3-cm ulcerative skin lesions around the left eye and oral commissure, liver and lung congestion, moderate sanguinal pericardial and cavitary effusion, cerebral swelling and congestion, and empty stomach. We collected postmortem tissue samples of the heart, lung, trachea, spleen, liver, kidney, adrenal gland, skin, skeletal muscle, mesenteric lymph node, pancreas, tongue, esophagus, stomach, small intestines, and brain (cerebrum) and fixed them in 10% neutral buffered formalin for 2 weeks. Histology

Author affiliations: North Slope Borough, Utqiagvik, Alaska, USA (R. Stimmelmayr); University of Alaska, Fairbanks, Alaska, USA (R. Stimmelmayr); Marine Mammal Pathology Services, Olney, Maryland, USA (D. Rotstein); US Department of Agriculture Animal and Plant Health Inspection Service, Ames, Iowa, USA (M.K. Torchetti); Alaska Department of Environmental Conservation, Anchorage, Alaska, USA (R. Gerlach)

DOI: https://doi.org/10.3201/eid3008.240481

[1]These authors contributed equally to this article.

Consultation Services (https://histocs.com) processed the tissue for routine histopathologic examination by staining with hematoxylin and eosin. We also collected oral, nasal, rectal, and brain swab samples and placed them in 2-mL cryovials, which we stored for 2 weeks at −50°C and shipped to the Alaska Environmental Health Laboratory in Anchorage, Alaska. Their personnel placed pooled swab specimens into brain–heart infusion broth. The primary histopathologic finding was a granulocytic and mononuclear meningoencephalitis with microgliosis, neuronal necrosis, neuronophagia, vasculitis, and parenchymal rarefaction (Figure, panel A). Other findings were pulmonary edema, focal lipid pneumonia, and multifocal ulcerative dermatitis.

Pooled swab specimens tested negative for the influenza virus matrix gene by PCR at the Washington Animal Disease Diagnostic Laboratory (Pullmans, WA, USA), which is a National Animal Health Laboratory Network facility. The root cause of negative PCR results is unclear because subsequent sequence analysis did not indicate assay failure. However, because of the cerebral lesions, we sent scrolls of formalin-fixed paraffin-embedded cerebral tissue to the Athens Disease Diagnostic Laboratory, University of Georgia (Athens, GA, USA), for immunohistochemistry to detect influenza A by using an influenza A virus polyclonal antibody (Abcam, https://www.abcam.com). Influenza A virus antigen was detected in cytoplasm of neurons and nuclei of microglial cells (Figure, panel B). We also sent scrolls of formalin-fixed paraffin-embedded cerebral tissue to the National Veterinary Services Laboratories (Ames, IA, USA), for molecular confirmation and virus genome characterization. HPAI virus genotype A3, a fully Eurasian influenza virus, was identified; this genotype was initially detected in Alaska in April 2022 and was the most frequently detected genotype in Alaska during August–December 2023. Reported markers for mammal adaptation were not identified. We deposited full genome sequences for the polar bear virus (A/polar bear/Alaska/23–0381234/2023) in GenBank (accession nos. PP820319–26) and GISAID (https://www.gisaid.org; accession no. EPI_ISL_18976667).

This detection of HPAI virus was in the southern Beaufort Sea subpopulation, 1 of 19 circumpolar polar bear subpopulations. During July–August 2023, three short-tailed shearwater seabirds (*Ardenna tenuirostris*) that tested positive for HPAI H5N1 clade 2.3.4.4b were found dead near Point Barrow, where the polar bear in this study was found. The shearwaters' virus genotype shared 9 common single-nucleotide polymorphisms (SNPs) with the polar bear virus and was representative of the virus circulating in that area at the time rather than a direct source of the polar bear infection. In addition, in August 2023, a small mortality event from avian influenza occurred among common murre seabirds (*Uria aalge*) in Dillingham Census Area in Alaska; that virus genotype also shared 8–9 common SNPs, further supporting regional virus circulation. Polar bears are primarily dependent on seals as a food source but will prey on birds and eggs; thus, virus exposure from consumption of infected birds is possible, but infection via an olfactory route cannot be excluded (*8*).

Support does not exist for ongoing HPAI virus–associated illness and death in free-ranging polar bears in Alaska's North Slope Borough; in 2023, swab specimens from 3 other dead polar bears tested negative for influenza virus by PCR (Appendix, https://wwwnc.cdc.gov/EID/article/30/8/24-0481-App1.pdf). As for black bears with HPAI H5N1 virus infections (*9*), brain lesions were the major histopathologic findings in this case. It is not unexpected for clade 2.3.4.4b virus–infected mammals with neurologic signs to have respiratory samples test negative (*10*), possibly because of different exposure routes, such as digestive, olfactory, or respiratory routes (*8*). The HPAI H5 goose/Guangdong lineage has been shown to be more neuropatho-

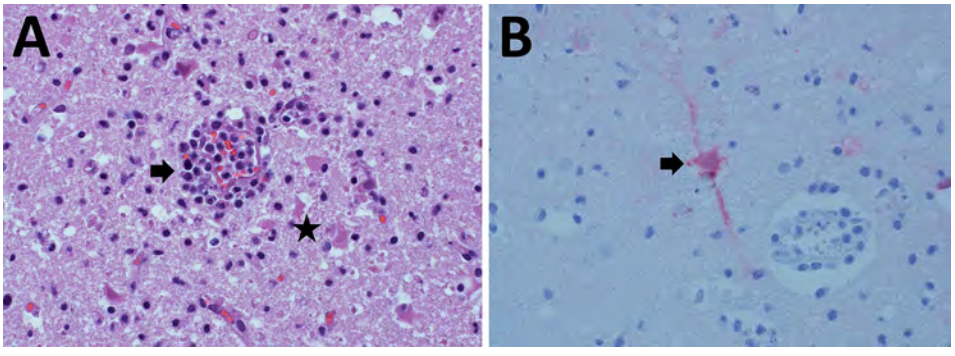

Figure. Histologic analysis of brain tissue from a dead free-ranging polar bear infected with highly pathogenic avian influenza virus A(H5N1) clade 2.3.4.4b, Alaska, USA. A) Hematoxylin and eosin staining of brain tissue section showing meningoencephalitis. Arrow indicates mixed inflammatory cells within and around blood vessels and hypertrophied vascular endothelial cells. Star indicates necrotic neurons and increased number of microglial cells within the parenchyma. Original magnification ×400. B) Arrow indicates influenza A virus within the neuronal perikaryon (red staining) observed by immunohistochemistry of formalin-fixed paraffin-embedded brain sections. Original magnification ×400.

genic than other influenza A viruses in mammals (*8*), including the H5N1 clade 2.3.4.4b virus (*11*,*12*).

Other notable findings in this case were pulmonary edema, lipid pneumonia, and ulcerative skin lesions. Pulmonary edema as a gross lesion and on histologic analysis was a consistent finding in 3 domestic cats with H5N1 clade 2.3.4.4b infections (*13*) but has been infrequently reported in wild mesocarnivores (*10*). Lipid pneumonia was documented in subsistence-harvested polar bears in the southern Beaufort Sea and is considered unrelated (D. Rotstein, unpub. data). Ulcerative skin lesions not caused by trauma are rarely documented in subsistence-harvested southern Beaufort Sea polar bears (R. Stimmelmayr, unpub. data); those lesions have not been reported in terrestrial mammals infected with the H5 clade 2.3.4.4b lineage (*10*) but have been reported in pinnipeds infected with H3N8 virus (*14*).

Conclusions

Genome analysis of influenza viruses originating from wildlife in Alaska has shown both unreassorted and reassorted viruses. HPAI virus genotype A3 was likely introduced into Alaska via the East Asia–Australia Flyway as early as November 2021 (*15*) and has been detected in a few backyard premises; in many wild birds, including California condors (*Gymnogyps californianus*) in Arizona; and several mammals (red fox, fishers, martens, racoons, and brown bears) along the Pacific Flyway.

In the Arctic, wildlife and other wild subsistence foods play a pivotal role in the health, well-being, and food security of northern indigenous communities. Therefore, subsistence harvesting of animals infected with HPAI viruses, including polar bears, poses a zoonotic risk and affects traditional food safety and food security. Continued community and hunter-based participation in wildlife health surveillance is key to detecting emerging pathogens and other One Health issues in the Arctic.

Acknowledgments

We thank the hunters and communities in the North Slope Borough who keep us informed about what they see when traveling the ocean and land; all of our subsistence and wildlife research assistant staff, as well as department leadership for their continued support of the NSB DWM wildlife health research program; Hon Ip for his support during the investigation; Histology Pathology Services for their slide preparation and rapid responsiveness; and staff in the Histology Laboratory in the Department of Pathology at the University of Georgia College of Veterinary Medicine for their immunohistochemistry expertise.

Marine mammal tissues were collected under US Fish and Wildlife Service (permit no. MA80164B-0).

The findings and conclusions in this publication are those of the authors and should not be construed to represent any official US Department of Agriculture or US Government determination or policy.

About the Author

Dr. Stimmelmayr is a wildlife veterinarian and research biologist with the North Slope Borough Department of Wildlife Management in Utqiagvik, Alaska. Her research interests focus on marine and terrestrial wildlife health and diseases within a One Health context of indigenous circumpolar hunting societies.

References

1. US Department of Agriculture, Animal and Plant Health Inspection Service. Detections of highly pathogenic avian influenza in mammals [cited 2024 Feb 12]. https://www.aphis.usda.gov/livestock-poultry-disease/avian/avian-influenza/hpai-detections/mammals
2. Boedeker NC, Nelson MI, Killian ML, Torchetti MK, Barthel T, Murray S. Pandemic (H1N1) 2009 influenza A virus infection associated with respiratory signs in sloth bears (*Melursus ursinus*). Zoonoses Public Health. 2017;64:566–71. https://doi.org/10.1111/zph.12370
3. Bessière P, Gaide N, Croville G, Crispo M, Fusade-Boyer M, Abou Monsef Y, et al. High pathogenicity avian influenza A(H5N1) clade 2.3.4.4b virus infection in a captive Tibetan black bear (*Ursus thibetanus*): investigations based on paraffin-embedded tissues, France, 2022. Microbiol Spectr. 2024;12:e0373623. https://doi.org/10.1128/spectrum.03736-23
4. Li D, Zhu L, Cui H, Ling S, Fan S, Yu Z, et al. Influenza A(H1N1)pdm09 virus infection in giant pandas, China. Emerg Infect Dis. 2014;20:480–3. https://doi.org/10.3201/eid2003.131531
5. Naidenko SV, Ivanov EA, Mordvintsev IN, Platonov NG, Ershov RV, Rozhnov VV. Seropositivity for different pathogens in polar bears (*Ursus maritimus*) from Barents Sea Islands. Biol Bull Russ Acad Sci. 2013;40:779–82. https://doi.org/10.1134/S1062359013090082
6. Ramey AM, Cleveland CA, Hilderbrand GV, Joly K, Gustine DD, Mangipane B, et al. Exposure of Alaska brown bears (*Ursus arctos*) to bacterial, viral, and parasitic agents varies spatiotemporally and may be influenced by age. J Wildl Dis. 2019;55:576–88. https://doi.org/10.7589/2018-07-173
7. Hemert CV, Spivey TJ, Uher-Koch BD, Atwood TC, Sinnett DR, Meixell BW, et al. Survey of Arctic Alaskan wildlife for influenza A antibodies: limited evidence for exposure of mammals. J Wildl Dis. 2019;55:387–98. https://doi.org/10.7589/2018-05-128
8. Bauer L, Benavides FFW, Veldhuis Kroeze EJB, de Wit E, van Riel D. The neuropathogenesis of highly pathogenic avian influenza H5Nx viruses in mammalian species including humans. Trends Neurosci. 2023;46:953–70. https://doi.org/10.1016/j.tins.2023.08.002
9. Jakobek BT, Berhane Y, Nadeau MS, Embury-Hyatt C, Lung O, Xu W, et al. Influenza A(H5N1) virus infections in 2

free-ranging black bears (*Ursus americanus*), Quebec, Canada. Emerg Infect Dis. 2023;29:2145–9. https://doi.org/10.3201/eid2910.230548
10. Elsmo EJ, Wünschmann A, Beckmen KB, Broughton-Neiswanger LE, Buckles EL, Ellis J, et al. Highly pathogenic avian influenza A(H5N1) virus clade 2.3.4.4b infections in wild terrestrial mammals, United States, 2022. Emerg Infect Dis. 2023;29:2451–60. https://doi.org/10.3201/eid2912.230464
11. Alkie TN, Cox S, Embury-Hyatt C, Stevens B, Pople N, Pybus MJ, et al. Characterization of neurotropic HPAI H5N1 viruses with novel genome constellations and mammalian adaptive mutations in free-living mesocarnivores in Canada. Emerg Microbes Infect. 2023;12:2186608. https://doi.org/10.1080/22221751.2023.2186608
12. Bordes L, Vreman S, Heutink R, Roose M, Venema S, Pritz-Verschuren SBE, et al. Highly pathogenic avian influenza H5N1 virus infections in wild red foxes (*Vulpes vulpes*) show neurotropism and adaptive virus mutations. Microbiol Spectr. 2023;11:e0286722. https://doi.org/10.1128/spectrum.02867-22
13. Sillman SJ, Drozd M, Loy D, Harris SP. Naturally occurring highly pathogenic avian influenza virus H5N1 clade 2.3.4.4b infection in three domestic cats in North America during 2023. J Comp Pathol. 2023;205:17–23. https://doi.org/10.1016/j.jcpa.2023.07.001
14. Anthony SJ, St Leger JA, Pugliares K, Ip HS, Chan JM, Carpenter ZW, et al. Emergence of fatal avian influenza in New England harbor seals. mBio. 2012;3:e00166–12. https://doi.org/10.1128/mBio.00166-12
15. Youk S, Torchetti MK, Lantz K, Lenoch JB, Killian ML, Leyson C, et al. H5N1 highly pathogenic avian influenza clade 2.3.4.4b in wild and domestic birds: introductions into the United States and reassortments, December 2021–April 2022. Virology. 2023;587:109860. https://doi.org/10.1016/j.virol.2023.109860

Address for correspondence: Raphaela Stimmelmayr, North Slope Borough, Department of Wildlife Management, PO Box 69, Ahkovak St 1795, Utqiagvik, AK 99723, USA; email: raphaela.stimmelmayr@north-slope.org

etymologia

Microbiota [mī′′-krō-bī′-ō-′tə], microbiome [mī′′-krō-bī′-ōm]

Julia Memrava Cabrera, Daniel F.M. Monte

From the Greek micro- (small) and -bios (life), microbiota was coined in the late 19th Century to denote the microorganisms residing in a specific environment. During the 20th Century, microbiota became more specifically associated with the microorganisms inhabiting the human body. Today, the term encompasses the collective genetic material of microorganisms, spanning viruses, archaea, bacteria, and fungi, and the intricate ecosystems of microorganisms, including commensal, symbiotic, and pathogenic ones, that exist within or on the human body or other environmental niches. Exploring microbiota and its implications in various aspects has rapidly gained momentum as a dynamic field of research.

The term microbiome was defined by Whipps and colleagues in 1988 as the collective genomes of microorganisms. However, Joshua Lederberg (Figure), a US molecular biologist, played a pivotal role in coining the term as we know it today. His journey from a precocious young scientist to a Nobel laureate and advocate for ethical science reflects the interconnectedness of language, curiosity, and scientific discovery. Lederberg's fascination with science also extended to writing science fiction, using the genre to explore complex scientific concepts through imaginative storytelling. In fact, microbiome is a combination of microbe and biome (bi- [life] + -ome [mass]) to describe the microbial ecosystem, which encompasses not only genomes but also the broader microbial environment. Microbiome, born from the fusion of linguistic roots and a thirst for knowledge, continues to shape our understanding of the microbial world and its profound impact on human health and biology.

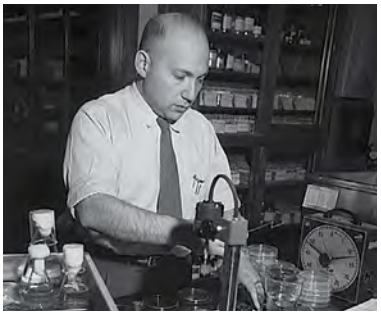

Figure. Molecular biologist and Nobel laureate Joshua Lederberg in his laboratory in Wisconsin, 1958. Dr. Lederberg played a pivotal role in coining the term microbiome as we know it today. Public domain image from the National Library of Medicine.

Sources

1. Dorland's illustrated medical dictionary. 32nd ed. Philadelphia: Elsevier Saunders; 2012.
2. Berg G, Rybakova D, Fischer D, Cernava T, Vergès MC, Charles T, et al. Microbiome definition re-visited: old concepts and new challenges. Microbiome. 2020;8:103. https://doi.org/10.1186/s40168-020-00875-0
3. Lederberg J, Mccray AT. 'Ome sweet 'omics—a genealogical treasury of words. Scientist. 2001;15:8–9.
4. Liu X. Microbiome. Yale J Biol Med. 2016;89:275–6.
5. Marchesi JR, Ravel J. The vocabulary of microbiome research: a proposal. Microbiome. 2015;3:31. https://doi.org/10.1186/s40168-015-0094-5

Address for correspondence: Daniel F.M. Monte, Department of Animal Science, College for Agricultural Sciences, Federal University of Paraiba, Areia, 58397000, Brazil; email: monte_dfm@alumni.usp.br

DOI: https://doi.org/10.3201/eid3008.230677

Rustrela Virus in Wild Mountain Lion (*Puma concolor*) with Staggering Disease, Colorado, USA

Karen A. Fox, Angele Breithaupt, Martin Beer, Dennis Rubbenstroth, Florian Pfaff

We identified a rustrela virus variant in a wild mountain lion (*Puma concolor*) in Colorado, USA. The animal had clinical signs and histologic lesions compatible with staggering disease. Considering its wide host range in Europe, rustrela virus should be considered as a cause for neurologic diseases among mammal species in North America.

On May 12, 2023, Colorado Parks and Wildlife (Denver, CO, USA) received a report of an ≈1-year-old free-ranging female mountain lion (*Puma concolor*) with signs of severe hind leg ataxia and paresis. The lion had been observed in a residential area of Douglas County, Colorado, USA (Appendix Figure 1, https://wwwnc.cdc.gov/EID/article/30/8/24-0411-App1.pdf). The animal was reluctant to rise and had markedly decreased capacity to move or bear weight on the hind end (Video, https://wwwnc.cdc.gov/EID/article/30/8/24-0411-V.htm). The animal appeared depressed but was still responsive to stimuli. Wildlife officers tranquilized the animal and then euthanized it by gunshot to the chest to prevent destruction of neurologic tissues. We conducted a postmortem investigation including necropsy, histopathology, immunohistochemistry, molecular diagnostics, and metatranscriptome sequencing to investigate potential causes of the disease.

The Study

Prenecropsy radiology revealed no skeletal abnormalities to explain the clinical signs observed. Necropsy results indicated poor body condition and mild bruising at the torso and limbs. The stomach contained only pine needles. Histopathology demonstrated severe nonsuppurative meningoencephalomyelitis (Appendix). The leptomeninges were multifocally and markedly expanded by lymphocytes and histiocytes in both brain and spinal cord (Figure 1). Virchow-Robin perivascular spaces were expanded by dense cuffs of lymphocytic to lymphohistiocytic infiltrates up to 20 cell layers thick in nearly all regions of the brain (Figure 1, panels A–C) and spinal cord. Inflammation was largely restricted to the leptomeninges and gray matter, and only minimal in the white matter (Figure 1, panels A, B). Affected sections also demonstrated scattered neuronal necrosis, gliosis, and loose glial nodules (Figure 1, panels B, E, G), partially leading to an irregular architecture (Figure 1, panel G). The cerebellar cortex showed no indication of inflammation or degenerative process (Figure 1, panel I)

Initial diagnostic tests did not detect feline panleukopenia virus, canine distemper virus, West Nile virus, *Toxoplasma gondii*, influenza A virus, rabies virus, or feline infectious peritonitis virus in the central nervous system (Appendix Table 1). We used pooled brain and spinal cord tissue to extract total RNA (Appendix), then conducted metatranscriptome sequencing to obtain sequence fragments (reads). We used those fragments to de novo assemble a single contiguous sequence (contig) with homology to known sequences of rustrela virus (RusV). The contig represented the whole viral genome and matched RusV reference strains. We submitted the annotated RusV genome sequence to the International Nucleotide Sequence Database Collaboration (https://www.insdc.org; accession no. PP025855).

We adapted real-time reverse transcription PCR primers and probe for RusV (*1*) by using degenerate bases for consensus homology to the Colorado mountain lion–derived sequence and European RusV sequences (Appendix Table 2). Those adapted methods

Author affiliations: Colorado State University College of Veterinary Medicine and Biomedical Sciences, Fort Collins, Colorado, USA (K.A. Fox); Colorado Parks and Wildlife, Fort Collins (K.A. Fox); Friedrich-Loeffler-Institut, Greifswald-Insel Riems, Germany (A. Breithaupt); Institute of Diagnostic Virology, Friedrich-Loeffler-Institut, Greifswald-Insel Riems (M. Beer, D. Rubbenstroth, F. Pfaff)

DOI: https://doi.org/10.3201/eid3008.240411

showed RusV RNA in a pooled sample of brain and spinal cord from the mountain lion, with a cycle threshold value of 20.3.

RusV (*Rubivirus strelense*), a member of the family *Matonaviridae*, was recently identified as the cause of staggering disease (*1*), a usually fatal neurologic syndrome in cats. Since the 1970s, staggering disease has been documented in domestic cats in Europe, predominantly in Sweden and Austria (*2*–*6*). Affected cats show a consistent combination of histologic lesions and clinical signs, including hind limb ataxia or paresis, and nonsuppurative meningoencephalitis

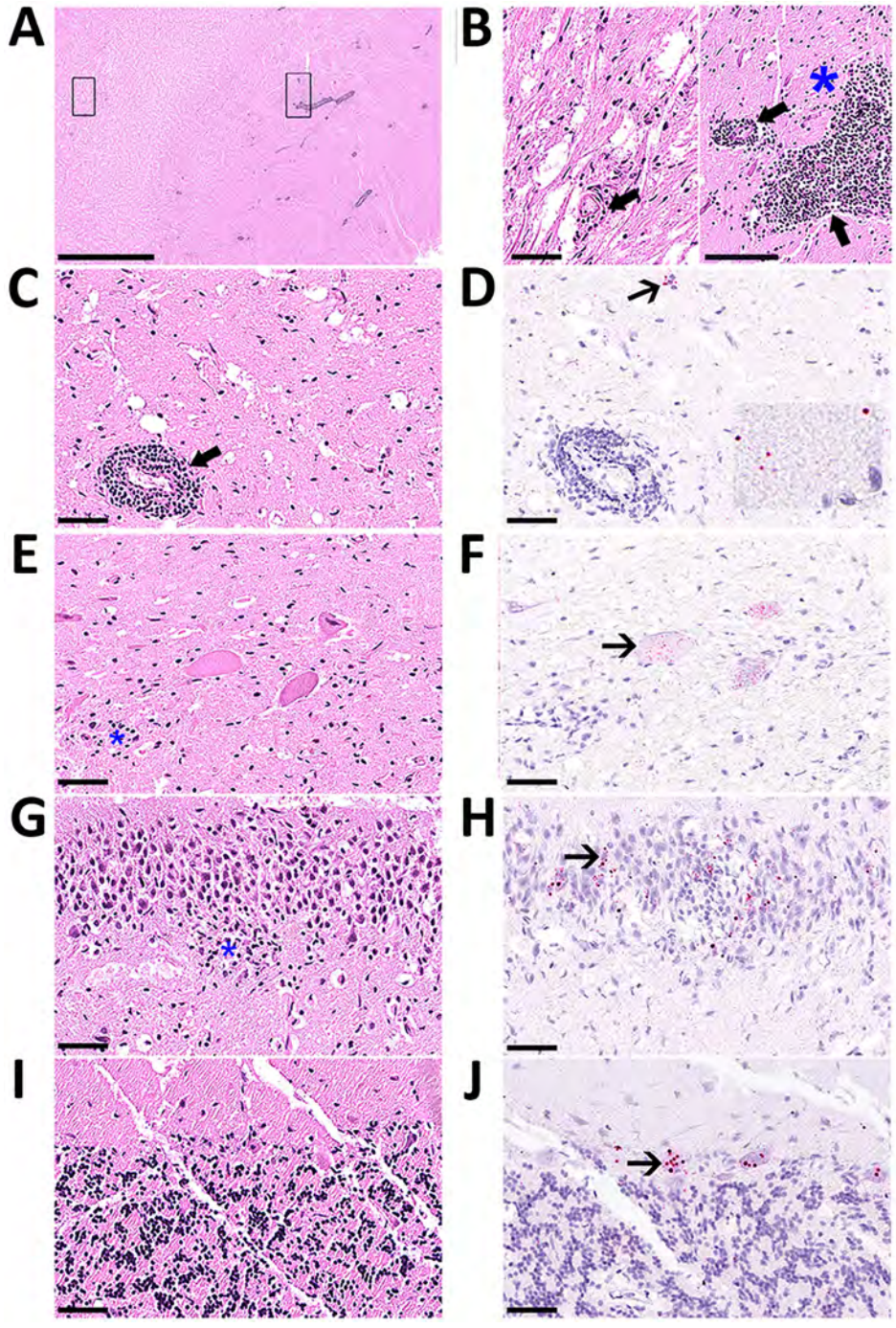

Figure 1. Histology of brain and spinal cord used to detect rustrela virus (RusV) in wild mountain lion (*Puma concolor*) with staggering disease, Colorado, USA. RusV RNA was detected by RNAscope Reagent Kit-Red (Advanced Cell Diagnostics/bio-techne, https://www.bio-techne.com) in situ hybridization**.** All sections demonstrate artifactual clefting of the neuropil due to freezing of the tissue postmortem. A) Cerebral cortex with perivascular cuffing and mild gliosis of the white and gray matter; boxes indicate detailed areas in panel B. Scale bar indicates 2.5 mm. B) The white matter (left panel) is minimally affected by perivascular lymphohistiocytic infiltrates (bold arrow), compared with the gray matter (right panel), also showing gliosis (asterisk). Scale bar indicates 100 µm. C) Midbrain affected by perivascular cuffing. Scale bar indicates 50 µm. D) Midbrain showing chromogenic labeling (fast red) of RusV in neuronal cell bodies (slender arrow) and in the neuropil (inlay). Scale bar indicates 50 µm. E) Spinal cord with 3 motor neurons showing variable degree of degeneration/necrosis and also gliosis (asterisk). Scale bar indicates 50 µm. F) Spinal cord with affected motor neurons with RusV RNA detection. Scale bar indicates 50 µm. G) Hippocampus exhibiting irregular architecture of the granule layer and gliosis (asterisk). Scale bar indicates 50 µm. H) Hippocampus with numerous RusV RNA signals in neurons of the granule cell layer in areas with or without irregular architecture. Scale bar indicates 50 µm. I) Cerebellum, no indication for inflammation or any degenerative process. Scale bar indicates 50 µm. J) Cerebellum with abundant RusV RNA labeling in Purkinje cells. Scale bar indicates 50 µm. A–C, E, G, I) Hematoxylin-eosin staining; D, F, H, I) RNAscope in situ hybridization with probes against the nonstructural protein–coding region of RusV, counterstained with Mayer's hematoxylin.

restricted to the gray matter but not affecting white matter or the cerebellar cortex (*1*,*4*,*5*). A similar syndrome was reported in cats from Alabama, USA, in 1979 but the etiology remained obscure (*7*). In Germany, RusV has been detected in a broad range of zoo animals with neurologic disorders, including lions (*Panthera leo*) (*8*–*11*).

Because initial diagnostic tests were negative in this case, and history, histopathology, and metatranscriptome sequencing suggested staggering disease, we sent tissue samples and sequence data from the mountain lion to the Friedrich-Loeffler-Institut (Greifswald-Insel Riems, Germany) for additional analyses. To demonstrate an association between the lesions and the virus, we used previously developed in situ hybridization methods for RusV (*1*,*6*) (Appendix), which demonstrated RusV RNA in all regions of the brain and nearly all levels of the spinal cord, irrespective of an inflammatory reaction. Only lumbosacral nerve roots (cauda equina) tested negative. RusV-specific RNA localized in neuronal cell bodies (Figure 1, panels D, F, H, J), disseminated within the neuropil of the gray matter (Figure 1, panel D, inlay) and, to a lesser extent, in the white matter. We found particularly abundant or large, dot-like signals in the granule cell layer of the hippocampus (Figure 1, panel H), and in Purkinje cells of the cerebellum (Figure 1, panel J), similar to findings from staggering disease cases in cats from Europe (*4*).

The overall architecture of the viral genome of the novel RusV from Colorado matched those of known RusV (Appendix Figure 2). The mean pairwise nucleotide identity between the novel RusV sequence and sequences from Germany was 69.9% and between sequences from Austria and Sweden was 68.9%; the sequences from Europe shared 76.7% identity among each other (Figure 2, panel A). The mean pairwise amino acid identities of the nonstructural and structural polyproteins ranged from 75.6% to 78.1% between the novel RusV sequence and the sequences from Europe (Figure 2, panel A). The genetic diversity was not equally distributed over the genome; part of the protease and the intergenic region showed especially high levels of sequence variations (Appendix Figure 2).

We performed phylogenetic analysis to compare the RusV sequence from Colorado with appropriate reference strains using an amino acid alignment of the structural polyprotein (Appendix). Those findings suggested classification of the novel RusV as a member of the family *Matonaviridae*, genus *Rubivirus*, placing it basal to the known RusV sequences detected in Germany, Sweden, and Austria (Figure 2, panel B). The basal position of the novel RusV in relation to all other known RusV is also supported by phylogeny based on the whole-genome nucleotide sequence (Appendix Figure 3).

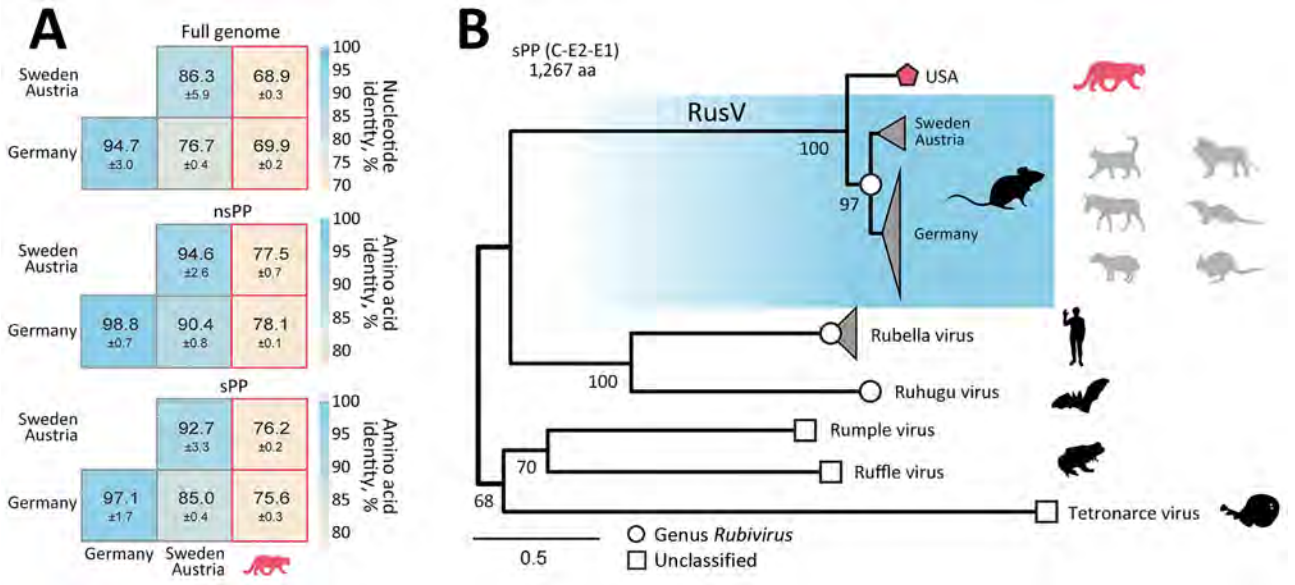

Figure 2. Sequence similarity and phylogenetic position of RusV in wild mountain lion (*Puma concolor*) with staggering disease, Colorado, USA. A) Mean pairwise sequence identity between the novel Colorado RusV and RusV sequences from Germany, Austria, and Sweden. Pairwise identity was based on nucleotide sequence alignments of the full genome or amino acid alignments of the nsPP and sPP. B) The sPP amino acid sequences of appropriate references from rubiviruses (circle) or currently unclassified matonavirids (square) were aligned with the novel RusV (pentagon). Phylogenetic tree was calculated using IQ-TREE (http://www.iqtree.org). Host species are depicted as silhouettes. For RusV, the potential reservoir (dark) and spillover hosts (light) are depicted. Scale bar indicates substitutions per site. nsPP, nonstructural polyprotein; sPP, structural polyprotein.

Conclusions

Our results demonstrate the presence of a RusV variant in North America that is divergent from those previously described from Europe. The clinical signs, histologic lesions, and infected target cells observed for the wild mountain lion in Colorado, USA, meet the case definition for staggering disease. A causative role for RusV is likely, further supporting previous work identifying RusV as the causative agent of staggering disease in domestic cats from Austria, Sweden, and Germany (*1*,*6*), and in lions from zoologic collections in Germany (*10*).

This report is limited to a single case of staggering disease in Colorado. To determine whether RusV is enzootic in this region, we recommend further investigations, including retrospective RusV testing of tissues from feline encephalitis cases of unknown causes in North America. Surveillance for RusV in small rodents might identify a local reservoir host because rodents of the genus *Apodemus* have been identified as likely RusV reservoir hosts in Europe through real-time reverse transcription PCR and sequencing of mice brain tissues (*1*,*8*,*9*,*12*,*13*). Although *Apodemus* mice are not indigenous to North America, several genera of small rodents are found throughout Colorado (*14*,*15*) and could serve as candidates for further screenings. In addition, future studies should consider that the zoonotic potential of RusV has not been determined.

Of note, a remarkably broad range of other mammalian RusV hosts has been identified in Germany, including equids, mustelids, rodents, and marsupials (*8*,*9*,*11*,*12*), raising concerns about a zoonotic potential of RusV (*8*,*9*). Given the wide host range of the virus in Europe, RusV should be considered as a possible cause for neurologic diseases in all mammal species in North America.

Acknowledgments

We thank Melanie Kaknes and Matt Martinez for submitting this case, Erica Rhinehart for providing video footage, Dan Tripp for advice on small mammal populations in Colorado, and Robin Brandt for pathology technical assistance.

About the Author

Dr. Fox is a veterinary anatomic pathologist at the Colorado State University Veterinary Diagnostic Laboratories. Her research interests include identification of emerging disease syndromes in Colorado wildlife and development of diagnostic strategies to inform wildlife management.

References

1. Matiasek K, Pfaff F, Weissenböck H, Wylezich C, Kolodziejek J, Tengstrand S, et al. Mystery of fatal 'staggering disease' unravelled: novel rustrela virus causes severe meningoencephalomyelitis in domestic cats. Nat Commun. 2023;14:624. https://doi.org/10.1038/s41467-023-36204-w
2. Lundgren A-L. Feline non-suppurative meningoencephalomyelitis. A clinical and pathological study. J Comp Pathol. 1992;107:411–25. https://doi.org/10.1016/0021-9975(92)90015-M
3. Kronevi T, Nordström M, Moreno W, Nilsson PO. Feline ataxia due to nonsuppurative meningoencephalomyelitis of unknown aetiology. Nord Vet Med. 1974;26:720–5.
4. Weissenböck H, Nowotny N, Zoher J. Feline meningoencephalomyelitis ("staggering disease") [in Austrian]. Wien Tierarztl Monatsschr. 1994;81:195–201.
5. Nowotny N, Weissenböck H. Description of feline nonsuppurative meningoencephalomyelitis ("staggering disease") and studies of its etiology. J Clin Microbiol. 1995;33:1668–9. https://doi.org/10.1128/jcm.33.6.1668-1669.1995
6. Weiss V, Weidinger P, Matt J, Weissenbacher-Lang C, Nowotny N, Weissenböck H. Rustrela virus-associated encephalomyelitis ('staggering disease') in cats from eastern Austria, 1994–2016. Viruses. 2023;15:1621. https://doi.org/10.3390/v15081621
7. Vandevelde M, Braund KG. Polioencephalomyelitis in cats. Vet Pathol. 1979;16:420–7. https://doi.org/10.1177/030098587901600404
8. Bennett AJ, Paskey AC, Ebinger A, Pfaff F, Priemer G, Höper D, et al. Author correction: relatives of rubella virus in diverse mammals. Nature. 2020;588:E2. https://doi.org/10.1038/s41586-020-2897-1
9. Bennett AJ, Paskey AC, Ebinger A, Pfaff F, Priemer G, Höper D, et al. Relatives of rubella virus in diverse mammals. Nature. 2020;586:424–8. https://doi.org/10.1038/s41586-020-2812-9
10. de le Roi M, Puff C, Wohlsein P, Pfaff F, Beer M, Baumgärtner W, et al. Rustrela virus as putative cause of nonsuppurative meningoencephalitis in lions. Emerg Infect Dis. 2023;29:1042–5. https://doi.org/10.3201/eid2905.230172
11. Voss A, Schlieben P, Gerst S, Wylezich C, Pfaff F, Langner C, et al. Rustrela virus infection—an emerging neuropathogen of red-necked wallabies (*Macropus rufogriseus*). Transbound Emerg Dis. 2022;69:4016–21. https://doi.org/10.1111/tbed.14708
12. Pfaff F, Breithaupt A, Rubbenstroth D, Nippert S, Baumbach C, Gerst S, et al. Revisiting rustrela virus: new cases of encephalitis and a solution to the capsid enigma. Microbiol Spectr. 2022;10:e0010322. https://doi.org/10.1128/spectrum.00103-22
13. Nippert S, Rubbenstroth D, Geers JA, Ebinger A, Hoffmann D, Breithaupt A, et al. Continuous presence of genetically diverse rustrela virus lineages in yellow-necked field mouse reservoir populations in northeastern Germany. Virus Evol. 2023;9:vead048. https://doi.org/10.1093/ve/vead048
14. Armstrong DM, Fitzgerald JP, Meaney CA. Mammals of Colorado. 2nd ed. Boulder (CO): University Press of Colorado; 2011.
15. Armstrong DM. Rocky Mountain Mammals. 3rd ed. Boulder (CO): University Press of Colorado; 2008.

Address for correspondence: Karen A. Fox, Colorado State University Veterinary Diagnostic Laboratories, 2450 Gillette Dr, 1644 Campus Delivery, Fort Collins, CO 80526, USA; email: 661karen.fox@colostate.edu

Hepatitis B Virus Reactivation after Switch to Cabotegravir/Rilpivirine in Patient with Low Hepatitis B Surface Antibody

Eisuke Adachi,[1] Ayako Sedohara,[1] Kotaro Arizono, Kazuaki Takahashi, Amato Otani, Yoshiaki Kanno, Makoto Saito, Michiko Koga, Hiroshi Yotsuyanagi

A patient in Japan with HIV began antiretroviral therapy because of acute hepatitis B virus (HBV) 15 years ago, with low hepatitis B surface antibody, and experienced breakthrough HBV reactivation 4 months after switching from bictegravir/emtricitabine/tenofovir alafenamide to cabotegravir/rilpivirine. An immune escape mutation, E164V, was identified in the isolated HBV DNA.

The 2013 guidelines outlined by the Centers for Disease Control and Prevention indicate in cases where hepatitis B surface antibody (anti-HBs) titers fall below the cut off value of 10.0 mIU/mL, administration of booster vaccinations is generally not required, barring certain exceptions, such as immunocompromised persons (*1*). This recommendation is based on the understanding that exposure to hepatitis B virus (HBV) typically triggers B lymphocytes, culminating in the production of adequate antibody levels within a short timeframe. However, the effectiveness of this antibody response following HBV exposure depends on the persons immune status. The primary goal in managing chronic hepatitis B is to achieve an undetectable hepatitis B surface antigen (HBsAg) level. Cases where seroconversion from HBsAg to anti-HBs occurs is considered a functional cure, although, the risk for de novo reactivation persists and is not eliminated (*2*).

Isolated hepatitis B core antibody (anti-HBc) positivity, defined as antigen negative, anti-HBs negative, and anti-HBc positive, is considered a risk factor for occult HBV infection (*3*) and de novo HBV reactivation (*4*), indicating 2 distinct pathogenic pathways. The first scenario involves HBsAg negativity resulting from treatment or spontaneous resolution, without subsequent seroconversion to anti-HBs. The second scenario occurs when anti-HBs levels decline below the threshold of detection after initially testing positive. When anti-HBs levels decline, exposure-induced boosting is expected to provide a preventive effect.

We describe the case of a patient with HIV whose anti-HBs titers declined below the threshold of detection after an initial confirmation of anti-HBs positivity. The patient's medications were changed from bictegravir/emtricitabine/tenofovir alafenamide (B/F/TAF) to cabotegravir/rilpivirine (CAB/RPV). His HBsAg positivity recurred, and he reverted to being an HBV carrier.

Ethics approval was granted by the ethics board of the Institute of Medical Science, University of Tokyo (approval no. 2022-48-1128). The patient gave consent for publication in accordance with the policies of Emerging Infectious Diseases and the International Committee of Medical Journal Editors.

The Case

A 52-year-old man with HIV had contracted an acute HBV infection 15 years earlier. Antiretroviral therapy (ART) consisting of tenofovir disoproxil fumarate/emtricitabine (TDF/FTC) and lopinavir/ritonavir (LPV/RTV) was initiated at the time, and the acute hepatitis rapidly improved. The patient's liver enzymes normalized 2 months after beginning ART, and he tested negative for HBV DNA and HBsAg 4 months after beginning ART (Table 1). Anti-HBs titers were detected at 2.03 IU/mL 9 months after beginning ART, and it was believed that his acute

Author affiliation: The University of Tokyo, Tokyo, Japan

DOI: https://doi.org/10.3201/eid3008.240019

[1]These first authors contributed equally to this article.

Table 1. Laboratory values over time of a person in Japan with HIV after diagnosis of an acute HBV infection, from diagnosis to 12 years*

	Time from HBV diagnosis							
Category	0 mo	1 mo	3 mo	9 mo	5 y	6 y	8 y	12 y
ART regimen	NA	TDF/FTC+LPV/RTV	TDF/FTC	TDF/FTC	TDF/FTC	TDF/FTC	TDF/FTC	B/F/TAF
Laboratory values								
Anti-HBs, IU/mL†	20.8	0.00	N/A	2.03	N/A	18.6	8.55	9.34
HBsAg, mIU/mL‡	119,533	68,065	552	0.00	0.00	0.00	0.00	0.00
Anti-HBe, inhibition %§	Negative	Negative	Negative	Negative	Negative	NA	NA	NA
HBeAg, S/CO¶	1,840	1,290	2.5	Negative	Negative	NA	NA	NA
HBV DNA, log copies/mL	>8.8	6.8	3.8	ND	ND	ND	NA	ND
ALT, U/L	418	937	8	17	23	17	57	66
Total bilirubin, mg/dL	0.3	0.5	0.5	0.5	0.7	0.3	0.4	0.4
HBcrAg, log U/mL#	NA	NA	NA	NA	NA	NA	NA	Negative

*ALT, alanine aminotransferase; anti-HBe, hepatitis B e-antibody; anti-HBs, hepatitis B surface antibody; ART, antiretroviral therapy; B/F/TAF, bictegravir/emtricitabine/tenofovir alafenamide; HBcrAg, hepatitis B core-related antigen; HBeAg, hepatitis B e-antigen; HBsAg, hepatitis B surface antigen; HBV, hepatitis B virus; LPV/RTV, lopinavir/ritonavir; mIU, milli-IU; NA, not applicable; ND, not detected; RPV, rilpivirine; S/CO, signal-to-cutoff ratio; TDF/FTC, tenofovir disoproxil fumarate/emtricitabine.
†Cutoff value 10 IU/mL.
‡Cutoff value 10 mIU/mL.
§Cutoff value 50% inhibition.
¶Cutoff value 1.0 S/CO.
#Cutoff value 3.0 log U/mL.

hepatitis B did not transition into a chronic HBV infection. His anti-HBs titers were again detected at 18.6 IU/mL 6 years after the initial diagnosis of the acute HBV infection. There was no reactivation of HBV while on stable ART containing TDF/FTC or TAF/FTC. Two years after the confirmation of seroconversion, his anti-HBs levels decreased below the cutoff value but remained around 8.0 mIU/mL. He tested positive for anti-HBc.

After 14 years of ART, the patient expressed a preference to change to a long-acting injectable ART. We considered 3 additional factors before making this medication change: the patient did not become an HBV carrier after his acute hepatitis B diagnosis, his HBsAg and his HBV DNA had remained undetectable for >10 years, and his anti-HBs had declined only after initial positive confirmation. His hepatitis B core-related antigen, which is shown to remain positive longer than HBsAg and HBV DNA in acute hepatitis B infections (*5*,*6*), was negative. After a 1-month lead-in with oral CAB/RPV, his ART was changed to an injectable CAB/RPV.

The patient's liver enzyme levels increased to alanine aminotransferase (ALT) 103 U/L (reference range 4–44 U/L) 4 months after switching to CAB/RPV. Both his HBsAg and HBV DNA tested positive again, while the level of anti-HBs decreased to nearly zero (Table 2). The probability of reinfection with a novel HBV strain was considered low because his sexual partner was on ART containing tenofovir during this period and the patient denied any other potential exposures. The patient's CD4 count was 512

Table 2. Laboratory values over time of a person in Japan with HIV 2 years before changing ART regimen to CAB/RPV and the period while on CAB/RPV, showing HBV reactivation in month 4*

	Time from ART change								
Category	–2 y	0 mo	1 mo	2 mo	4 mo	6 mo	8 mo	10 mo	14 mo
ART regimen	B/F/TAF	CAB/RPV oral	CAB/RPV injectable	CAB/RPV	CAB/RPV	CAB/RPV	CAB/RPV	CAB/RPV	B/F/TAF
Laboratory values									
Anti-HBs, IU/mL†	N/A	6.57	5.65	8.78	0.20	0.20	0.00	0.13	0.00
HBsAg, mIU/mL‡	0.00	0.00	0.00	0.00	816	90,332	124,890	143,785	131,765
Anti-HBe, inhibition %§	NA	NA	NA	Negative	6.16	31.1	54.4	56.0	55.3
HBeAg, S/CO¶	NA	NA	NA	Negative	60.5	404	680	835	915
HBV DNA, log copies/mL	ND	NA	NA	NA	3.9	NA	NA	NA	8.2
ALT, U/L	66	25	0	25	103	158	40	32	27
Total bilirubin, mg/dL	0.4	0.6	0.5	0.6	0.5	0.6	0.6	0.7	0.4
HBcrAg, Log U/mL#	NA	NA	Negative	NA	NA	NA	NA	NA	>7.1

*ALT, alanine aminotransferase; anti-HBe, hepatitis B e-antibody; anti-HBs, hepatitis B surface antibody; ART, antiretroviral therapy; B/F/TAF, bictegravir/emtricitabine/tenofovir alafenamide; CAB, cabotegravir; HBcrAg, hepatitis B core-related antigen; HBeAg, hepatitis B e-antigen; HBsAg, hepatitis B surface antigen; HBV, hepatitis B virus; NA, not applicable; ND, not detected; RPV, rilpivirine.
†Cutoff value 10 IU/mL.
‡Cutoff value 10 mIU/mL.
§Cutoff value 50% inhibition.
¶Cutoff value 1.0 S/CO.
#Cutoff value 3.0 log U/mL.

Table 3. Results of HBV DNA genome analysis on HBV strain isolated during hepatitis B reactivation in a person with HIV after changing antiretroviral therapy regimen to cabotegravir/rilpivirine*

Category	Region				
	S gene	P gene	Pre-S1/pre-S2/S	X gene	Precore/core
Position	155–835	2307–3221, 1–1623	2854–3221, 1–835	1374–1838	1814–2458/1901–2458
Size, bp	681	2538	1203	465	645
Mutations					
Vaccine-escape	E164V	NA	NA	NA	NA
Drug-resistant	NA	ND	NA	NA	NA
Promoter	NA	NA	NA	NA	ND
Other	NA	NA	ND	ND	T1858C,† T1674C†

*The full length of the HBV isolate was 3,221 bp. HBV, hepatitis B virus; NA, not applicable; ND, not detected.
†These mutations are typically observed in genotype A2.

cells/μL, indicating sufficient immune function. The patient's liver enzymes returned to within reference ranges 4 months later, whereas the HBsAg and HBV DNA remained elevated. The patient's ART regimen was switched to B/F/TAF 14 months after the change to CAB/RPV because of concerns of a concurrent chronic HBV infection.

We cloned 2 full-length HBV isolates and determined the genome sequences from serum samples obtained at 2 intervals: the first after 4 months of treatment with CAB/RPV, coinciding with the re-positivity of HBsAg, and the second 14 months after treatment with CAB/RPV (Appendix, https://wwwnc.cdc.gov/EID/article/30/8/24-0019-App1.pdf). Our genomic analysis revealed identical clones of genotype A2, and we observed no increases in mutations after reactivation (Table 3). Of note, E164V was identified within the S region and is recognized as a vaccine-escape mutation (Appendix Figure) (*7*). No drug resistance–associated mutations were observed in the polymerase region.

There are multiple explanations for the re-emergence of HBsAg in this case. The mostly likely explanation is our patient did not attain a functional cure of HBV. The reduction in HBsAg might have been because of ART containing TDF/FTC or TAF/FTC instead of acquired immunity against HBV, implying that anti-HBs levels were inadequate. After switching to CAB/RPV, the drugs no longer suppressed HBV. The exposure to reactivated HBV did not adequately boost the anti-HBs levels, which lead to breakthrough reactivation. Another potential explanation is a de novo reactivation of HBV independent of switching to CAB/RPV. However, we were unable to find documented cases of de novo HBV reactivation among persons on stable ART or with a stable immune status. Furthermore, whereas de novo HBV reactivation typically leads to severe hepatitis (*8*), our patient remained asymptomatic, with only a marginal elevation in transaminase levels.

E164V in the S region is known as a vaccine-escape mutation and is frequently identified in patients with occult HBV infection or de novo HBV reactivation (*9*,*10*). Cases of breakthrough infection are extremely rare worldwide, and it is not clear whether a single mutation is responsible for immune escape. In patients with occult HBV infection, escape mutations other than E164V are typically detected alongside other mutations (*10*,*11*).

HBV reactivation has been reported in patients with low CD4 counts (*12*,*13*). Cases have also been reported of HBV DNA detection at very low levels with negative HBsAg after switching to ART regimens without anti-HBV drugs (*14*). Our patient had a sufficient CD4 count for immunity and a history of anti-HBc and anti-HBs positivity, and still we found his HBV reactivated with re-emergence of HBsAg. We expect our patient will undergo the seroconversion of HBsAg again with ART containing F/TAF. Nonetheless, ART without tenofovir or lamivudine is not an option for this patient in the future.

Conclusions

Below the cutoff value, the preventive effect of anti-HBs may not be sufficient to prevent reactivation. Vaccination may be beneficial for patients with isolated anti-HBc positivity, even if their anti-HBs levels have declined since their initial anti-HBs positivity was confirmed (*15*). For many years, ART containing tenofovir or lamivudine has been widely used worldwide; however, providers are increasingly using ART regimens that do not include anti-HBV drugs. Healthcare providers must consider the potential scenario where the detection of anti-HBs might be a consequence of HBV suppression through ART containing anti-HBV drugs and not indicative of a functional cure. Switching to ART regimens without anti-HBV drugs should be approached with caution.

Nucleotide sequence data are registered in the GenBank database (accession nos. LC789983 and LC789984).

Author contributions: project design, E.A.; manuscript drafting, E.A.; clinical course review, E.A., M.S., and H.Y.; manuscript revision, E.A., M.S., and H.Y.; patient

management, E.A., A.O., Y.K., M.S., M.K., and H.Y.; genomic analysis, A.S., K.A., and K.T. All authors approved the final manuscript.

About the Author

Dr. Adachi is an infectious disease physician with the University of Tokyo and specializes in HIV/AIDS research.

References

1. Schillie S, Murphy TV, Sawyer M, Ly K, Hughes E, Jiles R, et al.; Centers for Disease Control and Prevention. CDC guidance for evaluating health-care personnel for hepatitis B virus protection and for administering postexposure management. MMWR Recomm Rep. 2013; 62:1–19.
2. Honda T, Yamada N, Murayama A, Shiina M, Aly HH, Kato A, et al. Amino acid polymorphism in hepatitis B virus associated with functional cure. Cell Mol Gastroenterol Hepatol. 2021;12:1583–98. https://doi.org/10.1016/j.jcmgh.2021.07.013
3. Firnhaber C, Viana R, Reyneke A, Schultze D, Malope B, Maskew M, et al. Occult hepatitis B virus infection in patients with isolated core antibody and HIV co-infection in an urban clinic in Johannesburg, South Africa. Int J Infect Dis. 2009;13:488–92. https://doi.org/10.1016/j.ijid.2008.08.018
4. Dickson RC, Everhart JE, Lake JR, Wei Y, Seaberg EC, Wiesner RH, et al.; The National Institute of Diabetes and Digestive and Kidney Diseases Liver Transplantation Database. Transmission of hepatitis B by transplantation of livers from donors positive for antibody to hepatitis B core antigen. Gastroenterology. 1997;113:1668–74. https://doi.org/10.1053/gast.1997.v113.pm9352871
5. Kuhns MC, Holzmayer V, McNamara AL, Anderson M, Cloherty GA. Hepatitis B seroconversion revisited: new insights into the natural history of acute hepatitis B virus (HBV) infection from quantitative and highly sensitive assays and novel biomarkers. Virol J. 2021;18:235. https://doi.org/10.1186/s12985-021-01706-w
6. Wong DK, Tanaka Y, Lai CL, Mizokami M, Fung J, Yuen MF. Hepatitis B virus core-related antigens as markers for monitoring chronic hepatitis B infection. J Clin Microbiol. 2007;45:3942–7. https://doi.org/10.1128/JCM.00366-07
7. Ma Q, Wang Y. Comprehensive analysis of the prevalence of hepatitis B virus escape mutations in the major hydrophilic region of surface antigen. J Med Virol. 2012;84:198–206. https://doi.org/10.1002/jmv.23183
8. Lubel JS, Angus PW. Hepatitis B reactivation in patients receiving cytotoxic chemotherapy: diagnosis and management. J Gastroenterol Hepatol. 2010;25:864–71. https://doi.org/10.1111/j.1440-1746.2010.06243.x
9. Ye Q, Shang SQ, Li W. A new vaccine escape mutant of hepatitis B virus causes occult infection. Hum Vaccin Immunother. 2015;11:407–10. https://doi.org/10.4161/21645515.2014.994461
10. Anastasiou OE, Almpani F, Herrmann A, Gerken G, Ditschkowski M, Ciesek S. HBV reactivation in allogeneic stem cell transplant recipients: risk factors, outcome, and role of hepatitis B virus mutations. Hepatol Commun. 2017;1:1014–23. https://doi.org/10.1002/hep4.1118
11. Lazarevic I, Banko A, Miljanovic D, Cupic M. Immune-escape hepatitis B virus mutations associated with viral reactivation upon immunosuppression. Viruses. 2019;11:778. https://doi.org/10.3390/v11090778
12. Mican R, Busca Arenzana C, Vasquez J, Daroca G, Perez-Valero I, Martin-Carbonero L. Hepatitis B reactivation after tenofovir withdrawal in an HIV-infected patient with history of cured hepatitis B virus infection and poor immunological status. AIDS. 2021;35:1707–8. https://doi.org/10.1097/QAD.0000000000002941
13. Vasishta S, Dieterich D, Mullen M, Aberg J. Brief Report: Hepatitis B infection or reactivation after switch to 2-drug antiretroviral therapy: a case series, literature review, and management discussion. J Acquir Immune Defic Syndr. 2023;94:160–4. https://doi.org/10.1097/QAI.0000000000003239
14. Welford E, Yin J, Hill L, Wooten D. A case series of low-level HBV viremia after switching to long-acting injectable cabotegravir/rilpivirine in patients with HIV, hepatitis B core antibody positivity, and hepatitis B surface antigen negativity. In: Abstracts of IDweek 2022; Washington, DC, USA; 2022 Oct 19–23. Abstract 1583. Arlington (VA): Infectious Diseases Society of America; 2022.
15. Piroth L, Launay O, Michel ML, Bourredjem A, Miailhes P, Ajana F, et al.; ANRS HB EP03 CISOVAC Study Group. Vaccination against hepatitis B virus (HBV) in HIV-1–infected patients with isolated anti-HBV core antibody: the ANRS HB EP03 CISOVAC prospective study. J Infect Dis. 2016;213:1735–42. https://doi.org/10.1093/infdis/jiw011

Address for correspondence: Eisuke Adachi, IMSUT Hospital, 4-6-1 Shirokanedai, Minato-ku, Tokyo 108-8639, Japan; email: e-adachi@ims.u-tokyo.ac.jp

Characterization of Influenza D Virus Reassortant Strain in Swine from Mixed Pig and Beef Farm, France

Stéphane Gorin,[1] Gautier Richard,[1] Séverine Hervé, Eric Eveno, Yannick Blanchard, Agnès Jardin, Nicolas Rose, Gaëlle Simon

Influenza D virus was isolated from pigs on a mixed pig and beef farm in France. Investigation suggested bull-to-pig transmission and spread among pigs. The swine influenza D virus recovered was a reassortant of D/660 and D/OK lineages. Reported mutations in the receptor binding site might be related to swine host adaptation.

Influenza D virus (IDV) was initially isolated in 2011 from a pig with influenza-like symptoms (*1*). IDV has been identified globally in various species, including humans, without respiratory disease association according to serologic data (*2*,*3*) and sequencing from nasal washes (*4*). Cattle are the main IDV reservoir worldwide, including in France (*5*). Sow herds in France have tested positive for IDV antibodies, but IDV has not been isolated (*6*). We describe detection of IDV in fattening pigs in France and the accompanying genetic data for the swine origin IDV strain.

The Study

The sampled farm houses both pigs and cattle and is in the Brittany region of France. The pig herd operation is a farrow-to-finish system with 2 distinct barns: the first barn houses the sows and growing pigs in the nursery sectors and some of the fattening rooms (B1), and the other barn serves as the primary fattening barn (B2) (Figure 1). The pig herd had onset of chronic respiratory disorders that affected pigs in the nursery and fattening stages. The respiratory symptoms included sneezing and coughing.

Author affiliations: French Agency for Food, Environmental and Occupational Health & Safety, Ploufragan, France (S. Gorin, G. Richard, S. Hervé, E. Eveno, Y. Blanchard, N. Rose, G. Simon); CEVA Santé Animale, Libourne, France (A. Jardin)

DOI: https://doi.org/10.3201/eid3008.240089

A livestock veterinarian sampled tracheobronchial secretions from 7 fattening pigs (16 weeks of age) in October 2022. Pooled samples were submitted to the PathoSense laboratory (Ghent University, Merelbeke, Belgium) for sequencing (Oxford Nanopore Technologies, https://nanoporetech.com), which yielded results suggestive of an IDV infection. We then confirmed the presence of IDV genome in the tracheobronchial secretions by polymerase basic 1–gene qualitative reverse transcription PCR, as previously described (*1*). We successfully propagated strain D/swine/France/29-220655/2022 on swine testis cells. We confirmed viral growth by using polymerase basic 1–gene qualitative reverse transcription PCR and hemagglutination activity on chicken red blood cells (*6*).

We visited the farm in December 2022 to collect information about the layout and management. Our visit enabled us to assess the presence and spread of IDV in the pig barns. Because B2 had side air inlets close (7–10 m) to the bull shelter, we hypothesized that IDV was transmitted from the bovine reservoir to fattening pigs either through this air intake or from clothing and equipment used between both livestock sectors. We were unable to restrain the bulls for sampling, but the breeder emphasized the occurrence of respiratory signs, specifically coughing, in young bull calves. Those signs developed shortly after the arrival of the bull calves at 6 months of age. Because the calves originated from Pays de la Loire, the region with the highest serologic IDV prevalence in cattle and small ruminants in France (*7*), we considered a link between the signs and an IDV infection. We collected nasal swabs and blood

[1]These first authors contributed equally to this article.

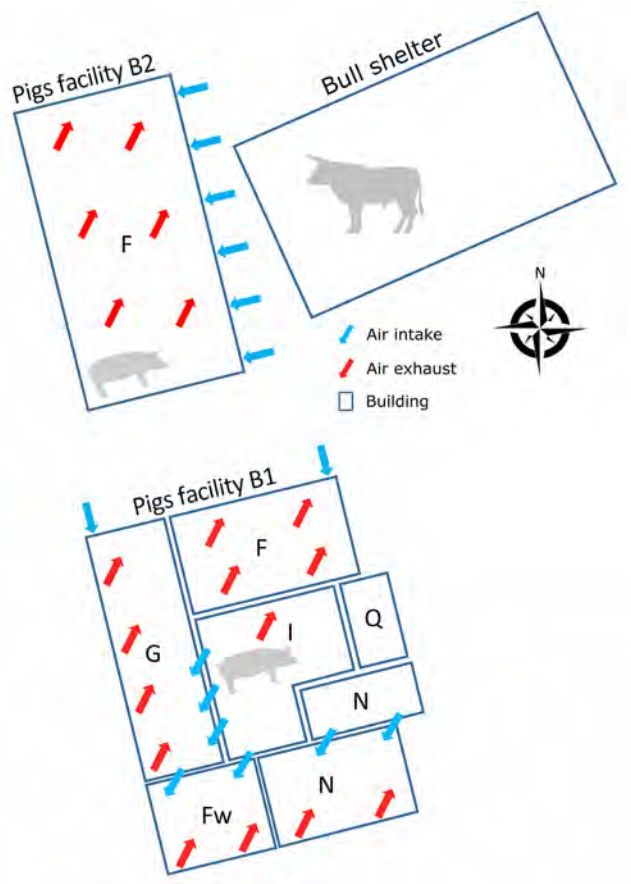

Figure 1. Schematic of a mixed pig and beef farm where influenza D virus was detected in pigs, France. Numbers of pigs in B1: F, n = 120 gilts; G + I, n = 160 sows and a few males; N, n = 960 (2 groups of 480 pigs, 5 and 10 weeks of age). Numbers of pigs in B2: F, n = 1,440 (3 groups of 480 pigs of 15, 20, and 25 weeks of age). F, fattening; Fw, farrowing room; G, gestation room; I, insemination room; N, nursery; Q, quarantine.

samples from 30 pigs with influenza-like illness: 10 pigs from the nursery at 10 weeks of age (B1), 10 pigs from fattening at 15 weeks of age (B2), and 10 pigs from fattening at 25 weeks of age (B2). The 25-week-old pigs were from the same group as the 7 pigs sampled in October that were IDV positive. IDV genome was not detected in nasal swab samples. We tested for IDV antibodies in serum by using a hemagglutination inhibition assay and used the D/swine/France/29-220655/2022 strain as an antigen (*8*). The results indicated that the pigs exposed to IDV in October 2022 had seroconverted (Table), suggesting IDV spread within the group. In the nursery (B1), 10% of the serum was positive for IDV antibodies, indicating that IDV might also have circulated in the B1 facility among piglets or farrowing sows. The sows would have transmitted some passive immunity to piglets, and that immunity could be detected at the end of the postweaning period.

We sequenced the isolated D/swine/France/29-220655/2022 strain (Appendix, https://wwwnc.cdc.gov/EID/article/30/8/24-0089-App1.pdf) and conducted phylogenetic analysis. Our analysis revealed that the hemagglutinin-esterase fusion (HEF) sequence of D/swine/France/29-220655/2022 classified within the D/660 lineage. This lineage is closely related to contemporary bovine IDV strains in Italy but distantly related to recent bovine strains in France, which belong to the D/OK lineage (Appendix Figure). Whole-genome phylogeny also classified D/swine/France/29-220655/2022 within the D/660 lineage, again showing proximity to Italian bovine IDV strains (Figure 2, panel A). However, individual analysis of the 6 internal genomic segments revealed that 1 segment, the nucleoprotein-encoding gene, belonged to the D/OK lineage rather than D/660. This analysis indicated that D/swine/France/29-220655/2022 is a reassortant strain (Figure 2, panel B).

When aligned to the 151 publicly available IDV HEF amino acids sequences, D/swine/France/29-220655/2022 contained 2 unique mutations in the receptor binding site (RBS), A236V/A252V and R268K/R284K. We based amino-acid coordinates on previously published data (*9*) or GenBank multisequence alignment and translation to proteins (Figure 3, panel A). Those mutations are located close to the 230 helix and the 270 loop, which are essential structures forming the IDV HEF RBS open channel (*9*). Hydrophobicity is increased by the A252V mutation and can potentially change HEF RBS affinity to different receptors (Figure 3, panel B) without changing the global 3D structure of the protein.

Conclusions

In our study, we isolated a swine IDV strain in France, confirming serologic proof of IDV circulation in pig

Table. Hemagglutination inhibition test results for the detection of influenza D virus antibodies against D/swine/France/29-220655/2022 in serum sampled from pigs housed on a mixed pig and beef farm in France, December 2022*

Growth stage, location	Age of pigs, wk	No. pigs sampled	HI titer range (mean)†	Positivity, %
Nursery, B1	10	10	<10–20	10
Fattening, B2	15	10	<10–10	0
Fattening, B2	25	10	20–160 (66)	100

*B1, nursery barn; B2, primary fattening barn; HI, hemagglutination inhibition.
†Positive threshold = 20.

livestock (*6*). When considering the epidemiologic investigation of the mixed pig and beef farm, we believe there was a transmission of IDV from bulls to pigs. The D/swine/France/29-220655/2022 strain displayed an HEF associated with the D/660 clade. The D/660 clade has become increasingly prevalent in Europe since 2019, after a decline in the previously dominant D/OK clade (*10*–*12*). In addition, we found that D/swine/France/29-220655/2022 was a reassortant strain that included a nucleoprotein gene from the D/OK lineage. This reassortant strain likely emerged in bovine species before transmission to swine. Reassortment could have taken place in bulls housed in the assembly center before being dispatched to fattening farms, or in a farrowing farm that delivered animals to the study farm. Either case would imply co-circulation of D/660 and D/OK clades at some point in France, similar to other European countries (*11*,*12*). Because other reassortant strains belonging to D/660 but displaying D/OK genes have been isolated from cattle in Italy (*10*), the reassortant IDV might have been imported.

Of interest, D/swine/France/29-220655/2022 HEF exhibited 2 unique mutations (A252V and R284K) located in the RBS. The HEF receptor-binding cavity is known to form an open channel between the 230 helix and 270 loop that could be responsible for IDV broad-cell tropism (*9*). By increasing HEF RBS hydrophobicity, an A252V mutation might have promoted virus binding to pig cell receptors and subsequent uptake, demonstrating an adaptation to the pig host. Single-point mutations related to hydrophobicity

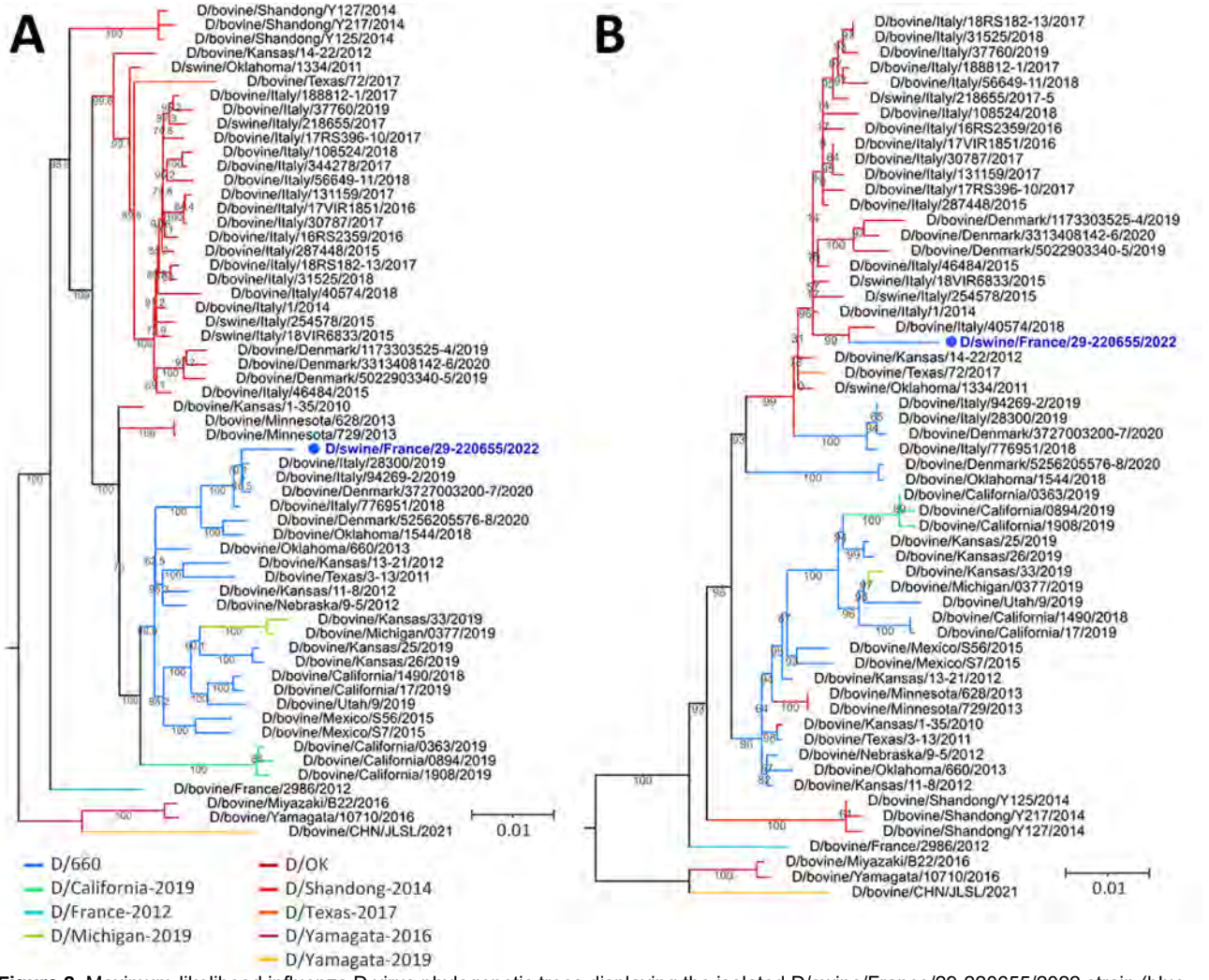

Figure 2. Maximum-likelihood influenza D virus phylogenetic trees displaying the isolated D/swine/France/29-220655/2022 strain (blue text) recovered from pigs at a mixed pig and beef farm in France. A) Whole-genome coding sequences phylogeny. B) Nucleoprotein coding sequences phylogeny. Numbers along branches indicate IQ-TREE2 (http://www.iqtree.org) ultra-fast bootstraps branch support. Scale bar indicates substitutions per site.

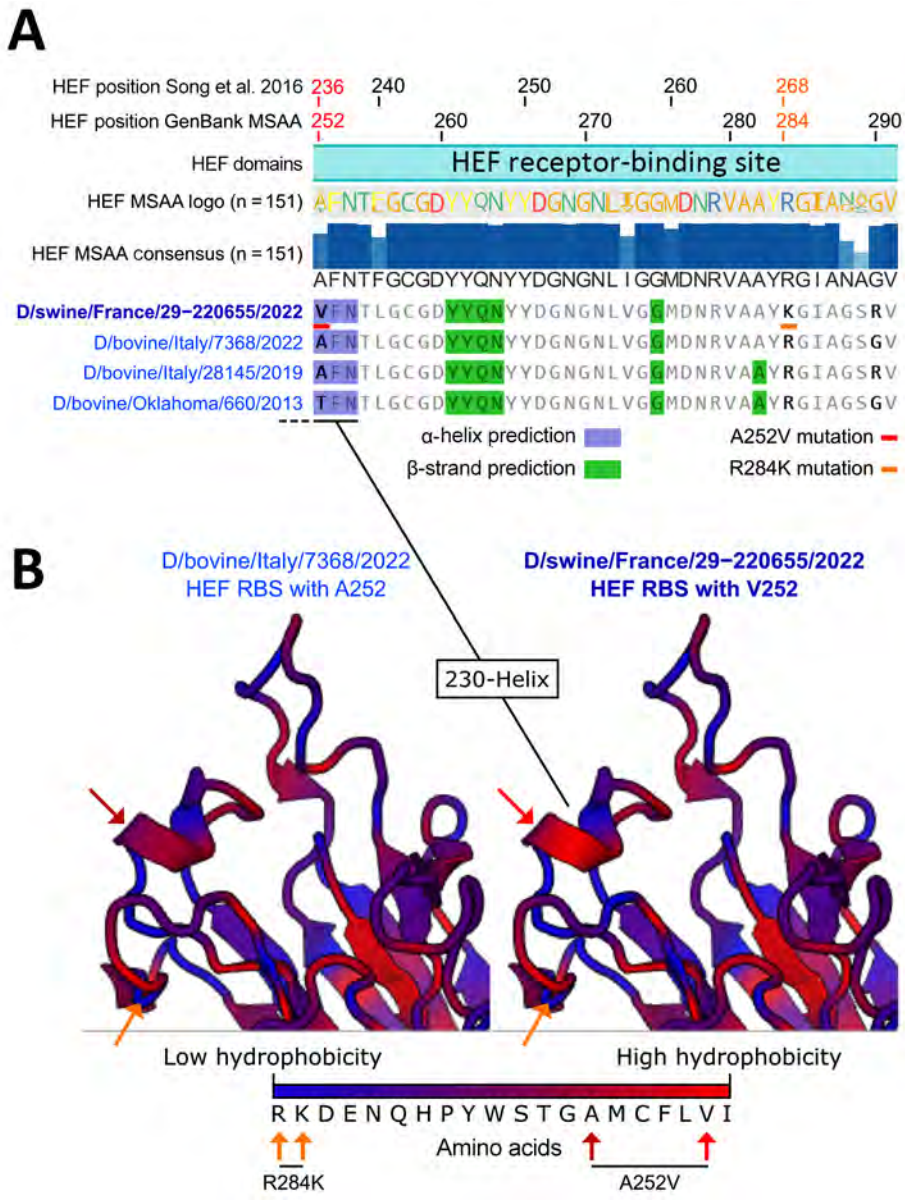

Figure 3. Alignments of hemagglutinin-esterase fusion protein sequences and structure prediction of the receptor-binding site of the influenza D virus strain recovered from swine in France. A) HEF sequence alignment and 2D structure prediction. From top to bottom: amino acid coordinates based on previously published research (9), amino acid coordinates based on GenBank MSAA and translation to protein, HEF domain based on previously published research (9), HEF sequence logo based on amino acid occurrence in the 151 HEF sequence alignment, HEF consensus sequence and percentage of amino occurrence in the 151 HEF sequence alignment, and representative HEF sequences from the D/660 lineage and their predicted secondary structures. Blue highlights indicate residues involved in α-helices and green highlights residues involved in β-strands. Red (A236V/A252V) and orange (R268K/R284K) underlines or arrows indicate unique mutations identified in D/swine/France/29-220655/2022. B) Predicted RBS structure of D/swine/France/29-220655/2022 compared with the closely related D/bovine/Italy/7368/2022. Blue colors on the protein 3D structures depict low hydrophobicity and red colors depict high hydrophobicity. HEF, hemagglutinin-esterase fusion; MSAA, multisequence alignment; RBS, receptor-binding site.

changes, such as threonine to isoleucine, in RBS were shown to enable adaptation to new hosts in influenza C viruses, which also could be the case for IDV HEF (*13*). The reported mutations might have contributed to the spread of the virus among pigs within the fattening unit, as shown by the serologic data.

Our case shows that IDV can be transmitted from bovines to swine and adapt to its new host through potential specific mutations enhancing intraspecies transmission. This adaptation process is similar to findings from a previous study (*14*). Replicating such a pig–calves IDV transmission experiment by using a strain such as D/swine/France/29-220655/2022 could help validate our findings. The proliferation and spread of IDV in swine could be an issue for animal health. Surveillance for IDV should be incorporated with influenza A virus surveillance, particularly in mixed pig and beef herds or in pig herds situated near bovine livestock.

Acknowledgments

We thank the farm owner and the livestock veterinarian for their support of this study.

About the Author

Dr. Richard is a researcher in molecular epidemiology at the swine virology immunology unit and National Reference Laboratory for swine influenza, France. His research interests include swine influenza virus evolution.

References

1. Hause BM, Ducatez M, Collin EA, Ran Z, Liu R, Sheng Z, et al. Isolation of a novel swine influenza virus from Oklahoma in 2011 which is distantly related to human influenza C viruses. PLoS Pathog. 2013;9:e1003176. https://doi.org/10.1371/journal.ppat.1003176
2. Trombetta CM, Montomoli E, Di Bartolo I, Ostanello F, Chiapponi C, Marchi S. Detection of antibodies against influenza D virus in swine veterinarians in Italy in 2004. J Med Virol. 2022;94:2855–9. https://doi.org/10.1002/jmv.27466
3. Trombetta CM, Marchi S, Manini I, Kistner O, Li F, Piu P, et al. Influenza D virus: serological evidence in the Italian population from 2005 to 2017. Viruses. 2019;12:30. https://doi.org/10.3390/v12010030
4. Leibler JH, Abdelgadir A, Seidel J, White RF, Johnson WE, Reynolds SJ, et al. Influenza D virus exposure among US cattle workers: a call for surveillance. Zoonoses Public Health. 2023;70:166–70. https://doi.org/10.1111/zph.13008
5. Ducatez MF, Pelletier C, Meyer G. Influenza D virus in cattle, France, 2011–2014. Emerg Infect Dis. 2015;21:368–71. https://doi.org/10.3201/eid2102.141449
6. Gorin S, Fablet C, Quéguiner S, Barbier N, Paboeuf F, Hervé S, et al. Assessment of influenza D virus in domestic pigs and wild boars in France: apparent limited spread within swine populations despite serological evidence of breeding sow exposure. Viruses. 2019;12:25. https://doi.org/10.3390/v12010025
7. Oliva J, Eichenbaum A, Belin J, Gaudino M, Guillotin J, Alzieu J-P, et al. Serological evidence of influenza D virus circulation among cattle and small ruminants in France. Viruses. 2019;11:516. https://doi.org/10.3390/v11060516
8. World Organisation for Animal Health. Influenza A viruses of swine. In: Manual of diagnostic tests and vaccines for terrestrial animals, 12th edition. Paris: The Organisation; 2023. p. 1–18.
9. Song H, Qi J, Khedri Z, Diaz S, Yu H, Chen X, et al. An open receptor-binding cavity of hemagglutinin-esterase-fusion glycoprotein from newly-identified influenza D virus: basis for its broad cell tropism. PLoS Pathog. 2016;12:e1005411. https://doi.org/10.1371/journal.ppat.1005411
10. Chiapponi C, Faccini S, Fusaro A, Moreno A, Prosperi A, Merenda M, et al. Detection of a new genetic cluster of influenza D virus in Italian cattle. Viruses. 2019;11:1110. https://doi.org/10.3390/v11121110
11. Gaudino M, Chiapponi C, Moreno A, Zohari S, O'Donovan T, Quinless E, et al. Evolutionary and temporal dynamics of emerging influenza D virus in Europe (2009–22). Virus Evol. 2022;8:081.
12. Goecke NB, Liang Y, Otten ND, Hjulsager CK, Larsen LE. Characterization of influenza D virus in Danish calves. Viruses. 2022;14:423. https://doi.org/10.3390/v14020423
13. Szepanski S, Gross HJ, Brossmer R, Klenk HD, Herrler G. A single point mutation of the influenza C virus glycoprotein (HEF) changes the viral receptor-binding activity. Virology. 1992;188:85–92. https://doi.org/10.1016/0042-6822(92)90737-A
14. Kaplan BS, Falkenberg S, Dassanayake R, Neill J, Velayudhan B, Li F, et al. Virus strain influenced the interspecies transmission of influenza D virus between calves and pigs. Transbound Emerg Dis. 2021;68:3396–404. https://doi.org/10.1111/tbed.13943

Address for correspondence: Gaëlle Simon, Laboratoire de Ploufragan-Plouzané-Niort, Rue des Fusillés, Zoopôle Les Croix, BP 53, 22440 Ploufragan, France; email: gaelle.simon@anses.fr

Spatiotemporal Modeling of Cholera, Uvira, Democratic Republic of the Congo, 2016–2020

Ruwan Ratnayake, Jackie Knee, Oliver Cumming, Jaime Mufitini Saidi, Baron Bashige Rumedeka, Flavio Finger, Andrew S. Azman, W. John Edmunds, Francesco Checchi,[1] Karin Gallandat[1]

We evaluated the spatiotemporal clustering of rapid diagnostic test–positive cholera cases in Uvira, eastern Democratic Republic of the Congo. We detected spatiotemporal clusters that consistently overlapped with major rivers, and we outlined the extent of zones of increased risk that are compatible with the radii currently used for targeted interventions.

Cholera outbreaks affect communities that lack access to safe water and adequate sanitation (*1*). Spatiotemporal clustering patterns of cholera indicate a high risk of transmission to the neighboring households of new cases (*2*,*3*). Case-area targeted interventions (CATI), consisting of early, multisectoral response within a 100–500-meter radius around case-households, have been proposed to attenuate clustered transmission (*4*). CATIs, driven by water, sanitation, and hygiene interventions, played a major role in response strategies in Haiti and Yemen, and CATIs including oral cholera vaccination helped suppress outbreaks after vaccination campaigns in Cameroon (*5*,*6*). In the Democratic Republic of the Congo (DRC), health officials evaluated water, sanitation, and hygiene targeting strategies within 500 meters around households with cholera cases (*7*). In Kalemie, DRC, and N'Djamena, Chad, researchers estimated a 200-meter zone of increased risk of infection around cholera cases in the first 5 days (*2*). As CATIs become part of routine practice (*4*,*5*), more insight is needed in delineating the spatiotemporal risk zones required to achieve a substantive effect on transmission.

In Uvira, a city in eastern DRC affected by protracted conflict, population displacement, and flooding, cholera is endemic, and stable transmission is punctuated by seasonal outbreaks (*8*). Citywide interventions include an ongoing piped water supply program with household tap installation beginning in late 2019 (*9*) and mass vaccination in mid-2020 (*10*). Using an enhanced surveillance system with rapid diagnostic testing (RDT), we investigated the location, timing, and prediction of clusters to identify outbreaks earlier and trigger early response. We estimated the extent of spatiotemporal zones of increased risk around cases as a proxy for the ideal radius of CATIs.

The Study

We analyzed suspected cases of cholera during 2016–2020 in patients at cholera treatment centers managed by the Uvira Health Zone. Beginning in April 2016, rectal swab samples were collected from suspected cases and RDT tested (Crystal VC O1/O139; Arkray Inc., https://www.arkray.co.in) after a 6-hour enrichment in alkaline peptone water. We classified cases by avenue of residence (i.e., enumeration areas of mean size 1,177 [range 180–5,711] based on 2017 population sizes) (town of Uvira census data, 2018, unpub. data). We used 2 methods to evaluate spatiotemporal clustering. The space–time scan statistic describes local clustering, where cases exceed expected density within a given area, to identify spatiotemporal clusters and assign relative

Author affiliations: London School of Hygiene & Tropical Medicine, London, UK (R. Ratnayake, J. Knee, O. Cumming, W.J. Edmunds, F. Checchi, K. Gallandat); Ministère de la Santé Publique, Division Provinciale de la Santé du Sud-Kivu, Zone de Santé d'Uvira, Uvira, Democratic Republic of the Congo (J.M. Saidi, B.B. Rumedeka); Epicentre, Paris, France (F. Finger); Johns Hopkins Bloomberg School of Public Health, Baltimore, Maryland, USA (A.S. Azman); Geneva University Hospitals, Geneva, Switzerland (A.S. Azman)

DOI: http://doi.org/10.3201/eid3008.231137

[1]These senior authors contributed equally to this article.

risk comparing observed versus expected cases inside and outside the cluster (*11*). To assess capacity for early detection of outbreaks, we simulated real-time detection by scanning prospectively (using few cases) and compared the delay with retrospective scanning (using more cases). We calculated the proportion of years that avenues were included in clusters during 2016–2020. The tau statistic (τ) describes global clustering, or the overall tendency for cases to occur near other cases in time and space (*12*), by using a relative risk of an individual in the population within a given distance band (i.e., 100–150 meters) from an incident case, compared with the risk for any individual in the population, becoming a potentially transmission-related case. This statistic suggests the geographic and temporal extents of increased infection risk. We defined the high-risk and elevated-risk zones as the radius where the moving average's lower 95% CI (high risk) and point estimate (elevated risk) cross 1.0 for ≥30 consecutive meters. We based the main analyses on enriched RDT-positive cases. We conducted sensitivity analyses using suspected cases, and given the use of enumeration areas, using simulated household locations (Appendix, https://wwwnc.cdc.gov/EID/article/30/8/23-1137-App1.pdf). We carried out analyses in R software v.4.1.2 (The R Foundation for Statistical Computing, https://www.r-project.org) by using the rsatscan v.1.0.5 (combined with SaTScan v.10.0.2) and IDSpatialStats v.0.3.12 packages.

Among 5,447 suspected cases, 3,456 (63.4%) were tested and 1,493 (43.2%) were RDT positive. We detected 26 significant spatiotemporal clusters (Table). Mean cluster radius was 652 (range 308–1582) meters, mean size was 20 (range 4–48) cases, and mean duration was 24.8 (range 1–58) days. Clustering occurred in similar locations annually (Figure 1). The first day of a retrospectively detected cluster usually anticipated a seasonal outbreak within 1 week, except for 2016 and 2017, when few cases were RDT tested (Figure 2, panel A). The median delay to the early outbreak signal was 1 day (interquartile range 0–3, maximum 23 days), and median size at signal detection was 3 cases (interquartile range 2–7, maximum 21 cases). Large clusters persisted across 2016–2020 and overlapped with major rivers in north-central and southern Uvira (Figure 2, panel B). We observed no changes in cluster locations in 2019, after household tap implementation began (Figures 1, panels D, E). Sensitivity analysis of suspected cases found more clusters

Table. Statistically significant spatiotemporal clusters of RDT-positive cholera cases detected through annual scanning at the avenue level, Uvira, Democratic Republic of the Congo, 2016−2020*

Year	No.	Cases observed: expected	Population at risk	RR†	Cluster radius, meters	Cluster start date	Cluster duration, d	Signal delay, d‡	Size at signal, no. cases
2016	1	20:1	30,553	20.9§	1,140	Aug 5	18	8	11
	2	28:3	34,232	10.5§	497	Jun 25	48	0	2
	3	17:1	30,758	13.8§	717	Jul 22	23	5	12
	4	15:1	31,240	11.9§	758	Jun 29	23	1	4
	5	4:0	6,579	344.4§	376	Apr 9	1	0	3
	6	14:2	30,082	8.8§	668	Jul 21	30	0	3
	7	9:1	27,452	12.6¶	368	Jul 26	14	3	4
2017	1	48:4	51,012	13.0§	811	Aug 7	40	2	2
	2	32:2	43,992	16.4§	657	Aug 20	23	1	13
	3	32:4	49,794	7.7§	880	Aug 23	44	0	2
	4	13:1	51,016	16.4§	378	Dec 24	7	0	2
	5	12:2	50,635	7.6¶	368	Aug 23	15	12	2
2018	1	20:1	28,884	26.6§	1,116	Oct 26	13	6	9
	2	11:1	31,204	22.7§	475	Feb 13	7	0	3
	3	8:0	25,148	40.6§	662	Aug 28	3	0	4
	4	7:0	17,345	18.6¶	308	Nov 10	10	1	3
2019	1	23:1	33,751	18.6§	743	Sep 10	18	1	7
	2	21:3	33,162	9.0§	755	Sep 7	35	0	12
	3	12:1	16,210	12.3§	309	Apr 27	29	1	2
	4	11:1	16,495	13.2§	527	Sep 7	24	0	2
	5	6:0	15,001	27.8¶	368	Jun 30	6	0	2
2020	1	42:6	60,378	7.8§	1,048	Jul 29	58	2	3
	2	27:3	42,423	8.7§	599	Jul 15	46	23	21
	3	17:1	56,029	19.1§	1,582	Feb 20	9	0	2
	4	30:5	63,207	6.5§	343	May 30	46	2	6
	5	32:6	63,593	5.8§	501	Jun 1	55	4	6

*RDT, rapid diagnostic test; RR, relative risk.
†p values indicate the statistical significance of clusters derived from Monte Carlo simulations.
‡Signal delay indicates the number of days between retrospective detection date with all available data and the earliest prospective detection date.
§p<0.001.
¶p<0.05.

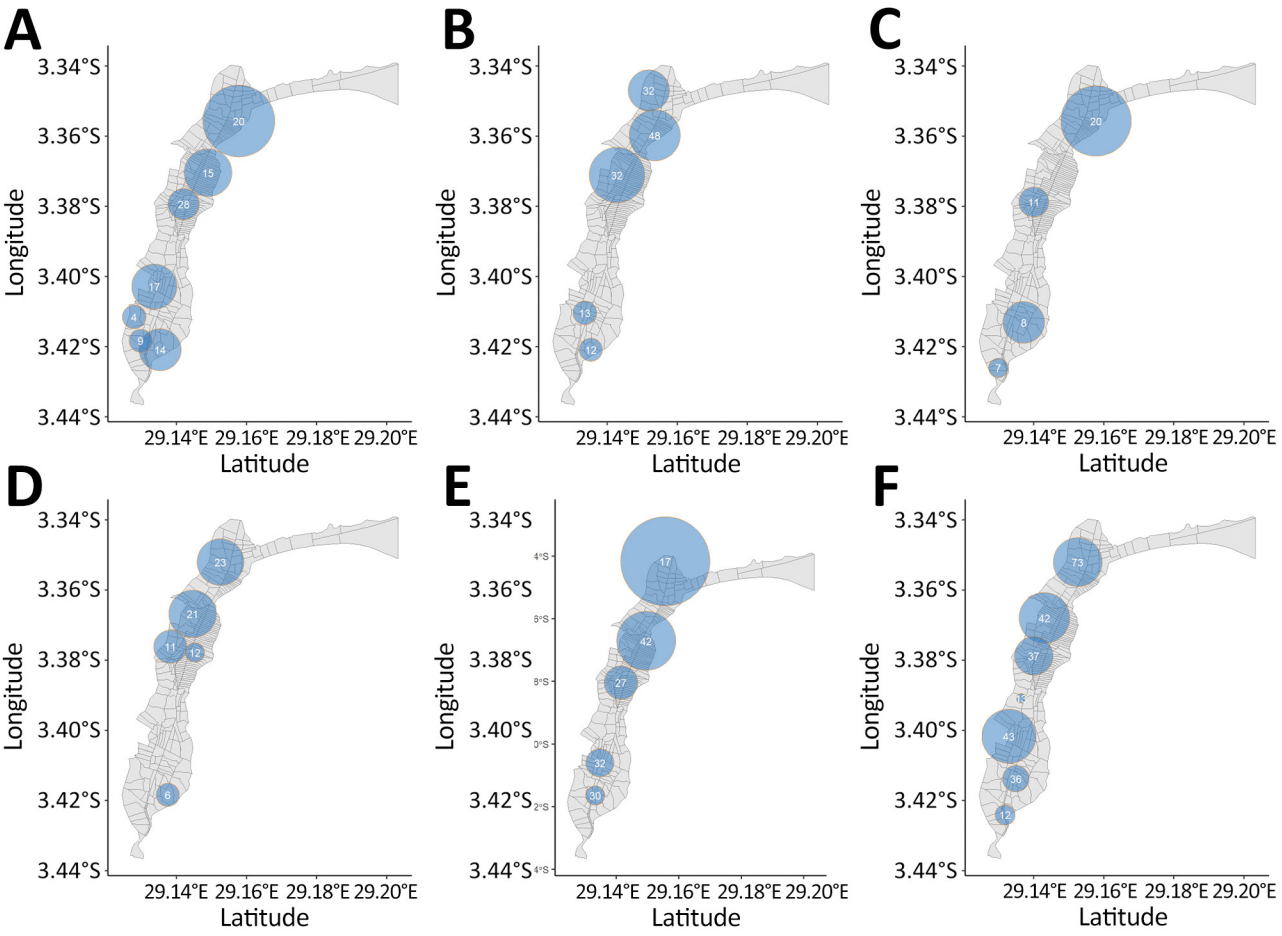

Figure 1. Spatial distribution of spatiotemporal clusters of rapid diagnostic test–positive cholera cases at the avenue level, Uvira, Democratic Republic of the Congo, 2016–2020. A) 2016; B) 2017; C) 2018; D) 2019; E) 2020; F) 2016–2020. Clusters have a relative risk >1 (p<0.05). The sizes of the light blue circles depict the spatial radius and the numbers of cases are shown inside the circles.

(n = 32) in similar locations with similar mean radii (668 [range 331–1,557] meters), larger mean size (42 [range 6–130] cases), and longer duration (27.8 [range 1–59] days) (Appendix Table 2, Figure 5).

In 2016–2020, within 5 days after cases began, the high-risk zone extended to 1,105 meters, and risk remained elevated up to 1,665 meters (maximum moving average τ = 1.8, 95% CI 1.4–2.3) (Figure 3, panel A). During days 1–4, which is more realistic for response, risk zones remained similar (Figure 3, panel D). In 2020, the high-risk zone extended to 585 meters and risk remained elevated up to 1,915 meters (τ = 1.8, 95% CI 1.0–2.9) (Figure 3, panel B). During days 1–4, the risk zones were 425 meters (high risk) and 1,915 meters (τ = 1.7, 95% CI 1.1–2.6) (Figure 3, panel E). Results were similar when we used simulated household locations (during days 0–4) with a moving average τ≥2.0 at 75–275 meters (τ = 2.4, 95% CI 1.7–3.3) and high-risk zone radius (1,415 meters) (Appendix Table 1, Figure 4). Annual results showed lower high-risk (425 meters, except 2017, when it was 875 meters) and elevated (1,125–1,485 meters) zone ranges and no discernable changes after 2019, when household tap implementation began (Appendix Figure 6). Using suspected cases from 2020, the trends remained similar (Figure 3, panels E, F).

Conclusions

We detected spatiotemporal clustering of cholera outbreaks during 2016–2020 in Uvira, DRC, that could inform early mitigation of seasonal outbreaks. The clustering methods produced aligned results compatible with a high-risk radius of ≤500 meters, as previously used for CATI in DRC (*7*,*13*) and similar to clustering in Matlab, Bangladesh, and coastal Sabah, Malaysia (500 meters, ≈5 days after cases began) (*3*,*14*). For RDT-positive cases within 5 days after cases began, we estimated a 1,105-meter high-risk radius, showing that a ≤1,000-meter risk window is optimal. Scan

statistics detected a similar mean cluster radius of 650 meters. The simulated real-time scanning usually signaled an outbreak with a 1-day median delay, which would enable early control.

We used enriched RDT-positive cases to increase specificity, but among study limitations is that we relied on medically attended cases at a cholera treatment center, biasing toward severely dehydrated case-patients and against milder cases. The spatial resolution misses case-pair distances <420 meters, where 5% of distances fell, although simulation of household locations showed similar trends with even higher (τ) across smaller radii. Circular scan statistics have reduced sensitivity to outline the shape of elliptical clusters (potentially along Uvira's coastline), but detection appeared unaffected (*11*).

Conspicuously, the clusters endured annually and overlapped with Uvira's 3 major rivers. According to surveys in 2016, 2017, and 2021, households in those clusters commonly use rivers as a primary water source (K. Gallandat et al., unpub. data) because piped water has remained inconsistent (*15*). Combined with

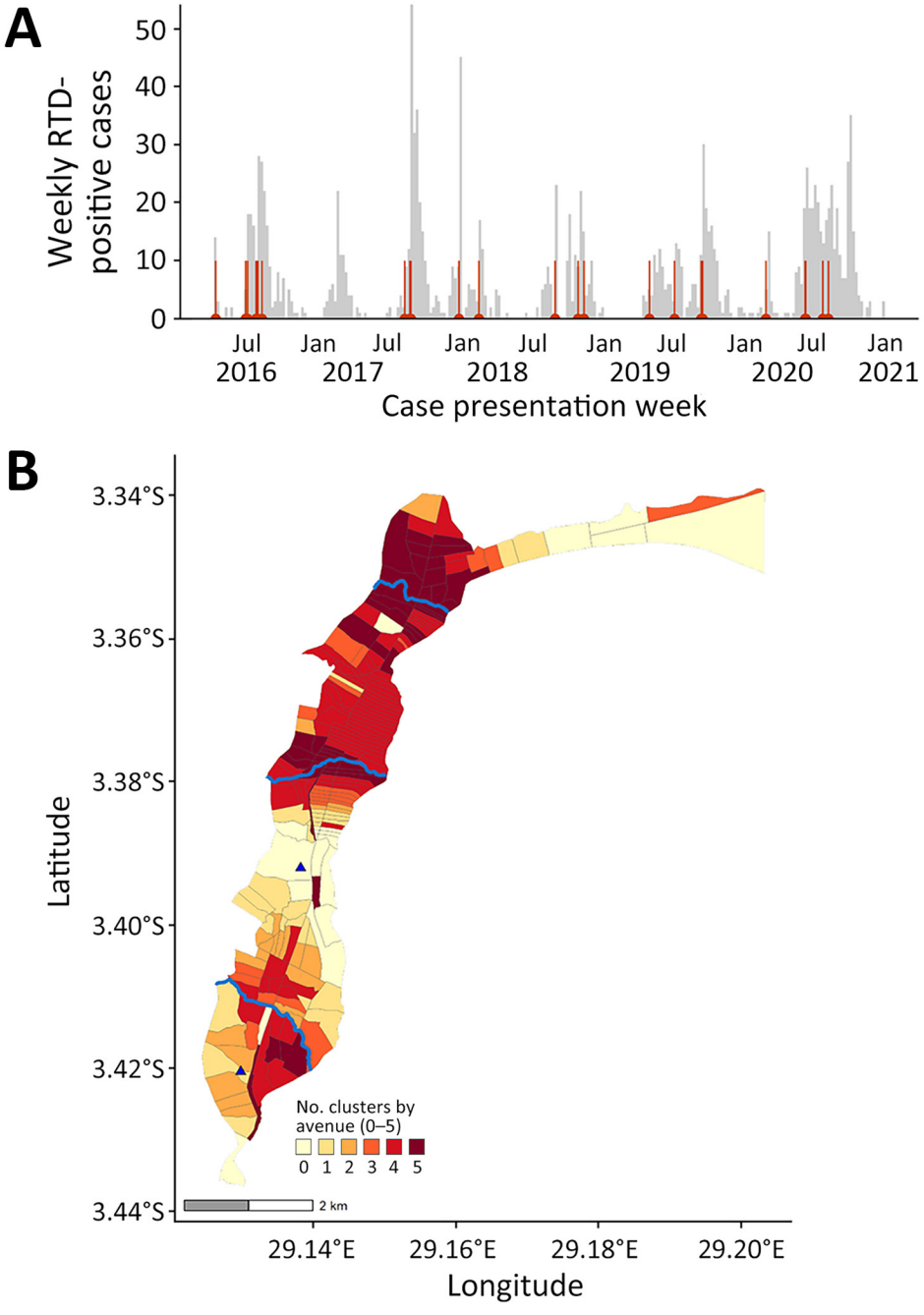

Figure 2. Epidemic curve and cluster persistence in study of spatiotemporal modeling of cholera, Uvira, Democratic Republic of the Congo, 2016–2020. A) Epidemic curve shows weekly numbers of RDT-positive cholera cases based on week of onset and start dates of 26 clusters (red vertical lines). B) Cluster persistence within avenues for RDT-positive cases showing the number of years affected by clustering within avenues and proximity to rivers (blue lines, top to bottom: Kalimabenge River, Mulongwe River, Kanvinvira River). Blue triangles indicate cholera treatment center (top) and unit (bottom). RDT, rapid diagnostic test.

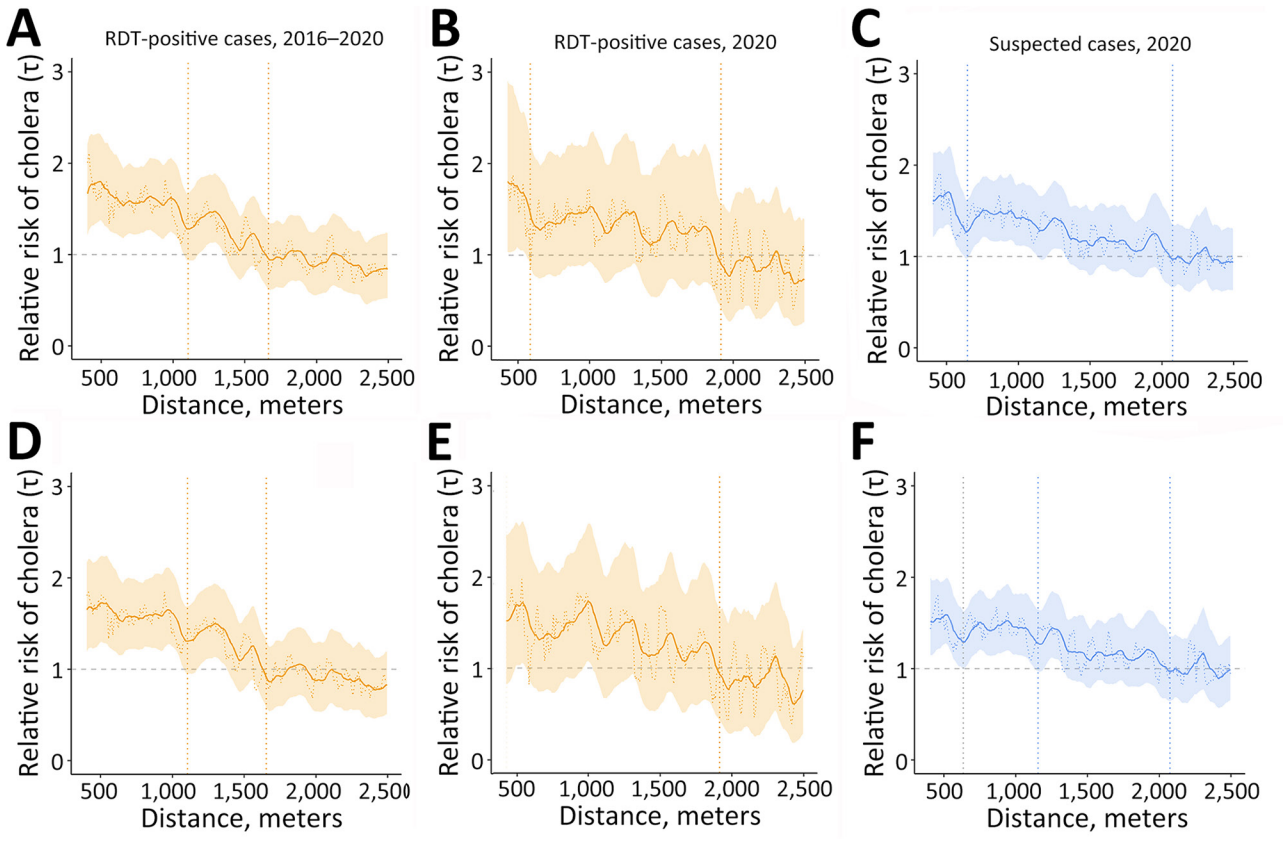

Figure 3. Moving average estimates for RDT-positive and suspected cholera cases in study of spatiotemporal modeling of cholera, Uvira, Democratic Republic of the Congo, 2016–2020. Moving average estimates of (relative risk) and 95% CIs (shading) are shown with point estimates (dashed horizontal lines) for days 0–4 (panels A–C) and days 1–4 (panels, D–F), for RDT-positive cases (orange) and suspected cases (blue), using 1,000 bootstrap samples. The vertical dashed lines indicate the spatial extent of the zone of high-risk where the lower 95% CI crossed 1.0 for ≥30 meters consecutively (first line) and zone of elevated risk where the point estimate crossed 1.0 for ≥30 meters consecutively (second line). RDT, rapid diagnostic test.

the high population density and inadequate sanitation, close-contact, fecal–oral transmission is amplified, producing recurrent clustering. Preventive measures, including piped water and vaccination, could be reinforced in cluster locations. CATI could address containment for new cases in less affected areas to prevent larger outbreaks. Because lakeside cities like Uvira may regularly seed regional outbreaks, targeted disease control strategies may bring substantial public health benefits.

Acknowledgments

We thank the Uvira Health Zone and cholera treatment center/unit (CTC/CTU) collaborators for the support provided to testing and data collection, often under difficult circumstances. We thank John Giles for advice on implementing the IDSpatialStats package. Last, we thank the patients who participated in the main study.

All data and code produced are available online at https://github.com/ruwanepi/Uvira_spatiotemporal.

R.R. is funded by a Doctoral Foreign Study Award from the Canadian Institutes of Health Research (award no. DFS-164266). The trial on which this study sources its data was co-funded by the French Agency for Development (ref. no. EVA/364-2015) and the Veolia Foundation (ref. no. 13/14 HD 1123).

Ethics approval was provided by the London School of Hygiene and Tropical Medicine (#10603-5) and the University of Kinshasa School of Public Health (#ESP/CE/173B/2022) as an amendment to the primary study for which the cholera case data was collected (*9*).

About the Author

Dr. Ratnayake is an infectious disease epidemiologist with a background in public health in humanitarian crises.

This analysis was part of his PhD at the London School of Hygiene and Tropical Medicine on the spatial modelling and field evaluation of case-area targeted interventions for cholera outbreaks. His research links field epidemiology and mathematical modelling to improve public health responses for vulnerable and crisis-affected populations.

References

1. World Health Organization. Multi-country outbreak of cholera: external situation report #11. Geneva, Switzerland; February 12, 2024. [cited 2024 July 2] https://www.who.int/publications/m/item/multi-country-outbreak-of-cholera--external-situation-report--11---12-february-2024
2. Azman AS, Luquero FJ, Salje H, Mbaïbardoum NN, Adalbert N, Ali M, et al. Micro-hotspots of risk in urban cholera epidemics. J Infect Dis. 2018;218:1164–8. https://doi.org/10.1093/infdis/jiy283
3. Debes AK, Ali M, Azman AS, Yunus M, Sack DA. Cholera cases cluster in time and space in Matlab, Bangladesh: implications for targeted preventive interventions. Int J Epidemiol. 2016;45:2134–9. https://doi.org/10.1093/ije/dyw267
4. Ratnayake R, Finger F, Azman AS, Lantagne D, Funk S, Edmunds WJ, et al. Highly targeted spatiotemporal interventions against cholera epidemics, 2000-19: a scoping review. Lancet Infect Dis. 2021;21:e37–48. https://doi.org/10.1016/S1473-3099(20)30479-5
5. Bulit G, Ramos M. Response to cholera outbreaks: case-area targeted interventions (CATI) and community outbreak response teams (CORT) guidelines. New York: UNICEF; 2020. [cited 2024 July 2] https://www.washcluster.net/node/30201
6. Ouamba JP, Fouda Mbarga N, Ciglenecki I, Ratnayake R, Tchiasso D, Finger F, et al. Implementation of targeted cholera response activities, Cameroon. Bull World Health Organ. 2023;101:170–8. https://doi.org/10.2471/BLT.22.288885
7. Bompangue D, Moore S, Taty N, Impouma B, Sudre B, Manda R, et al. Description of the targeted water supply and hygiene response strategy implemented during the cholera outbreak of 2017–2018 in Kinshasa, DRC. BMC Infect Dis. 2020;20:226. https://doi.org/10.1186/s12879-020-4916-0
8. Ingelbeen B, Hendrickx D, Miwanda B, van der Sande MAB, Mossoko M, Vochten H, et al. Recurrent cholera outbreaks, Democratic Republic of the Congo, 2008–2017. Emerg Infect Dis. 2019;25:856–64. https://doi.org/10.3201/eid2505.181141
9. Gallandat K, Macdougall A, Jeandron A, Mufitini Saidi J, Bashige Rumedeka B, Malembaka EB, et al. Improved water supply infrastructure to reduce acute diarrhoeal diseases and cholera in Uvira, Democratic Republic of the Congo: results and lessons learned from a pragmatic trial. PLoS Negl Trop Dis. 2024;18:e0012265. https://doi.org/10.1371/journal.pntd.0012265
10. Malembaka EB, Bugeme PM, Hutchins C, Xu H, Hulse JD, Demby MN, et al. Effectiveness of one dose of killed oral cholera vaccine in an endemic community in the Democratic Republic of the Congo: a matched case-control study. Lancet Infect Dis. 2024;24:514–22. https://doi.org/10.1016/S1473-3099(23)00742-9
11. Kulldorff M, Heffernan R, Hartman J, Assunção R, Mostashari F. A space-time permutation scan statistic for disease outbreak detection. PLoS Med. 2005;2:e59. https://doi.org/10.1371/journal.pmed.0020059
12. Lessler J, Salje H, Grabowski MK, Cummings DA. Measuring spatial dependence for infectious disease epidemiology. PLoS One. 2016;11:e0155249. https://doi.org/10.1371/journal.pone.0155249
13. Ratnayake R, Peyraud N, Ciglenecki I, Gignoux E, Lightowler M, Azman AS, et al.; Epicentre and MSF CATI Working Group. Effectiveness of case-area targeted interventions including vaccination on the control of epidemic cholera: protocol for a prospective observational study. BMJ Open. 2022;12:e061206. https://doi.org/10.1136/bmjopen-2022-061206
14. Maluda MCM, Johnson E, Robinson F, Jikal M, Fong SY, Saffree MJ, et al. The incidence, and spatial trends of cholera in Sabah over 15 years: Repeated outbreaks in coastal areas. PLOS Glob Public Health. 2024;4:e0002861. https://doi.org/10.1371/journal.pgph.0002861
15. Gaiffe M, Dross C, Bwenge Malembaka E, Ross I, Cumming O, Gallandat K. A fuzzy inference-based index for piped water supply service quality in a complex, low-income urban setting. Water Res. 2023;243:120316. https://doi.org/10.1016/j.watres.2023.120316

Address for correspondence: Ruwan Ratnayake, London School of Hygiene & Tropical Medicine, Keppel St, London WC1E 7HT, UK; email: ruwan.ratnayake@lshtm.ac.uk

Surge in Ceftriaxone-Resistant *Neisseria gonorrhoeae* FC428-Like Strains, Asia-Pacific Region, 2015–2022

Leshan Xiu, Lulu Zhang, Junping Peng

Ceftriaxone-resistant *Neisseria gonorrhoeae* FC428-like strains have disseminated across the Asia-Pacific region, with a continuous rise in prevalence during 2015–2022. To mitigate the effect of these strains, we advocate for enhanced molecular diagnostics, expanded surveillance networks, and a regionally coordinated effort to combat the global spread of FC428-like strains.

Neisseria gonorrhoeae infections represent an urgent public health threat, compounded by the alarming surge in strains resistant to ceftriaxone, the last line of defense for gonorrhea treatment (*1*). Before 2015, ceftriaxone resistance and treatment failures were sporadically reported globally. However, since 2015, the ceftriaxone-resistant FC428 clone carrying the mosaic *penA*-60.001 allele, initially identified in Japan (*2*), has spread nationally and internationally. Given this context, the World Health Organization's global surveillance of gonococcal antimicrobial resistance (AMR) needs to urgently expand internationally to provide essential data for developing effective management guidelines and public health policies (*3*).

The Asia-Pacific region, housing two thirds of the world's population and 10 of the least developed countries (*4*), is recognized as a regional hotspot for the emergence and spread of AMR. Indeed, recent evidence indicates that AMR in gonococci typically originates in an area the World Health Organization has deemed the Western Pacific Region before subsequently spreading internationally (*5*). Understanding the prevalence and dissemination of FC428-like Schoostrains in the Asia-Pacific region is therefore crucial for studying their origins and implementing measures to curtail their ongoing global spread. Our study offers a comprehensive analysis of the global spread of the ceftriaxone-resistant FC428-like strains, with a focus on prevalence, genetic diversity, and geographic distribution.

Author affiliations: School of Global Health, Shanghai Jiao Tong University School of Medicine, Shanghai, China (L. Xiu); National Institute of Pathogen Biology, Chinese Academy of Medical Sciences & Peking Union Medical College, Beijing, China (L. Zhang, J. Peng)

DOI: http://doi.org/10.3201/eid3008.240139

The Study

We acquired a sample library of FC428-like strains, incorporating data from our previously published effort (*6*), publicly available worldwide information collected over an 8-year period (*7*), and previously unpublished data from a comprehensive surveillance program in China conducted during 2019–2021 (National Center for Biotechnology Information Sequence Read Archive accession no. PRJNA560592). We identified 214 FC428-like strains across 14 countries (Appendix Table, Figure, https://wwwnc.cdc.gov/EID/article/30/8/24-0139-App1.pdf), most from Asia (186 strains), followed by Europe (21 strains), Oceania (4 strains), and North America (3 strains), suggesting circulation in the Asia-Pacific region (Figure 1). The prevalence of FC428-like strains has continuously increased during 2015–2022 (Figure 1, panel A), possibly because of an actual increase in cases but also potentially because of advancements in sequencing technology and increased use of more straightforward AMR tests. In a surveillance initiative for FC428-like strains, researchers determined minimal inhibitory concentrations for ceftriaxone (*8*). In another study, researchers categorized isolates as ceftriaxone susceptible or ceftriaxone resistant according to the latest clinical breakpoints (version 14.0) from the European Committee on Antimicrobial Susceptibility Testing (*9*). Based on those breakpoints, ceftriaxone resistance is defined as a MIC of ≥0.25 mg/L. Antimicrobial susceptibility analysis on 210 strains

revealed that 195 (92.86%) displayed a ceftriaxone-resistant phenotype, and 15 strains exhibited susceptibility. Caution is warranted when interpreting the clinical relevance of ceftriaxone resistance with *penA*-60.001. We classified 211 FC428-like strains (3 strains lacking sequence information) into 23 multilocus sequence typing sequence types (STs) (Appendix Table). ST1903 was predominant (44.08%, 93/211), followed by ST13871 (10.90%, 23/211), ST1600 (7.11%, 15/211), ST7365 (6.64%, 14/211), ST8123 (5.69%, 12/211), and ST7363 (5.21%, 11/211).

We obtained whole-genome sequence data from either our previously unpublished dataset or those we downloaded from public databases (Appendix Table). We extracted total genomic DNA from each bacterial isolate by using the QIAamp DNA Mini Kit (QIAGEN, https://www.sigmaaldrich.com) and prepared libraries for sequencing by using the Nextera XT DNA Library Preparation Kit (Illumina, https://www.illumina.com). We used the Illumina NovaSeq 6000 platform to execute sequencing. As of November 23, 2023, we could identify only 158 (73.83%) of the 214 FC428-like strains on the basis of available whole-genome sequencing data. The Asia-Pacific region hosted the most FC428-like strain genomes (86.08%, 136/158). We linked the remaining 22 strains, isolated from outside the Asia-Pacific region, to infections associated with travel or contact history in that region, suggesting a potential epidemiologic link. We generated a concatenate superset of single-nucleotide polymorphisms to measure genetic variations, following previously described methods (*6*). We then constructed a maximum-likelihood phylogenetic tree based on genomewide single-nucleotide polymorphisms by using PhyML 3.0. We conducted a whole-genome phylogenetic analysis, categorizing 158 strains into 2 major lineages and 10 distinct clades (Figure 2). Lineage A accounted for 51.9% (82/158), comprising clade 1, primarily isolated in Japan, and clade 2, mainly composed of FC428-like strains isolated in China. Lineage B consisted of 8 clades isolated from 12 different countries, but primarily from Cambodia and Vietnam. FC428-like strains from Europe, Oceania, and North America appeared interspersed in the lineage B phylogeny, suggesting multiple introductions of FC428-like strains into those countries.

Strains from different countries exhibited diverse STs, suggesting a common ancestry for these FC428-like strains that subsequently disseminated and evolved in other areas. China and Cambodia displayed the richest variety of sequence types. The diversity within the FC428-like population mirrors the global population, indicating potential multiple sources for lineages found within regional collections. Traditional sequence types have evolved further into FC428-like strains, particularly those susceptible to ceftriaxone, through the acquisition of *penA*-60.001 and homologous recombination of the core genome, resulting in the emergence of new clones with increased resistance. Those events lead to development of new clones at the global level, followed by the erosion of signals of clonality through recombination and, in some identifiable cases, the formation of new clonal clusters.

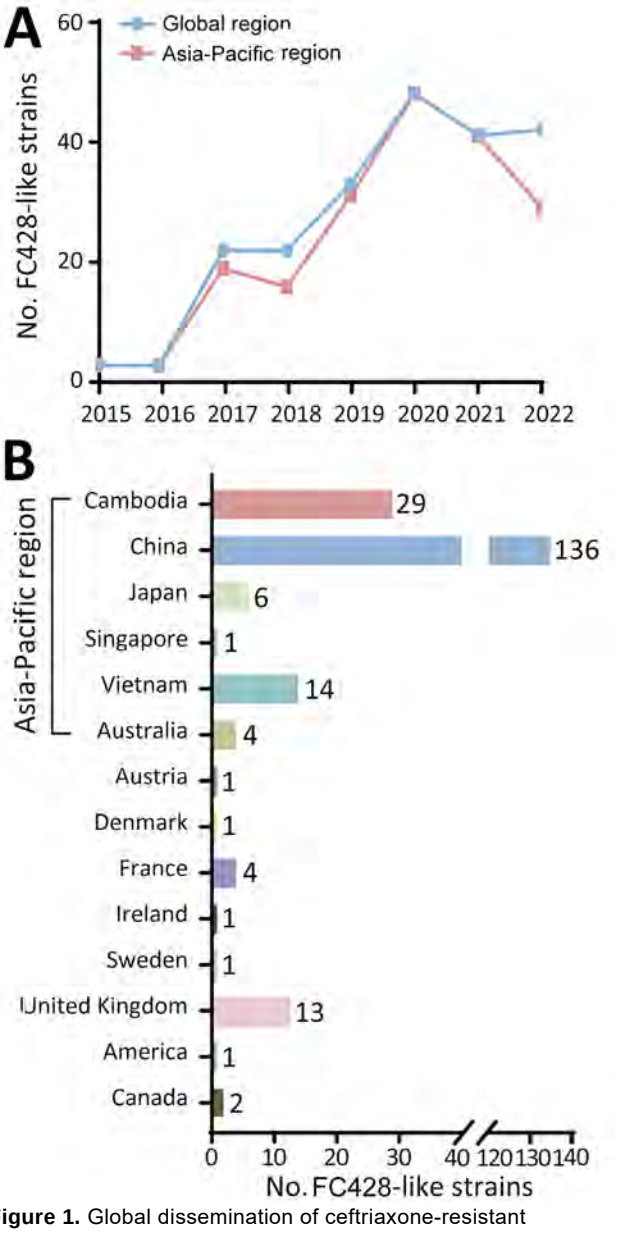

Figure 1. Global dissemination of ceftriaxone-resistant *N. gonorrhoeae* FC428-like strains. A) Trends in the prevalence of FC428-like strains from global and Asia-Pacific regions during 2015–2022. B) Number of FC428-like strains identified across 14 countries.

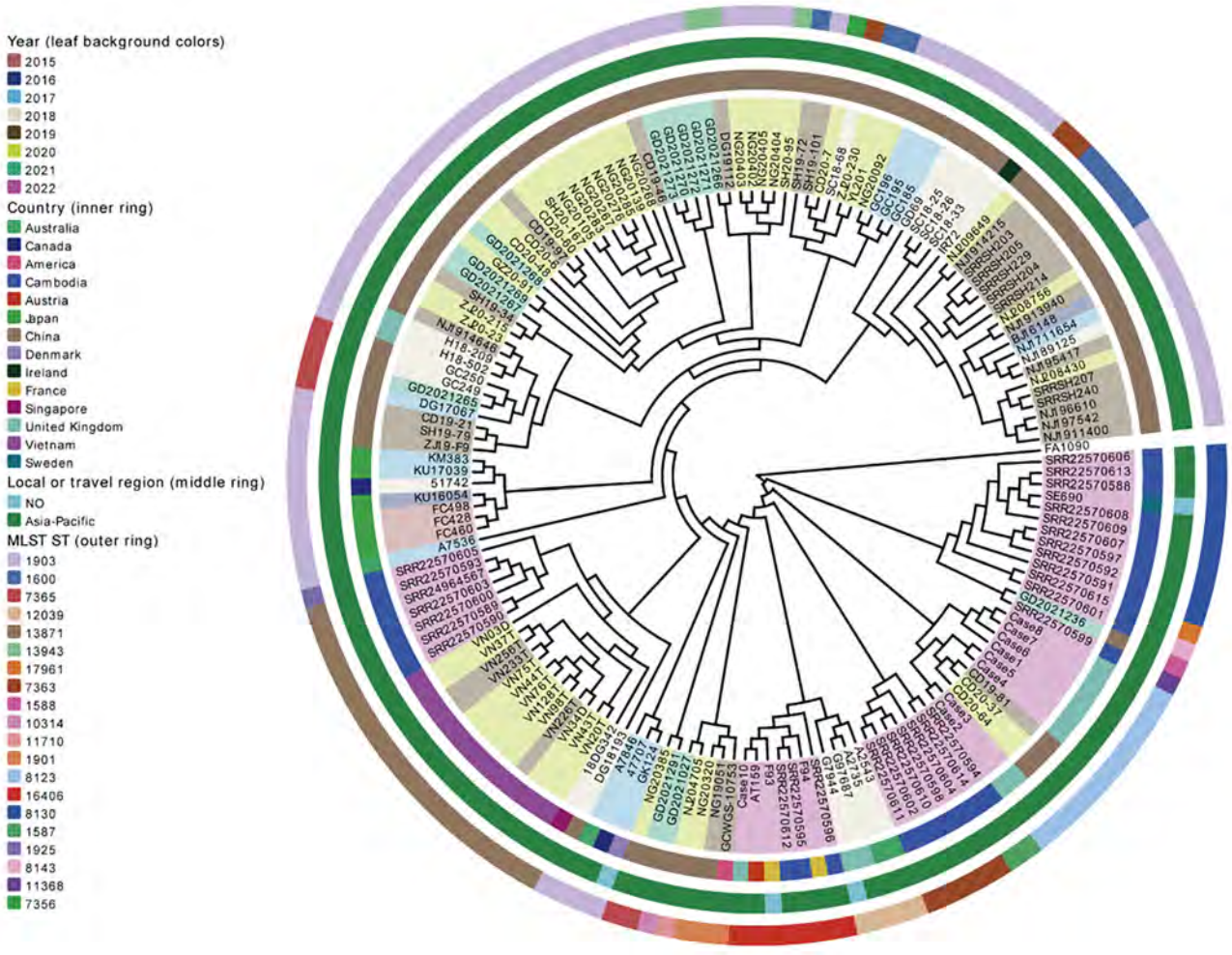

Figure 2. Phylogenetic analysis of globally disseminated gonococcal FC428-like strains from a study of the surge in ceftriaxone-resistant *Neisseria gonorrhoeae* FC428-like strains in the Asia-Pacific region, 2015−2022.. MLST, multilocus sequence typing; ST, sequence type.

To mitigate the effect of newly emerged and future clones, additional research is required to understand the evolutionary mechanisms involved in the emergence of the new *N. gonorrhoeae* lineages that contribute to global dissemination over relatively short timeframes. Large-scale genomic data provide valuable insights into the identification and characterization of FC428-like strains, enhancing our understanding of their global distribution and associated epidemiologic links. The strains forming lineage B phylogeny are sourced primarily from Cambodia and Vietnam, again highlighting distinct epidemiologic links (*10*,*11*). This reinforcing evidence strengthens the argument for the interconnectedness of FC428-like strains across different regions and underscores the significance of international travel and contact in their dissemination.

Conclusions

Effective disease control measures are crucial for addressing *N. gonorrhoeae* infections, given the substantial increase in identifying persons with ceftriaxone-resistant FC428-like strains observed globally over the past decade (*12*). This study provides insights into the prevalence, genetic diversity, and geographic distribution of these strains, contributing to a collective understanding of the current state of AMR in *N. gonorrhoeae* and the strategies needed to address this pressing public health issue.

Ceftriaxone resistance mediated by the *penA*-60.001 allele has been increasing, emphasizing the need for closer attention to identifying and surveilling of FC428-like strains. How, then, do we tackle the threat of ceftriaxone-resistant FC428-like strains? First, in addition to continuing to use antimicrobial susceptibility testing methods to detect novel resistance

mechanisms, we recommend expanding access to molecular diagnostics (*13*) to provide routine ceftriaxone-resistant testing as a minimum for all persons investigated for gonorrhea. Tailoring regimens on the basis of individual resistance profiles could maximize therapeutic efficacy while minimizing the risk of contributing to further resistance. Second, governments in the Asia-Pacific region should build on existing networks and local public health laboratories to expand capacity for ongoing surveillance and contribute data to the global fight against AMR (*3*). Deploying genomic AMR surveillance as a leapfrog technology (*1*,*14*), skipping over the targeted-molecular expansion of isolate-based phenotypic surveillance, can differentiate between strains within closely related clades dominating in specific countries, enabling detailed transmission mapping surpassing limitations of standard typing methods. Third, creating an enabling environment supported by appropriate resourcing is essential to fostering multisectoral partnerships to drive innovative solutions delivered through responsive and well-resourced health services. Finally, a regionally coordinated effort, driven by clear targets and sustainability, and built on a framework that facilitates communication and governance, will strengthen the fight against the global dissemination of ceftriaxone-resistant *N. gonorrhoeae* FC428-like strains.

This work was sponsored by Shanghai Pujiang Program (22PJD035), the China Medical Board (23-526), the CAMS Innovation Fund for Medical Sciences (2021-I2M-1-038), Nonprofit Central Research Institute Fund of Chinese Academy of Medical Sciences (2019PT310029 and 2023PT31004), and the Fundamental Research Funds for the Central Universities (3332021092).

About the Author

Dr. Xiu is an assistant professor in the School of Global Health, Shanghai Jiao Tong University School of Medicine. His research program bridges infectious diseases and clinical microbiology, with projects focused on evolution of antimicrobial resistance and molecular epidemiology in *Neisseria gonorrhoeae*.

References

1. Sánchez-Busó L, Yeats CA, Taylor B, Goater RJ, Underwood A, Abudahab K, et al. A community-driven resource for genomic epidemiology and antimicrobial resistance prediction of Neisseria gonorrhoeae at Pathogenwatch. Genome Med. 2021;13:61. https://doi.org/10.1186/s13073-021-00858-2
2. Lee K, Nakayama SI, Osawa K, Yoshida H, Arakawa S, Furubayashi KI, et al. Clonal expansion and spread of the ceftriaxone-resistant Neisseria gonorrhoeae strain FC428, identified in Japan in 2015, and closely related isolates. J Antimicrob Chemother. 2019;74:1812–9. https://doi.org/10.1093/jac/dkz129
3. Unemo M, Lahra MM, Escher M, Eremin S, Cole MJ, Galarza P, et al. WHO global antimicrobial resistance surveillance for *Neisseria gonorrhoeae* 2017-18: a retrospective observational study. Lancet Microbe. 2021;2:e627–36. https://doi.org/10.1016/S2666-5247(21)00171-3
4. Yam ELY, Hsu LY, Yap EP, Yeo TW, Lee V, Schlundt J, et al. Antimicrobial resistance in the Asia Pacific region: a meeting report. Antimicrob Resist Infect Control. 2019;8:202. https://doi.org/10.1186/s13756-019-0654-8
5. Unemo M, Bradshaw CS, Hocking JS, de Vries HJC, Francis SC, Mabey D, et al. Sexually transmitted infections: challenges ahead. Lancet Infect Dis. 2017;17:e235–79. https://doi.org/10.1016/S1473-3099(17)30310-9
6. Yuan Q, Li Y, Xiu L, Zhang C, Fu Y, Jiang C, et al. I dentification of multidrug-resistant Neisseria gonorrhoeae isolates with combined resistance to both ceftriaxone and azithromycin, China, 2017-2018. Emerg Microbes Infect. 2019; 8:1546–9. https://doi.org/10.1080/22221751.2019.1681242
7. Ouk V, Pham CD, Wi T, van Hal SJ, Lahra MM, group ECw. The Enhanced Gonococcal Surveillance Programme, Cambodia. Lancet Infect Dis. 2023;23:e332-e3. https://doi.org/10.1016/S1473-3099(23)00479-6
8. Xiu L, Wang L, Li Y, Hu L, Huang J, Yong G, et al. Multicentre clinical evaluation of a molecular diagnostic assay to identify Neisseria gonorrhoeae infection and detect antimicrobial resistance. Int J Antimicrob Agents. 2023; 61:106785. https://doi.org/10.1016/j.ijantimicag.2023.106785
9. The European Committee on Antimicrobial Susceptibility Testing. Breakpoint tables for interpretation of MICs and zone diameters. Version 14. 2024 [cited 2024 Jan 1] https://www.eucast.org/clinical_breakpoints
10. Day M, Pitt R, Mody N, Saunders J, Rai R, Nori A, et al. Detection of 10 cases of ceftriaxone-resistant Neisseria gonorrhoeae in the United Kingdom, December 2021 to June 2022. Euro Surveill. 2022; 27:2200803. https://doi.org/10.2807/1560-7917.ES.2022.27.46.2200803
11. Maubaret C, Caméléna F, Mrimèche M, Braille A, Liberge M, Mainardis M, et al. Two cases of extensively drug-resistant (XDR) Neisseria gonorrhoeae infection combining ceftriaxone-resistance and high-level azithromycin resistance, France, November 2022 and May 2023. Euro Surveill. 2023;28:2300456. https://doi.org/10.2807/1560-7917.ES.2023.28.37.2300456
12. Lahra MM, Ryder N, Whiley DM. A new multidrug-resistant strain of Neisseria gonorrhoeae in Australia. N Engl J Med. 2014;371:1850–1. https://doi.org/10.1056/NEJMc1408109
13. Tickner JA, Lahra MM, Whiley DM. The need for a commercial test using the penA60 allele to identify ceftriaxone-resistant Neisseria gonorrhoeae. Lancet Infect Dis. 2022; 22:1271–2. https://doi.org/10.1016/S1473-3099(22)00520-5
14. Golparian D, Unemo M. Now Is the Time to Implement Whole Genome Sequencing in the Global Antimicrobial Resistance Surveillance for Neisseria gonorrhoeae? EClinicalMedicine. 2019;7:11–2. https://doi.org/10.1016/j.eclinm.2019.02.002

Address for correspondence: Leshan Xiu, School of Global Health, Shanghai Jiao Tong University School of Medicine, 227 South Chongqing Rd, Shanghai 200025, China; email: xiuls001@hotmail.com; Junping Peng, National Institute of Pathogen Biology, Chinese Academy of Medical Sciences & Peking Union Medical College, No. 16 Tianrong St, Daxing District, Beijing 102629, China; email: pengjp@hotmail.com.

Real-Time Enterovirus D68 Outbreak Detection through Hospital Surveillance of Severe Acute Respiratory Infection, Senegal, 2023

Mamadou Malado Jallow, Marie Pedapa Mendy, Mamadou Aliou Barry, Moussa Moise Diagne, Samba Niang Sagne, Fatime Tall, Jean Baptisse Niokhor Diouf, Ndiendé Koba Ndiaye, Davy Kiori, Sara Sy, Déborah Goudiaby, Cheikh Loucoubar, Gamou Fall, Hervé Kadjo, Maël Bessaud, Ndongo Dia

In December 2023, we observed through hospital-based surveillance a severe outbreak of enterovirus D68 infection in pediatric inpatients in Dakar, Senegal. Molecular characterization revealed that subclade B3, the dominant lineage in outbreaks worldwide, was responsible for the outbreak. Enhanced surveillance in inpatient settings, including among patients with neurologic illnesses, is needed.

Enterovirus D68 (EV-D68) has emerged as a major public health concern because of its association with outbreaks of severe acute respiratory illness (SARI), acute flaccid myelitis (AFM), and acute flaccid paralysis (AFP), particularly among children and persons with underlying respiratory conditions (*1*). The virus was discovered in 1962 in California, USA, in 4 children with SARI (*2*); originally named Fermon virus, it was later reclassified under enterovirus species D and serotype 68 (*3*). Before 2014, EV-D68 was reported only sporadically; a total of 699 confirmed cases in Europe, Africa, and southeast Asia were reported during 1970–2013 (*4*). However, in recent years, a notable increase in the frequency and scale of EV-D68 outbreaks has been observed, prompting heightened surveillance and public health responses. In 2014, a large outbreak of EV-D68 infection that was associated with severe respiratory illness (*5*) and, in some cases, neurologic complications such as AFP occurred in the United States and in other parts of the world (*6*). More than 2,000 cases of EV-D68 infection were reported in 20 countries during that period (*2*). After the 2014 outbreak, other waves of EV-D68 infections were observed in 2016, 2018, and 2022; outbreaks were reported in several parts of the world, including the countries Sweden (*7*), Japan (*8*), and Finland (*9*).

In Senegal, few EV-D68 infection cases were detected in 2014 (*10*). In 2016, an outbreak of novel subclade B3 infections in outpatients with influenza-like illness and AFP (*11*) were reported. Since 2016, the virus has been detected sporadically through community surveillance of respiratory infections until December 2023, when a notable upsurge of EV-D68 infections in pediatric inpatients occurred. We report on an outbreak of severe EV-D68 infections in pediatric patients in Dakar, Senegal, and describe the clinical characteristics of EV-D68 cases identified in this outbreak.

The Study

In 2015, in collaboration with Senegal's Ministry of Health, the Institut Pasteur of Dakar initiated in hospital-based surveillance of SARI in referral hospitals in the capital of Dakar through its National Influenza Centre (NIC) and its Unit of Epidemiology Clinical Research and Data Sciences (Figure 1) to enable the Ministry of Health to quickly detect and alert any of

Author affiliations: Institut Pasteur de Dakar, Dakar, Senegal (M.M. Jallow, M.P. Mendy, M.A. Barry, M.M. Diagne, S.N. Sagne, N.K. Ndiaye, D. Kiori, S. Sy, D. Goudiaby, C. Loucoubar, G. Fall, N. Dia); Hôpital des enfants Albert Royer de Fann, Dakar (F. Tall); Hôpital Roi Baudoin de Guediawaye, Dakar (J.B.N. Diouf); Institut Pasteur de Côte d'Ivoire, Abidjan, Côte d'Ivoire (H. Kadjo); Institut Pasteur Paris, Paris, France (M. Bessaud)

DOI: https://doi.org/10.3201/eid3008.240410

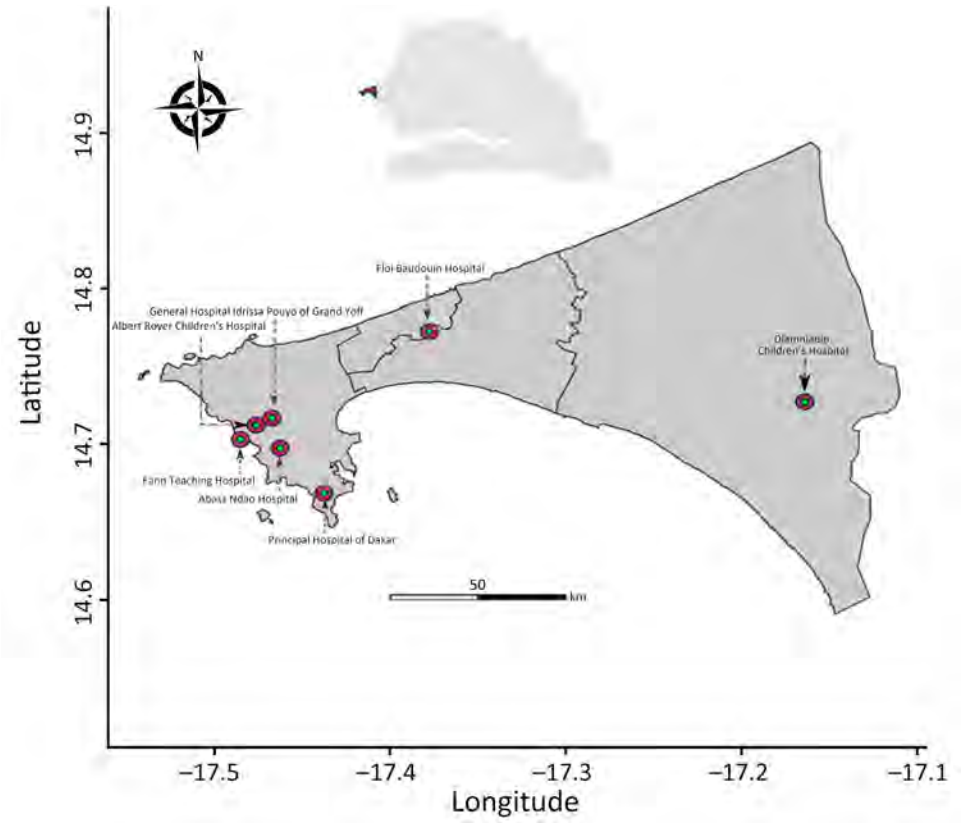

Figure 1. Referral hospitals contributing to the hospital-based surveillance of severe acute respiratory infection (red circles), Dakar, Senegal, 2023. Inset map show study area in Senegal.

abnormal health event. As part of this routine surveillance, which falls within the scope of the Sentinel Syndromic Surveillance in Senegal's network activities, we collected swab samples (nasopharyngeal, oropharyngeal, or both) from hospitalized patients with SARI and promptly transported the specimens at a controlled temperature (4°C–8°C) to NIC to screen for respiratory pathogens, as detailed by Jallow et al. (*12*). We then typed all enterovirus-positive samples by using 1-step real-time reverse transcription PCR (rRT-PCR) by using primers and a probe specific to EV-D68, as previously described (*10*). We genetically

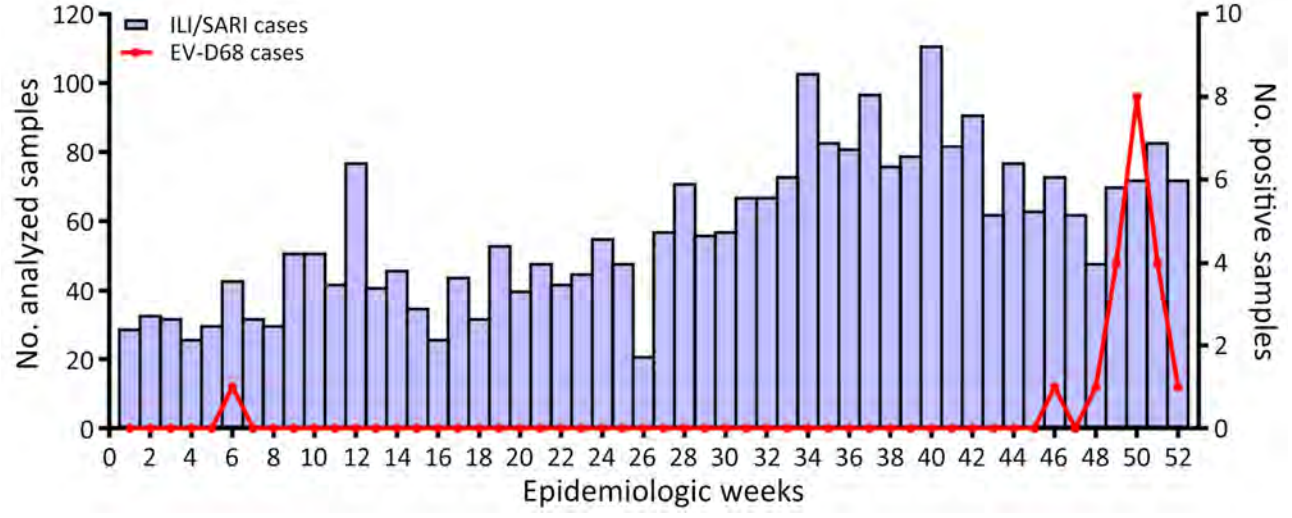

Figure 2. Weekly distribution of EV-D68 in patients with acute respiratory infection, Dakar Senegal, 2023. Bars represent the number of samples tested for each epidemiologic week. Line indicates number samples positive for EV-D68. Scales for the y-axes differ substantially to underscore patterns but do not permit direct comparisons. EV-D68, enterovirus D68; ILI, influenza-like illness; SARI, severe acute respiratory illness.

characterized all EV-D68 isolates by using whole-genome sequencing on an Illumina sequencing platform (https://www.illumina.com) with the Twist Respiratory Virus Research Panel (Twist Biosciences, https://www.twistbioscience.com), as previously described (*12*). This study was conducted as part of SARI hospital-based surveillance with approval from the National Ethical Committee of Senegal's Ministry of Health.

In December 2023, NIC noticed an increase in the positivity rate of enterovirus (0% in January, 1.1% from February to November, and 6.9% in December) in SARI samples, even though the number of specimens tested monthly remained relatively unchanged. The typing of enterovirus-positive samples identified EV-D68 as the predominant virus implicated in this upsurge of cases. Of the 2,986 nasopharyngeal samples from patients with influenza-like illness and

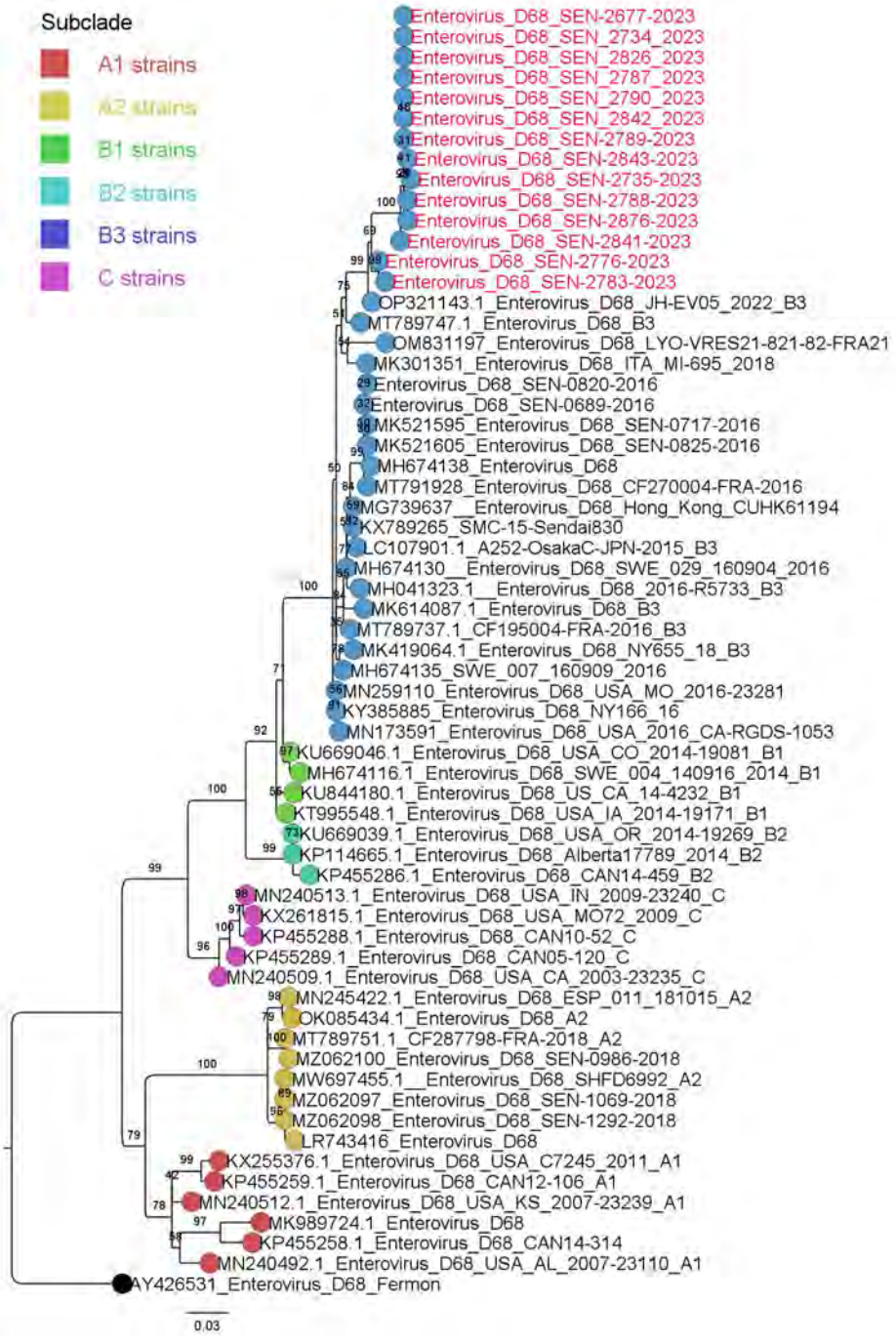

Figure 3. Maximum-likelihood phylogenetic tree based on the nucleotide sequences of major capsid protein gene region of enterovirus D68 from Senegal (red text) and reference sequences. Tree was constructed by using IQ-TREE2 2.0.6 (http://www.iqtree.org) and visualized by using Figtree 1.4.4 (http://tree.bio.ed.ac.uk/software/figtree). Statistical significance was tested by using 1,000 bootstrapping replicates. Software was used to define the correct model used. Tree is rooted by the Fermon strain. Scale bar indicates substitutions per site.

SARI collected at the different sentinel sites during January–December 2023, a total of 45 (1.5%) tested positive for enterovirus (Appendix, https://wwwnc.cdc.gov/EID/article/30/8/24-0410-App1.pdf). We detected EV-D68 in 20 (44.4%) of the enterovirus-positive specimens, and most cases (8 [40%]) were recorded during epidemiologic week 50 (Figure 2). The proportion of specimens in which EV-D68 was detected increased from 0.04% during February–September (1/2,338) to 0.7% in November (2/295) and 5.8% in December (17/291). The 20 patients in whom EV-D68 was detected were all children ≤6 years of age (median age 2 years); 65% (13/20) of cases were in girls and 35% (17/20) in boys. Almost all children with confirmed EV-D68 infection (18/20 [90%]) were inpatients with SARI who had been admitted to 2 referral hospitals, Roi Baudouin hospital (11 [55%]) in a suburb of Dakar and Albert Royer Children's Hospital (7 [35%]) in Dakar. The primary reason for hospitalization was bronchiolitis for 30% (6/20), acute bronchitis for 10% (2/20), pneumonia for 30% (6/20), and asthma exacerbation for 20% (4/20). One patient was found to have an underlying medical condition (prematurity). Nearly half (9 [45%]) of children with confirmed EV-D68 infection needed supplemental oxygen. The common clinical characteristics at the time of admission were cough (15 [75%]), breathing difficulties (15 [75%]), fever (9 [45%]), wheezing (5 [25%]), tachypnea (4 [20%]), rhinitis (3 [15%]), and apnea (2 [10%]). Although EV-D68 can cause AFM and other neurologic complications, children infected with EV-D68 during this outbreak had no neurologic symptoms, unlike those described in reports from Europe (*13*) and the United States (Colorado) in 2014 (*14*).

Eight children were co-infected with rhinovirus (6 children), bocavirus (1 child), or human metapneumovirus (1 child). We also encountered mixed infections with *Haemophilus infuenzae* (2 children) and *Streptococcus pneumoniae* (2 children).

For the molecular characterization, we successfully obtained 14 complete EV-D68 genomes and deposited them into GenBank (accession nos. PP838726–39). We initially used the enterovirus online genotyping tool (https://www.rivm.nl/mpf/typingtool/enterovirus) for genotype predictions of EV-D68 strains. The genotyping tool classified all EV-D68 sequences into the sub-genogroup B3. We undertook phylogenetic analysis to further confirm this assignment. The maximum-likelihood phylogenetic tree based on major capsid protein gene region sequences clearly shows that all EV-D68 strains from this outbreak belonged to the B3 lineage, which has been the main subclade of EV-D68 circulating in Senegal since 2016 (Figure 3). However, this B3 lineage circulated at a very low level in 2022, when the A2 subclade emerged and was the dominant strain. By using BLAST (https://blast.ncbi.nlm.nih.gov), we found that the B3 strains from our study were closely related to B3 strains of EV-D68 that circulated in the United States (Maryland) in 2022 (*15*), showing nucleotide similarity of 97.8%–99.37%.

One limitation of this study is that almost all cases of EV-D68 were detected on the basis of samples collected from only 2 referral hospitals in Dakar, which might not reflect the actual incidence of EV-D68 infection for this outbreak. Therefore, active surveillance in inpatient settings across more areas would probably give a more accurate picture of EV-D68 infection in Senegal. Despite this limitation, our study identified an outbreak of EV-D68 in Senegal in real-time, whereas all previous cases were identified in retrospective studies.

Conclusions

We observed a sudden onset of an EV-D68 outbreak in Dakar that was exceptionally intense and lasted from epidemiologic weeks 48 through 52 of 2023. The outbreak was caused by the B3 lineage, which has been circulating in Senegal since 2016, and all infected patients were children ≤6 years of age, most of whom required hospitalization. Given the ability of EV-D68 to cause AFM and AFP, this upsurge of EV-D68 infections in pediatric inpatients underscores the need for enhanced surveillance in inpatient settings across more areas, including collecting respiratory specimens from patients with neurologic illnesses.

Acknowledgments

We acknowledge the Ministry of Health of Senegal for its support and all the SARI sentinel sites healthcare workers. We convey special thanks to Sandra Corre and Quentin Lacour for their unwavering support.

This study was supported by the Institutes Pasteur Network (grant no. ACIP 275-2019) though the Pasteur Institutes' International Division.

About the Author

Mr. Jallow is a final-year PhD student at the Virology Department of the Institute Pasteur of Dakar, Senegal. His research interests include the molecular epidemiology of respiratory viruses, particularly influenza viruses at the human–animal interface. Dr. Dia is head of the Virology Department of the Institute Pasteur of Dakar, Senegal. His primary research focuses on respiratory viral diseases and their implications for public health.

References

1. Sanjay RE, Sabeena S, Robin S, Shaji JT, Jayakrishnan MP, Suresh EKK, et al. Genetic analysis of enterovirus D68 associated with pneumonia in children from South India. J Med Microbiol. 2021;70. https://doi.org/10.1099/jmm.0.001356
2. Holm-Hansen CC, Midgley SE, Fischer TK. Global emergence of enterovirus D68: a systematic review. Lancet Infect Dis. 2016;16:e64–75. https://doi.org/10.1016/S1473-3099(15)00543-5=
3. Abdul-Rahman T, Nazir A, Khater B, Pyrpyris N, Wireko AA, Miteu DG, et al. Increased rhinovirus/enterovirus infections including EV-D68 in the United States, a challenge for healthcare providers amidst influenza virus infection and the COVID-19 pandemic. Postgrad Med J. 2023;99:372–4. https://doi.org/10.1093/postmj/qgad016
4. Dyrdak R, Mastafa M, Hodcroft EB, Neher RA, Albert J. Intra- and interpatient evolution of enterovirus D68 analyzed by whole-genome deep sequencing. Virus Evol. 2019;5:vez007. https://doi.org/10.1093/ve/vez007
5. Messacar K, Abzug MJ, Dominguez SR. 2014 outbreak of enterovirus D68 in North America. J Med Virol. 2016;88:739–45. https://doi.org/10.1002/jmv.24410
6. Sejvar JJ, Lopez AS, Cortese MM, Leshem E, Pastula DM, Miller L, et al. Acute flaccid myelitis in the United States, August–December 2014: results of nationwide surveillance. Clin Infect Dis. 2016;63:737–45. https://doi.org/10.1093/cid/ciw372
7. Dyrdak R, Grabbe M, Hammas B, Ekwall J, Hansson KE, Luthander J, et al. Outbreak of enterovirus D68 of the new B3 lineage in Stockholm, Sweden, August to September 2016. Euro Surveill. 2016;21:30403. https://doi.org/10.2807/1560-7917.ES.2016.21.46.30403
8. Ikuse T, Aizawa Y, Yamanaka T, Habuka R, Watanabe K, Otsuka T, et al. Outbreak of enterovirus D68 among children in Japan—worldwide circulation of enterovirus D68 clade B3 in 2018. Pediatr Infect Dis J. 2021;40:6–10. https://doi.org/10.1097/INF.0000000000002889
9. Peltola V, Österback R, Waris M, Ivaska L, Tähtinen PA, Laine M, et al. Enterovirus D68 outbreak in children, Finland, August–September 2022. Emerg Infect Dis. 2023;29:1258–61. https://doi.org/10.3201/eid2906.221795
10. Fall A, Jallow MM, Kebe O, Kiori DE, Sy S, Goudiaby D, et al. Low circulation of subclade A1 enterovirus D68 strains in Senegal during 2014 North America outbreak. Emerg Infect Dis. 2019;25:1404–7. https://doi.org/10.3201/eid2507.181441
11. Fall A, Ndiaye N, Jallow MM, Barry MA, Touré CSB, Kebe O, et al. Enterovirus D68 subclade B3 circulation in Senegal, 2016: detection from influenza-like illness and acute flaccid paralysis surveillance. Sci Rep. 2019;9:13881. https://doi.org/10.1038/s41598-019-50470-z
12. Jallow MM, Diagne MM, Sagne SN, Tall F, Diouf JBN, Boiro D, et al. Respiratory syncytial virus in pediatric patients with severe acute respiratory infections in Senegal: findings from the 2022 sentinel surveillance season. Sci Rep. 2023;13:20404. https://doi.org/10.1038/s41598-023-47015-w
13. Benschop KS, Albert J, Anton A, Andrés C, Aranzamendi M, Armannsdóttir B, et al. Re-emergence of enterovirus D68 in Europe after easing the COVID-19 lockdown, September 2021. Euro Surveill. 2021;26:2100998. https://doi.org/10.2807/1560-7917.ES.2021.26.45.2100998
14. Aliabadi N, Messacar K, Pastula DM, Robinson CC, Leshem E, Sejvar JJ, et al. Enterovirus D68 infection in children with acute flaccid myelitis, Colorado, USA, 2014. Emerg Infect Dis. 2016;22:1387–94. https://doi.org/10.3201/eid2208.151949
15. Fall A, Han L, Abdullah O, Norton JM, Eldesouki RE, Forman M, et al. An increase in enterovirus D68 circulation and viral evolution during a period of increased influenza like illness, The Johns Hopkins Health System, USA, 2022. J Clin Virol. 2023;160:105379. https://doi.org/10.1016/j.jcv.2023.105379

Address for correspondence: Ndongo Dia, Institut Pasteur Dakar 36, Avenue Pasteur, B.P. 220, Dakar, Senegal; email: ndia@pasteur.sn

Macrolide-Resistant *Mycoplasma pneumoniae* Infections among Children before and during COVID-19 Pandemic, Taiwan, 2017–2023

Tsung-Hua Wu, Yu-Ping Fang, Fang-Ching Liu, Hui-Hsien Pan, Yu-Ying Yang, Chiah-Sing Song, Chun-Yi Lee

Before the COVID-19 pandemic, *Mycoplasma pneumoniae* infections emerged during spring to summer yearly in Taiwan, but infections were few during the pandemic. *M. pneumoniae* macrolide resistance soared to 85.7% in 2020 but declined to 0% during 2022–2023. Continued molecular surveillance is necessary to monitor trends in macrolide-resistant *M. pneumoniae*.

Mycoplasma pneumoniae is a major cause of respiratory tract infections, particularly in children and young adults. *M. pneumoniae* accounts for 10%–30% of community-acquired pneumonia (*1*). Macrolides are the primary treatment, but since 2000, macrolide-resistant *M. pneumoniae* (MRMP) strains have increased substantially, especially in Asia (*2*,*3*). However, a global study indicated a decline in *M. pneumoniae* detections during 2017–2021, which researchers attributed to the impact of nonpharmaceutical COVID-19 measures on *M. pneumoniae* transmission (*4*).

In Taiwan, MRMP prevalence rose from 12.3%–24% before 2017 to 54%–88% during 2017–2020 (*5*–*7*). Multilocus sequence typing (MLST) is a valuable tool for epidemiologic surveillance, offering high discriminatory ability to identify the shift of circulating strain types (*8*–*10*). We used MLST to analyze the genetic diversity and macrolide resistance prevalence of *M. pneumoniae* in hospitalized children in Taiwan during 2017–2023. This study was approved by the institutional review board of Show Chwan Memorial Hospital (approval nos. 1051007 and 1091104).

Author affiliations: Show Chwan Memorial Hospital, Changhua, Taiwan (T.-H. Wu, Y.-Y. Yang); College of Medicine, National Chung Hsing University, Taichung, Taiwan (T.-H. Wu, C.-Y. Lee); Chang Bing Show Chwan Memorial Hospital, Changhua (Y.-P. Fang, C.-S. Song, C.-Y Lee); Jen-Ai Hospital, Taichung (F.-C. Liu); Taichung Veterans General Hospital, Taichung (H.-H. Pan)

DOI: https://doi.org/10.3201/eid3008.231596

The Study

Our study spanned 2 phases: phase 1 was March 2017–June 2019, and phase 2 was March 2020–December 2023. After obtaining the necessary consent, we enrolled children ≤18 years of age at 4 central hospitals in Taiwan: Show Chwan Memorial Hospital (739 beds), Chang Bing Show Chwan Memorial Hospital (946 beds), Jen-Ai Hospital (644 beds), and Chung Shan Medical University Hospital (1,023 beds). We enrolled children with acute respiratory tract infections who tested *M. pneumoniae* IgM–positive via Biocardä (AniBiotech, https://anibiotech.fi). We collected nasopharyngeal or oropharyngeal swab specimens, stored them, and cultured for *M. pneumoniae*. We performed MLST typing on positive cultures confirmed by PCR as true *M. pneumoniae* infections.

We cultured specimens in SP-4 medium and incubated at 37°C in 5% CO_2 for 14 days (*11*). We used the QIAamp DNA Blood Mini Kit (QIAGEN, https://www.qiagen.com) to extract DNA and confirmed *M. pneumoniae* by real-time PCR targeting the repMp1 gene (*12*). We further analyzed *M. pneumoniae* isolates, including single-base mutations in the 23S rRNA gene and MLST on the basis of 8 housekeeping genes (*8*). We used goeBURST software (https://phyloviz.readthedocs.io/en/latest/data_analysis.html) to explore relationships among sequence types (STs).

Among 770 nasopharyngeal or oropharyngeal samples collected during the study period,

Table 1. Annual and seasonal distribution of macrolide-resistant *Mycoplasma pneumoniae* infections among children before and during the COVID-19 pandemic, Taiwan, 2017–2023*

Year	No. positive cases (%)					p value†
	Total no. cases	Spring, Mar–May	Summer, Jun–Aug	Autumn, Sep–Nov	Winter, Dec–Feb	
2017	67 (43.23)	13 (30.23)	9 (21.43)	21 (65.63)	24 (63.16)	<0.001
2018	54 (58.06)	17 (65.38)	18 (81.82)	4 (57.14)	15 (39.47)	0.010
2019	17 (38.64)	4 (14.29)	13 (81.25)	ND	ND	NA
2020	21 (16.80)	8 (61.54)	7 (41.18)	6 (12.50)	0	<0.001
2021	10 (13.33)	10 (24.39)	0	0	0	0.016
2022	16 (11.59)	11 (28.21)	2 (12.50)	3 (4.05)	0	0.002
2023	24 (17.14)	5 (13.51)	13 (37.14)	3 (9.38)	3 (8.33)	0.008
Total	209 (27.14)	68 (29.96)	62 (41.61)	37 (18.14)	42 (22.11)	<0.001
p value‡	<0.001					

*The study period ended December 2023. NA, not applicable; ND, no data.
†p value by Fisher exact test to examine the relationship between season and infection.
‡p value by X^2 test to examine the relationship between year and infection.

209 (27.1%) were confirmed *M. pneumoniae* cases. By comparing the annual and seasonal distribution of *M. pneumoniae* respiratory tract infections, we noted significant yearly differences (p<0.001) and an outbreak that occurred during 2017–2018 (Table 1). Seasonal prevalence also varied significantly (p<0.001); average positivity rates were 30% in spring, 41.6% in summer, 18.1% in autumn, and 22.1% in winter. *M. pneumoniae* was detected year-round, but primarily during March–August (Figure 1, panel A). During the COVID-19 pandemic, detection rates notably declined.

Among the 209 *M. pneumoniae*–positive isolates, 74 (35.4%) were macrolide-resistant. Annual resistance rates ranged from 12.5% in 2017 to 85.7% in 2020, then dropped to 18.2% in 2021 and 0% in 2022 and 2023 (Figure 1, panel B). Among macrolide-resistant isolates, 72 (97.3%) had the A2063G mutation, and 2 (2.7%) had the A2063T mutation.

We submitted all 209 confirmed *M. pneumoniae* strains for molecular analysis, and 155 were identified by MLST, revealing 12 different STs (Appendix Table). ST3 was the most prevalent at 38.2%, followed by ST17 at 19.1%. However, 54 (25.8%) strains could not be successfully genotyped due to the failure of amplification and sequencing of the *pgm* locus. Of the 74 macrolide-resistant isolates, the leading STs were ST3 (49%) and ST17 (8%), but ST3 was the most common in MRMP during 2017–2019 (Figure 2, panel A). Among 135 macrolide-susceptible isolates, ST33 (33%), ST17 (25%), and ST9 (3%) were predominant (Figure 2, panel B). ST17 was more common in macrolide-susceptible than in macrolide-resistant isolates (p = 0.003), and ST3 was more prevalent in macrolide-resistant isolates (p = 0.002). However, we found no correlation between the dynamic proportion of macrolide resistance and ST3, although a notable percentage of macrolide-resistant strains within ST3 were detected during 2017–2019 (Table 2).

We identified 2 clonal complexes (CCs) in the goeBURST analysis (Figure 2, panel C), which included data from 140 strains. Of those 2 CC clusters, most (96%) STs belonged to CC1, which included the most frequently detected STs, ST3 and ST17. CC2 comprised 5 (4%) strains and included 2 STs, ST33 and ST26.

Conclusions

During 2017–2023, we observed changes in *M. pneumoniae* infection rates, alterations in STs, and shifts in antimicrobial resistance. Nonpharmaceutical interventions during the pandemic mitigated the transmission of respiratory pathogens besides SARS-CoV-2 (*13*). In our study, we noted a substantial decrease in *M. pneumoniae* detection during 2021, and no positive cases were recorded during June 2021–February 2022, coinciding with the height of the pandemic period in Taiwan, a finding that aligns with those reported in a global survey (*4*).

MRMP infections have increased greatly worldwide, particularly in the Western Pacific region (*14*). In Taiwan, prior studies noted a substantial rise in macrolide resistance rates from 12%–24% during 2011–2016 to 54%–88% during 2017–2020 (*5*–*7*). However, in our study, MRMP prevalence decreased rapidly to 0%–18.2% during 2021–2023. During the 2011–2012 outbreak in Japan, the MRMP detection rate soared to 90% (*9*). After that outbreak, the number of MRMP strains decreased, reaching 14.3% in 2018, whereas China and South Korea continued to report high resistance rates from 2014 to 2018 (*10*,*15*).

ST3 within CC1 is a globally successful clone and was prevalent in Japan, China, South Korea, Cuba, Germany, and Taiwan at rates from 30% to 70% during 2002–2022 (Appendix Figure). A previous study in Taiwan showed high macrolide resistance rates for ST3 (93.5%) and ST17 (82.1%) (*7*). In contrast, ST17 was more common among the macrolide-susceptible cases in our study and had a resistance rate of only 15%.

Recent data indicate shifts in *M. pneumoniae* sequence types: in Japan, ST3 and ST14 were largely replaced by ST7 and ST33 in 2018–2019, reducing macrolide resistance by 11.3% (*9*). However, South Korea did not have a notable decrease in its macrolide resistance rate (78.5%) during 2019–2020, and ST3 remained dominant (*10*). Our findings show no substantial shifts in ST distribution in Taiwan but a notable change in the ratio of macrolide-resistant to macrolide-susceptible within ST3, possibly reducing the overall resistance rate (Table 2).

The first limitation of our study is that an 8-month gap in data collection occurred during July 2019–February 2020, which might have caused a slight underestimation of cases. Second, we only enrolled patients who tested positive for *M. pneumoniae* IgM, which might underestimate the actual number of *M. pneumoniae* infections. We did not investigate the clinical manifestations

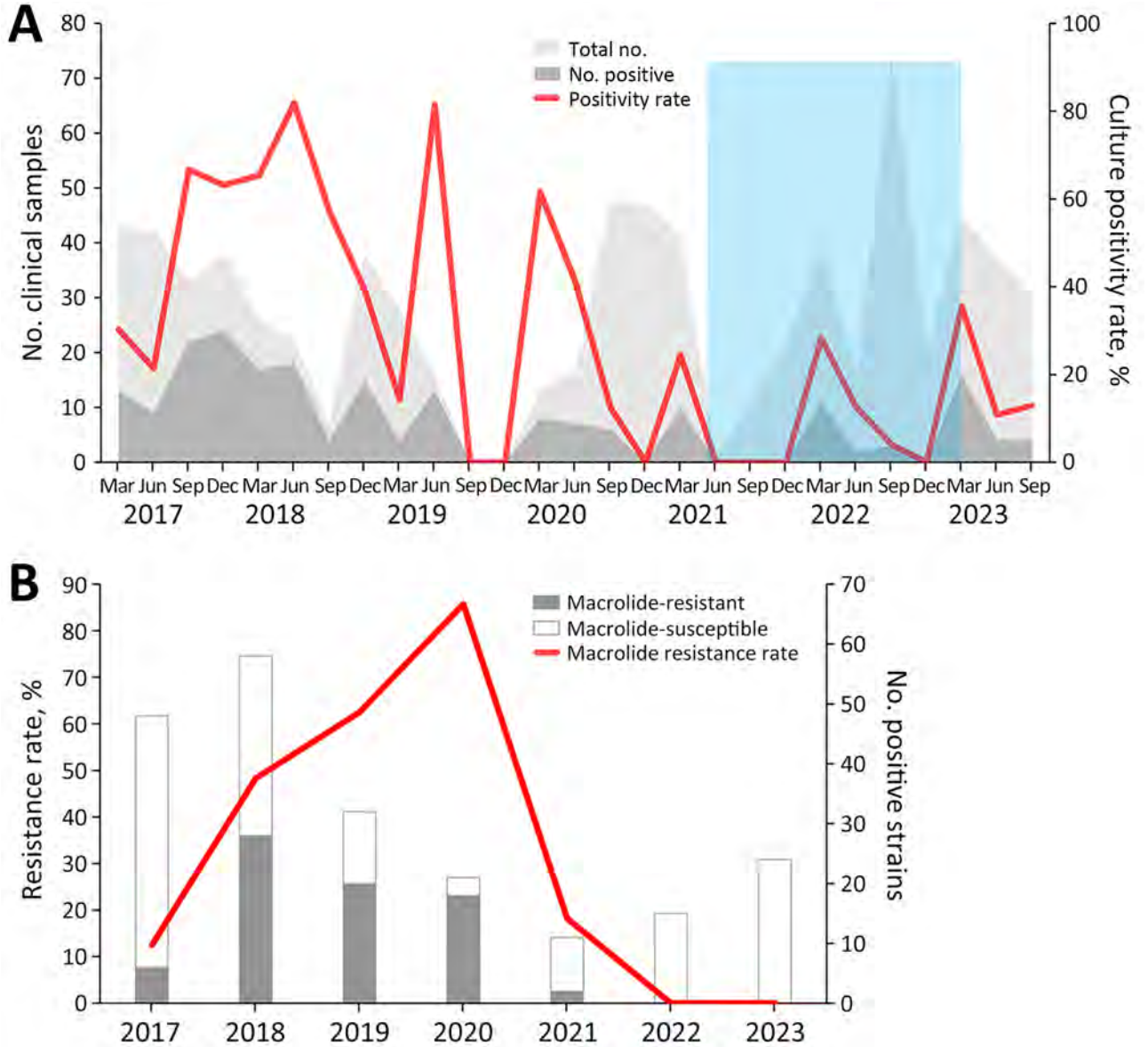

Figure 1. Dynamic distribution of macrolide-resistant *Mycoplasma pneumoniae* infections among children before and during the COVID-19 pandemic, Taiwan, 2017–2023. A) *M. pneumoniae* infections were detected throughout the year, primarily from March to August. An *M. pneumoniae* outbreak occurred during 2017–2018. The *M. pneumoniae* detection rate substantially declined during the COVID-19 pandemic, 2021–2022. Light gray background represents 770 IgM-positive participants; dark gray background represents 209 cases confirmed by culture and PCR. Blue shading indicates timeframe of nonpharmaceutical interventions during the COVID-19 pandemic. B) Among 211 isolates, macrolide resistance was observed in 74 (35.1%) isolates. The resistance rate was 12.5% in 2017, increased to 48.3% in 2018, and to 62.5% in 2019, and reached 85.7% in 2020. Subsequently, the rate decreased to 18.2% in 2021 and dropped to 0% in 2022 and 2023.

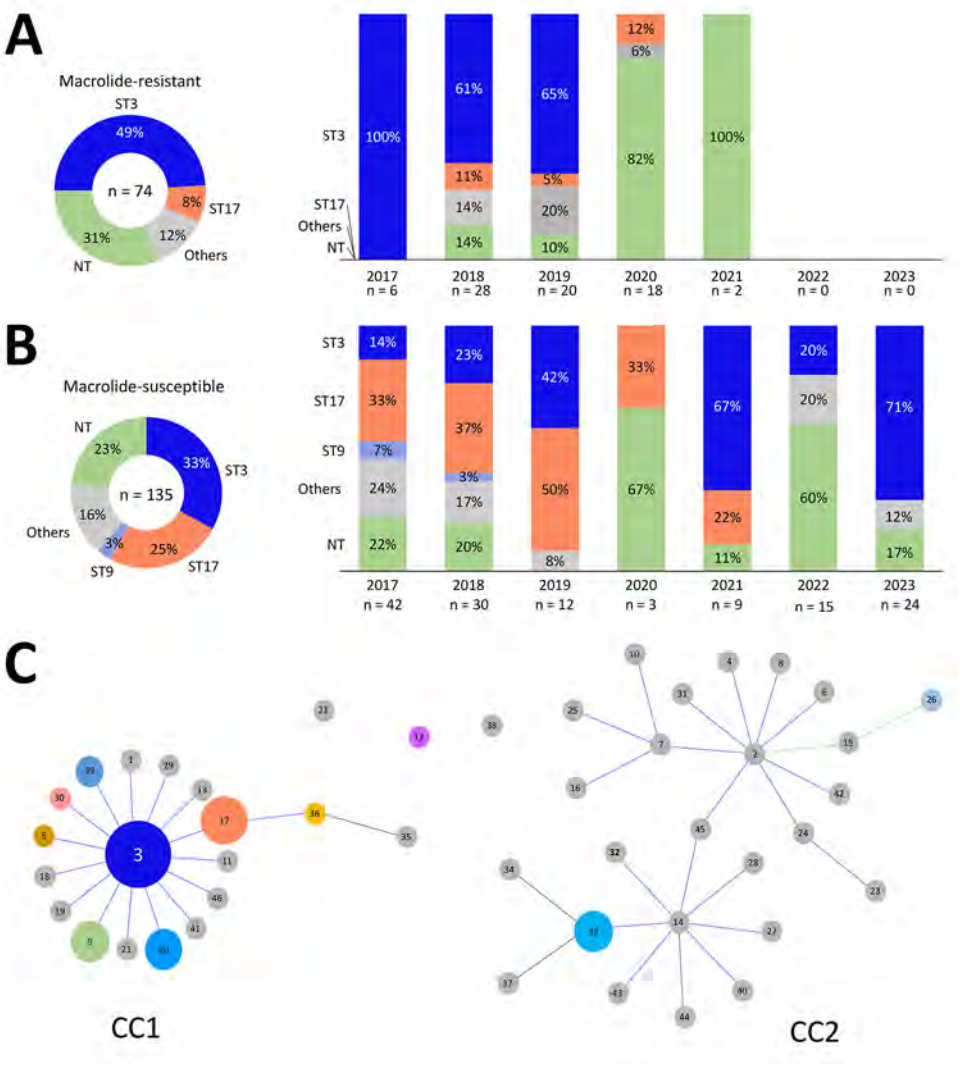

Figure 2. Relationships between year of isolation, ST, and genotype distribution in a study of macrolide-resistant *Mycoplasma pneumoniae* infections among children before and during the COVID-19 pandemic, Taiwan, 2017–2023. A) Macrolide-resistant *M. pneumoniae* isolates (n = 74) and 5 identified STs: ST3, ST17, ST26, ST33, and ST36. Macrolide resistance substantially decreased after 2021. ST3 was the predominant strain in macrolide-resistant isolates, especially during 2017–2019. B) Macrolide-susceptible *M. pneumoniae* isolates (n = 135) and 10 identified STs: ST3, ST17, ST9, ST5, ST12, ST20, ST30, ST33, ST39, and ST46. ST17 was the predominant strain during 2017–2019. ST3 was the most common strain and was distributed across all years. C) The relationship between *M. pneumoniae* CC and ST depicted by goeBURST (https://phyloviz.readthedocs.io/en/latest/data_analysis.html). The data, comprising 144 strains from Taiwan (2017–2023) and previously reported STs (shown in gray) from PubMLST (https://pubmlst.org), demonstrate the genetic relationships within the dataset analyzed by the goeBURST algorithm. The size of each circle is proportional to the number of isolates for each ST, and most STs belonged to CC1, including the leading 2 STs, ST3, and ST17. Green sections indicate *M. pneumoniae* strains could not be successfully identified using multilocus sequence typing. CC, clonal complex; NT, nontypable; ST, sequence type.

in patients who tested IgM-negative. Third, although the trend toward resistant strains was evident, the absolute number of resistant strains was small. Fourth, some strains failed at the *pgm* locus, and on the basis of other known loci, those strains are most likely to be either ST3 or ST17. That issue might have been to the result of low bacterial loads and fragile DNA that hindered the successful amplification of the 1,072-bp *pgm* locus via nested PCR. Recent advances have made whole-genome sequencing a promising tool for future *M. pneumoniae* research, especially in identifying genotypes linked to macrolide resistance or virulence.

Table 2. Distribution of macrolide susceptibility of sequence type 3 and 17 isolates in a study of macrolide-resistant *Mycoplasma pneumoniae* infections among children before and during the COVID-19 pandemic, Taiwan, 2017–2023

	Year, no. (%) isolates						
Macrolide susceptibility	2017	2018	2019	2020	2021	2022	2023
Sequence type 3							
Resistant	6 (50)	17 (70.8)	13 (72.2)	0	0	0	0
Susceptible	6 (50)	7 (29.2)	5 (27.8)	0	6 (100)	3 (100)	17 (100)
Total no. isolates	12	24	18	0	6	3	17
Sequence type 17							
Resistant	0	3 (21.4)	1 (14.3)	2 (66.7)	0	0	0
Susceptible	14 (100)	11 (78.6)	6 (85.7)	1 (33.3)	2 (100)	0	0
Total no. isolates	14	14	7	3	2	0	0

In conclusion, *M. pneumoniae* respiratory tract infections in Taiwan exhibit seasonality, and prevalence decreased after the COVID-19 pandemic. Simultaneously, MRMP incidence experienced a sharp decline after 2021. Although ST3 remains the most prevalent *M. pneumoniae* strain and is associated with macrolide resistance, global data still lack evidence of correlation between STs and macrolide resistance. Thus, continued molecular surveillance is necessary to monitor those trends.

Acknowledgments

We thank the patients who graciously consented to participate in this study, as well as all the clinicians who contributed by taking samples.

About the Author

Dr. Wu is a pediatrician in Show Chwan Memorial Hospital, Changhua, Taiwan. His primary research interest is infectious diseases, particularly *Mycoplasma pneumoniae*.

References

1. Principi N, Esposito S, Blasi F, Allegra L; Mowgli Study Group. Role of *Mycoplasma pneumoniae* and *Chlamydia pneumoniae* in children with community-acquired lower respiratory tract infections. Clin Infect Dis. 2001;32:1281–9. https://doi.org/10.1086/319981
2. Morozumi M, Ubukata K, Takahashi T. Macrolide-resistant *Mycoplasma pneumoniae*: characteristics of isolates and clinical aspects of community-acquired pneumonia. J Infect Chemother. 2010;16:78–86. https://doi.org/10.1007/s10156-009-0021-4
3. Pereyre S, Goret J, Bébéar C. *Mycoplasma pneumoniae*: current knowledge on macrolide resistance and treatment. Front Microbiol. 2016;7:974. 10.3389/fmicb.2016.00974 https://doi.org/10.3389/fmicb.2016.00974
4. Meyer Sauteur PM, Beeton ML, Uldum SA, Bossuyt N, Vermeulen M, Loens K, et al.; ESGMAC–MyCOVID Study Team. *Mycoplasma pneumoniae* detections before and during the COVID-19 pandemic: results of a global survey, 2017 to 2021. Euro Surveill. 2022;27:2100746. https://doi.org/10.2807/1560-7917.ES.2022.27.19.2100746
5. Wu HM, Wong KS, Huang YC, Lai SH, Tsao KC, Lin YJ, et al. Macrolide-resistant *Mycoplasma pneumoniae* in children in Taiwan. J Infect Chemother. 2013;19:782–6. https://doi.org/10.1007/s10156-012-0523-3
6. Kuo CY, Tsai WC, Lee HF, Ho TS, Huang LM, Shen CF, et al.; Taiwan Pediatric Infectious Disease Alliance (TPIDA). The epidemiology, clinical characteristics, and macrolide susceptibility of *Mycoplasma pneumoniae* pneumonia in children in Southern Taiwan, 2019–2020. J Microbiol Immunol Infect. 2022;55:611–9. https://doi.org/10.1016/j.jmii.2021.09.010
7. Hung H-M, Chuang C-H, Chen Y-Y, Liao W-C, Li S-W, Chang IY-F, et al. Clonal spread of macrolide-resistant Mycoplasma pneumoniae sequence type-3 and type-17 with recombination on non-P1 adhesin among children in Taiwan. Clin Microbiol Infect. 2021;27:1169.e1–6. https://doi.org/10.1016/j.cmi.2020.09.035
8. Brown RJ, Holden MT, Spiller OB, Chalker VJ. Development of a multilocus sequence typing scheme for molecular typing of *Mycoplasma pneumoniae*. J Clin Microbiol. 2015;53:3195–203. https://doi.org/10.1128/JCM.01301-15
9. Morozumi M, Tajima T, Sakuma M, Shouji M, Meguro H, Saito K, et al. Sequence type changes associated with decreasing macrolide-resistant *Mycoplasma pneumoniae*, Japan. Emerg Infect Dis. 2020;26:2210–3. https://doi.org/10.3201/eid2609.191575
10. Lee JK, Choi YY, Sohn YJ, Kim KM, Kim YK, Han MS, et al. Persistent high macrolide resistance rate and increase of macrolide-resistant ST14 strains among *Mycoplasma pneumoniae* in South Korea, 2019–2020. J Microbiol Immunol Infect. 2022;55:910–6. https://doi.org/10.1016/j.jmii.2021.07.011
11. Tully JG. New laboratory techniques for isolation of *Mycoplasma pneumoniae*. Yale J Biol Med. 1983;56:511–5.
12. Dumke R, Schurwanz N, Lenz M, Schuppler M, Lück C, Jacobs E. Sensitive detection of *Mycoplasma pneumoniae* in human respiratory tract samples by optimized real-time PCR approach. J Clin Microbiol. 2007;45:2726–30. https://doi.org/10.1128/JCM.00321-07
13. Mendez-Brito A, El Bcheraoui C, Pozo-Martin F. Systematic review of empirical studies comparing the effectiveness of non-pharmaceutical interventions against COVID-19. J Infect. 2021;83:281–93. https://doi.org/10.1016/j.jinf.2021.06.018
14. Kim K, Jung S, Kim M, Park S, Yang HJ, Lee E. Global trends in the proportion of macrolide-resistant *Mycoplasma pneumoniae* infections: a systematic review and meta-analysis. JAMA Netw Open. 2022;5:e2220949. https://doi.org/10.1001/jamanetworkopen.2022.20949
15. Zhao F, Li J, Liu J, Guan X, Gong J, Liu L, et al. Antimicrobial susceptibility and molecular characteristics of *Mycoplasma pneumoniae* isolates across different regions of China. Antimicrob Resist Infect Control. 2019;8:143. https://doi.org/10.1186/s13756-019-0576-5

Address for correspondence: Chun-Yi Lee, Department of Pediatrics, Chang Bing Show Chwan Memorial Hospital, No. 6 Lu-Kung Rd, Chang Bing Industrial Center, Lu-Kang, Changhua 505, Taiwan; email: lee821083@gmail.com

Group B *Streptococcus* Sequence Type 103 as Human and Bovine Pathogen, Brazil

Laura M.A. Oliveira, Leandro C. Simões, Chiara Crestani, Natália S. Costa, José Carlos F. Pantoja, Renata F. Rabello, Sérgio E.L. Fracalanzza, Lucia M. Teixeira, Uzma B. Khan, Dorota Jamrozy, Stephen Bentley, Tatiana C.A. Pinto, Ruth N. Zadoks

Group B *Streptococcus* sequence type 103 is known primarily as a bovine mastitis pathogen. In Brazil, it has circulated in cattle and humans since the 1990s. It lacks *scp*B and, in humans, was found only among carriage isolates. Bovine–human interspecies transmission may have contributed to its evolution and spread.

Group B *Streptococcus* (GBS) is a major cause of life-threatening neonatal infections and bovine mastitis (*1*). The GBS population is composed of host-specialist lineages, such as sequence type (ST) 17, and host-generalist lineages, such as ST23 (*2*). ST103 is common among bovine GBS (bGBS) in Europe (*3*,*4*), Colombia (*5*), and China (*6*); reports of human GBS (hGBS) ST103 are rare and mostly limited to Asia (*7*–*9*). This difference may reflect limitations to host or geographic range or may be attributable to surveillance efforts. We investigated the molecular epidemiology of GBS STs in humans and cattle in Brazil.

The Study

We extracted genomic DNA from hGBS (carriage n = 416, disease n = 39) and bGBS (milk n = 151, environment n = 5) isolates collected in Brazil during 1978–2021 (Table 1) by using the DNeasy Blood & Tissue Kit (QIAGEN, https://www.qiagen.com). We generated whole-genome sequences at the Wellcome Sanger Institute (Hixton, UK; https://www.gbsgen.net) or at MicrobesNG (Birmingham, UK; https://microbesng.com) by using the Illumina NovaSeq platform (https://www.illumina.com). We used the sequences to predict ST, capsular types, antimicrobial resistance (AMR), and surface protein profiles (Alpha, Alp1, Alp2/3, Rib, Srr1, Srr2, pilus islands PI1, PI-2A1, PI-2A2, and PI-2B, and HvgA) with GBS Typer version 1.0.11 (https://github.com/sanger-bentley-group/GBS-Typer-sanger-nf), and to detect *scp*B gene carriage by using BLASTn (https://blast.ncbi.nlm.nih.gov) and GenBank reference sequence AF327852.1. We performed whole-genome alignment by using Snippy v4.6.0 (https://github.com/tseemann/snippy) and constructed a phylogenetic tree with RAxML as implemented in Gubbins version 3.3.1 (https://github.com/nickjcroucher/gubbins).

We included only GBS isolates assigned to ST103 in this study. Of the 611 isolates tested, 67 (11%) isolates belonged to ST103 (17 hGBS isolates, 1990–2020; 50 bGBS, 1999–2021) (Table 2), which showed that ST103 hGBS circulated in Brazil in parallel with bGBS well before it was reported elsewhere (*7*–*9*). In accordance with previous studies (*2*,*4*), ST103 isolates mostly belonged to serotype Ia, with 1 exception (hGBS, serotype II), which was also the only *ssr*1-negative isolate (Figure 1). Although rare, capsular switching can occur in GBS and may impair the effectiveness of future polysaccharide vaccines (*10*).

The core-genome phylogeny showed 10 clusters, largely representing either host or, for bGBS, farm of origin, and 3 singletons (Figure 1). Some bGBS (clusters D and E) were more closely related to hGBS (clusters B, C, and F) than to other bGBS (clusters G, I, and J) (Figure 1). The hGBS were distributed across 4 clusters and 3 singletons. Clusters B (n = 2 isolates), C

Author affiliations: Federal University of Rio de Janeiro, Rio de Janeiro, Brazil (L.M.A. Oliveira, L.C. Simões, N.S. Costa, S.E.L. Fracalanzza, L.M. Teixeira, T.C.A. Pinto); Pasteur Institut, Paris, France (C. Crestani); Universidade Estadual Paulista Júlio de Mesquita Filho, São Paulo, Brazil (J.C.F. Pantoja); Fluminense Federal University, Rio de Janeiro (R.F. Rabello); Wellcome Sanger Institute, Hinxton, UK (U.B. Khan, D. Jamrozy, S. Bentley); University of Sydney, Camden, New South Wales, Australia (R.N. Zadoks)

DOI: http://doi.org/10.3201/eid3008.231575

Table 1. Origin of GBS isolates recovered from human and bovine samples submitted to whole-genome sequencing, Brazil*

Host	Clinical source	Region	Collection year	ST103 GBS	Non-ST103 GBS
Human†	Anovaginal carriage‡	Rio de Janeiro	1979–2021	14	329
	Oropharynx§	Rio de Janeiro	1978–2014	2	8
	Umbilical swab	Rio de Janeiro	2001	0	1
	Semen	Rio de Janeiro	2017–2018	1	61
	Urine	Rio de Janeiro	1990–2019	0	16
		São Paulo	2009	0	3
		Porto Alegre	2006	0	5
		Cuiabá	2009	0	2
	Invasive disease specimens¶	Rio de Janeiro	1990–2021	0	13
Bovine	Milk	Rio de Janeiro#	1987–2007	17	38
		Minas Gerais**	1996–2021	6	51
		São Paulo††	1987–2021	23	16
	Farm environment	Minas Gerais‡‡	2010	4	1

*GBS, group B *Streptococcus*; ST, sequence type.
†Human isolates were epidemiologically unrelated.
‡Anovaginal carriage: anovaginal specimens collected from pregnant women between the 35th and 37th gestational weeks during routine antenatal care.
§Oropharynx: throat swab.
¶Invasive disease specimens: blood, cerebrospinal fluid, cerebrospinal fluid, bronchoalveolar lavage, peritoneal fluid, bone, abscess.
#Isolates represent 18 farms and 53 cows.
**Isolates represent 21 farms and 46 cows.
††Isolates represent 6 farms and 21 cows.
‡‡Isolates represent 1 farm and 5 environmental samples.

(n = 2), and F (n = 8) formed a clade with bGBS clusters D and E and were detected throughout the period studied (1990–2020) (Figure 1). Cluster H (n = 2), which is located on a long branch in the phylogeny, included 2 historical strains isolated in 1990 from human oropharynx samples.

Some accessory genome traits were consistent across the entire phylogeny, whereas others differed between or within host species. All isolates carried pilus island PI-2B, as previously decribed (*2*,*4*). All hGBS and bGBS isolates lacked the *scp*B gene, which encodes C5a peptidase and is crucial for GBS adhesion and invasion of human cells (*11*). The absence of *scp*B gene may explain why ST103 was only found among carriage isolates in humans, although a larger sample size or in vitro studies would be needed to provide statistical or mechanistic support for that hypothesis.

The Alpha protein gene was absent in clusters nearest to the tree root, regardless of host, year or, for bGBS, farm of isolation, suggesting that the element was acquired later by the diverged subpopulation (clusters A–F). By contrast, the lactose operon was consistently present in all bGBS but not in all hGBS, suggesting either multiple loss or acquisition events in those host-associated clusters. The ability to ferment lactose, as mediated by the Lac.2 operon, drives GBS adaptation to the bovine udder (*2*). Presence

Table 2. Distribution of group B *Streptococcus* ST103 isolates from human and bovine samples, Brazil*

Host	Sample	No. isolates	Accession nos. (ENA/GenBank)
Human	Anovaginal	14	ERR9738291†, ERR9738561†, ERR9738563†, ERR9738359†, ERR9738596†, ERR9738481, ERR9738404†‡, ERR9738442†, ERR9738474, ERR9738564, ERR9738631, ERR9738643, ERR9937783†, ERR9937793
	Oropharynx	2	ERR9738674, ERR9738675
	Semen	1	ERR9738366
Bovine	Milk	46	ERR9738322, ERR9937866, ERR9937886, ERR9937890, ERR9937910, ERR9937940, ERR9738322, ERR9937792, ERR9937904, ERR9937944, ERR9937946, ERR9937948, ERR9937950, ERR9937952, ERR9937954, ERR9937956, ERR9937966, ERR9937968, ERR9937970, ERR9937972, ERR9937974, ERR9937976, ERR9937978, ERR9937980, ERR9937936, ERR9937703, ERR9937937, ERR9937705, ERR9937707, ERR9937939, BioProject ID: PRJNA1086968 (JBBHGR000000000, JBBHGQ000000000, JBBHGP000000000, JBBHGO000000000, JBBHGN000000000, JBBHGM000000000, JBBHGL000000000, JBBHGK000000000, JBBHGJ000000000, JBBHGI000000000, JBBHGH000000000, JBBHGG000000000, JBBHGF000000000, JBBHGE000000000, JBBHGD000000000, JBBHGC000000000)
	Farm environment	4	ERR9937891, ERR9937699, ERR9937892, ERR9937893

*ST103 identified from 619 human and bovine isolates collected in Brazil during 1978–2021. All ST103 isolates were negative for *scpB*. All bovine isolates were lactose fermenting, as were 8 human isolates from anovaginal samples. All but 1 isolate belonged to serotype Ia. ENA, European Nucleotide Archive; ST, sequence type.
†Human isolates positive for lactose fermentation.
‡Human isolate belonging to serotype II.

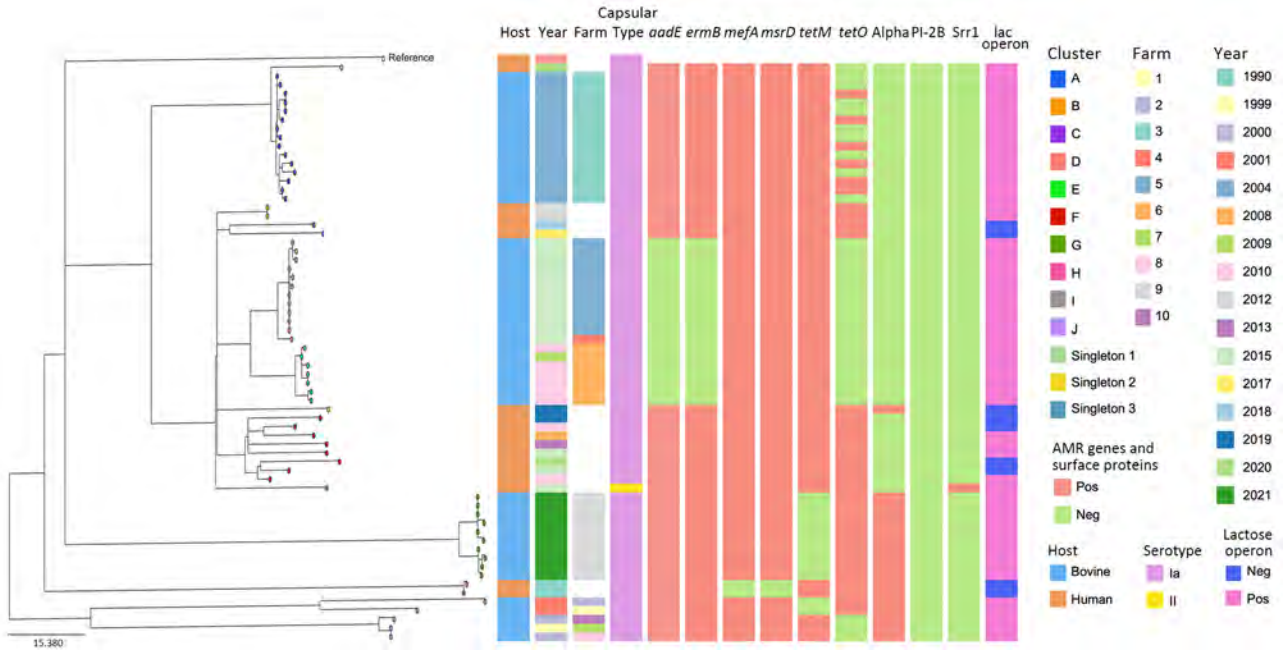

Figure 1. Phylogeny of group B *Streptococcus* isolates belonging to ST103 recovered from cattle and human populations in Brazil, 1990–2021. The tree was built based on single-nucleotide polymorphisms extracted from an alignment outside recombination regions, created by mapping reads of each isolate to the sequence of the ST103 reference strain GBS85147 (GenBank accession no. CP010319.1). Scale bar indicates substitutions per site. AMR, antimicrobial resistance; neg, negative; pos, positive; ST, sequence type.

of Lac.2 and the phenotypic ability to ferment lactose are relatively rare in human isolates (*4*,*12*). In our study, all bGBS and almost half of hGBS (n = 8, 47%) were able to ferment lactose, suggesting bovine-to-human transmission with subsequent loss of Lac.2 in the absence of selective pressure for its maintenance in the human niche. This finding contrasts with an earlier study, which suggested a human origin of bovine ST103 (*3*). In-depth analysis of the evolution of this clade using a larger collection of isolates across a broad geographic range would be needed to determine the timing and direction of host jumps.

We observed the greatest variability in accessory genome content in AMR genes. In bGBS, *tet*O was the most common resistance gene, followed by *tet*M, but never in combination. In hGBS, AMR genes were rarely found (Figure 1); this finding is in contrast to many other human-associated GBS lineages, which have a high prevalence of tetracycline resistance genes (*13*). In addition to *tet*O, bGBS clusters D and E also carried *erm*B and *aad*E on a variant of ICESag37 (OP508056), an integrative conjugative element associated with AMR and virulence genes, with a median nucleotide similarity of 86% (Figure 2). Overall, prevalence of AMR genes was higher in bGBS than in hGBS (88% vs. 17.6% of isolates carrying ≥1 AMR gene). Sampling bias might have contributed to this finding; several herds were represented by multiple isolates, which formed monophyletic clusters with homogeneous AMR profiles, as expected based on contagious transmission of bGBS within dairy herds. Nevertheless, we detected AMR in bGBS in every single herd, and AMR prevalence in bGBS would still be higher than in hGBS if each herd was represented by a single isolate, indicating a true biologic effect. The high prevalence of AMR among bGBS may be driven by the overuse of antimicrobial drugs in dairy herds in emerging economies like that of Brazil (*1*), where macrolides, tetracycline, and aminoglycosides are among the most commonly used antimicrobial drugs for treatment and prevention of clinical mastitis (*14*).

Vaccination is desirable to prevent hGBS and bGBS disease without reliance on antimicrobial drugs, but no human or bovine vaccines are licensed yet. Promising candidates for a human maternal vaccine include both polysaccharide-protein conjugate and protein subunit strategies. Surveillance of capsular types and surface proteins of emerging GBS lineages, including in low- and middle-income countries, is crucial to inform vaccine design, which can impair vaccine effectiveness. In our study, all ST103 strains were associated with serotype Ia and PI-2B, Srr1, and Alpha surface proteins, which are among the most immunogenic vaccine targets (*15*).

Conclusions

GBS is a multihost pathogen, able to adapt to different niches. The phylogeny of ST103 and the presence of the lactose operon in hGBS suggest that interspecies transmission (bovine-to-human) might have contributed to the evolution of ST103 in Brazil. In addition, our results suggest that the presence of the pilus variant PI-2B and absence of the *scp*B gene are common markers of ST103 in Brazil, irrespective of host species. The lack of *scp*B may limit the virulence of GBS ST103 in humans, which in turn may have contributed to its underreporting, especially in countries or studies that focus on clinical isolates. Additional studies at population and mechanistic level would be needed to fully understand the origin, evolution, epidemiology, and virulence potential of this emerging clade, but our results show that ST103 is more common in hGBS than previously described and that it has been circulating in Brazil at least since the 1990s.

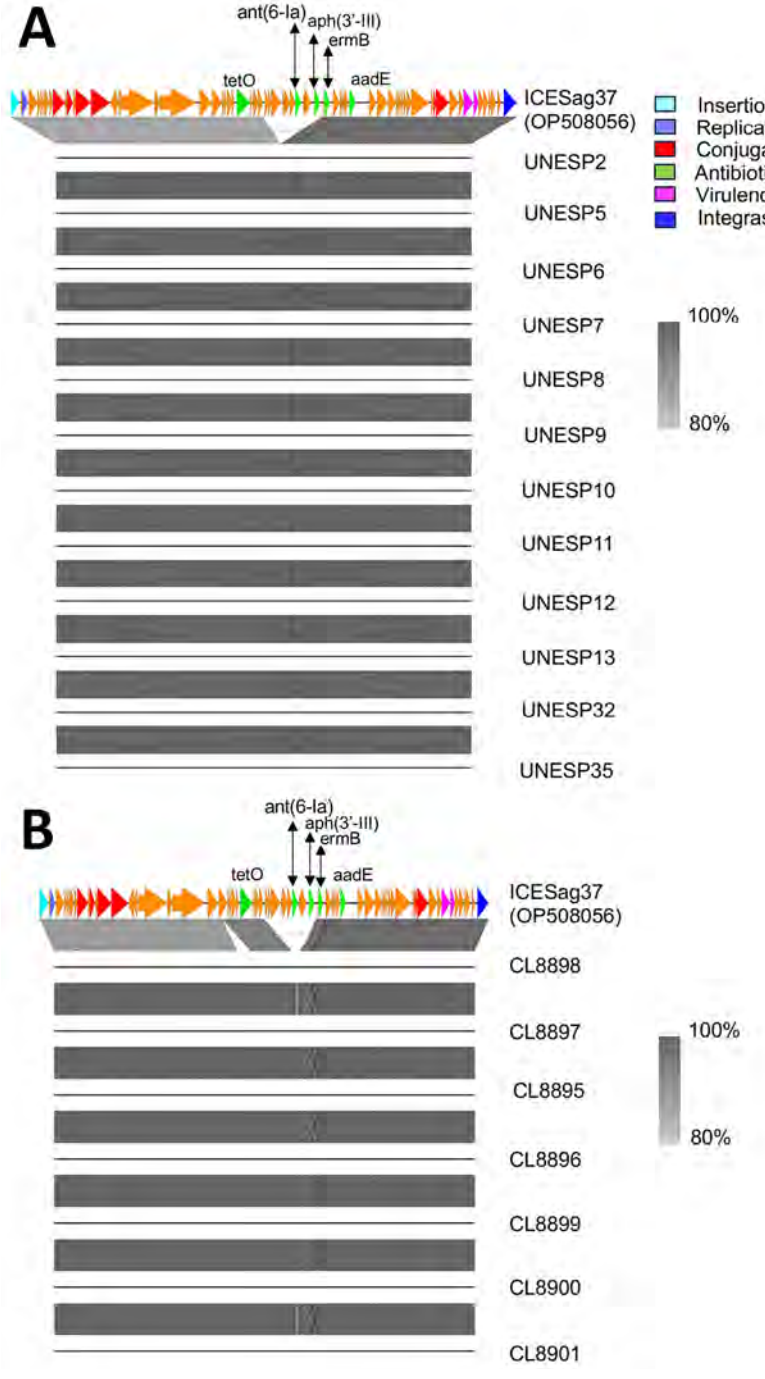

Figure 2. Alignment of nucleotide sequences of bovine group B *Streptococcus* isolates belonging to ST103 collected in Brazil with ICESag37, an integrative conjugative element associated with antimicrobial resistance and virulence genes. A) Sequence alignment for cluster D isolates (n = 12). B) Sequence alignment for cluster E isolates (n = 7). The analysis used Easyfig version 2.2 to perform BLASTn (https://blast.ncbi.nlm.nih.gov) comparisons between isolates in clusters D and E against the reference ICEsag37 (GenBank accession no. OP508056). Arrows indicate mobility genes and conjugal transfer proteins (red), *rep*A initiator genes (purple), critical site-specific recombinase (blue), antibiotic resistance genes (green), and other ICE genes (orange). Aminoglycoside genes normally found in ICESag37 (*ant*(6–1a) and *aph*(3-III)) are missing from the bovine isolates.

This work was supported by the International Veterinary Vaccinology Network (IVVN) Fellowship Programme and the JUNO project (https://www.gbsgen.net) through a Bill and Melinda Gates Foundation grant (INV-010426).

About the Author

Dr. Oliveira is a postdoctoral researcher at the Microbiology Institute of the Federal University of Rio de Janeiro, Brazil. Her primary research interests include investigating the molecular epidemiology, antimicrobial resistance markers, and virulence traits of GBS isolated from humans and animals to improve the surveillance and diagnosis of infectious diseases and to inform control strategies and vaccine design.

References

1. Oliveira LMA, Simões LC, Costa NS, Zadoks RN, Pinto TCA. The landscape of antimicrobial resistance in the neonatal and multi-host pathogen group B *Streptococcus:* review from a One Health perspective. Front Microbiol. 2022;13:943413. https://doi.org/10.3389/fmicb.2022.943413
2. Richards VP, Velsko IM, Alam MT, Zadoks RN, Manning SD, Pavinski Bitar PD, et al. Population gene introgression and high genome plasticity for the zoonotic pathogen *Streptococcus agalactiae.* Mol Biol Evol. 2019;36:2572–90. https://doi.org/10.1093/molbev/msz169
3. Crestani C, Forde TL, Lycett SJ, Holmes MA, Fasth C, Persson-Waller K, et al. The fall and rise of group B *Streptococcus* in dairy cattle: reintroduction due to human-to-cattle host jumps? Microb Genom. 2021;7:000648. https://doi.org/10.1099/mgen.0.000648
4. Lyhs U, Kulkas L, Katholm J, Waller KP, Saha K, Tomusk RJ, et al. *Streptococcus agalactiae* serotype IV in humans and cattle, northern Europe. Emerg Infect Dis. 2016;22:2097–103. https://doi.org/10.3201/eid2212.151447
5. Cobo-Ángel C, Jaramillo-Jaramillo AS, Lasso-Rojas LM, Aguilar-Marin SB, Sanchez J, Rodriguez-Lecompte JC, et al. *Streptococcus agalactiae* is not always an obligate intramammary pathogen: molecular epidemiology of GBS from milk, feces, and environment in Colombian dairy herds. PLoS One. 2018;13:e0208990. https://doi.org/10.1371/journal.pone.0208990
6. Yang Y, Liu Y, Ding Y, Yi L, Ma Z, Fan H, et al. Molecular characterization of *Streptococcus agalactiae* isolated from bovine mastitis in eastern China. PLoS One. 2013;8:e67755. https://doi.org/10.1371/journal.pone.0067755
7. Boonyayatra S, Wongsathein D, Tharavichitkul P. Genetic relatedness among *Streptococcus agalactiae* isolated from cattle, fish, and humans. Foodborne Pathog Dis. 2020;17:137–43. https://doi.org/10.1089/fpd.2019.2687
8. Shen L, Huang M, Xie N. Experimental study on *Streptococcus agalactiae* genotype and erythromycin resistance in neonatal sepsis. Cell Mol Biol. 2022;67:100–6. https://doi.org/10.14715/cmb/2021.67.6.14
9. Hsu JF, Chen CL, Lee CC, Lien R, Chu SM, Fu RH, et al. Characterization of group B *Streptococcus* colonization in full-term and late-preterm neonates in Taiwan. Pediatr Neonatol. 2019;60:311–7. https://doi.org/10.1016/j.pedneo.2018.07.015
10. Bellais S, Six A, Fouet A, Longo M, Dmytruk N, Glaser P, et al. Capsular switching in group B *Streptococcus* CC17 hypervirulent clone: a future challenge for polysaccharide vaccine development. J Infect Dis. 2012;206:1745–52. https://doi.org/10.1093/infdis/jis605
11. Franken C, Haase G, Brandt C, Weber-Heynemann J, Martin S, Lämmler C, et al. Horizontal gene transfer and host specificity of beta-haemolytic streptococci: the role of a putative composite transposon containing *scp*B and *lmb.* Mol Microbiol. 2001;41:925–35. https://doi.org/10.1046/j.1365-2958.2001.02563.x
12. Sørensen UB, Poulsen K, Ghezzo C, Margarit I, Kilian M. Emergence and global dissemination of host-specific *Streptococcus agalactiae* clones. MBio. 2010;1:e00178-10. https://doi.org/10.1128/mBio.00178-10
13. Da Cunha V, Davies MR, Douarre PE, Rosinski-Chupin I, Margarit I, Spinali S, et al.; DEVANI Consortium. *Streptococcus agalactiae* clones infecting humans were selected and fixed through the extensive use of tetracycline. Nat Commun. 2014;5:4544. https://doi.org/10.1038/ncomms5544
14. Tomazi T, Dos Santos MV. Antimicrobial use for treatment of clinical mastitis in dairy herds from Brazil and its association with herd-level descriptors. Prev Vet Med. 2020;176:104937. https://doi.org/10.1016/j.prevetmed.2020.104937
15. McGee L, Chochua S, Li Z, Mathis S, Rivers J, Metcalf B, et al. Multistate, population-based distributions of candidate vaccine targets, clonal complexes, and resistance features of invasive group B streptococci within the United States, 2015–2017. Clin Infect Dis. 2021;72:1004–13. https://doi.org/10.1093/cid/ciaa151

Address for correspondence: Laura M.A. Oliveira, Av. Carlos Chagas Filho, 373 Bl I Room I02-028, Cidade Universitária, , Instituto de Microbiologia Paulo de Goes, Universidade Federal do Rio de Janeiro, Rio de Janeiro 21941-902, Brazil; email: lauraoliveira@micro.ufrj.br

Recurrent Occupational Hantavirus Infections Linked to Feeder Rodent Breeding Farm, Taiwan, 2022

Kung-Ching Wang, Chih-Kai Chang, Shu-Fen Chang, Pei-Yun Shu, Hsi-Chieh Wang, Shin-Wei Su, Fang-Ling Lin, Chung-Yu Wang, Chia-ping Su[1]

We investigated 2 acute cases and 1 previous case of Seoul hantavirus infection in workers in a feeder rodent breeding farm in Taiwan. Prevalence of hantavirus IgG among the tested feeder rats was 37.5%. Appropriate prevention measures, including using disinfection protocols and personal protective equipment, are crucial to lowering risk.

Each year in Taiwan, hantaviruses cause 0–4 human cases of hemorrhagic fever with renal syndrome (HFRS) (*1*). *Rattus norvegicus* rats are a notable local reservoir host for Seoul virus (SEOV), a hantavirus causing HFRS, but SEOV also is found in other rat species, such as *Rattus rattus*, *R. flavipectus*, and *R. losea* (*2*). Humans can be exposed to hantaviruses by inhaling aerosolized virus from rodent urine or feces or by being bitten by an infected rodent (*3*). SEOV is not known to spread from person to person.

Rodent-to-rodent transmission occurs through biting or scratching or by exposure from contaminated materials, such as bedding (*4*). Vertical transmission is less likely because rodent progeny are protected by maternal antibodies (*5*). Since 2013, human hantavirus infections transmitted by pet rats have been reported in countries in Europe and the United States (*6*,*7*). In the Netherlands, quantitative reverse transcription PCR (RT-PCR) testing revealed 12.2% positivity among feeder rats not linked to human SEOV cases (*8*). The feeder rodent industry involves cultivating and selling live and frozen rats and mice, primarily as food for reptiles and birds of prey. Although hantavirus infections have occurred in laboratory workers working with rats, little information has existed about hantaviruses in workers at feeder rodent breeding farms (*9*).

In October 2022, hantavirus infection in a man in his 30s (case-patient A) was reported to the Taiwan Centers for Disease Control (TCDC; Taipei, Taiwan); diagnosis was confirmed by a 4-fold increase in serum IgG from acute- to convalescent-phase serum samples. Initially, the patient manifested fever, generalized malaise, and clinically confirmed coagulopathy and acute renal failure. Upon learning that he worked at a feeder rodent breeding farm, our team sought source and other epidemiologic data to help prevent disease transmission. Because our outbreak investigation involved a notifiable disease, the study was exempt from institutional review board approval. We obtained approval from the Institutional Animal Care and Use Committee at the National Taiwan University College of Medicine and College of Public Health (approval no. 20220344).

The Study

At the time of disease diagnosis, the farm employed 5 workers (including case-patient A) and had ≈12,000 feeder mice (*Mus musculus*) and 2,200 feeder rats (*R. norvegicus*) (Appendix, https://wwwnc.cdc.gov/EID/article/30/8/23-0875-App1.pdf). The owner had introduced no new rodents since 2017. The breeding room in the farm building was an enclosed space (Figure 1). Feeder mice and rats were housed in different racks (Figure 2). Workers were required to wear face masks and gloves when working, but no protocol existed for hand hygiene.

Author affiliations: Taiwan Centers for Disease Control, Ministry of Health and Welfare, Taipei, Taiwan (K.-C. Wang, C.-K. Chang, S.-F. Chang, P.-Y. Shu, C.-p. Su); Institute of Environmental and Occupational Health Sciences, National Taiwan University (H.-C. Wang, S.-W. Su, F.-L. Lin, C.-Y. Wang); National Tsing Hua University School of Medicine, Hsinchu, Taiwan (C.-p. Su)

DOI: https://doi.org/10.3201/eid3008.230875

[1]Current affiliation: New Taipei Municipal TuCheng Hospital, New Taipei City, Taiwan.

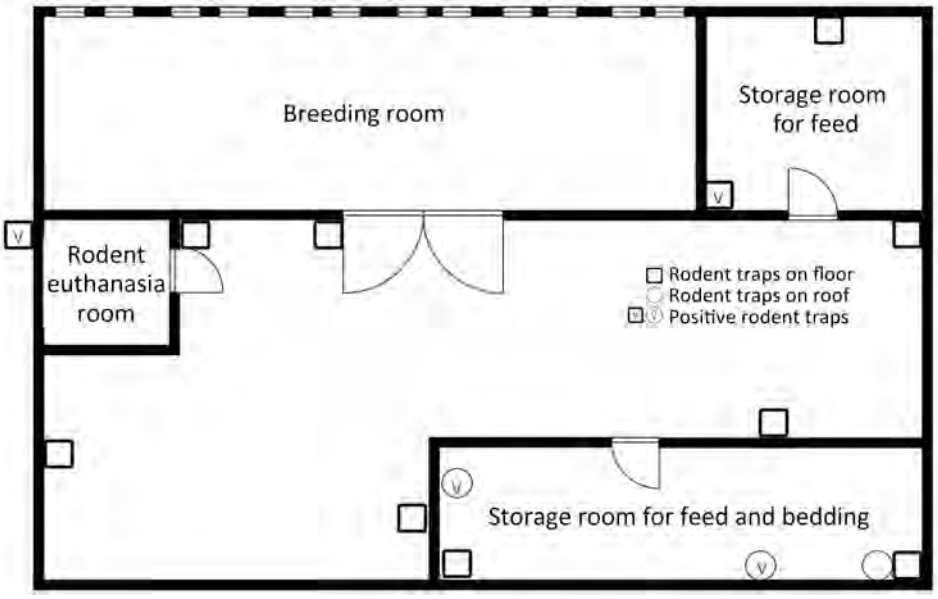

Figure 1. Floor plan of feeder rodent breeding farm and locations where positive feeder rodents were captured in study of recurrent occupational hantavirus infections at the farm, Taiwan.

We trapped wild rodents during November 5–9, 2022, ≈18 days after the initial case-patient was reported. Fourteen traps around the farm captured 5 wild rats, all *R. tanezumi*. We also randomly tested 40 feeder mice and 8 feeder rats (Appendix); 3 feeder *R. norvegicus* rats (37.5%) tested positive for hantavirus IgG, whereas all the feeder mice and wild rats tested negative (Table). The owner agreed to humane killing of all feeder rats on the farm on November 19, but the mice colony was not eradicated, and unused bedding and feed were retained. The rat colony was not replenished until February 2023, after later diagnosis of a second worker, case-patient B.

The other 4 workers on the farm reported no hantavirus symptoms during interviews. We also collected and tested blood samples. On the basis of IgM and IgG findings, previous infection wasindicated in 1 worker; results for other workers were negative.

We began wild rodent control using rodenticide and traps on November 9. The rack and floor were disinfected with 5,000 ppm bleach; rat tubs were washed, disinfected, and stored. The enclosed breeder room showed no signs of wild rat activity. Cracks noted in storage rooms for rat feed and bedding were sealed. Thereafter, the owner used bleach to clean used rodent tubs (5,000 ppm) and the racks and floor (1,000 ppm).

Figure 2. Racks (A) and tubs (B) used at a rodent breeding farm linked to study of recurrent occupational hantavirus infections, Taiwan.

On January 15, 2023, fever and retro-orbital pain developed in case-patient B, who worked at the farm but had tested negative in November 2022. Blood tests revealed thrombocytopenia and elevated liver enzyme levels. We diagnosed case-patient B with hantavirus infection on the basis of a positive IgM titer and a 4-fold rise in IgG titer from acute- to convalescent-phase serum samples. RT-PCR showed hantavirus RNA in her blood. Genomic sequencing data submitted to GenBank (accession no. OR734632) matched with the SEOV nucleoprotein gene.

The farm had ≈12,000 feeder mice and no feeder rats when the second investigation began on February 10, 2023. We placed 91 traps around the farm and neighborhood and captured 8 wild rats; 1 *R. norvegicus* rat tested positive for hantavirus IgG. We conducted wild rodent control in the neighborhood and discussed with the farm owner the importance of hand hygiene measures and using personal protective equipment (PPE).

Conclusions

We identified recurrent hantavirus infections in 2 workers on a feeder rodent breeding farm, even though all feeder rats were humanely killed after the first case had been reported. Previous laboratory studies showed that rodents can transmit the virus horizontally through infected bedding (*5*). Because the colony received no additional rodents from 2017 through the end of our testing, the breeder room is enclosed, and we found no signs of wild rat activity, we suspect that the virus was introduced to the breeder colony by infected bedding or feed and then spread through biting and scratching.

The duration between last exposure and onset of symptoms in case-patient B was 8 weeks. Given incubation for SEOV infection can take up to 8 weeks, case-patient B might have become infected before the infected feeder rats were killed but not diagnosed because of the long incubation period. However, we cannot exclude possible infection from wild rodents or remaining contaminated bedding and feed (*2*).

Hantavirus infection has been associated with occupational exposure. Several high-risk occupational fields have been identified, including agriculture, forestry, biology fieldwork, and laboratory work (*10*,*11*). Wearing appropriate PPE is crucial because of potentially severe or fatal outcomes. According to the US Office of Animal Care and Use of the National Institutes of Health, rodent facilities should classify their activities as low, moderate, or high risk, and workers should match appropriate PPE use with risk level (*12*). Rodent breeding farms should regularly monitor colony animals for hantavirus infection and maintain ongoing pest control to minimize presence of wild rodents. Staff should wear gloves when handling live or frozen rodents, used bedding, and soiled cages. Proper handwashing should promptly follow glove removal. In a zoonotic outbreak, personnel should wear PPE such as respirators, gloves, washable coveralls, and appropriate footwear. Regular disinfection with bleach or other commercial disinfectants that can effectively kill enveloped viruses is also crucial to prevent environmental contamination (*13*).

Table. Results of diagnostic testing of rodents for Seoul virus, by date trapped, in study of recurrent occupational hantavirus infections linked to feeder rodent breeding farm, Taiwan*

Species	No. IgG-positive/no. tested (%)	
	2022 Nov 5–9	2023 Feb 11–13
Feeder rodents		
Mus musculus	0/40 (0)	NA
Rattus norvegicus	3/8 (37.5)	NA
Wild rodents		
Rattus tanezumi	0/5 (0)	NA
Rattus norvegicus	NA	1/3 (33.3)
Suncus murinus	NA	0/5 (0)

*NA, not applicable.

HFRS symptoms include fever, headache, muscle aches, and abdominal pain. One study in the United States showed that only 41% of hantavirus case-patients developed an acute illness (*14*). HFRS can manifest in various nonspecific ways, so knowledge of potential animal or environmental exposure is crucial for identifying hantavirus disease in workers.

Among limitations of this study, we did not test feeder rat organ tissues for hantavirus with RT-PCR, so we were unable to compare viral sequences from case-patients and rats. Also, because we did not test environmental samples, such as bedding and feed, we obtained no direct evidence of virus origin. Finally, we did not test feeder rodents after case-patient B was diagnosed.

In summary, our findings emphasize that rodent breeding facilities should implement preventive measures such as disinfection protocols and use of PPE. Those actions would lower risk for hantavirus infections among persons working around infected rodents.

Acknowledgments

The authors thank their partners at the Department of Health, Changhua County Government, for their dedicated outbreak investigation and efforts that made this study possible.

About the Author

Dr. Wang is a medical officer in the Centers for Disease Control, Ministry of Health and Welfare, Taiwan. Her primary interest is infectious disease epidemiology.

References

1. Taiwan Centers for Disease Control. Hantavirus syndrome [cited 2023 Oct 3]. https://www.cdc.gov.tw/En/Category/ListContent/bg0g_VU_Ysrgkes_KRUDgQ?uaid=FRCHC1QNnvZMrohYrWLGNQ
2. Center for Food Security and Public Health. Hantavirus disease [cited 2023 Mar 24]. https://www.cfsph.iastate.edu/Factsheets/pdfs/hantavirus.pdf
3. Centers for Disease Control and Prevention. Hemorrhagic fever with renal syndrome (HFRS) [cited 2023 Apr 6]. https://www.cdc.gov/hantavirus/hcp/clinical-overview/hfrs.html
4. World Organisation for Animal Health. Hantaviruses [cited 2023 Jan 19]. https://www.woah.org/app/uploads/2021/05/hantaviruses-infection-with.pdf
5. Jonsson CB, Figueiredo LT, Vapalahti O. A global perspective on hantavirus ecology, epidemiology, and disease. Clin Microbiol Rev. 2010;23:412–41. https://doi.org/10.1128/CMR.00062-09
6. Shepherd JG, Blunsum AE, Carmichael S, Smollett K, Maxwell-Scott H, Farmer ECW, et al. Seoul virus associated with pet rats, Scotland, UK, 2019. Emerg Infect Dis. 2021;27:2677–80. https://doi.org/10.3201/eid2710.211298
7. Kerins JL, Koske SE, Kazmierczak J, Austin C, Gowdy K, Dibernardo A; Seoul Virus Working Group; Canadian Seoul Virus Investigation Group (Federal); Canadian Seoul Virus Investigation Group (Provincial); Contributors. Outbreak of Seoul virus among rats and rat owners—United States and Canada, 2017. MMWR Morb Mortal Wkly Rep. 2018;67:131–4. https://doi.org/10.15585/mmwr.mm6704a5
8. Cuperus T, de Vries A, Hoornweg TE, Fonville M, Jaarsma RI, Opsteegh M, et al. Seoul virus in pet and feeder rats in the Netherlands. Viruses. 2021;13:443. https://doi.org/10.3390/v13030443
9. Lee HW, Johnson KM. Laboratory-acquired infections with Hantaan virus, the etiologic agent of Korean hemorrhagic fever. J Infect Dis. 1982;146:645–51. https://doi.org/10.1093/infdis/146.5.645
10. Zhang YZ, Dong X, Li X, Ma C, Xiong HP, Yan GJ, et al. Seoul virus and hantavirus disease, Shenyang, People's Republic of China. Emerg Infect Dis. 2009;15:200–6. https://doi.org/10.3201/eid1502.080291
11. de St Maurice A, Ervin E, Schumacher M, Yaglom H, VinHatton E, Melman S, et al. Exposure characteristics of hantavirus pulmonary syndrome patients, United States, 1993–2015. Emerg Infect Dis. 2017;23:733–9. https://doi.org/10.3201/eid2305.161770
12. National Institutes of Health Office of Animal Care and Use. Guidelines for personnel protection in animal facilities [cited 2023 May 4]. https://oacu.oir.nih.gov/system/files/media/file/2022-12/d2-Personal_Protective_Equipment.pdf
13. Pet Advocacy Network. Best management practices for feeder rodent production and distribution [cited 2023 Oct 4]. https://petadvocacy.org/wp-content/uploads/2022/07/Feeder-Rodent-Industry-BMP-July-2017-Pet-Advocacy-Network.pdf
14. Knust B, Brown S, de St Maurice A, Whitmer S, Koske SE, Ervin E, et al.; Multistate Seoul Virus Outbreak Investigation Team. Seoul virus infection and spread in United States home-based ratteries: rat and human testing results from a multistate outbreak investigation. J Infect Dis. 2020;222:1311–9. https://doi.org/10.1093/infdis/jiaa307

Address for correspondence: Chia-ping Su, New Taipei Municipal TuCheng Hospital, No. 6, Sec. 2, Jincheng Rd, Tucheng District, New Taipei City 236, Taiwan; email: sigbird@gmail.com

Crimean-Congo Hemorrhagic Fever Virus Kinetics in Serum, Saliva, and Urine, Iran, 2018

Malihe Metanat, Seyed Dawood Mousavi Nasab, Tahmineh Jalali, Fahimeh Bagheri Amiri, Neda Sadat Torab Jahromi, Mahsa Tavakoli, Mohammad Hassan Pouriayevali, Mohammad Mehdi Gouya, Mostafa Salehi-Vaziri

Little is known about using noninvasive samples for diagnosing Crimean-Congo hemorrhagic fever (CCHF). We investigated detection of CCHF virus in serum, saliva, and urine samples. Our results indicate that serum is the best sample type for CCHF diagnosis; saliva can be used for noninvasive sampling.

Crimean-Congo hemorrhagic fever (CCHF), caused by CCHV virus (CCHFV), is an emerging disease that has been listed by the World Health Organization as a priority pathogen (*1*). Including noninvasive samples such as saliva and urine in testing can improve the current CCHF diagnostic algorithm. The World Health Organization has emphasized investigating the usefulness of alternative, noninvasive sample types, such as urine and oral fluid, for diagnosing and monitoring CCHF. For this study, we analyzed the utility of saliva and urine samples for laboratory diagnosis of CCHF by comparing real-time reverse transcription PCR (rRT-PCR) results for serially collected saliva, urine, and serum samples from CCHF patients in Iran. To provide additional information about the kinetics of CCHFV, we investigated the presence of RNA and antigen in saliva, urine, and serum samples, and IgM in serum samples. Ethics committees of the Zahedan University of Medical Sciences approved this study (IR.zaums.REC.1397.425).

The Study

We collected serum, saliva, and urine samples from 22 CCHF patients in Iran in 2018. Fourteen (63.6%) patients were male; mean age was 30.59 (SD = 12.83) years. We extracted viral RNA by using the QIAGEN QIAamp Viral RNA Mini Kit (https://www.qiagen.com) and the Fast-Track Diagnostics CCHF rRT-PCR (Siemens, https://www.siemens.com). We detected CCHFV IgM using a Vector-Best VectoCrimean-CCHF IgM Kit and antigens using a Vector-Best CCHFV-antigen ELISA Kit (https://en.vector-best.ru). We performed all experiments in a Biosafety Level 2-plus laboratory. We used GraphPad PRISM software (https://www.graphpad.com) for data analysis.

We subjected serum, saliva, and urine samples from the 22 CCHF patients to rRT-PCR to identify CCHFV RNA, antigen ELISA for antigens, and IgM ELISA for IgM. We tested 39 serum, 37 saliva, and 42 urine samples using rRT-PCR and detected CCHFV RNA in all 3 types of samples but with different detection rates and time frames. Overall, 35/39 (89.74%) serum samples tested positive. We detected CCHFV RNA in 2 serum samples as early as day 0 and 1 serum sample as late as day 41. Overall, 25/37 (67.57%) saliva samples tested positive. We detected CCHFV RNA as early as day 2 in 2 saliva samples and as late as day 13 in 1 saliva sample. Only 3/42 (7.14%) urine samples tested positive (Figure 1). We detected viral RNA as early as day 1 in 1 urine sample and as late as day 10 in 1 urine sample.

For further analysis, we categorized positive samples by days after symptom onset into 4 groups: 0–4, 5–9, 10–14, and ≥15 days (Table). In serum samples, the rRT-PCR positivity rate was high through day 14: 100% on days 0–4, 90.9% on days 5–9, and 100% on days 10–14. The positivity rate decreased substantially thereafter to 25% during days ≥15. rRT-PCR positivity rate for saliva samples gradually increased from 55.6% on days 0–4 to 83.3% on days 10–14; we observed no positive results during days ≥15. Rate of

Affiliations: Zahedan University of Medical Sciences, Zahedan, Iran (M. Metanat, N.S. Torab Jahromi); Pasteur Institute of Iran, Tehran, Iran (S.D. Mousavi Nasab, T. Jalali, F. Bagheri Amiri, M. Tavakoli, M.H. Pouriayevali, M. Salehi-Vaziri); Iran University of Medical Sciences, Tehran (M.M. Gouya)

DOI: https://doi.org/10.3201/eid3008.240036

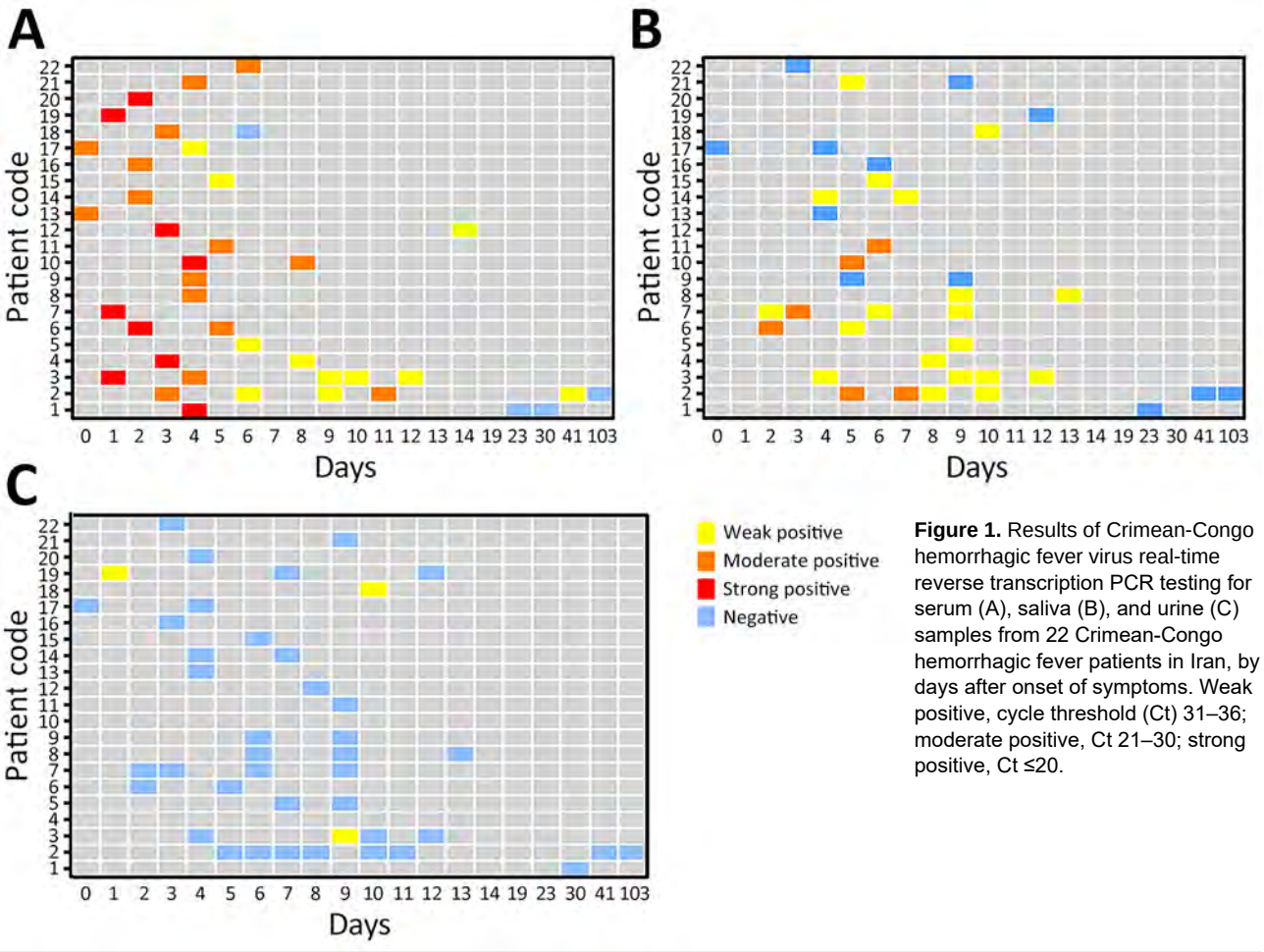

Figure 1. Results of Crimean-Congo hemorrhagic fever virus real-time reverse transcription PCR testing for serum (A), saliva (B), and urine (C) samples from 22 Crimean-Congo hemorrhagic fever patients in Iran, by days after onset of symptoms. Weak positive, cycle threshold (Ct) 31–36; moderate positive, Ct 21–30; strong positive, Ct ≤20.

positivity in urine samples was very low during the first 2 weeks of the disease, and we observed no positive samples during days ≥15.

We tested 21 serum, 39 saliva, and 42 urine samples using Vector-Best CCHFV-antigen ELISA. Eight (38.10%) of 21 serum, 2/39 (5.13%) saliva, and 0/42 (0.0%) urine samples tested positive for CCHFV antigen (Figure 2). We detected CCHFV antigen as early as day 0 in 1 serum sample and as late as day 5 in 1 serum sample. In contrast, we detected CCHFV antigen in only 2 saliva samples on days 5–9, and no urine samples tested positive for CCHFV antigen. Antigen ELISA results were 100% positive in serum samples through day 5 of disease onset but declined substantially after that (Table).

We analyzed 35 serum samples using a Vector-Best VectoCrimean-CCHF IgM kit. Of those serum samples, 22 (62.85%) were positive. On day 2, 1 serum sample tested positive for CCHFV IgM; by day 6, all 22 serum samples had tested positive for CCHFV IgM (Figure 3). The IgM positivity rate using CCHFV-IgM ELISA increased substantially during days 5–9 and reached 100% by days 10–14. We tested no samples for IgM during days ≥15 (Table).

Our results showed that serum provides most suitable sample type for identifying CCHFV RNA. From highest to lowest, rRT-PCR positivity rates were 89.74% in serum, 67.57% in saliva, and 7.14% in urine. In line with our results, 1 study (2) identified CCHFV RNA in blood, saliva, and urine samples; highest

Table. Positivity rate for Crimean-Congo hemorrhagic fever virus by real-time reverse transcription PCR and ELISA in serum, saliva, and urine samples from patients in Iran

Days after disease onset	PCR-positive samples (%)			Antigen ELISA–positive samples (%)			IgM ELISA–positive serum samples (%)
	Serum	Saliva	Urine	Serum	Saliva	Urine	
0–4	20/20 (100)	5/9 (55.6)	1/12 (8.3)	7/7 (100)	0/9 (0)	0/11 (0)	6/18 (33.3)
5–9	10/11 (90.9)	15/19 (78.9)	1/20 (5)	1/6 (16.7)	2/20 (10)	0/21 (0)	12/13 (92.3)
10–14	4/4 (100)	5/6 (83.3)	1/7 (14.3)	0/4 (0)	0/7 (0)	0/7 (0)	4/4 (100)
≥15	1/4 (25)	0/3 (0)	0/3 (0)	0/4 (0)	0/3 (0)	0/3 (0)	Not tested

positivity was observed in blood (100%, n = 8/8), followed by saliva (83%, n = 5/6) and urine (66%, n = 2/3). Similarly, another study (*3*), from Kosovo, identified CCHFV RNA in 66.66% of serum and 42.85% of urine samples from CCHF patients. In a study from India (*4*), viral RNA was detected in blood and urine samples, but the viral load in urine was lower. In a study conducted in Spain (*5*), viral RNA was detected in different sample types, including serum, saliva, and vaginal secretions, but not in urine. In our study, we detected viral RNA on different days after the onset of disease in all 3 evaluated sample types, but the widest diagnostic window (days 0–41) was related to serum samples. The study from Spain (*5*) also showed that CCHFV RNA can be detected in plasma samples through day 20 after onset of the disease. As in our review, the study from Kosovo (*3*) reported the lengthy persistence (36 days) of viral RNA in serum.

We detected CCHFV antigen in serum and saliva but not urine samples. Although viral antigen was detectable in serum and urine samples, the positivity rate was much lower compared with the rate when tested for viral RNA. Only 38.1% of serum samples and 5.13% of saliva samples were positive for CCHFV antigen, supporting results from other studies suggesting the lower sensitivity of antigen ELISA compared with rRT-PCR testing (*6*,*7*).

The genetic diversity of CCHF viruses can negatively affect the results of rRT-PCR (*8*). Therefore, targeting IgM along with viral RNA can be helpful to increase the sensitivity of the diagnosis. In our study, IgM was detectable in serum from the second day of the disease and, from day 6 onward, all serum samples were positive for IgM. Of note, CCHFV antibodies cannot be detected in fulminant CCHF patients (*9*,*10*). Therefore, interpretation of serologic tests should be considered in the context of the patient's clinical and laboratory data.

Conclusion

This study showed that CCHF virus can be identified in serum, saliva, and urine samples. However, for laboratory diagnosis of acute CCHFV infection, the best sample type was serum and the best target was viral RNA. Between saliva and urine as noninvasive samples, saliva might be the more suitable option for genome identification.

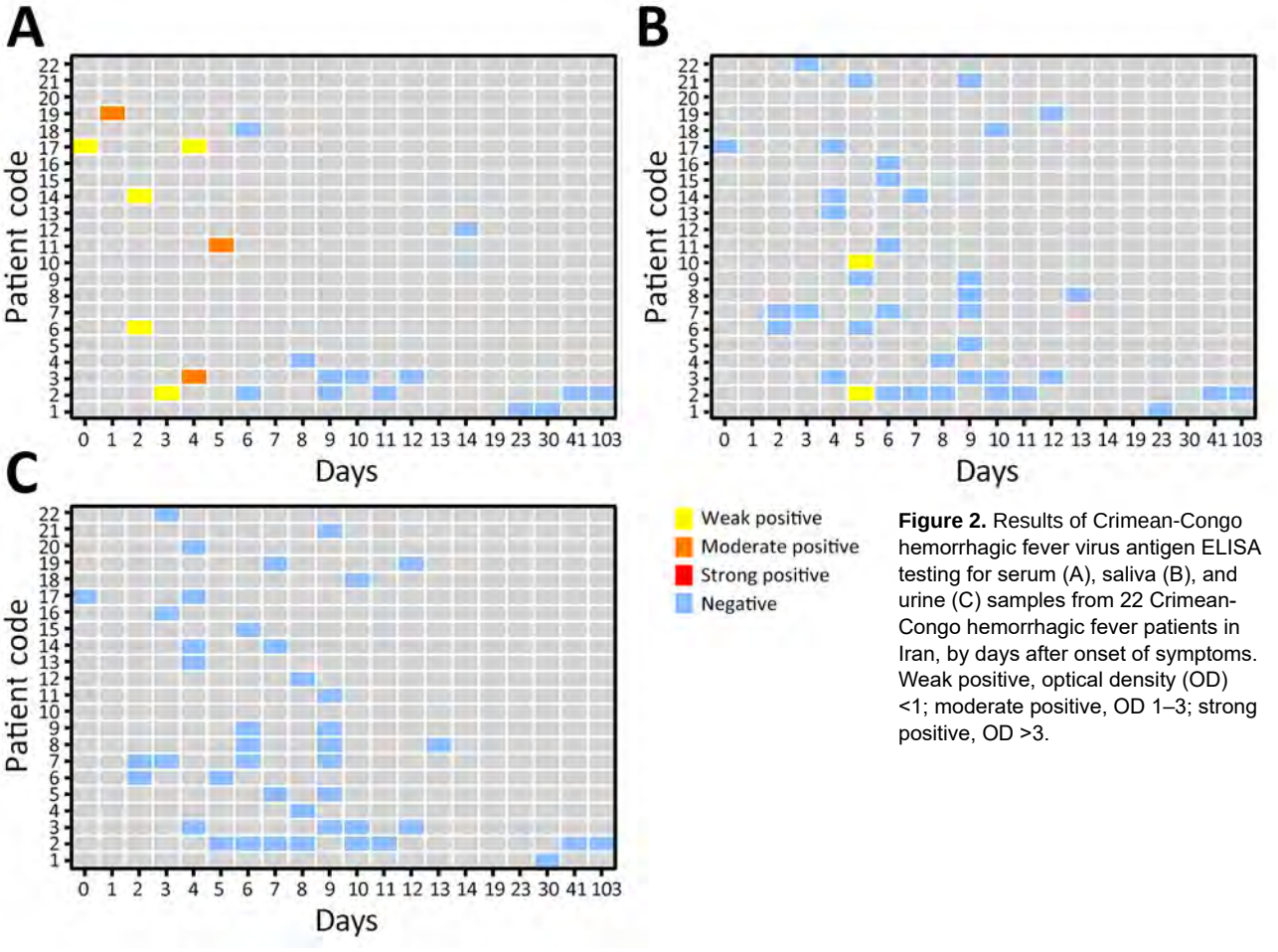

Figure 2. Results of Crimean-Congo hemorrhagic fever virus antigen ELISA testing for serum (A), saliva (B), and urine (C) samples from 22 Crimean-Congo hemorrhagic fever patients in Iran, by days after onset of symptoms. Weak positive, optical density (OD) <1; moderate positive, OD 1–3; strong positive, OD >3.

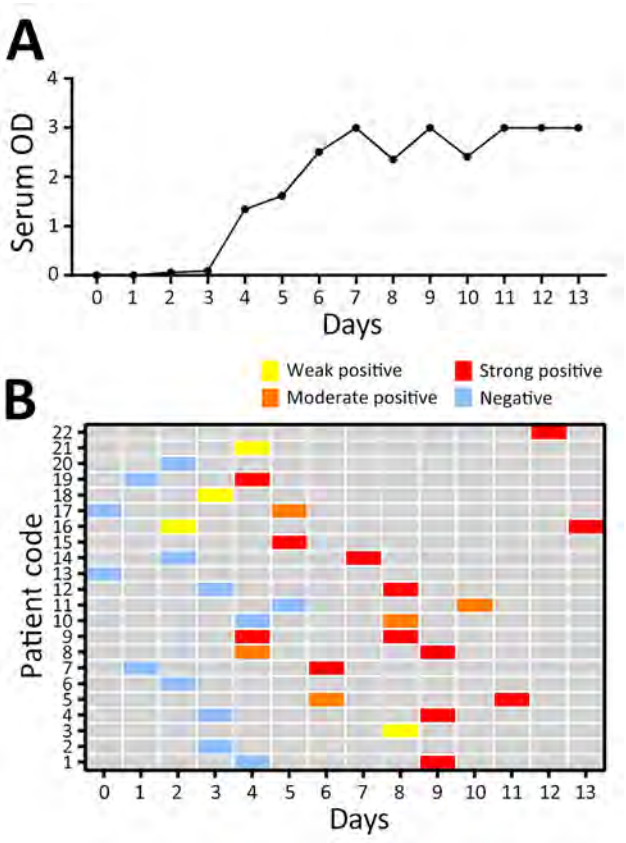

Figure 3. Results of Crimean-Congo hemorrhagic fever virus IgM antigen ELISA testing for serum samples from 22 Crimean-Congo hemorrhagic fever patients in Iran, by days after disease onset. A) Mean of detected OD in serum samples per day. B) IgM ODs. Weak positive, optical density (OD) <1; moderate positive, OD 1–3; strong positive, OD >3.

Acknowledgments

The authors thank all collaborators, especially the personnel of the Department of Arboviruses and Viral Hemorrhagic Fevers, Pasteur Institute of Iran, for their contributions to the study.

This study was financially supported by the Iran Center for Communicable Diseases Control, Ministry of Health and Medical Education, Tehran, Iran.

About the Author

Dr. Metanat is a physician specializing in infectious diseases and a researcher at the Zahedan University of Medical Sciences, Iran. Her main interests focus on epidemiology and control of infectious diseases.

References

1. Sorvillo TE, Rodríguez SE, Hudson P, Carey M, Rodríguez LL, Spiropoulou CF, et al. Towards a sustainable One Health approach to Crimean–Congo hemorrhagic fever prevention: focus areas and gaps in knowledge. Trop Med Infect Dis. 2020;5:113. https://doi.org/10.3390/tropicalmed5030113
2. Bodur H, Akinci E, Ongürü P, Carhan A, Uyar Y, Tanrici A, et al. Detection of Crimean-Congo hemorrhagic fever virus genome in saliva and urine. Int J Infect Dis. 2010;14:e247–9. https://doi.org/10.1016/j.ijid.2009.04.018
3. Thomas S, Thomson G, Dowall S, Bruce C, Cook N, Easterbrook L, et al. Review of Crimean Congo hemorrhagic fever infection in Kosova in 2008 and 2009: prolonged viremias and virus detected in urine by PCR. Vector Borne Zoonotic Dis. 2012;12:800–4.
4. Mourya DT, Yadav PD, Shete AM, Gurav YK, Raut CG, Jadi RS, et al. Detection, isolation and confirmation of Crimean-Congo hemorrhagic fever virus in human, ticks and animals in Ahmadabad, India, 2010–2011. PLoS Negl Trop Dis. 2012;6:e1653. https://doi.org/10.1371/journal.pntd.0001653
5. Negredo A, de la Calle-Prieto F, Palencia-Herrejón E, Mora-Rillo M, Astray-Mochales J, Sánchez-Seco MP, et al.; Crimean Congo Hemorrhagic Fever@Madrid Working Group. Autochthonous Crimean-Congo hemorrhagic fever in Spain. N Engl J Med. 2017;377:154–61. https://doi.org/10.1056/NEJMoa1615162
6. Shrivastava N, Kumar JS, Yadav P, Shete AM, Jain R, Shrivastava A, et al. Development of double antibody sandwich ELISA as potential diagnostic tool for rapid detection of Crimean-Congo hemorrhagic fever virus. Sci Rep. 2021;11:14699. https://doi.org/10.1038/s41598-021-93319-0
7. Saijo M, Tang Q, Shimayi B, Han L, Zhang Y, Asiguma M, et al. Antigen-capture enzyme-linked immunosorbent assay for the diagnosis of Crimean-Congo hemorrhagic fever using a novel monoclonal antibody. J Med Virol. 2005;77:83–8. https://doi.org/10.1002/jmv.20417
8. Bente DA, Forrester NL, Watts DM, McAuley AJ, Whitehouse CA, Bray M. Crimean-Congo hemorrhagic fever: history, epidemiology, pathogenesis, clinical syndrome and genetic diversity. Antiviral Res. 2013;100:159–89. https://doi.org/10.1016/j.antiviral.2013.07.006
9. Kaya S, Elaldi N, Kubar A, Gursoy N, Yilmaz M, Karakus G, et al. Sequential determination of serum viral titers, virus-specific IgG antibodies, and TNF-α, IL-6, IL-10, and IFN-γ levels in patients with Crimean-Congo hemorrhagic fever. BMC Infect Dis. 2014;14:416. https://doi.org/10.1186/1471-2334-14-416
10. Salehi-Vaziri M, Baniasadi V, Jalali T, Mirghiasi SM, Azad-Manjiri S, Zarandi R, et al. The first fatal case of Crimean-Congo hemorrhagic fever caused by the AP92-like strain of the Crimean-Congo hemorrhagic fever virus. Jpn J Infect Dis. 2016;69:344–6. https://doi.org/10.7883/yoken.JJID.2015.533

Address for correspondence: Mostafa Salehi-Vaziri, Department of Arboviruses and Viral Hemorrhagic Fevers (National Ref Lab), Pasteur Institute of Iran, 69 Pasteur Ave, 1316943551 Tehran, Iran; email: mostafavaziri1985@gmail.com, m.salehi@pasteur.ac.ir

Multiplex Dual-Target Reverse Transcription PCR for Subtyping Avian Influenza A(H5) Virus

Malaya K. Sahoo, Ingrid E.A. Morante, ChunHong Huang, Daniel Solis, Fumiko Yamamoto, Uzoamaka C. Ohiri, Daniel Romero, Benjamin A. Pinsky

An increased risk for human infection with avian influenza A(H5N1) viruses is of concern. We developed an internally controlled, dual-target reverse transcription PCR for influenza A(H5) subtyping. This test could be used to detect influenza A(H5) in clinical samples.

Highly pathogenic avian influenza (HPAI) viruses cause high mortality rates in wild birds and farmed poultry, and their potential for adaptation to humans remains a major pandemic threat (*1*). In 2021, a notable increase in avian influenza activity occurred, driven by the emergence of influenza A(H5N1) clade 2.3.4.4b viruses (*2*,*3*). Suspected mammal-to-mammal transmission during outbreaks among seals and minks led to concerns regarding the escalation of risk to humans (*4*–*7*). In 2024, the virus was identified in dairy cows in the United States (*8*), and exposure to infected cows has resulted in transmission to humans (*9*). To prepare for possible additional human cases, we developed an internally controlled, dual-target H5 subtyping quantitative reverse transcription PCR (qRT-PCR) based on primer–probe sequences from the World Health Organization (*10*). We evaluated this qRT-PCR by using synthesized nucleic acids, cultured avian and human virus isolates, and clinical upper respiratory specimens collected from patients with influenza A virus infection.

The Study

We identified previously published primer–probe sets from the World Health Organization that target different regions of the influenza A(H5) hemagglutinin (HA) gene for combination into a dual-target H5 subtyping qRT-PCR (Appendix Table 1, https://wwwnc.cdc.gov/EID/article/30/8/24-0785-App1.pdf) (*10*). We introduced minor sequence changes to account for recent clade 2.3.4.4b diversity, and simultaneously, to limit primer–probe complexity (Table 1). We evaluated these primers and probes against complete North American H5 clade 2.3.4.4b HA gene sequences in the GISAID database (https://www.gisaid.org) during January 1, 2022–May 29, 2024, and found that 99.8% (5,975/5,987) of sequences aligned with a maximum of 1 mismatch to primer–probe set 1 and 97.7% (5,972/5,990) aligned with a maximum of 1 mismatch to primer–probe set 2 (Appendix Tables 2, 3). We observed no primer–probe mismatches compared with the influenza A H5 sequences obtained from persons with H5 infections in the United States (4 persons as of May 29, 2024) (Appendix Tables 4, 5). We combined the primer–probe sets in multiplex with primers–probes for the influenza A matrix (M) gene for pan–influenza A detection and with primers–probes for RNase P as an internal control (*11*).

We determined the 95% lower limit of detection (LLOD) by using single-stranded DNA (ssDNA) encoding the H5 target sequences from HPAI virus clade 1 (GenBank accession no. JQ966928, A/condor/Guangdong/139/2003 [H5N1]) (*12*) and clade 2.3.4.4b (GenBank accession no. OP499866, A/red-tailed hawk/Kansas/W22–198/2022 [H5N1]) viruses (Appendix Table 6). The primer–probe target regions of this clade 2.3.4.4b H5 sequence are identical to the recent H5 sequences from dairy cows and humans. We combined the 2 clade 1 ssDNA targets at equal copy numbers; we did the same with the clade 2.3.4.4b ssDNA targets. We also combined these H5 clade mixes at equal copy numbers with ssDNA encoding the pan–influenza A M gene target. We then diluted the clade 1 ssDNA mix and clade 2.3.4.4b ssDNA mix to 2, 1, and 0.5 copies/μL in pooled influenza

Author affiliations: Stanford Health Care Clinical Virology Laboratory, Stanford, California, USA (M.K. Sahoo, I.E.A. Morante, U.C. Ohiri, D. Romero, B.A. Pinsky); Stanford University School of Medicine, Stanford (C. Huang, D. Solis, F. Yamamoto, B.A. Pinsky)

DOI: https://doi.org/10.3201/eid3008.240785

Table 1. Primers and probes used in study of multiplex dual-target reverse transcription PCR for subtyping avian influenza A(H5) virus*

Target	Name	Sequence, 5′ → 3′	Final concentration
A(H5)	FluA_H5_v4_1F	TACCAGATACTGTCAATTTATTCAAC	400 nM
	FluA_H5_v4_1R	GTAACGACCCATTGGAGCACATCC	400 nM
	FluA_H5_v4_1Prb.FAM	FAM-CTGGCAATC/ZEN/ATG**R**T**R**GCTGGTCT-3IABkFQ	200 nM
	FluA_H5_v4_2F	TGGGTACCATCATAGCAATGAGCA	400 nM
	FluA_H5_v4_2R	AACTCCCTTCCAACTGCCTCAAA	400 nM
	FluA_H5_v4_2Prb.FAM	FAM-TGGGTACGC/ZEN/TGCGGACAAAGAATCCA-3IABkFQ	200 nM
A (M)	Pan-FluA-F	GACC**R**ATCCTGTCACCTCTGAC	400 nM
	Pan-FluA -R	AGGGCATT**Y**TGGACAAA**K**CGTCTA	400 nM
	Pan-FluA -prb_Q705	Q705-TGCAGTCCTCGCTCACTGGGCACG- BHQ-3	200 nM
Human RNase P	RNase P Fwd	AGATTTGGACCTGCGAGCG	100 nM
	RNase P Rev	GAGCGGCTGTCTCCACAAGT	100 nM
	RNase P Probe CF560	CF560-TTCTGACCTGAAGGCTCTGCGCG-BHQ-1	50 nM

*H5 probes were purchased from Integrated DNA Technologies (https://www.idtdna.com). The probes contain the internal quencher, ZEN, in addition to the 3′ Iowa BHQ FQ (3IABkFQ) (proprietary to Integrated DNA Technologies). Influenza A (M) and human RNase P probes were purchased from Biosearch Technologies (https://www.biosearchtech.com). Bold type indicates mixed bases. BHQ, Black Hole Quencher; CF560, CalFluor 560; FAM, 6-carboxyfluorescein; M, matrix gene; Q705, Quasar 705.

A–negative eluates extracted from clinical upper respiratory specimens. We then performed the H5 subtyping qRT-PCR (Appendix). We tested 20 replicates at each level for both mixes. The 95% LLOD for the H5 target was 2.5 copies/µL (95% CI 1.8–5.3 copies/µL) for the clade 1 ssDNA mix and <0.5 copies/µL (we were unable to calculate 95% CI) for the clade 2.3.4.4b ssDNA mix.

We also evaluated the H5 subtyping multiplex qRT-PCR by using genomic RNA from a clade Eur-Asian non-goose/GuangDong (Gs/Gd) isolate, Kilbourne F181, A/duck/Singapore/645/1997 (H5N3). We assigned this genomic RNA an estimated concentration in copies/µL by using the clade 2.3.4.4b ssDNA as standard curve, then diluted it to 2, 1, and 0.5 copies/µL in pooled influenza A–negative eluates. We tested 20 replicates at each level. The 95% LLOD for the H5 target was 0.6 copies/µL (95% CI 0.5–0.7 copies/µL). In addition, we tested 10-fold serial dilutions from 4.6 to 0.6 $\log_{10}$ copies/mL of the Kilborne F181 genomic RNA in duplicate (Appendix Figure), which indicated 0.97 reaction efficiency for the H5 target.

We then evaluated the H5 subtyping qRT-PCR by using genomic RNA from additional H5 viruses, including 5 low pathogenicity avian influenza non-Gs/Gd isolates from the United States (Table 2). We tested each eluate in duplicate. Although we detected H5 RNA in all reactions, the difference in mean cycle threshold (Ct) values between the H5 and pan–influenza A (M gene) targets varied widely (range 0.6–9.9 cycles). Testing the H5 primer–probe sets individually revealed that the US non-Gs/Gd genomic RNAs were detected only by primer–probe set 1. The A/mallard/Minnesota/16-041335-3/2016 (H5N2) eluate showed the greatest Ct difference, consistent with the highest number of H5 primer–probe mismatches in primer–probe set 1 (9 mismatches) (Appendix Tables 5, 6).

To determine specificity, we tested genomic RNA from cultured human and avian virus isolates encoding non-H5 HA genes (Table 3). We detected the pan–influenza A target in all eluates; median Ct value was 17.3 (range 13.6–20.7). We did not detect the H5 target in any eluates.

We performed further specificity experiments by using residual upper respiratory swab samples in viral transport media submitted for clinical respiratory virus testing. We conducted this work with Stanford Institutional Review Board approval (protocol no. 68234); individual consent was waived. We evaluated 100 samples collected

Table 2. Avian influenza A(H5) virus genomic RNA used to evaluate inclusivity in study of multiplex dual-target reverse transcription PCR for subtyping avian influenza A(H5) virus*

Genome	Clade	GenBank accession no.	H5 Ct	M Ct	Ct difference
Kilbourne F181, A/duck/Singapore/645/1997 (H5N3)	EA-non-Gs/Gd	NA	18.3	17.7	0.6
A/quail/California/14-012546-1/2014 (H5N8)	Am-non-Gs/Gd	NA	22.9	19.0	3.9
A/mallard/Minnesota/16-041335-3/2016 (H5N2)	Am-non-Gs/Gd	MH546659	32.1	22.3	9.9
A/emperor goose/Alaska/17-004479-1/2016 (H5N2)	Am-non-Gs/Gd	MH546451	26.8	23.3	3.6
A/glaucous-winged gull/Alaska/16-041335-19/2016 (H5N2)	Am-non-Gs/Gd	MH546475	23.3	21.8	1.5
A/northern pintail/Alaska/16-041335-5/2016 (H5N2)	Am-non-Gs/Gd	MH546883	20.9	19.1	1.9

*Kilbourne F181 genomic RNA was obtained from BEI Resources (https://www.beiresources.org). Am-non-Gs/GD A(H5) genomic RNA was obtained from the US Department of Agriculture. The genomic RNA from these influenza A(H5) viruses was diluted 1:10 buffer AVE plus carrier RNA (QIAGEN, https://www.qiagen.com) and tested in duplicate. Ct values are means. Am-non-Gs/Gd, non-goose/GuangDong from the United States; Ct, cycle threshold; EA-non-Gs/Gd, Eurasian non-goose/GuangDong; M, matrix gene; NA, not available.

Table 3. Non-H5 human and avian influenza A virus genomic RNA used to evaluate H5 specificity in study of multiplex dual-target reverse transcription PCR for subtyping avian influenza A(H5) virus*

HA gene	Genome	BEI catalog no.
H1	A/Brisbane/59/2007 (H1N1)	NR-20080
H1 pdm09	A/California/04/2009 (H1N1)pdm09	NR-14689
H2	A/duck/Germany/1215/1973 (H2N3)	NR-2762
H3	A/Brisbane/10/2007 (H3N2)	NR-20081
H4	A/duck/Czechoslovakia/1956 (H4N6)	NR-43012
H6	A/shearwater/Australia/1/1973 (H6N5)	NR-43014
H8	A/turkey/Ontario/6118/1968 (H8N4)	NR-43015
H9	A/turkey/Wisconsin/1/1966 (H9N2)	NR-43016
H10	A/chicken/Germany/N/1949 (H10N7)	NR-2765
H11	A/duck/Memphis/546/1974 (H11N9)	NR-43017
H12	A/duck/Alberta/60/1976 (H12N5)	NR-43018
H13	A/gull/Maryland/704/1977 (H13N6)	NR-43019
H14	A/mallard/Astrakhan/263/1982 (H14N5)	NR-43020
H15	A/shearwater/Australia/2576/1979 (H15N9)	NR-43021
H16	A/shorebird/Delaware/172/2006 (H16N3)	NR-43022

*All genomic RNA obtained from BEI Resources (https://www.beiresources.org). The genomic RNA from these influenza A (H5) viruses was diluted 1:10 in buffer AVE plus carrier RNA (QIAGEN, https://www.qiagen.com). HA, hemagglutinin; pdm09, pandemic 2009.

during the 2022–2023 respiratory virus season that were positive for influenza A by using routine clinical methods (98 by using Hologic Panther Fusion [Hologic, https://www.hologic.com] and 2 by using Cepheid GeneXpert [Cepheid, https://www.cepheid.com]), including 29 known co-infections (13 respiratory syncytial virus [RSV], 7 rhinovirus, 3 adenovirus, 3 human metapneumovirus, 1 parainfluenza-3, 1 parainfluenza 4, and 1 with both RSV and rhinovirus). In addition, we tested 55 upper respiratory samples collected in April 2024 that were negative for influenza A, influenza B, RSV, parainfluenza virus 1–4, rhinovirus, adenovirus, and human metapneumovirus on the Panther Fusion by using the H5 subtyping qRT-PCR. We extracted total nucleic acids from 400 μL and eluted them in 60 μL buffer AVE on the BioRobot EZ1 (Qiagen) by using the EZ1 virus mini kit 2.0, according to the manufacturer's recommendations. We detected the pan–influenza A target in 97.0% (97/100) of the influenza A–positive samples; median Ct value was 24.1 (range 12.6–37.7). All 3 of the samples that were not detected in the pan–influenza A channel of the H5 multiplex had detectable RNase P (Ct values of 22.5, 18.7, and 20.8), indicating adequate extraction and the absence of inhibitors. The original influenza A Ct values (Panther Fusion) for those 3 samples were 41.4, 38.0, and 38.2. Upon repeat testing, influenza A RNA was detected only in the sample with the lowest original Ct value for influenza A (C_t 34.8) by the H5 multiplex. None of those influenza A–positive samples had detectable H5 RNA. Of the respiratory virus panel negative samples, all had detectable RNase P; median Ct value was 23.9 (range 17.7–29.8). None of the panel negative samples had detectable H5 RNA.

Conclusions

HPAI H5 viruses, particularly clade 2.3.4.4b viruses, pose an emerging pandemic threat. This internally controlled dual-target influenza A(H5) qRT-PCR demonstrated high analytical performance and could be used to directly test samples from patients with suspected HPAI A(H5) virus infection or as a secondary test to subtype known influenza A–positive samples after routine respiratory virus testing. The dual-target design reduces the likelihood of false negatives, as evidenced by detection of low pathogenicity avian influenza H5 viruses with substantial target mismatch. However, continuous sequence surveillance and updating of the primer–probe sets will be required to ensure that this assay accounts for ongoing viral evolution (*13*).

Acknowledgments

We thank Erica Spackman for providing genomic RNA from US avian influenza A(H5) non-goose/GuangDong isolates.

We obtained additional influenza A genomic RNA through the Biodefense and Emerging Infections Research Resources Repository, National Institute for Allergy and Infectious Diseases, National Institutes of Health.

About the Author

Dr. Sahoo is senior bioinformatic staff scientist in the Stanford Health Care Clinical Virology Laboratory. His research involves the design and evaluation of nucleic acid amplification and sequencing assays for the diagnosis and characterization of infectious diseases.

References

1. Morens DM, Park J, Taubenberger JK. Many potential pathways to future pandemic influenza. Sci Transl Med. 2023; 15:eadj2379. https://doi.org/10.1126/scitranslmed.adj2379

2. Sun Y, Zhang T, Zhao X, Qian J, Jiang M, Jia M, et al. High activity levels of avian influenza upwards 2018–2022: a global epidemiological overview of fowl and human infections. One Health. 2023;16:100511. https://doi.org/10.1016/j.onehlt.2023.100511
3. Szablewski CM, Iwamoto C, Olsen SJ, Greene CM, Duca LM, Davis CT, et al. Reported global avian influenza detections among humans and animals during 2013–2022: comprehensive review and analysis of available surveillance data. JMIR Public Health Surveill. 2023;9:e46383. https://doi.org/10.2196/46383
4. Kniss K, Sumner KM, Tastad KJ, Lewis NM, Jansen L, Julian D, et al. Risk for infection in humans after exposure to birds infected with highly pathogenic avian influenza A(H5N1) virus, United States, 2022. Emerg Infect Dis. 2023;29:1215–9. https://doi.org/10.3201/eid2906.230103
5. Gilbertson B, Subbarao K. Mammalian infections with highly pathogenic avian influenza viruses renew concerns of pandemic potential. J Exp Med. 2023;220:e20230447. https://doi.org/10.1084/jem.20230447
6. Puryear W, Sawatzki K, Hill N, Foss A, Stone JJ, Doughty L, et al. Highly pathogenic avian influenza A(H5N1) virus outbreak in New England seals, United States. Emerg Infect Dis. 2023;29:786–91. https://doi.org/10.3201/eid2904.221538
7. Agüero M, Monne I, Sánchez A, Zecchin B, Fusaro A, Ruano MJ, et al. Highly pathogenic avian influenza A(H5N1) virus infection in farmed minks, Spain, October 2022. Euro Surveill. 2023;28:2300001. https://doi.org/10.2807/1560-7917.ES.2023.28.3.2300001
8. Burrough ER, Magstadt DR, Petersen B, Timmermans SJ, Gauger PC, Zhang J, et al. Highly pathogenic avian influenza A(H5N1) clade 2.3.4.4b virus infection in domestic dairy cattle and cats, United States, 2024. Emerg Infect Dis. 2024;30:1335–43. https://doi.org/10.3201/eid3007.240508
9. Uyeki TM, Milton S, Abdul Hamid C, Reinoso Webb C, Presley SM, Shetty V, et al. Highly pathogenic avian influenza A(H5N1) virus infection in a dairy farm worker. N Engl J Med. 2024;390:2028–9. https://doi.org/10.1056/NEJMc2405371
10. World Health Organization. WHO information for molecular diagnosis of influenza virus—update. 2021 Feb 7 [cited 2023 Jun 25]. https://www.who.int/teams/global-influenza-programme/laboratory-network/quality-assurance/eqa-project/information-for-molecular-diagnosis-of-influenza-virus
11. Huang C, Sahoo MK, Verghese M, Sibai M, Solis D, Mfuh KO, et al. Interepidemic respiratory syncytial virus during the COVID-19 pandemic. Microbiol Spectr. 2022;10:e0094722. https://doi.org/10.1128/spectrum.00947-22
12. Jiao P, Yuan R, Song Y, Wei L, Ren T, Liao M, et al. Full genome sequence of a recombinant H5N1 influenza virus from a condor in southern China. J Virol. 2012;86:7722–3. https://doi.org/10.1128/JVI.01043-12
13. Kandeil A, Patton C, Jones JC, Jeevan T, Harrington WN, Trifkovic S, et al. Rapid evolution of A(H5N1) influenza viruses after intercontinental spread to North America. Nat Commun. 2023;14:3082. https://doi.org/10.1038/s41467-023-38415-7

Address for correspondence: Benjamin A. Pinsky, Stanford University School of Medicine, 3375 Hillview Ave, Palo Alto, CA 94304, USA; email bpinsky @stanford.edu

ST913-IVa-t991 Methicillin-Resistant *Staphylococcus aureus* among Pediatric Patients, Israel

Moti Baum, Einav Anuka, Maya Davidovich-Cohen, Assaf Rokney

In Israel, prevalence of sequence type 913, staphylococcal cassette chromosome *mec*IVa, *spa* type t991 methicillin-resistant *Staphylococcus aureus* lineage has surged among pediatric populations, predominantly in Arab and Orthodox Jewish communities. Antimicrobial resistance patterns vary by demographics. This lineage's spread and microevolution in the Middle East underscore the need for ongoing surveillance.

In 2010, a new methicillin-resistant *Staphylococcus aureus* (MRSA) clone, belonging to the clonal complex (CC) 913, Panton-Valentine leukocidin (PVL)–negative, staphylococcal cassette chromosome *mec* type IV, was isolated from Bedouin children in Israel (*1*). In 2012, isolates of CC913 were further analyzed, and their *spa* type was revealed as t991. Four t991 isolates were identified in hospitals across Israel, indicating the spread of the clone to communities beyond the Bedouin population in southern Israel (*2*). In 2015, a total of 12 t991 isolates were obtained from 280 patients (*3*), and in 2019, a total of 6 t991 isolates were obtained from 112 patients (*4*), mainly from children.

Since 2015, MRSA isolates of *spa* type t991 have emerged to become one of the main lineages in hospitals and health maintenance organizations in Israel. However, despite its significance, comprehensive characterization of *spa* type t991 clone is lacking. We explore its genomic context and antibiotic profile in this study.

The Study

During 2012–2020, the *S. aureus* national reference laboratory of Israel received a total of 4,646 MRSA isolates, obtained from skin and soft tissue infections (SSTIs), that were classified into 284 different *spa* types. Types t002, t008, and t032 were the most prevalent; t002 comprised 25% of total MRSA SSTI isolates, t008 comprised 15%, and t032, 5%. During that period, the proportion of t991 MRSA gradually increased to 13% of total MRSA SSTI isolates, whereas the leading *spa* types in MRSA SSTIs (t002 and t008) remained stable (Appendix Figure 1, https://wwwnc.cdc.gov/EID/article/30/8/23-0981-App1.pdf). During that period, 689 *S. aureus* samples of *spa* type t991, *mecA*-positive, PVL-negative, were received at the *S. aureus* national reference laboratory (Appendix). Most of the samples (406, 70%) were isolated from SSTIs; 66% isolates were from patients <5 years of age (p = 0.0001), whereas 4% were isolated from patients >60 years of age. In addition, most patients resided in localities associated with Arab and Orthodox Jewish populations (*5*). The number of t991 MRSA isolates from SSTI and blood increased dramatically, from 5 in 2012 to 180 in 2019 and 146 in 2020 (https://microreact.org/project/r4dFwJGXudh3gfyWtE1f87-t991final) (Figure 1).

We conducted whole-genome sequencing on 20 t991 MRSA isolates that were selected (Appendix Table), along with 3 t991 MRSA isolates from Germany (*6*,*7*). The isolates clustered into 4 separate clades (Figure 2). Clade A consisted of the 3 t991 isolates from Germany and is 130 whole-genome multilocus sequence typing (wgMLST) alleles distant from the first isolate of clade B, which consisted of 7 isolates from patients who lived in the Negev and were admitted to the same hospital. Clade C consisted of 5 isolates from patients residing in the Jerusalem district. Clade D consisted of 8 isolates, 7 of which were from Orthodox Jewish patients.

We tested 116 t991 MRSA isolates for phenotypic susceptibility by using the broth microdilution method (Figure 3). Isolates from patients living in Arab localities were more resistant to erythromycin and chloramphenicol, whereas those isolated from patients living in Jewish localities showed higher resistance to gentamicin, ciprofloxacin, levofloxacin, and

Author affiliation: Ministry of Health, Jerusalem, Israel

DOI: http://doi.org/10.3201/eid3008.230981

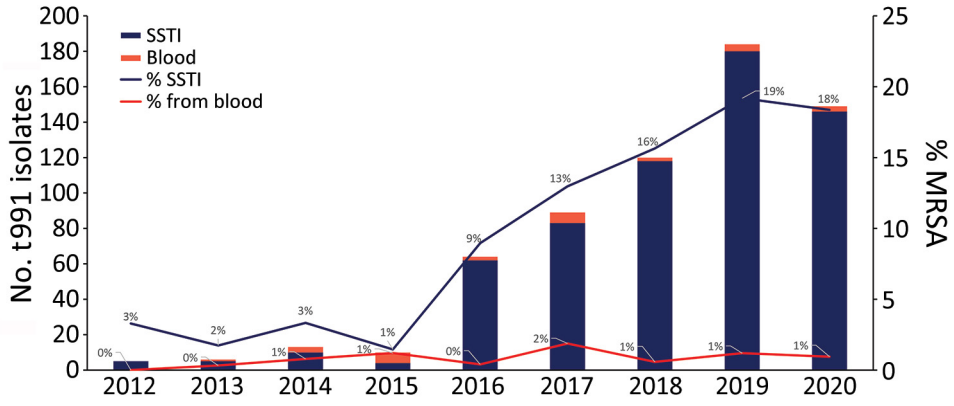

Figure 1. t991 MRSA isolates isolated from blood and SSTIs among patients in Israel during 2012–2020. Left y-axis represents number of t991 isolates isolated and right y-axis represents the relative part from total MRSA SSTI or blood isolates. MRSA, methicillin-resistant *Staphylococcus aureus*; SSTI, skin and soft tissue infection.

moxifloxacin (Appendix Figure 2). That tendency was statistically significant for chloramphenicol (p = 0.01) and gentamicin (p = 0.01).

We found 9 antimicrobial resistance (AMR) determinants, 8 AMR genes and 1 point mutation, among the 20 t991 MRSA sequences (Figure 4). Overall,

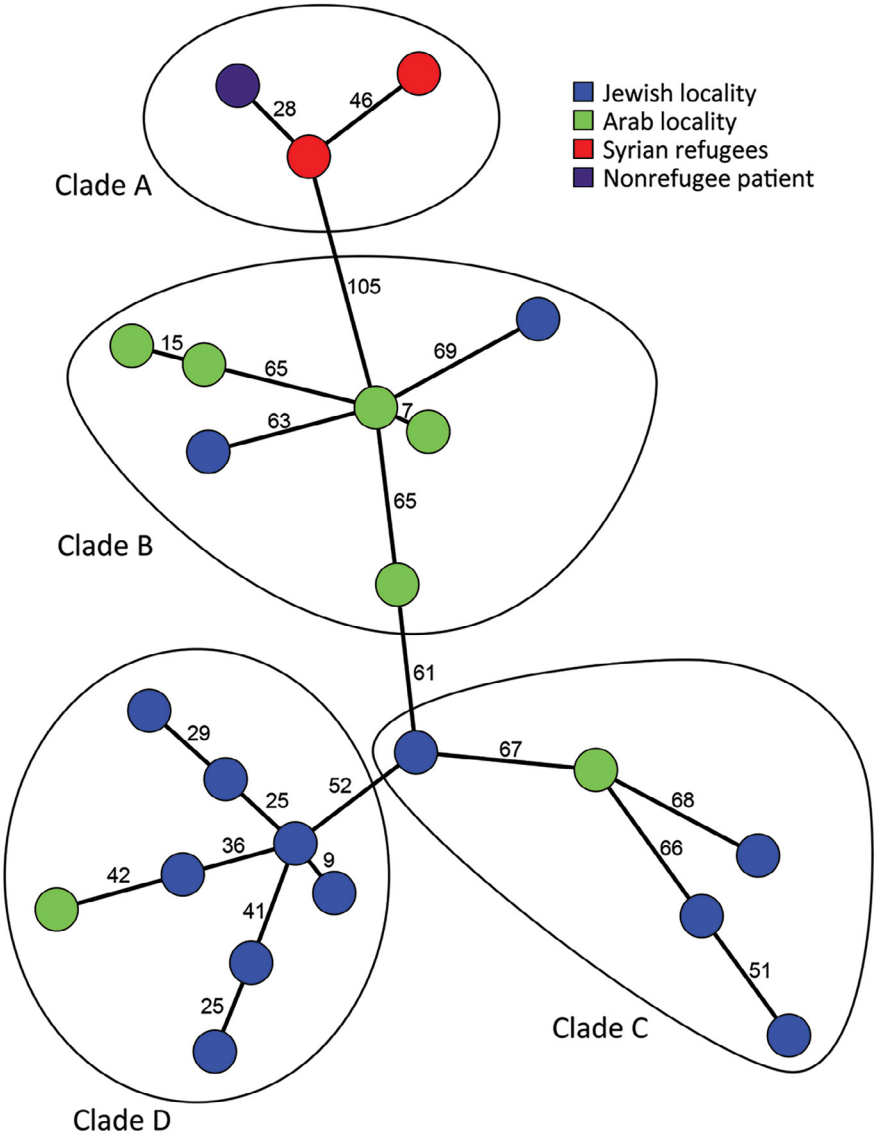

Figure 2. Phylogenetic relationships between 23 t991 MRSA genomes isolated in Israel and Germany. The figure shows a minimum spanning tree, created in Bionumerics software (https://www.bionumerics.com), based on 3,904 wgMLST allele IDs of sequenced t991 MRSA isolates. Each node represents an isolate; numbers along branches connecting nodes indicate the numbers of allelic differences between isolates. The isolates are further divided into 4 clades (A–D). MRSA, methicillin-resistant *Staphylococcus aureus;* wgMLST whole-genome multilocus sequence typing.

correlation between genotype prediction based on WGS and phenotypic AMR was 99% with a sensitivity of 94% and specificity of 100%. All discrepancies were associated with an absence of resistance determinant among phenotypically resistant isolates. No data for quinolone resistance genes or mutational resistance were predicted by the BioNumerics (https://www.bionumerics.com) or AMRFinder (https://github.com/ncbi/amr/releases/tag/amrfinder_v3.10.21) algorithms. In addition, we did not test phenotypic resistance against mupirocin.

We compared virulence profiles of 20 WGS t991 isolates with 3 t991 isolates from Germany, community-acquired MRSA USA300, and USA400 (*8*) as a reference using the functional genotyping tool of Bionumerics version 8.0. The main difference in virulence gene profile is reflected in the group of genes associated with adherence (Appendix Figure 3). In addition, virulence profiles can be grouped into 6 patterns on the basis of the presence of specific adherence factor genes in the genomes (Appendix Figure 4). We found no correlation between virulence profile and AMR, age, sex, residence location, or association with 1 of the genomic clades.

Next, to assess the genetic relationship of t991 isolates to other MRSA strains circulating worldwide, we created GrapeTree on the pubMLST site (https://pubmlst.org/organisms/staphylococcus-aureus) based on wgMLST data of representative local MRSA t991 strain (SA14675) along with 37,883 *S. aureus* global isolates (Appendix Figure 5) (*9*). The closest node to strain SA14675 is at a distance of 74 wgMLST alleles and is composed of 7 isolates. The next closest node is at a distance of 1,486 wgMLST alleles and composed of isolates that belong mainly to CC1.

Conclusions

Most t991 cases were isolated from young patients who live in strictly Orthodox and Arab localities. A possible explanation for this phenomenon is a similar lifestyle of the 2 sectors, characterized by overcrowding and large families. Regarding the evolution of this clone and its spread into the population, this strain appears to have evolved by multiple different genetic events. This assumption is supported by several findings. First, t991 MRSA isolates demonstrated classification into 4 distinct clades on the basis of geographic location and sectoral association; we noted genetic variation and weak clonality evident from the considerable distances between nodes, even within the same clade. Second, antibiotic resistance patterns vary between isolates obtained from patients who live in Jewish and Arab localities (Appendix Figure 2). Finally, *spa* type t991 composition is very short; it consists of 3 repeats (07-33-23) and can be formed as a result of genetic rearrangement of numerous MRSA strains harboring longer *spa* type repeats in which the repeats of *spa* type t991 from a part of their repeat succession. Worldwide phylogenetic analysis indicates that t991 MRSA stands out as a distinct emerging lineage because it appears considerably distant from most strains included in the GrapeTree (Appendix Figure 5).

Phenotypic AMR data for global isolates were available for 2 isolates (*7*,*10*). One isolate obtained in Kuwait was resistant to erythromycin, clindamycin, trimethoprim, and fusidic acid (*10*), and the

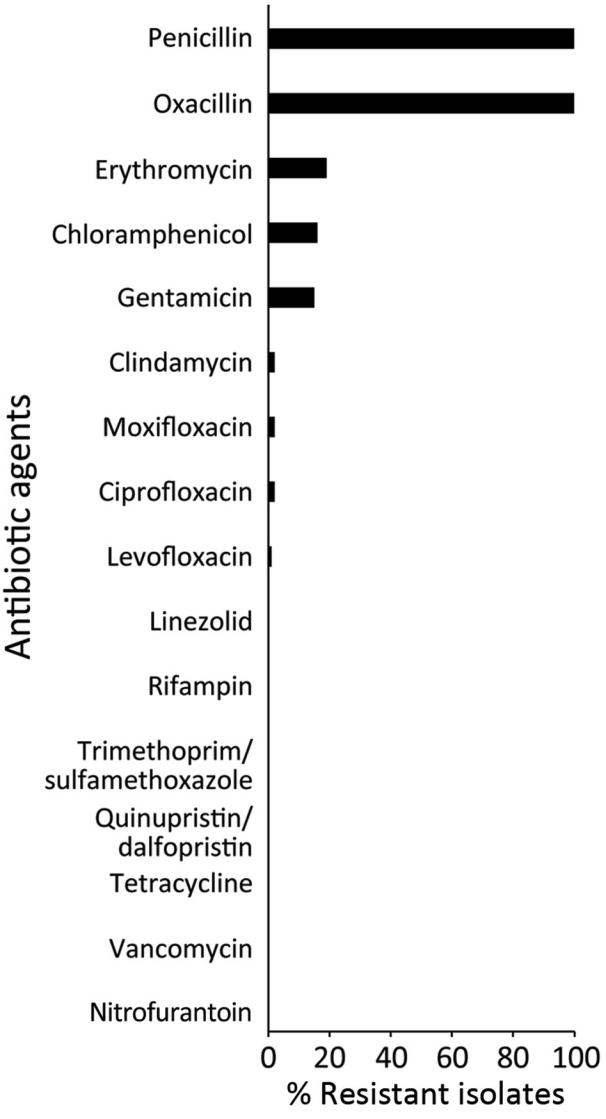

Figure 3. Percentage of resistant isolates to antibacterial agents among 116 t991 MRSA isolates from Israel tested for antimicrobial susceptibility using the broth microdilution method. MRSA, methicillin-resistant *Staphylococcus aureus.*

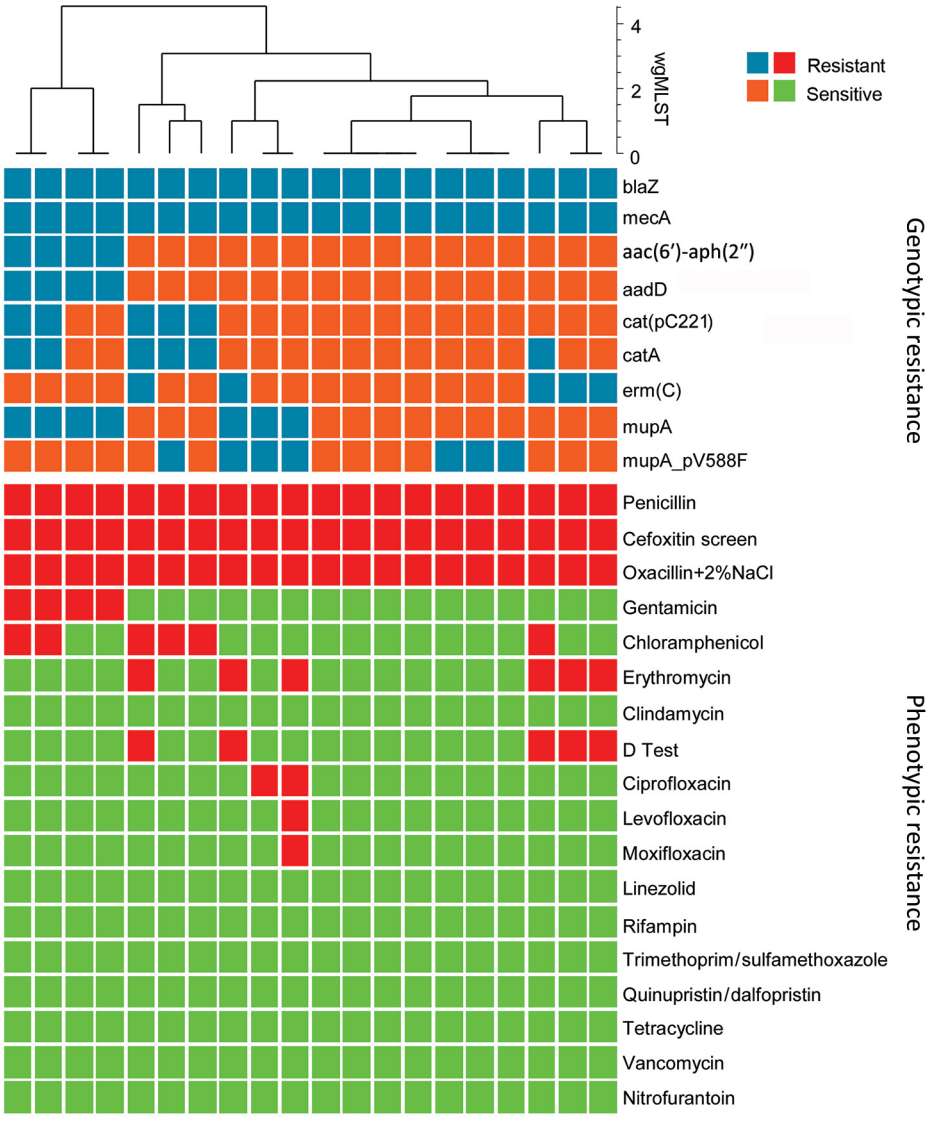

Figure 4. Comparison of genotypic and phenotypic resistance patterns of 20 t991 MRSA isolates from Israel tested using whole-genome sequencing. Blue tiles represent presence of resistance gene and orange tiles absence of resistance gene; red tiles represent antimicrobial resistance and green tiles antimicrobial sensitivity. Clustering is based on wgMLST data and generated by BioNumerics software (https://www.bionumerics.com). wgMLST, whole-genome multilocus sequence typing.

other was isolated in Germany from a refugee from Syria (*7*) and was resistant to erythromycin, clindamycin, and tetracycline. Out of the 116 tested t991 isolates, none showed resistance to tetracycline by antimicrobial susceptibility. For 2 isolates, we observed phenotypic resistance for erythromycin and chloramphenicol without prediction of AMR determinant. Close inspection of those isolates revealed they were actually positive for *ermC* and *cat*, and their sequences were fragmented into multiple contigs. Consistent with previous publications (*10*–*12*), all isolates tested, except for the strain from the Syria refugee (*7*), were positive for *eta*, a toxin responsible for skin infections seen mainly among young patients (*3*,*4*,*7*). Those findings are in accordance with the observation that t991 MRSA is predominantly isolated from children.

In conclusion, our study shows the emergence of t991 MRSA in Israel. These strains affect mainly pediatric populations, and a geographic distribution is limited mainly to the Middle East. The epidemiologic and genomic information our research provides will assist further investigation on the origin and dissemination of this clone.

About the Author

Dr. Baum is head of the National Staphylococcus Reference Laboratory at the Ministry of Health, Israel. His interests include genomic epidemiology and infectious diseases.

References

1. Adler A, Givon-Lavi N, Moses AE, Block C, Dagan R. Carriage of community-associated methicillin-resistant *Staphylococcus aureus* in a cohort of infants in southern

Israel: risk factors and molecular features. J Clin Microbiol. 2010;48:531–8. https://doi.org/10.1128/JCM.02290-08
2. Adler A, Chmelnitsky I, Shitrit P, Sprecher H, Navon-Venezia S, Embon A, et al. Molecular epidemiology of methicillin-resistant *Staphylococcus aureus* in Israel: dissemination of global clones and unique features. J Clin Microbiol. 2012;50:134–7. https://doi.org/10.1128/JCM.05446-11
3. Biber A, Parizade M, Taran D, Jaber H, Berla E, Rubin C, et al. Molecular epidemiology of community-onset methicillin-resistant *Staphylococcus aureus* infections in Israel. Eur J Clin Microbiol Infect Dis. 2015;34:1603–13.
4. Hadyeh E, Azmi K, Seir RA, Abdellatief I, Abdeen Z. Molecular characterization of methicillin resistant *Staphylococcus aureus* in West Bank–Palestine. Front Public Health. 2019;7:130. https://doi.org/10.3389/fpubh.2019.00130
5. Shadmi E, Khatib M, Spitzer S. The COVID-19 Israeli tapestry: the intersectionality health equity challenge. Isr J Health Policy Res. 2023;12:17. https://doi.org/10.1186/s13584-023-00567-8
6. Kossow A, Stühmer B, Schaumburg F, Becker K, Glatz B, Möllers M, et al. High prevalence of MRSA and multi-resistant gram-negative bacteria in refugees admitted to the hospital—but no hint of transmission. PLoS One. 2018;13:e0198103. https://doi.org/10.1371/journal.pone.0198103
7. Creutz I, Busche T, Layer F, Bednarz H, Kalinowski J, Niehaus K. Evaluation of virulence potential of methicillin-sensitive and methicillin-resistant *Staphylococcus aureus* isolates from a German refugee cohort. Travel Med Infect Dis. 2022;45:102204. https://doi.org/10.1016/j.tmaid.2021.102204
8. Thurlow LR, Joshi GS, Richardson AR. Virulence strategies of the dominant USA300 lineage of community-associated methicillin-resistant *Staphylococcus aureus* (CA-MRSA). FEMS Immunol Med Microbiol. 2012;65:5–22. https://doi.org/10.1111/j.1574-695X.2012.00937.x
9. Zhou Z, Alikhan NF, Sergeant MJ, Luhmann N, Vaz C, Francisco AP, et al. GrapeTree: visualization of core genomic relationships among 100,000 bacterial pathogens. Genome Res. 2018;28:1395–404. https://doi.org/10.1101/gr.232397.117
10. Boswihi SS, Udo EE, Monecke S, Mathew B, Noronha B, Verghese T, et al. Emerging variants of methicillin-resistant *Staphylococcus aureus* genotypes in Kuwait hospitals. PloS One. 2018;13:e0195933. https://doi.org/10.1371/journal.pone.0195933
11. Monecke S, Coombs G, Shore AC, Coleman DC, Akpaka P, Borg M, et al. A field guide to pandemic, epidemic and sporadic clones of methicillin-resistant *Staphylococcus aureus*. PloS One. 2011;6:e17936. https://doi.org/10.1371/journal.pone.0017936
12. Azarian T, Cella E, Baines SL, Shumaker MJ, Samel C, Jubair M, et al. Genomic epidemiology and global population structure of exfoliative toxin A–producing *Staphylococcus aureus* strains associated with staphylococcal scalded skin syndrome. Front Microbiol. 2021;12:663831. https://doi.org/10.3389/fmicb.2021.663831

Address for correspondence: Moti Baum, Ministry of Health Ya'akov Eliav 9, Jerusalem, Israel; email: moti.baum@moh.gov.il

Emayella augustorita, New Member of Pasteurellaceae, Isolated from Blood Cultures of Septic Patient

Sylvain Meyer, Valentin Tilloy, Sylvaine Durand-Fontanier, Thomas Lafon, Fabien Garnier, Christian Martin, Marie-Cécile Ploy, Olivier Barraud

Author affiliations: Laboratoire de Bactériologie-Virologie-Hygiène, CHU Limoges, Limoges, France (S. Meyer, F. Garnier, C. Martin, M.-C. Ploy, O. Barraud); Université Limoges, UMR INSERM 1092, Limoges (S. Meyer, F. Garnier, C. Martin, M.-C. Ploy, O. Barraud); Centre National de Référence des Herpèsvirus, Limoges (V. Tilloy); Service de Chirurgie Digestive, CHU Limoges, Limoges (S. Durand-Fontanier); Service d'Accueil des Urgences, CHU Limoges, Limoges (T. Lafon).

DOI: https://doi.org/10.3201/eid3008.231651

We report discovery of a new bacterial genus and species of the family Pasteurellaceae by using phylogenetic and metabolic analysis. The bacterium, *Emayella augustorita*, was isolated from blood cultures of a patient in France diagnosed with an adenocarcinoma of the intestines and who was treated with a biliary prosthesis placement.

Pasteurellaceae bacteria have been identified in many vertebrates as members of the microbiota but can occasionally cause human infections (*1*). Currently, the family Pasteurellaceae contains 34 genera and 105 species (https://pasteurellaceae.eu). Few acquired antibiotic resistances are reported (occasionally β-lactamases, macrolides, tetracyclines, or fluoroquinolones), but recently some strains were reported to have multidrug resistance profiles (*2*–*4*). We describe a new bacterium belonging to the Pasteurellaceae family isolated from positive blood cultures of a septic patient.

A 74-year-old woman was admitted January 2022 to the emergency department at the Limoges teaching hospital in France. She reported complaints of an occlusive syndrome with nausea, vomiting, and fever. She was previously diagnosed in 2015 with an adenocarcinoma of the small intestine with metastases in the lungs and liver with biliary compression. After multiple chemotherapies and surgeries, she was diagnosed with severe bacteremia of digestive origin (Figure). A metallic biliary prosthesis through a biliary drain was placed in December 2021. No documentation of any contact with farm animals or pets was reported.

We conducted an abdominal computed tomography scan that detected a hepatic lesion with a heterogeneous hypodense area of the tip of the VI segment of the liver on the path of the biliary drain, suggesting a biloma. Laboratory results showed evidence of possible infection with a total leukocyte count of 24.4 × 10^9 leukocytes/L (reference range 3.78–9.42 × 10^9 leukocytes/L) and a C-reactive protein result of 150 mg/L (reference range <5 mg/L). Two blood cultures were collected, and we initiated empiric antibiotic therapy with ceftriaxone-metronidazole (Figure). Four blood culture bottles, aerobic and anaerobic incubation detected growth after 16 hours of incubation. A Gram stain of the positive bottles showed a short gram-negative rod (Appendix Figure 1, https://wwwnc.cdc.gov/EID/article/30/8/23-1651-App1.pdf). Small, bright colonies grew in a 5% CO_2 atmosphere on blood agar and PolyVitex plates (bioMérieux, https://www.biomerieux.com) after 24 hours of incubation at 35°C (Appendix Figure 1). We attempted bacterial identification by using matrix-assisted laser desorption/ionization time-of-flight mass spectrometry (bioMérieux) and did not match any known bacterial species. We determined MICs by using E-tests (bioMérieux) on Mueller Hinton agar with 5% horse blood (bioMérieux) for amoxicillin/clavulanic acid, piperacillin/tazobactam, cefotaxime, levofloxacin, and trimethoprim/sulfamethoxazole, according to pharmacokinetic-pharmacodynamic EUCAST breakpoints

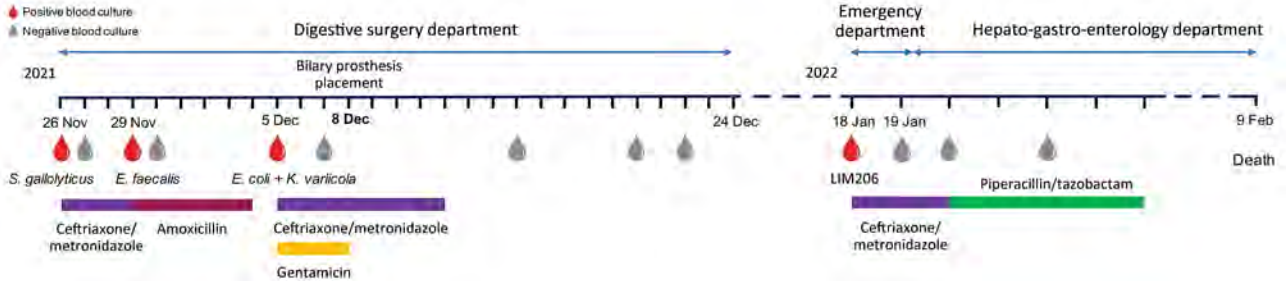

Figure. Timeline of main events for case report on the isolation of *Emayella augustorita*, a novel bacterium of the *Pasteurellaceae* family recovered from a patient with sepsis, France. *E. coli*, *Escherichia coli*; *E. faecalis*, *Enterococcus faecalis*; *K. variicola*, *Klebsiella variicola*; *S. gallolyticus*, *Streptococcus gallolyticus*.

Table. MIC values observed for LIM206, *Emayella augustorita*, a novel bacteria of the Pasteurellaceae family recovered from a patient with sepsis, France*

Antibiotic	PK/PD breakpoints, mg/L†	MIC, mg/L
Amoxicillin	2–8	0.75
Amoxicillin + clavulanic acid	2–8	0.75
Piperacillin + tazobactam	8–16	1.0
Cefotaxime	1–2	0.032
Levofloxacin	0.5–1	0.064
Trimethoprim/sulfamethoxazole	0.5	0.004

*PK/PD, pharmacokinetics/pharmacodynamics.
†All breakpoints were from EUCAST except for trimethoprim/sulfamethoxazole, which was epidemiologic cutoff value.

(https://www.eucast.org). No phenotypic resistance was detected (Table). The patient's successive blood cultures became negative, but her general status worsened, leading to death in February 2022 (Figure).

Sanger sequencing of the whole 16S rRNA gene (Genbank accession no. OR046993) did not show sufficient identification (94.78% similarity with *Pasteurella oralis*). A 16S phylogenetic tree confirmed the result but also emphasized the wrong affiliation of genera in this family (Appendix Figure 2). Because of the low identity percentage (<97%), we conducted whole-genome sequencing by using the Ion GeneStudio S5 Plus platform (ThermoFisher Scientific, https://www.fishersci.com), as previously described (*5*). The genome size was 2.68 Mbp, and the total DNA guanine and cytosine mol% content was 45.3 mol%. Annotation identified 2462 coding sequence, 45 tRNA, and 6 rRNA. No resistance genes were detected (Appendix). We identified the type strain as LIM206 (Genbank accession no. JAWHQP010000000).

A phylogenetic tree based on single nucleotide polymorphisms comparison between whole genomes of different Pasteurellaceae species showed LIM206 was placed on a separate branch from all other genera. The average nucleotide identity between LIM206 and the closest members that shared a phylogenetic branch was 73.48% with *Actinobacillus succinogenes*, 74.09% with *Basfia succiniciproducens*, 72.13% with *Lonepinella koalarum*, 73.20% with *Mesocricetibacter intestinalis*, and 72.13% with *Pasteurella bettyae* (Appendix Figure 3). Results of those combined analyses suggested LIM206 belonged to a new species and a new genus of Pasteurellaceae. We conducted multilocus sequence analysis on 16S rRNA, *infB*, *recN*, *rpoA*, and *rpoB* genes according to previous recommendations (*6*,*7*) (Appendix). LIM206 was separated from existing genera of Pasteurellaceae and closely linked to *A. succinogenes* and *B. succiniciproducens* (Appendix Figure 4). To confirm the new genus, we conducted amino acid identity analysis and found a maximum amino acid identity value of 77.67% with *Basfia succiniciproducens* (Appendix Figure 5). This identity value was considered below the genus identity threshold of ≈83% compared to other Pasteurellaceae genera.

We compared the biochemical characteristics of LIM206 to those of different species of the Pasteurellaceae family (Appendix Table 1). We detected the presence of urease activity, the acidification of L-arabinose and D-xylose, and the absence of acidification of D-mannitol and D-trehalose, which are not frequently observed in Pasteurellaceae. Those characteristics are absent in the genetically closest species (*8*,*9*).

In conclusion, we report the description of a new genus and species of the Pasteurellaceae family found in blood cultures of a septic patient in France followed for metastatic adenocarcinoma of the intestines. We derived the genus name *Emayella* from the word enamel; the species name *augustorita* is in reference to the Roman name of Limoges. The bacterium is a short gram-negative coccoid to rod shape. It is catalase negative, oxidase positive, nonmotile, fermentative, capnophilic, and nonhemolytic. The bacterium does not require β-nicotinamide adenine dinucleotide or hemin-factors for growth.

About the Author

Dr. Meyer is a clinical microbiologist at the Limoges University Hospital Center, France. His research focuses on molecular bacteriology, clinical metagenomics, and antibiotic resistance.

References

1. Chien Y-C, Huang Y-T, Liao C-H, Chien J-Y, Hsueh P-R. Clinical characteristics of bacteremia caused by *Haemophilus* and *Aggregatibacter* species and antimicrobial susceptibilities of the isolates. J Microbiol Immunol Infect. 2021;54:1130–8. https://doi.org/10.1016/j.jmii.2020.12.002
2. Michael GB, Bossé JT, Schwarz S. Antimicrobial resistance in *Pasteurellaceae* of veterinary origin. Microbiol Spectr. 2018;6:6.3.02. https://doi.org/10.1128/microbiolspec.ARBA-0022-2017
3. Van Driessche L, Vanneste K, Bogaerts B, De Keersmaecker SCJ, Roosens NH, Haesebrouck F, et al. Isolation of drug-resistant *Gallibacterium anatis* from calves with unresponsive bronchopneumonia, Belgium. Emerg Infect Dis. 2020;26:721–30. https://doi.org/10.3201/eid2604.190962
4. Saiz-Escobedo L, Cadenas-Jiménez I, Olmos R, Carrera-Salinas A, Berbel D, Càmara J, et al. Detection of $bla_{CTX-M-15}$ in an integrative and conjugative element in four extensively drug-resistant *Haemophilus parainfluenzae* strains causing

urethritis. Int J Antimicrob Agents. 2023;62:106991. https://doi.org/10.1016/j.ijantimicag.2023.106991
5. Mairi A, Meyer S, Tilloy V, Barraud O, Touati A. Whole genome sequencing of extended-spectrum beta-lactamase-producing *Klebsiella pneumoniae* isolated from neonatal bloodstream infections at a neonatal care unit, Algeria. Microb Drug Resist. 2022;28:867–76. https://doi.org/10.1089/mdr.2021.0337
6. Kuhnert P, Korczak BM. Prediction of whole-genome DNA-DNA similarity, determination of G+C content and phylogenetic analysis within the family *Pasteurellaceae* by multilocus sequence analysis (MLSA). Microbiology. 2006;152:2537–48. https://doi.org/10.1099/mic.0.28991-0
7. Chun J, Oren A, Ventosa A, Christensen H, Arahal DR, da Costa MS, et al. Proposed minimal standards for the use of genome data for the taxonomy of prokaryotes. Int J Syst Evol Microbiol. 2018;68:461–6. https://doi.org/10.1099/ijsem.0.002516
8. Kuhnert P, Scholten E, Haefner S, Mayor D, Frey J. *Basfia succiniciproducens* gen. nov., sp. nov., a new member of the family *Pasteurellaceae* isolated from bovine rumen. Int J Syst Evol Microbiol. 2010;60:44–50. https://doi.org/10.1099/ijs.0.011809-0
9. Christensen H, Nicklas W, Bisgaard M. Investigation of taxa of the family *Pasteurellaceae* isolated from Syrian and European hamsters and proposal of *Mesocricetibacter intestinalis* gen. nov., sp. nov. and *Cricetibacter osteomyelitidis* gen. nov., sp. nov. Int J Syst Evol Microbiol. 2014;64:3636–43. https://doi.org/10.1099/ijs.0.067470-0

Address for correspondence: Sylvain Meyer, Laboratoire de Bactériologie-Virologie-Hygiène, CHU de Limoges, 2 Avenue Martin Luther King, 87042 Limoges CEDEX, France; email: sylvain.meyer@unilim.fr

Persistence of Influenza H5N1 and H1N1 Viruses in Unpasteurized Milk on Milking Unit Surfaces

Valerie Le Sage,[1] A.J. Campbell,[1] Douglas S. Reed, W. Paul Duprex, Seema S. Lakdawala

Author affiliations: University of Pittsburgh, Pittsburgh, Pennsylvania, USA (V. Le Sage, D.S. Reed, W.P. Duprex); Emory University School of Medicine, Atlanta, Georgia, USA (A.J. Campbell, S.S. Lakdawala)

DOI: https://doi.org/10.3201/eid3008.240775

[1]These first authors contributed equally to this article.

Examining the persistence of highly pathogenic avian influenza A(H5N1) from cattle and human influenza A(H1N1)pdm09 pandemic viruses in unpasteurized milk revealed that both remain infectious on milking equipment materials for several hours. Those findings highlight the risk for H5N1 virus transmission to humans from contaminated surfaces during the milking process.

Highly pathogenic avian influenza A(H5N1) virus was detected in US domestic dairy cattle in late March 2024, after which it spread to herds across multiple states and resulted in at least 3 confirmed human infections (*1*). Assessment of milk from infected dairy cows indicated that unpasteurized milk contained high levels of infectious influenza virus (*2*; L.C. Caserta et al., unpub. data, https://doi.org/10.1101/2024.05.22.595317). Exposure of dairy farm workers to contaminated unpasteurized milk during the milking process could lead to increased human H5 virus infections. Such infections could enable H5 viruses to adapt through viral evolution within humans and gain the capability for human-to-human transmission.

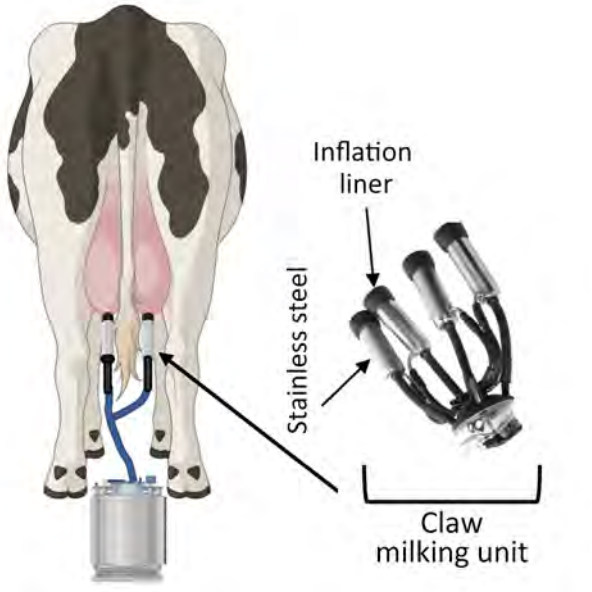

Figure 1. Illustration of milking unit surfaces tested in a study of persistence of influenza H5N1 and H1N1 viruses in unpasteurized milk. Before attaching the milking unit (claw), a dairy worker disinfects the teat ends, performs forestripping of each teat to detect abnormal milk, and then wipes each teat with a clean dry towel. Workers then attach the milking unit to the cow teats. A pulsation system opens and closes the rubber inflation liner (at left) around the teat to massage it, mimicking a human stripping action. A vacuum pump is controlled by a variable speed drive and adjusts the suction to allow milk to flow down a pipeline away from the cow into a bulk tank or directly onto a truck. Additional sources of exposure to humans include handling of raw unpasteurized milk collected separately from sick cows or during the pasteurization process. Schematic created in BioRender (https://www.biorender.com).

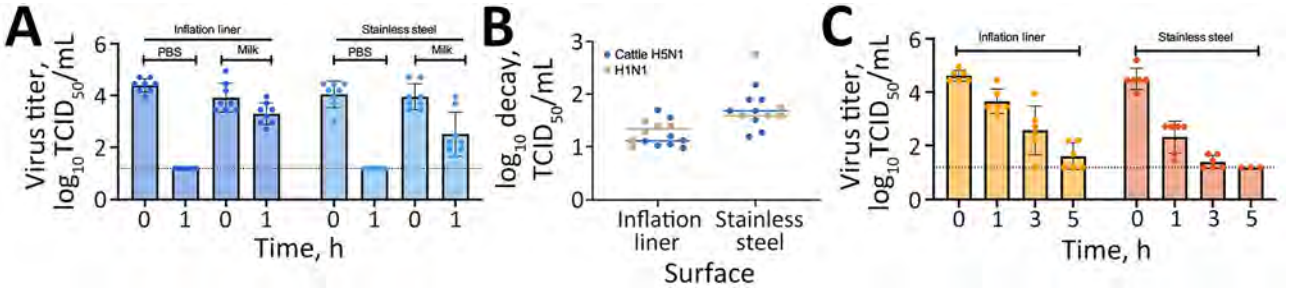

Figure 2. Viral titers in a study of persistence of influenza H5N1 and H1N1 viruses in unpasteurized milk on milking unit surfaces. A) Viral titers of bovine A(H5N1) virus diluted 1:10 in unpasteurized milk or PBS and deposited as ten 1-μL droplets onto the indicated surfaces. Droplets were recovered immediately after deposition (time 0) or after 1 hour of aging at 70% relative humidity (RH) at 21°C. Colored dots indicate measurements for each droplet; error bars indicate SD. Horizontal dotted lines indicate the theoretical limits of detection. B) Comparison of log decay values of H5N1 and H1N1 viruses in unpasteurized milk at 70% RH for 1 hour on rubber inflation liners and stainless steel. Decay was calculated as a ratio of the viral titer at time 0 divided by the titer after 1 hour. Colored symbols indicate measurements for each droplet. Horizonal lines indicate median values. C) Viral titers of the H1N1 virus diluted 1:10 in unpasteurized milk on the 2 surfaces at 70% RH for 0, 1, 3, or 5 hours at 23.6°C–25°C. Each symbol is a replicate of ≥2 biologic replicates using 2 distinct lots of unpasteurized milk performed in triplicate. Virus titer was calculated using the traditional $TCID_{50}$ assay on MDCK cells. Colored dots indicate measurements for each droplet; error bars indicate SD. Horizontal dotted lines indicate the theoretical limits of detection. All raw data are available at https://doi.org/10.6084/m9.figshare.c.7242034.v1. PBS, phosphate buffered saline; $TCID_{50}$, 50% tissue culture infectious dose.

The milking process is primarily automated and uses vacuum units, commonly referred to as clusters or claws, which are attached to the dairy cow teats to collect milk (Figure 1) (*3*). However, several steps in the milking process require human input, including forestripping, whereby workers manually express the first 3–5 streams of milk from each teat by hand. Forestripping stimulates the teats for optimal milk letdown, improves milk quality by removing bacteria, and provides an opportunity to check for abnormal milk. The forestripping process can result in milk splatter on the floor of the milking parlor and surrounding equipment and production of milk aerosols.

After forestripping, each teat is cleaned and dried by hand before the claw is installed. During milking, a flexible rubber inflation liner housed within the stainless-steel shell of the claw opens to enable the flow of milk and closes to exert pressure on the teat to stop the flow of milk (Figure 1). When the flow of milk decreases to a specific level, the claw automatically releases (*3*), at which point residual milk in the inflation liner could spray onto dairy workers, equipment, or the surrounding area. Of note, milking often takes place at human eye level; the human workspace is physically lower than the cows, which increases the potential for infectious milk to contact human workers' mucus membranes. No eye or respiratory protection is currently required for dairy farm workers, but recommendations have been released (*4*).

Influenza virus persistence in unpasteurized milk on surfaces is unclear, but information on virus persistence is critical to understanding viral exposure risk to dairy workers during the milking process. Therefore, we analyzed the persistence of infectious influenza viruses in unpasteurized milk on surfaces commonly found in milking units, such as rubber inflation liners and stainless steel (Figure 1).

For infectious strains, we used influenza A(H5N1) strain A/dairy cattle/TX/8749001/2024 or a surrogate influenza A(H1N1)pdm09 pandemic influenza virus strain, A/California/07/2009. We diluted virus 1:10 in raw unpasteurized milk and in phosphate-buffered saline (PBS) as a control. As described in prior studies (*5*–*7*), we pipetted small droplets of diluted virus in milk or PBS onto either stainless steel or rubber inflation liner coupons inside an environmental chamber. We then collected virus samples immediately (time 0) or after 1, 3, or 5 hours to detect infectious virus by endpoint titration using a 50% tissue culture infectious dose assay (*7*). To mimic environmental conditions within open-air milking parlors in the Texas panhandle during March–April 2024, when the virus was detected in dairy herds, we conducted persistence studies using 70% relative humidity.

We observed that the H5N1 cattle virus remained infectious in unpasteurized milk on stainless steel and rubber inflation lining after 1 hour, whereas infectious virus in PBS fell to below the limit of detection after 1 hour (Figure 2, panel A). That finding indicates that unpasteurized milk containing H5N1 virus remains infectious on materials within the milking unit. To assess whether a less pathogenic influenza virus could be used as a surrogate to study viral persistence on milking unit materials, we compared viral decay between H5N1 and H1N1 in raw milk over 1 hour on rubber inflation liner and stainless-steel surfaces (Figure

2, panel B). The 2 viruses had similar decay rates on both surfaces, suggesting that H1N1 can be used as a surrogate for H5N1 cattle virus in studies of viral persistence in raw milk. Further experiments examining H1N1 infectiousness over longer periods revealed viral persistence in unpasteurized milk on rubber inflation liner for at least 3 hours and on stainless steel for at least 1 hour (Figure 2, panel C). Those results indicate that influenza virus is stable in unpasteurized milk and that influenza A virus deposited on milking equipment could remain infectious for >3 hours.

Taken together, our data provide compelling evidence that dairy farm workers are at risk for infection with H5N1 virus from surfaces contaminated during the milking process. To reduce H5N1 virus spillover from dairy cows to humans, farms should implement use of personal protective equipment, such as face shields, masks, and eye protection, for workers during milking. In addition, contaminated rubber inflation liners could be responsible for the cattle-to-cattle spread observed on dairy farms. Sanitizing the liners after milking each cow could reduce influenza virus spread between animals on farms and help curb the current outbreak.

This article was preprinted at https://www.medrxiv.org/content/10.1101/2024.05.22.24307745v1.

Acknowledgments

We thank the Lakdawala lab members, Centers of Excellence for Influenza Research and Response (CEIRR) risk assessment pipeline meeting attendees, Rachel Duron, and Linsey Marr for useful feedback.

This project was funded in part with federal funds from the National Institute of Allergy and Infectious Diseases, National Institutes of Health, Department of Health and Human Services, under contract no. 75N93021C00015 and a National Institutes of Health award (no. UC7AI180311) from the National Institute of Allergy and Infectious Diseases supporting the operations of the University of Pittsburgh Regional Biocontainment Laboratory in the Center for Vaccine Research. H5N1 studies were performed in accordance with select agent permit no. 20230320-074008 at the University of Pittsburgh.

About the Author

Dr. Le Sage is a research assistant professor at the University of Pittsburgh Center for Vaccine Research, Pittsburgh, Pennsylvania, USA. Her research interests include elucidating the requirements for influenza virus transmission and assessing the pandemic potential of emerging influenza viruses.

References

1. Centers for Disease Control and Prevention. H5N1 bird flu: current situation summary [cited 2024 Jun 13]. https://www.cdc.gov/flu/avianflu/avian-flu-summary.htm
2. Burrough ER, Magstadt DR, Petersen B, Timmermans SJ, Gauger PC, Zhang J, et al. Highly pathogenic avian influenza A(H5N1) clade 2.3.4.4b virus infection in domestic dairy cattle and cats, United States, 2024. Emerg Infect Dis. 2024;30:1335–43. https://doi.org/10.3201/eid3007.240508
3. Odorčić M, Rasmussen MD, Paulrud CO, Bruckmaier RM. Review: Milking machine settings, teat condition and milking efficiency in dairy cows. Animal. 2019;13(S1):s94–9. https://doi.org/10.1017/S1751731119000417
4. Centers for Disease Control and Prevention. Avian influenza (bird flu): reducing risk for people working with or exposed to animals [cited 2024 Jun 20]. https://www.cdc.gov/bird-flu/prevention/worker-protection-ppe.html
5. Qian Z, Morris DH, Avery A, Kormuth KA, Le Sage V, Myerburg MM, et al. Variability in donor lung culture and relative humidity impact the stability of 2009 pandemic H1N1 influenza virus on nonporous surfaces. Appl Environ Microbiol. 2023;89:e0063323. https://doi.org/10.1128/aem.00633-23
6. Kormuth KA, Lin K, Qian Z, Myerburg MM, Marr LC, Lakdawala SS. Environmental persistence of influenza viruses is dependent upon virus type and host origin. MSphere. 2019;4:e00552-19. https://doi.org/10.1128/mSphere.00552-19
7. Kormuth KA, Lin K, Prussin AJ II, Vejerano EP, Tiwari AJ, Cox SS, et al. Influenza virus infectivity is retained in aerosols and droplets independent of relative humidity. J Infect Dis. 2018;218:739–47. https://doi.org/10.1093/infdis/jiy221

Address for correspondence: Seema Lakdawala, Emory University School of Medicine, 1510 Clifton Rd, Rm 3121, Rollins Research Center, Atlanta, GA 30322, USA; email: seema.s.lakdawala@emory.edu; or Valerie Le Sage, Center for Vaccine Research, University of Pittsburgh School of Medicine, Biomedical Science Tower 3, Rm 9052, 3501 Fifth Ave, Pittsburgh, PA 15213, USA; email: valerie.lesage@pitt.edu

Panton-Valentine Leukocidin–Positive *Staphylococcus aureus* in Family and Pet Cat

Astrid Bethe, Anne-Kathrin Schink, Julian Brombach, Lennard Epping, Torsten Semmler, Susanne Reinhardt, Ernst Molitor, Svenja Müller, Julian Balks, Robin Köck, Stefan Schwarz, Birgit Walther,[1] Antina Lübke-Becker[1]

Author affiliations: Freie Universität Berlin, Berlin, Germany (A. Bethe, A.-K. Schink, J. Brombach, S. Schwarz, A. Lübke-Becker); German Environment Agency, Berlin (A. Bethe, B. Walther); Laboratory Diagnostics Germany, Cuxhaven, Germany (A.-K. Schink); Robert Koch Institute, Berlin (L. Epping, T. Semmler, B. Walther); Kleintierpraxis am Kenntemichplatz, Troisdorf, Germany (S. Reinhardt); University Hospital, Bonn, Germany (E. Molitor, S. Müller, J. Balks); Universitätsmedizin, Essen, Germany (R. Köck)

DOI: https://doi.org/10.3201/eid3008.231255

Continued detection of Panton-Valentine leukocidin–positive *Staphylococcus aureus* in samples from a family with severe repeated skin infections and their pet cat suggests transmission between the family and the cat. Decolonizing the pet led to successful elimination of the bacteria from the household. Clinicians should consider pet cats as possible reinfection sources.

Panton-Valentine leucocidin (PVL)–producing *Staphylococcus aureus* (PVL-SA) is typically associated with skin and soft tissue infections, such as abscesses (*1*). Transmission occurs between persons in close contact, often causing clusters of community-onset infections, especially within families (*1*). PVL-SA contains the genes *lukS* and *lukF*, which encode 2 toxin components capable of forming a pore-like octamer on neutrophil membranes, leading to cell lysis, local inflammation, and tissue damage (*2*). Because staphylococci colonize the nares, pharynx, and skin, infection reemergence occurs in the case of abrasions or wounds, enabling PVL-SA to cross the skin barrier. Topical decolonization of the skin and other body sites during or after acute PVL-SA infections is part of the therapy (*3*). In this article, we describe the successful decolonization of a family in Germany, comprising 2 adults and 2 children, who experienced severe recurrent PVL-SA infections and multiple unsuccessful decolonization attempts with increased hygiene measurements over an extended period.

[1]These authors contributed equally to this article.

The consultant laboratory for methicillin-resistant staphylococci in veterinary practice and clinic (CL-MRS-VPC), located at the institute of microbiology and epizootics, Freie Universität Berlin, was contacted in January 2022 because a family affected by severe repeated soft tissue infections caused by PVL-SA had undergone 3 unsuccessful decolonization attempts. Everyone in the family had experienced multiple (5–15/person) skin abscesses caused by PVL-SA since 2017. The 3 unsuccessful ambulatory decolonization attempts of the family were performed by the University Hospital in Bonn, Germany, according to a standard protocol (Charité, https://hygiene.charite.de/forschung/arbeitsgruppen/ag_pvl_bildender_staphylococcus_aureus). A review and assessment of possible reinfection sources by the clinicians led to the initial sampling of 2 household cats. Samples from both cats (oral, nasal, inguinal, perianal, and rectal) were screened at CL-MRS-VPC.

We cultured all swab samples as previously described (*4*). We identified the *S. aureus* isolates by using matrix-assisted laser desorption/ionization time-of-flight mass spectrometry (Bruker, https://www.bruker.com). We conducted antimicrobial susceptibility testing by using the VITEK2 system (bioMérieux, https://www.biomerieux.com) and Clinical and Laboratory Standards Institute clinical breakpoints (*5*). We used PCR on the *S. aureus* isolates recovered to detect PVL-encoding genes (*lukF* and *lukS*) (*6*). We isolated methicillin-susceptible *S. aureus* (MSSA) from the oral cavity and nostrils of both cats. Cat 1 was confirmed as a carrier of PVL-positive MSSA, and cat 2 carried PVL-negative MSSA (Table; Figure). We further investigated whether the feline MSSA strains were circulating in the family by conducting whole-genome sequencing of both feline strains and PVL-positive and PVL-negative MSSA strains obtained from samples of the human family members (Table).

We performed a de novo assembly of the paired-end reads and annotated the resulting genomes as previously described (*7*). We generated an alignment of the maximum common genome from the study set to identify single-nucleotide polymorphisms (SNPs). The SNP analyses showed close clonal relationships of both the PVL-MSSA, assigned to sequence type 8 (range 10–12 SNPs), and the PVL-negative MSSA strains, assigned to sequence type 45 (range 1–7 SNPs), isolated from human and feline samples. The *lukS* and *lukF* genes of the PVL-MSSA isolate shared 100% nucleotide sequence identity and coverage with the corresponding genes in strain USA300 FPR3757 (GenBank accession no. 87125858), an epidemic clone of community-acquired methicillin-resistant *S. aureus* (*8*).

Table. Antimicrobial susceptibility testing results of *Staphylococcus aureus* isolates recovered from a family who had repeated soft-tissue infections caused by Panton-Valentine leukocidin–producing *S. aureus* and their pet cats*

Isolate	IMT51844	IMT51843	IMT51535	IMT51669	IMT51533	IMT51534	IMT51668	IMT51681
Source	Child	Parent	Cat 2	Cat 2	Cat 1	Cat 1	Cat 1	Cat 1
Sample site	Nose	Inguinal	Mouth	Nose	Mouth	Nose	Nose	Nose
Date	2021 Nov	2021 Nov	2022 Mar	2022 Mar	2022 Mar	2022 Mar	2022 Mar	2022 Mar
ST	45	8	45	45	8	8	8	8
PVL	–	+	–	–	+	+	+	+
Antimicrobial drug MIC, µg/mL								
CIP	0.12	16	0.12	0.25	16	16	16	16
ENR	0.12	4	0.12	0.12	4	4	4	4
MAR	0.25	16	0.25	0.25	16	16	16	16
GEN	1	0.25	0.5	1	0.25	0.25	1	0.25
SXT	0.06/1.19	0.06/1.19	0.06/1.19	0.06/1.19	0.06/1.19	0.06/1.19	0.06/1.19	0.06/1.19
TET	0.25	32	0.5	1	64	32	32	64
DOX	0.5	4	0.5	0.5	4	4	4	4
PEN	0.03	0.03	0.03	0.03	0.03	0.06	0.06	0.06
AMP	0.12	0.12	0.25	0.12	0.12	0.12	0.25	0.25
AMC	0.25/0.12	0.25/0.12	0.25/0.12	0.25/0.12	0.25/0.12	0.25/0.12	0.25/0.12	0.25/0.12
OXA	0.12	0.25	0.12	0.25	0.25	0.25	0.5	0.25
ERY	1	≥64	0.5	0.5	≥64	32	≥64	≥64
CLI	0.25	0.25	0.25	0.25	0.12	0.12	0.25	0.12

*AMC, amoxicillin/clavulanate; AMP, ampicillin; CIP, ciprofloxacin; CLI, clindamycin; DOX, doxycycline; ENR, enrofloxacin; ERY, erythromycin; GEN, gentamicin; MAR, marbofloxacin; OXA, oxacillin; PEN, penicillin; PVL, Panton-Valentine leukocidin; ST, sequence type; SXT, sulfamethoxazole/trimethoprim; TET, tetracycline; +, positive; –, negative.

According to regulations in Germany for research with animal subjects, attempts to decolonize cats by using amoxicillin/clavulanate do not need approval (Landesamt für Gesundheit und Soziales, Berlin, pers. comm., letter, 2023 Feb 6). We performed an initial attempt to decolonize the cats on the basis of antimicrobial susceptibility testing results involving oral administration of amoxicillin/clavulanate for 10 days (Figure). The decolonization attempt was accompanied by hand washing and isolation of the cats indoors.

Samples from cat 2 were negative for *S. aureus* after 10 days, but cat 1, which was PVL-SA–positive, required a second course of antimicrobial drugs (Figure). Because cat 1 refused oral administration of antimicrobial drugs for the second decolonization, a 14-day course of amoxicillin was administered parenterally. Swab samples from cat 1 taken on days 58 and 79 after the second decolonization yielded negative results (Figure). A fourth attempt to decolonize the entire family was conducted in parallel and was successful, according to samples taken from the family 1 week, 3 months, and 6 months after decolonization.

When recurrent PVL-SA–associated soft tissue infections occur within a family and increased hygiene measures and decolonization attempts are repeatedly unsuccessful, clinicians should consider that

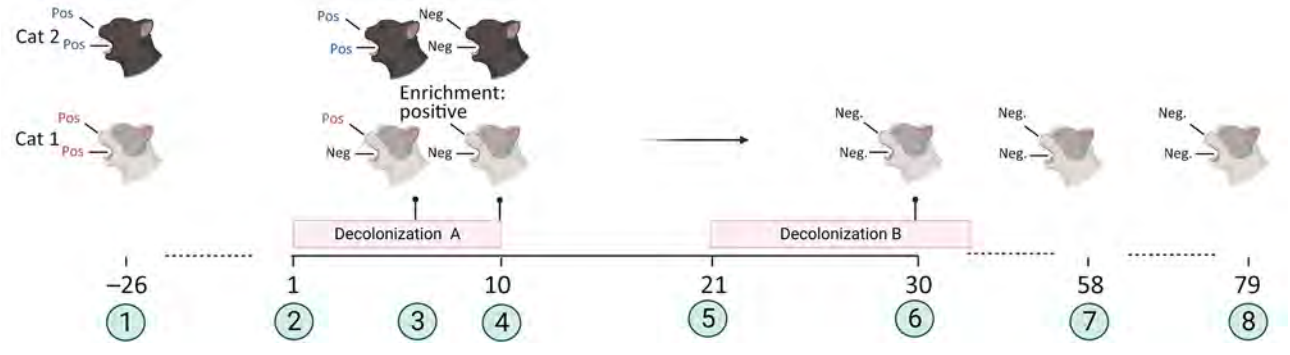

Figure. Timeline and overview of a successful decolonization attempt of 2 household cats colonized with methicillin-susceptible *Staphylococcus aureus*, Germany. The family suffered from repeated soft-tissue infections caused by PVL-SA. Cat 1 was colonized with PVL-SA; cat 2 was colonized with PVL-negative SA. Decolonization period A consisted of oral administration of amoxicillin/clavulanic acid for 10 days. Decolonization period B consisted of parenteral administration of amoxicillin for 14 days. 1, initial screening for SA; 2, start of decolonization period A; 3, screening results at day 7 of decolonization period A; 4, screening results at day 10 of decolonization period A; 5, start of decolonization period B; 6, screening result of cat 1 during decolonization period B; 7, screening results on day 58 from the start of decolonization period A; 8, screening results on day 79 from the start of decolonization period A. Red text indicates positive for PVL-SA; blue text indicates positive for PVL-negative *S. aureus*. Figure created with Biorender (https://www.biorender.com; license BW 27.06.2023). Enrichment: Neg, negative for *S. aureus*; Pos, positive; Positive, positive for PVL-SA after enrichment step in liquid medium; PVL, Panton-Valentine leukocidin; PVL-SA, PVL-positive *S. aureus*.

pets may be involved in the transmission circle. Because the close phylogenetic relationship of the human and feline isolates in this case strongly suggested transmission, our findings highlight the importance of considering colonized or infected pets as a potential source of reinfection for humans during *S. aureus* decolonization attempts, as previously reported (*9*,*10*). In such cases, cat decolonization attempts require antimicrobial drugs that are well tolerated and approved as first-line treatments in veterinary medicine. Feasibility of treatment and animal welfare of the feline outpatients should be taken into consideration.

Access to the genome alignment study set generated can be found at https://www.ncbi.nlm.nih.gov/bioproject/PRJNA859770.

This research was financially supported by the German Federal Ministry of Education and Research for #1Health-PREVENT (grant nos. 01KI2009D and 01KI2009F) within the German Research Network of Zoonotic Diseases.

About the Author

Dr. Bethe is a veterinary microbiologist at the Freie Universität Berlin. Her research interests include clinical microbiology, antimicrobial stewardship, and antimicrobial resistant bacteria.

References

1. Von Dach E, Diene SM, Fankhauser C, Schrenzel J, Harbarth S, François P. Comparative genomics of community-associated methicillin-resistant *Staphylococcus aureus* shows the emergence of clone ST8-USA300 in Geneva, Switzerland. J Infect Dis. 2016;213:1370–9. https://doi.org/10.1093/infdis/jiv489
2. Shallcross LJ, Fragaszy E, Johnson AM, Hayward AC. The role of the Panton-Valentine leucocidin toxin in staphylococcal disease: a systematic review and meta-analysis. Lancet Infect Dis. 2013;13:43–54. https://doi.org/10.1016/S1473-3099(12)70238-4
3. Leistner R, Hanitsch LG, Krüger R, Lindner AK, Stegemann MS, Nurjadi D. Skin infections due to Panton-Valentine leukocidin–producing *S. aureus*. Dtsch Arztebl Int. 2022;119:775–84.
4. Hanselman BA, Kruth SA, Rousseau J, Weese JS. Methicillin-resistant *Staphylococcus aureus* colonization in schoolteachers in Ontario. Can J Infect Dis Med Microbiol. 2008;19:405–8. https://doi.org/10.1155/2008/284239
5. Clinical and Laboratory Standards Institute. Performance standards for antimicrobial disk and dilution susceptibility tests for bacteria isolated from animals. 5th ed. CLSI supplement VET01S. Wayne (PA): The Institute; 2020.
6. Lina G, Piémont Y, Godail-Gamot F, Bes M, Peter MO, Gauduchon V, et al. Involvement of Panton-Valentine leukocidin–producing *Staphylococcus aureus* in primary skin infections and pneumonia. Clin Infect Dis. 1999;29:1128–32. https://doi.org/10.1086/313461
7. Huber C, Stamm I, Ziebuhr W, Marincola G, Bischoff M, Strommenger B, et al. Silence as a way of niche adaptation: *mec*C-MRSA with variations in the accessory gene regulator (*agr*) functionality express kaleidoscopic phenotypes. Sci Rep. 2020;10:14787. https://doi.org/10.1038/s41598-020-71640-4
8. Diep BA, Gill SR, Chang RF, Phan TH, Chen JH, Davidson MG, et al. Complete genome sequence of USA300, an epidemic clone of community-acquired methicillin-resistant *Staphylococcus aureus*. Lancet. 2006;367:731–9. https://doi.org/10.1016/S0140-6736(06)68231-7
9. Vincze S, Brandenburg AG, Espelage W, Stamm I, Wieler LH, Kopp PA, et al. Risk factors for MRSA infection in companion animals: results from a case–control study within Germany. Int J Med Microbiol. 2014;304:787–93. https://doi.org/10.1016/j.ijmm.2014.07.007
10. Sing A, Tuschak C, Hörmansdorfer S. Methicillin-resistant *Staphylococcus aureus* in a family and its pet cat. N Engl J Med. 2008;358:1200–1. https://doi.org/10.1056/NEJMc0706805

Address for correspondence: Antina Lübke-Becker, Freie Universität Berlin, Robert-von-Ostertag-Str. 7, 14163, Berlin, Germany; email: antina.luebke-becker@fu-berlin.de

Rare Case of *Echinostoma cinetorchis* Infection, South Korea

Sooji Hong, Hyejoo Shin, Yoon-Hee Lee, Sung-Jong Hong, So-Ri Kim, Youn-Kyoung Kim, Young-Jin Son, Jeong-Gil Song, Jong-Yil Chai, Bong-Kwang Jung

Author affiliations: MediCheck Research Institute, Korea Association of Health Promotion, Seoul, South Korea (S. Hong, H. Shin, Y.-H. Lee, J.-Y. Chai, B.-K. Jung); Convergence Research Center for Insect Vectors, Incheon National University, Incheon, South Korea (S.-J. Hong); Dr. Song Jeong-Gil's Internal Medical Clinic, Pyeongtaek, South Korea (S.-R. Kim, Y.-K. Kim, Y.-J. Son, J.-G. Song); Seoul National University College of Medicine, Seoul (J.-Y. Chai)

DOI: http://doi.org/10.3201/eid3008.240289

A woman in South Korea who underwent a colonoscopy for occasional gastrointestinal discomfort had 4 adult flukes of *Echinostoma cinetorchis* showing 37 collar spines around the oral sucker recovered from the terminal ileum through the ascending colon. Partial gene sequencing showed high identity with *E. cinetorchis*.

Echinostomes are zoonotic intestinal flukes infecting birds and mammals worldwide (*1*,*2*). Adult echinostomes generally inhabit the small intestines of the definitive host and attach to the mucosal surface, causing pathological changes that include inflammation of the mucosa, bleeding, and ulceration (*1*). *Echinostoma cinetorchis* infects humans, dogs, cats, rodents, chickens, and ducks in South Korea, Japan, China, Taiwan, and Vietnam (*1*,*2*). The second intermediate hosts—that is, the source of infection for definitive hosts—include freshwater snails, fish, and amphibians (*1*). Human *E. cinetorchis* infection has been relatively rare and reported in only a few patients who had abdominal pain, diarrhea, weakness, and weight loss (*1*,*3*). We report the case of a woman in South Korea infected with *E. cinetorchis* whereby adult flukes were recovered through colonoscopy and identified by morphologic and molecular analyses.

A 69-year-old woman with occasional gastrointestinal discomfort, indigestion, constipation, and diarrhea visited Dr. Song Jeong-Gil's Internal Medicine Clinic, Pyeongtaek, Gyeonggi, South Korea, in October 2023. Laboratory examinations revealed overall blood counts, liver function markers, renal function indicators, and lipid profiles were within reference ranges. Feces examination revealed negative results for protozoa and helminths.

Colonoscopy showed 4 actively motile adult trematodes in the mucosa of the ileum, cecum, and ascending colon (Figure 1, panel A). A physician removed the worms with grasping forceps and transferred them to the MediCheck Research Institute, Korea Association of Health Promotion (Seoul, South Korea), for morphologic and molecular identification. Two of the 4 worms were intact, and the remaining 2 were broken during the clipping of the worms. Researchers observed the intact worms by using a light microscope after fixation with 10% formalin under coverslip pressure and stained with acetocarmine (Figure 1, panels B, C).

The worms were elongated and spindle-shaped, measuring ≈6.75 mm in length and 2.25 mm in width (both average measurements at the ovarian level. The worms had 37 collar spines (Figure 1, panel B), of which 24 were arranged in a single row, consisting of 6 corners and 6 laterals on each side, and the additional

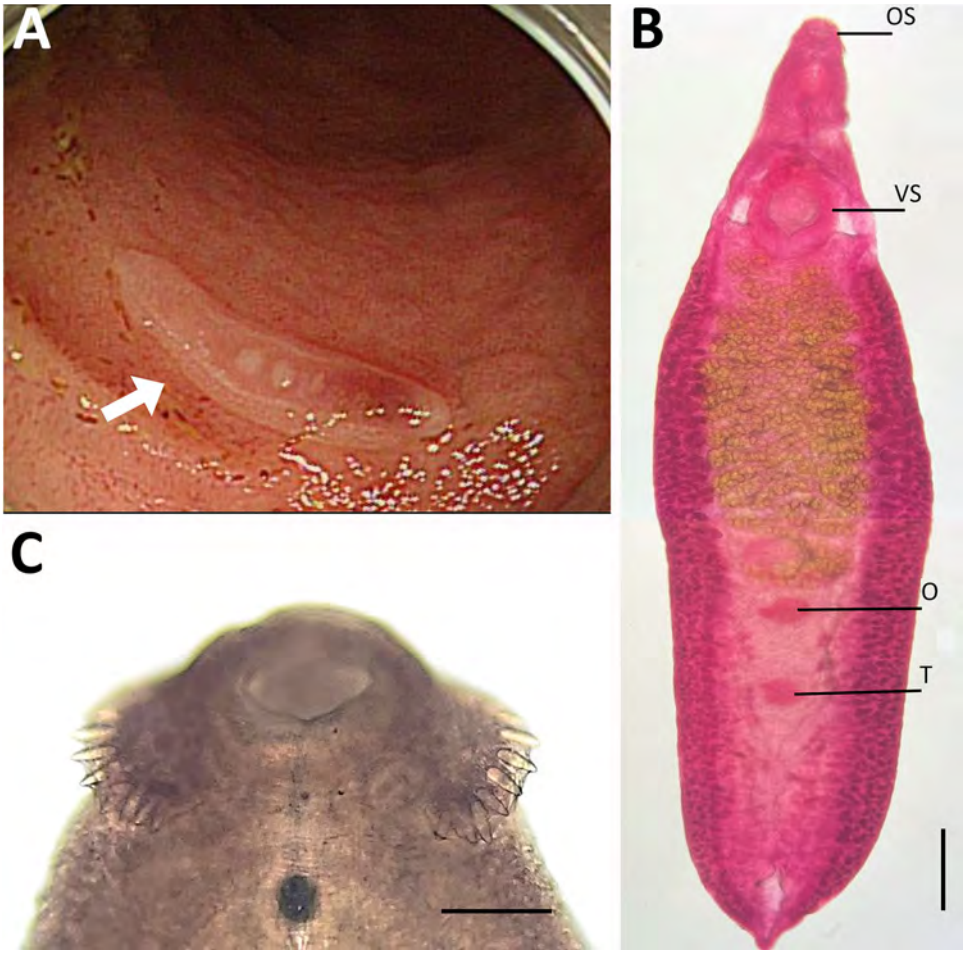

Figure 1. Analysis of a worm identified as *Echinostoma cinetorchis* removed during colonoscopy from a 69-year-old woman in South Korea. A) Colonoscopy image showing a moving trematode in the mucosa of the descending colon. B) Whole body of the worm. Scale bar = 0.6 mm. C) Head part of the worm showing collar spines (37 in total number) on the head collar around the oral sucker, by which it could be morphologically identified as a 37-collar-spined echinostome. Scale bar = 0.1 mm). O, ovary; OS, oral sucker; T, testis; VS, ventral sucker.

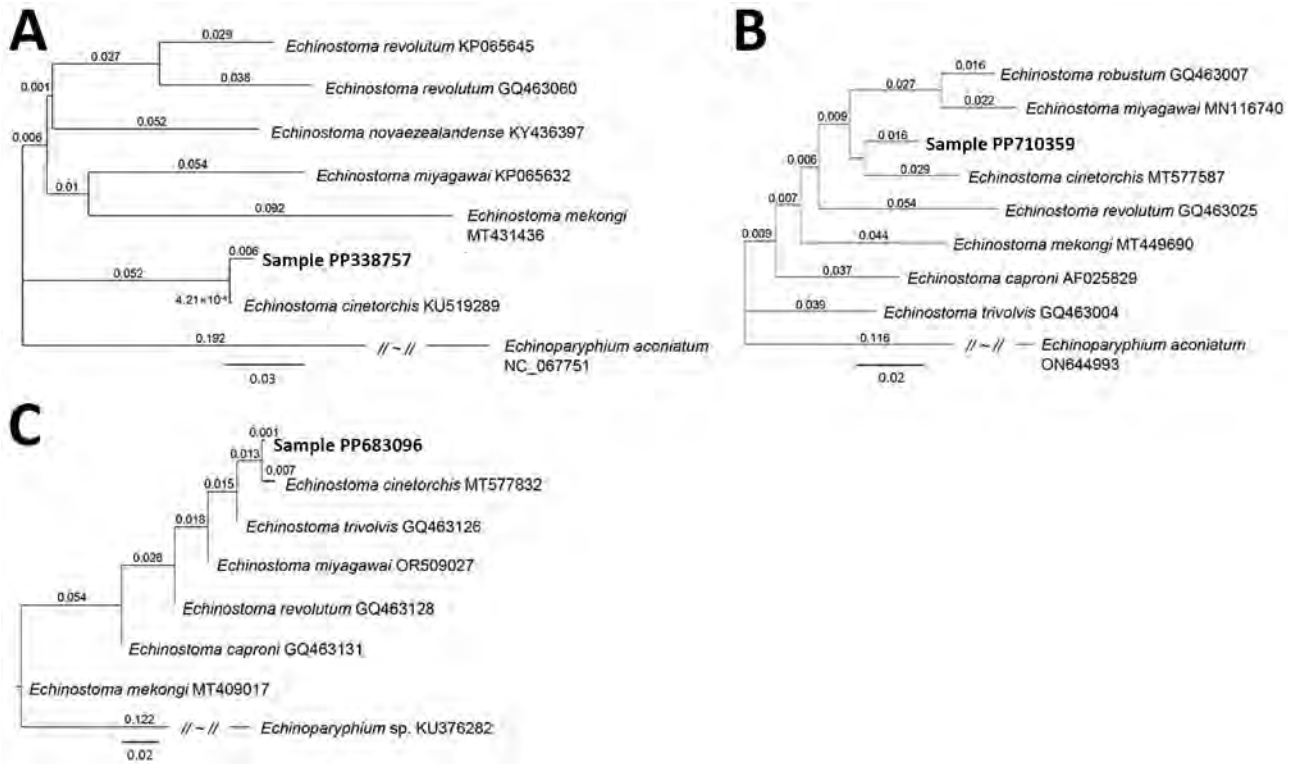

Figure 2. Phylogenetic trees of a worm identified as *Echinostoma cinetorchis* removed during colonoscopy from a 69-year-old woman in South Korea (bold text). Trees were based on nucleotide sequences of the NADH dehydrogenase 1 gene (A), cytochrome c oxidase subunit 1 mitochondrial gene (B), and internal transcribed spacer region (C) of the worm in comparison with various echinostome species deposited in GenBank (accession numbers shown), inferred by the neighbor-joining method (1,000 bootstrap replications) using the Geneious Prime Program 2023.1.2. (Geneious, https://www.geneious.com). *Echinoparyphium aconiatum* (NADH dehydrogenase 1 and cytochrome c oxidase subunit 1 mitochondrial genes) and *Echinoparyphium* sp. (internal transcribed spacer) were used as the outgroups. Scale bars indicate evolutionary distance.

13 dorsal spines were arranged in 2 alternating rows. The vitellaria were follicular and distributed mainly in lateral fields from the posterior margin of the ventral sucker to the posterior end of the body. One or both testes were absent in 3 of the 4 specimens (1 specimen had 2 testes), unlike other echinostome species, which usually have 2 testes. Intrauterine eggs (n = 10) were yellowish and operculated, measuring an average of 110 μm in length and 63 μm in width. The patient was prescribed a single dose of praziquantel (10 mg/kg).

We preserved the 2 broken worms in 70% ethanol for molecular studies. We isolated genomic DNA from the worm segments by using the DNeasy Blood and Tissue kit (QIAGEN, https://www.qiagen.com). We partially amplified (398 bp) the NADH dehydrogenase 1 (*ND*1) regions by using the standard PCR protocol with GenomicsOne 5X PCR Premix (GenomicsOne, https://www.donginbio.com) and 10 pmol of forward and reverse primers to detect *Echinostoma* spp. (*4*). We directly sequenced the PCR product at Macrogen Inc. (Seoul, Korea). Sequencing revealed 99.7% identity of our specimens (GenBank accession no. PP338757) with the sequences of *E. cinetorchis* deposited in GenBank (accession no. KU519289) (Figure 2, panel A). We obtained phylogenetic trees based on sequences of partial cytochrome c oxidase subunit 1 mitochondrial gene (*CO*1) (185 bp) and internal transcribed spacer (ITS) region (ITS1–5.8S-ITS2) (657 bp). Our sample for *CO*1 (accession no. PP710359) was 95.7% identical to *E. cinetorchis* (accession no. MT577587) (Figure 2, panel B), and our sample for the ITS region (accession no. PP683096) was 98.3% identical to *E. cinetorchis* (accession no. MT577832) (Figure 2, panel C).

In South Korea, few human infection cases with *E. cinetorchis* have been identified through adult worm recovery by purging with magnesium sulfate or through gastrointestinal endoscopy (*1*,*3*). Our diagnosis of *E. cinetorchis* infection was determined by adult worm recovery through colonoscopy, followed by morphologic and molecular analyses. Most adult echinostomes, such as *Isthmiophora hortensis*, reside in the upper portion of the small intestine or occasionally in the pyloric area of the stomach (*5*–*10*). In comparison, 2 endoscopy cases of *E. cinetorchis* infection

(*3*), including our case, have identified the presence of worms in the colon. This unique location of echinostome flukes in humans might be a distinguishing feature for *E. cinetorchis* infection.

Freshwater snails are first as well as second intermediate hosts for *E. cinetorchis* (*1*). Large-sized snail species in particular (e.g., *Cipangopaludina*) and freshwater fish are potential sources of human infections. Our patient reported that she had sold snails and freshwater fish on the street and often consumed them raw or undercooked. Thus, the infection source for our patient might have been 1 or both kinds of intermediate hosts.

In countries where human echinostome infections are found, physicians should include echinostomiasis among the differential diagnoses of diseases causing nonspecific gastrointestinal problems. Public education regarding the hazards associated with consuming raw or undercooked snails or fish in these regions also would be useful in reducing *E. cinetorchis* infections.

Acknowledgments

We appreciate the staff at Dr. Song Jeong-Gil's Internal Medicine Clinic, Pyeongtaek, Korea, who helped with the management of this patient.

About the Author

Ms. Sooji Hong is a clinical pathologist and researcher at MediCheck Research Institute, Korea Association of Health Promotion, Seoul, Korea. Her primary research interest is parasite fauna study based on molecular methods, and she recently performed studies on the intestinal microbiome fauna of cats and dogs infected with parasites.

References

1. Chai JY. Human intestinal flukes: from discovery to treatment and control. Dordrecht (the Netherlands): Springer Nature; 2019. p. 1–549.
2. Chai JY, Jung BK. General overview of the current status of human foodborne trematodiasis. Parasitology. 2022; 149:1262–85. https://doi.org/10.1017/S0031182022000725
3. Jung WT, Lee KJ, Kim HJ, Kim TH, Na BK, Sohn WM. A case of *Echinostoma cinetorchis* (Trematoda: Echinostomatidae) infection diagnosed by colonoscopy. Korean J Parasitol. 2014;52:287–90. https://doi.org/10.3347/kjp.2014.52.3.287
4. Morgan JAT, Blair D. Mitochondrial ND1 gene sequences used to identify echinostome isolates from Australia and New Zealand. Int J Parasitol. 1998;28:493–502. https://doi.org/10.1016/S0020-7519(97)00204-X
5. Chai JY, Hong ST, Lee SH, Lee GC, Min YI. A case of echinostomiasis with ulcerative lesions in the duodenum. Korean J Parasitol. 1994;32:201–4. https://doi.org/10.3347/kjp.1994.32.3.201
6. Hamamoto T, Kawasaki H, Maejima J, Hirai K. A case of *Echinostoma hortense* infection diagnosed by the upper gastrointestinal endoscopy [in Japanese]. Nihon Shokakibyo Gakkai Zasshi. 1997;94:487–91.
7. Lee OJ, Hong SJ. Gastric echinostomiasis diagnosed by endoscopy. Gastrointest Endosc. 2002;55:440–2. https://doi.org/10.1067/mge.2002.121193
8. Cho CM, Tak WY, Kweon YO, Kim SK, Choi YH, Kong HH, et al. A human case of *Echinostoma hortense* (Trematoda: Echinostomatidae) infection diagnosed by gastroduodenal endoscopy in Korea. Korean J Parasitol. 2003;41:117–20. https://doi.org/10.3347/kjp.2003.41.2.117
9. Chang YD, Sohn WM, Ryu JH, Kang SY, Hong SJ. A human infection of *Echinostoma hortense* in duodenal bulb diagnosed by endoscopy. Korean J Parasitol. 2005;43:57–60. https://doi.org/10.3347/kjp.2005.43.2.57
10. Sah R, Khadka S, Hamal R, Poudyal S. Human echinostomiasis: a case report. BMC Res Notes. 2018;11:17. https://doi.org/10.1186/s13104-018-3133-z

Address for correspondence: Bong-Kwang Jung, MediCheck Research Institute, Korea Association of Health Promotion, Seoul 07572, South Korea; email: mulddang@snu.ac.kr

Vibrio mimicus Lineage Carrying Cholera Toxin and *Vibrio* Pathogenicity Island, United States and China

Sergio Mascarenhas Morgado, Fernanda dos Santos Freitas, Erica Lourenço da Fonseca, Ana Carolina Paulo Vicente

Author affiliation: Instituto Oswaldo Cruz, Rio de Janeiro, Brazil

DOI: https://doi.org/10.3201/eid3008.240252

Vibrio mimicus bacteria have caused sporadic cases and outbreaks of cholera-like diarrhea throughout the world, but the association of lineages with such events is unexplored. Genomic analyses revealed *V. mimicus* lineages carrying the virulence factors cholera toxin and toxin coregulated pilus, one of which has persisted for decades in China and the United States.

Vibrio mimicus bacteria are native to aquatic environments but have the potential to cause diseases in animals and humans, such as gastroenteritis

and cholera-like diarrhea (*1*). In *Vibrio cholera* bacteria, the main toxigenic factor is cholera toxin (CTX), which is encoded by *ctx*A and *ctx*B genes and is part of the bacteriophage CTXΦ. The acquisition of CTXΦ phage by *V. cholerae* bacteria was associated with the toxin coregulated pilus (TCP), which is involved in intestinal colonization and aggregation. This virulence factor is encoded in an operon in the *Vibrio* pathogenicity island 1 (VPI-1), and *tcp*A is the main structural subunit of that pilus. In addition to TCP, VPI-1 also harbors the *acf*A-D operon, which also plays a role in colonization (*2*).

In 2004, the largest documented foodborne outbreak of *V. mimicus* occurred in Thailand, in which 306 persons experienced symptoms including diarrhea, abdominal pain, and vomiting (*3*), but the virulome associated with these strains was not verified. In 2010, in the United States, a cluster of severe diarrheal diseases was caused by *V. mimicus* strains carrying CTX (*4*). In 2019, *V. mimicus* bacteria caused a seafood-associated outbreak in Florida (USA), in which the patients experienced severe diarrhea, although the strains were CTX-negative (*5*). However, the virulome of most genomes analyzed (n = 33) was not explored, leaving a gap regarding the association of the strains or lineages with virulence factors. To fill this gap, we analyzed 44 *V. mimicus* genomes, 35 from GenBank and 9 environmental genomes from Brazil and Japan that we sequenced by using an Illumina Hiseq 2500, assembled by using SPAdes 3.15.2 (https://github.com/ablab/spades), and then analyzed by using Abricate (http://github.com/tseemann/abricate) and the Comprehensive Antibiotic Resistance Database (https://card.mcmaster.ca) and the

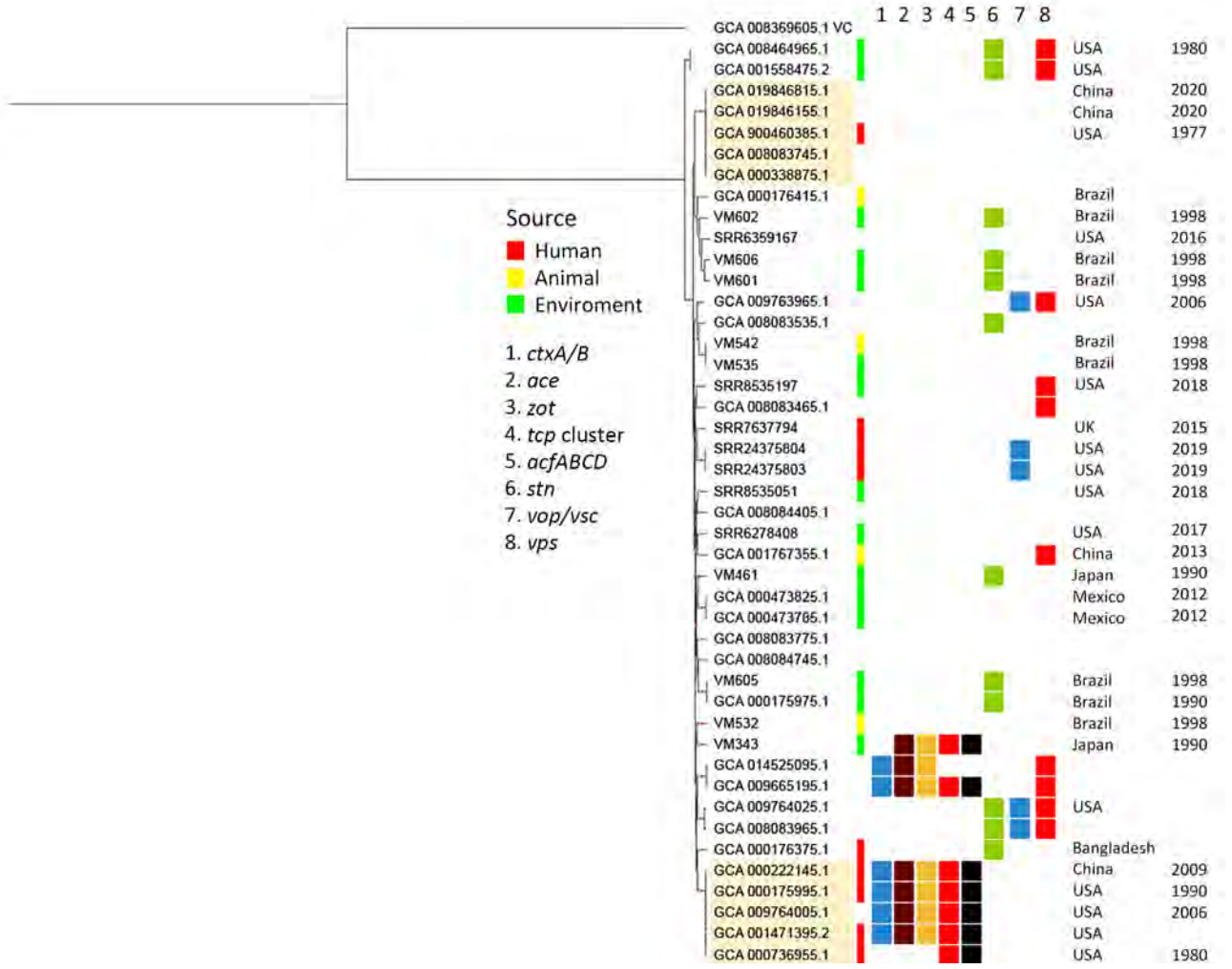

Figure. Maximum-likelihood phylogenetic tree of 44 *Vibrio mimicus* bacteria genomes from the United States and China. The best evolutionary model (general time reversible plus base frequencies plus ascertainment bias correction plus FreeRate model with 8 categories) was selected on the basis of the Bayesian information criterion. The beige highlighted clusters represent the main ones sharing genomes from China and the United States. Red circles on branches represent >70% bootstrap.

Virulence Factor Database (http://www.mgc.ac.cn/VFs/main.htm).

The phylogenetic analysis based on the core genome revealed clusters; the 2 main clusters had genomes that had been circulating in China and the United States for decades (Figure). These 2 clusters are characterized by distinct virulomes; 1 co-harbored *ctx*A, *ctx*B, *ace*, *zot*, TCP, and *acf*A-D (mainly clinical genomes), whereas the other did not have any of those genes. The lineage carrying those virulence genes has persisted for ≥3 decades (1980–2009), infecting persons in China and the United States. The other lineage, which lacks these virulence factors, also was identified in China (2020) and the United States (1977 [human source]). Another interesting cluster of genomes is the one that covers Brazil (1998 [animal source]) and the United States (2016 [environmental source]).

Our analysis indicates that *V. mimicus* lineages are disseminated and persist in distinct sources in space and time. In addition, another set of 3 related genomes (VM343, GCA_014525095.1, and GCA_009665195.1) also possessed CTX, TCP, or both, which suggests loss or partial acquisition of the pathogenicity islands of these elements. Of note, other genomes belonging to the same lineage (Figure) appear to have acquired the *ctx*A or *ctx*B genes from different sources; GCA_000175995.1, GCA_001471395.2, and GCA_009764005.1 (United States) possessed the *ctx*B2 genotype (El Tor [Australia]), whereas GCA_000222145.1 (China) had the *ctx*B1 genotype (classical [strain 569B]). Regarding the TCP cluster, analyses in blastn (https://blast.ncbi.nlm.nih.gov) revealed that all *tcp*A sequences, except for VM343, were identical and differed from the classical and El Tor genotypes. The *tcp*A allele carried by most genomes has also been characterized in nonpandemic clinical *V. cholerae* strains from the United States (*6*), whereas the *tcp*A allele of VM343 (Japan [environmental source]) is unique.

We identified several other virulence genes in the genomes (Appendix, https://wwwnc.cdc.gov/EID/article/30/8/24-0252-App1.pdf). We highlight the presence of the heat-stable enterotoxin gene (NAG-ST), identified throughout the phylogeny, and gene clusters related to exopolysaccharide production (*vps*) and the type III secretion system (T3SS) (*vop*, *vsc*, and *vcr*). We identified T3SS only in genomes that did not carry CTX, TCP, or both, including those from the 2019 outbreak in Florida (*5*), but 2 closely related genomes (1 of which was identified in the United States) co-carried the T3SS and NAG-ST genes. Because T3SS is a syringe-like protein secretion apparatus, the co-occurrence of this system with a diarrhea-associated toxin could increase the pathogenicity of these strains.

Our findings show that *V. mimicus* strains are spread throughout the world and that some of them carry a virulome comparable to that of *V. cholerae* bacteria. The virulome of environmental and clinical strains is apparently not heterogeneous (*5*), even with the analysis of the new environmental genomes. However, those findings may represent just the tip of the iceberg, given the bias regarding the locality of available genomes. Therefore, more genomic data must be generated to determine whether specialized clinical strains of *V. mimicus* exist, as they do for *V. cholerae* bacteria. Furthermore, the environmental and clinical genomes possessed a set of common virulence genes, suggesting that environmental strains have the potential to cause disease in humans. Because *V. mimicus* already possesses an intrinsic virulome, with the potential to cause disease, the acquisition of virulence determinants such as CTX, TCP, or both could specialize certain lineages, as revealed in our analysis by the clinical lineages that carry these determinants.

This study was financed by Fundação Carlos Chagas Filho de Amparo à Pesquisa do Estado do Rio de Janeiro (grant no. SEI-260003/019688/2022).

The *Vibrio mimicus* whole-genome sequences from this study were deposited in GenBank under the accession nos. JAZHPO000000000 (VM343), JAZHPP000000000 (VM461), JAZHPQ000000000 (VM532), JBAKBZ000000000 (VM535), JAZHPR000000000 (VM542), JBAKBY000000000 (VM601), JBAKBX000000000 (VM602), JBAKBW000000000 (VM605), and JAZHPS000000000 (VM606).

Author contributions: Conceptualization, methodology, writing (original draft), writing (review and editing), and funding acquisition, A.C.V.; methodology, formal analysis, writing (original draft), writing (review and editing), S.M.; writing (review and editing), É.F.; investigation, F.F. All authors have read and approved the manuscript.

About the Author

Dr. Sergio is a postdoctoral fellow in bioinformatics at the Oswaldo Cruz Institute in Rio de Janeiro, Brazil. His primary research interests include genomic surveillance of environmental and clinical bacteria and the exploration of their resistomes, virulomes, and mobilomes.

References

1. Yu Z, Wang E, Geng Y, Wang K, Chen D, Huang X, et al. Complete genome analysis of *Vibrio mimicus* strain SCCF01, a highly virulent isolate from the freshwater catfish. Virulence. 2020;11:23–31. https://doi.org/10.1080/21505594.2019.1702797

2. Kumar A, Das B, Kumar N. *Vibrio* pathogenicity island-1: the master determinant of cholera pathogenesis. Front Cell Infect Microbiol. 2020;10:561296. https://doi.org/10.3389/fcimb.2020.561296
3. Chitov T, Kirikaew P, Yungyune P, Ruengprapan N, Sontikun K. An incidence of large foodborne outbreak associated with *Vibrio mimicus*. Eur J Clin Microbiol Infect Dis. 2009;28:421–4. https://doi.org/10.1007/s10096-008-0639-7
4. Kay MK, Cartwright EJ, Maceachern D, McCullough J, Barzilay E, Mintz E, et al. *Vibrio mimicus* infection associated with crayfish consumption, Spokane, Washington, 2010. J Food Prot. 2012;75:762–4. https://doi.org/10.4315/0362-028X.JFP-11-410
5. Alam MT, Stern SR, Frison D, Taylor K, Tagliamonte MS, Nazmus SS, et al. Seafood-associated outbreak of *ctx*-negative *Vibrio mimicus* causing cholera-like illness, Florida, USA. Emerg Infect Dis. 2023;29:2141–4. https://doi.org/10.3201/eid2910.230486
6. Tay CY, Reeves PR, Lan R. Importation of the major pilin *tcp*A gene and frequent recombination drive the divergence of the *Vibrio pathogenicity* island in *Vibrio cholerae*. FEMS Microbiol Lett. 2008;289:210–8. https://doi.org/10.1111/j.1574-6968.2008.01385.x

Address for correspondence: Sergio Morgado, Instituto Oswaldo Cruz, Rio de Janeiro, Av Brasil 4365, Rio de Janeiro 21040-360, Brazil; email: sergio.morgado@ioc.fiocruz.br

Fecal Microbiota Transplantation for Severe Infant Botulism, China

Chaonan Fan,[1] Rubo Li,[1] Lijuan Wang, Kechun Li, Xinlei Jia, Hengmiao Gao, Bike Zhang, Xuefang Xu, Suyun Qian

Author affiliations: Beijing Children's Hospital, Capital Medical University, National Center for Children's Health, Beijing, China (C. Fan, R. Li, L. Wang, K. Li, X. Jia, H. Gao, S. Qian); National Key Laboratory of Intelligent Tracking and Forecasting for Infectious Diseases, National Institute for Communicable Diseases Control and Prevention, Center for Disease Control and Prevention, Infectious Disease Prevention and Control Institute, Beijing (B. Zhang, X. Xu)

DOI: https://doi.org/10.3201/eid3008.231702

[1]These authors contributed equally to this article.

Infant botulism in a 4-month-old boy in China who continued to excrete toxins for over a month despite antitoxin therapy was further treated with fecal microbiota transplantation. After treatment, we noted increased gut microbial diversity and altered fecal metabolites, which may help reduce intestinal pH and enhance anti-inflammatory capabilities.

Infant botulism is caused by ingesting *Clostridium botulinum* spores and characterized by symmetric descending paralysis, which can progress to respiratory failure in severe cases (*1*). Specific therapies include intravenous administration of botulism immune globulin (BIG-IV or BabyBIG, https://infantbotulism.org/general/babybig.php) or botulinum antitoxin. However, BIG-IV and BabyBIG are unavailable in some countries, including China (*2*). Even after clinical signs have been alleviated through antitoxin therapy, some children may continue to excrete *C. botulinum* and its neurotoxin (BoNT) in their feces over a prolonged period, heightening the potential for relapse and transmission to others (although relatively rare) (*3*,*4*). Hence, effective treatments that promote clearance of intestinal *C. botulinum* spores are needed. During March–May 2021, we treated severe infant botulism in a 4-month-old boy in China who had continued excreting toxins for >1 month after clinical signs disappeared after antitoxin therapy. The study was approved by the Ethics Committee of Beijing Children's Hospital (2023-E-149-R).

Five days before admission to Beijing Children's Hospital (Beijing, China), the previously healthy infant exhibited intermittent fever, lethargy, poor appetite, and constipation, followed by respiratory distress. After intubation and mechanical ventilation in the emergency department, the patient was admitted to the pediatric intensive care unit. During examination, his pupils were dilated (≈4 mm) and had sluggish light reflexes but no signs of meningeal irritation. In addition, his muscle strength and tone were low. A series of tests excluded central nervous system infections, metabolic disorders, and other potential causes. By day 3 of hospitalization, the diagnosis of infant botulism was confirmed by detection of BoNT nucleic acid (serotype B) in fecal samples. Subsequently, we were able to obtain botulism antitoxin (monovalent type B) and administer it by intravenous injection of 2 mL (5,000 IU) 2×/day. Substantial improvement in clinical signs was observed by day 7 of hospitalization, and complete resolution was achieved by day 15.

Nevertheless, through day 33, multiple fecal samples tested for botulinum nucleic acid by real-time

Table. Analysis of *Clostridium botulinum* and botulinum neurotoxin in 4-month-old boy with infant botulism, Beijing, China*

Fecal sample no.	Days after admission	Sample classification	Real-time PCR result	Isolated strain	Mouse bioassay result
A1	3	Before FMT	BoNTB	B	BoNTB
A2	23	Before FMT	BoNTB	B	BoNTB
A3	27	Before FMT	BoNTB	B	BoNTB
A4	32	Before FMT	BoNTB	B	BoNTB
A5	33	Before FMT	BoNTB	B	BoNTB
A6	34	FMT1	Negative	B	Negative
A7	36	FMT3	Negative	Negative	Negative
A8	37	FMT4	Negative	Negative	Negative
A9	38	After FMT	Negative	Negative	Negative
A10	39	After FMT	Negative	Negative	Negative
A11	182	Follow-up	Negative	Negative	Negative

*BoNTB, *Clostridium botulinum* neurotoxin B; FMT, fecal microbiota transplantation.

PCR and for BoNT by mouse bioassays (*5*) remained positive (Table). Consequently, during days 34–37 of hospitalization, the infant received a fecal microbiota transplantation (FMT; donor identification D024) at a dose of 20 mL via rectal enema daily for 4 consecutive days. During that time, he experienced low-grade fever and mild coughing, but his body temperature returned to reference range after FMT. After the third FMT (on day 36 after admission), test results for BoNT nucleic acid and mouse bioassays in feces were all negative (Table).

We conducted epidemiologic investigations for the exclusively breastfed patient and isolated *C. botulinum* from his home environment; serologic and genetic types matched those in his feces. After discharge, he was followed up for 6 months and exhibited good growth and development without any relapse.

We analyzed gut microbiota composition and fecal metabolomics of 10 fecal samples (5 time points before and after FMT) (Figure; Appendix Figure 1, https://wwwnc.cdc.gov/EID/article/30/8/23-1702-App1.pdf). Use of 16S rRNA sequencing revealed increased α diversity of the gut microbiota after FMT, indicated by the Abundance-based Coverage Estimator and Shannon indices (*6*). At the genus level, relative abundance of *Enterococcus* and *Lactobacillus* was decreased and that of *Collinsella* and *Holdemanella* was increased. Although 16S rRNA sequencing cannot directly detect *C. botulinum*, the taxonomic group to which *C. botulinum* belongs (*Clostridium_sensus_stricto_18*) was also reduced. Ultra-high performance liquid chromatography–tandem mass spectrometry further revealed statistically significant alterations in 53 fecal metabolites after FMT; primarily implicated metabolic pathways were α-linolenic acid and linoleic acid metabolism, bile acid biosynthesis, bile acid metabolism, branched-chain amino acid metabolism, and butyrate metabolism. Correlation analyses indicated that changes in those metabolites were closely associated with alterations in the gut microbiota (Appendix Figure 2).

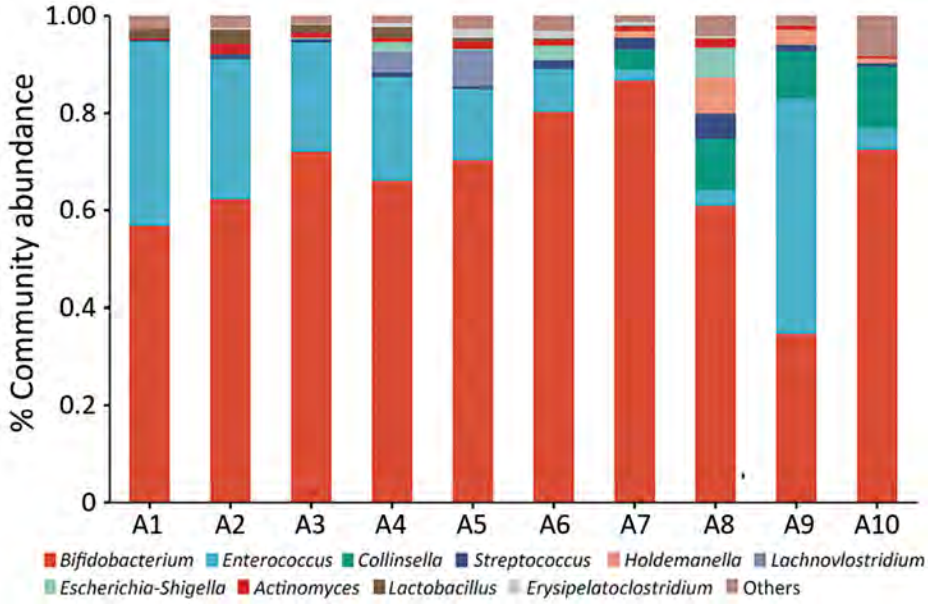

Figure. Relative gut microbiota abundance at the genus level before and after fecal microbiota transplantation (FMT) in 4-month-old boy with infant botulism, Beijing, China. The collected fecal samples (A1–A10) included 5 samples before FMT (A1–A5), 3 samples during FMT (A6–A8), and 2 samples after FMT (A9–A10), as shown in the Table.

Infants with infant botulism may continue to excrete *C. botulinum* and BoNT for weeks or even months (*7*). The simpler gut microbiota with fewer taxa and the deficiency of bile acids in infants might contribute to the overgrowth of *C. botulinum* spores and their persistent excretion in the intestine (*8*). Our study illustrated increased gut microbiota diversity after FMT, concurrently accompanied by increased bile acid, potentially shifting the function of the microbiota–bile acid axis (*9*). Moreover, the increased production of metabolites, such as organic acids and docosapentaenoic acid, may help reduce intestinal pH and enhance anti-inflammatory capabilities (*10*). However, whether the restoration of gut microbiota diversity and changes in fecal metabolites are directly associated with the disappearance of *C. botulinum* spores is not clear. Because our study lacked a control group and solely represents an observational phenomenon, we cannot provide causal evidence for the effectiveness of FMT in treating infant botulism. Interventions such as fecal transplantation are recommended for children with infant botulism who continue to produce toxins for a long time.

Acknowledgment

We thank all nurses and doctors in the Beijing Children's Hospital pediatric intensive care unit.

The study was funded by the National Key Research and Development Program of China (2021YFC2600501), Beijing Research Ward Project (BCRW202101), and Beijing Municipal Natural Science Foundation (7222057).

About the Author

Dr. Fan is currently an associate researcher at the Children's Hospital Affiliated with Capital Medical University, specializing in critical illness and infections in children.

References

1. Goldberg B, Danino D, Levinsky Y, Levy I, Straussberg R, Dabaja-Younis H, et al. Infant botulism, Israel, 2007–2021. Emerg Infect Dis. 2023;29:235–41. https://doi.org/10.3201/eid2902.220991
2. O'Horo JC, Harper EP, El Rafei A, Ali R, DeSimone DC, Sakusic A, et al. Efficacy of antitoxin therapy in treating patients with foodborne botulism: a systematic review and meta-analysis of cases, 1923-2016. Clin Infect Dis. 2017;66(suppl_1):S43–56. https://doi.org/10.1093/cid/cix815
3. Glauser TA, Maguire HC, Sladky JT. Relapse of infant botulism. Ann Neurol. 1990;28:187–9. https://doi.org/10.1002/ana.410280214
4. Aminian KSG, Gulati P. Recurrent infant botulism complicated by necrotizing enterocolitis. Pediatr Neurol. 2023;143:77–8. https://doi.org/10.1016/j.pediatrneurol.2023.03.006
5. Pellett S, Tepp WH, Johnson EA. Critical analysis of neuronal cell and the mouse bioassay for detection of botulinum neurotoxins. Toxins (Basel). 2019;11:713. https://doi.org/10.3390/toxins11120713
6. Wan Y, Yuan J, Li J, Li H, Yin K, Wang F, et al. Overweight and underweight status are linked to specific gut microbiota and intestinal tricarboxylic acid cycle intermediates. Clin Nutr. 2020;39:3189–98. https://doi.org/10.1016/j.clnu.2020.02.014
7. Yu PA, Lin NH, Mahon BE, Sobel J, Yu Y, Mody RK, et al. Safety and improved clinical outcomes in patients treated with new equine-derived heptavalent botulinum antitoxin. Clin Infect Dis. 2017;66(suppl_1):S57–64. https://doi.org/10.1093/cid/cix816
8. Huhtanen CM. Bile acid inhibition of *Clostridium botulinum*. Appl Environ Microbiol. 1979;38:216–8. https://doi.org/10.1128/aem.38.2.216-218.1979
9. Wahlström A, Sayin SI, Marschall HU, Bäckhed F. Intestinal crosstalk between bile acids and microbiota and its impact on host metabolism. Cell Metab. 2016;24:41–50. https://doi.org/10.1016/j.cmet.2016.05.005
10. Liu Y, Wu H, Wang T, Shi X, He H, Huang H, et al. Paeonol reduces microbial metabolite α-hydroxyisobutyric acid to alleviate the ROS/TXNIP/NLRP3 pathway-mediated endothelial inflammation in atherosclerosis mice. Chin J Nat Med. 2023;21:759–74. https://doi.org/10.1016/S1875-5364(23)60506-0

Address for correspondence: Xuefang Xu, National Key Laboratory of Intelligent Tracking and Forecasting for Infectious Diseases, National Institute for Communicable Diseases Control and Prevention, Chinese Center for Disease Control and Prevention, Changping, Beijing 102206, China; email: xuxuefang@icdc.cn; Suyun Qian, Pediatric Intensive Care Unit, Beijing Children's Hospital, Capital Medical University, National Center for Children's Health, No. 56 Nan-Li-Shi Road, Beijing 100045, China; email: syqian2020@163.com

Infective SARS-CoV-2 in Skull Sawdust at Autopsy, Finland

Jonas N. Kantonen, Suvi Kuivanen,[1] Teemu Smura, Henri Puttonen, Eliisa Kekäläinen, Antti Sajantila, Liisa Myllykangas, Anu Kantele, Olli Vapalahti, Mikko I. Mäyränpää,[2] Olli Carpén[2]

Author affiliations: University of Helsinki, Helsinki, Finland (J.N. Kantonen, S. Kuivanen, T. Smura, H. Puttonen, E. Kekäläinen, A. Sajantila, L. Myllykangas, A. Kantele, O. Vapalahti, M.I. Mäyränpää, O. Carpén); Helsinki University Central Hospital, Helsinki (J.N. Kantonen, H. Puttonen, E. Kekäläinen, L. Myllykangas, A. Kantele, O. Vapalahti, M.I. Mäyränpää, O. Carpén); Finnish Institute for Health and Welfare, Helsinki (A. Sajantila)

DOI: https://doi.org/10.3201/eid3008.240145

We assessed the distribution of SARS-CoV-2 at autopsy in 22 deceased persons with confirmed COVID-19. SARS-CoV-2 was found by PCR (2/22, 9.1%) and by culture (1/22, 4.5%) in skull sawdust, suggesting that live virus is present in tissues postmortem, including bone. Occupational exposure risk is low with appropriate personal protective equipment.

Autopsies afford simultaneous access to all tissues and body compartments. The unique opportunity for extensive sampling during autopsy enables several research questions to be addressed. Early in the COVID-19 pandemic, autopsies were rare, mainly because of presumed transmission risk and shortage of personal protective equipment (PPE), and suspicions that autopsies might be of limited value (*1*,*2*).

Autopsies pose an occupational infectious hazard to the personnel involved in a pathogen-dependent manner. For example, *Mycobacterium tuberculosis* deserves particular attention as a major cause of airborne infections in autopsies that puts pathologists at a 100–200-fold risk for infection compared with the general public (*3*). Viable SARS-CoV-2 has been detected in tissues for prolonged periods after death from COVID-19 (*4*). However, to our knowledge, no confirmed occupational cases of COVID-19 transmitted at autopsies have been reported.

Protection against aerosols remains a challenge in autopsy settings. Bone sawing is a major source of aerosols that can carry pathogens. Sawing of the skull is a standard procedure in every routine autopsy to enable access to the brain. SARS-CoV-2 has previously been documented in bone tissues in 2 reported cases, neither of which were in the skull (*5*). Here, we present results of SARS-CoV-2 analyses from 22 deceased persons with PCR-confirmed COVID-19 and detail our experience of managing the occupational hazards associated with COVID-19 autopsies.

Our study belongs to the Clin_COVID-19 master study approved by the Helsinki University Hospital Ethics committee (approval no. HUS/1238/2020). All autopsies were clinical (nonforensic) and conducted in compliance with research laws and regulations in Finland, after consent from the next of kin.

The postmortem examinations were conducted in the pathology department of the HUS Diagnostic Center in Meilahti, Helsinki, Finland. The series comprised 22 PCR-confirmed cases (any positive airway sample from nasopharynx, bronchi, lungs, tonsils, sclera, or airway-associated cervical or parabronchial lymph nodes) of SARS-CoV-2 identified during 2021–2022 that had skull sawdust sampled during autopsy. Testing was carried out in the pathology and virology laboratories by using accredited and previously published methods (*6*) (Appendix, https://wwwnc.cdc.gov/EID/article/30/8/24-0145-App1.pdf). All autopsies encompassed a neuropathological examination and a collection of swabs/fresh tissues from airway, nonairway, and central nervous system (CNS) categories. In addition, swab samples were collected from skull sawdust and the contaminated autopsy table with the organ block. Each tissue was sampled with separate sterile equipment. PCR-positive samples were cultured using VeroE6 cells to assess for infective SARS-CoV-2.

We detected SARS-CoV-2 by reverse transcription PCR in 22/22 (100%) airway, 10/22 (45.5%) nonairway, 0/22 CNS, 2/22 (9.1%) skull sawdust, and 13/22 (59.1%) autopsy table samples (Table). The virus was culturable in 13/22 (59.1%) airway, 2/22 (9.1%) nonairway, 1/22 (4.5%) skull sawdust, and 3/22 (13.6%) autopsy table samples.

Among the personnel present at COVID-19 autopsy procedures, no cases of COVID-19 resulting from occupational exposure were identified. Serologic screening results of all persons involved in COVID-19 autopsies (n = 5) in June 2020 were negative, and none showed PCR positivity when tested during symptoms.

Our findings revealed that SARS-CoV-2 was detectable by PCR in 9.1% and by viral culture in 4.5% of skull sawdust samples, suggesting the presence of live virus and a risk, although low, of infective viruses becoming aerosolized. We could not identify previous

[1]Current affiliation: Charité-Universitätsmedizin Berlin, Berlin, Germany.

[2]These senior authors contributed equally to this article.

Table. SARS-CoV-2 distribution among cohort of 22 autopsied deceased persons with COVID-19 who had skull sawdust sampling, Finland*

	Airway		Nonairway		CNS PCR	Skull sawdust		Autopsy table	
Case no.	PCR	Culture	PCR	Culture	and culture	PCR	Culture	PCR	Culture
1	+	–	–	–	–	–	–	+	–
2	+	–	–	–	–	–	–	–	–
3	+	–	–	–	–	–	–	–	–
4	+	–	–	–	–	–	–	–	–
5	+	–	–	–	–	–	–	–	–
6	+	+	–	–	–	–	–	+	–
7	+	+	+	–	–	–	–	+	–
8	+	+	+	–	–	–	–	–	–
9†	+	+	+	–	–	+	+	+	–
10	+	+	–	–	–	–	–	+	–
11	+	+	+	+	–	–	–	+	–
12	+	+	–	–	–	+	–	–	–
13	+	–	–	–	–	–	–	–	–
14	+	+	+	+	–	–	–	+	–
15	+	+	+	–	–	–	–	+	+
16	+	+	+	–	–	–	–	+	+
17	+	–	–	–	–	–	–	+	–
18	+	+	+	–	–	–	–	+	–
19	+	–	+	–	–	–	–	+	–
20	+	+	+	–	–	–	–	–	–
21	+	–	–	–	–	–	–	–	–
22	+	+	–	–	–	–	–	+	+
Positive samples/total no. samples (%)	22/22 (100)	13/22 (59.1)	10/22 (45.5)	2/22 (9.1)	0/22	2/22 (9.1)	1/22 (4.5)	13/22 (59.1)	3/22 (13.6)

*The pooled sample category per patient was considered positive if a single positive tissue sample of that category was found (copy number cutoff value 10; Appendix, https://wwwnc.cdc.gov/EID/article/30/8/24-0145-App1.pdf). Airway refers to tissues relating to the airway system (i.e., nasopharynx, bronchi, lungs, tonsils, sclera, and airway-associated cervical and parabronchial lymph nodes). Autopsy table refers to the contaminated autopsy table and the outer surfaces of the organ block, representing the main working area and target of showering with water. Only a limited number of cases showed culture positivity (Ct value reduction after culture compared with initial Ct value; Appendix) in general; skull positivity was scarce, whereas the autopsy table was more often positive by both PCR and viral culture.
†Test results showed culture positivity in the cranial sawdust sample and low-level nonairway PCR-positivity limited to skeletal muscle and salivary gland tissues, indicating limited systemic viral involvement (Appendix Table).

work examining cranial sawdust for the presence of pathogens, but our results align with a previous study showing SARS-CoV-2 PCR positivity for 4.5% of goggles and no masks tested after autopsy (*7*).

The sample size for our study was limited but represents a consecutive and nonselected series of cases at a single institution. We did not directly assess aerosols, but given that bone sawing is the only high-energy technique used, and considering the findings from a previous study (*7*), the presence of concomitant other sources of infective aerosols in the autopsy room is unlikely. The personnel present during COVID-19 autopsies were not systematically tested, but symptomatic persons were extensively PCR tested for SARS-CoV-2 during the study period (2020–2022). In addition, skull sawdust samples might not consist solely of bone and could contain adjacent tissues because of anatomy, particularly the frontal sinus, which is lined with respiratory epithelium. Skullcap sawing has the potential to generate infective aerosols, but in our experience, general autopsy safety measures are effective. The absence of positive findings in our CNS samples give confidence in the sterility of our sampling technique, thereby making other sources of contamination in the skull sawdust samples less likely.

Pandemic preparedness should encompass plans for early, rapid autopsies to acquire vital data at the onset. General safety measures appear adequate for most pathogens encountered during autopsy, including SARS-CoV-2 (*3*). However, early testing for pathogens in skull sawdust, along with other tissues, could prove beneficial in further assessing the risk for occupational infections resulting from autopsies during future pandemics.

Acknowledgments

We thank Mira Utriainen and Leena Palmunen for their excellent work on PCR and viral culture in the BioSafety Level 3 laboratory and personnel at Helsinki University Central Hospital Diagnostic Center and the University of Helsinki for excellent technical assistance.

Funding was a provided by a DeLaval COVID donation, the Juho Vainio Foundation, and a Fazer COVID donation.

About the Author

Dr. Kantonen is a certified pathologist and medical doctor performing research at the University of Helsinki, Finland. His research interests focus on the use of autopsies for medical research.

References

1. Ledford H. Autopsy slowdown hinders quest to determine how coronavirus kills. Nature. 2020 May 7. https://doi.org/10.1038/d41586-020-01355-z
2. Fineschi V, Aprile A, Aquila I, Arcangeli M, Asmundo A, Bacci M, et al.; Scientific Society of Hospital Legal Medicine of the National Health System (COMLAS); Italian Society of Anatomical Pathology and Cytology (SIAPEC). Management of the corpse with suspect, probable or confirmed COVID-19 respiratory infection—Italian interim recommendations for personnel potentially exposed to material from corpses, including body fluids, in morgue structures and during autopsy practice. Pathologica. 2020;112:64–77.
3. Kritselis M, Remick DG. Universal precautions provide appropriate protection during autopsies of patients with infectious diseases. Am J Pathol. 2020;190:2180–4. https://doi.org/10.1016/j.ajpath.2020.08.005
4. Plenzig S, Bojkova D, Held H, Berger A, Holz F, Cinatl J, et al. Infectivity of deceased COVID-19 patients. Int J Legal Med. 2021;135:2055–60. https://doi.org/10.1007/s00414-021-02546-7
5. Jurek T, Rorat M, Szleszkowski Ł, Tokarski M, Pielka I, Małodobra-Mazur M. SARS-CoV-2 viral RNA is detected in the bone marrow in post-mortem samples using RT-LAMP. Diagnostics (Basel). 2022;12:515. https://doi.org/10.3390/diagnostics12020515
6. Corman VM, Landt O, Kaiser M, Molenkamp R, Meijer A, Chu DK, et al. Detection of 2019 novel coronavirus (2019-nCoV) by real-time RT-PCR. Euro Surveill. 2020;25:2000045. https://doi.org/10.2807/1560-7917.ES.2020.25.3.2000045
7. Brandner JM, Boor P, Borcherding L, Edler C, Gerber S, Heinemann A, et al. Contamination of personal protective equipment during COVID-19 autopsies. Virchows Arch. 2022;480:519–28. https://doi.org/10.1007/s00428-021-03263-7

Address for correspondence: Jonas N. Kantonen, University of Helsinki, Haartmaninkatu 3 C 323, 00290 Helsinki, Finland; email: jonas.kantonen@helsinki.fi

Novel Genotypes of Highly Pathogenic Avian Influenza H5N1 Clade 2.3.4.4b Viruses, Germany, November 2023

Ann Kathrin Ahrens, Anne Pohlmann, Christian Grund, Timm Harder, Martin Beer

Author affiliation: Friedrich-Loeffler-Institut, Greifswald–Insel Riems, Germany

DOI: https://doi.org/10.3201/eid3008.240103

Several subtypes and many different genotypes of highly pathogenic avian influenza viruses of subtype H5 clade 2.3.4.4b have repeatedly caused outbreaks in Germany. Four new highly pathogenic avian influenza genotypes emerged in November 2023 after reassortment with low pathogenicity precursors, replacing genotype BB, which had dominated in Europe since 2022.

Germany has experienced repeated outbreaks of highly pathogenic avian influenza (HPAI) viruses (HPAIVs) of clade 2.3.4.4b of the H5 goose/Guangdong lineage since 2016, causing devastating losses to wild bird biodiversity and the poultry production sector (*1*). Since 2016, seasonal outbreaks or cases increased during the winter season and decreased to zero in summer. Seasonality terminated in 2021, when HPAIV H5 became endemic in wild birds in Germany and the rest of Europe (*2*). Along with an increasing incidence, genetic diversity expanded, resulting in a high number of new genotypes (*3*).

During summer 2023, genotype Ger-02-23-N1.1 (BB based on the European Union nomenclature [*4*,*5*]), a reassortment with a gull-derived H13 virus, dominated HPAI cases caused by outbreaks in colony breeders (*6*). Sporadically, older genotypes (Ger-10-21-N1.5 and Ger-12-22-N1.1) were identified, accompanied by some viruses that could not be assigned to a proper genotype because of incomplete genome covering. After the breeding season ended, incidence decreased (84 cases in July, 16 in August, 10 in September, and 3 in October). In addition, increasing numbers of low pathogenicity avian influenza (LPAI) viruses (LPAIVs) were detected during active and passive wild bird monitoring, representing the autumnal, bird migration–related upsurge of avian influenza virus infections in Germany. Since November, the number of HPAIV H5 cases has increased to a still moderate but substantially higher level (29 in November).

We analyzed the genotypes of HPAI and LPAI viruses by using full-genome sequencing. Sequencing

procedures of HPAI and LPAI viruses (*7*) and methods for genotype differentiation including the reference sequences have been described previously (*8*). We analyzed 244 sequences from 33 viruses collected from late May to late November 2023, of which 22 originated from wild birds, 5 from poultry, and 6 from captive birds. We found various LPAIVs and 16 HPAIVs of H5N1 subtype in the resulting sequences (Table).

All HPAIV H5 sequences from viruses collected in November clustered differently from genotype Ger-02-23-N1.1 (BB) that dominated during the summer of 2023. None of those genotypes, including genome segments from viruses that could not be sequenced to completion, were detected after November 2023. Instead, we identified 4 new genotypes. Four viruses grouped with the HPAIV H5N1 genotype Ger-11-23-N1.1 (DB) (reference A/herring gull/Germany-NI/2023AI08764/2023) with a new reassorted polymerase basic 1 (PB1) gene similar to LPAIVs detected in a zoo in Germany (LPAI A/flamingo/Germany-ST/2023AI08233/2023 [H5N2]). One virus (reference A/barnacle goose/Germany-SH/2023AI08822/2023) was associated with genotype Germany Ger-11-23-N1.2 (AB) with a reassorted PB1 gene. Two viruses from Germany clustered with Ger-11-23-N1.3 (DG) (reference A/chicken/Germany-NI/2023AI08838/2023) containing the PB1 gene of Ger-11-23-N1.2 and a new reassorted polymerase basic 2 and polymerase acidic genes, which were also found in LPAIVs from a wild duck in Germany in October 2023 (type strain LPAI A/wild duck/Germany-NW/2023AI07895/2023 [H3N8]) and November 2023 (LPAI A/Eurasian Wigeon/Germany-MV/2023AI08762/2023 [H5N2]). Two sequences formed a new reassortant for Germany, Ger-11-23-N1.4 (DA) (reference A/common crane/Germany-HH/2023AI08835/2023) with new PB1, polymerase basic 2, and nonstructural gene segments (Appendix Figures 1, 2, https://wwwnc.cdc.gov/EID/article/30/8/24-0103-App1.pdf).

Table. Number of HPAI and LPAI virus subtypes identified from 244 sequences from 33 viruses collected in Germany, late May to late November 2023*

Subtype	Wild birds	Poultry	Captive birds
HPAI H5N1†	12	4	
LPAI H11N9			1
LPAI H2N3	1		
LPAI H3N8	3		
LPAI H4N6			2
LPAI H5N2†	1		2
LPAI H5N3	1		
LPAI H5N4		1	
LPAI H6N4	1		
LPAI H9N2	3		1

*HPAI, highly pathogenic avian influenza; LPAI, low pathogenicity avian influenza.

In conclusion, our study shows a high number of emerging new HPAIV H5 clade 2.3.4.4b genotypes in November 2023 and identified related LPAIVs circulating at the same time in the same area, which may have served as reassortment partners. These findings highlight the continued promiscuity of currently circulating HPAI H5 strains of clade 2.3.4.4b and the need for genotypic surveillance of both HPAIVs and LPAIVs.

This work was funded in part by the German Federal Ministry of Education and Research within the project PREPMEDVET (grant no. 13N15449), by the European Union under the Horizon 2020 Programme (grant agreement VEO no. 874735) and under the Horizon Europe Programme (grant agreement KAPPA-FLU no. 101084171).

All sequences from this study are available in the public GISAID (https://www.gisaid.org) EpiFlu database (accession nos. 18432788–9, 18432793, 18435608–12, 18458714–6, 18458718, 18458720, 18458722, 18463193–4, 18526630–5, 18745067–74, 18745076–7, and 18745086).

The authors declare no conflicts of interest in this work.

About the Author

Dr. Ahrens is a junior scientist at the Institute of Diagnostic Virology at the German Federal Institute for Animal Health (Friedrich-Loeffler-Institut). Her research interests include avian influenza viruses, from virus isolation up to real-time sequencing.

References

1. King J, Harder T, Conraths FJ, Beer M, Pohlmann A. The genetics of highly pathogenic avian influenza viruses of subtype H5 in Germany, 2006–2020. Transbound Emerg Dis. 2020.
2. Pohlmann A, King J, Fusaro A, Zecchin B, Banyard AC, Brown IH, et al. Has epizootic become enzootic? Evidence for a fundamental change in the infection dynamics of highly pathogenic avian influenza in Europe, 2021. MBio. 2022;13:e0060922. https://doi.org/10.1128/mbio.00609-22
3. Kandeil A, Patton C, Jones JC, Jeevan T, Harrington WN, Trifkovic S, et al. Rapid evolution of A(H5N1) influenza viruses after intercontinental spread to North America. Nat Commun. 2023;14:3082. https://doi.org/10.1038/s41467-023-38415-7
4. European Food Safety Authority, European Centre for Disease Prevention and Control, European Reference Laboratory for Avian Influenza, Adlhoch C, Fusaro A, Gonzales JL, et al. Avian influenza overview March–April 2023. EFSA J. 2023;21:8039. https://doi.org/10.2903/j.efsa.2023.8039
5. European Food Safety Authority, European Centre for Disease Prevention and Control, European Reference Laboratory for Avian Influenza, Adlhoch C, Fusaro A, Gonzales JL, et al. Avian influenza overview September–December 2023. EFSA J. 2023;21:8539. https://doi.org/10.2903/j.efsa.2023.8539

6. Pohlmann A. HPAIV genotypes in Germany. 2022 Sep 30 [cited 2024 May 21]. https://zenodo.org/records/7078789
7. King J, Harder T, Beer M, Pohlmann A. Rapid multiplex MinION nanopore sequencing workflow for influenza A viruses. BMC Infect Dis. 2020;20:648. https://doi.org/10.1186/s12879-020-05367-y
8. Pohlmann A, Harder T. Genotype differentiation of highly pathogenic avian influenza viruses (HPAIV) of the goose/Guangdong lineage in Germany—derivation and deployment of reference sequences. 2023 Aug 10 [cited 2021 May 21]. https://zenodo.org/records/8233815

Address for correspondence: Martin Beer, Friedrich-Loeffler-Institut, Südufer 10, 17493 Greifswald–Insel Riems, Germany; email: martin.beer@fli.de

COMMENT LETTER

Transmission and Surveillance of Rat Hepatitis E Virus in Swine

Matheus Filgueira Bezerra, Maria Gabriela Oliveira da Paz, Edmilson Ferreira de Oliveira-Filho, Christian Robson de Souza Reis

Author affiliations: Oswaldo Cruz Foundation, Recife, Pernambuco, Brazil (M.F. Bezerra, M.G.O. da Paz, C.R.D.S. Reis); Humboldt-Universität zu Berlin, Berlin, Germany (E.F. de Oliveira-Filho).

DOI: https://doi.org/10.3201/eid3008.240484

To the Editor: The study by Rios-Muñoz et al. reporting rat hepatitis E virus (HEV) RNA in swine feces contains intriguing findings with the potential to change our understanding of rat HEV transmission routes (*1*). One relevant aspect highlighted by the authors is that limited prior evidence of rat HEV infection in swine might be partially explained by the lack of rat HEV serology tests for pigs. The low genomic homology between rat HEV and other HEV (<60%) makes most of the commercially available HEV-based tests ineffective in detecting rat HEV (*2*,*3*).

Such findings are exciting but must be interpreted with caution because some gaps remain to be addressed. Pigs can feed on small mammal remains and even prey on rodents, which means detecting rat HEV RNA in pig feces does not conclusively indicate an infection. To rule out the possibility of viral detection because of contaminated food, it is necessary to detect the virus in other tissues, such as blood or liver (*3*). Of note, a substantial proportion of the positive samples in the study by Rios-Muñoz et al. exhibited high cycle threshold values, which might be suggestive of residual viral RNA. Furthermore, considering the hypothesis that both viruses could be transmitted through contaminated swine meat, it remains unclear why rat HEV infection in humans is uncommon when compared with other HEV.

Nevertheless, from our perspective, these findings suggest the possibility of approaching swine as a sentinel species. If results are confirmed in additional eco-epidemiologic studies, sampling swine stools could offer valuable public health information. Insights from other rodentborne diseases, such as bubonic plague, underscore the benefits of a surveillance strategy focused on sentinel species rather than primary hosts (*4*). Sampling rodents is logistically more challenging and expensive than for domestic animals, but surveillance of sentinel species is typically more efficient in predicting the dissemination of zoonotic diseases at early stages.

About the Author

Dr. Bezerra currently works a technologist at the Plague National Reference Laboratory, Aggeu Magalhães Institute, Recife, Brazil. His research interests include bubonic plague, epidemiology, laboratory diagnosis of zoonotic diseases, and genomic surveillance.

References

1. Rios-Muñoz L, Gonzálvez M, Caballero-Gomez J, Castro-Scholten S, Casares-Jimenez M, Agulló-Ros I, et al. Detection of rat hepatitis E virus in pigs, Spain, 2023. Emerg Infect Dis. 2024;30:823–6. https://doi.org/10.3201/eid3004.231629
2. Chen Z, Li G, Situ J, Li Z, Guo S, Huang Y, et al. Redeveloping antigen detection kits for the diagnosis of rat hepatitis E virus. J Clin Microbiol. 2023;61:e0071023. https://doi.org/10.1128/jcm.00710-23
3. Johne R, Plenge-Bönig A, Hess M, Ulrich RG, Reetz J, Schielke A. Detection of a novel hepatitis E-like virus in faeces of wild rats using a nested broad-spectrum RT-PCR. J Gen Virol. 2010;91:750–8. https://doi.org/10.1099/vir.0.016584-0
4. Rajerison M, Andrianaivoarimanana V, Ratsitorahina M, Rahelinirina S, Chanteau S, Telfer S, et al. Field assessment of dog as sentinel animal for plague in endemic foci of Madagascar. Integr Zool. 2021;16:886–92. https://doi.org/10.1111/1749-4877.12541

Address for correspondence: Matheus Bezerra, Oswaldo Cruz Foundation, Avenida Professor Moraes Rego, s/n, Recife/PE 50740-465, Brazil; email: matheus.bezerra@fiocruz.br

Gustav Klimt (1862–1918). *The Tree of Life, Stoclet Frieze,* (1905–1909 (detail). Oil, gold leaf, mosaic on canvas, 77 in x 40 in/195 cm x 102 cm (combined dimensions for 3 panels). Museum of Applied Arts, Vienna, Austria. Photo credit: Album/Art Resource. Digital image from Art Resource, New York, New York, USA.

The Tree of Life, Archetype and Artifice

Byron Breedlove

The tree of life is an archetype woven into various mythological, religious, philosophical, and shamanistic traditions around the world, as well as a concept underpinning some scientific efforts to depict the diversity of life. It is also a tantalizing subject for visual artists, and this month's cover image features an example, *The Tree of Life,* from the *Stoclet Frieze* by Gustav Klimt.

Author affiliation: Centers for Disease Control and Prevention, Atlanta, Georgia, USA

DOI: https://doi.org/10.3201/eid3008.AC3008

Klimt was born in 1862 in Baumgarten, Austria, then a small village near Vienna. His artistic talents were apparent from a young age, and when just 14 years old, he attended the Vienna School of Arts and Crafts on a scholarship. His brother Ernst later joined him, and they focused on becoming architectural painters. After graduation in 1883, the Klimt brothers and fellow artist Franz Matsch formed a successful studio, named Künstler-Compagnie (Artists' Company), which received commissions for creating murals and art for public spaces such as theaters and museums.

An uncredited online biography of Klimt recounts, "Their most notable works during this time were the mural at the Vienna Burgtheater and the ceiling above the staircase at the Kunsthistorisches Museum. The group was honored for their achievements in 1888, when they received the Golden Order of Merit from Austro-Hungarian Emperor Franz Josef I."

After Gustav Klimt's father and brother, both named Ernst, both died in 1892, Klimt shifted to more personal and less traditional artistic pursuits. In 1897, he was among the Austrian artists who formed the Vienna Secession, a movement that favored symbolism and allegory over realism. Art historian Dusan Nikolic wrote, "Under the presidency of Klimt, they founded the Union of Austrian Artists Vienna Secession, intending to educate society through future-oriented artistic concepts and infusing life with art." Rifts among this group began, and Nikolic noted that Klimt, "whose style became a combination of natural elements with large areas of abstract geometrical ornament," and other prominent members who also favored abstract style over realism left the movement in 1908.

The *Stoclet Frieze* is among the best-known works from Klimt's "Golden Phase," which started a few years before he broke from the Vienna Secession. A wealthy Belgian couple, Adolphe and Suzanne Stoclet, commissioned Klimt to design a series of mosaics for the dining room at their Palais Stoclet in Brussels. Klimt's panels depict a standing female figure, a central panel known as *The Tree of Life*, and a couple embracing (Figure). Klimt worked on that intricate ornamental mosaic for 5 years, incorporating semiprecious stones, gilded tiles, enamel, marble, ceramics, gold leaf, and other opulent materials. Art historian A.N. Hodge noted that it showcases Klimt's "mastery of mosaic, a technique he had intensely studied on his recent trip to Ravenna [Italy]."

The center panel features a mosaic of a golden tree with curling, spiraling branches, festooned with recurring decorative shapes. The tree grows from an ochre patch of earth, and dazzling jeweled flowers cluster around the trunk. Klimt's opulent and luminescent tree celebrates the continuity and complexity of life. Perched on a lower branch is a large black bird that contrasts with the brightly shimmering gold background, perhaps intended by Klimt as a symbol of death.

Klimt's tree is symbolic, but in the biological sciences, the tree motif proved, for a time, a useful working artifice. Charles Darwin wrote, "The affinities of all the beings of the same class have sometimes been represented by a great tree. I believe this simile largely speaks the truth." Science writer David Quammen explores this topic in his book *The Tangled Tree: A Radical New History of Life* and documents how trees have been used to categorize the diversity of life forms that

Figure. *Stoclet Frieze* by Gustav Klimt, depicting a standing female figure, a central panel known as *The Tree of Life*, and a couple embracing.

emerged and evolved from some common ancestral microbe billions of years ago. Quammen discusses trees sketched by Charles Darwin and Ernst Haeckel in the 17th Century, provides example of trees from the 18th- and 19th-Century scientific literature, and shows modern iterations created by 20th-Century scientists.

Modern evolutionary classification is a rapidly changing science, especially regarding microbial life. In 1977, a team of researchers lead by biophysicist Carl Woese announced their discovery of a new, distinct category of microbial life now known as Archaea. Woese's work made previous trees of life obsolete and new depictions of such trees, including his own, more contorted. Scientists now categorize life on earth into 3 domains: Bacteria, Archaea, and Eukaryota. Those domains are further subdivided into 6 kingdoms: Animalia, Plantae, Fungi, Protista, Archaebacteria, and Eubacteria.

Mapping life's diversity via the tree motif was further complicated after the 20th-Century discovery of horizonal gene transfer—that is, the movement of DNA between organisms instead of transmission from parent to offspring. Such sideways transfer occurs across species and across kingdoms, blurring those boundaries, and contributes to the spread of antimicrobial resistance. Quammen notes that "the tree hypothesis works poorly for the history of bacteria and archaea, with all their sideways exchanges; and it works imperfectly for everything else."

This month's issue of *Emerging Infectious Diseases* focuses on the diversity of life, and an article by Stefanie Duller and Christine Moissl-Eichinger examines how archaea in the human microbiome are linked to various diseases, "though archaea are generally considered nonpathogenic." Other articles discuss a range of emerging infections from various kingdoms, including different bacterial, fungal, and viral agents.

In his 1999 article Phylogenetic Classification and the Universal Tree, biologist W. Ford Doolittle stated, "Molecular phylogeneticists will have failed to find the 'true tree,' not because their methods are inadequate or because they have chosen the wrong genes, but because the history of life cannot properly be represented as a tree. However, taxonomies based on molecular sequences will remain indispensable, and understanding of the evolutionary process will ultimately be enriched, not impoverished." Even if the tree motif does not serve as an accurate artifice to illustrate the diversity of life, especially at the microbial level, Klimt's *The Tree of Life* resonates as a celebration of this archetypal image.

Bibliography

1. Cooper JC. An illustrated encyclopaedia of traditional symbols. London: Thames and Hudson Ltd.; 1978. p. 176–9.
2. Darwin C. Natural selection (Chapter IV). In: On the origin of species, 1st edition [cited 2024 Jul 10]. https://www.gutenberg.org/files/1228/1228-h/1228-h.htm
3. Doolittle WF. Phylogenetic classification and the universal tree. Science. 1999;284:2124–9. https://doi.org/10.1126/science.284.5423.2124
4. Duller S, Moissl-Eichinger C. Archaea in the human microbiome and potential effects on human infectious disease. Emerg Infect Dis. 2024;30:1505–13. https://doi.org/10.3201/eid3008.240181
5. Gustav Klimt. Biography.com. [cited 2024 Jun 30]. https://www.biography.com/artists/gustav-klimt
6. Hodge AN. Gustav Klimt. London: Arcturus Publishing; 2019.
7. Nikolic D. Viennese visionary: the life and art of Gustav Klimt [cited 2024 Jul 30] https://www.thecollector.com/life-and-art-of-gustav-klimt
8. Quammen D. The tangled tree: a radical new history of life. New York: Simon & Schuster, Inc.; 2018.
9. The Tree of Life,, Stoclet Frieze, 1905 by Gustav Klimt [cited 2024 June 30]. https://www.gustav-klimt.com/The-Tree-Of-Life.jsp
10. Balch WE, Magrum LJ, Fox GE, Wolfe RS, Woese CR. An ancient divergence among the bacteria. J Mol Evol. 1977;9:305–11. https://doi.org/10.1007/BF01796092
11. Wolfe S. The life and paintings of Gustav Klimt. Artland Magazine [cited 2024 Jun 30]. https://magazine.artland.com/gustav-klimt-life-paintings

Address for correspondence: Byron Breedlove, EID Journal, Centers for Disease Control and Prevention, 1600 Clifton Rd NE, Mailstop H16-2, Atlanta, GA 30329-4018, USA; email: wbb1@cdc.gov

EMERGING INFECTIOUS DISEASES®

Upcoming Issue • Parasitic Diseases

- Morphologic and Molecular Identification of Human Ocular Infection Caused by *Pelecitus* species, Thailand
- Molecular Confirmation of *Taenia solium* Taeniasis in Child, Timor-Leste
- Clinical Aspects and Disease Severity of *Streptococcus dysgalactiae* Subspecies *equisimilis* Bacteremia, Finland
- Loop-Mediated Isothermal Amplification Assay to Detect Invasive Malaria Vector *Anopheles stephensi* Mosquitoes
- Emergence of Extensively Drug-Resistant *Neisseria gonorrhoeae,* France, 2023
- Co-Circulation of Genetically Distinct High Pathogenicity Avian Influenza A(H5N5) and (H5N1) Viruses in Crows, Hokkaido, Japan
- Mosquitoes as Vectors of Buruli Ulcer Based on Transmission of Ross River/ Barmah Forest Virus and *Mycobacterium ulcerans*, Australia
- Fatal Case of *Naegleria fowleri* Primary Amebic Meningoencephalitis from Indoor Surfing Center, Taiwan, 2023
- Clinical Significance, Species Distribution, and Temporal Trends of Nontuberculous Mycobacteria, Denmark, 1991–2022

Complete list of articles in the September issue at https://wwwnc.cdc.gov/eid/#issue-313

Earning CME Credit

To obtain credit, you should first read the journal article. After reading the article, you should be able to answer the following, related, multiple-choice questions. To complete the questions (with a minimum 75% passing score) and earn continuing medical education (CME) credit, please go to http://www.medscape.org/journal/eid. Credit cannot be obtained for tests completed on paper, although you may use the worksheet below to keep a record of your answers.

You must be a registered user on http://www.medscape.org. If you are not registered on http://www.medscape.org, please click on the "Register" link on the right hand side of the website.

Only one answer is correct for each question. Once you successfully answer all post-test questions, you will be able to view and/or print your certificate. For questions regarding this activity, contact the accredited provider, CME@medscape.net. For technical assistance, contact CME@medscape.net. American Medical Association's Physician's Recognition Award (AMA PRA) credits are accepted in the US as evidence of participation in CME activities. For further information on this award, please go to https://www.ama-assn.org. The AMA has determined that physicians not licensed in the US who participate in this CME activity are eligible for AMA PRA Category 1 Credits™. Through agreements that the AMA has made with agencies in some countries, AMA PRA credit may be acceptable as evidence of participation in CME activities. If you are not licensed in the US, please complete the questions online, print the AMA PRA CME credit certificate, and present it to your national medical association for review.

Article Title

Archaea in the Human Microbiome and Potential Effects on Human Infectious Disease

CME Questions

1. Which of the following member of the archaea family is most commonly found in human feces?

A. Methanobrevibacteroralis
B. Mycobacterium massisiliense
C. Melica smithii
D. Thermoplasma-like spp.

2. What byproduct is most commonly associated with archaea?

A. Hydrogen
B. Nitrogen
C. Methane
D. Bicarbonate

3. Which of the following statements regarding the potential role of archaea as human pathogens most accurate?

A. They are directly implicated in causing infections of multiple organ systems
B. They are most clearly pathogenic in the presence of bacteria such as *Escherichia coli*
C. They are mostly considered nonpathogenic
D. They are not pathogenic and instead have been demonstrated to be vital to digestion and circulatory health

4. Archaea are most associated with pathologic processes at which of the following anatomic sites?

A. Oral cavity
B. Lungs
C. Skin
D. Central nervous system

Earning CME Credit

To obtain credit, you should first read the journal article. After reading the article, you should be able to answer the following, related, multiple-choice questions. To complete the questions (with a minimum 75% passing score) and earn continuing medical education (CME) credit, please go to http://www.medscape.org/journal/eid. Credit cannot be obtained for tests completed on paper, although you may use the worksheet below to keep a record of your answers.

You must be a registered user on http://www.medscape.org. If you are not registered on http://www.medscape.org, please click on the "Register" link on the right hand side of the website.

Only one answer is correct for each question. Once you successfully answer all post-test questions, you will be able to view and/or print your certificate. For questions regarding this activity, contact the accredited provider, CME@medscape.net. For technical assistance, contact CME@medscape.net. American Medical Association's Physician's Recognition Award (AMA PRA) credits are accepted in the US as evidence of participation in CME activities. For further information on this award, please go to https://www.ama-assn.org. The AMA has determined that physicians not licensed in the US who participate in this CME activity are eligible for AMA PRA Category 1 Credits™. Through agreements that the AMA has made with agencies in some countries, AMA PRA credit may be acceptable as evidence of participation in CME activities. If you are not licensed in the US, please complete the questions online, print the AMA PRA CME credit certificate, and present it to your national medical association for review.

Article Title

Retrospective Study of Infections with *Corynebacterium diphtheriae* Species Complex, French Guiana, 2016–2021

CME Questions

1. Which of the following statements regarding the epidemiology of corynebacteria infections in the current study is most accurate?

A. > 90% of infections with *Corynebacterium diphtheriae* were cutaneous
B. Infections with *C. diphtheriae* and *C. ulcerans* nearly equally common
C. About half of cases of *C. diphtheriae* infection were tox-positive
D. There was a gradual decline in the annual number of corynebacteria cases between 2016 and 2022

2. Which of the following statements regarding the clinical presentation of patients with corynebacteria infection in the current study is most accurate?

A. The mean age of patients was 76 years old
B. More female patients had infection than male patients
C. 35% of patients with infection had a history of immunosuppression
D. Two-thirds of patients with infection were up-to-date on diphtheria vaccination

3. What was the most common anatomic site of cutaneous infections with *C. diphtheriae* in the current study?

A. Upper extremities
B. Lower extremities
C. Head
D. Abdomen

4. Which of the following statements regarding the clinical management and outcomes of patients with cutaneous infection with *C. diphtheriae* in the current study is most accurate?

A. 12% of cutaneous *C.diphtheriae* cases were treated with dressing care alone
B. The most commonly used antibiotic was doxycycline
C. 61% of patients experienced an unfavorable outcome
D. 25% of patients received diphtheria antitoxin

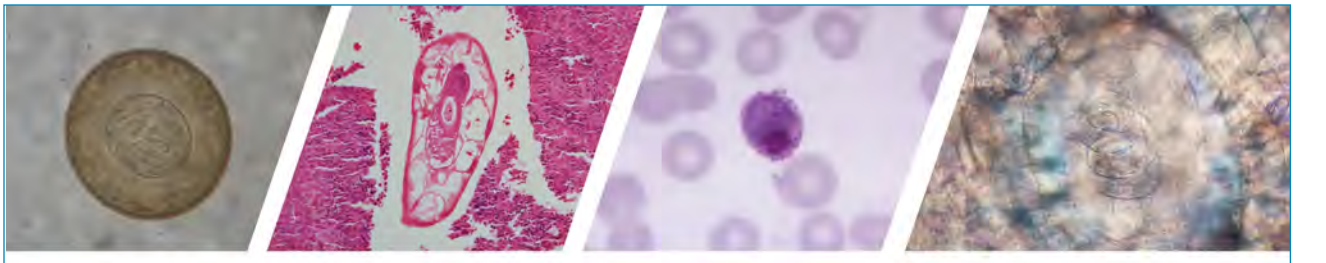

DPDx

Diagnostic Assistance and Training in Laboratory Identification of Parasites

A free service of CDC available to laboratorians, pathologists, and other health professionals in the United States and abroad

- Diagnosis from photographs of worms, histological sections, fecal, blood, and other specimen types
- Expert diagnostic review
- Formal diagnostic laboratory report
- Submission of samples via secure file share

Visit the DPDx website for information on laboratory diagnosis, geographic distribution, clinical features, parasite life cycles, and training via Monthly Case Studies of parasitic diseases.

www.cdc.gov/dpdx
dpdx@cdc.gov

U.S. Department of Health and Human Services
Centers for Disease Control and Prevention

CS272346-DE